UNIVERSITY OF TASMANIA

Towards the Isolation of α-*N*-Metallated Free *N*-Heterocyclic Carbenes

by

Mei Yi Leow, BSc (Hons)

A thesis submitted in fulfilment of the requirements for the degree of Doctor of Philosophy at the University of Tasmania

School of Natural Sciences

University of Tasmania

February 2019

Candidate statement

This thesis contains no material which has been accepted for a degree or diploma by the University or any other institution, except by way of background information and duly acknowledged in the thesis, and to the best of my knowledge and belief no material previously published or written by another person except where due acknowledgement is made in the text of the thesis, nor does the thesis contain any material that infringes copyright.

This thesis may be made available for loan and limited copying and communication in accordance with the Copyright Act 1968.

Mei Yi Leow

February 2019

Statement of Co-Authorship

The following people and institutions contributed to the publication of work undertaken as part of this thesis:

Mei Yi Leow, School of Natural Sciences = **Candidate**
Curtis C. Ho, University of Tasmania = **Author 1**
Michael G. Gardiner, University of Tasmania = **Author 2**
Alex C. Bissember, University of Tasmania = **Author 3**

Author details and their roles:

Review article: Non-Classical Anionic Naked N-Heterocyclic Carbenes: Fundamental Properties and Emerging Applications in Synthesis and Catalysis
Located in Chapter 1

Candidate was the primary author and drafted significant parts of the paper. Candidate contributed approximately 60 % to the literature review and the preparation of the paper.
Author 1 contributed approximately 20 % to the literature review and the drafting of the paper.
Authors 2 and 3 contributed to the determination of the scope for the paper and refinement of the work by critically revising the paper.

We the undersigned agree with the above stated "proportion of work undertaken" for the above published peer-reviewed manuscript contributing to this thesis:

Signed: _____

Dr Michael G. Gardiner
Supervisor
School of Natural Sciences
University of Tasmania

Professor Mark Hunt
Dean of Natural Sciences
School of Natural Sciences
University of Tasmania

Acknowledgements

First and foremost, I am profoundly grateful to my supervisors Assoc Prof Michael Gardiner and Dr Alex Bissember for their continual guidance and mentorship. Through their generosity, I have received every opportunity for growth, and I sincerely hope that I have done them justice with this work.

I am also indebted to Dr Nathan Kilah for his meticulous critique of one chapter, and his help with navigating the often arcane world of crystallography.

Furthermore, I would like to thank Dr Richard Wilson and Dr David Nichols for conducting the mass spectrometry analyses, and Dr Thomas Rodemann for performing the elemental analyses.

For every fleeting moment of success, there have been weeks and months when the challenges felt insurmountable. I owe a great deal to my friends and family, whose small kindnesses provided temporary reprieve during those troubled times.

Of the many individuals who have helped me, knowingly or not, there are two who deserve a special mention:

My loyal friend and lab ally, the relentlessly optimistic Dr Curtis Ho, with whom many base bath conversations and inside jokes were shared. Thank you for lifting both my spirits and anything that weighed more than 20 kg;

And Kieran – first buddy, and soon husband – who firmly believed the best of me when I could not. If nothing else, this book is the reason we met, and that alone will have made it worth the journey.

Abstract

Great strides have been made in the synthesis and understanding of *N*-heterocyclic carbenes (NHCs). This has led to tremendous success in their use in catalytic transformations, either directly or as ligands for transition metals. Although NHCs spanning a vast range of *N*-heterocycle classes are known, those derived from imidazolium and benzimidazolium frameworks are especially popular for their steric and electronic tunability. The two *N*-substituents constitute major sites for structural modification, and currently, NR,NR (R = alkyl, aryl), NR,NH, NH,NH and naked N,NR substitution patterns are known.

This work attempts to expand the scope of free benzimidazolium-derived NHCs to include NM,NR (M = metal) types. These free NM,NR NHCs may possess capabilities for dual catalysis as a result of the proximal Lewis acidic metal centre and Lewis basic free carbene. A modular *N*,*N'*,*N''*,*N'''*-tetradentate bis(benzimidazolyl) ligand framework "MeRLH$_2$" (R = bridging group) designed specifically for the demonstration of proof-of-concept would coordinatively saturate the metal centre, preventing its migration to the adjacent carbene site and thus preserving the α-*N*-metallated free NHC motif. The figure below illustrates the proposed formation of the target NHC from a precursor MeRLH$_2$ complex, with the desired free NM,NR NHC motif highlighted in blue.

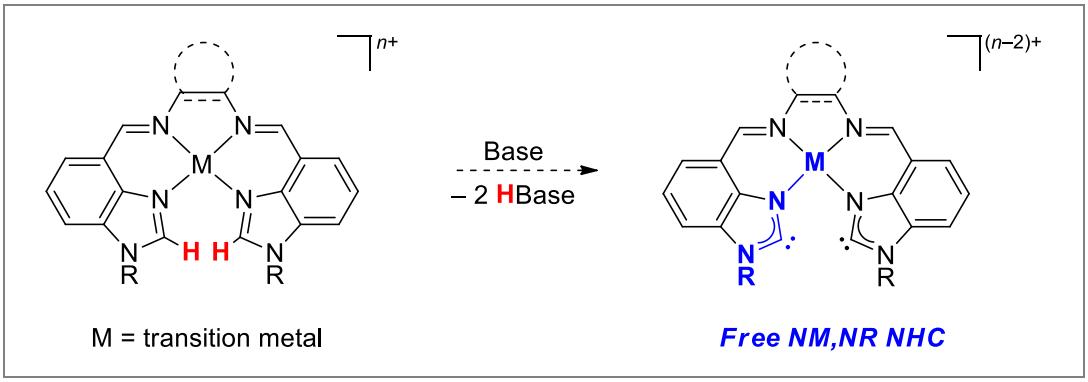

Synthetic pathways towards a C_2-symmetric ethylene-bridged bis(benzimidazolyl) ligand Me(en)LH$_2$ from three different precursors, namely 2-amino-3-nitrophenol, 2-amino-3-nitrotoluene and methyl 2-amino-3-nitrobenzoate, are described. An efficient protocol for the multigram-scale synthesis of Me(en)LH$_2$ was successfully established. The preparation of its respective cyclohexyl- and phenylene-bridged analogues, MeCyLH$_2$ and MePhLH$_2$ are also discussed. The challenges encountered during attempts to

prepare them as free ligands are circumvented using metal-templated condensation of the cyclic diamines and key precursor aldehyde.

A series of nickel(II), copper(II), cobalt(II), silver(I), zinc(II) and palladium(II) complexes of these novel *N*,*N'*,*N''*,*N'''*-tetradentate bis(benzimidazolyl) ligands was synthesised. Their suitability as precursors to the free NM,NR NHC was assessed based on their stability, solubility, geometric and spectroscopic properties. In accordance with initial predictions, the palladium(II) complexes were shown to be the prime candidate for further studies, as they consistently exhibited square planar coordination geometries, diamagnetic behaviour, and in some cases, greater stability compared to their nickel(II), copper(II), cobalt(II) or silver(I) counterparts. Counterion effects in the nickel(II), copper(II) and cobalt(II) complexes and the structural impacts of bridging group variations in the nickel(II) and palladium(II) complexes of $MeRLH_2$ are also discussed.

NMR-scale deprotonation trials using a range of inorganic and organic bases were conducted on the palladium(II) suite of complexes $[PdMeRLH_2](OTf)_2$ (R = en, Cy, Ph). The results suggest that the NM,NR NHC decomposes too rapidly to be observed or isolated. Increasing the rigidity of the bridging group between the imine donor atoms failed to prevent decomposition. However, base-assisted deuterium exchange experiments with $[PdMe(en)LH_2](OTf)_2$ support the transient existence of the NM,NR NHC. It is suspected that competitive deprotonation at the aldimines and the limited solubility of these complexes in inert solvents both contributed to the formation of complex product mixtures. Alternative approaches to the NM,NR NHC such as simultaneous complexation/deprotonation with alkylmetal reagents or stepwise deprotonation-then-complexation were found to be unsuccessful.

These findings suggest that future endeavours to isolate a free NM,NR NHC may benefit from replacing the benzimidazolyl core structure with imidazolyls, which have more acidic C2 protons; increasing steric bulk around the ligand for improved solubility, and eliminating other potential deprotonation sites on the ligand.

Publications and presentations

Parts of Chapter 1 have been published in a peer-reviewed open access journal. The article is included in the appendix:

Review article

Non-Classical Anionic Naked *N*-Heterocyclic Carbenes: Fundamental Properties and Emerging Applications in Synthesis and Catalysis

M. Y. Leow, C. C. Ho, M. G. Gardiner, A. C. Bissember, *Catalysts*, 2018, **8**, 620.

This work has also been presented at the following conferences:

Poster

Novel *N*-Bound Platinum Complexes Featuring Proximal Free *N*-Heterocyclic Carbenes

M. Y. Leow, M. G. Gardiner, A. C. Bissember, *27th International Conference on Organometallic Chemistry*, 17 – 22 July 2016, Melbourne, Australia.

Oral presentation

Towards the Isolation of an α-*N*-Metallated Free *N*-Heterocyclic Carbene

M. Y. Leow, A. C. Bissember, M. G. Gardiner, *11th Australasian Organometallics Meeting*, 16 – 19 January 2018, Perth, Australia.

Table of contents

Abbreviations

Å	Angstrom, 10^{-10} m
Ad	Adamantyl, $–C_{10}H_{15}$
AIBN	2,2’-Azobisisobutyronitrile
app.	Apparent
aq	Aqueous
atm	Atmosphere, 1.01325×10^5 Pa
Bim	Benzimidazole
Boc	*tert*-Butoxycarbonyl
BPO	Benzoyl peroxide
ca.	Circa
CAAC	Cyclic (alkyl)(amino)carbene
CAN	Ceric ammonium nitrate
cat	Catalyst
CD_2Cl_2	Deuterated dichloromethane
$CDCl_3$	Deuterated chloroform
COE	Cyclooctene
COD	1,5-Cyclooctadiene
COSY	(Homonuclear) Correlation spectroscopy
Cy	Cyclohexyl, $–C_6H_{11}$
d	Doublet (NMR spectroscopy)
DABCO	1,4-Diazabicyclo[2.2.2]octane
dba	Dibenzylideneacetone

DBDMH	1,3-Dibromo-5,5-dimethylhydantoin
DBU	1,8-Diazabicyclo[5.4.0]undec-7-ene
dd	Doublet of doublets (NMR spectroscopy)
d_6-DMSO	Deuterated dimethyl sulfoxide
d_8-THF	Deuterated tetrahydrofuran
dipp	1,3-Diisopropylphenyl
DMAP	Dimethylaminopyridine
DMF	*N*,*N*-Dimethylformamide
DMP	Dess–Martin periodinane, 1,1,1-triacetoxy-1,1-dihydro-1,2-benziodoxol-3(1*H*)-one
DMPU	*N*,*N′*-Dimethylpropyleneurea
DMSO	Dimethyl sulfoxide
EI-MS	Electron impact ionisation mass spectrometry
en	Ethylenediamine
eq	Equivalent(s)
ESD	Estimated standard deviation
ESI-MS	Electrospray ionisation mass spectrometry
EtOH	Ethanol
FAB	Fast atom bombardment
h	Hour
HMBC	Heteronuclear multiple bond correlation
HRMS	High resolution mass spectrometry
HSQC	Heteronuclear single quantum correlation
IAd	1,3-Di-1-adamantylimidazol-2-ylidene

I(*i*Pr)	1,3-Diisopropylimidazol-2-ylidene
*i*Pr	Isopropyl, –$CH(CH_3)_2$
IPr	1,3-Bis(diisopropyl)phenylimidazol-2-ylidene
*i*PrOH	Isopropanol
IR	Infrared
I*t*Bu	1,3-Di-*tert*-butylimidazol-2-ylidene
L	Ligand
liq	Liquid
m	Multiplet (NMR spectroscopy)
M	Metal
MeOH	Methanol
min	Minute
mp	Melting point
NBS	*N*-Bromosuccinimide
*n*Bu	*n*-Butyl
NHC	*N*-heterocyclic carbene
NMR	Nuclear magnetic resonance
OAc	Acetate, CH_3COO^-
OTf	Triflate (trifluoromethanesulfonate, –OSO_2CF_3)
Pd/C	Palladium on carbon
Ph	Phenyl, –C_6H_5
ppm	Parts per million
rt	Room temperature
s	Singlet (NMR spectroscopy)

SC-XRD	Single crystal X-ray diffraction
SIMes	1,3-Bis(2,4,6-trimethylphenyl)-4,5-dihydroimidazol-2-ylidene
t	Triplet (NMR spectroscopy) **OR** time
*t*Bu	*tert*-Butyl
TFA	Trifluoroacetic acid
THF	Tetrahydrofuran
TLC	Thin layer chromatography
TMP	2,2,6,6-Tetramethylpiperidine
TON	Turnover number

General experimental considerations

General remarks

All air-sensitive manipulations were performed under an atmosphere of high purity argon using standard Schlenk techniques, and/or in a high purity nitrogen-filled glovebox. Glassware was heated under vacuum and backfilled with argon to ensure the exclusion of air and moisture from these reactions. All solvents were of analytical grade or higher. Toluene, THF, 40/60 petroleum spirits were dried by passage through alumina columns in an Innovative Technologies solvent purifier, and stored over sodium mirrors. Anhydrous MeOH (≥99.8 % purity) and anhydrous DMSO (≥99.9 % purity) were purchased from Sigma-Aldrich and stored in ampoules over 3 Å molecular sieves. Deuterated solvents for NMR spectroscopy were purchased from Cambridge Isotope Laboratories. Anhydrous d_6-DMSO and CD_3CN were obtained by distillation over CaH_2 under an argon atmosphere and stored over molecular sieves under N_2 before use. C_6D_6 was distilled over sodium/benzophenone and stored under N_2. All reagents were purchased from commercial suppliers and used as received or prepared according to a reported procedure unless stated otherwise. 2-Amino-3-nitrotoluene, methyl 2-amino-3-nitrobenzoate, Dess–Martin periodinane, and (1*R*,2*R*)-(−)-1,2-diaminocyclohexane were purchased from Combi-Blocks. Palladium(II) acetate was purchased from Precious Metals Online. *N*-bromosuccinimide was recrystallised from water before use.

Instrumentation

NMR spectroscopic data were recorded at 293 K on a Bruker Avance III NMR spectrometer operating at 400 MHz (^{1}H) or 100 MHz (^{13}C), or on a Bruker Avance III spectrometer 600 MHz spectrometer operating at 600 MHz (^{1}H) or 150 MHz (^{13}C). NMR spectra were referenced against the ^{1}H or ^{13}C resonance of the residual solvent peak(s).

Elemental analyses for nitrogen, carbon, hydrogen and sulfur were performed by Dr Thomas Rodemann from the Central Science Laboratory at the University of Tasmania (CSL UTas), using a Thermo Finnigan EA 1112 Series Flash Elemental Analyser. High resolution ESI-MS analyses were conducted by Dr Richard Wilson, also of CSL UTas, using a Thermo Fisher Scientific LTQ-Orbitrap high resolution mass spectrometer. Samples were introduced by

infusion at 5 µl per minute using positive mode electrospray ionisation, with an applied voltage of 4 kV. Full scan data (*m*/*z* range 150 – 2000 at a resolution of 60 000) and reported values for M+H or M+Na ions were based on the averaged spectrum of 20 successive scans.

Low resolution ESI-MS analyses were conducted by Dr David Nichols from CSL UTas using a Waters Acquity® H-class UPLC system coupled to a Waters Xevo® triple quadrupole mass spectrometer (Waters Corporation, Milford, MA). Analyses were undertaken using direct infusion of sample dissolved in methanol, and analysed by full scan mass spectrometry in positive electrospray ionisation mode. Electrospray ionisation was performed with a capillary voltage of ±2.7 kV and individual cone voltages. The desolvation temperature was 450 °C, using nitrogen as the nebulising gas at 950 L/h and cone gas at 50 L/h.

Low and high resolution EI-MS analyses were also performed by Dr David Nichols, employing a Kratos Concept ISQ mass spectrometer operated on Mach 3 software. An accelerating voltage of 8 kV was used at a 25 s per decade scan rate. The sample was introduced by a direct insertion probe with a source temperature of 200 °C. Low resolution full scan data was acquired at a mass resolution of 2000, whereas high resolution mass spectra were acquired at a mass resolution of 10 000 via peak matching (10 % valley definition) using PFK as an internal reference.

Single crystal X-ray diffraction

X-ray data were collected at 100 K (unless otherwise stated) to approximately 0.84 Å resolution on a Bruker AXS D8 Quest diffractometer employing Cu-Kα radiation (λ = 1.54178 Å), or on the MX1/MX2 beamlines of the Australian Synchrotron.[1] Crystals were mounted on a Hampton Scientific cryoloop. Structure solution and refinement were achieved by direct methods with SHELXT[2] and full matrix least squares routines against F^2 with SHELXL-97 respectively, on the OLEX2[3] graphical user interface. Non-hydrogen atoms were modelled with anisotropic displacement parameters, whereas hydrogen atoms were located in calculated positions and refined using a riding atom model. C–H distances were fixed at 0.95 Å (sp^2 CH), 0.99 Å (CH_2) and 0.98 Å (CH_3). The thermal parameters of all hydrogen atoms were estimated as $U_{iso}(H) = 1.2U_{eq}(C)$, except for CH_3 where $U_{iso}(H) = 1.5U_{eq}(C)$.

References

1 T. M. McPhillips, S. E. McPhillips, H.-J. Chiu, A. E. Cohen, A. M. Deacon, P. J. Ellis, E. Garman, A. Gonzalez, N. K. Sauter, R. P. Phizackerley, S. M. Soltis and P. Kuhn, *J. Synchrotron Radiat.*, 2002, **9**, 401–406.

2 G. M. Sheldrick, *Acta Crystallogr. Sect. C Struct. Chem.*, 2015, **71**, 3–8.

3 O. V. Dolomanov, L. J. Bourhis, R. J. Gildea, J. A. K. Howard and H. Puschmann, *J. Appl. Crystallogr.*, 2009, **42**, 339–341.

1 Introduction

1.1 Carbenes: Definition, structure, and general properties

The structure and behaviour of carbenes have captured the imagination of chemists for decades. Although initially regarded as transient intermediates that were too reactive to be isolated,[1–6] enormous advances in the field have enabled the successful isolation of a staggering variety of stable free carbenes.[7–10] Many carbenes and their complexes have found practical applications in synthesis,[11–15] medicine,[16,17] and materials chemistry.[18–24]

By definition, a carbene is any compound bearing a neutral, divalent carbon atom with only six valence electrons.[7,25] Four of these electrons form the two C–X bonds (X = C, H, heteroatom). The electronic configuration of the two remaining non-bonding electrons dictates the geometry and reactivity of the carbene, as illustrated in Figure 1.1.

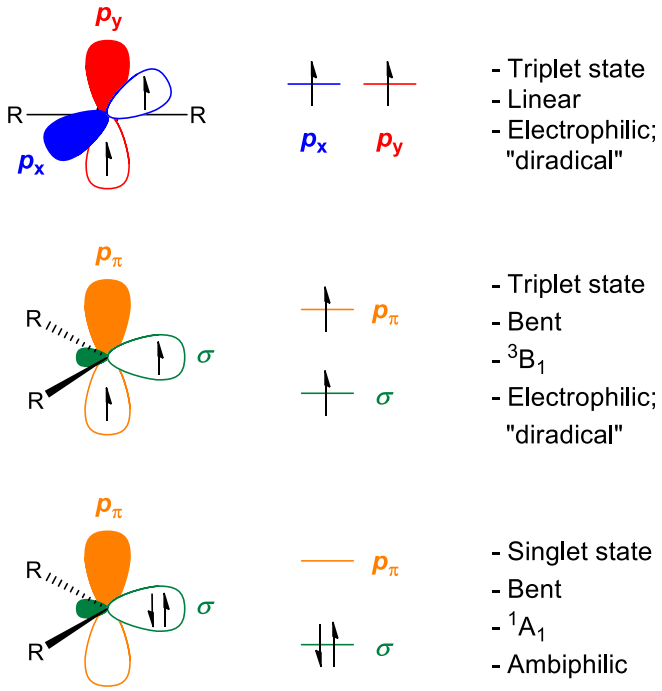

Figure 1.1 *The effects of hybridisation and spin multiplicity on the geometry and reactivity of carbenes.*

In cases where the carbene centre is *sp*-hybridised, each of the degenerate *p* orbitals are singly occupied by non-bonding electrons with the same spin, resulting in a spin multiplicity of 3; hence the label “triplet state”. As a

consequence of *sp*-hybridisation, the carbene centre adopts a linear geometry. Given that each *p* orbital can accept another electron of opposite spin, it is unsurprising that linear carbenes mimic the reactivity of diradicals.

Highly unstable by nature, linear carbenes are uncommon. Carbenes typically adopt a bent geometry, reflecting the sp^2-hybridised nature of the carbene centre. Here, the *p* orbitals are no longer degenerate: One of the *p* orbitals acquires some degree of *s* character and becomes lower in energy than the other *p* orbital, which remains largely unchanged. The two orbitals are usually denoted σ and p_π respectively.

Now, two main possibilities exist for the assignment of the non-bonding electrons. In the first instance, the electrons have parallel spins and separately occupy the σ and p_π orbitals. This gives rise to a triplet ground state ($^3B_1$). Alternatively, the non-bonding electrons may be spin-paired in the σ orbital, leaving the higher energy p_π orbital unoccupied. Since this creates a ground state spin multiplicity of 1, it is referred to as the singlet state ($^1A_1$). Singlet carbenes possess an ambiphilic character: Nucleophilicity is attributed to the fully occupied σ orbital, whereas electrophilicity arises from the presence of the vacant p_π orbital. It is conceivable for the non-bonding electrons in singlet carbenes to occupy the p_π orbital instead of the σ orbital, but this is usually the least stable of the two states.

The ground state multiplicity of a carbene is governed by the relative energies of the σ and p_π orbitals. A large energy separation of 2 eV or more will favour the singlet state, whereas an energy difference less than 1.5 eV will lead to the triplet state.[26] The steric and electronic properties of the carbene substituents heavily influence the energies of the σ and p_π orbitals. Bulky substituents will generally stabilise all carbenes kinetically, regardless of multiplicity. In the absence of other geometric constraints, increasing the steric bulk of the substituents can also widen the carbene bond angle, bringing it closer to linearity, thus favouring the triplet state.[27]

It is widely accepted that σ-electron-withdrawing substituents can inductively stabilise the carbene σ orbital by increasing its *s* character, without altering the p_π orbital (Figure 1.2). This results in a larger σ—p_π gap, which in turn stabilises the singlet state. In the reverse case, σ-electron-donating substituents reduce the size of the σ—p_π gap, and thus the triplet state is favoured.

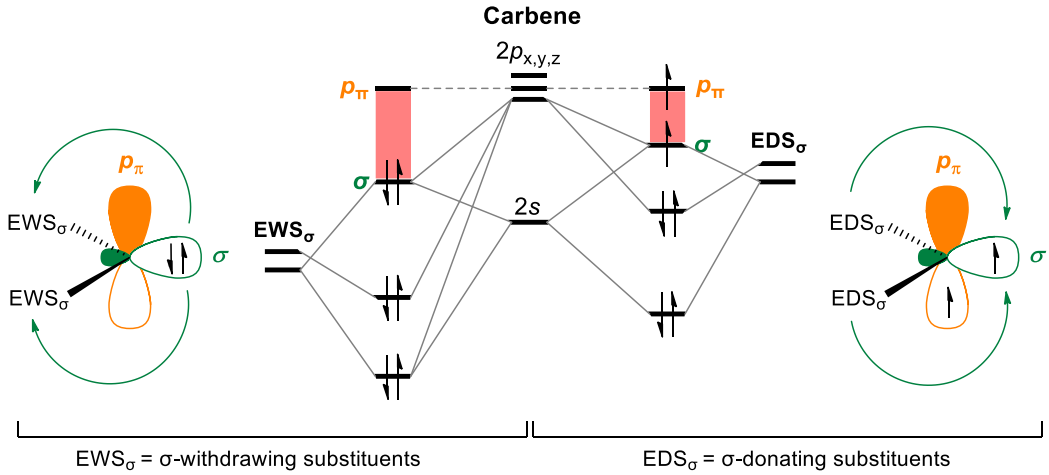

Figure 1.2 *Perturbation orbital diagrams showing the influence of inductive effects on the size of the σ—p_π gap (highlighted in red) with σ-withdrawing or σ-donating substituents.*

In addition to the inductive effects described above, singlet carbenes are also subject to mesomeric effects; namely, the interactions between any of the carbene's orbitals and the *p* or *π* orbitals of its substituents (Figure 1.3).[7] Due to the more favourable overlap between these orbitals, mesomeric effects tend to be more dominant than *σ* orbital interactions. These effects are manifested in the degree of bending in carbenes. Interaction with the lone pair of a π-electron donating substituent (halides, —NR_2, —PR_2, —OR, —SR, and —SR_3, for instance) increases the energy of the vacant p_π orbital of the carbene. As the *σ* orbital is generally unaffected by this interaction, this results in a net increase in the size of the *σ*—p_π gap and a highly bent singlet state is favoured, as exemplified in the case of stable diaminocarbenes, and transient dimethoxy-[28,29] and dihalocarbenes.[30–32]

Conversely, the presence of π-electron withdrawing substituents (such as —COR, —CN, —CF_3, —BR_2, —SiR_3, —PR_3^+, and so on) is predicted to result in the formation of linear carbenes which are, interestingly, in the singlet state.[33,34] The symmetric interaction between the vacant orbitals of the substituent and the p_y orbital of the carbene breaks the degeneracy of the carbene's p_x and p_y orbitals. Although the p_x orbital is not affected, this ultimately widens the *σ*—p_π gap, which then allows for the stabilisation of the singlet state. Where both π-electron donating and withdrawing substituents are present, the carbene benefits from the combined effects of both interactions, which raises the energy of its p_y

orbital while lowering the energy of its p_x orbital. Once again, the singlet state is favoured, but the resulting geometry is quasi-linear.[35,36]

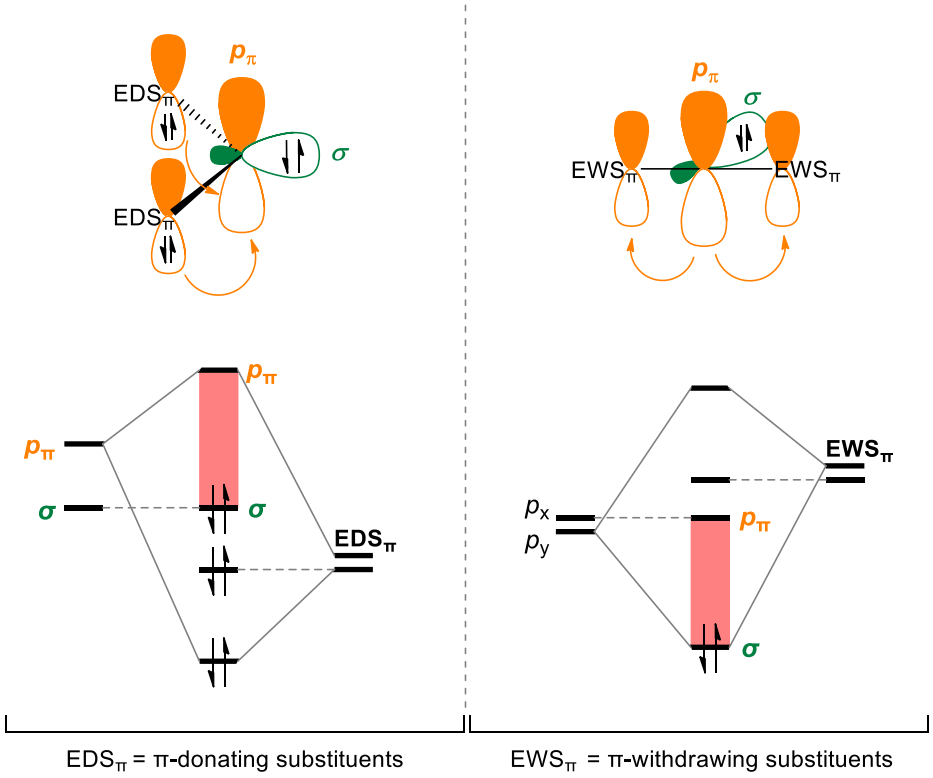

Figure 1.3 *Perturbation orbital diagrams showing the influence of mesomeric effects on the size of the σ—p_π gap (highlighted in red) with π-donating or π-withdrawing substituents.*

In all three substitution scenarios discussed above, mesomeric effects stabilise the singlet state over the triplet state. It is therefore unsurprising that singlet carbenes are far more common than triplet carbenes. Presently, diaminocarbenes are arguably the largest family of singlet carbenes, and for good reason: As a whole, they are more stable and thus more easily synthesised than other carbenes. Their enhanced stability is mainly attributed to electronegative α-nitrogen atoms, which mitigates electron deficiency at the carbon centre by π-donation while inductively stabilising the carbene lone pair.

1.2 Discovering *N*-heterocyclic carbenes: A realm of structural possibilities

The term *N*-heterocyclic carbene (NHC) applies to any ring system which includes at least one nitrogen atom and one carbene carbon. Reported in 1991 by Arduengo and coworkers,[37] the first free NHC was also the first stable,

crystalline free carbene (IAd **1**, Scheme 1.1). To the surprise of the chemical community at the time, free carbene **1** demonstrated remarkable thermal stability, capable of withstanding temperatures up to its melting point of 240 °C without observable decomposition. The successful isolation and crystallographic characterisation of IAd marked a major turning point in the field. As such, NHCs hold a special place in the history of carbenes.

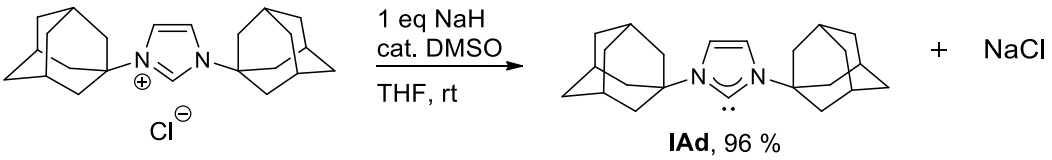

1

Scheme 1.1 *Synthesis of the first stable, crystalline free carbene, IAd by deprotonation of 1,3-di-1-adamantylimidazolium chloride.*

Decades before, the pioneering work of Hans-Werner Wanzlick laid the groundwork for the synthesis of IAd. In 1960, he reported that the thermolysis of imidazolidine **2** produced a colourless crystalline solid.[38] Based on the molecular weight of that material, which he determined to be in between that of the free carbene **3** and its dimer **4**, he proposed that the free carbene — formed via the α-elimination of chloroform from **2** — existed in equilibrium with entetraamine **4** (Scheme 1.2). Although subsequent cross-metathesis experiments provided conclusive evidence against the presence of the free carbene in equilibrium,[39] Wanzlick's report was the first hint that stable carbenes could be prepared from *N*-heterocycles.

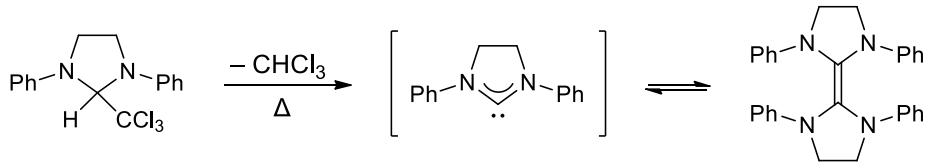

2 **3** **4**

Scheme 1.2 *Wanzlick's proposed free carbene–dimer equilibrium following the thermally induced elimination of chloroform from an imidazolidine.*

Undeterred, Wanzlick and others resumed the search for free carbenes, shifting their focus to unsaturated imidazolium systems. The move was met with some success. Wanzlick[40] and Öfele[41] found that imidazolium salts could be deprotonated *in situ* by metal salts bearing basic acetato or hydrido ligands (Scheme 1.3 a,b). The resulting carbenes in **6** and **8** were stabilised upon

coordination to the metal centre, which improved their ease of handling and facilitated efforts to characterise them. It should be emphasised that the stabilising effect of the metal centre is not trivial. Many carbenes that are difficult to access in their free form are often conveniently obtained as their metal complexes. For example, recall that attempts to isolate **3** were thwarted by its preference for its dimeric form, which was itself air-sensitive. However, it can be trapped as a bench-stable platinum(II) complex, by heating a xylene solution of **2** or **4** in the presence of a chloride-bridged platinum(II) dimer (Scheme 1.3 c).[42]

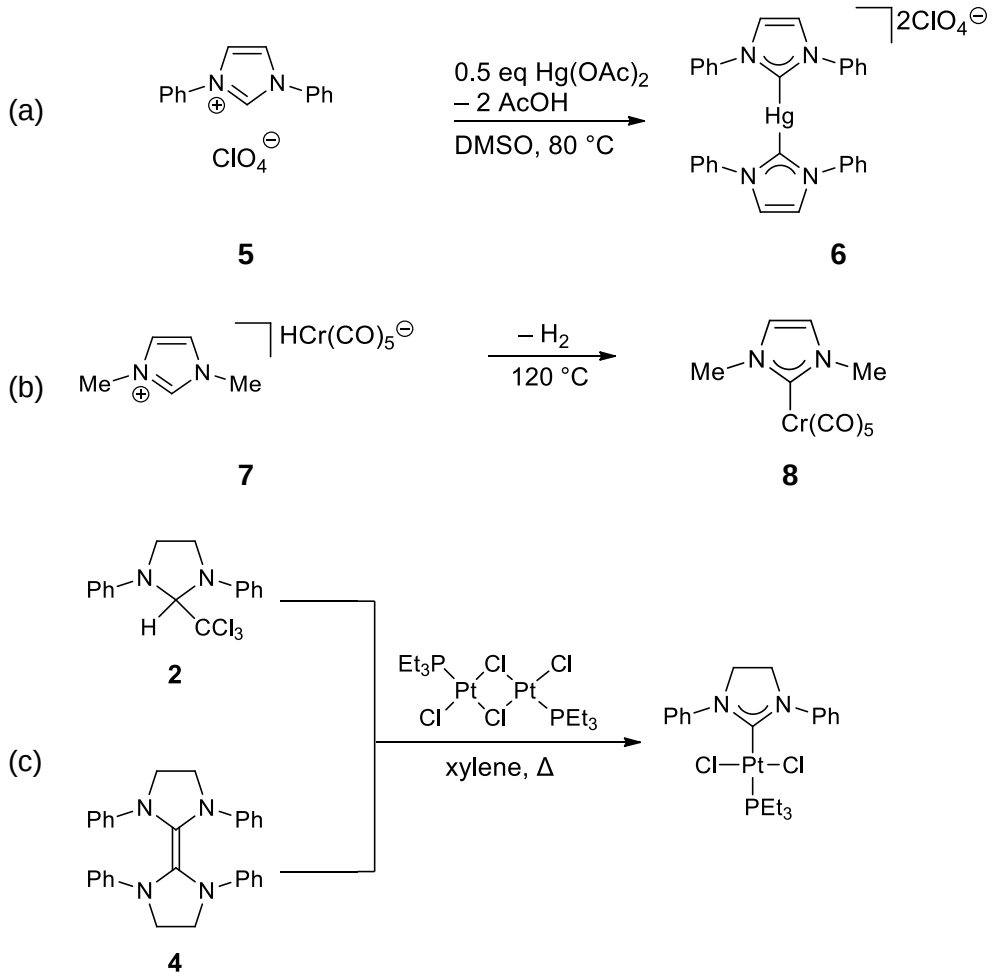

Scheme 1.3 (a) *Wanzlick's synthesis of the first mercury–NHC complex by deprotonation of an imidazolium salt by a basic metal salt.* ***(b)*** *Öfele's synthesis of the first chromium–NHC complex using a similar approach.* ***(c)*** *Trapping an imidazolidine-based NHC as a platinum complex.*

Encouraged by these findings, Wanzlick and Schönherr turned their attention to tetraphenylimidazolium perchlorate **9**. They reasoned that deprotonation of **9**

was unlikely to result in a dimeric species as it would break the aromaticity of the system, and the steric interaction between the *N*-phenyl groups on each monomer unit would make it additionally unfavourable.

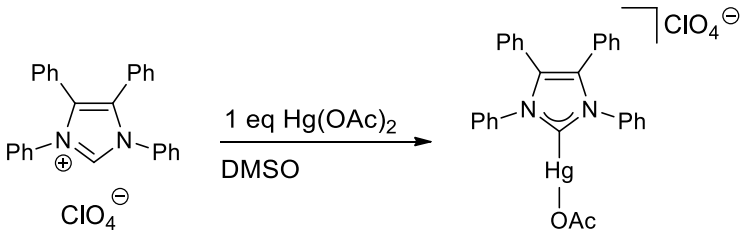

9 **10**

Scheme 1.4 *Synthesis of a mercury(II) acetate tetraphenylimidazolium NHC complex.*

The reaction of **9** with an equimolar amount of mercury(II) acetate afforded the expected mono-NHC complex **10** (Scheme 1.4).[43] Assured that carbene formation from the tetraphenylimidazolium system was feasible, they proceeded to deprotonate the imidazolium salt **9** with potassium *tert*-butoxide. In lieu of observing or isolating the proposed free carbene intermediate directly, the reaction mixture was treated with water, from which diimine **11** was isolated in 16 % yield after recrystallisation (Scheme 1.5). It was presumed that the diimine was the water/CO_2 elimination product of the hydrolysed/oxidised free carbene, and thus served as indirect evidence of the formation of the latter. They did not report the detection of any dimers of the free NHC derived from **9**.

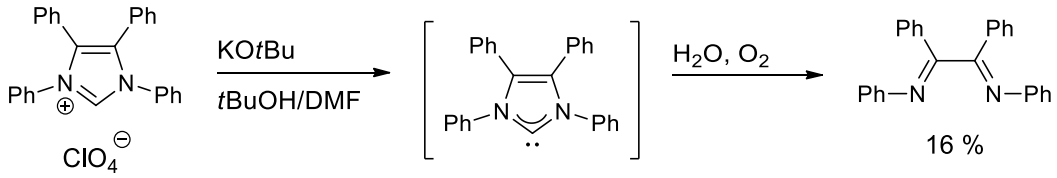

9 **11**

Scheme 1.5 *Indirect observation of a free carbene by quenching with water in air to form a diimine.*

Together with the success of IAd, these observations gave the impression that very bulky *N*-substituents were essential to stabilise free NHCs. However, this misconception was quickly overturned. The following year after IAd was reported, Arduengo and colleagues isolated 1,3,4,5-tetramethylimidazol-2-ylidene, IMe **13a** (Scheme 1.6).[44] This too proved to be stable under anhydrous

conditions, conclusively demonstrating that the electronic contribution of the α-amino groups was far more influential to the carbene's stability than any steric protection offered by the wingtip substituents. Even 1,3-dimethylimidazol-2-ylidene **13b** was sufficiently stable to be observed in solution by NMR.

The similar ease with which *N*-aryl substituted imidazol-2-ylidenes **13c**–**e** could be synthesised quickly ruled out the presence of special electronic effects that phenyl substituents might exert on the imidazole nitrogen centres, preventing them from stabilising the carbene centre. They were all crystalline solids which were stable up to their closely distributed melting points of between 150 – 158 °C, at which point they suffered decomposition. **13d-e** would degrade in solution over the course of several days, but no dimers were detected in their decomposition products. Indeed, imidazol-2-ylidenes seem strongly disinclined to dimerise, with one of the few exceptions being when the imidazolium units are linked by two *n*-butyl bridges on the ring nitrogens.[45]

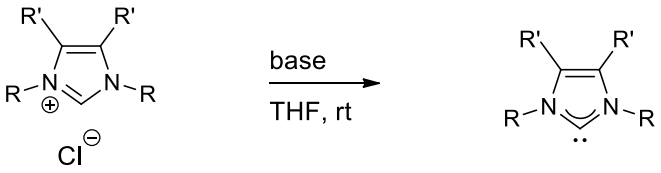

12a-**e** **13a**-**e**

12a R = Me, R' = Me
12b R = Me, R' = H
12c R = Mes, R' = H
12d R = 4-methylphenyl, R' = H
12e R = 4-chlorophenyl, R' = H

13a R = Me, R' = Me
13b R = Me, R' = H
13c R = Mes, R' = H
13d R = 4-methylphenyl, R' = H
13e R = 4-chlorophenyl, R' = H

Scheme 1.6 *Preparation of a series of alkyl and aryl-substituted free NHCs from imidazolium chlorides.*

In theory, the higher coplanarity of the *p*-tolyl substituents and the imidazole ring of **13d** could enable a π-effect as a result of greater conjugation between the three rings, in addition to any σ-effects that also exist in **13c**, whose bulkier mesityl substituents must be twisted out of the imidazole plane to accommodate the *o*-methyl groups. However, there was no significant difference in the stabilities of the two species. Likewise, replacing the methyl group in **13d** with a chlorine atom had little effect on the structure or stability of the resulting carbene, **13e**. It seemed that tetraphenylimidazol-2-ylidene would be a realistic goal. Indeed, Arduengo eventually devised a modified procedure that led to its

isolation.[46] It was believed that Wanzlick's chlorate salt **9** was prone to contamination by hydrogen sulfate anions or water. The use of an imidazolium chloride precursor effectively circumvented this issue.

Thus far, it appeared that imidazol-2-ylidenes could tolerate both alkyl and aromatic backbone and wingtip substituents, and that aromatic substituents did not necessarily confer greater stability to the carbene. What proved to be more effective was the introduction of strongly σ-withdrawing substituents on the 4- and 5-positions. For instance, 1,3-dimesityl-4,5-dichloroimidazol-2-ylidene **14** was markedly more stable than its non-halogenated precursor, IMes **13c** (Scheme 1.7).[47] The decrease in the basicity of the carbene lone pair in **14** was so dramatic; not only could it tolerate exposure to acidic solvents like chloroform and dichloromethane (which would be rapidly deprotonated by IMes), but it was also air-stable for two days.

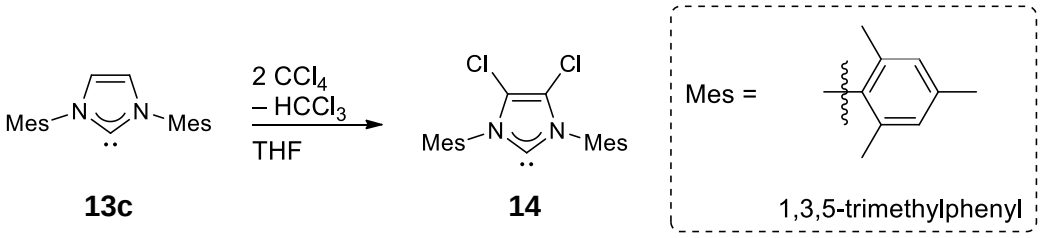

13c **14**

Scheme 1.7 *Synthesis of air-stable 4,5-dichloroimidazol-2-ylidene **14** by chlorination of IMes with carbon tetrachloride.*

Arduengo's discoveries also spawned the aggressive pursuit of free carbenes derived from *N*-heterocycles other than imidazole. In 1995, the group of Enders and Teles prepared the first 1,2,4-triazol-5-ylidene **17** (Scheme 1.8).[48] This was accomplished via the addition of sodium methoxide to the triazolium salt **15** to give the neutral 5-methoxy-1,3,4-triphenyl-4,5-dihydro-1*H*-1,2,4-triazole **16**. When subjected to reduced pressure at 80 °C, triazole **16** undergoes the endothermic α-elimination of methanol, affording the free carbene **17** in quantitative yield. This was also the first successful adaptation of Wanzlick's strategy for producing free carbenes by the liberation of a stable, volatile byproduct.

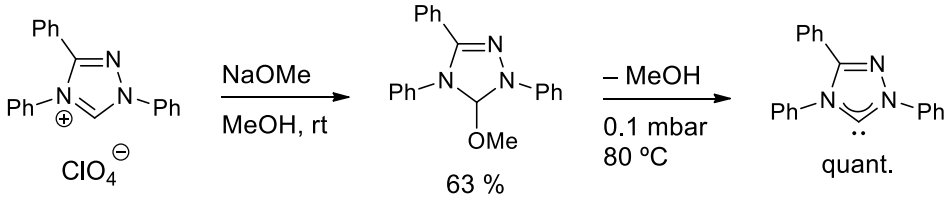

15 **16** **17**

Scheme 1.8 *Enders' et al. synthesis of the first triazole-based NHC by α-elimination of methanol.*

In the same year, Arduengo and colleagues successfully isolated the imidazolin-2-ylidene **19** (Scheme 1.9).[49] In contrast to its predecessor IAd **1**, carbene **19** lacks a double bond between C4 and C5. Thus, it is commonly abbreviated to SIMes to reflect the saturated nature of its carbon backbone. Its synthesis was analogous to that of **1**: The parent imidazolinium salt **18** was deprotonated with a strong hydride base in THF, and the insoluble potassium chloride byproduct was removed by filtration. The pure carbene was obtained in good yield upon recrystallisation from hexane. Notably, SIMes and IAd exhibited comparable stability in air- and moisture-free conditions. The former could be melted between 107 to 109 °C without suffering decomposition.

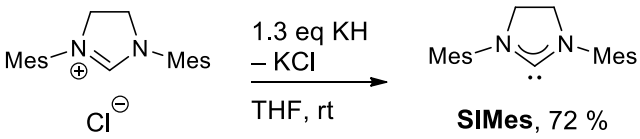

18 **19**

Scheme 1.9 *Preparation of the first imidazolin-2-ylidene SIMes.*

The study of NHCs was rapidly gaining momentum, for the first thiazole-2-ylidene was reported soon after. Once again, it was Arduengo's group who laid claim to its isolation. Using the synthetic strategy developed for the preparation of IAd and SIMes, they were able to generate carbene **21** in good yield by the direct deprotonation of its thiazolium salt precursor **20** (Scheme 1.10).[50] The deprotonation of azolium salts gradually came to represent a fairly general route to free NHCs.

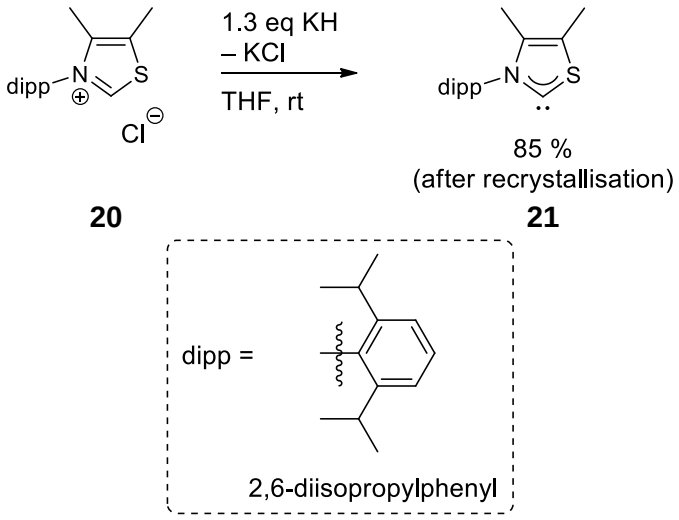

Scheme 1.10 *Preparation of the first free carbene derived from a thiazole scaffold.*

X-ray diffraction studies showed that the solid-state structure of **21** shared the planar ring structure of imidazol-2-ylidenes and imidazolin-2-ylidenes, despite the replacement of one of the nitrogen atoms with a larger sulfur atom. This did however have implications for its reactivity; it was more difficult to handle. While the robustness of the imidazole-type NHCs did not seem contingent on the steric bulk of the wingtip substituents, this proved critical for the thiazole-based analogues, which only have protection on one side. **21** reportedly dimerises in the presence of trace amounts of a proton source. Its less bulky *N*-mesityl analogue could be observed in a cold solution but dimerises rapidly upon warming to room temperature, whereas the least sterically hindered *N*-methyl analogue was observed exclusively in its dimeric form.

Attempts to replace the sulfur heteroatom in thiazol-2-ylidenes with other chalcogens have met with limited success. Although complexes of oxazole[51–55] and benzoxazole-based[56–62] NHCs are known, no free carbenes of this kind or its phosphorus analogues have been reported. The study of their relatively stable acyclic congeners[63,64] **22**–**24** (Figure 1.4) provides some insight as to why.

Firstly, their spectroscopic and structural properties strongly suggest that only the nitrogen atom is involved in π-donation into the vacant p_π orbital of the carbene. The $C_{carbene}$–N bond lengths are comparable to those observed in classical diaminocarbenes, and the nitrogen atom is perfectly planar relative to the carbene atom. Furthermore, both *N*-alkyl substituents possessed distinct resonances in the ^{1}H NMR spectra, a tell-tale sign of restricted rotation about the

$C_{carbene}$–N bond. Altogether, this supports the existence of a strong interaction between the nitrogen lone pair and the carbene p_π orbital.

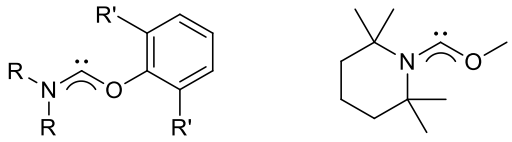

22a R = *i*Pr, R' = *t*Bu
22b R = Me, R' = *t*Bu
22c R = *i*Pr, R' = Me

23

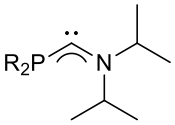

24a R = $N(Cy)_2$
24b R = $N(iPr)_2$
24c R = Ph
24d R = *t*Bu

Figure 1.4 *Examples of acyclic aminooxycarbenes* ***22a-c*** *and* ***23****, and (amino)(phosphino)carbenes* ***24a-d****.*

The lesser influence of the phosphorus or oxygen atom is evident in the elongated $C_{carbene}$–P or $C_{carbene}$–O bonds, which is indicative of their minimal π-character. In the X-ray structure of **24a**, the lone pair of the pyramidalised phosphorus atom is oriented perpendicular to the vacant carbene orbital, precluding electron donation from the former to the latter.[64] When the O or P heteroatoms are not confined within a ring, the flexibility of the substituents can compensate for the reduced electronic stabilisation by adopting a conformation that best shields the carbene centre. The persistent cyclic 6-membered N–C–P carbene **25** has been observed in solution by NMR spectroscopy, but is kinetically unstable and will undergo a formal C–H insertion into the *tert*-butyl group on the mesityl moiety to give **26** (Scheme 1.11).[65]

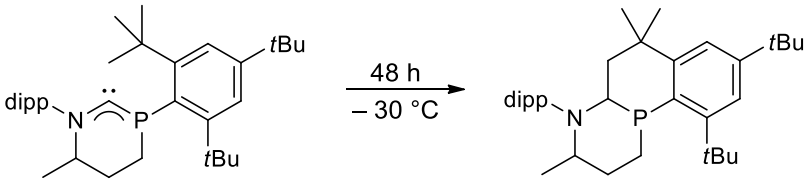

25 **26**

Scheme 1.11 *Quantitative C–H insertion by a persistent N,P carbene at low temperature.*

Although all the carbenes discussed so far possess two adjacent heteroatoms, this too was not a steadfast requirement for an isolable carbene. In 2001, Bertrand and coworkers reported that the deprotonation of iminium salt **27** gave the (aryl)(amino)carbene **28**, which was sufficiently stable in solution at −50 °C to be observed by ^{13}C NMR spectroscopy.[66] Upon warming to room temperature,

carbene **28** rapidly inserted into the C–H bond of an ortho-*t*-butyl group to give indane **29** (Scheme 1.12). Such behaviour had not been observed for diaminocarbenes, and reflects the expected decrease in carbene perturbation that results from having only one electron-active substituent.

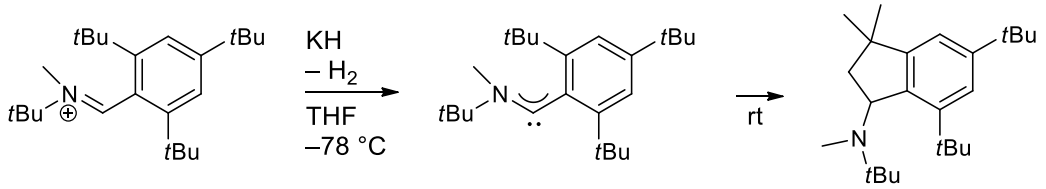

27 **28** **29**

Scheme 1.12 *Synthesis of an (aryl)(amino)carbene and its subsequent C–H insertion at room temperature.*

Capitalising on the unreactive nature of C–F bonds towards carbene insertion, they replaced the ortho-*t*-butyl groups with trifluoromethyl groups, which enabled the isolation of free (aryl)(amino)carbenes **31a**-**c** in near quantitative yields at room temperature (Scheme 1.13).

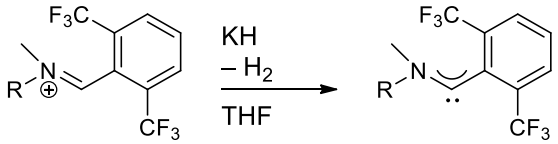

30a-**c** **31a**-**c**

30a R = *t*Bu **31a** R = *t*Bu
30b R = Ad **31b** R = Ad
30c R = *i*Pr **31c** R = *i*Pr

Scheme 1.13 *Preparation of (aryl)(amino)carbenes that are isolable at room temperature.*

Building upon earlier work where they synthesised an acyclic bis(diisopropyl)amino carbene **32** (Scheme 1.14),[67] the Bertrand group also prepared the first cyclic (alkyl)(amino)carbenes (CAACs) **33**–**35** (Figure 1.5).[68]

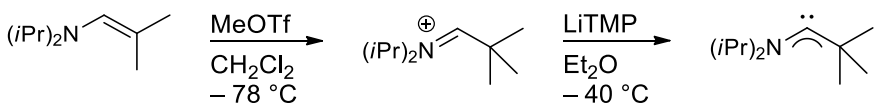

32

Scheme 1.14 *Synthesis of an (alkyl)(amino)carbene **32** via deprotonation of an iminium salt, accessible by methylation of the corresponding enamine.*

Since the quaternary α-carbon in CAACs carries two wingtip substituents, it offers the carbene centre greater steric protection than an sp^2 nitrogen. The alkyl group is a stronger σ-donor but weaker π-acceptor than an amino group, which makes these N–C–C carbenes both more nucleophilic and more electrophilic than their N–C–N counterparts.

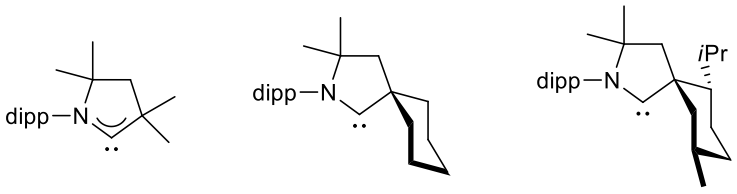

33 **34** **35**

Figure 1.5 *Cyclic (alkyl)(amino)carbenes **33**, with the simplest quaternary α-carbon; **34**, with a spiro-cyclohexyl "flexible wing"; and **35**, featuring a rigid, extremely bulky wing.*

Consequently, (alkyl)(amino)carbenes can mimic certain aspects of transition metal reactivity such as H_2 activation under mild conditions (Scheme 1.15 b,c),[69] whereas diaminocarbenes are not electrophilic enough to do so in the absence of a catalyst (Scheme 1.15 a).[70] Even more impressively, (alkyl)(amino)carbenes can insert into the N–H bond of ammonia (Scheme 1.15 b,c),[69] a feat of which few species are capable. In contrast, most transition metals simply form Lewis acid-base adducts with NH_3, while cyclic diaminocarbenes are stable as solutions in liquid ammonia.[71]

It is noteworthy that compared to diaminocarbenes, which typically exhibit ^{13}C NMR resonances between 200 – 300 ppm for the carbenic atom, the signals for CAACs and (amino)(phosphino)carbenes are markedly more downfield (>300 ppm).

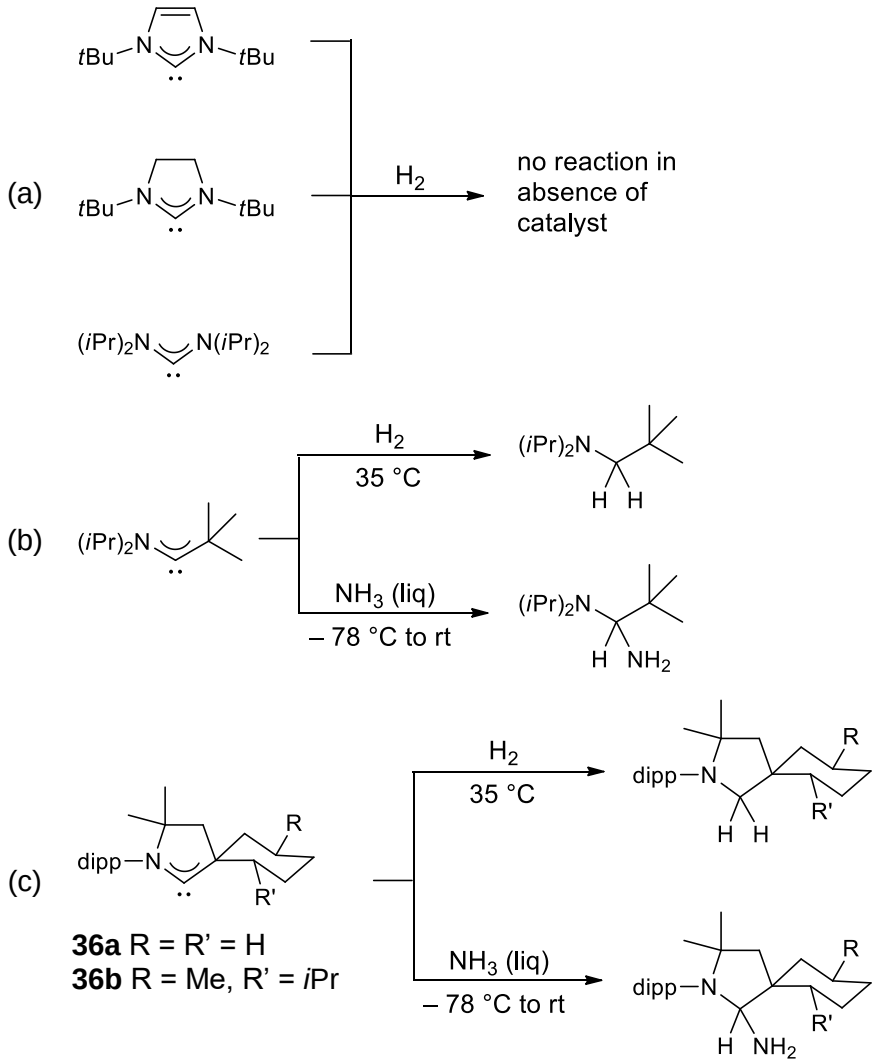

Scheme 1.15 (a) *Cyclic and acyclic diaminocarbenes are inert towards H_2. In contrast, acylic* ***(b)*** *and cyclic* ***(c)*** *(alkyl)(amino)carbenes readily undergo insertion with H_2 and liquid ammonia.*

Very recently, the Bertrand group was credited with yet another landmark achievement in the study of NHCs: The isolation of the first crystalline monosubstituted carbene (Scheme 1.16).[72] **37** is reportedly stable in its solid form for up to one month at room temperature, provided it is stored under an inert atmosphere. The immense steric bulk of the sole benzo[*c*]pyrrolidino substituent is critical to the ability of **37** to resist dimerisation.

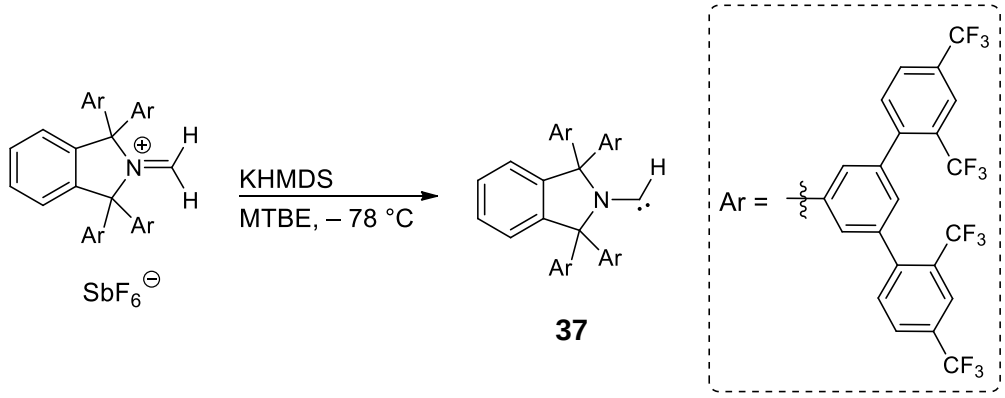

Scheme 1.16 *Synthesis of the first stable monosubstituted carbene.*

The isolation of benzannulated five-membered NHCs again presented its own unique challenges. Treating a benzimidazolium salt with a strong base or reducing a benzimidazolin-2-thione with Na/K alloy produces the corresponding entetraamine if the *N*-substituents are insufficiently bulky to prevent this (Scheme 1.17 a).[73–75] Instead, the first free NHC of this kind, **41** was accessed via the Na/K reduction of a neopentyl-substituted benzimidazolin-2-thione **40**.[75] When the same strategy was applied to the minimally hindered *N*-methyl analogue **38**, the dimer **39** obtained. Even then, the product was shown to be sensitive to the reaction solvent. In THF, the presumed carbene intermediate was spontaneously reduced to the benzimidazoline **42**, necessitating the use of toluene, a more inert solvent, to isolate the free carbene (Scheme 1.17 b).

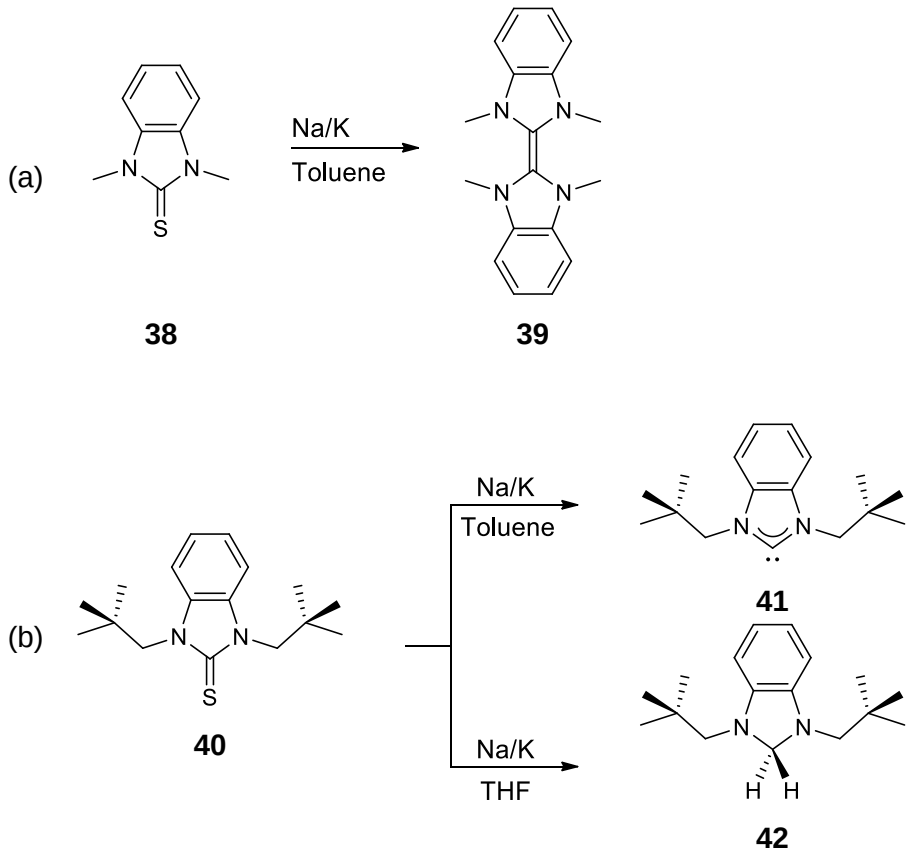

38 **39** **40** **41** **42**

Scheme 1.17 *The Na/K reduction of benzimidazolin-2-thiones bearing different N-substituents affords the:* ***(a)*** *corresponding dimer* ***39*** *for the N-methyl analogue 38;* ***(b)*** *free carbene* ***41*** *in toluene, but the benzimidazoline* ***42*** *in THF for the N-neopentyl analogue* ***40****.*

An interesting outcome of the isolation of these benzimidazol-2-ylidenes was that the equilibrium between free carbenes and their dimers could finally be observed. Earlier, Denk and colleagues[76] showed that backbone-saturated entetraamines **43** and **44** formed mixtures of the metathesis products **45** in statistical ratios except for the phenyl/*o*-tolyl substituted dimer **45d** previously studied by Lemal et al (Scheme 1.18).[39] However, the mixed olefin products could also be accounted for by [2+2]-cycloaddition or [2+2]-cycloreversion of the entetraamines.

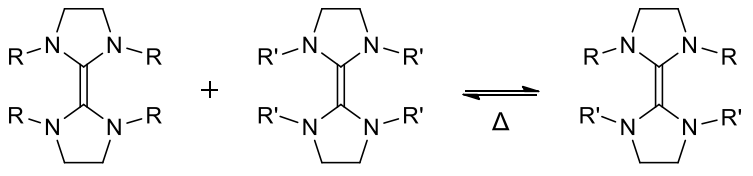

43 **44** **45**

	R	**R'**
45a	Me	Et
45b	Me	*i*Pr
45c	Et	*i*Pr
45d	Ph	pTol

Scheme 1.18 *Formation of mixed olefin products from symmetrical entetraamines.*

Fortunately, the structural and spectroscopic properties of benzimidazol-2-ylidenes display properties that are intermediate to those of the imidazolin- and imidazol-2-ylidenes. While less hindered examples of the former readily dimerise, the latter tend to remain in the monomeric state. Denk's metathesis experiments show that if the olefin bridge of the dimers **45a**-**d** dissociates to form the free carbenes, it does so very rapidly. The dibenzotetraazafulvene **46** on the other hand, will slowly convert into the free carbene **47** at ambient temperature until the equilibrium concentration is reached (Scheme 1.19).[77] Lemal and coworkers likewise observed the same equilibrium in solution for the *N*-methyl and *N*-ethyl dibenzotetraazafulvenes.[78] However, these less bulky analogues had to be heated above 100 °C for significant dissociation to occur, then quickly quenched and maintained at −50 °C to prevent reversion to the dimeric state for the diagnostic carbenic resonance to be detected by ^{13}C NMR spectroscopy. The simultaneous observation of both species under the rigorous exclusion of electrophiles finally provided convincing evidence of Wanzlick's equilibrium.

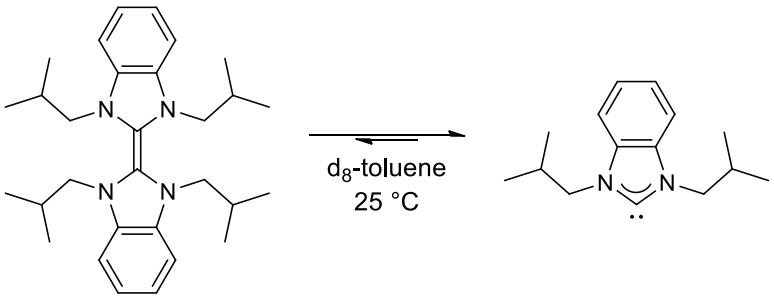

46 **47**

Scheme 1.19 *The slow equilibration of dimer **46** into free carbene **47** in solution, observed by ^{1}H NMR spectroscopy.*

In spite of the ever-growing variety of NHCs, the popularity of imidazolium-based carbenes has endured nearly three decades on. Generally, they are more stable than their thiazolium or oxazolium counterparts, and are easily accessible from their imidazolium salts, which in turn can be prepared from readily available starting materials and well-developed syntheses.

1.3 The significance and classification of *N*,*N*'-substitution patterns in imidazol-2-ylidenes

Far from remaining mere laboratory curiosities, imidazolium-based NHCs have found applications as organocatalysts and ligands for metal complexes, thus assuring continued interest in their development. Their reactivity is first and

foremost a result of their exceptionally strong σ-donor ability, but the astounding variety of transformations they can effect is related to their structural diversity, which allows each carbene to be tailored to a particular purpose.

NHCs are frequently compared to phosphines, another important class of ligands which are similarly prized for their strong σ-donor ability. The key difference between the two lies in the orientation of the steric bulk around the metal centre. The *N*-substituents on NHCs will surround the metal centre in a fan- or umbrella-like fashion, permitting extensive shielding of the active site, whereas the phosphine substituents are arranged in a cone shape, away from the metal centre (Figure 1.6).[79] Accordingly, the calculated values for % buried volume is often higher for NHC complexes than it is for phosphine complexes.[80] Other advantages of NHCs over phosphines often include better air and moisture tolerance of their derived complexes, higher C–M versus C–P bond dissociation energies,[81–83] and less toxic or malodorous precursor reagents.

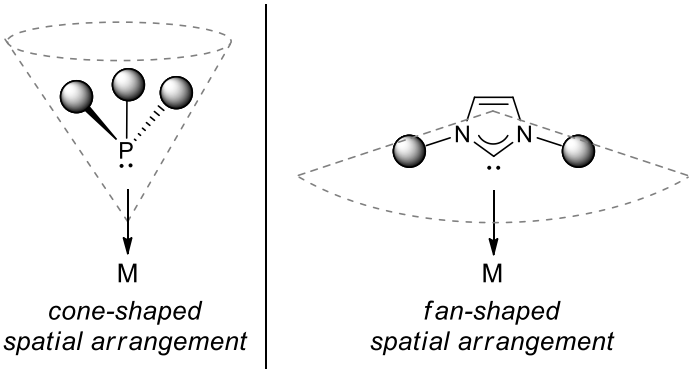

Figure 1.6 *The orientation of substituents on phosphines and NHCs gives rise to different steric environments around the coordinated metal centre.*

By design, it is easier to independently tune the sterics and electronics of an NHC than it is for a phosphine. There are fewer points of modification on the latter, and they are all directly attached to the phosphorus centre. In contrast, there are two points of modification on the imidazolium NHC; namely, the C4–C5 backbone and the *N*-substituents. Typically, the *N*-substituents serve to regulate the steric environment around the carbene centre, but they may also carry important electronic effects. These substituents may participate in bonding to the metal centre, or interact with other substrates.

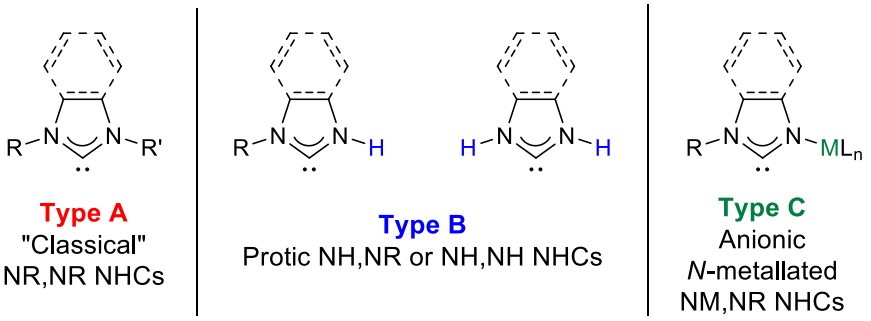

Figure 1.7 *Broad classes of N,N'-substitution patterns for imidazolium-derived NHCs.*

Thus, it can be useful to categorise imidazolium-based NHCs based on their *N*,*N* substitution pattern (Figure 1.7). The NR,NR substituted type A, also known as classical NHCs, is most common. It is possible to replace one or both of these R groups with a proton to give NH,NR or NH,NH substitution patterns, as seen in type B protic carbenes. Of particular interest to us are those of the NM,NR/H variety, where one of the nitrogen centres is coordinated to a metal (type C). These three classes will be discussed in detail in subsequent sections.

1.4 Type A or "classical" NR,NR NHCs and their complexes

1.4.1 Classical free carbenes: Synthesis, and structural and spectroscopic trends

At present, there are few general routes for the preparation of free classical NHCs, all of which have been mentioned in the previous section (Scheme 1.20). The deprotonation of an azolium salt with a strong base remains, by far and large, the most widely used route to access free carbenes. Attractive for its simplicity, the success of this strategy has been greatly facilitated by the wealth of existing literature describing the preparation of azolium compounds.[84]

The reduction of thiones[75,85] and α-elimination of small molecules[86] are less commonly used. A limitation of the thione reduction method is the need for very strong reducing agents such as elemental sodium and/or potassium, or potassium graphite, which may necessitate prolonged reaction times or elevated temperatures. The α-elimination method lacks broad appeal as the preparation of the required 4-imidazolines from their parent imidazolium salts may introduce additional steps into the synthetic sequence.

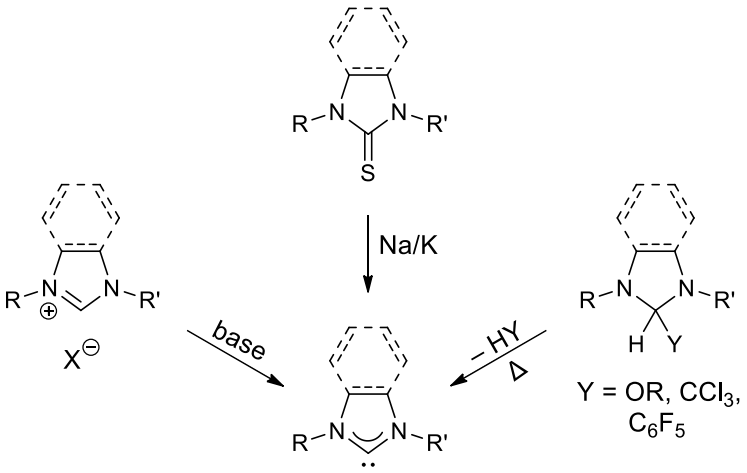

Scheme 1.20 *General routes to free classical NHCs.*

The conversion of an imidazolium salt into a free NHC is marked by characteristic structural and spectroscopic changes.[37,44] The N–C2–N angle at the carbene centre shrinks, while the N1(3)–C2, N1–C5 and N3–C4 bonds are lengthened. The most diagnostic change, however, is the drastic downfield shift of the carbenic atom in the ^{13}C NMR spectrum. The protons on C4 and C5, if present, typically exhibit an upfield shift in the ^{1}H NMR spectrum upon carbene formation. Although imidazole ring retains its planarity, these changes are consistent with diminished π-delocalisation in the system.

Within the classical free carbenes, there are subtler trends: The ^{13}C NMR shifts for the carbenic atom range between 210 – 220 ppm for the imidazol-2-ylidenes, 220 – 230 ppm for benzimidazol-2-ylidenes, and 238 – 245 ppm for imidazolin-2-ylidenes.[87] N–C2–N angles are smallest for the imidazol-2-ylidenes and widest for their unsaturated cousins, while those for the benzimidazol-2-ylidenes lie somewhere in between.

1.4.2 Classical NHC complexes: Synthesis, and structural and spectroscopic trends

It has been known since the early work in carbene chemistry that free carbenes are much less stable towards air, moisture and heat than their metal-bound counterparts. The formation of the carbene-metal bond is highly thermodynamically favourable, and this is reflected in the much greater ease and methodological scope of the preparation of these complexes, relative to the free carbenes. A snapshot of some commonly used methods for preparing classical

NHC complexes are presented in this section (Scheme 1.21), but extensive reviews have been published elsewhere.[7,88,89]

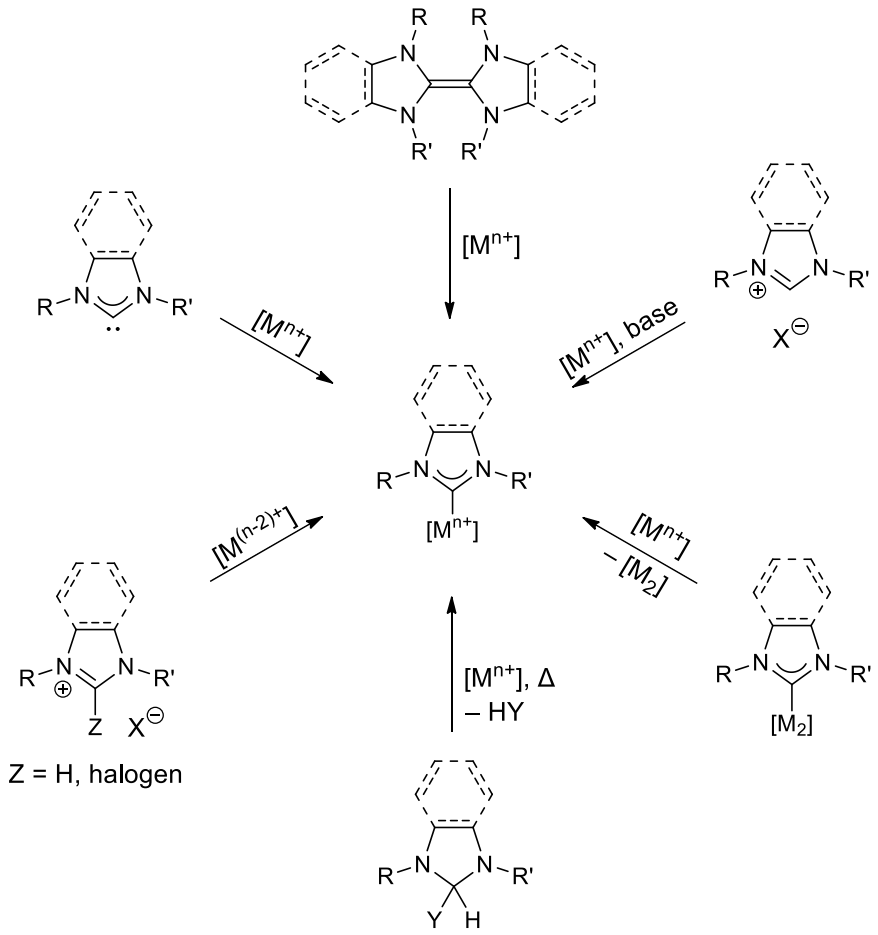

Scheme 1.21 *Generic strategies for the preparation of classical NHC complexes.*

The most direct route to NHC complexes involves the coordination of free NHCs to a metal precursor.[90] However, this route is not widely applicable as many free NHCs are unstable and have short lifetimes even when handled at low temperatures under an inert atmosphere, if they are isolable at all.[91,92] As seen in work pioneered by Lappert, it is also possible access these complexes by metal cleavage of entetraamines.[42,74,93,94] More recently, this strategy has been applied in the preparation of coordinatively unsaturated biphenyl-linked bis(benzimidazole-2-ylidene)iron(II) complexes.[95] The main drawback of this approach is the difficult in obtaining the entetraamines, which are often troublesome to purify and readily undergo subsequent rearrangement, presumably via a [1,3]-radical mechanism,[96] or dealkylation to give bis(imidazoles).[97]

To avoid this, most NHC complexes are made by the *in situ* deprotonation of azolium salts in the presence of a suitable metal source, which effectively trap the NHC as its complex. Favoured for its general applicability, another benefit of this approach is that it permits the use of much milder bases, since the equilibrium lies strongly in favour of the NHC complex, the thermodynamic product. The source of the base may be external, or from basic ligands on the metal precursor.[98–100] However, the long reflux periods associated with many of these procedures can lead to the formation of decomposition products. For some NHC/metal combinations, the method is low yielding, or fails entirely.

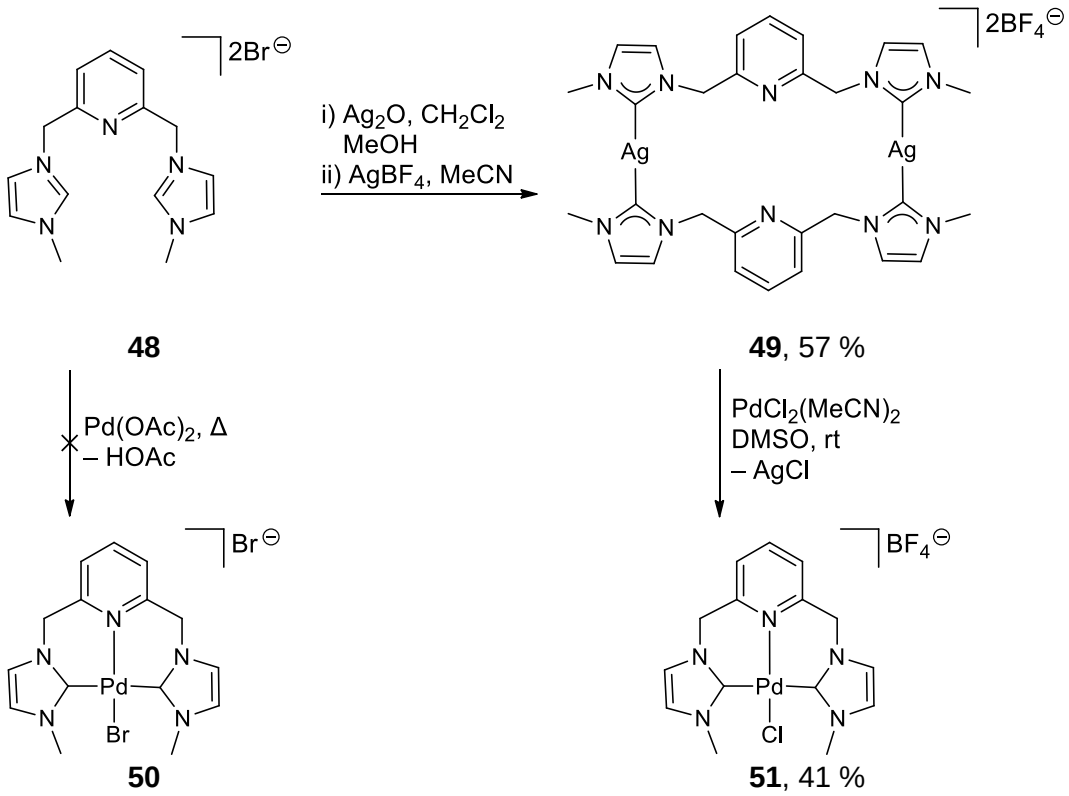

Scheme 1.22 *Synthesis of a palladium(II) NHC complex by transmetallation of a silver(I) NHC adduct.*

Transmetallation of a preformed NHC complex with another metal source is a milder alternative method that can cleanly provide higher yields of the desired complex, and often tolerates air and moisture. Since silver–carbene bonds are quite labile, silver NHC complexes are often used as transfer agents.[101,102] These transfer agents are usually prepared by the reaction of silver(I) oxide with the desired azolium salt.[103] The precipitation of highly insoluble silver halide salts can be used to drive the subsequent transmetallation reaction. In a fitting example described by Cavell and coworkers, the direct reaction of imidazolium

salt **48** with $Pd(OAc)_2$ results in a complex mixture with no trace of NHC complex **50** (Scheme 1.22).[104] Fortunately, the silver(I) complex **49** formed readily, and the palladium(II) complex **51** was obtained following successful NHC transfer.

Under basic phase transfer catalyst conditions, it may even be possible to reuse the silver halide byproduct to generate more carbene transfer agents in a pseudo-catalytic process.[105] Other metals have been known to be effective, albeit less well-explored, carbene transfer agents. Some examples include the tungsten, chromium and molybdenum carbonyl complexes which Liu and coworkers used for the transfer of imidazolin-2-ylidenes onto other transition metal ions.[106,107] They noted that the carbene transfer reaction proceeds more efficiently when π-bonding *N*-substituents are present. Even nickel(II) NHC complexes have shown promise as carbene transfer agents.[108]

The thermolysis of NHC adducts in the presence of a metal source is particularly useful in cases where it is desirable to exclude bases from the complexation entirely.[94,109–111] Such adducts can be regarded as "protected" forms of free NHCs.

Lastly, another well-established approach to classical NHC complexes relies on the oxidative insertion of a low valent metal into a C2–Z bond (where Z = halogen,[112] H[113,114]) of an azolium cation. This method is also applicable to backbone saturated azolium salts such as **52**, furnishing the bromopalladium(II) complex **53** in good yield after heating with a palladium(0) source for 6 hours (Scheme 1.23).[115] This method bypasses the need for harshly basic or reducing conditions, but with the caveat of requiring low valent metal precursors such as $Ni(COD)_2$, which must be handled under air- and moisture-free conditions.

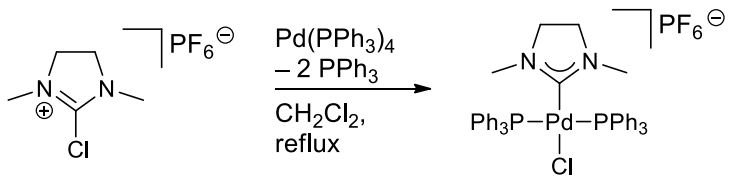

52 **53**, 72 %

Scheme 1.23 *NHC complex synthesis by oxidative addition of zero-valent palladium to a 2-chloro-substituted imidazolinium salt.*

Solid-state structural analyses of NHC–metal complexes indicate slight shortening of the C2–N1(3) bonds and widening of the N–C2–N angle relative to the free carbene.[90] Bond formation between a free classical NHC and a metal

results in electron density being drawn away from the carbene centre, towards the Lewis acidic metal. By ^{13}C NMR spectroscopy, this is usually observed as an upfield shift for the carbene resonance.[90,116] The carbene resonance is prone to downfield shifts when located *trans* to a strongly donating ligand, a property which provides a convenient quantitative measure of the second ligand's donor ability.[117]

1.4.3 Catalytic applications of free classical NHCs and their complexes

NHCs make up a class of powerful nucleophilic organocatalysts for the activation of electrophiles, most commonly the carbonyl group in aldehydes or ketones (Figure 1.8). In many cases, the free carbene is generated *in situ* from its azolium salt for ease of handling.

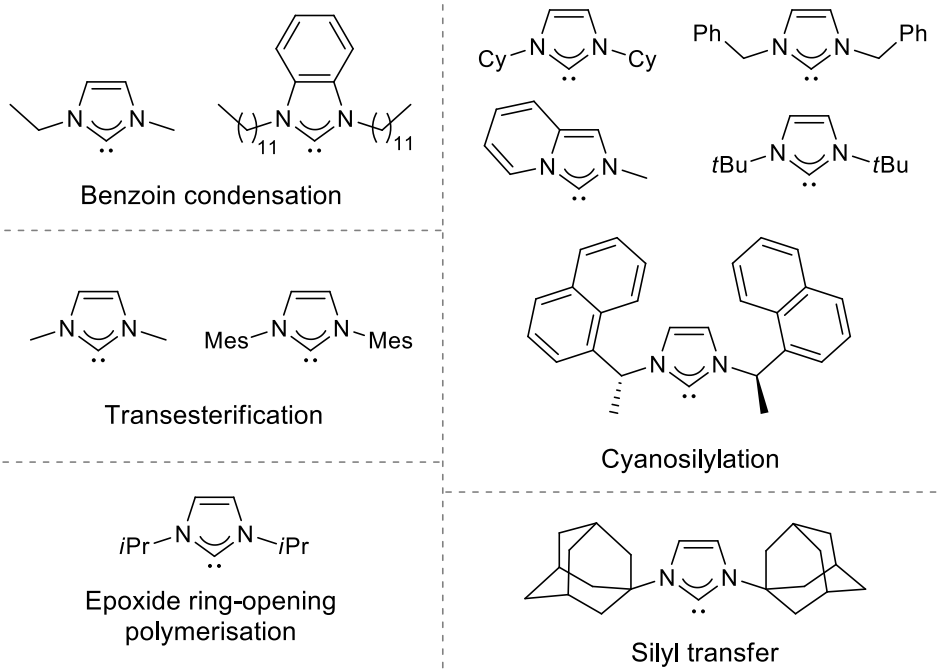

Figure 1.8 *Selection of NHCs responsible for various organocatalytic processes.*

The benzoin condensation[118,119] and the Stetter reaction[120,121] are two classic examples of NHCs in organocatalysis. NHCs derived from thiazolium and triazolium salts are generally preferred for these reactions, though some imidazolium-derived NHC catalysts are also known to perform well.[122] Benzimidazolium-derived NHCs with long chain *N*-alkyl substituents enable the benzoin condensation of aromatic aldehydes to take place in water, presumably due to their ability to form micelles.[123]

Maruoka and coworkers discovered that some NHCs could efficiently catalyse the cyanosilylation of aldehydes, ketones and imines.[124] Even at low catalyst loadings, the 1,2-addition of trimethylsilyl cyanide to carbonyl and imine substrates proceeded in excellent yields to give the desired congested cyanohydrin trimethylsilyl ethers. The groups led by Song[125] and Sato expanded the substrate and catalyst scope while maintaining impressive conversion rates, and even achieved some degree of enantioselectivity in the addition by using a chiral NHC.[126]

Hedrick and coworkers reported good conversion rates at 25 °C for the transesterification of methyl benzoate with a primary or secondary alcohol, or a diol with IMe as the catalyst.[127] This was exploited in the self-condensation of straight chain alcohol esters to form polyesters. Nolan and coworkers showed that NHC-catalysed transesterification could be generalised to esters that were activated, sterically hindered, acidic or α,β-unsaturated.[128]

Many NHCs are also highly efficient catalysts for polymer synthesis, such as epoxide ring-opening polymerisation. α,ω-Heterodifunctionalised poly(ethylene oxide) oligomers with reactive alcohol or silyl terminal groups could be obtained with excellent control of molar masses and dispersities.[129] This can also be achieved under solvent-free conditions.[130] Unlike organometallic catalysts, these NHC catalysts do not leave unwanted metallic residues in the polymeric product.

As a final example, IAd could be employed as an organocatalyst for the room temperature silyl transfer from trialkylsilyl ketene acetals to ketones, giving the silyl enol ether product in near quantitative yields.[131]

NHCs have been awarded the title “privileged” ligands for good reason. Apart from phosphines, few other ligands have demonstrated such a broad scope of applicability. Due to the strongly σ-donating nature of NHCs, they were initially regarded as phosphine mimics. It seems natural then that the use of NHC complexes as catalysts began in areas where phosphine complexes were known to perform very well, such as olefin metathesis (Figure 1.9). Grubbs and coworkers found that for many substrates, the ring-closing metathesis (RCM) activity of NHC complexes **54** and **55** either rivalled or outperformed their predecessors **56** and molybdenum[132] complex **57**, which were the leading RCM catalysts at the time.[111,133] The ability of Ru–NHC complexes to form tri- and tetrasubstituted cycloalkenes were also superior to that of their phosphine analogues.[134]

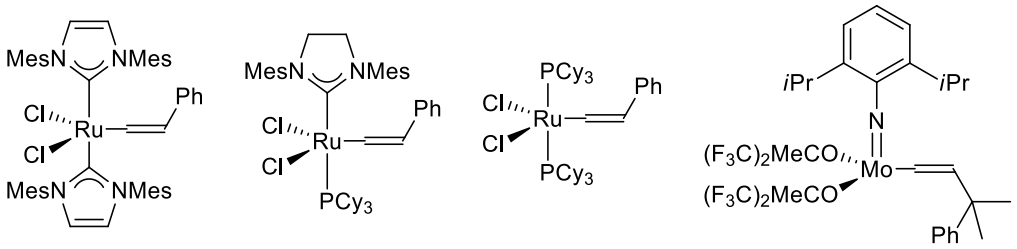

54 **55** **56** **57**

Figure 1.9 *Ruthenium NHC complexes and their older generation phosphine and molybdenum catalysts for ring-closing metathesis.*

The use of NHC complexes in organometallic catalysis has long since outgrown the confines of RCM. In the present day, they have a particularly strong presence in cross-coupling reactions. NHC complexes of palladium can mediate the C–C cross coupling of aryl chlorides and aryl triflates with a range of arylboronic acids.[135] Palladium(II) complexes bearing *N*-pyrimidyl NHC were not only highly active in the Mizoroki-Heck reaction of allyl bromide with bromoarenes, but they could also activate the C–H bond in methane to produce methanol in the presence of $K_2S_2O_8$ as the oxidant.[136]

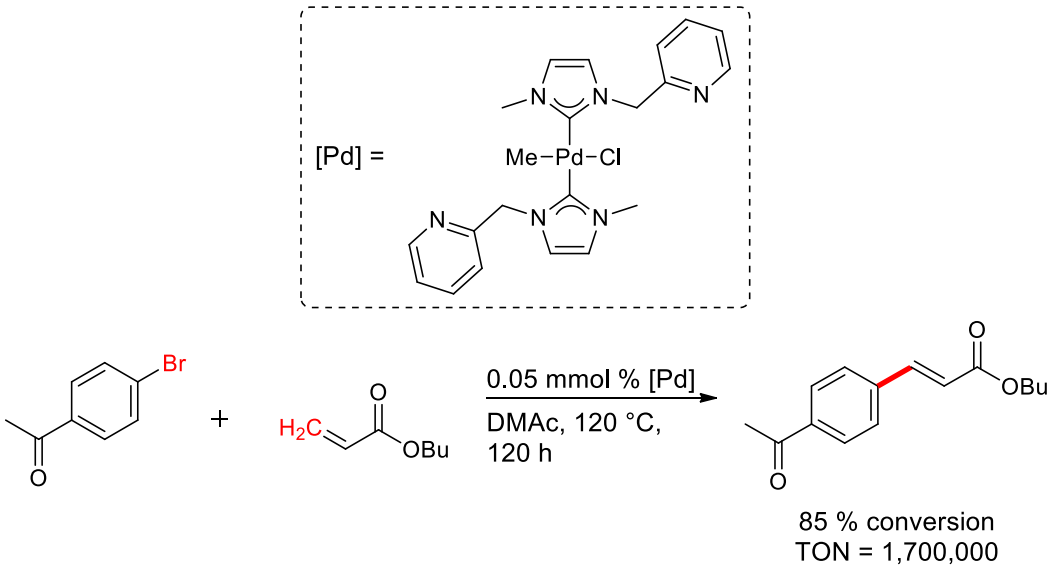

Scheme 1.24 *Highly efficient Heck coupling catalysed by a palladium(II) NHC complex featuring pendant donor N-substituents.*

The relative ease of adding structural complexity to the NHC scaffold facilitates the design of highly functionalised metal-NHC complexes that are fine-tuned for catalytic performance. Palladium(II) catalysts bearing NHC ligands with hemilabile donor-functionalised *N*-substituents were used in Heck, Suzuki and Sonogashira coupling reactions of acetophenone to great effect. Turnover

numbers (TON) of up to 1,700,000 could be achieved with sub-micromolar equivalents of catalyst (Scheme 1.24).[103]

A ruthenium(II) NHC complex with a pendant amine arm catalyses the hydrogenation of esters at relatively mild conditions, and theoretical studies indicate that the NH group interacts with the ester carbonyl through hydrogen bonding as part of a bifunctional mechanism.[137]

Peris and coworkers added a remote ferrocenyl group fused to the NHC backbone of a gold(I) complex.[138] The ferrocenyl unit functions as a redox switch, which allows the electron donating ability of the NHC ligand to be tuned according to the oxidation state of the iron centre. The subtle decrease in the donor ability of the NHC upon oxidation is sufficient to produce measurable increases in catalytic activity for the hydroamination of terminal alkynes, and the cyclisation of alkynes with furans.

1.5 Type B or protic NH,NR and NH,NH NHC complexes

The previous section highlighted ways in which the *N*-substituents in classical NHCs can enhance reactivity on the metal centre through donor-functionalised N wingtips. On the other hand, replacing one or both of those substituents with a proton enables hydrogen bonding with other substrates, a feature which has been exploited as a means for improving selectivity in catalytically active complexes. These protic NHCs can also serve as precursors to classical NHCs. The synthesis, properties and reactivity of protic NHCs are still underdeveloped compared to classical NHCs, and have been the subject of several excellent reviews.[139–141]

1.5.1 Protic NHC complexes: Synthesis, and structural and spectroscopic trends

The most acidic proton in a NH,NR or NH,NH imidazolium salt resides on the nitrogen, not the C2 carbon. Instead of producing the free carbene, treatment of such a salt with base results in regioselective deprotonation of the nitrogen and isomerisation into the corresponding imidazole. Unsurprisingly, this has prevented the isolation of protic NHCs in their free form; to this date, they are only known as their complexes. In principle, these protic NHC complexes could isomerise into the *N*-coordinated imidazole complex, but this is seldom observed in practice (Scheme 1.25).[142] While imidazole is more thermodynamically stable than its protic free NHC tautomer, the high energy barrier calculated for the required 1,2-hydrogen shift suggests that the latter is often kinetically

favoured,[143,144] with occasional exceptions.[145–147] Theoretical studies of the relative stabilities of the *C*-bound and *N*-bound tautomers suggest that factors such as strongly π-basic metal centres, hydrogen bond formation at the NH site(s), and the absence of ligands with a strong *trans* influence located *trans* to the C/N binding site will stabilise the *C*-form over the *N*-form.[146,148]

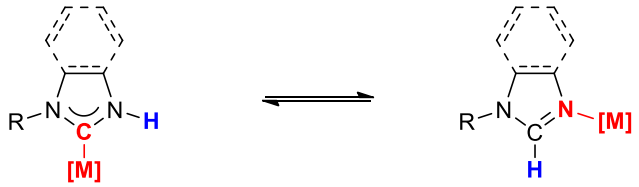

***C*-bound tautomer**
Protic NHC complex

***N*-bound tautomer**
Imidazolyl complex

Scheme 1.25 *Tautomeric forms of imidazole-type protic NHC complexes.*

Consequently, other strategies were developed to access protic NHC complexes, such as the metal-templated cyclisation of isocyanides and nitrogen-containing nucleophiles (Scheme 1.26). Under basic conditions, a pre-coordinated metal isocyanide may be reacted with phenylisocyanate or phenylthioisocyanate to give protic NHC complexes bearing exocyclic olate and thiolate functions, respectively.[149] These versatile backbone substituents may undergo further alkylation or acylation, or act as monodentate donors. 2-Bromoethylamine[150] and aziridine[151] may also be used as cyclisation partners to form protic imidazolidin-2-ylidenes. In cases where the isocyanide and nucleophile are contained within the same molecule, protic NHC complexes may be accessed via intramolecular 1,2-addition across the C–N triple bond. This approach has been particularly successful in the preparation of backbone saturated[152] and benzannulated protic NHCs.[153,154] In a variation of this method, the isocyanide complex is generated *in situ* from an amino-phosphinimine ligand.[155] One carbonyl ligand on a group VI metal carbonyl is deoxygenated by the phosphinimine at room temperature, forming the isocyanide complex which then undergoes intramolecular attack by the amine. Five- and six-membered protic NHC complexes with saturated backbones can be formed in this way. However, this approach may fail for aromatic amines, or when ligands other than carbonyl are present.[156]

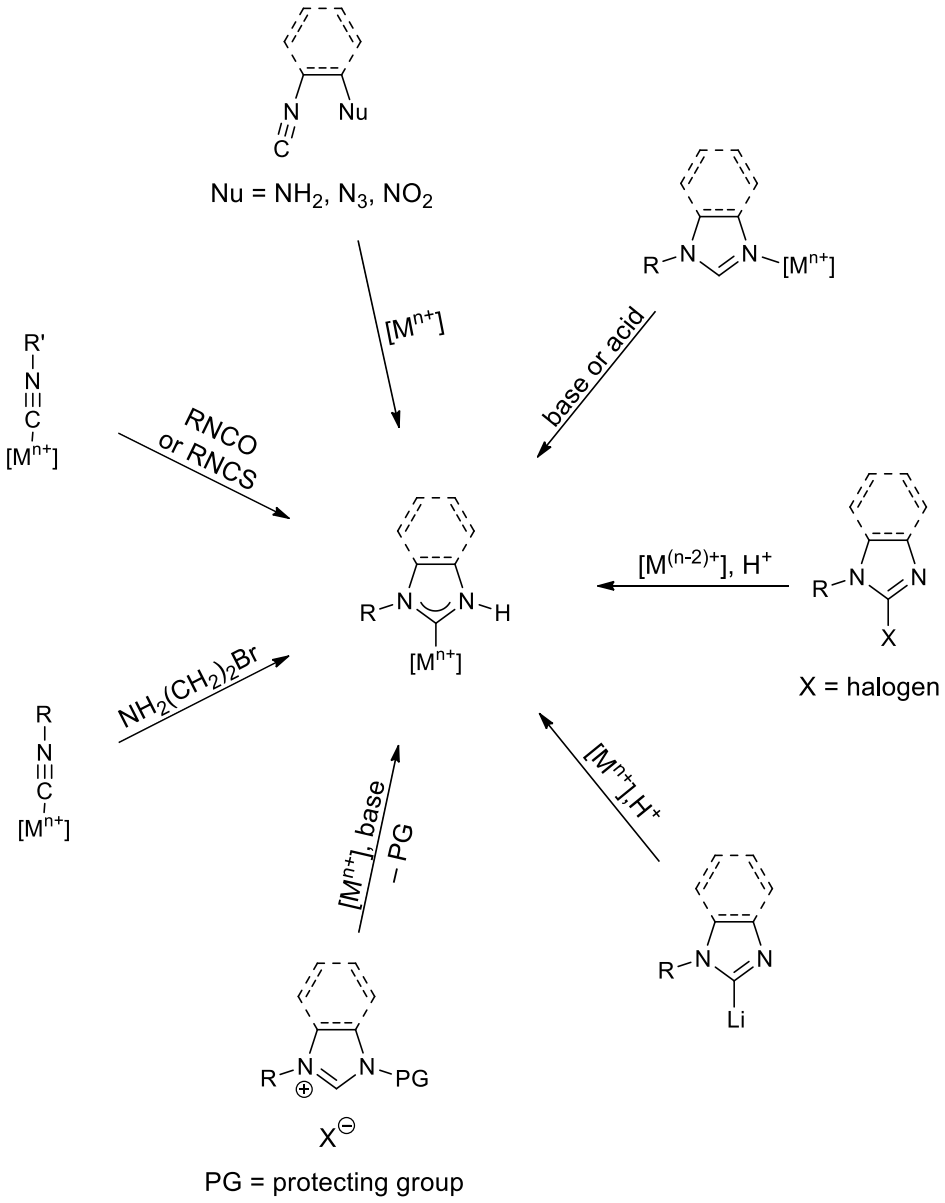

Scheme 1.26 *Synthetic strategies towards protic NHC complexes.*

Where the synthesis of benzannulated targets is concerned, an azide group is typically used as a synthon for the amine nucleophile: a crucial modification, as free 2-aminophenyl isocyanide spontaneously cyclises to form benzimidazole. Upon coordination of the isocyanide to a metal centre, the azide is converted into an amine, after which cyclisation into the carbene readily occurs. Azide reductions are often effected via a Staudinger-type reaction, unless the phosphinimine intermediate cannot be hydrolysed, or the tertiary phosphines used to generate the phosphinimine may preferentially coordinate to the metal centre instead (Scheme 1.27). Michelin and coworkers have observed that the isocyanide-coordinated metal ion must be coordinatively saturated or bound to

sterically hindered ancillary ligands for the Staudinger reaction to proceed.[157] NaI/$FeCl_3$[153] and Zn/NH_4Cl/H_2O[158] were found to be suitable alternatives as azide reducing agents. When 2-nitrophenyl isocyanide is used in place of the azide, NH,NOH substituted carbenes are obtained if the reduction is carried out with hydrazine hydrate instead of tin/HCl.[159]

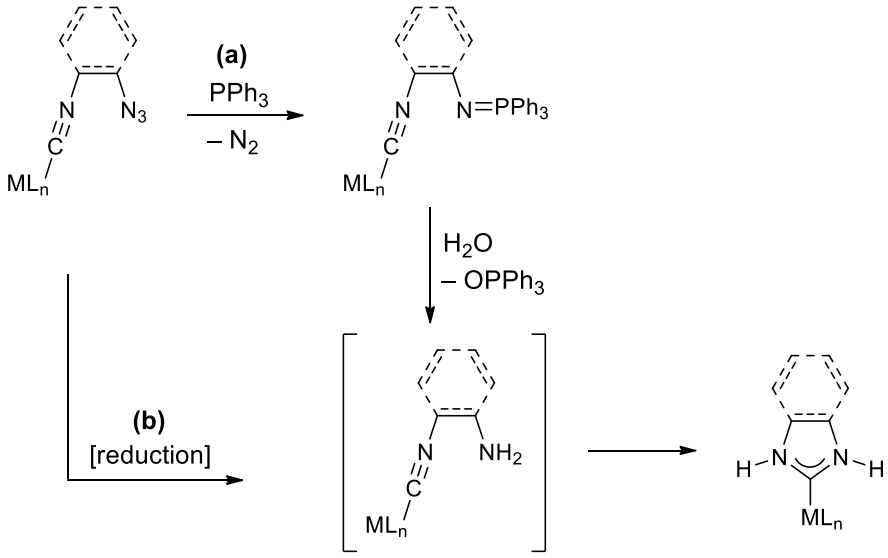

Scheme 1.27 *Conversion of an azide to an amine via* ***(a)*** *the Staudinger reaction or* ***(b)*** *one-step reduction, followed by intramolecular cyclisation into the protic NHC complex.*

One major drawback of this approach is the challenging synthesis of β-functionalised isocyanides. It is conceptually simpler to convert an *N*-metallated imidazolyl or otherwise pre-coordinated complex into its protic NHC tautomer, usually with the assistance of base,[160] acid,[161] or a chelating director[162–170] (Scheme 1.28). The use of a tether not only encourages the formation of the protic NHC, but also stabilises it by preventing reverse tautomerisation into the *N*-metallated form.[167]

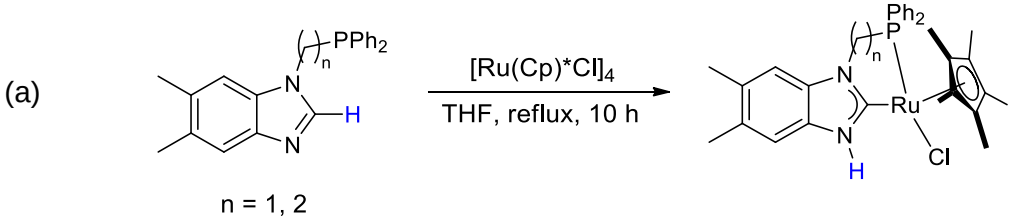

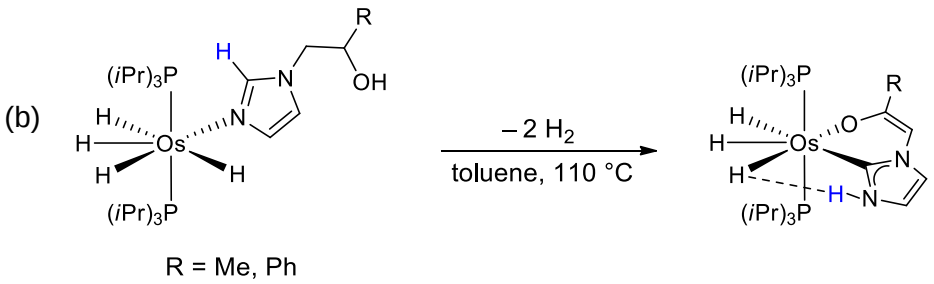

Scheme 1.28 *Synthesis of protic NHC complexes by tautomerisation of neutral azolyl ligands, facilitated by* ***(a)*** *phosphine*[162] *or* ***(b)*** *oxygen pendant donors.*[163]

The carbene can also be generated by the oxidative addition of metals to 2-haloimidazoles followed by protonation of the nitrogen.[171–174] Neutral azoles which have been lithiated at the C2 position may undergo transmetallation to give imidazolate complexes, which furnish protic NHC complexes upon protonation of the unsubstituted nitrogen.[175–178] Otherwise, the conventional procedure of deprotonating azolium salts in the presence of a metal source can be modified by installing a labile *N*-protecting group, which is later cleaved to reveal the protic NHC complexes (Scheme 1.26). Silane[179] and benzoyl[180] protecting groups have been successfully employed in this manner, and both can be conveniently displaced by alcoholysis.

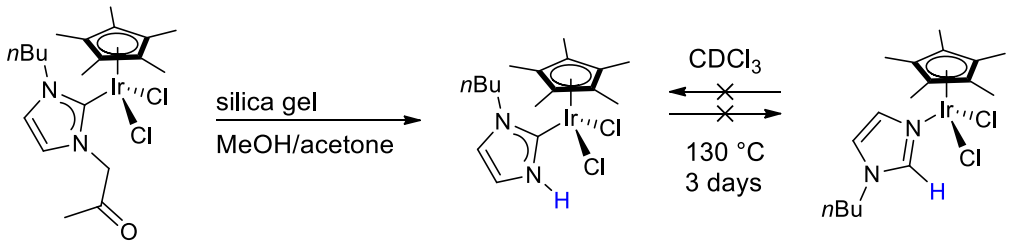

Scheme 1.29 *Cleavage of a 2-oxopropyl group yields a protic NHC complex which is inaccessible by tautomerisation of the corresponding N-metallated imidazolyl complex.*

Protic NHC complexes of iridium(III) in particular have been prepared by the removal of 2-oxopropyl protecting groups through heterogeneous N–C bond cleavage on silica gel.[142,181] Interestingly, a protection/deprotection strategy involving the 2-oxopropyl group enabled access to the protic NHC complex where the attempted C/N tautomerisation from the *N*-bound iridium(III) complex failed (Scheme 1.29).[142]

The replacement of an alkyl group on a nitrogen atom of an imidazol-2-ylidene with a proton creates electronic differences that are structurally and spectroscopically evident. The ^{13}C NMR shifts for the carbenic carbon in protic NHC complexes tend to appear further upfield than those for classical NHC complexes; resonances falling within the 140 – 170 ppm region are not unusual.[142,166,175] A systematic downfield shift also occurs when protic imidazolinium-type NHC complexes undergo *N*-alkylation.[152] The carbene–metal bond is consistently longer in protic NHC complexes than in their NR,NR-type counterparts, which indicates weaker σ-donor ability in protic NHCs compared to classical NHCs.[152,154,159] Exceptions to the carbene–metal bond elongation may occur if *N*-alkylation results in the confinement of the carbene fragment within a macrocyclic structure. In such instances, the chelate effect may force the carbenic atom and the coordinated metal centre closer together.[182,183]

The presence of the NH site on a protic carbene can have direct consequences on the solid state molecular arrangement of its complexes. Fehlhammer and coworkers observed that the ligand arrangement around the metal centre in tetrakis(1-methylimidazol-2-ylidene)palladium(II) iodide did not minimise steric interactions between the *N*-methyl groups; rather, it was more strongly influenced by hydrogen bonding interactions between the NH site and the iodide counterions.[175]

1.5.2 Practical significance of protic NHC complexes

Since the defining feature of a protic NHC is the presence of an NH site directly adjacent to the carbene centre, it comes as no surprise that all the applications unique to this class of NHC involve, at least to some degree, the ability of the NH site to undergo substitutions, participate in hydrogen bonding or exhibit acid–base chemistry.

Early reports of post-synthetic modifications on protic NHCs mostly revolved around simple *N*-alkylations to give NR,NR-type NHC complexes. Allyl,[152] ethyl and propargyl groups have been successfully installed (Scheme 1.30).[155]

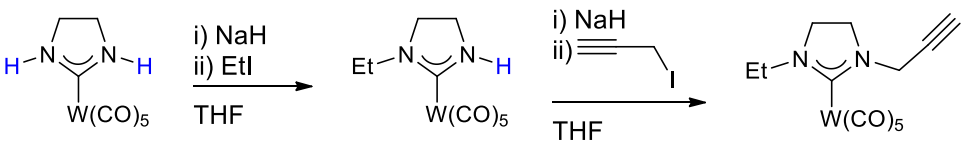

Scheme 1.30 *Stepwise N-alkylation of a protic carbene to give an asymmetrically substituted imidazolin-2-ylidene complex.*[155]

N-functionalisation on protic NHCs became more than an alternative route to NR,NR-type complexes when the potential for metal-templated structural elaborations of ligands was recognised. The synthesis of macrocyclic complex **59** by linking the four carbene units on the pre-formed homoleptic complex **58** neatly avoids any size control issues that might arise from attempting to prepare the free macrocycle (Scheme 1.31).[182]

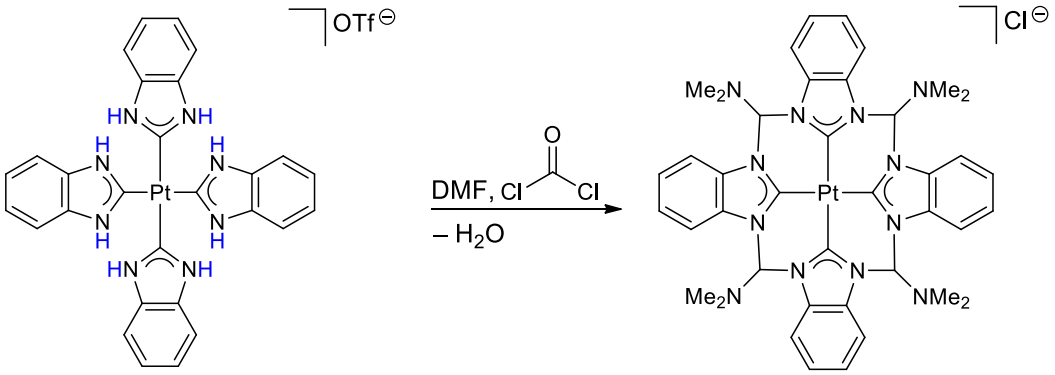

58 **59**

Scheme 1.31 *Construction of a "molecular square" macrocycle by template-controlled linkage of four protic NHCs.*[182]

Enhanced control over the stereochemistry of the ligand can be achieved if it is constructed by building upon a coordinated protic NHC. Consider the tridentate mixed phosphine ligand in **61** (Scheme 1.32 b). Synthetic routes to similar 11-membered ligands are limited by the need for very dilute reaction mixtures, the narrow scope of linkers between the phosphorus atoms, and the formation of multiple diastereomers.[184] Only the *all-syn* isomer is capable of binding to a metal centre in a tridentate fashion, but the *syn-anti* isomer is the most thermodynamically stable (Scheme 1.32 a).[185] The latter must be heated at high temperatures to induce conversion into the former. Fortunately, a more elegant option exists: The *all-syn* tridentate ligand can obtained exclusively via an intramolecular S_N2_{Ar} type substitution of the coordinated phosphine at the NHC fragment in **60** (Scheme 1.32 b).[186]

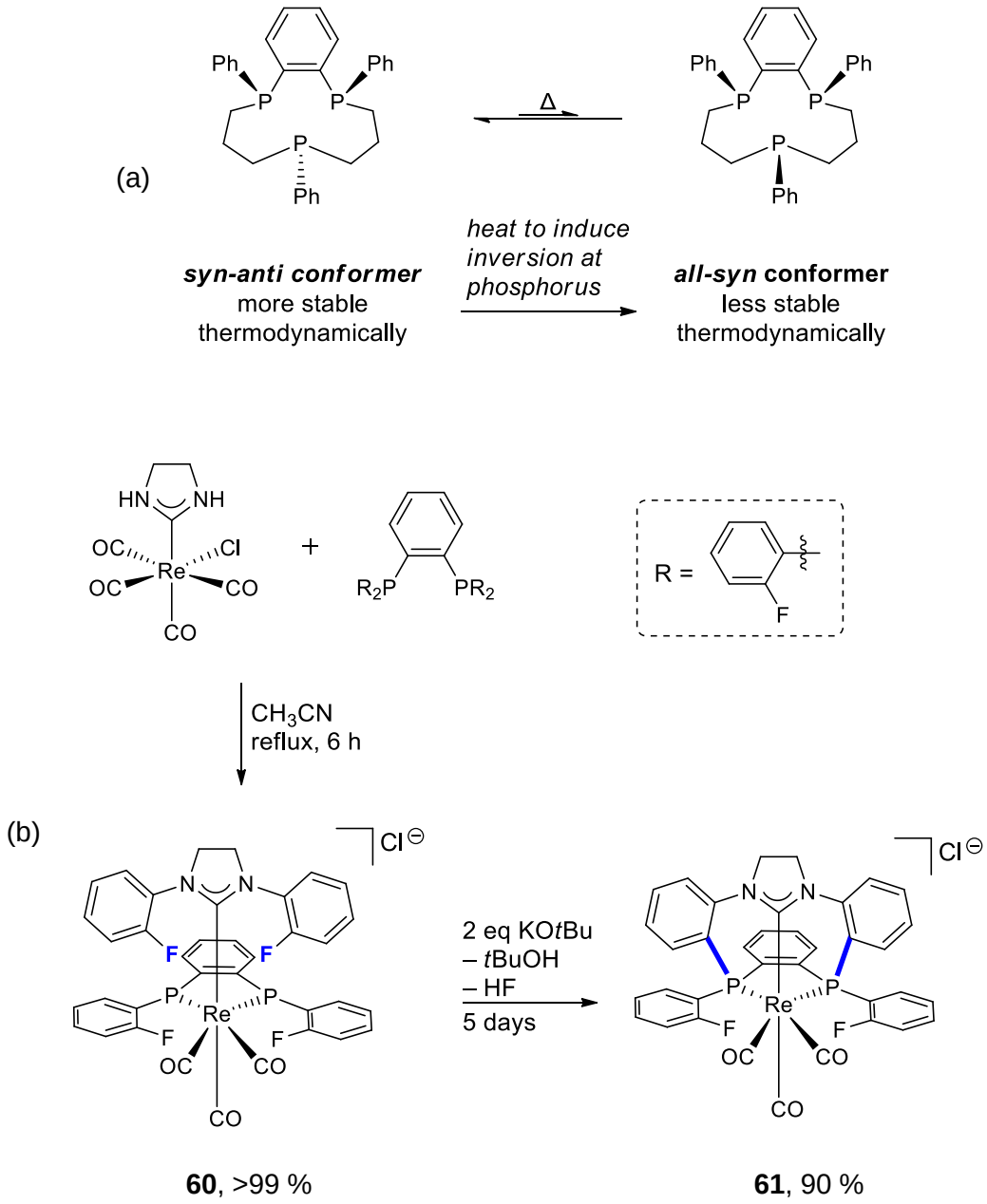

Scheme 1.32 (a) *The difficulty in selectively synthesising the desired conformer of tridentate P-donor macrocycles can be overcome by* ***(b)*** *conducting a metal-templated linkage of two phosphorus donors to a protic NHC.*

Protic NHCs have been implicated as important intermediates in certain catalytic transformations. Based on empirical and computational data, the rhodium(I)-catalysed intramolecular C–C coupling of pendant alkenyl-functionalised benzimidazoles is thought to proceed via the protic NHC complex **62** as the catalyst resting state (Scheme 1.33).[187,188]

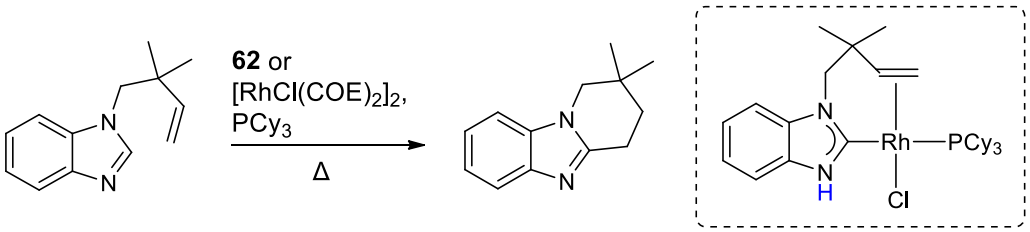

62

Scheme 1.33 *Intramolecular C–C coupling catalysed by a protic NHC complex of rhodium(I), which can also be generated in situ.*

Subsequent insertion of the alkenyl group into the Rh–C bond, followed by an intramolecular proton transfer from the carbene ring nitrogen to the metal centre, then C–H reductive elimination affords an annulated heterocycle as the product. The catalyst resting state is regenerated upon C–H activation of another benzimidazole by the rhodium species. A similar complex **63** also appears to be an intermediate in a related rhodium-catalysed arylation where benzimidazole is used as the substrate (Scheme 1.34).[189]

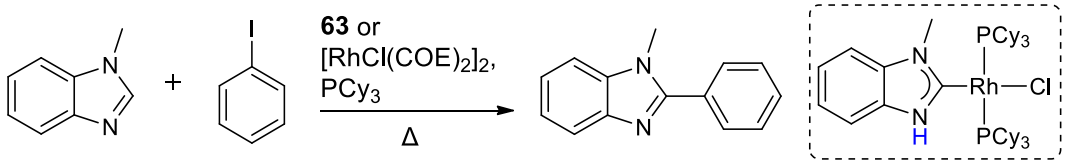

63

Scheme 1.34 *Rhodium(I) may undergo C–H activation at the C2 position of benzimidazole to form the active catalyst for subsequent C-arylation.*

It is uncertain whether the arylation of every *N*-heterocycle tested also occurs via a protic carbene intermediate. However, the fact that protic NHC complex **64** is formed under conditions not unlike those for olefin coupling with dihydroquinazolines is a compelling sign that this mechanism is not solely operative for benzimidazoles (Scheme 1.35).[190]

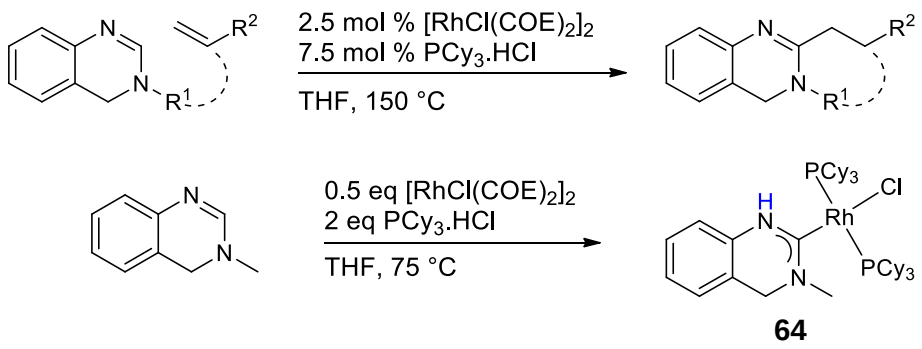

64

Scheme 1.35 *Intramolecular C–C coupling of pendant alkenyl-functionalised dihydroquinazolines may proceed via a protic NHC intermediate similar to* ***64****, which is formed in an irreversible reaction at temperatures lower than those required for the olefin coupling.*

In addition to being a key intermediate in some reaction mechanisms, protic NHC complexes have been more purposefully deployed in synthesis. The hydrogen bond donating abilities of the NH site in protic NHC complexes are well-documented in their solid state structures and crystal packing.[164,191] These abilities are also evident in their solution state behaviour, and can be monitored by the NH chemical shift changes in ^{1}H and ^{15}N NMR spectroscopy.[162,191] After finding that tungsten complex **65** forms hydrogen-bonded aggregates with DMPU in solution, Hahn and coworkers identified the potential of the NH group to act as a supramolecular recognition site.[176] This can be a beneficial feature in catalysis, a point which they illustrate by using 1-dodecene and 3-butenoic acid ester as competing substrates in a hydrogenation experiment. The carbonyl functionality on the ester is capable of accepting a hydrogen bond from the NH site in **66**, thus forming an additional point of interaction between the catalyst and the substrate. The greater affinity of **66** for the ester over 1-dodecene translates to a significantly higher conversion rate of the latter into the hydrogenated product.

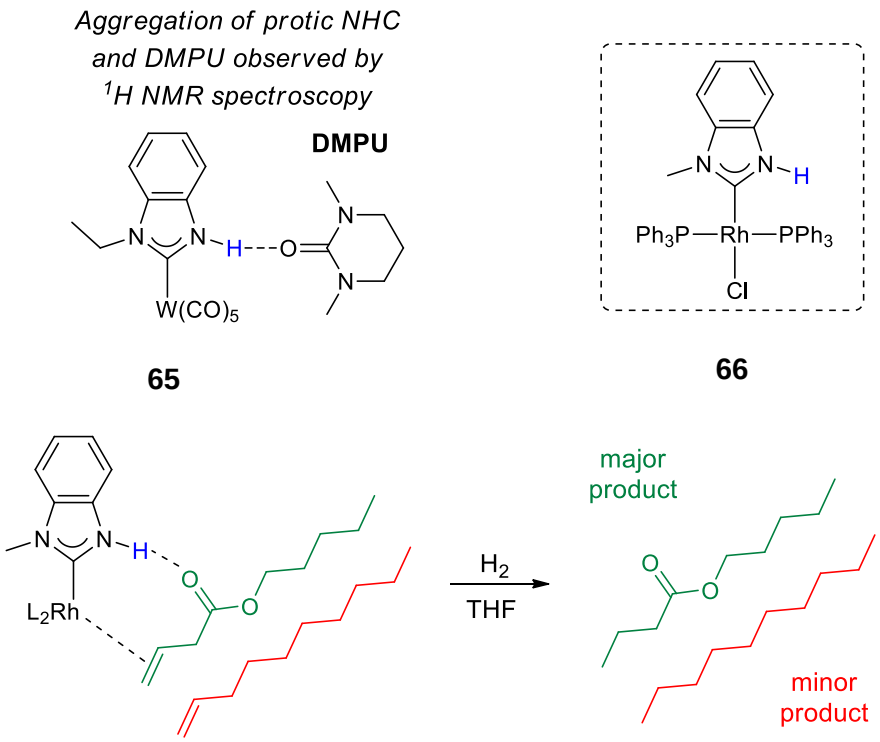

Scheme 1.36 *Molecules bearing hydrogen bond acceptors can interact with the NH wingtip of a protic NHC. These interactions enabled the recognition and preferential hydrogenation of a carbonyl-functionalised olefin by* ***66****.*

Aside from enabling molecular recognition through hydrogen bonding, protic NHC ligands can actively participate in catalytic transformations by reversible deprotonation at the acidic NH site. For instance, *N*-(2-pyridyl)benzimidazole can be allylated at the C2 position to give **71** in a ruthenium-catalysed dehydrative C–C coupling reaction (Scheme 1.37).[164] Presumably, the catalytic cycle begins with Ru insertion into the C2–H bond of benzimidazole to give the isolable intermediate **67**, which then coordinates to allyl alcohol. Next, it is suggested that the NH proton and hydroxyl group in **68** are lost as water to give the imidazol-2-yl complex **69**. The elimination is expected to be a facile process due to the dual binding mode of the alcohol in **68** that is evocative of **66** from Hahn et al.'s competitive hydrogenation experiment. Reductive elimination of the heterocycle from **70** (a species that is also obtainable from the stoichiometric reaction of **67** and allyl alcohol) occurs in the presence of excess benzimidazole and the cycle repeats itself.

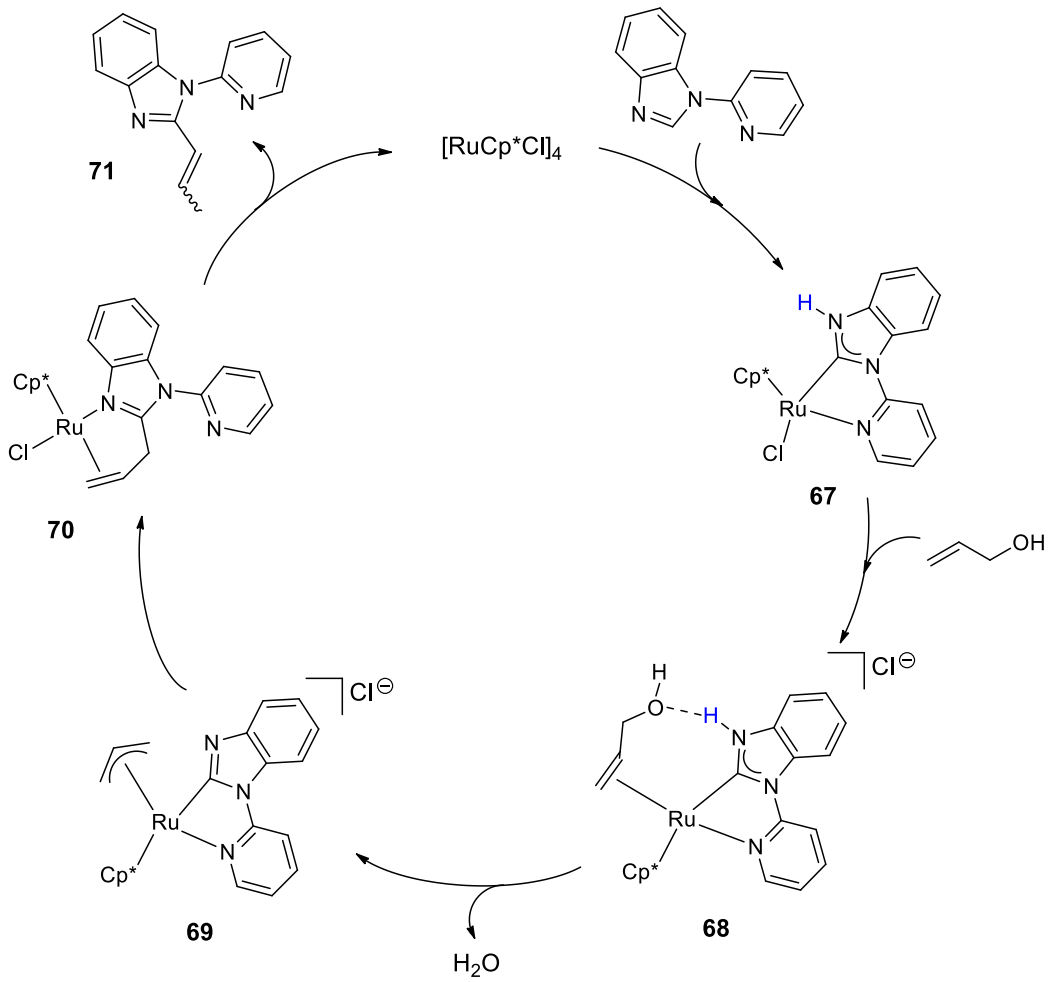

Scheme 1.37 *Catalytic dehydrative C–C coupling of a benzimidazole and allyl alcohol.*

Thus far, the cases discussed involve chemical changes that take place primarily on the NHC ligand, such as imidazolyl/NHC tautomerisation or NH deprotonation. More sophisticated catalytic systems which are forthcoming involve reactions between the NH wingtip and the carbene-coordinated metal centre, causing changes in the formal oxidation state of the latter. Consider the example of ligand **72**, which reacts with $[Ir(COD)_2]BF_4$ to give a mixture of the NHC species **73** and a number of iridium(III) hydrides, as evidenced by ^1H NMR spectroscopy (Scheme 1.38).[192] The hydride species may arise from C–H activation at either of the two positions ortho to the 2-pyridyl group. Tautomerisation of the hydride species into NHC complex **73** is not possible if the oxidative addition of iridium occurs across the C–H bond at the 4-position. Blocking the 4-position with a methyl substituent will prevent this from occurring, but one hydride species **75** still forms in addition to the NHC **74**.

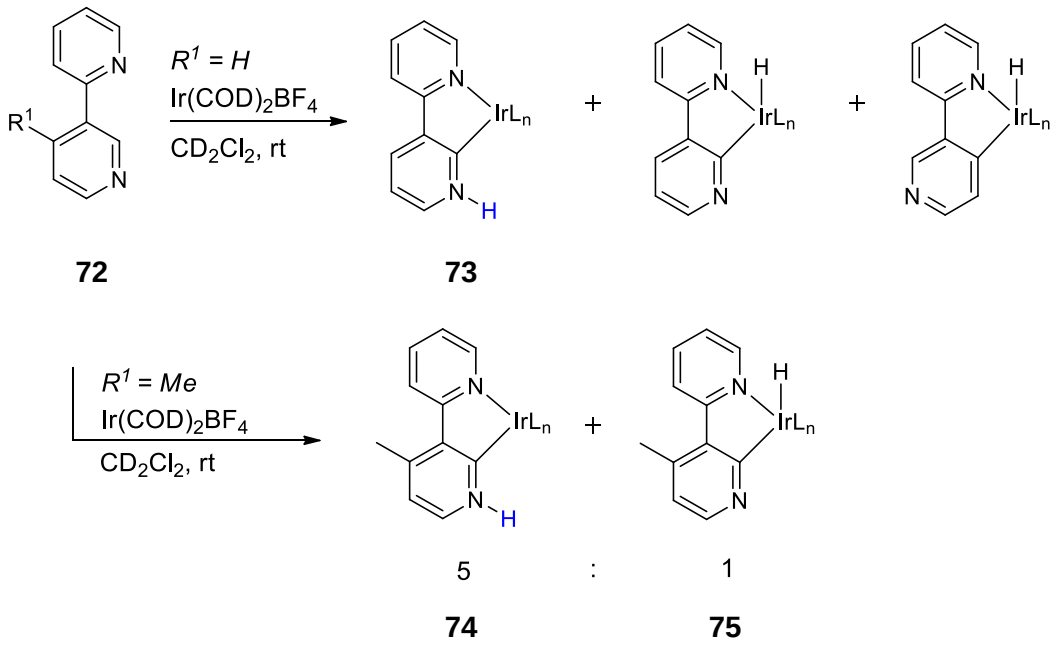

Scheme 1.38 *Formation of iridium NHC and hydride species.*

The NHC tautomer can be stabilised by hydrogen bonding to an amide carbonyl α to the protonated nitrogen. This simple modification is so effective at promoting tautomerisation that the NHC **77** is obtained from the amide-functionalised ligand **76** in near quantitative yields, even when the 4-position is left unblocked (Scheme 1.39).

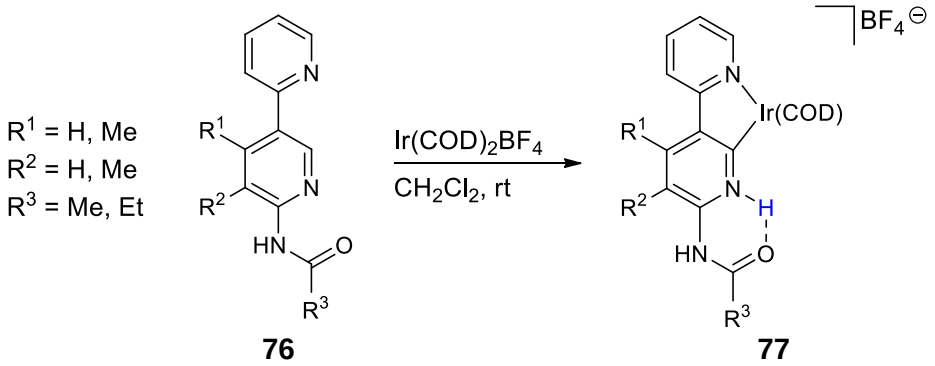

Scheme 1.39 *Hydrogen bonding induced **s**elective formation of the NHC tautomer over the hydride tautomer.*

These findings provided inspiration for the idea of an interconvertible iridium(I) NHC and iridium(III) hydride catalyst. The 1,3-migration of the hydride in **79** onto the pyridine nitrogen is an equilibrium process, the thermodynamics of which can be tuned by controlling the extent of hydrogen bonding stabilisation that is available to the NHC isomer **78** (Scheme 1.40).[193] Hydrogen bonding – and thus

the equilibrium concentration of the NHC species – can be attenuated by using counterions or solvents which are poorer hydrogen bond acceptors. Electron-rich ancillary ligands help stabilise the iridium(III) metal centre, therefore shifting the equilibrium towards the hydride species **79**.

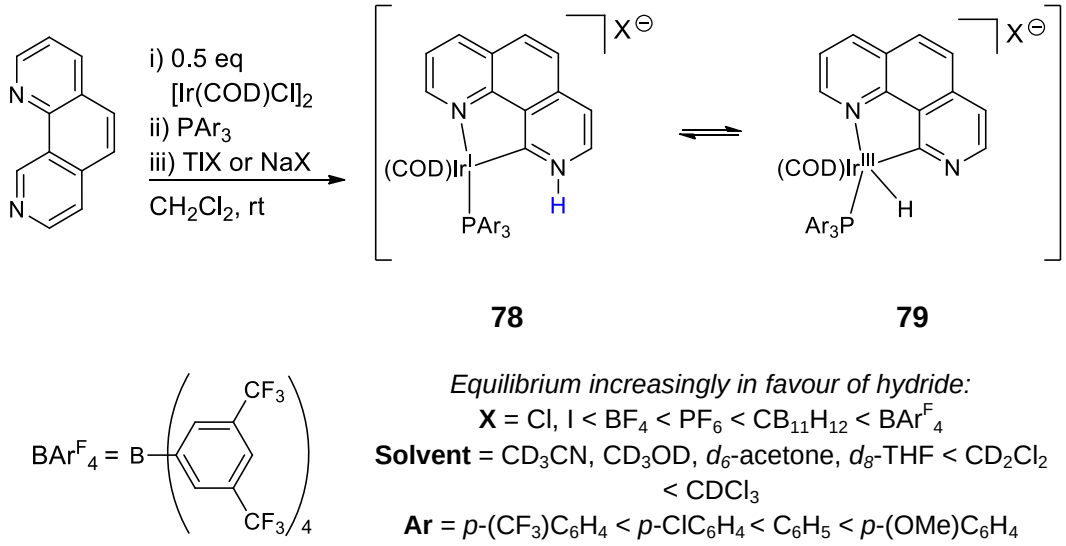

78 **79**

Equilibrium increasingly in favour of hydride:
X = Cl, I < BF_4 < PF_6 < $CB_{11}H_{12}$ < BAr^F_4
Solvent = CD_3CN, CD_3OD, d_6-acetone, d_8-THF < CD_2Cl_2 < $CDCl_3$
Ar = *p*-$(CF_3)C_6H_4$ < *p*-ClC_6H_4 < C_6H_5 < *p*-$(OMe)C_6H_4$

Scheme 1.40 *The equilibrium between an iridium(I) NHC complex **78** and its iridium(III) hydride tautomer **79** can be tuned by changing the counterion, solvent or ancillary ligand.*

Grotjahn and coworkers elaborated upon this concept of switchable oxidation states by proposing that protic NHC complexes can also be transformed into bifunctional ambident reactants (Scheme 1.41).[166] The hydride in **80** can be abstracted to create a vacant coordination site on the metal ion. This vacant site and the proximal basic nitrogen of **81** make up a dual functionality complex, capable of metal–ligand cooperation to induce bond-breaking in another substrate to give **82**.

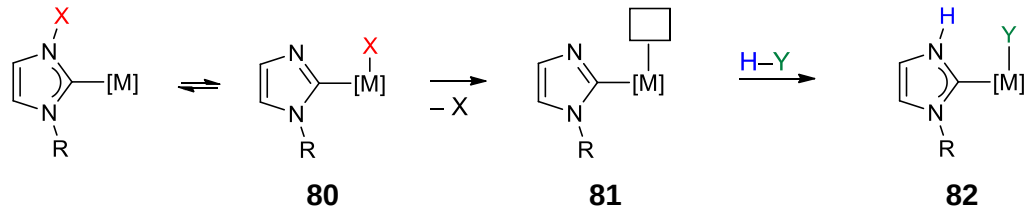

80 **81** **82**

NHC/hydride tautomerisation for X = H	Vacant site creation by hydride abstraction	Cooperative substrate activation by basic ring nitrogen and coordinatively unsaturated metal centre

Scheme 1.41 *Key reactivity modes resulting in bifunctional ambident reactivity, derived from protic NHC complexes.*

To demonstrate proof-of-concept for bifunctional ambident reactivity, they deprotonated protic NHC complex **83** to form **84**. In the presence of $KB(C_6F_5)_4$, **84** produces **85** and **87** upon exposure to hydrogen gas or acetylene respectively (Scheme 1.42). Presumably, chloride abstraction results in a transient, bifunctional complex **86**, which subsequently activates H_2 or the C–H bond in acetylene. The heterolysis took place at room temperature, highlighting the powerful reactivity of these bifunctional intermediates. H_2 activation was also observed under similar conditions for the analogous iridium(III) complex with a benzannulated NHC.[170]

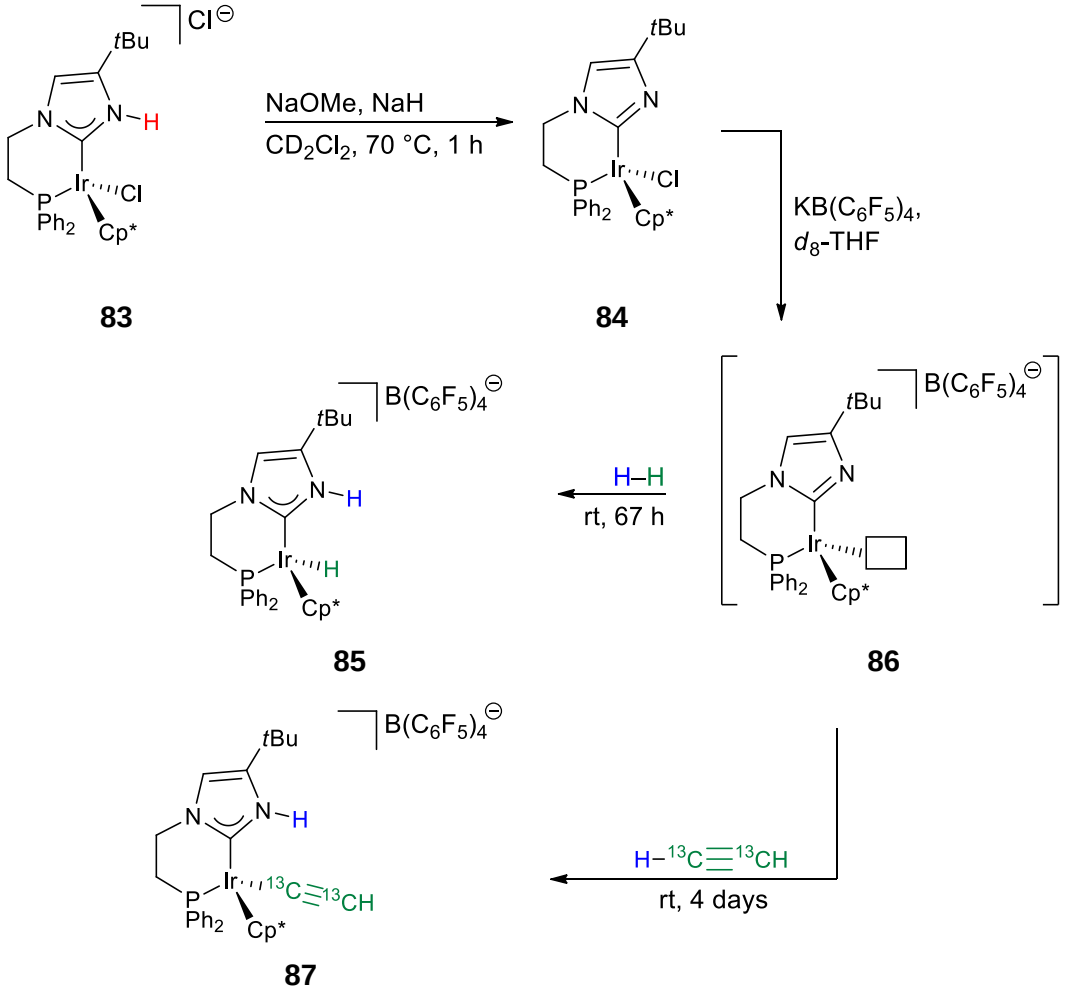

Scheme 1.42 *Bifunctional ambident reactivity of an iridium NHC complex capable of C–H and H_2 activation.*

Although the iridium complex **83** and its hydride derivative showed little catalytic behaviour, the ruthenium congeners **88** and **89** performed very well as catalysts for the transfer hydrogenation of acetophenone in isopropanol (Scheme 1.43).[165]

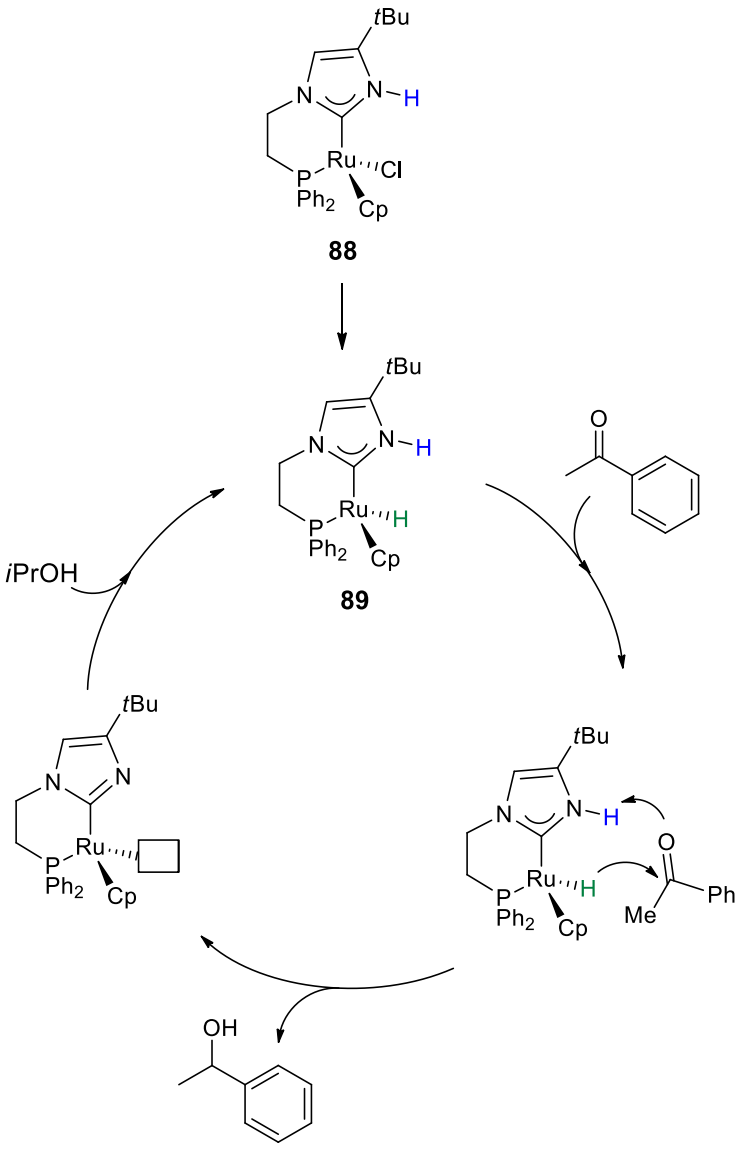

Scheme 1.43 *Proposed catalytic cycle for the transfer hydrogenation of acetophenone. Conditions: iPrOH at 70 °C using either 0.05 mol % **88** and 0.2 mol % KOH for 24 hours, or 1.0 mol % **89** for 3 hours.*

The active catalyst **89** can be generated *in situ* from **88** if a catalytic amount of base is added, or pre-formed by metathesis of **88** with sodium hydride (Scheme 1.44).

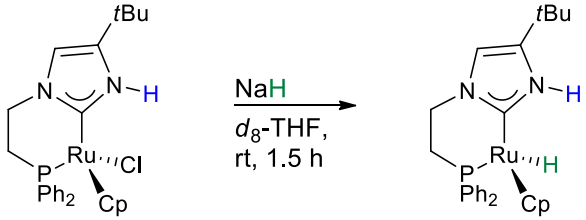

88 **89**

Scheme 1.44 *Hydride transfer at a ruthenium centre to give a hydride complex.*

Bidentate bis(imidazol-2-ylidene) iridium(III) complex **90** showed promising catalytic activity in the transfer hydrogenation of some alkenones into alcohols, and shared similar reactivity rates with **91a**-**b** in the conjugate reduction of an α,β-unsaturated ketone (Scheme 1.45).[194] The good chemoselectivity observed in the transfer hydrogenations is attributed to the ability of the protic NHC complexes to form hydrogen bonds with the alkenone substrates.

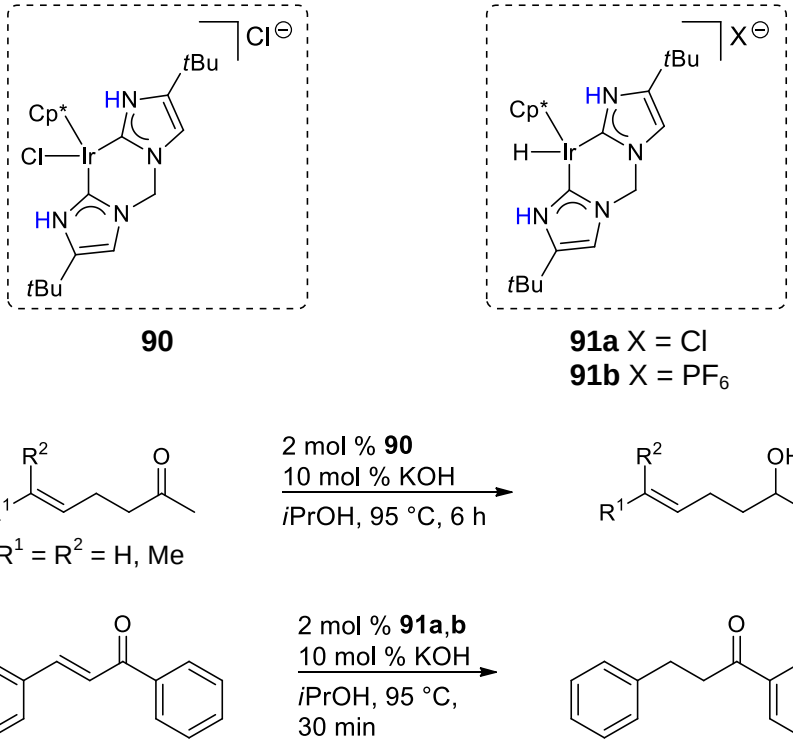

90

91a X = Cl
91b X = PF_6

Scheme 1.45 *Catalytic transfer hydrogenation reactions with bidentate protic NHC complexes of iridium(III).*

Meanwhile, preliminary reactivity studies of the platinum(II) pincer protic NHC complex **92** reveal that it can catalytically add O–H to phenylacetylene to form phenylacetaldehyde (Scheme 1.46 a), whereas the same reaction with 1-hexyne gives a 4:1 mixture of 1-hexanal and 2-hexanone (Scheme 1.46 b).[191] The

apparent selectivity for the anti-Markovnikov hydration products makes this system a strong candidate for further development. Successful ligand exchanges with CO, ethylene, nitriles and amines at the metal active site suggest a wide scope of potential substrates for these catalytically active protic NHC complexes.

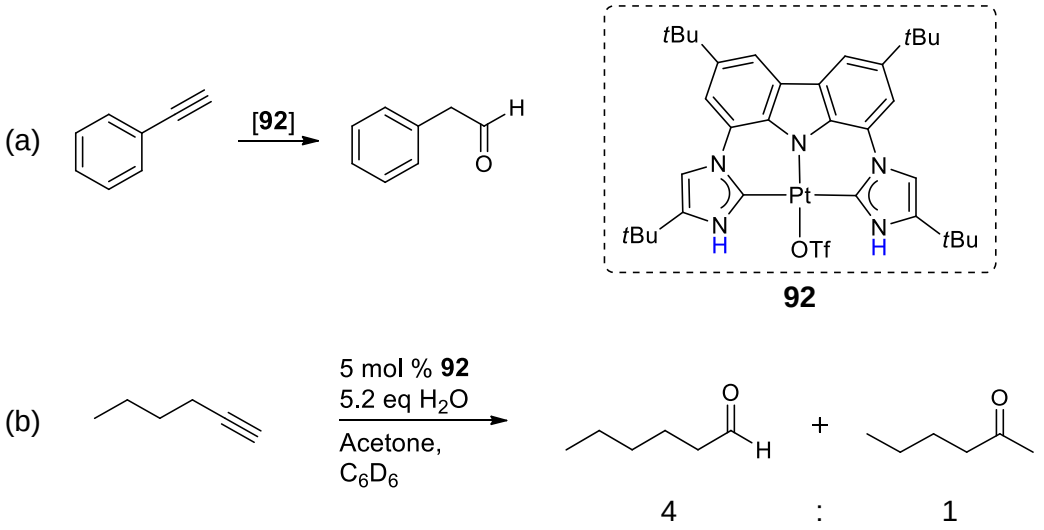

Scheme 1.46 *Platinum-catalysed hydration of* ***(a)*** *phenylacetylene and* ***(b)*** *1-hexyne, resulting in the selective formation of the anti-Markovnikov products.*

A tungsten complex bearing a saturated protic NHC and alkyne ligands was reported to be catalytically active in the polymerisation of diphenylacetylene.[156] A recent review extolled the properties of polydiphenylacetylenes that made them suitable for sensor and actuator applications.[195] This shows that protic NHCs may have commercial value in fields like material science.

The utility of protic NHC complexes extends beyond catalytic applications. The synthesis of protic NHCs from the cyclisation of metal-coordinated isocyanides tolerates a fairly wide scope of amine partners, including amino acids and derivatives thereof. This may be exploited in the development of improved protein labelling techniques. Heavy metal atoms such as tungsten may be introduced into a protein structure by converting any amino acid side chains into protic NHC complexes, thus greatly facilitating X-ray structure determination and protein topography studies.[196]

Unlike classical NHCs which tend to function as mere spectator ligands, the true strength of protic NHCs as ligands lies in their non-innocent behaviour. Their fundamental reactivity provides access to a rich variety of functionalised species

which lend themselves well to catalytic applications, as illustrated by the examples discussed here. As the understanding of their preparation and reactivity improves, their application in chemical synthesis will hopefully become more widespread, bringing forth new aspects of chemistry to explore.

1.6 Type C or naked N,NR NHCs and their *C,N*-bimetallic complexes

Studies involving protic NHCs have uncovered, often inadvertently, interesting structures which constitute a third class of NHCs where one of the ring nitrogens is unsubstituted. Some examples appeared in the previous section. These so-called “naked N”,NR NHCs (hereinafter abbreviated as N,NR NHCs) carry a formal negative charge on the unsubstituted nitrogen, and thus may be considered anionic NHCs. It must be emphasised that in this work, the term “anionic NHCs” refers to NHCs where the negative charge is shared or carried by the ring heteroatom adjacent to the carbene and not on a remote anionic substituent on the NHC,[197–201] although the latter are often labelled the same way in the literature. The scope of the discussion is further limited to imidazole-type anionic NHCs with an N,NR substitution pattern, thus excluding mixed normal/abnormal classical NR,NR NHCs which are anionic because the azolium salt has been deprotonated at two different sites.[202–205]

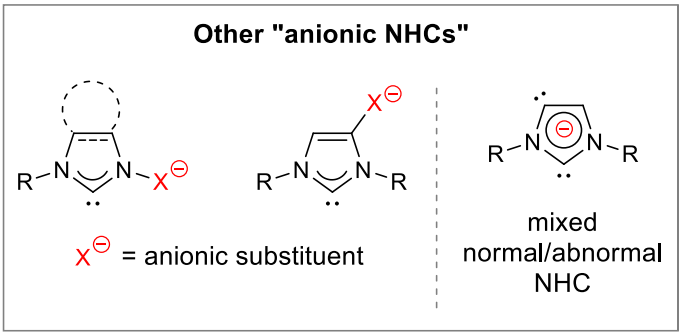

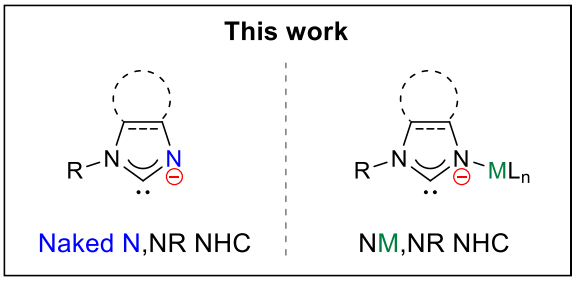

Examples of N,NR NHCs are rarely encountered as their high reactivity makes them difficult to isolate, although they may be invoked as intermediates in a reaction.[176,206,207] They are usually obtained as their complexes, where both the

carbene and the anionic nitrogen are coordinated to metal ions. Those will be referred to as “NM,NR NHC” complexes.

These azol-2-yl type compounds have been known for some time before they became more widely recognised as anionic NHCs within the chemical community. As early as 1995, Boche and colleagues described a dimeric lithiated thiazol-2-yl compound **93** as a formyllithium equivalent (Figure 1.10).[208] In contrast to common organolithium reagents such as methyl- or butyllithium where the alkyl component is closely regarded as a carbanion, they argue that **93** exhibits singlet carbene character in its crystal structure. A comparison with thiazole revealed that **93** experienced lengthening of the C2–N and C2–S bonds and shrinking of the N–C2–S angle from 115.1(8) ° to 107.9(2) °, which mirrors the structural trends going from an imidazolium cation to an imidazol-2-ylidene. While the C2–N1 and C2–N3 bonds in imidazol-2-ylidenes are usually identical in length, a meaningful comparison cannot be made for **93**, which has two different heteroatoms attached to the carbene.

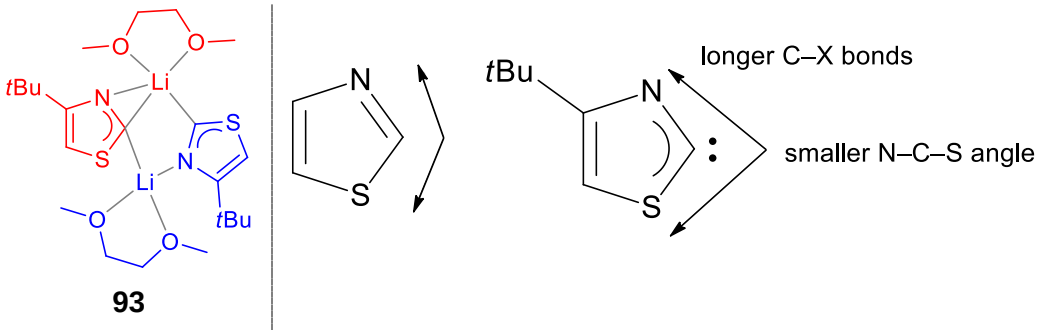

Figure 1.10 *Lithiation of 4-tert-butylthiazole results in pronounced structural differences compared to the parent thiazole that would be consistent with a carbene-like product.*

Hahn and co-workers were perhaps the first to introduce the term “anionic NHC” when they presented **96**, one of the products isolated from the oxidative addition of zero-valent Group 10 metals to 2-chloro-*N*-methylbenzimidazole (Scheme 1.47).[209] They had previously alluded to the intermediacy of an anionic benzimidazole in the synthesis of protic NHC complexes via this oxidative addition route.[171,210] In the absence of a proton source such as NH_4BF_4, oxidative addition does not lead to the protic NHC complexes **94** or **95**. Instead, the N,NR NHC complex **96** and its dimer **97** were obtained in a 4:1 ratio. The reaction of $[Pt(PPh_3)_4]$ and 2-chloro-*N*-picolylbenzimidazole also afforded a similar dimeric

product, implying that the formation of N(M),NR complexes under aprotic conditions may be generalised to other 2-halobenzimidazoles.[210]

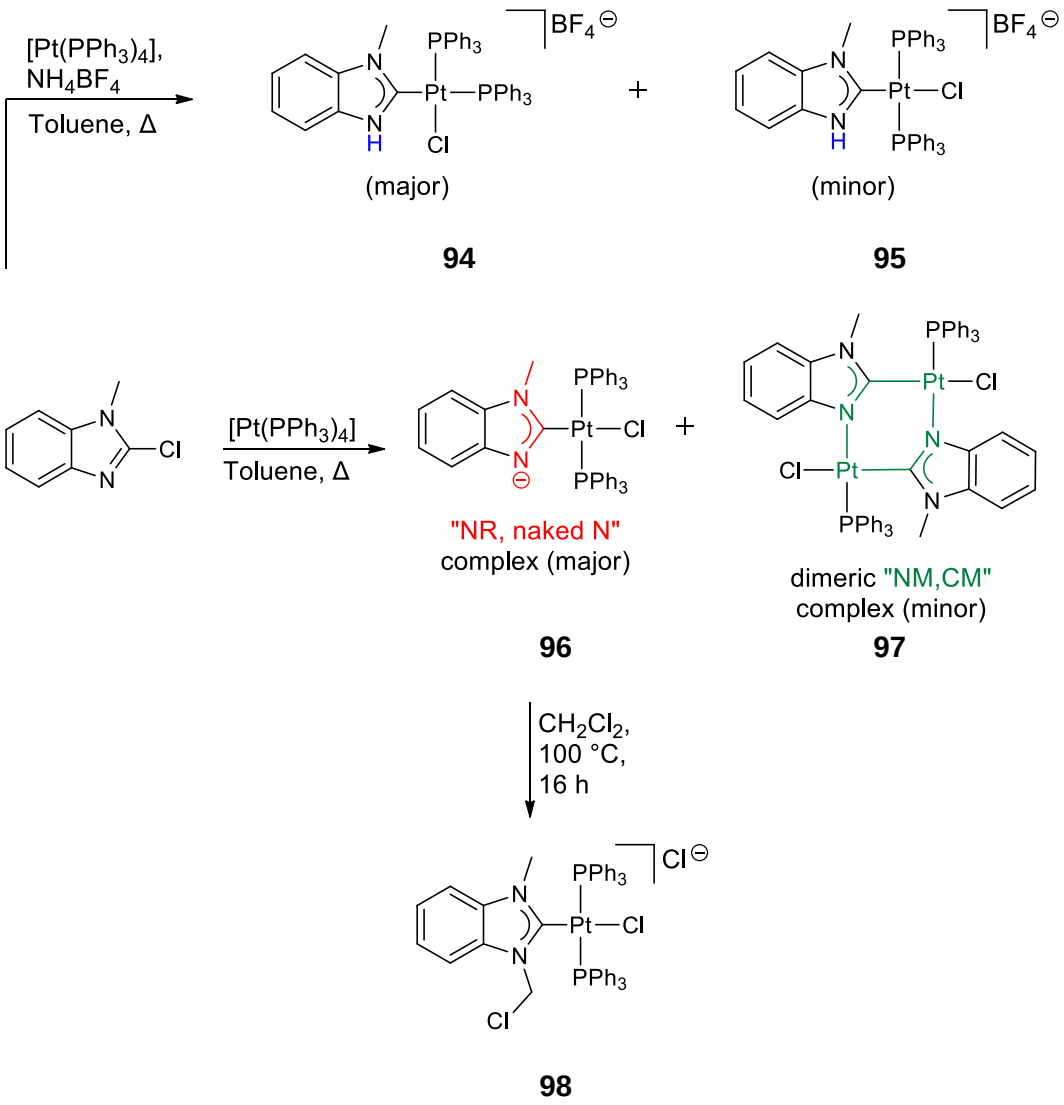

Scheme 1.47 *Reaction products of the oxidative addition of platinum(0) to 2-chloro-N-methylbenzimidazole with and without a proton source.*

This is a timely juncture to revisit a question posed when imidazol-2-ylidenes were first discovered: Does deprotonation give rise to a carbene or a carbanion? The Arduengo group endeavoured to answer this question using a combination of theoretical and experimental approaches. If the deprotonated azol-2-yl under study is indeed a carbanion, one would surely observe regions of high electron density or localised negative charge on a carbon that also participates in π-bonding interactions. However, Mulliken charge calculations for imidazol-2-ylidene estimate that most of the negative charge is borne by the nitrogen

atoms, and only a small amount is found on the carbene atom.[211] Electron density maps derived from neutron diffraction data of IMe **12a** showed that most of the electron density within the ring was localised on the nitrogen atoms, a predictable result in view of nitrogen's higher electronegativity relative to carbon.[212] The π-electron densities surrounding the C2–N and exocyclic C–N bonds are similarly low, indicating that bonds connected to C2 have minimal double bond character. A minima for π-electron density was found on C2. In addition, deformation density maps reveal a concentrated region of electron density at C2 in the plane of the molecule which evolves into a pronounced deficit above the plane. This is consistent with C2 having an in-plane lone pair and a vacant π-orbital. In contrast, other endocyclic atoms exhibit little distortion in their nuclear positions. The electron density maps generated by DFT were in excellent agreement with the empirically derived maps, suggesting that accurate models of electron distribution in NHCs can be made this way. All the evidence favours the interpretation of IMe as a carbene rather than a carbanion.

It seems fair to draw on the same structural and electronic reasoning used by Boche and Arduengo to establish whether or not the N,NR NHC complex **96** is a carbene. From a structural point of view, **96** is perhaps best described as having partial azole and partial NHC character. *N*-Methyladamantylbenzimidazole and benzimidazole will be used as references for the parent azole, as structural data for 2-chloro-*N*-methylbenzimidazole is not available. The key bond lengths and angles are summarised in Table 1.1.

Table 1.1 *Key structural and spectroscopic comparisons for NH,NR; N,NR and NR,NR NHC complexes against reference benzimidazoles.*

Parameter	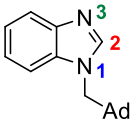	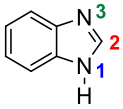	**95**, N3 = protonated[171]	**96**, N3 = naked	**98** N3 = alkylated
N1–C2–N3 (°)	114.83(11)[213]	114.41(17)	107.1(4)	111.37(17)	106.7(2)
C2–N1, $\mathbf{b_1}$ (Å)	1.3629(14)[213]	1.345(2)	1.350(6)	1.389(2)	1.351(3)
C2–N3, $\mathbf{b_2}$ (Å)	1.3096(14)[213]	1.312(2)	1.349(6)	1.319(3)	1.364(3)
$\mathbf{b_1} - \mathbf{b_2}$ (Å)	0.053	0.033	0.001	0.070	0.013
C2–Pt (Å)	-	-	1.972(4)	1.987(2)	1.973(2)
^{13}C NMR δ_{C2} (ppm)	144.3 ($CDCl_3$)[214]	141.9 (d_6-DMSO)	157.8 (CD_2Cl_2)	149.4 (CD_2Cl_2)	163.3 (CD_2Cl_2)

Compared to the neutral azoles, the N1–C2–N3 angles in **95** and **98** are smaller, a feature that is associated with NHC formation. The same decrease in the N1–C2–N3 angle is observed for **96**, albeit to a lesser extent. The C2–Pt bond lengths in **96**, its protonated form **95** and the chloromethylated form **98** are within very close range of each other, signifying that all three heterocycles possess similar donor/acceptor properties. This could mean that like the other two, **96** is also a carbene.

As mentioned previously, another telling sign of NHC formation is C2–N1 and C2–N3 bonds that are of roughly equal lengths, but longer than the corresponding bonds in neutral azoles. This change is evident for the NHC complexes **95** and **98**, with a marked lengthening of the C2–N3 bond that ultimately results in a negligible difference between the C2–N1 and C2–N3 bond lengths. In **96** however, the C2–N3 bond becomes significantly longer than that in the neutral azoles and the NHC complexes, while its C2–N1 bond length is typical of neutral azoles. The disparity in C2–N1 and C2–N3 bond lengths for **96** exceeds the values observed for neutral azoles. C2–N1 and C2–N3 bond length asymmetry appears to be characteristic of anionic azol-2-yl ligands in general.[164,186]

Based solely on the stark difference in the C2–N1 and C2–N3 bond lengths, Hahn and colleagues initially assigned the structure in Figure 1.11 b to **96**, where the C2 atom and short C2–N1 bond are represented as an acyl-like anion and a double bond respectively. However, this interpretation was contradicted by their natural bonding orbital (NBO) charge calculations for the N,NR NHC ligand in **96**. The calculated NBO charges suggest that the region of highest electron density is found on N3 followed by N1, whereas C2 appears to be electron deficient. DFT calculations support this, with the results indicating that the maximum negative electrostatic potential (of comparable value to Cl^-) is located close to N2. Overall, the NBO and DFT models of **96** are more consistent with a carbene flanked by an anionic nitrogen, as depicted in Figure 1.11 a.

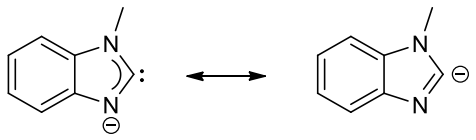

(a) (b)

Figure 1.11 *Possible* ***(a)*** *carbenic and* ***(b)*** *carbanionic resonance contributors for the N,NR ligand moiety in* ***96.***

It is clear that the C2 resonance appears further upfield in the ^{13}C NMR spectrum of **96** than for **95** and **98**. Although an extreme downfield shift is usually expected for a carbenic resonance, this may not necessarily suggest that the C2 in **96** is not a carbene. Rather, the upfield position of the resonance may be viewed be a consequence of greater shielding experienced by C2, due to the higher electron density surrounding the adjacent anionic nitrogen. The upfield shift in the C2 resonance going from an NH(R),NR NHC complex to an N(M),NR NHC species has also been observed for other metals.[170]

Finally, the reactivity of **96** further supports the assignment of the negative charge on N3 instead of C2. The dinuclear species **97** results from adduct formation between the Lewis basic unsubstituted nitrogen and the Lewis acidic metal centre in a second molecule of **96**. The anionic nitrogen in **96** is strongly nucleophilic, and will attack electrophiles such as dichloromethane to produce the classical NHC complex **98**. On the whole, the structural, electronic and reactivity data provide sufficient justification that **96** can be considered an anionic NHC. However, the term has not been widely adopted, possibly due to the challenges involved in making the subtle distinction between a carbanion and an anionic carbene. Most N(M),NR NHC compounds in the literature are still named azol-2-yls.

1.7 The preparation and utility of NM,NR NHC complexes

N,NR NHC complexes are probably most easily prepared by deprotonation of an NH,NR NHC complex with a suitable base.[164,165,170] Recall an earlier example from Scheme 1.42, where treatment of the protic NHC complex **83** with NaOMe and NaH gives the N,NR NHC complex **84**.[166] As discussed, **84** can activate acetylene and H_2. Similar to protic NHCs, **84** can undergo *N*-methylation with methyl triflate to give a classical NR,NR NHC complex. The Ir–C2 bond length in **84** measures 2.059(3) Å, around 0.033 Å longer than the corresponding bond in **83**. This perhaps suggests that in this case, the anionic NHC is a slightly weaker donor than its protic NHC congener. The iridium(III) centre in the related hydride

99 could be reduced to iridium(I) by hydride abstraction using *n*BuLi (Scheme 1.48). The resulting lithium adduct **100** is an NM,NR NHC complex with its carbene resonance appearing at 150 ppm, almost 20 ppm downfield to that of **99**. Interestingly, the reaction of **100** with methyl triflate or 1-iodobutane leads to alkylation at the metal instead of the nitrogen, simultaneously oxidising the metal centre to iridium(III).

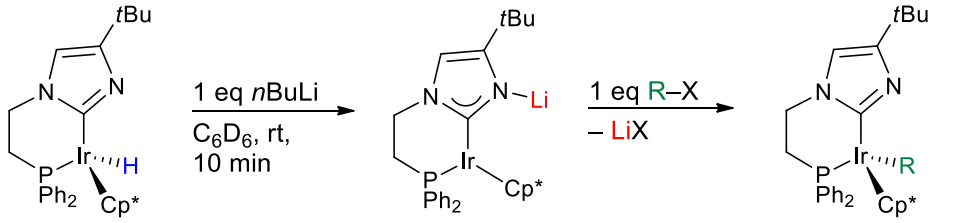

Scheme 1.48 *Reduction at the iridium centre of an N,NR NHC complex to give a NM,NR complex, which can undergo alkylation on the metal.*

The utility of such heterobimetallic NM,NR NHC complexes comes partly from their susceptibility to ligand exchange on the NHC-bound metal centre, particularly when the exchange is driven by the precipitation of an insoluble lithium salt. The conversion of **100** into **101a**,**b** is rapid and high yielding, even at temperatures well below 0 °C. The *N*-lithiated ruthenium complex **103** reacts with ethylene in a similar manner, affording the ethylene complex **104** (Scheme 1.49).[165] On the other hand, adding H_2 to **103** gives the protic NHC/hydride complex **102**.

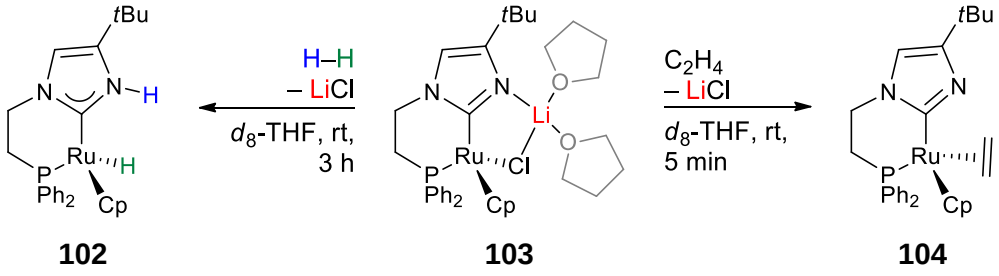

Scheme 1.49 *Elimination of the N-coordinated metal in a heterobimetallic NM,NR NHC complex facilitates ligand exchange at the metal centre.*

In some cases however, metathesis occurs exclusively on N3, and the NHC-bound metal centre is left unchanged when inorganic metal salts are used. Therefore, NM,NR NHC complexes may allow access to a variety of

heterobimetallic complexes with bridging NHC ligands. Cossairt and Flowers highlighted the potential of NM,NR NHC complexes as ligand transfer agents, beginning with the *N*-lithiation of the tridentate bis(carbene) complex **105** (Scheme 1.50).[168] Transmetallation of the lithiated product **106** with cobalt or iron gives rise to new NM,NR NHC complexes such as **107**.

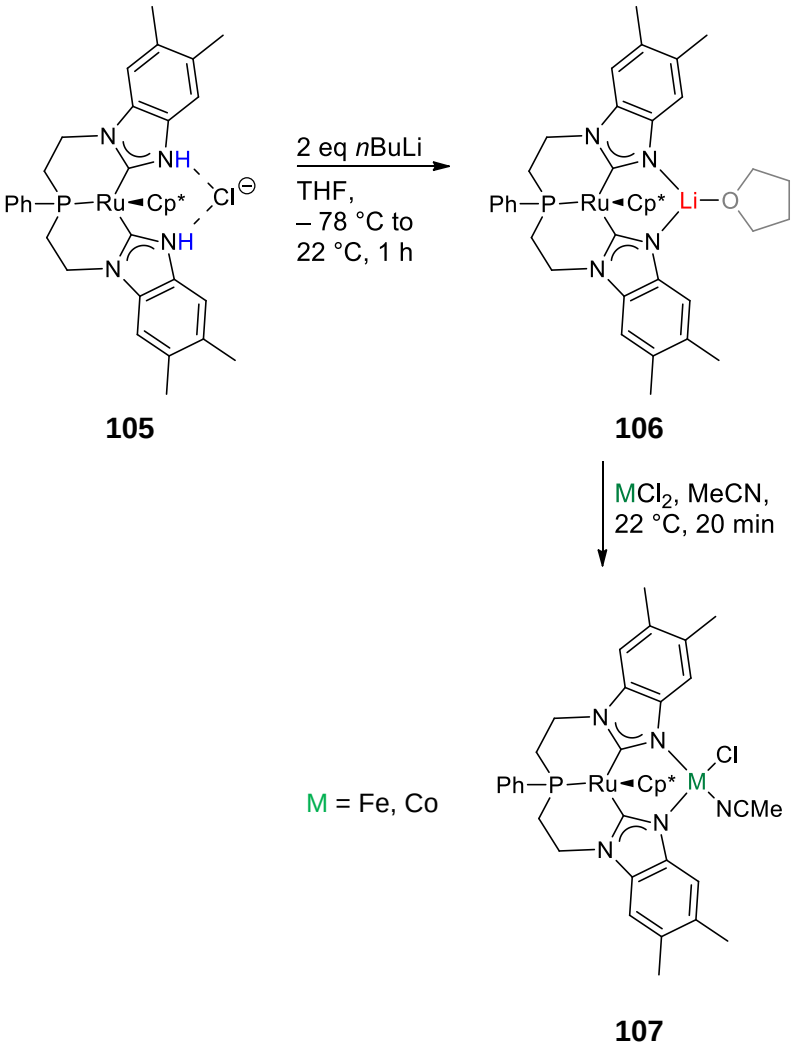

Scheme 1.50 *Transmetallation at the anionic nitrogen site in NM,NR NHC complexes.*

The anionic NHC complex **109** can be made from the ruthenium nitrosyl complex **110** using the aforementioned base-assisted deprotonation method. However, the Brønsted acidity of the NH unit on a protic NHC complex can also be exploited under base-free conditions to give an N,NR NHC complex. The addition of a stoichiometric equivalent of $AgNO_2$ to the protic NHC complex **108** results in chloride abstraction by silver(I). This is followed by intramolecular proton migration, generating a nitrosyl ligand from the nitrite ion in a dehydrative

process that culminates in the formation of **109** after anion exchange with excess KOTf (Scheme 1.51).[164]

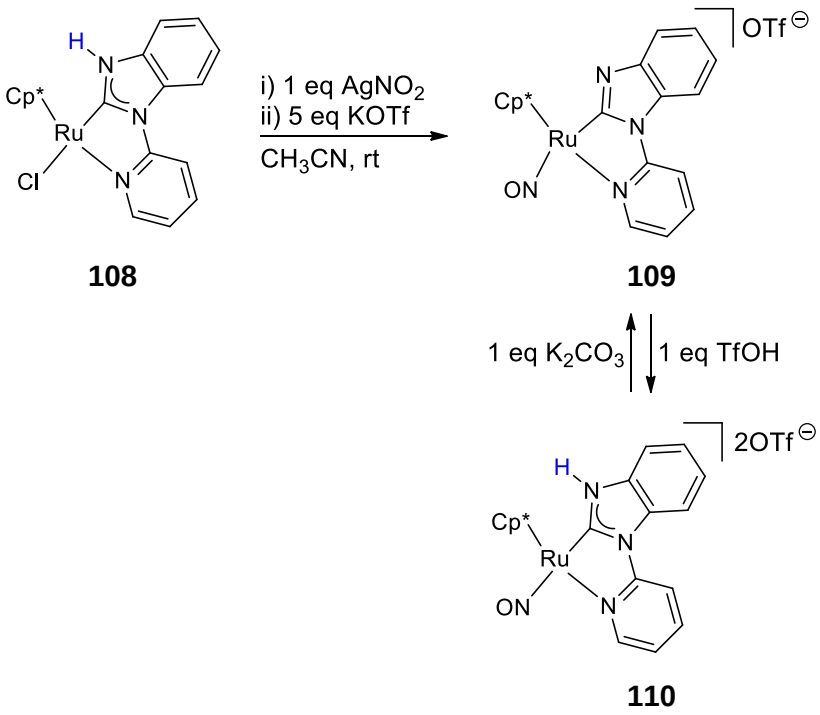

108 **109** **110**

Scheme 1.51 *Formation of N,NR NHC complex **109** from protic NHC complexes **108** and **110** via dehydrative conversion of a nitrite ion into a nitrosyl ligand under neutral conditions, or base-assisted deprotonation.*

Another method that has been used to access N,NR NHC complexes is the deprotonation and tautomerisation of an imidazole that is coordinated to a metal centre. The tris(*N*-methylimidazolyl)rhenium(I) complex **111a** can be deprotonated with KHMDS to give the N,NR NHC complex **112**, whose structure was verified by NMR spectroscopy and single crystal X-ray diffraction (Scheme 1.52).[160] A resonance at 182.4 ppm in the ^{13}C NMR spectrum was assigned to C2 in **112**, the furthest downfield of all the N,NR NHC complexes discussed so far. Protonation with strong acids such as triflic or trifluoroacetic acid yielded the NH,NR NHC species **113**, confirming the presence of the naked nitrogen in **112**.

A topological analysis of the Laplacian of the electron density was performed for **112** and **113** using X-ray diffraction data. **112** and **113** both exhibited large non-bonded charge concentrations perpendicular to the plane at N3. **112** also displayed an in-plane non-bonded charge concentration of similar magnitude at N3. However, the same was not true of **113**, which showed a smaller bonded

charge concentration instead. These observations corroborate the presence of an in-plane lone pair on N3 for **112**, which is replaced by an N–H covalent interaction in **113**.

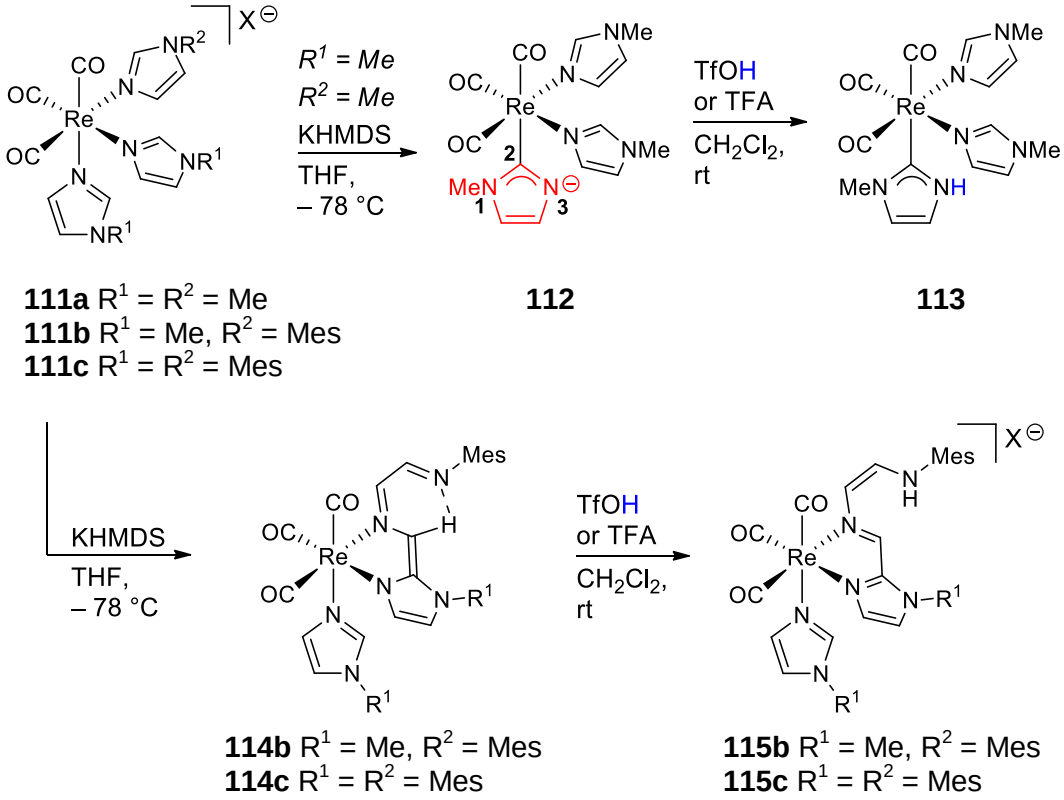

Scheme 1.52 *Substituent-dependent formation of an N(H),NR NHC complex or ring-opening at an N-alkylimidazole rhenium(I) complex.*

Curiously, the *N*-substituents on the imidazole ligands have considerable bearing on the deprotonation outcome. When one or all of the methyl groups in **111a** are replaced with a mesityl group, treatment with KHMDS results in ring opening of an *N*-mesitylimidazole unit. It is believed that deprotonation took place at the C2 position of one of the *N*-mesitylimidazole ligands, swiftly followed by intramolecular attack of the NCHN on an adjacent imidazole ligand by this C2 site. C–C coupling between the C2 atoms of two imidazole ligands and ensuing ring-opening furnished **114b** and **114c** as the products. The amido-like nitrogen in **114b**-**c** can then be converted into the amine with the addition of acid to obtain **115b** and **115c** in good yields.

Mechanistic probes using DFT suggest that the *N*-mesityl group enhances electron delocalisation in, and thus stabilises, the transition state for the ring-opening step.[215] The identity of the metal centre also influences the

outcome: while ring-opening/C–C coupling is shown to be favourable for rhenium, imidazolyl formation is the preferred pathway for molybdenum and manganese systems.[207]

The N,NR NHC complex **112** can undergo a second metallation with $[AuCl(PPh_3)_2]$ to give the NM,NR NHC complex **116** (Scheme 1.53).[215] Notably, the imidazolyl fragment tautomerises into the Re–*N*-bound form to accommodate the *C*-binding preference of Au(I), a result that is paralleled in the molybdenum system.[207]

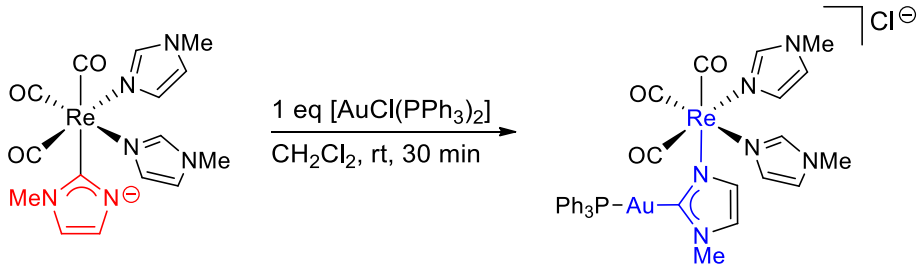

112 **116**

Scheme 1.53 *Auration of an N,NR rhenium(I) complex involving tautomerisation of the imidazolyl ligand.*

A similar phenomenon has been observed in a manganese/gold system by Ruiz and coworkers (Scheme 1.54).[206] The manganese(I) imidazole complex **117** can be transformed into the protic NHC complex **119**. It was proposed that the deprotonation of **117**$[ClO_4]$ gives an *N*-bound NHC **I**, which isomerises into the *C*-bound form **II**. Neither of these intermediates could be isolated, although the transition was marked by a shift of the CO bands to lower frequencies in the infrared spectrum. **I** is calculated to be 13.55 kcal mol^{-1} less stable than **II**, which may account for the fact that type **II** imidazolyl complexes have been isolated elsewhere, but type **I** complexes have not.[216]

Metallation of the NHC complex **119** is accomplished under basic conditions. Presumably, the soft gold(I) centre initially coordinates to the hard anionic nitrogen on the NHC ligand, but undergoes spontaneous 1,2-migration in order to bind with the softer carbene donor to afford the heterobimetallic product **118**. The Mn–N bond in **118** can be cleaved with perchloric acid to give the gold(I) protic NHC complex **120**. This demonstrates that NM,NR NHC complexes of manganese(I) may serve as NH,NR carbene transfer agents for gold(I), providing a complementary approach to the Ag_2O transfer method which is

limited to NR,NR NHCs. The strategy depicted in Scheme 1.54 for forming manganese(I) protic NHC complexes can be extended to benzannulated heterocycles such as benzimidazole and benzoxazole, although their use as carbene transfer agents is currently prevented by the instability of the corresponding manganese(I)/gold(I) heterobimetallic complexes.[217]

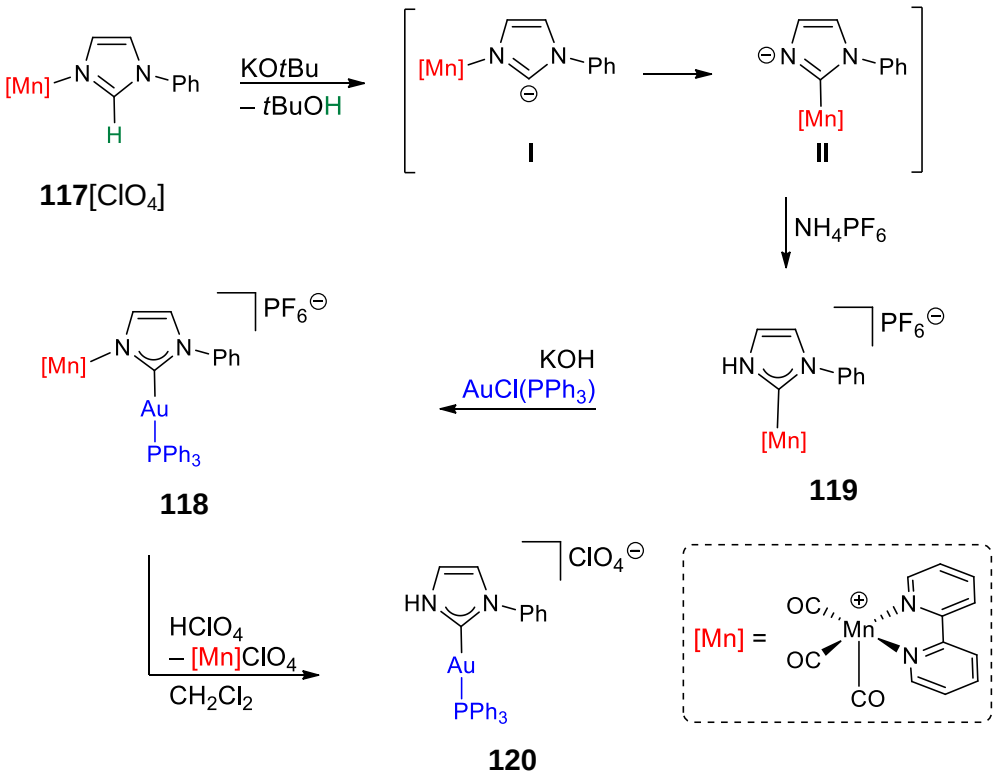

Scheme 1.54 *Carbene transfer from a manganese(I) complex onto a gold(I) centre via the heterobimetallic intermediate* ***118****.*

In a somewhat isolated example, Radius and Hering obtained the N,NR NHC platinum(II) complex **121** by degradation of an NHC (Scheme 1.55).[218] The reaction of [Pt(PPh_3)$_2$(η^2-C_2H_4)] with excess I(*i*Pr) in *n*-hexane precipitates **122** as the product, but in more polar solvents such as toluene or benzene, the homoleptic bis(NHC) platinum complex remains in solution and reacts with another molecule of I(*i*Pr) to give **121**. Radius and Hering did not consider the imidazolyl fragment in **121** a carbene, partly on account of the elongated Pt–$C_{imidazolyl}$ bond relative to the Pt–C_{NHC} bond. However, they acknowledged that the elongation may be due to the *trans* influence of the hydride ligand, and that a similar Pt–C_{NHC} bond length[219] had been reported for an abnormal NHC complex.

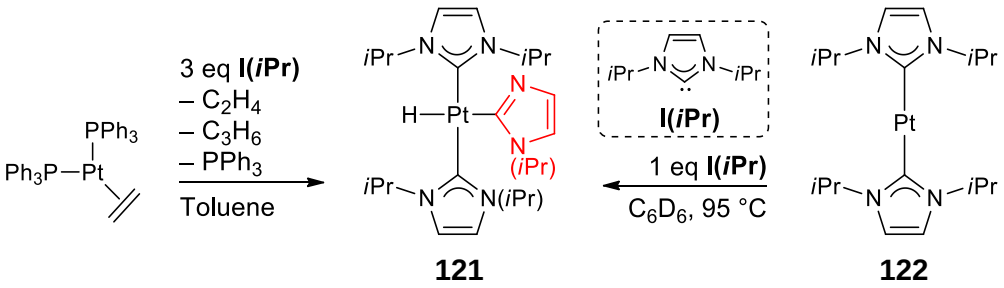

Scheme 1.55 *Platinum-mediated dealkylation of an NHC to afford N,NR complex* ***121****.*

Presently, some degree of uncertainty remains surrounding the exact nature of these azol-2-yl ligands. Cogent arguments have been presented for both sides of the carbene–carbanion debate. Since both are resonance forms of each other, it is possible that these assignments are strongly dependent on the identity of the coordinated metal and have to be made on a case-by-case basis. The uranyl complex **123** exhibits exceptionally short U–C bonds and an extreme downfield ^{13}C NMR peak that is most consistent with a carbanionic imidazolyl ligand (Scheme 1.56).[220] In contrast, the M–C bonds lengths in the isomerised iron(II) and cobalt(II) derivatives **124a**,**b** fall within the normal range for their respective NHC complexes. The new U–N bond is slightly shorter than those previously observed for U–$N_{imidazole}$ complexes, which may be ascribed to the presence of a negative charge on the nitrogen atom. This suggests that the imidazolyl ligand adopts the carbanionic resonance form when coordinated to the hard uranyl centre, but undergoes electronic reconfiguration to become the carbene when bound to softer transition metal ions.

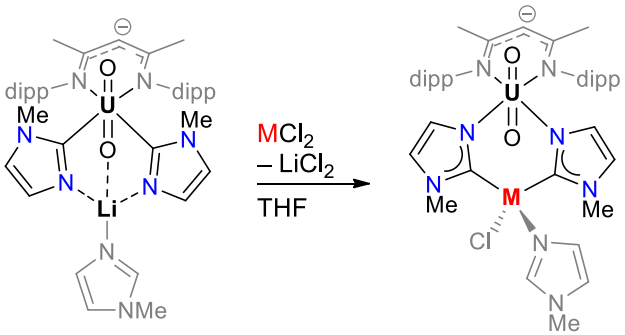

123

124a M = Fe
124b M = Co

Scheme 1.56 *Metallation and tautomerisation of a uranyl imidazolyl complex.*

The N,NR imidazolyl bridging ligand has been used as a supramolecular building block in the construction of Cu_2O nanoclusters and one-dimensional polymeric chains held together by Cu–Cu and Au–NHC contacts.[221]

1.8 The case for pursuing a free NM,NR NHC

Tantalising hints of the existence of free NM,NR NHCs are embedded throughout the literature. Ruiz and coworkers speculated that one such species (**I**, Scheme 1.54) may be an intermediate formed during the deprotonation of **117**, prior to N–C migration of the manganese(I) ion.[206] It is conceivable that deprotonation and rhenium(I) migration onto the C centre from **111a** proceeds via an NM,NR free NHC species (Scheme 1.52).

Our interest in isolating an NM,NR free NHC was first piqued by one particular theoretical study, which in turn was based on two independent reports of copper(I)-catalysed carboxylation from the Hou and Nolan groups respectively. Hou and coworkers performed the direct insertion of CO_2 into the C2–H bond of various *N*-heterocycles under fairly mild conditions (Scheme 1.57).[222]

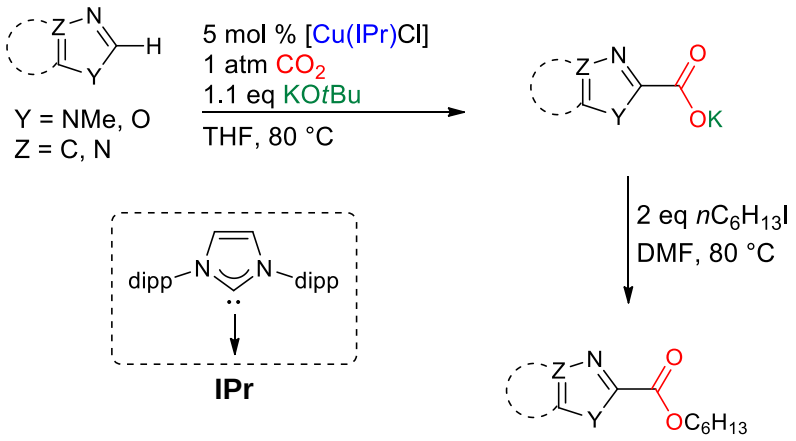

Scheme 1.57 *Direct copper(I)-catalysed carboxylation of aromatic C–H bonds.*

Likewise, Cazin and Nolan used the closely related [Cu(IPr)(OH)] catalyst to install ester functionalities onto heteroarenes and polyfluorinated benzenes. They were also able to apply the same chemistry to carboxylate N–H bonds of imidazoles, pyrazoles and even oxygen-containing heterocycles such as 2-oxazolidinone.[223]

Based on two copper(I) intermediates **125** and **126** isolated from the stoichiometric carboxylation of benzoxazole, Hou and coworkers proposed the catalytic cycle below. The proposed mechanism comprised three main steps:

First, the activation of the heterocyclic C–H bond by copper(I), followed by CO_2 insertion into the Cu–C bond, and finally salt metathesis with KO*t*Bu to regenerate the active catalyst [Cu(IPr)(O*t*Bu)] and produce a potassium carboxylate salt, which yields the ester product after alkylation.

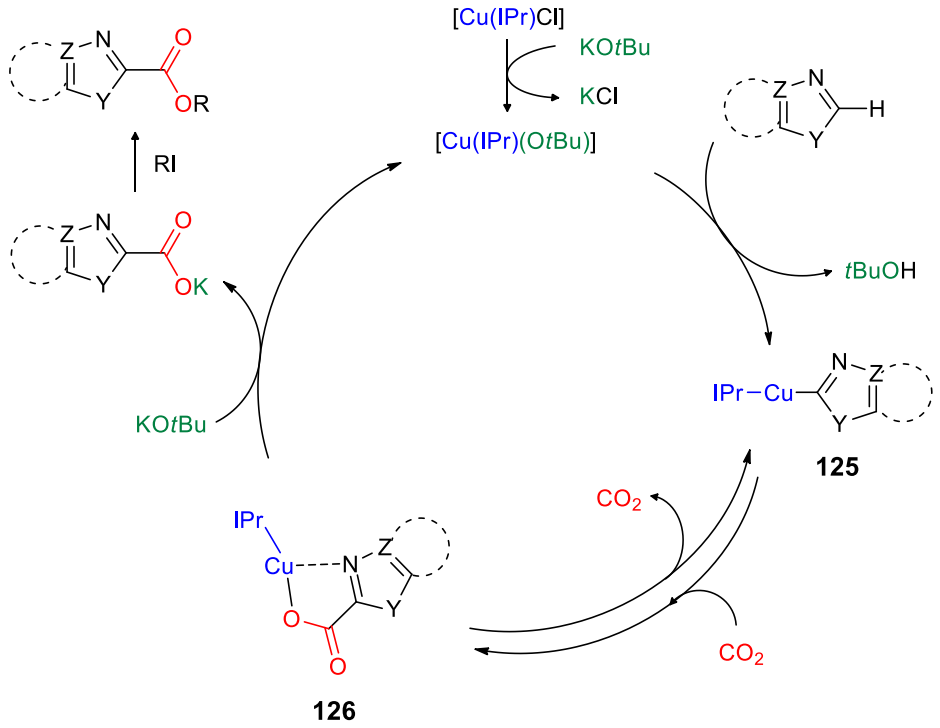

Scheme 1.58 *Proposed mechanism for the copper(I)-catalysed direct carboxylation of aromatic N-heterocycles.*

Although it is cheap, abundant and low in toxicity, CO_2 is a notoriously inert reagent due to its high thermodynamic stability. Hou and Nolan's works represent significant advances in the development of efficient and functional group tolerant methods to employ CO_2 in synthesis, and have positive implications for future technologies involving carbon capture, storage and reuse. Keenly aware of the incentives to better understand the carboxylation process, Ariafard and coworkers conducted a detailed DFT investigation of each step in Hou et al.'s proposed mechanism.[224] The following results are based on the carboxylation of benzoxazole by Nolan and colleagues' [Cu(IPr)(OH)] catalyst. Similar pathways were calculated for oxazole and thiazole substrates.

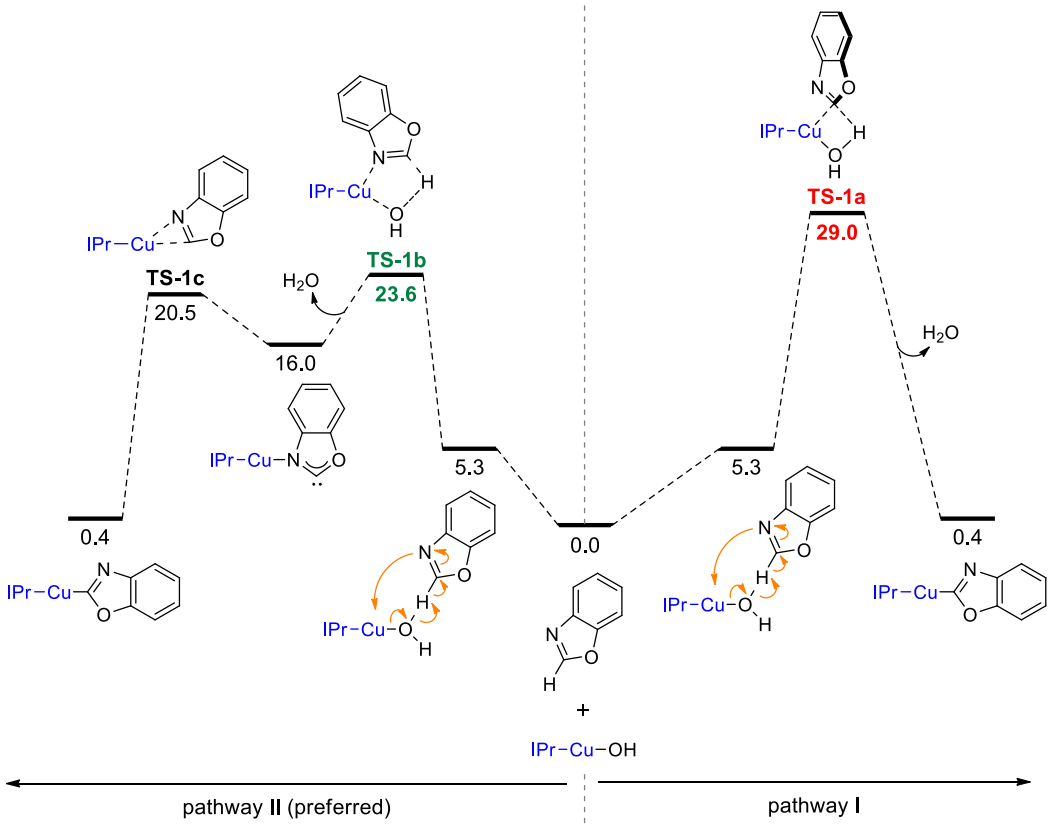

Figure 1.12 *Computed energy profiles for two possible pathways for the protonolysis of [Cu(IPr)(OH)] by benzoxazole. Relative free energies are given in kcal/mol.*

Two possible pathways were identified for the first step of the catalytic cycle, namely the protonolysis of [Cu(IPr)(OH)] by benzoxazole to form a copper(I) benzoxazole complex (Figure 1.12). Pathway I proceeds via a four-membered transition structure **TS-1a**, where proton transfer from benzoxazole to the OH ligand and benzoxazolyl migration to the copper atom occur simultaneously. Alternatively, the reaction may occur via pathway II, which contains transition structure **TS-1b** where the copper atom interacts with the nitrogen instead of the carbon atom of benzoxazole during proton transfer to OH. The loss of H_2O from **TS-1b** yields a free NM,NR NHC, which then isomerises into the *C*-metallated benzoxazolyl. Since **TS-1b** and **TS-1c** are lower in energy than **TS-1a**, it is expected that pathway II is more kinetically favourable than pathway I.

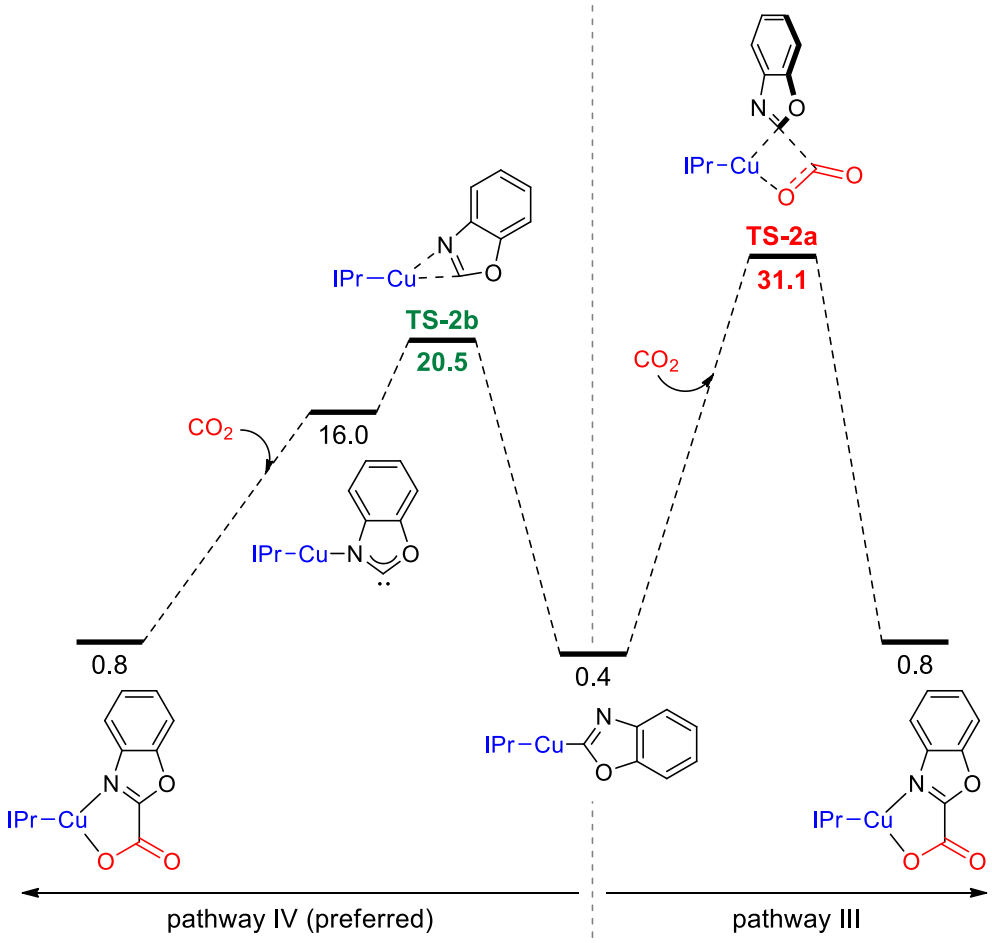

Figure 1.13 *Computed energy profiles for two possible CO_2 activation pathways from a copper(I) benzoxazolyl complex. Relative free energies are given in kcal/mol.*

The second step in the catalytic sequence concerns the insertion of CO_2 into the Cu–C bond of the copper(I) benzoxazolyl complex, resulting in a copper carboxylate complex (Figure 1.13). The more conventional pathway III involves the nucleophilic attack of the Cu–C σ bond on the electrophilic carbon atom in CO_2, which has the four-membered transition structure **TS-2a**. The calculated energy barrier for this process is fairly high. However, Ariafard and colleagues were able to identify a second pathway with a lower energy barrier. This new pathway IV begins with the isomerisation of the copper(I) benzoxazolyl complex into its *N*-metallated form. Remarkably, the resulting free NM,NR NHC is so much more nucleophilic than the Cu–C σ-bond that the nucleophilic attack on CO_2 is barrierless. The free NM,NR NHC route also appeared to be the most energetically favourable for the analogous CO_2 activation by gold(I).[225,226]

These findings highlight the dual functionality nature of free NM,NR NHCs, which contain a Lewis acidic metal centre and Lewis basic free carbene, and how they may be exploited in cooperative catalysis. There are other examples of transformations which are co-catalysed by an organometallic complex and a free NHC. Yu and Zhang claim that a polyNHC dendrimer can serve as both a ligand and a catalyst in the direct carboxylation into the C–H bond of terminal alkynes, enabling the synthesis of functionalised propiolic acids (Figure 1.14).[227] They observed that the carboxylation of their model substrate, 4-nitro-1-ethynylbenzene proceeded most efficiently when only half an equivalent (relative to the polyNHCs) was used. The yield of the propiolic acid product dropped sharply when a stoichiometric amount of CuCl was used, whereas no reaction occurred when the polyNHC was used without any CuCl. This led them to believe that both the copper–NHC complex and the free NHC were required for optimal catalytic performance. Presumably, the [Cu(NHC)Cl] and free NHC fragments activate the terminal alkyne and CO_2 respectively in the presence of base. The NHC carboxylate coordinates to a nearby copper atom, facilitating the nucleophilic attack of the acetylide carbanion on the carboxylate carbon. This links the alkyne and carboxyl segments of the propiolic acid, which can be exchanged for another alkyne unit at the copper centre.

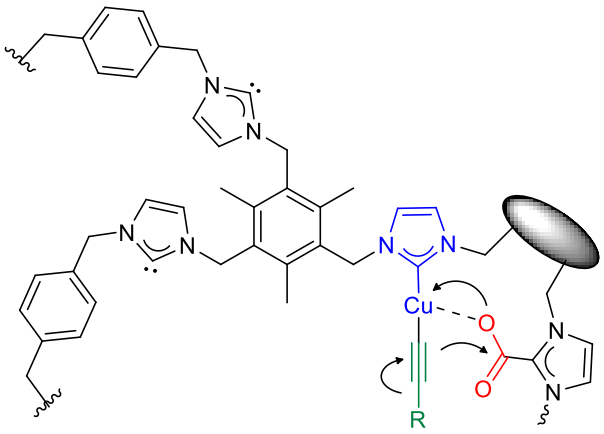

Figure 1.14 *Cooperative CO_2 insertion into the C–H bond of terminal alkynes by copper(I) and a free carbene on a polyNHC scaffold.*

In Yu and Zhang's dendrimer, the copper-NHC and free NHC are remote from each other. In Hou and Nolan's systems however, the two functional sites in the putative free NM,NR NHC intermediate are directly adjacent to each other. This is akin to the bifunctional ambident complexes pioneered by Grotjahn and coworkers (Scheme 1.42, Scheme 1.43). In fact, one might view free NM,NR

NHCs as the *N*-metallated tautomer of structures **80** and **81** (Scheme 1.41). It has already been shown that complexes bearing structural motifs like **81** can activate H_2 and acetylene, suggesting that there may be something to gain from positioning the two complementary functions close to each other. Given the general usefulness of the bifunctional ambident reactivity concept and encouraging evidence for the role of NM,NR free NHCs in powerful carboxylation chemistry, there is a strong case for the pursuit and study of these species. Their reactivity could potentially be harnessed in the activation of inert small molecules other than CO_2.

So far, free NM,NR NHCs have eluded isolation. The astute reader may have observed that in the examples shown, there is nothing preventing the metal ion from migrating to the carbene and forming the thermodynamically favoured complex. DFT calculations estimate the energy separation between the copper–benzoxazolyl free NM,NR NHC and its less energetic *C*-bound isomer at 15.4 kcal/mol (Figure 1.13, Figure 1.14). Perhaps with the appropriate structural modifications, this gap can be reduced to the point that the free NM,NR NHC is stable enough to be isolated. Ideally, the barrier to tautomerisation should be high, so that the free NM,NR NHC does not convert into the *C*-bound complex. Since similar issues are encountered in the synthesis of protic NHC complexes, it may be possible to borrow strategies from that, such as using chelating pendant donors to fix the metal centre onto a desired position. Chapter 2 details the full design rationale for a proof-of-concept free NM,NR NHC.

1.9 Aims

The aim of this project is to demonstrate proof of concept that a free NM,NR NHC can indeed be isolated, enabling the study of its structure and reactivity to inform the synthesis of more free NM,NR NHCs that are capable of catalysis. To achieve this, the following four-stage plan has been devised:

a) Design a proof-of-concept target ligand on which the free NM,NR NHC is to be generated;
b) Develop and optimise a scalable synthesis for this proof-of-concept ligand;
c) Perform screening of various transition metals to determine the most suitable complex of the proof-of-concept ligand for deprotonation trials;
d) Subject the proof-of-concept complex to deprotonation with base to isolate the free NM,NR NHC.

1.10 References

1 M. Hermann, *Ann. der Chemie und Pharm.*, 1855, **95**, 211–225.

2 A. Geuther, *Ann. der Chemie und Pharm.*, 1862, **123**, 121–122.

3 E. Buchner and T. Curtius, *Ber. Dtsch. Chem. Ges.*, 1885, **18**, 2377–2379.

4 H. Staudinger and O. Kupfer, *Ber. Dtsch. Chem. Ges.*, 1911, **44**, 2194–2197.

5 H. Staudinger and O. Kupfer, *Ber. Dtsch. Chem. Ges.*, 1912, **45**, 501–509.

6 W. von E. Doering and A. K. Hoffmann, *J. Am. Chem. Soc.*, 1954, **76**, 6162–6165.

7 D. Bourissou, O. Guerret, F. P. Gabbaï and G. Bertrand, *Chem. Rev.*, 2000, **100**, 39–92.

8 M. Melaimi, M. Soleilhavoup and G. Bertrand, *Angew. Chem. Int. Ed.*, 2010, **49**, 8810–8849.

9 Y. Canac, M. Soleilhavoup, S. Conejero and G. Bertrand, *J. Organomet. Chem.*, 2004, **689**, 3857–3865.

10 W. Kirmse, *Angew. Chem. Int. Ed.*, 2004, **43**, 1767–1769.

11 J. W. Herndon, *Coord. Chem. Rev.*, 2000, **206**–**207**, 237–262.

12 M. N. Hopkinson, C. Richter, M. Schedler and F. Glorius, *Nature*, 2014, **510**, 485–496.

13 S. Díez-González, N. Marion and S. P. Nolan, *Chem. Rev.*, 2009, **109**, 3612–3676.

14 D. Enders, O. Niemeier and A. Henseler, *Chem. Rev.*, 2007, **107**, 5606–5655.

15 S. P. Nolan, Ed., *N-Heterocyclic Carbenes*, Wiley-VCH Verlag GmbH & Co. KGaA, Weinheim, Germany, 2014.

16 K. M. Hindi, M. J. Panzner, C. a Tessier, C. L. Cannon and W. J. Youngs,

Chem. Rev., 2009, **109**, 3859–3884.

17 L. Oehninger, R. Rubbiani and I. Ott, *Dalton Trans.*, 2013, **42**, 3269–3284.

18 N. E. Kamber, W. Jeong, R. M. Waymouth, R. C. Pratt, B. G. G. Lohmeijer and J. L. Hedrick, *Chem. Rev.*, 2007, **107**, 5813–5840.

19 L. Mercs and M. Albrecht, *Chem. Soc. Rev.*, 2010, **39**, 1903.

20 C. M. Crudden, J. H. Horton, I. I. Ebralidze, O. V. Zenkina, A. B. McLean, B. Drevniok, Z. She, H.-B. Kraatz, N. J. Mosey, T. Seki, E. C. Keske, J. D. Leake, A. Rousina-Webb and G. Wu, *Nat. Chem.*, 2014, **6**, 409–414.

21 H. Ismaili and M. S. Workentin, *Chem. Commun.*, 2011, **47**, 7788.

22 O. Schuster, L. Mercs and M. Albrecht, *CHIMIA Int. J. Chem.*, 2010, **64**, 184–187.

23 K. A. Williams, A. J. Boydston and C. W. Bielawski, *J. Royal Soc. Interface*, 2007, **4**, 359–362.

24 E. F. Connor, G. W. Nyce, M. Myers, A. Möck and J. L. Hedrick, *J. Am. Chem. Soc.*, 2002, **124**, 914–915.

25 G. Bertrand, Ed., *Carbene Chemistry: From Fleeting Intermediates to Powerful Reagents*, Marcel Dekker, New York, 2002.

26 R. Hoffmann, *J. Am. Chem. Soc.*, 1968, **90**, 1475–1485.

27 B. C. Gilbert, D. Griller and A. S. Nazran, *J. Org. Chem.*, 1985, **50**, 4738–4742.

28 R. A. Moss, M. Włostowski, S. Shen, K. Krogh-Jespersen and A. Matro, *J. Am. Chem. Soc.*, 1988, **110**, 4443–4444.

29 X. M. Du, H. Fan, K. Krogh-Jespersen, R. A. Moss, S. Shen, J. L. Goodman, J. A. Lavilla, M. A. Kesselmayer and R. S. Sheridan, *J. Am. Chem. Soc.*, 1990, **112**, 1920–1926.

30 R. A. Mitsch, *J. Am. Chem. Soc.*, 1965, **87**, 758–761.

31 R. A. Moss and C. B. Mallon, *J. Am. Chem. Soc.*, 1975, **97**, 344–347.

32 S. Koda, *Chem. Phys. Lett.*, 1978, **55**, 353–357.

33 W. W. Schoeller, *J. Chem. Soc. Chem. Commun.*, 1980, 124–125.

34 L. Pauling, *J. Chem. Soc. Chem. Commun.*, 1980, 688–689.

35 C. Buron, H. Cornitzka, V. Romanenko and G. Bertrand, *Science*, 2000, **288**, 834–836.

36 Y. Canac, S. Conejero, B. Donnadieu, W. W. Schoeller and G. Bertrand, *J. Am. Chem. Soc.*, 2005, **127**, 7312–7313.

37 A. J. Arduengo, R. L. Harlow and M. Kline, *J. Am. Chem. Soc.*, 1991, **113**, 361–363.

38 H.-W. Wanzlick and E. Schikora, *Angew. Chem.*, 1960, **72**, 494–494.

39 D. M. Lemal, R. A. Lovald and K. I. Kawano, *J. Am. Chem. Soc.*, 1964, **86**, 2518–2519.

40 H. W. Wanzlick and H. J. Schönherr, *Angew. Chem. Int. Ed. Engl.*, 1968, **7**, 141–142.

41 K. Öfele, *J. Organomet. Chem.*, 1968, **12**, P42–P43.

42 D. J. Cardin, B. Cetinkaya, M. F. Lappert, L. Manojlović-Muir and K. W. Muir, *J. Chem. Soc. D*, 1971, **0**, 400–401.

43 H. J. Schönherr and H. W. Wanzlick, *Justus Liebigs Ann. Chem.*, 1970, **731**, 176–179.

44 A. J. Arduengo, H. V. R. Dias, R. L. Harlow and M. Kline, *J. Am. Chem. Soc.*, 1992, **114**, 5530–5534.

45 T. A. Taton and P. Chen, *Angew. Chem. Int. Ed. Engl.*, 1996, **35**, 1011–1013.

46 A. J. Arduengo III, J. R. Goerlich, R. Krafczyk and W. J. Marshall, *Angew. Chem. Int. Ed.*, 1998, **37**, 1963–1965.

47 A. J. Arduengo, F. Davidson, H. V. R. Dias, J. R. Goerlich, D. Khasnis, W. J. Marshall and T. K. Prakasha, *J. Am. Chem. Soc.*, 1997, **119**, 12742–12749.

48 D. Enders, K. Breuer, G. Raabe, J. Runsink, J. H. Teles, J. P. Melder, K. Ebel and S. Brode, *Angew. Chem. Int. Ed. Engl.*, 1995, **34**, 1021–1023.

49 A. J. Arduengo, J. R. Goerlich and W. J. Marshall, *J. Am. Chem. Soc.*, 1995, **117**, 11027–11028.

50 A. J. Arduengo, J. R. Goerlich and W. J. Marshall, *Liebigs Ann.*, 1997, **1997**, 365–374.

51 J. C. Cintrat, V. Léat-Crest, J. L. Parrain, E. Le Grognec, I. Beaudet, L. Toupet and J. P. Quintard, *Eur. J. Org. Chem.*, 2004, 4268–4279.

52 J. Ruiz, G. García, M. E. G. Mosquera, B. F. Perandones, M. P. Gonzalo and M. Vivanco, *J. Am. Chem. Soc.*, 2005, **127**, 8584–8585.

53 J. Zhang, J. Fu, X. Su, X. Wang, S. Song and M. Shi, *Chem. Asian J.*, 2013, **8**, 552–555.

54 J. A. Cabeza, I. Del Río, D. Miguel, E. Pérez-Carreño and M. G. Sánchez-Vega, *Organometallics*, 2008, **27**, 211–217.

55 T. J. Schmeier, A. Nova, N. Hazari and F. Maseras, *Chem. Eur. J.*, 2012, **18**, 6915–6927.

56 F. E. Hahn and M. Tamm, *Organometallics*, 1995, **14**, 2597–2600.

57 F. E. Hahn, D. Klusmann and T. Pape, *Eur. J. Inorg. Chem.*, 2008, 4420–4424.

58 C. C. Ko, C. O. Ng and S. M. Yiu, *Organometallics*, 2012, **31**, 7074–7084.

59 J. Barluenga, F. Aznar, B. Weyershausen, S. Garcí-Granda and E. Martín, *Chem. Commun.*, 1996, **222**, 2455–2456.

60 G. Boche, F. Bosold, H. Hermann, M. Marsch, K. Harms and J. C. W. Lohrenz, *Chem. Eur. J.*, 1998, **4**, 814–817.

61 F. E. Hahn and M. Tamm, *J. Chem. Soc. Chem. Commun.*, 1993, 842–844.

62 M. Schmidtendorf, T. Pape and F. E. Hahn, *Angew. Chem. Int. Ed.*, 2012, **51**, 2195–2198.

63 R. W. Alder, C. P. Butts and A. G. Orpen, *J. Am. Chem. Soc.*, 1998, 11526–11527.

64 N. Merceron, K. Miqueu, A. Baceiredo and G, *J. Am. Chem. Soc*, 2002,

124, 6806–6807.

65 G. D. Frey, M. Song, J.-B. Bourg, B. Donnadieu, M. Soleilhavoup and G. Bertrand, *Chem. Commun.*, 2008, 4711.

66 S. Solé, H. Gornitzka, W. W. Schoeller, D. Bourissou and G. Bertrand, *Science*, 2001, **292**, 1901–1903.

67 V. Lavallo, J. Mafhouz, Y. Canac, B. Donnadieu, W. W. Schoeller and G. Bertrand, *J. Am. Chem. Soc.*, 2004, **126**, 8670–8671.

68 V. Lavallo, Y. Canac, C. Präsang, B. Donnadieu and G. Bertrand, *Angew. Chem. Int. Ed.*, 2005, **44**, 5705–5709.

69 G. D. Frey, V. Lavallo, B. Donnadieu, W. W. Schoeller and G. Bertrand, *Science*, 2007, **316**, 439–441.

70 M. K. Denk, J. M. Rodezno, S. Gupta and A. J. Lough, *J. Organomet. Chem.*, 2001, **617**, 242–253.

71 W. A. Herrmann, M. Elison, J. Fischer, C. Köcher and G. R. J. Artus, *Chem. Eur. J.*, 1996, **2**, 772–780.

72 R. Nakano, R. Jazzar and G. Bertrand, *Nat. Chem.*, 2018, **10**, 1196–1200.

73 Z. Shi and R. P. Thummel, *J. Org. Chem.*, 1995, **60**, 5935–5945.

74 E. Çetinkaya, P. B. Hitchcock, H. Küçükbay, M. F. Lappert and S. Al-Juaid, *J. Organomet. Chem.*, 1994, **481**, 89–95.

75 F. E. Hahn, L. Wittenbecher, R. Boese and D. Bläser, *Chem. Eur. J.*, 1999, **5**, 1931–1935.

76 M. K. Denk, K. Hatano and M. Ma, *Tetrahedron Lett.*, 1999, **40**, 2057–2060.

77 F. E. Hahn, L. Wittenbecher, D. Le Van and R. Fröhlich, *Angew. Chem. Int. Ed.*, 2000, **39**, 541–544.

78 Y. Liu, P. E. Lindner and D. M. Lemal, *J. Am. Chem. Soc.*, 1999, **121**, 10626–10627.

79 R. H. Crabtree, *J. Organomet. Chem.*, 2005, **690**, 5451–5457.

80 R. Dorta, E. D. Stevens, N. M. Scott, C. Costabile, L. Cavallo, C. D. Hoff and S. P. Nolan, *J. Am. Chem. Soc.*, 2005, **127**, 2485–2495.

81 R. Dorta, E. D. Stevens, C. D. Hoff and S. P. Nolan, *J. Am. Chem. Soc.*, 2003, **125**, 10490–10491.

82 A. C. Hillier, W. J. Sommer, B. S. Yong, J. L. Petersen, L. Cavallo and S. P. Nolan, *Organometallics*, 2003, **22**, 4322–4326.

83 L. Cavallo, A. Correa, C. Costabile and H. Jacobsen, *J. Organomet. Chem.*, 2005, **690**, 5407–5413.

84 L. Benhamou, E. Chardon, G. Lavigne, S. Bellemin-Laponnaz and V. César, *Chem. Rev.*, 2011, **111**, 2705–2733.

85 N. Kuhn and T. Kratz, *Synthesis*, 1993, **1993**, 561–562.

86 G. W. Nyce, S. Csihony, R. M. Waymouth and J. L. Hedrick, *Chem. Eur. J.*, 2004, **10**, 4073–4079.

87 H. V. Huynh, in *The Organometallic Chemistry of N-heterocyclic Carbenes*, John Wiley & Sons, Ltd, Chichester, UK, 2017, pp. 17–51.

88 E. Peris, in *Topics in Organometallic Chemistry*, ed. F. Glorius, Springer, Berlin, Heidelberg, 2006, pp. 83–116.

89 F. E. Hahn and M. C. Jahnke, *Angew. Chem. Int. Ed.*, 2008, **47**, 3122–3172.

90 A. J. Arduengo, H. V. R. Dias, J. C. Calabrese and F. Davidson, *Organometallics*, 1993, **12**, 3405–3409.

91 A. Caballero, E. Díez-Barra, F. A. Jalón, S. Merino and J. Tejeda, *J. Organomet. Chem.*, 2001, **617**–**618**, 395–398.

92 A. Caballero, E. Díez-Barra, F. A. Jalón, S. Merino, A. M. Rodríguez and J. Tejeda, *J. Organomet. Chem.*, 2001, **627**, 263–264.

93 M. F. Lappert, *J. Organomet. Chem.*, 1988, **358**, 185–213.

94 D. J. Cardin, B. Cetinkaya, E. Cetinkaya and M. F. Lappert, *J. Chem. Soc., Dalton Trans.*, 1973, 514–522.

95 Y. Liu, M. Shi and L. Deng, *Organometallics*, 2014, **33**, 5660–5669.

96 J. E. Baldwin, S. E. Branz and J. A. Walker, *J. Org. Chem.*, 1977, **42**, 4142–4144.

97 C. Holtgrewe, C. Diedrich, T. Pape, S. Grimme and F. E. Hahn, *Eur. J. Org. Chem.*, 2006, 3116–3124.

98 C. Köcher and W. A. Herrmann, *J. Organomet. Chem.*, 1997, **532**, 261–265.

99 R. McKie, J. A. Murphy, S. R. Park, M. D. Spicer and S. Z. Zhou, *Angew. Chem. Int. Ed.*, 2007, **46**, 6525–6528.

100 H. Lebel, M. K. Janes, A. B. Charette and S. P. Nolan, *J. Am. Chem. Soc.*, 2004, **126**, 5046–5047.

101 I. J. B. Lin and C. S. Vasam, *Comments Inorg. Chem.*, 2004, **25**, 75–129.

102 I. J. B. Lin and C. S. Vasam, *Coord. Chem. Rev.*, 2007, **251**, 642–670.

103 D. S. McGuinness and K. J. Cavell, *Organometallics*, 2000, **19**, 741–748.

104 D. J. Nielsen, K. J. Cavell, B. W. Skelton and A. H. White, *Inorg. Chim. Acta*, 2002, **327**, 116–125.

105 H. M. J. Wang and I. J. B. Lin, *Organometallics*, 1998, **17**, 972–975.

106 S.-T. Liu, T.-Y. Hsieh, G.-H. Lee and S.-M. Peng, *Organometallics*, 1998, **17**, 993–995.

107 R.-Z. Ku, J.-C. Huang, J.-Y. Cho, F.-M. Kiang, K. R. Reddy, Y.-C. Chen, K.-J. Lee, J.-H. Lee, G.-H. Lee, S.-M. Peng and S.-T. Liu, *Organometallics*, 1999, **18**, 2145–2154.

108 B. Liu, X. Liu, C. Chen, C. Chen and W. Chen, *Organometallics*, 2012, **31**, 282–288.

109 T. M. Trnka, J. P. Morgan, M. S. Sanford, T. E. Wilhelm, M. Scholl, T.-L. Choi, S. Ding, M. W. Day and R. H. Grubbs, *J. Am. Chem. Soc.*, 2003, **125**, 2546–2558.

110 A. P. Blum, T. Ritter and R. H. Grubbs, *Organometallics*, 2007, **26**, 2122–2124.

111 M. Scholl, S. Ding, C. W. Lee and R. H. Grubbs, *Org. Lett.*, 1999, **1**, 953–

956.

112 A. J. Arduengo, D. Tapu and W. J. Marshall, *J. Am. Chem. Soc.*, 2005, **127**, 16400–16401.

113 T. Steinke, B. K. Shaw, H. Jong, B. O. Patrick and M. D. Fryzuk, *Organometallics*, 2009, **28**, 2830–2836.

114 M. Viciano, M. Poyatos, M. Sanaú, E. Peris, A. Rossin, G. Ujaque and A. Lledós, *Organometallics*, 2006, **25**, 1120–1134.

115 A. Fürstner, G. Seidel, D. Kremzow and C. W. Lehmann, *Organometallics*, 2003, **22**, 907–909.

116 W. Shih, C. Wang, Y. Chang, G. P. A. Yap and T. Ong, 2009, 1060–1067.

117 H. V. Huynh, Y. Han, R. Jothibasu and J. A. Yang, *Organometallics*, 2009, **28**, 5395–5404.

118 R. Breslow, *J. Am. Chem. Soc.*, 1958, **80**, 3719–3726.

119 C. A. Dvorak and V. H. Rawal, *Tetrahedron Lett.*, 1998, **39**, 2925–2928.

120 H. Stetter, *Angew. Chem. Int. Ed. English*, 1976, **15**, 639–647.

121 M. S. Kerr, J. R. de Alaniz and T. Rovis, *J. Am. Chem. Soc.*, 2002, **124**, 10298–10299.

122 L.-W. Xu, Y. Gao, J.-J. Yin, L. Li and C.-G. Xia, *Tetrahedron Lett.*, 2005, **46**, 5317–5320.

123 K. Iwamoto, M. Hamaya, N. Hashimoto and H. Kimura, *Tetrahedron Lett.*, 2006, **47**, 7175–7177.

124 T. Kano, K. Sasaki, T. Konishi, H. Mii and K. Maruoka, *Tetrahedron Lett.*, 2006, **47**, 4615–4618.

125 J. J. Song, F. Gallou, J. T. Reeves, Z. Tan, N. K. Yee, C. H. Senanayake and V. Preysing, *J. Org. Chem.*, 2006, **71**, 1273–1276.

126 Y. Suzuki, A. Bakar, K. Muramatsu and M. Sato, *Tetrahedron*, 2006, **62**, 4227–4231.

127 G. W. Nyce, J. A. Lamboy, E. F. Connor, R. M. Waymouth and J. L.

Hedrick, *Org. Lett.*, 2002, **4**, 3587–3590.

128 G. A. Grasa, R. M. Kissling and S. P. Nolan, *Org. Lett.*, 2002, **4**, 3583–3586.

129 J. Raynaud, C. Absalon, Y. Gnanou and D. Taton, *Macromolecules*, 2010, **43**, 2814–2823.

130 J. Raynaud, W. N. Ottou, Y. Gnanou and D. Taton, *Chem. Commun.*, 2010, **46**, 3203–3205.

131 J. J. Song, Z. Tan, J. T. Reeves, D. R. Fandrick, N. K. Yee and C. H. Senanayake, *Org. Lett.*, 2008, **10**, 877–880.

132 R. R. Schrock, J. S. Murdzek, G. C. Bazan, J. Robbins, M. Dimare and M. O'Regan, *J. Am. Chem. Soc.*, 1990, **112**, 3875–3886.

133 M. Scholl, T. M. Trnka, J. P. Morgan and R. H. Grubbs, *Tetrahedron Lett.*, 1999, **40**, 2247–2250.

134 L. Ackermann, A. Fürstner, T. Weskamp, F. J. Kohl and W. A. Herrmann, *Tetrahedron Lett.*, 1999, **40**, 4787–4790.

135 G. A. Grasa, M. S. Viciu, J. Huang, C. Zhang, M. L. Trudell and S. P. Nolan, *Organometallics*, 2002, **21**, 2866–2873.

136 D. Meyer, M. A. Taige, A. Zeller, K. Hohlfeld, S. Ahrens and T. Strassner, *Organometallics*, 2009, **28**, 2142–2149.

137 W. N. O. Wylie and R. H. Morris, *ACS Catal.*, 2013, **3**, 32–40.

138 S. Ibáñez, M. Poyatos, L. N. Dawe, D. Gusev and E. Peris, *Organometallics*, 2016, **35**, 2747–2758.

139 S. Kuwata and T. Ikariya, *Chem. Eur. J.*, 2011, **17**, 3542–3556.

140 M. C. Jahnke and F. E. Hahn, *Coord. Chem. Rev.*, 2015, **293**–**294**, 95–115.

141 S. Kuwata and F. E. Hahn, *Chem. Rev.*, 2018, **118**, 9462–9677.

142 X. Wang, H. Chen and X. Li, *Organometallics*, 2007, **26**, 4684–4687.

143 C. Heinemann and W. Thiel, *Chem. Phys. Lett.*, 1994, **217**, 11–16.

144 G. A. McGibbon, C. Heinemann, D. J. Lavorato and H. Schwarz, *Angew. Chem. Int. Ed. Engl.*, 1997, **36**, 1478–1381.

145 S. Burling, M. F. Mahon, R. E. Powell, M. K. Whittlesey and J. M. J. Williams, *J. Am. Chem. Soc.*, 2006, **128**, 13702–13703.

146 L. J. L. Häller and S. A. Macgregor, *Eur. J. Inorg. Chem.*, 2009, **2009**, 2000–2006.

147 Y. Han, Y. T. Hong and H. V. Huynh, *J. Organomet. Chem.*, 2008, **693**, 3159–3165.

148 G. Sini, O. Eisenstein and R. H. Crabtree, *Inorg. Chem.*, 2002, **41**, 602–604.

149 W. P. Fehlhammer, A. Völkl, U. Plaia and G. Beck, *Chem. Ber.*, 1987, **120**, 2031–2040.

150 R. A. Michelin, L. Zanotto, D. Braga, P. Sabatino and R. J. Angelici, *Inorg. Chem.*, 1988, **27**, 93–99.

151 R. A. Michelin, M. Mozzon, M. Zecca, B. Corain, O. Piazzi and G. Zanotti, *Inorg. Chim. Acta*, 1990, **174**, 3–7.

152 F. E. Hahn, V. Langenhahn and T. Pape, *Chem. Commun.*, 2005, **5**, 5390–5392.

153 O. Kaufhold, A. Flores-Figueroa, T. Pape and F. E. Hahn, *Organometallics*, 2009, **28**, 896–901.

154 F. E. Hahn, V. Langenhahn, N. Meier, T. Lügger and W. P. Fehlhammer, *Chem. Eur. J.*, 2003, **9**, 704–712.

155 C. Y. Liu, D. Y. Chen, G. H. Lee, S. M. Peng and S. T. Liu, *Organometallics*, 1996, **15**, 1055–1061.

156 R. Z. Ku, D. Y. Chen, G. H. Lee, S. M. Peng and S. T. Liu, *Angew. Chem. Int. Ed. Engl.*, 1997, **36**, 2631–2632.

157 M. Basato, F. Benetollo, G. Facchin, R. A. Michelin, M. Mozzon, S. Pugliese, P. Sgarbossa, S. M. Sbovata and A. Tassan, *J. Organomet. Chem.*, 2004, **689**, 454–462.

158 A. Flores-Figueroa, O. Kaufhold, K.-O. Feldmann and F. E. Hahn, *Dalton Trans.*, 2009, 9334–9342.

159 F. E. Hahn, C. G. Plumed, M. Münder and T. Lügger, *Chem. Eur. J.*, 2004, **10**, 6285–6293.

160 M. A. Huertos, J. Pérez, L. Riera and A. Menéndez-Velázquez, *J. Am. Chem. Soc.*, 2008, **130**, 13530–13531.

161 R. J. Sundberg, R. F. Bryan, I. F. Taylor and H. Taube, *J. Am. Chem. Soc.*, 1974, **96**, 381–392.

162 F. E. Hahn, A. R. Naziruddin, A. Hepp and T. Pape, *Organometallics*, 2010, **29**, 5283–5288.

163 B. Eguillor, M. A. Esteruelas, J. García-Raboso, M. Oliván, E. Oñate, I. M. Pastor, I. Peñafiel and M. Yus, *Organometallics*, 2011, **30**, 1658–1667.

164 K. Araki, S. Kuwata and T. Ikariya, *Organometallics*, 2008, **27**, 2176–2178.

165 V. Miranda-Soto, D. B. Grotjahn, A. L. Cooksy, J. A. Golen, C. E. Moore and A. L. Rheingold, *Angew. Chem. Int. Ed.*, 2011, **50**, 631–635.

166 V. Miranda-Soto, D. B. Grotjahn, A. G. DiPasquale and A. L. Rheingold, *J. Am. Chem. Soc.*, 2008, **130**, 13200–13201.

167 A. R. Naziruddin, A. Hepp, T. Pape and F. E. Hahn, *Organometallics*, 2011, **30**, 5859–5866.

168 S. E. Flowers and B. M. Cossairt, *Organometallics*, 2014, **33**, 4341–4344.

169 F. He, P. Braunstein, M. Wesolek and A. A. Danopoulos, *Chem. Commun.*, 2015, **51**, 2814–2817.

170 S. Cepa, C. Schulte To Brinke, F. Roelfes and F. E. Hahn, *Organometallics*, 2015, **34**, 5454–5460.

171 T. Kösterke, T. Pape and F. E. Hahn, *Chem. Commun.*, 2011, **47**, 10773.

172 H. Jin, P. Kluth and F. E. Hahn, *Eur. J. Inorg. Chem.*, 2017, **2017**, 2774–2781.

173 M. C. Jahnke and F. E. Hahn, *Chem. Lett.*, 2015, **44**, 226–237.

174 D. Brackemeyer, A. Hervé, C. Schulte To Brinke, M. C. Jahnke and F. E. Hahn, *J. Am. Chem. Soc.*, 2014, **136**, 7841–7844.

175 W. P. Fehlhammer, T. Bliß, J. Fuchs and G. Holzmann, *Z. Naturforsch. B: Chem. Sci.*, 1992, **59**, 79–89.

176 N. Meier, F. E. Hahn, T. Pape, C. Siering and S. R. Waldvogel, *Eur. J. Inorg. Chem.*, 2007, 1210–1214.

177 F. Bonati, A. Burini, B. R. Pietroni and B. Bovio, *J. Organomet. Chem.*, 1989, **375**, 147–160.

178 H. G. Raubenheimer, L. Lindeque and S. Cronje, *J. Organomet. Chem.*, 1996, **511**, 177–184.

179 E. Brendler, A. F. Hill and J. Wagler, *Chem. Eur. J.*, 2008, **14**, 11300–11304.

180 G. E. Dobereiner, C. A. Chamberlin, N. D. Schley and R. H. Crabtree, *Organometallics*, 2010, **29**, 5728–5731.

181 M. C. Jahnke, D. Brackemeyer, T. Pape and F. E. Hahn, *Heteroatom Chem.*, 2011, **22**, 476–490.

182 F. E. Hahn, V. Langenhahn, T. Lügger, T. Pape and D. Le Van, *Angew. Chem. Int. Ed.*, 2005, **44**, 3759–3763.

183 V. Blase, T. Pape and F. E. Hahn, *J. Organomet. Chem.*, 2011, **696**, 3337–3342.

184 E. P. Kyba, A. M. John, S. B. Brown, C. W. Hudson, M. J. McPhaul, A. Harding, K. Larsen, S. Niedzwiecki and R. E. Davis, *J. Am. Chem. Soc.*, 1980, **102**, 139–147.

185 E. P. Kyba, R. E. Davis, S. T. Liu, K. A. Hassett and S. B. Larson, *Inorg. Chem.*, 1985, **24**, 4629–4634.

186 O. Kaufhold, A. Stasch, T. Pape, A. Hepp, P. G. Edwards, P. D. Newman and F. E. Hahn, *J. Am. Chem. Soc.*, 2009, **131**, 306–317.

187 K. L. Tan, R. G. Bergman and J. A. Ellman, *J. Am. Chem. Soc.*, 2002, **124**, 3202–3203.

188 K. L. Tan, R. G. Bergman and J. A. Ellman, *J. Am. Chem. Soc.*, 2001, **123**, 2685–2686.

189 J. C. Lewis, S. H. Wiedemann, R. G. Bergman and J. A. Ellman, *Org. Lett.*, 2004, **6**, 35–38.

190 S. H. Wiedemann, J. C. Lewis, J. A. Ellman and R. G. Bergman, *J. Am. Chem. Soc.*, 2006, **128**, 2452–2462.

191 D. C. Marelius, E. H. Darrow, C. E. Moore, J. A. Golen, A. L. Rheingold and D. B. Grotjahn, *Chem. Eur. J.*, 2015, **21**, 10988–10992.

192 G. Song, Y. Li, S. Chen and X. Li, *Chem. Commun.*, 2008, 3558–3560.

193 G. Song, Y. Su, R. A. Periana, R. H. Crabtree, K. Han, H. Zhang and X. Li, *Angew. Chem. Int. Ed.*, 2010, **49**, 912–917.

194 J. L. Gomez-Lopez, D. Chávez, M. Parra-Hake, A. T. Royappa, A. L. Rheingold, D. B. Grotjahn and V. Miranda-Soto, *Organometallics*, 2016, **35**, 3148–3153.

195 Y.-J. Jin and G. Kwak, *Polym. Rev.*, 2017, **57**, 176–200.

196 U. Kernbach, M. Mühl, K. Polborn, W. P. Fehlhammer and G. Jaouen, *Inorg. Chim. Acta*, 2002, **334**, 45–53.

197 M. Liu, J. C. Namyslo, M. Nieger, M. Polamo and A. Schmidt, *Beilstein J. Org. Chem.*, 2016, **12**, 2673–2681.

198 V. César, N. Lugan and G. Lavigne, *J. Am. Chem. Soc.*, 2008, **130**, 11286–11287.

199 A. A. Danopoulos, K. Y. Monakhov and P. Braunstein, *Chem. Eur. J.*, 2013, **19**, 450–455.

200 S. T. Liddle, I. S. Edworthy and P. L. Arnold, *Chem. Soc. Rev.*, 2007, **36**, 1732–1744.

201 L. Benhamou, V. César, H. Gornitzka, N. Lugan and G. Lavigne, *Chem. Commun.*, 2009, **0**, 4720–4722.

202 M. Uzelac, A. Hernán-Gómez, D. R. Armstrong, A. R. Kennedya and E. Hevia, *Chem. Sci.*, 2015, **6**, 5719–5728.

203 Y. Wang, Y. Xie, M. Y. Abraham, P. Wei, H. F. I. Schaefer, P. v. R. Schleyer and G. H. Robinson, *J. Am. Chem. Soc.*, 2010, **132**, 14370–14372.

204 A. Jana, R. Azhakar, G. Tavčar, H. W. Roesky, I. Objartel and D. Stalke, *Eur. J. Inorg. Chem.*, 2011, 3686–3689.

205 D. R. Armstrong, S. E. Baillie, V. L. Blair, N. G. Chabloz, J. Diez, J. Garcia-Alvarez, A. R. Kennedy, S. D. Robertson and E. Hevia, *Chem. Sci.*, 2013, **4**, 4259–4266.

206 J. Ruiz and B. F. Perandones, *J. Am. Chem. Soc.*, 2007, **129**, 9298–9299.

207 M. Brill, J. Díaz, M. A. Huertos, R. López, J. Pérez and L. Riera, *Chem. Eur. J.*, 2011, **17**, 8584–8595.

208 G. Boche, C. Hilf, K. Harms, M. Marsch and J. C. W. Lohrenz, *Angew. Chem. Int. Ed. Engl.*, 1995, **34**, 487–489.

209 T. Kösterke, J. Kösters, E. U. Würthwein, C. Mück-Lichtenfeld, C. Schulte To Brinke, F. Lahoz and F. E. Hahn, *Chem. Eur. J.*, 2012, **18**, 14594–14598.

210 T. Kösterke, T. Pape and F. E. Hahn, *J. Am. Chem. Soc.*, 2011, **133**, 2112–2115.

211 D. A. Dixon and A. J. Arduengo, *J. Phys. Chem.*, 1991, **95**, 4180–4182.

212 A. J. Arduengo, D. A. Dixon, R. L. Harlow, H. V. R. Dias, W. T. Booster and T. F. Koetzle, *J. Am. Chem. Soc.*, 1994, **116**, 6812–6822.

213 J. Cernochová, M. Necas, I. Kuritka and R. Vícha, *Acta Crystallogr. E*, 2011, **E67**, 2906.

214 U. E. Hille, C. Zimmer, C. A. Vock and R. W. Hartmann, *ACS Med. Chem. Lett.*, 2011, **2**, 2–6.

215 M. A. Huertos, J. Pérez, L. Riera, J. Díaz and R. López, *Chem. Eur. J.*, 2010, **16**, 8495–8507.

216 J. Ruiz, B. F. Perandones, J. F. Van Der Maelen and S. García-Granda, *Organometallics*, 2010, **29**, 4639–4642.

217 J. Ruiz, Á. Berros, B. F. Perandones and M. Vivanco, *Dalton Trans.*, 2009, 6999.

218 F. Hering and U. Radius, *Organometallics*, 2015, **34**, 3236–3245.

219 G. C. Fortman, N. M. Scott, A. Linden, E. D. Stevens, R. Dorta and S. P. Nolan, *Chem. Commun.*, 2010, **46**, 1050.

220 M. F. Schettini, G. Wu and T. W. Hayton, *Chem. Commun.*, 2012, **48**, 1484–1486.

221 J. Ruiz, L. García, D. Sol and M. Vivanco, *Angew. Chem. Int. Ed.*, 2016, **55**, 8386–8390.

222 L. Zhang, J. Cheng, T. Ohishi and Z. Hou, *Angew. Chem. Int. Ed.*, 2010, **49**, 8670–8673.

223 I. I. F. Boogaerts, G. C. Fortman, M. R. L. Furst, C. S. J. Cazin and S. P. Nolan, *Angew. Chem. Int. Ed.*, 2010, **49**, 8674–8677.

224 A. Ariafard, F. Zarkoob, H. Batebi, R. Stranger and B. F. Yates, *Organometallics*, 2011, **30**, 6218–6224.

225 I. I. F. Boogaerts and S. P. Nolan, *J. Am. Chem. Soc.*, 2010, **132**, 8858–8859.

226 X. Zhang, Z. Geng, Y. Wang, X. Hou and D. Wang, *J. Mol. Catal. A Chem.*, 2012, **363**–**364**, 31–40.

227 D. Yu and Y. Zhang, *Proc. Natl. Acad. Sci. U.S.A.*, 2010, **107**, 20184–20189.

2 Synthesis of ligands for precursor complexes to free NM,NR NHCs

2.1 Design rationale for the MeRLH$_2$ target ligand system

The preceding chapter discussed several independent accounts which suggested that *C*-bound NHC complexes are more stable than their *N*-bound free carbene tautomers.[1–4] The reversal of the relative stabilities of these tautomers to favour the *N*-bound form must be accomplished in order to demonstrate proof-of-concept that the *N*-bound tautomer can be isolated. It was believed that this can be realised with some key structural modifications to the intermediate species **1** computed by Ariafard and colleagues.[5]

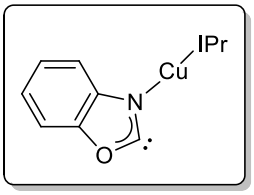

1

The heart of the chosen strategy outlined in Scheme 2.1 rests on the chelate effect, whereby a donor atom substituent is introduced to the C4 position to help direct and maintain the coordination of the metal centre to the ring nitrogen. Chelate ring strain can be minimised by extending the pendant donor arm to create a six-membered chelate ring instead of a five-membered ring.

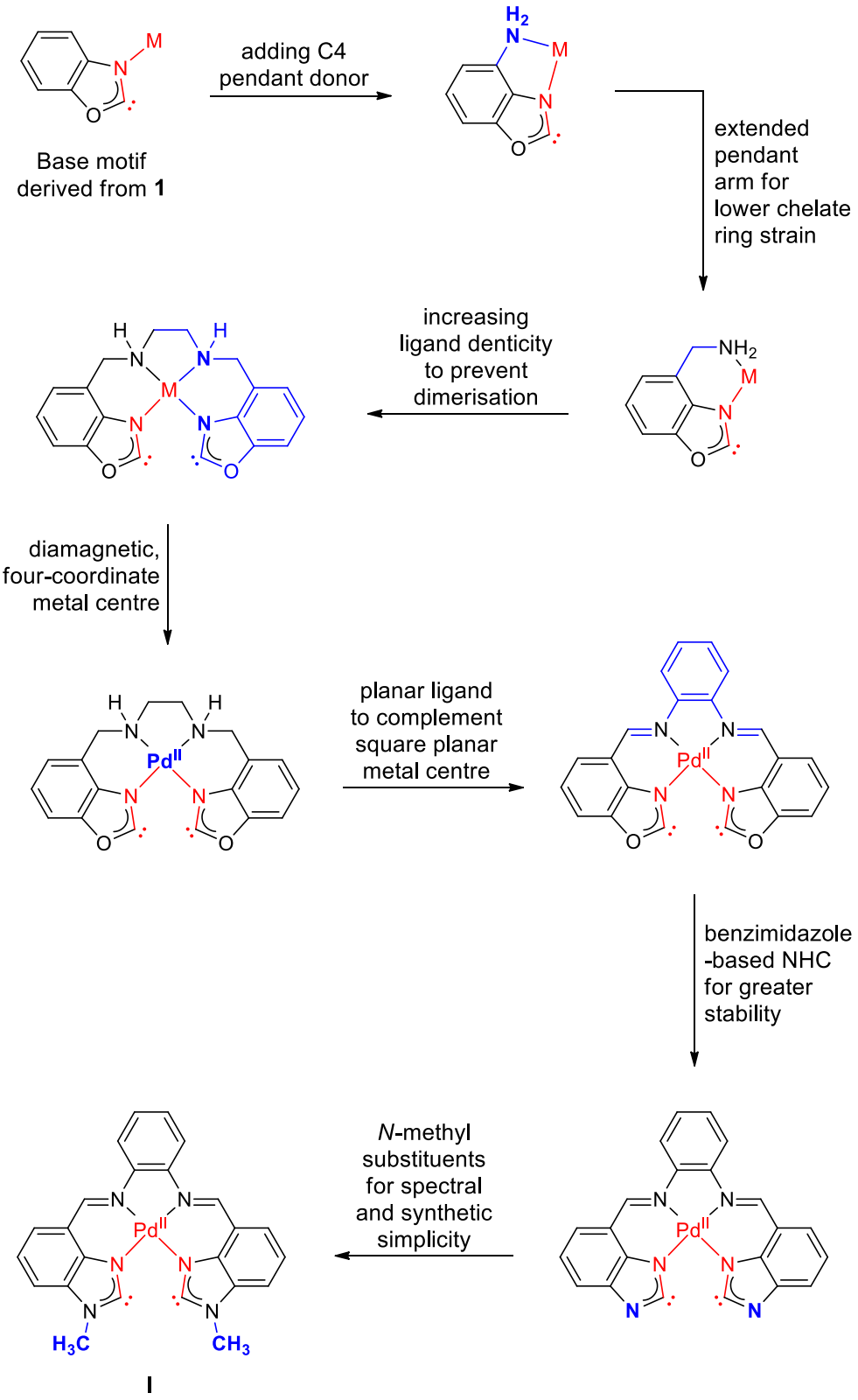

Scheme 2.1 *Design rationale for the proof-of-concept target complex.*

However, this bidentate complex may be prone to dimerisation, as Hahn and coworkers observed in some cases with N,NR NHC complexes (Scheme 2.2).[1] These N,NR NHC complexes are often difficult to isolate. Hence, their

corresponding dimeric NM,NR NHC complexes are more prevalent in the literature.[6,7] Here, the benefits of adopting a tetradentate ligand are twofold: The additional steric bulk around the metal centre prevents dimerisation by restricting intermolecular contact, while higher denticity augments the strength of the chelate effect. Meanwhile, the symmetrical motif increases the ligand's spectroscopic and synthetic simplicity.

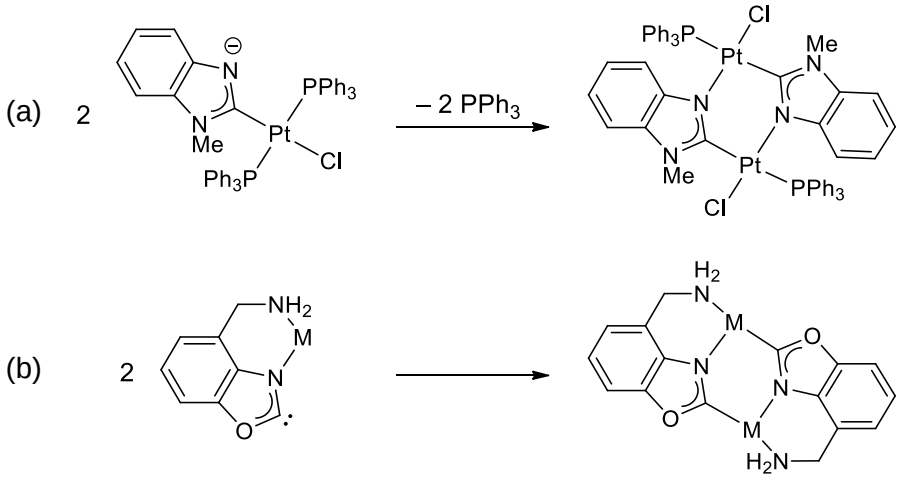

Scheme 2.2 (a) *Dimerisation of an N,NR NHC platinum complex reported by Hahn et al. An analogous reaction is predicted to occur with bidentate α-N-metallated free carbenes, as illustrated in* ***(b)****.*

The choice of metal centre was guided by several factors that are outlined below. In order to tailor the ligand design accordingly, the metal must exhibit highly predictable coordination geometry. It should preferably be diamagnetic, to facilitate characterisation of the complex by NMR spectroscopy. Ideally, the complex should be overall uncharged to preclude complications arising from anion scrambling, and potentially improve solubility. It logically follows that a metal with a +2 charge is required to balance the two negative charges of the heterocyclic motifs.

After taking these requirements into account, palladium(II) emerged as the prime candidate. In the readily accessible +2 oxidation state, palladium reliably adopts a square planar coordination geometry, which is especially attractive as it can be coordinatively saturated by the proposed tetradentate ligand. This further reduces the likelihood that coordinating solvents or counterions will compete with the ligand for coordination to the metal centre.

It stands to reason that a square planar palladium(II) centre is best complemented by a fully planar ligand. Ligand planarity can be enhanced by ensuring that all atoms within the ligand scaffold are sp^2 hybridised; namely, by linking the two imine pendant donors via a phenylene bridge. The result is a rigid complex that is conformationally restricted from undergoing dimerisation.

It is perhaps timely to recall that thus far, no free carbenes derived from oxazoles or benzoxazoles have been reported. Of the five-membered NHCs, only the diaminocarbenes have been isolable in their free form to any significant degree. Although structure **1** features a benzoxazol-2-ylidene, collective wisdom suggests that it would be prudent to replace it with the benzimidazol-2-ylidene to increase the stability of the free carbene moiety. Previous work with the ester-substituted benzoxazole **2** revealed that the benzoxazole ring was prone to hydrolysis (Scheme 2.3),[8] further affirming the selection of a benzimidazole ring, which is reputedly more robust. Finally, *N*-methyl substituents were chosen for ease of synthesis and spectroscopic simplicity.

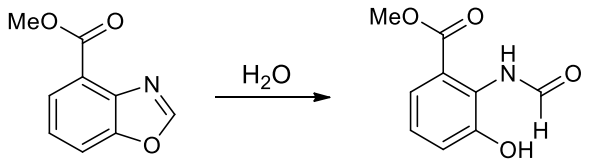

2 **3**

Scheme 2.3 *Spontaneous hydrolysis of 4-methyl ester benzoxazole **2** into the ring-opened formamidine **3**.*

In accordance with the $MeRLH_2$ naming convention described in Figure 2.1 a, the phenylene-bridged target ligand is dubbed $MePhLH_2$.

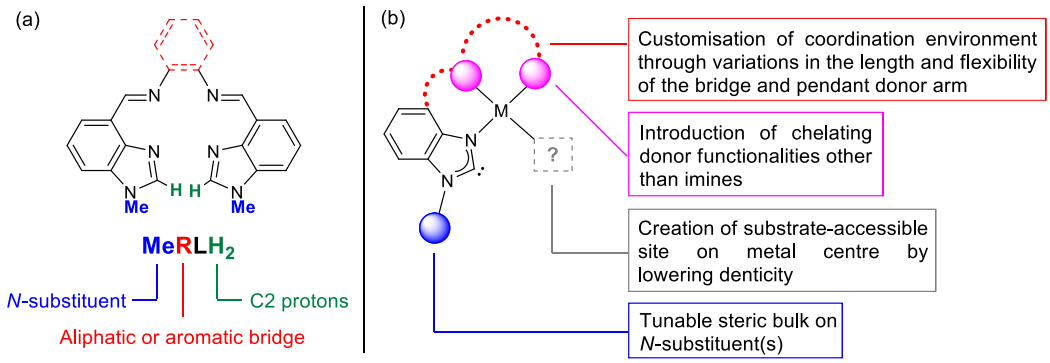

Figure 2.1 ***(a)*** *Nomenclature of the target free NM,NR NHC ligand precursors.* ***(b)*** *Potential points of structural modification in the $MeRLH_2$ ligand system.*

The previous chapter highlighted the potential for the free NM,NR NHC to be exploited in cooperative dual catalysis. However, this is unlikely to occur with the proof-of-concept complex in its present form, which has no vacant coordination sites on the metal centre to accommodate potential substrates. Furthermore, the carbenic sites are similarly inaccessible. Foreseeing this, the ligand was designed to be highly modular, thus enabling systematic modifications in the future (Figure 2.1 b). For example, coordinative unsaturation can be effected by removing the second benzimidazole unit to reduce ligand denticity, and a bulkier *N*-substituent may then compensate for the reduced steric protection around the carbene. The ligand can also be adapted to suit metals with different sizes or coordination geometries by changing the length and hybridisation of the linker unit between the pendant donors. Instead of nitrogen-based functional groups such as imines or amines, the pendant donors may also contain other heteroatoms: phosphines, ethers, or thioethers, to name a few.

2.2 Synthetic strategies towards $MeRLH_2$

The synthesis of the precursor to complex **I** can be divided into three key transformations, as shown in the following retrosynthetic analysis (Scheme 2.4): First, the construction of the benzimidazole ring; second, the formation of the bridged imine donors; and finally, the metallation of the ligand.

While designing target complex **I**, it became apparent that the length and flexibility of the linker between the aldimine units could influence the orientation of the benzimidazole units, which in turn affects the distance between the C2 atoms. This may alleviate the steric hindrance around the potential carbene

sites, and ultimately lower the stability of the free carbenes. As mentioned in the earlier section, it was predicted that a reduction in the steric protection offered by the opposing benzimidazole arm could be compensated for by an increase in the size of the benzimidazole *N*-substituents.

In order to study the structural and reactivity effects of the imine linker and *N*-substituents in detail, it will be necessary to compare analogues of **I** which differ at those sites. Thus, the synthetic strategy was designed to accommodate these variations with minimal procedural modifications. The simplest and most general method for preparing aldimines is the condensation of a primary amine with an aldehyde.[9,10] The bridge can be easily modified via this route by condensing two 4-formylbenzimidazoles with the desired diamine.

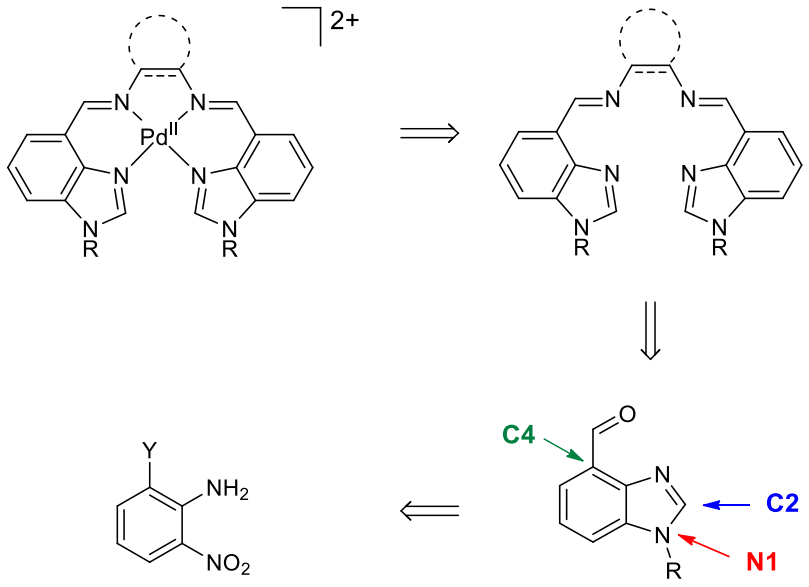

4 Y = OH
5 Y = Me
6 Y = COOMe

7a R = Boc
7b R = H
7c R = Me

Scheme 2.4 *Retrosynthetic analysis of the precursor cationic palladium(II) complex.*

Although general preparative methods for benzimidazoles are numerous and well-documented in the literature,[11] the requirement of a C4-substituent limited our choice of starting materials. Syntheses of 4-substituted benzimidazoles almost invariably proceed via 1,2,3-trisubstituted benzenes with ortho-diamines, which undergo cyclisation with a carbon source to form the *N*-heterocycle. The *N*1-substituent may be installed prior to or after ring closure. Therefore, the key

decision lay in the choice of substituent Y, which must be convertible into a formyl group.

Of all the commercially available 1,2,3-trisubstituted benzenes surveyed, **4**–**6** were selected on the basis of their affordability and potential for modification at Y. The following sections discuss the attempts to synthesise **7** from each of these candidates. The synthesis proved to be non-trivial: Although many routes to **7** seemed equally worthy at the outset, each one presented complications that were unique to the system at hand. Given that time was a scarce resource, most of these strategies were explored in parallel. The isolation of the target compound was a greater priority than the efficiency of the methods themselves, which were only optimised for multigram-scale synthesis at a later stage.

2.2.1 Routes from 2-amino-3-nitrophenol 4

Although aryl halides are excellent starting points for installing a wide scope of functional groups (largely due to developments in transition metal-mediated coupling chemistry),[12–15] commercially sourced ortho-diamines where Y = halogen were expensive. Synthesising these aryl halides from ortho-diamines is likely impractical, as regioselective halogenation can be difficult to achieve.

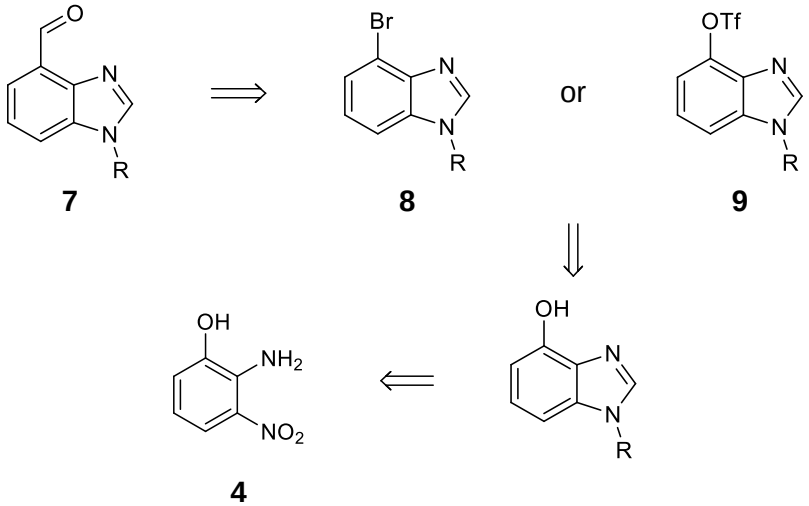

Scheme 2.5 *Retrosynthetic analysis showing potential transformations from phenol **4**.*

Phenol **4** appeared to be an attractive alternative, as it can be converted into aryl bromide **8** or pseudohalides such as triflate **9**, which may then undergo palladium-catalysed reductive carbonylation,[16–19] or lithium-halogen exchange

followed by an electrophilic quench with DMF[20–23] to form the target carbaldehyde **7** (Scheme 2.5). The successful preparation of **8** or **9** would of course bring opportunities to employ cross-coupling chemistry to incorporate other pendant donors containing motifs such as – but by no means not limited to – pyridine, phosphine, or imidazole. Cross-coupling reactions utilising phenol as the electrophile have been developed more recently, but these often require derivatisation of the phenolic group, and the scope of nucleophilic coupling partners remains relatively narrow.[24,25]

Before proceeding to reduce the nitro group of **4** into the amine, the protection of the phenol and amine as their respective acyl and *N*-Boc derivatives was initially attempted. This was mainly to ensure that alkylation occurred exclusively on the 3-amino group (Scheme 2.6).

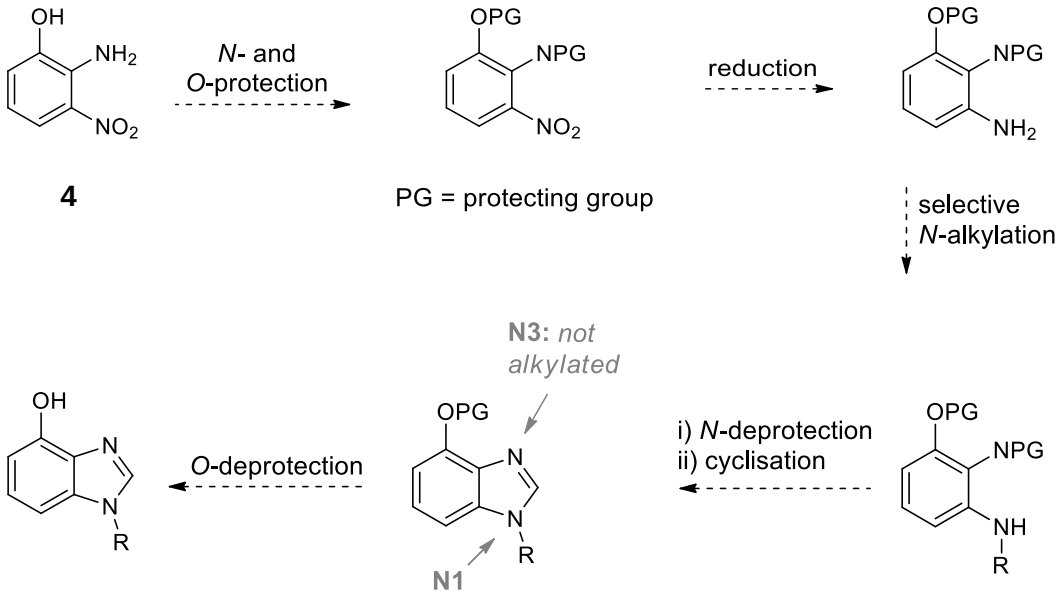

Scheme 2.6 *Overview of protect–alkylate–cyclise strategy towards N-alkyl-4-hydroxybenzimidazole. The potential formation of benzoxazole or N3-alkylated benzimidazole side products is avoided by protecting the phenol and aniline functions respectively.*

A secondary concern was that if **4** was reduced into the diamine prior to ring closure, *N*,*O*-cyclisation might take place to form a 4-aminobenzoxazole instead of the desired 4-hydroxybenzimidazole. Existing preparatory methods for 4-hydroxybenzimidazole from 2,3-diaminophenol indicate that the *N*,*N*-cyclisation is generally favoured over *N*,*O*-cyclisation, presumably because the amine is more nucleophilic than the phenolic centre.[26–30] Although the probability

of *N*,*O*-cyclisation is low, the phenol/amine double protection strategy could offer additional reassurance by eliminating the risk completely.

Somewhat unexpectedly, the treatment of **4** with 1.1 equivalents of Boc anhydride (Boc_2O) and a catalytic amount of 4-DMAP yielded primarily the *O*-Boc product **10**, with variable amounts of the intended *N*-Boc product **11** (Scheme 2.7). The structural assignment of **10** was made on the basis of its ^1H NMR spectrum, which featured a broad singlet integrating for 2H at 6.20 ppm. The only other singlet in the spectrum appeared at 1.57 ppm and had an integration of 9H, indicating that the Boc group had been successfully installed. The conspicuous absence of a peak for the phenol O*H* and the apparent retention of the amino group signal provided compelling evidence of *O*-protection. In addition, the IR spectrum of **10** contained a sharp, diagnostic band at 1765 cm^{-1}, which is consistent with the expected C=O stretching frequency in the intermediate range between alkyl and aryl carbonates.[31] The ^1H NMR spectrum of *N*-Boc product **11** is easily distinguished from that of **10**: The carbamate and phenolic protons appear as two distinct singlets, each integrating for 1H, at 9.10 and 9.16 ppm. Efforts to obtain suitable crystals of **10** or **11** for structural authentication by SC-XRD were unsuccessful.

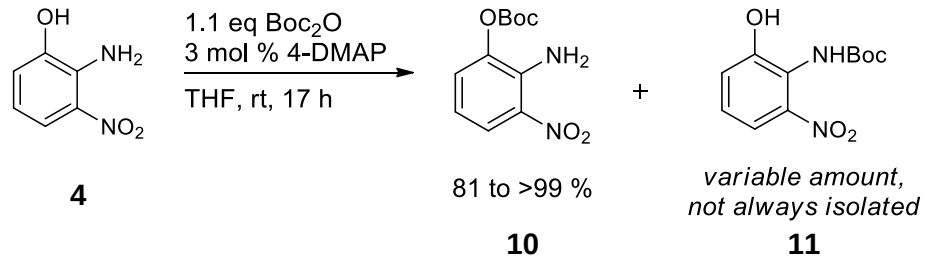

Scheme 2.7 *Preferential O- versus N-Boc protection for aminophenol **4**.*

Although the Boc protection of phenols is fairly common in the literature,[32–34] there are very limited reports of competing *O*- versus *N*-*tert*-butyloxycarbonylation in bifunctional systems. Fréchet and coworkers observed that in the absence of base, *p*-aminophenol selectively undergoes Boc protection at the amino functionality.[35] However, in the presence of NaOH, *tert*-butyloxycarbonylation occurs almost exclusively on the oxygen, possibly due to the higher nucleophilicity of the phenolate ion compared to the aniline nitrogen. Perhaps 4-DMAP is sufficiently basic to deprotonate the phenol in **4** and induce the same reaction. Another likely explanation is that the nitro

substituent draws electron density away from the adjacent amino group, to the extent that the latter becomes less nucleophilic than the phenol.

The full picture, however, may be more complicated. In a detailed investigation of the reaction of Boc_2O/4-DMAP with amino alcohol **12**, Basel and Hassner found evidence for indirect additional pathways stemming from an isolable carbamic-carbonic anhydride intermediate **13** (Scheme 2.8).[36] The carbamic-carbonic anhydrides generated from **12** are highly unusual outcomes for Boc protection reactions, and were characterised using ^{1}H and ^{13}C NMR spectroscopy and mass spectrometry. It was shown that **13** reacted with the free amino alcohol to generate an equal mixture of the *O*-Boc and *N*-Boc products **15** and **16** respectively. **13** can also undergo conversion into *O*-Boc **15** and the diBoc product **14** in the presence of 4-DMAP.

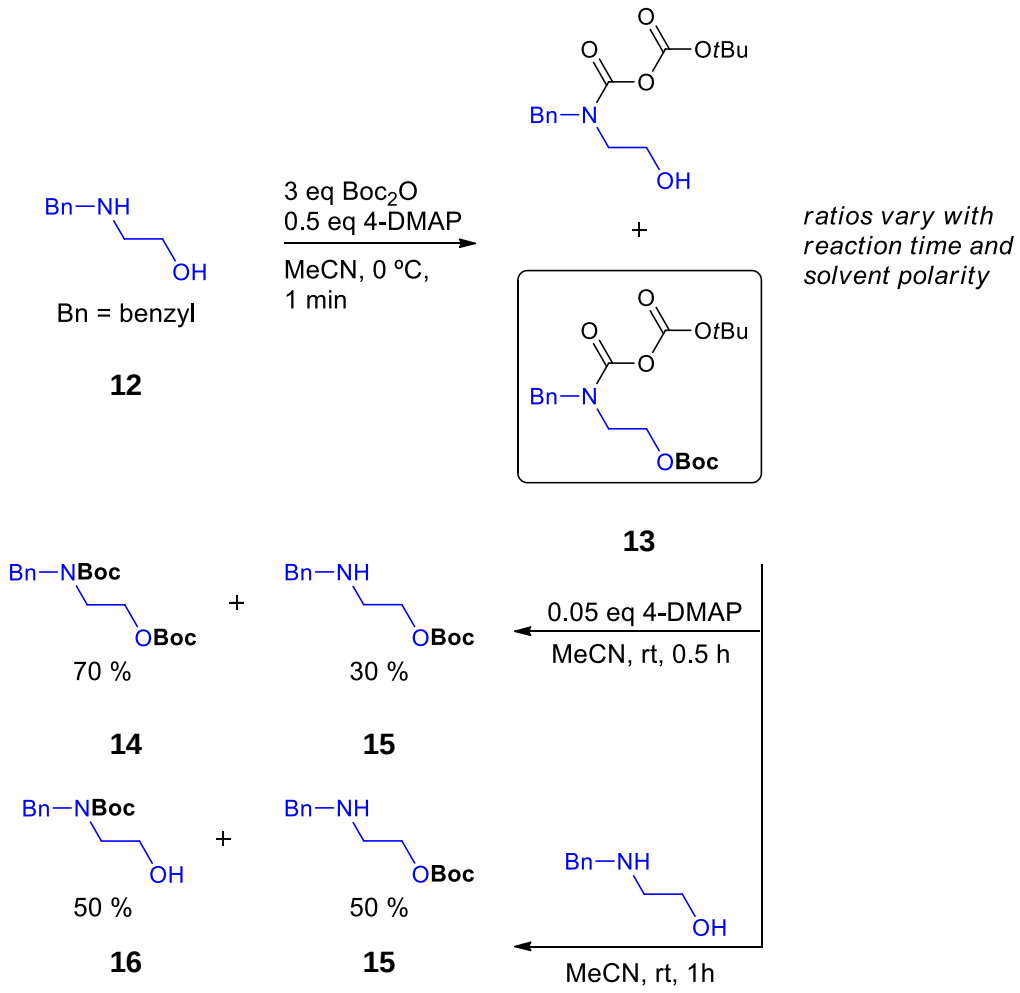

Scheme 2.8 *Formation of N- and O-Boc product mixtures via a carbamate-carbonic anhydride intermediate.*[36]

Due to their spectral similarities, **10** was initially mischaracterised as **11**, and subsequently reacted with 2.2 equivalents of acetic anhydride in refluxing glacial acetic acid with the intention of protecting the phenol as its acyl derivative. However, the ^{1}H NMR spectrum of the isolated product did not retain the upfield singlet integrating for 9H characteristic of the Boc *t*-butyl groups. Instead, the spectral data supported the formation of 2-methyl-4-nitrobenzoxazole **17** as the major product. The ^{1}H NMR spectrum of **17** exhibits only the three signals expected for the phenyl protons, and a singlet at 2.76 ppm integrating for 3H corresponding to the methyl group. No additional signals were observed when the spectrum was recorded in a non-exchanging solvent such as d_6-DMSO. Notably, the ^{13}C NMR spectrum of **17** featured a downfield signal at 168.0 ppm, which falls within the typical range for the C2 carbon of benzoxazoles. Repeat attempts of this reaction also led to the isolation of the mono-*N*-acylated product **19** and imide **18** along with benzoxazole **17** (Scheme 2.9).

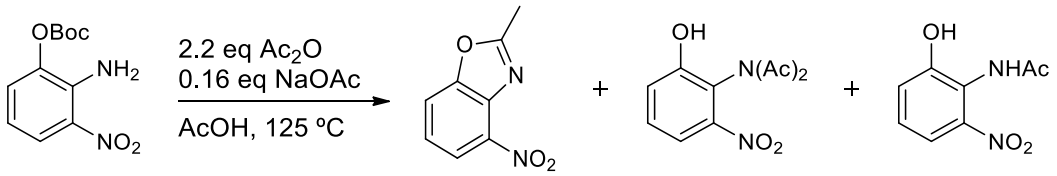

10 **17** **18** **19**

Approximate ratio 10 : 2 : 1

Scheme 2.9 *Acylation of a Boc-protected phenol resulting in the deprotection of the hydroxyl group, and formation of amide derivatives or 2-methyl-4-nitrobenzoxazole.*

Two new singlets integrating for 3H appeared at 2.21 and 2.30 ppm in the ^{1}H NMR spectrum of **18**, suggesting that the amino group had been doubly acylated, while a broad singlet integrating for 1H at 8.22 ppm indicated that the phenol had been deprotected under these harsh acidic conditions. Amide **19** is easily distinguished from imide **18** by the presence of two singlets at 9.12 and 9.18 ppm integrating for 1H each, which are indicative of a phenol and amide protons respectively.

Presumably, when carbonate cleavage in **10** occurs before the amine nitrogen is acylated for the second time, the phenol group in **19** attacks the electrophilic carbonyl of the amide and then furnishes benzoxazole **17** by intramolecular condensation. The formation of this benzoxazole side product highlights that

care must be taken to avoid *N*,*O*-cyclisation, and that acyl protecting groups may be unsuitable for this system.

Since it was relatively convenient to prepare and purify the *O*-Boc product **10**, the key objective of protecting both the phenol and aniline functions could still be met. The original approach could be reversed so that the phenol would be protected as the *O*-Boc derivative, while the aniline could be protected as acetamide **19**. Mono-acylation of the aniline without phenol regeneration and subsequent cyclisation might be possible under milder conditions. A THF solution of **10** was stirred with triethylamine, excess acetic anhydride, and a catalytic amount of 4-DMAP at room temperature. Unfortunately, the reaction gave complex mixtures whose composition varied between attempts. In all cases, no significant amounts of **19** or benzoxazole **17** were detected. It was concluded that the *N*,*O*-double protection strategy was unduly difficult to control, and therefore abandoned in search of more reliable routes.

Without protecting the aniline, the nitro group in the *O*-Boc aniline **10** was cleanly reduced into an amine by catalytic hydrogenation with 10 % palladium on carbon. Heating an acetonitrile solution of the resulting ortho-diamine and isopropyl bromide with K_2CO_3 and NaI resulted in a mixture of at least three isopropylated products, based on the three characteristic septets between 4.40 – 4.80 ppm visible in the ^{1}H NMR spectrum of the reaction mixture. This is perhaps suggestive of non-selective substitution at either or both of the nitrogen centres.

The *O*-Boc species **10** was then subjected to reductive amination with acetone and sodium borohydride, in hope that this *N*-alkylation pathway would demonstrate higher regioselectivity. By ^{1}H NMR spectroscopy, the major product was consistent with a mono-*N*-alkylated species, as indicated by the appearance of the C$H_{(isopropyl)}$ septet at 3.52 ppm and the C$H_{3(isopropyl)}$ doublet at 1.22 ppm integrating for 1H and 6H respectively, relative to the three CH_{phenyl} peaks. Nevertheless, the product proved troublesome to purify and once again, alternative routes were sought.

Given that protecting either one or both of the amino or hydroxyl groups in **4** did not mitigate the selectivity problems anticipated for the *N*-alkylation step, it seemed that while forming the benzimidazole prior to *N*-alkylation may not provide higher regioselectivity, it would at least improve step economy (Scheme 2.10).

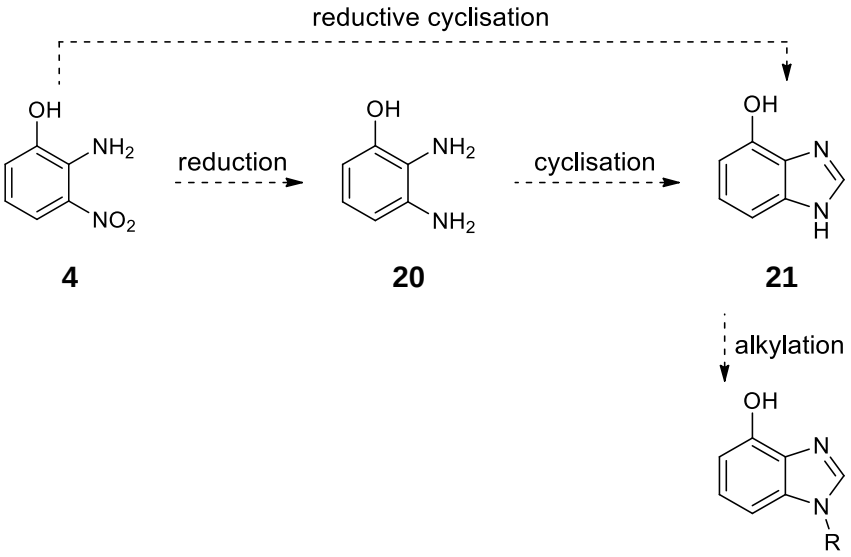

Scheme 2.10 *Overview of the reduce–cyclise–alkylate strategy towards N-alkyl-4-hydroxybenzimidazole.*

As a starting point, 0.2 equivalents of 10 % palladium on carbon were employed as the reducing agent for the aromatic nitro group. However, under 1 atm H_2 at room temperature, the reduction proved to be sluggish. Despite stirring for 3 days, only approximately 50 % conversion was observed by TLC. Agitating the reaction mixture for 3 hours at an increased H_2 pressure of 2.4 atm, and adding an additional 0.2 equivalents of 10 % palladium on carbon only increased the ratio of starting material to diaminophenol **20** to 1:8 by ^{1}H NMR spectroscopy. It was suspected that **20** was capable of coordination to the palladium particles, thus deactivating the catalyst. In order to overcome this, the catalyst loading was increased to 0.6 equivalents, and hydrochloric acid was added to protonate the diamine and prevent it from coordinating to the fresh palladium. Despite these measures, the product ratio only increased to 1:10 after stirring overnight at 1 atm H_2. An alternative catalyst, $Pd(dba)_2$ proved to be more effective. Even at ambient temperature under 1 atm H_2 and a lower catalyst loading of 5 mol %, the starting material was fully consumed within 16 hours. The reaction time could be reduced to 6 hours with only 1.5 mol % of $Pd(dba)_2$ when a pressure of 8.2 atm H_2 was applied. The expected diamine **20** was obtained as the major product, accompanied by a small amount of unidentified byproduct.

Ring closure of ortho-diamines such as **20** is generally accomplished at elevated temperatures using a formate orthoester[37,38] or formic acid[39,40] as the carbon source for C2-unsubstituted benzimidazoles. An acid catalyst is often employed. In the first attempt, **20** was heated to reflux in a fourfold excess of triethyl

orthoformate and a catalytic amount of sulfuric acid. A complex mixture was obtained, from which no starting material or 4-hydroxybenzimidazole **21** could be discerned in the ^{1}H NMR spectrum. More promising results were obtained from an adapted procedure[40] in which the reaction was performed with formic acid in a 5 N hydrochloric acid solution. The ^{1}H NMR spectrum of the product after basic workup showed one major species, featuring chemical shifts that were in reasonable agreement with the reported values[26] for **21**. Notably, there was a new singlet at 8.04 ppm integrating for 1H, which is suggestive of the C2 proton in **21**. However, the putative product could not be satisfactorily purified for unambiguous characterisation. Similar results were obtained from a method developed by Katritzky and coworkers,[26] using triethyl orthoformate and *p*-toluenesulfonic acid as the carbon source and catalyst respectively.

Another common approach to benzimidazole synthesis involves the reductive cyclisation of *ortho*-nitroanilines. Shen and coworkers reportedly synthesised 4-hydroxybenzimidazole in 75 % yield by reacting **4** with an excess of triethyl orthoformate in the presence of 10 % palladium on carbon and a catalytic amount of acetic acid.[41] However, in our hands, the ^{1}H NMR spectrum of the reaction mixture revealed only trace amounts of conversion under these conditions. Addition of a large excess of acetic acid failed to accelerate the rate of reductive cyclisation, and little change was observed after 14 hours. Substituting sodium formate as the hydrogen source as per a different one-pot reductive cyclisation procedure[42] produced no improvement, with **4** being fully recovered despite refluxing in 1:1 formic acid/triethyl orthoformate for 2.5 days. Although prior attempts to reduce the nitro group have indicated that the transformation is not as facile as expected, it was surprising to note that aminophenol **4** also resisted *N*,*O*-cyclisation under these conditions. No cyclisation products or intermediates were detected, even though 4-nitrobenzoxazole could be obtained quantitatively from **4** and trimethyl orthoformate with a catalytic amount of *p*-toluenesulfonic acid at 100 °C.[43]

2.2.2 Routes from 2-amino-3-nitrotoluene 5

While investigating routes to carbaldehyde **7** from **4**, routes from **5** were also being explored. It soon became apparent that syntheses beginning with **5** were more tractable, and our focus shifted to this approach. The transformations attempted were generally more selective without the interference of a nucleophilic hydroxyl substituent. Its replacement with a methyl group eliminates

the possibility of *N*,*O*-cyclisation and competitive *N*- versus *O*-alkylation during the synthetic sequence, voiding the need for any phenol protecting groups.

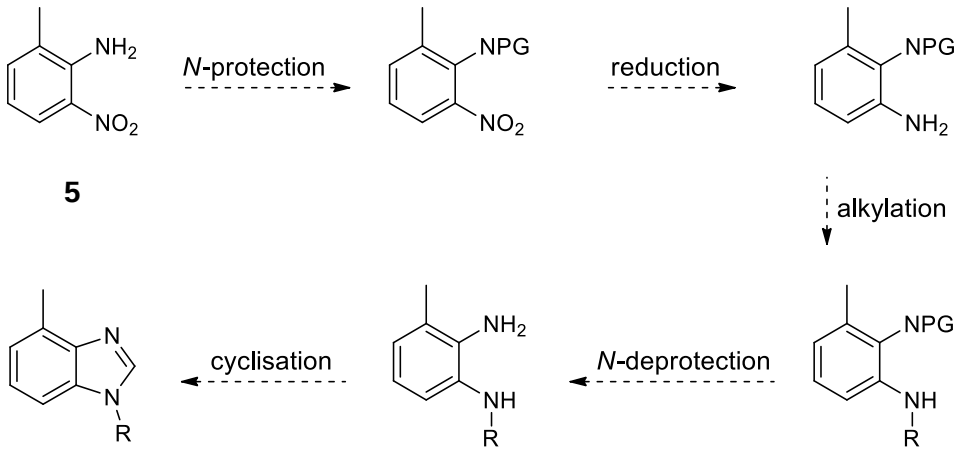

Scheme 2.11 *Overview of protect–alkylate–cyclise strategy from 2-amino-3-nitrotoluene.*

As was the case with aminophenol **4**, two routes were tested. The first route was designed to minimise the formation of *N*3-alkylated products (Scheme 2.11), while the second is analogous to the reduce–cyclise–alkylate strategy described for phenol **4** in Scheme 2.10. Following a conventional procedure for the Boc protection of aniline **5**, a 1:1 mixture of starting material and the doubly protected product **22** was obtained instead of the expected mono-Boc protected product (Scheme 2.12).

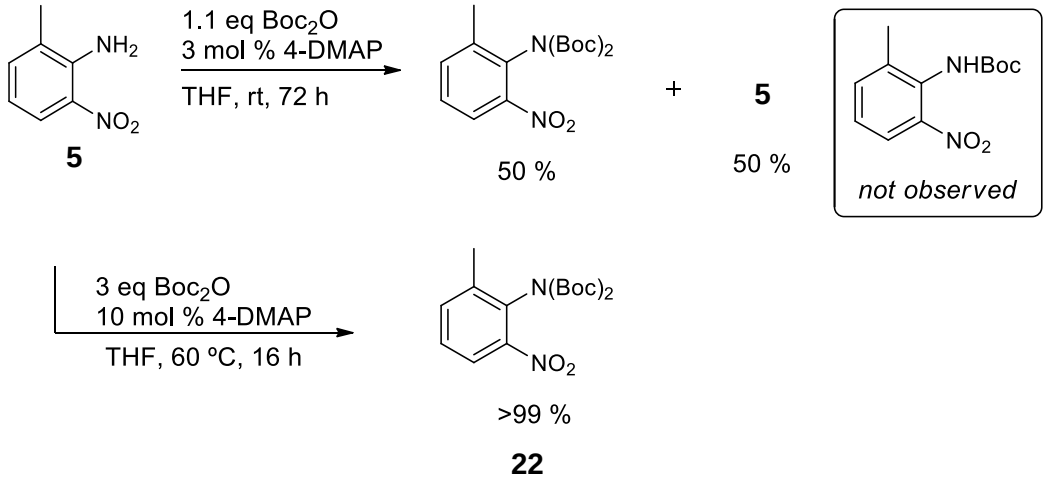

Scheme 2.12 *N-protection of 2-amino-3-nitrotoluene with a stoichiometric quantity or excess of Boc anhydride.*

This is also consistent with our observation that phenol **4** reacts with 2.1 equivalents of Boc_2O to give a 1:1 mixture of mono-*O*-Boc **10** and tri-Boc product **23**, with no trace of the expected *O*,*N*-di-Boc product (Scheme 2.13).

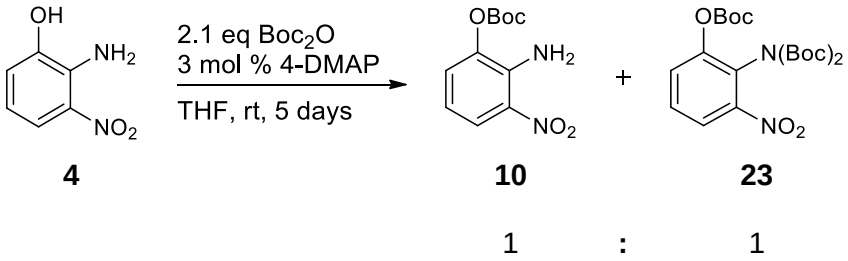

4 **10** **23**

1 : 1

Scheme 2.13 *The attempted synthesis of O,N-diBoc-protected aminophenol results in an equal mixture of mono- and triBoc-protected aminophenols.*

A survey of the literature revealed that this was not an irregular occurrence. In their efforts to prepare the mono-Boc derivatives of sterically hindered anilines bearing at least one ortho substituent, Darnbrough and coworkers found that existing procedures for Boc protection afforded only the di-Boc product and unreacted starting material when 1 equivalent of Boc_2O was used.[44] They postulated that the incorporation of the first Boc group occurs rather slowly but the resulting carbamate NH, being more acidic, enables rapid deprotonation and installation of the second Boc group. This necessitated the development of a two-step procedure from which the mono-Boc aryl amines could be reliably obtained. The aryl amines were treated with three equivalents of Boc_2O to quantitatively generate the di-Boc derivatives, which were then heated to reflux in methanol with excess potassium carbonate to effect the selective deprotection and yield the mono-Boc products.

As the objective was simply to render the aniline unavailable for alkylation, the double protection was not initially considered a disadvantage, so the deprotection step could be omitted. Subjecting aniline **5** to the double protection conditions published by Darnbrough and colleagues cleanly and quantitatively afforded di-Boc **22** as yellow oil. Colourless crystals of suitable quality for X-ray diffraction studies were formed from the oil after standing for several weeks. The resulting structure is depicted in Figure 2.2.

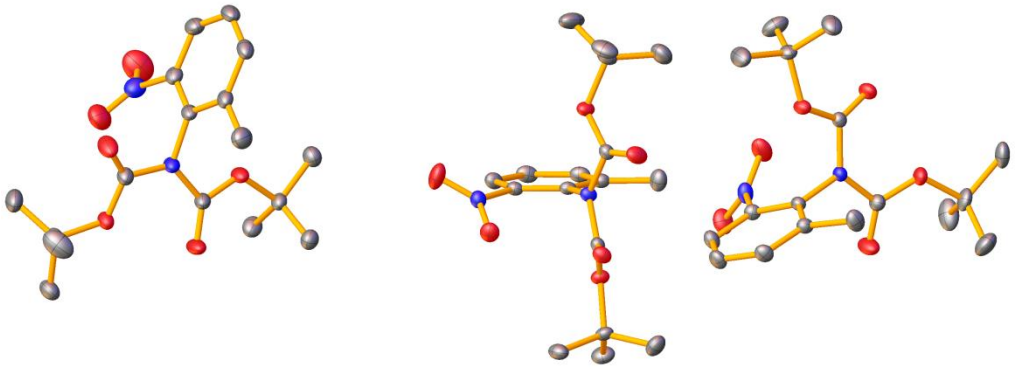

Figure 2.2 *Structure of the three chemically equivalent but crystallographically distinct molecules of 2-N(Boc)$_2$-3-nitrotoluene,* ***22*** *that make up the asymmetric unit. Thermal ellipsoids are shown at the 50 % probability level. Aryl and methyl hydrogens are omitted for clarity.*

Under 1 atm H_2 with a catalytic amount of Pd(dba)$_2$, **22** underwent almost no conversion into the desired amine **24**. Even after stirring overnight at an increased pressure of 8 atm H_2, only starting material was recovered (Scheme 2.14). Perhaps the large steric bulk of the two Boc groups shielded the nitro group from the palladium catalyst surface, preventing hydrogen transfer.

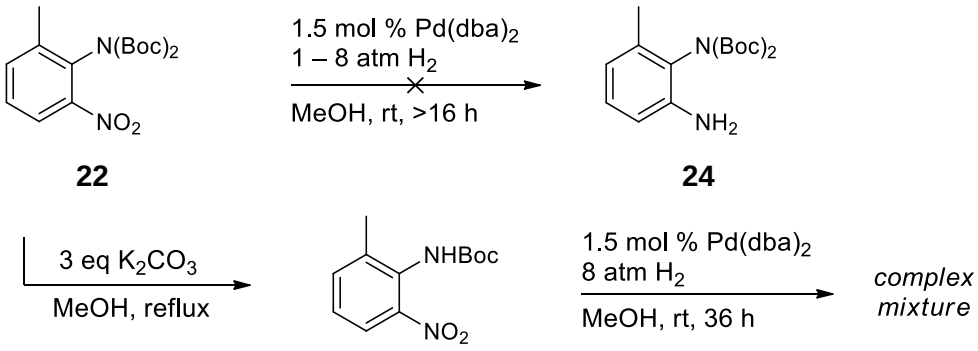

Scheme 2.14 *Unsuccessful reduction of the aromatic nitro group in carbamate-containing substrates.*

To reduce steric shielding around the nitro group, one of the Boc groups was selectively removed from **22**. The ^{1}H NMR spectrum of mono-Boc product **25** showed a decrease in the integration of the singlet corresponding to the *t*-butyl groups from 18H to 9H. **25** was then hydrogenated at elevated pressure (Scheme 2.14). Analysis of the resulting mixture by ^{1}H NMR spectroscopy revealed a complex array of products, with no residual trace of **25**. The

appearance of two broad singlets at 4.65 and 4.86 ppm suggest that some amine products may be present. Liu and coworkers noted that the reductive cyclisation of 3-COOEt-2-(*N*-Boc)nitrobenzene was slower and had poorer yields than the same reaction with the unprotected analogue.[41] This might indicate that the carbamate functionality may interfere with nitro reduction to some degree. It seems that the protect–alkylate–cyclise strategy carries many complications, even without the influence of the phenol group.

Meanwhile, the reduce–cyclise–alkylate route was progressing more smoothly. It was quickly discovered that the nitro reduction of **5** with $Pd(dba)_2$ also suffered from slow conversion at 1 atm H_2 at room temperature. Increasing the catalyst loading from 0.5 mol to 1.5 mol % failed to drive the reaction to completion within a reasonable time frame. The deactivation of the Pd catalyst by complexation with the diamine may once again be at play. Fortunately, increasing the H_2 pressure produced a corresponding increase in the rate of reduction. Under 8 atm of H_2, quantitative conversion of **5** into diamine **26** could be achieved within 4 – 6 hours.

Using a cyclisation procedure adapted from Katritzky and coworkers,[26] benzimidazole **27** was obtained in high yield from the reaction of diamine **26** with excess triethyl orthoformate and an organic acid catalyst (Scheme 2.15). There were marked differences between the ^1H NMR spectra of **26** and **27**; most importantly, the replacement of the broad singlet at 3.36 ppm corresponding to the four amino protons with a singlet at 8.12 ppm, which signified the C2 proton of the newly formed imidazole unit.

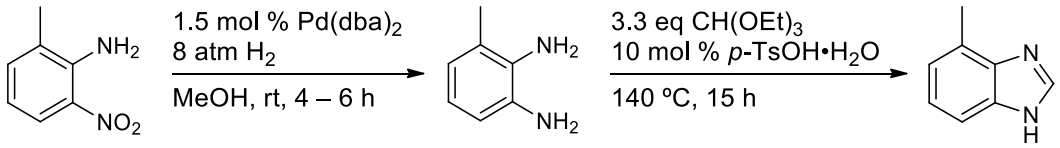

5 >99 % **26** 81 % **27**

Scheme 2.15 *Synthesis of 4-methylbenzimidazole.*

The ease of access to **27** was encouraging, and synthetic efforts shifted to the next step in the sequence: alkylation at the N1 position. As stated earlier in this chapter, it was anticipated that the target free carbene would benefit from kinetic stabilisation by a bulkier *N*-substituent. Therefore, isopropyl bromide was initially chosen over methyl iodide as the alkylating agent, although the latter would

likely result in higher yields. 4-Methylbenzimidazole was deprotonated with a slight excess of sodium hydride in DMF. Isopropyl bromide was added and the solution was stirred for 11 hours at 30 °C before being subjected to an aqueous workup to give **28** (Scheme 2.16). Proton and carbon resonances were assigned on the basis on two-dimensional NMR spectroscopy. The ^{1}H NMR spectrum of **28** bore the unmistakeable septet of the isopropyl methine proton at 4.58 ppm, for which correlations to the C2 and C7a carbon could be found in the ^{1}H-^{13}C HMBC spectrum. The *N*3-alkylated regioisomer was not observed. This is consistent with the findings of Howell and Rasmussen, who reported that C4-substituted benzimidazoles almost always demonstrate a strong preference for *N*-alkylation at N1 over N3.[45] While the ratio of N1 to N3 alkylation in C5- or C6-substituted benzimidazoles is closer to parity, with small deviations that are governed by electrostatic or thermodynamic effects, the regioselectivity of alkylation in C4-substituted benzimidazoles is largely determined by the steric interactions between the C4-substituent and the N3 site.

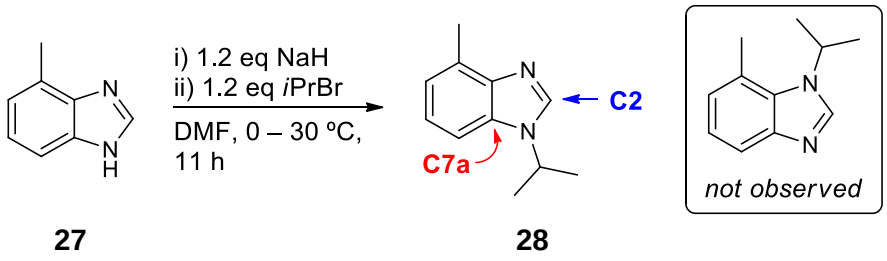

27 **28**

Scheme 2.16 *N1-isopropylation of 4-methylbenzimidazole.*

The prospect of preparing aldehyde **7** from benzimidazole **28** in a single step was highly desirable. The one-electron oxidant, ceric ammonium nitrate (CAN) has been successfully applied to the oxidation of alkylbenzenes into their corresponding aryl aldehydes or ketones.[46] Generally speaking, CAN-promoted oxidations of benzylic methyl groups are rapid and high-yielding,[47–50] although the presence of deactivating substituents may lead to lower yields.[51] Although one report warned that the oxidation may proceed very slowly for a methylbenzimidazole substrate,[52] this transformation was explored nevertheless. Unfortunately, the methyl group in **28** was unaltered after stirring with 4 equivalents of CAN in methanol/acetonitrile at room temperature for a week. The same reaction mixture was then warmed at 50 °C for 10 days. A new singlet emerged at 9.80 ppm in the ^{1}H NMR spectrum of the crude reaction mixture, along with a peak at 172.5 ppm in the ^{13}C NMR spectrum. This may be indicative of aldehyde formation; however, the reaction mixture contained a number of

other inseparable species and no definitive characterisation could be made based on the NMR spectra. The reproducibility of this reaction was also questionable: A subsequent attempt to perform and monitor the reaction on an NMR scale in CD_3OD at 50 °C showed virtually no change over a time span of two weeks.

Another useful derivative of the aromatic methyl group is its benzyl halide, an excellent electrophile for substitution reactions, and for which there are many reliable and general oxidation methods. The halogenation itself is usually accomplished with *N*-bromosuccinimide (NBS), a safer and more convenient alternative to Br_2, in what is sometimes known as the Wohl–Ziegler reaction.[53–57] Somewhat unexpectedly, it was found that the bromination of **28** occurred on the ring instead of the benzyl position. The reaction of **28** with 1.1 equivalents of NBS with AIBN as the radical initiator led mainly to one species presumed to be the C5-brominated product, with a small amount of the C7-brominated product (Scheme 2.17).

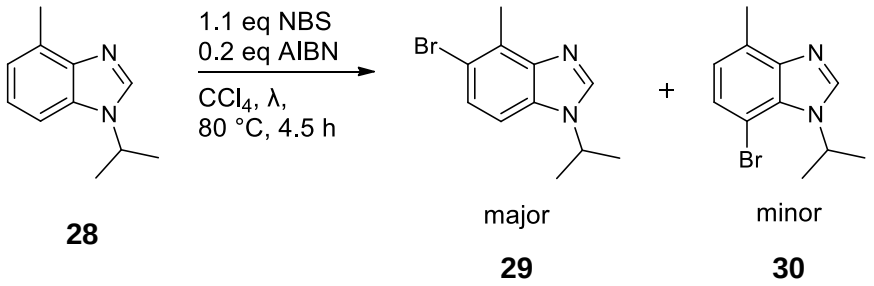

Scheme 2.17 *Ring bromination of benzimidazole **28** on C5 and C7.*

C6 bromination could be ruled out as it would produce two singlets for the phenyl ring protons in the ^{1}H NMR spectrum, as opposed to the two doublets that were observed for each species. This interpretation is also consistent with the tendency for a methyl group to act as an ortho (C5) or para (C7) director. It was presumed that the C5-brominated species is the major product, as the proximity of C7 to the isopropyl group would be less sterically favourable.

Although ring bromination with NBS is certainly not unheard of for benzimidazoles, it tends to occur at the C2 position.[58–60] In this case, the downfield singlets representing the C2 protons in **29** and **30** are still clearly visible in their ^{1}H NMR spectra. Smith and coworkers noted that when two equivalents of NBS are employed for the bromination of benzimidazole in dichloromethane, a second substitution occurs at C5 (after initial substitution at

C2) to give 2,5-dibromobenzimidazole.[59] The regioselectivity of this reaction can be controlled by solvent choice: It is possible to select for the C2-monobrominated product and avoid forming mixtures containing di- or tribrominated benzimidazoles by performing the reaction in THF.[60] When the C2 position is blocked, for example in 2-methylbenzimidazole, the bromination takes place exclusively at C5, affording 5-bromo-2-methylbenzimidazole in excellent yield.[59] There are very few examples of NBS bromination occurring solely on ring positions other than C2 for 1*H*-benzimidazoles. It appears that strongly activating substituents such as hydroxyl[61] or methoxy[62] groups are required to direct the ring bromination away from the C2 position (Scheme 2.18). Alternatively, the use of sulfonic-acid-functionalised silica as a catalyst may also encourage C5-monobromination in benzimidazole.[63]

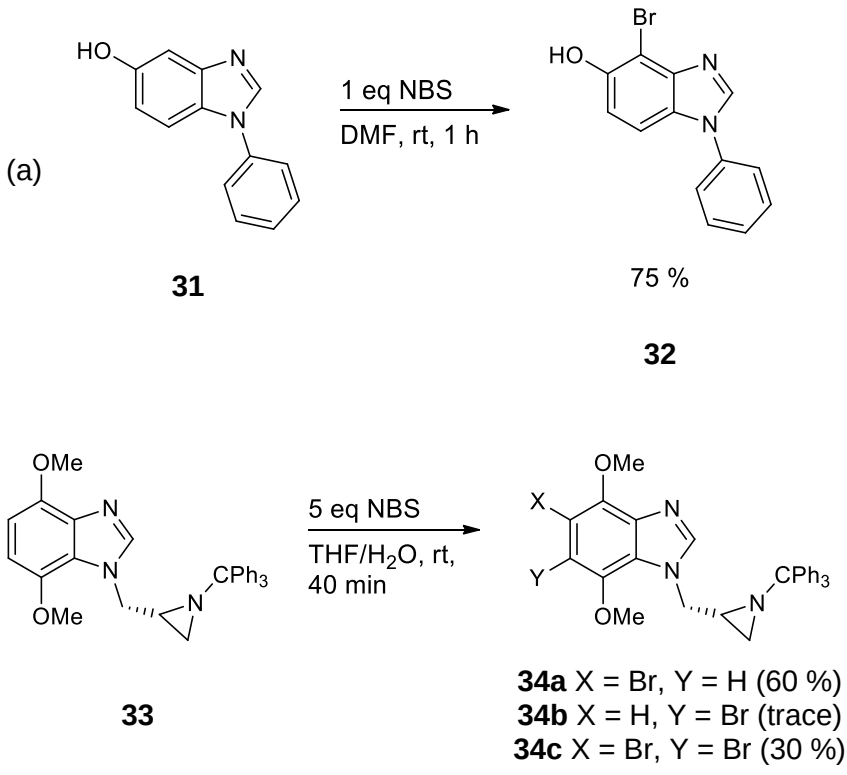

Scheme 2.18 *Ring bromination on 1H-benzimidazoles at positions other than C2 in* ***(a)*** *5-hydroxy-1-phenylbenzimidazole and* ***(b)*** *4,7-dimethoxybenzimidazole* ***33****.*

In any case, it still seemed unlikely that ring bromination would have occurred under the conditions used in this work. The substituents in **28** do not represent strong activators. Furthermore, there is general consensus in the literature that bromination at the benzylic position is favoured when light or a radical initiator such as benzoyl peroxide (BPO) is present.[55,64] It is mystifying that these

strategies proved unsuccessful for **28**, but worked well for the methyl-substituted benzimidazoles **35** and **37**. In those cases, the respective benzyl bromides **36** and **38** were obtained after treatment with NBS and BPO in refluxing CCl_4 (Scheme 2.19).[65,66]

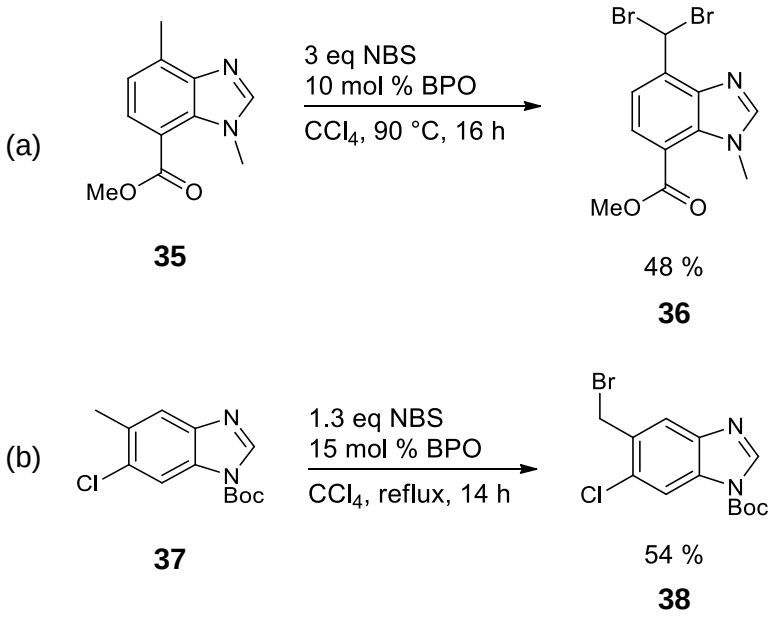

Scheme 2.19 *Regioselective bromination at the benzylic carbon for some methyl-substituted benzimidazoles.*

The use of 1,3-dibromo-5,5-dimethylhydantoin (DBDMH) as an alternative brominating agent to NBS was briefly explored. *N*-Heterocyclic substrates similar to benzimidazole such as pyrroloindoles and acridines have been successfully brominated at ortho-benzylic positions using DBDMH,[67–70] affording higher yields of the desired bromide than NBS in some cases.[71] Heating a solution of **28** with 1 equivalent of DBDMH and 10 mol % of AIBN in CCl_4 for 16 hours led to complete conversion of the starting material. The ^{1}H NMR spectrum of the crude product indicated the presence of two main species in a 2:3 ratio. Partial separation of these products could be achieved by flash chromatography on silica gel, enabling the identification of the major component as the C5-brominated product **29**. The ^{1}H NMR spectrum of the minor component comprises only two singlets in the aromatic region integrating for 1H each, a singlet at 2.66 ppm that was consistent with an intact benzylic CH_3, and two more resonances that were characteristic of the isopropyl group. The simplicity of the aromatic region suggests that bromination had occurred at two positions on the phenyl ring.

Since NBS and DBDMH both resulted in ring bromination, it was suspected that the problem lay with the substrate **28** and not the choice of brominating agent. Venkatraman's use of a *N*-(Boc)benzimidazole[66] (Scheme 2.19 b) prompted consideration of the electronic effects of the N1-substituent on the reactivity of the benzylic site. Perhaps it was also not entirely coincidental that successful brominations using DBDMH involved indoles which bear tosyl[68,69] or carbamate[67,70] *N*-substituents. Thus far, every reaction involving the *N*-isopropylbenzimidazole system has been problematic. In order to disfavour the electrophilic aromatic substitution pathway, it might be necessary to sequester the N1 lone pair with a substituent like the Boc group.

The Boc protection of 4-methylbenzimidazole **27** was easily accomplished with a slight excess of Boc_2O and a catalytic amount of 4-DMAP (Scheme 2.20). *N*-(Boc)-4-methylbenzimidazole **39** was obtained in 95 % yield as an orange oil. The identity of the product was verified by the appearance of a singlet integrating for 9H in the ^{1}H NMR spectrum, which is expected for the carbamate *t*-butyl group. The newly incorporated Boc group also gave rise to a strong carbonyl stretching band at 1746 cm^{-1} in the IR spectrum of **39**.

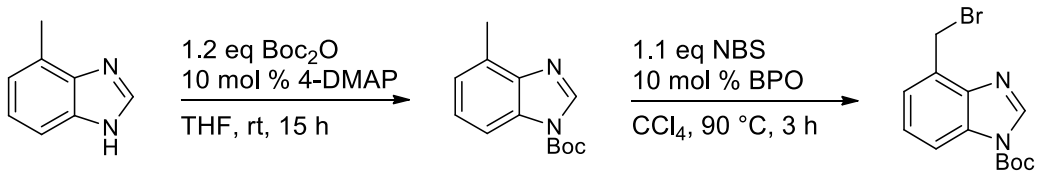

27 **39**, 95 % **40**, 94 %

Scheme 2.20 *Stepwise Boc protection and benzylic bromination of 4-methylbenzimidazole.*

Pleasingly, the results support the earlier hypothesis that benzylic bromination can be promoted by attenuating the N1 lone pair contribution to the ring system. **39** can be transformed into the benzyl bromide **40** in high yield using NBS and 10 mol % of AIBN or benzoyl peroxide (BPO) as the radical initiator (Scheme 2.20). In the ^{1}H NMR spectrum, the singlet at 2.67 ppm is replaced by another singlet integrating for 2H at 4.94 ppm, signifying the change of the methyl group into a methylene bromide.

The few reports which allow the direct comparison of AIBN and BPO as radical initiators generally find that both produce similar yields of the benzyl bromide (likewise observed in the preparation of **40**),[72–74] suggesting that they

could be used interchangeably. Although the literature examples presented here tend to employ BPO as the initiator, the application of AIBN in the same reaction is hardly uncommon.[75–80] In some cases, the use of AIBN enhances chemoselectivity for benzylic over ring bromination.[72] Here, AIBN was chosen for the earlier bromination experiments on the basis that its byproduct, isobutyronitrile might be more easily removed than benzoic acid. However, the bulk of the syntheses in this study later gravitated towards the use of BPO, in favour of its lower cost and wider commercial availability compared to AIBN.

The efficiency of the synthesis of **40** encouraged the exploration of ways to prepare its aldehyde derivative **7a**. As a starting point, **40** was subjected to a Kornblum oxidation[81] by heating to 100 °C in DMSO with a fivefold excess of $NaHCO_3$ for 1.5 hours. TLC analysis showed that all the benzyl bromide had been consumed, and the resulting mixture contained at least three new species that were more polar than the starting material. This inference was corroborated by ^{1}H NMR spectroscopy, in which three or four singlets were found in the >10 ppm region. Together, these observations imply the formation of multiple aldehyde species. The deprotected 4-formylbenzimidazole **7b** could be identified as one of the minor components in the spectrum, but no other component could be isolated in sufficient quantity and purity for unequivocal characterisation.

The pursuit of **7a** resumed with the conversion of the benzyl bromide **40** into the corresponding benzyl alcohol. This was achieved using an adapted literature procedure,[82] whereby **40** is heated to reflux in a dioxane/water mixture for 4 hours with an excess of a carbonate base (Scheme 2.21). $CaCO_3$ and $BaCO_3$ were both equally effective, but the former was preferred for its lower toxicity. Filtration of the carbonate from the reaction mixture and subsequent solvent removal gives **41** as a dark brown resin. Fortuitously, the Boc protecting group was cleaved under these conditions. The resonances for the Boc group were no longer present in the ^{1}H and ^{13}C NMR spectra of **41**. Instead, singlets integrating for 2H and 1H could be seen at 4.86 and 5.23 ppm, corresponding to a methylene and an adjacent hydroxyl group respectively. The hydroxyl resonance conspicuously lacked any correlations in the ^{1}H-^{13}C HSQC spectrum. The detection of a peak at *m/z* = 148 in the mass spectrum supports the formulation of **41**. The $CaCO_3$ hydrolysis method was also superior to another procedure using $NaHCO_3$/acetone/water at 56 °C, which showed little conversion by TLC after 5 hours and resulted in an intractable mixture after 46 hours. It must be noted that **41** cannot be purified by flash chromatography without suffering

significant losses due to its limited solubility and highly polar nature. For this reason, **41** was used directly in the next step.

Fortunately, the oxidation of the alcohol into the aldehyde was met with success on the first attempt. **41** was suspended in CH_2Cl_2 at 0 °C. Triethylamine and an approximately equimolar amount of Dess–Martin periodinane (DMP) were added to the brown mixture and stirred overnight at ambient temperature (Scheme 2.21). Upon aqueous workup, the desired aldehyde **7b** was obtained as an orange solid in 57 % yield over 4 steps from **27**, albeit with minor intractable impurities. A downfield singlet at 10.14 ppm in the ^{1}H NMR spectrum and 192.4 ppm peak in the ^{13}C NMR spectrum could be attributed to the formyl functionality, which also exhibited a strong C=O stretching band at 1682 cm^{-1} in the IR spectrum. As for its mass spectrum, the peak observed at *m/z* = 146 was consistent with the loss of two protons from the parent alcohol **41**.

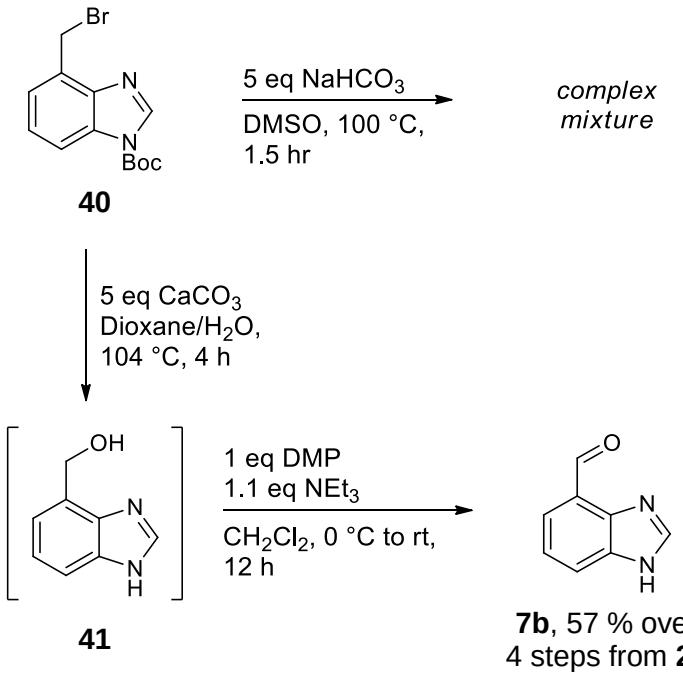

Scheme 2.21 *Stepwise hydrolysis and oxidation of a benzyl bromide provides access to the carbaldehyde **7b** where the Kornblum oxidation fails.*

The compounds **41** and **7b** have been previously prepared via an alternative route.[83] The spectral data presented here is in good agreement with the literature values. Kristensen and coworkers' synthesis of **7b** was achieved in only 8 % yield over 7 steps from 3-nitrophthalic anhydride, with the final two steps involving the $LiAlH_4$ reduction of 4-methyl ester benzimidazole into **41**, which is

then oxidised into **7b** using MnO_2 (Scheme 2.22). The route developed in this study therefore constitutes a higher yielding pathway to **7b** with improved step economy.

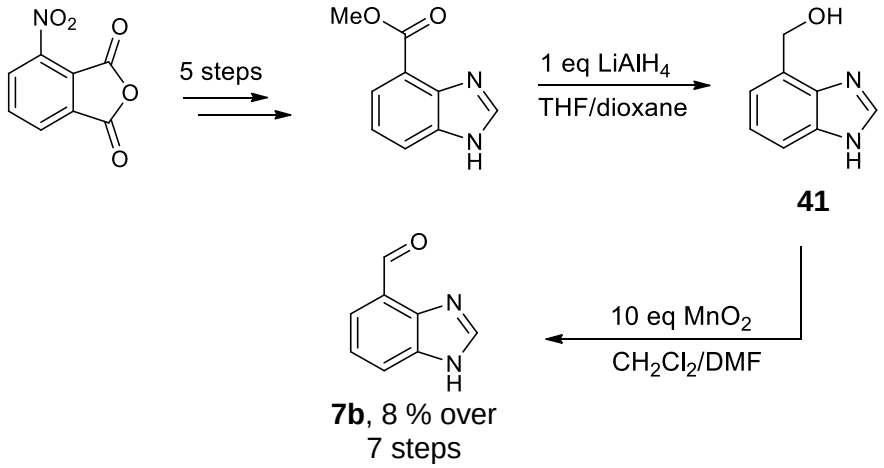

Scheme 2.22 *Kristensen et al.'s alternative synthesis of* ***7b*** *from 3-nitrophthalic anhydride.*[83]

The installation of the C4-formyl group meant that the *N*-Boc substituent had served its purpose. Although unintended, its removal during the hydrolysis step was optimistically regarded as a consolidation of two reaction steps. **7b** could now be *N*-alkylated, but efforts to do so turned out to be problematic (Scheme 2.23). The best results were obtained by subjecting **7b** to the conditions for the *N*-isopropylation of **27**. A crude aliquot of the reaction mixture after 16 hours at 30 °C revealed a 1:1 distribution of **7b** and **42** in its ^{1}H NMR spectrum, judging by the emergence of a second aldehyde singlet at 10.76 ppm, and a septet and doublet for the isopropyl fragment at 4.76 and 1.70 ppm respectively. Despite prolonging the reaction for another 21 hours at 60 °C with an additional 2.4 equivalents of isopropyl bromide, the maximum conversion observed by ^{1}H NMR spectroscopy was around 70 %. Performing the reaction in THF did not result in visible formation of *N*-isopropylated products, although a number of unidentified byproducts were observed at elevated temperatures. The formation of multiple side products was rampant in acetonitrile, even at room temperature. The base-induced β-elimination of isopropyl bromide was briefly contemplated as the cause for low yields of the alkylated product. However, conducting the isopropylation with a milder base, K_2CO_3 in acetonitrile at room temperature led only to the recovery of starting material. Switching to a less sterically demanding primary alkyl halide facilitated the *N*-alkylation of the benzimidazole. The reaction of **7b** with 1.2 equivalents of NaH and methyl iodide in THF showed

high conversion into the *N*-methylated product **7c** by ^{1}H NMR. However, it was difficult to separate **7c** from the contaminants that were present in the starting material.

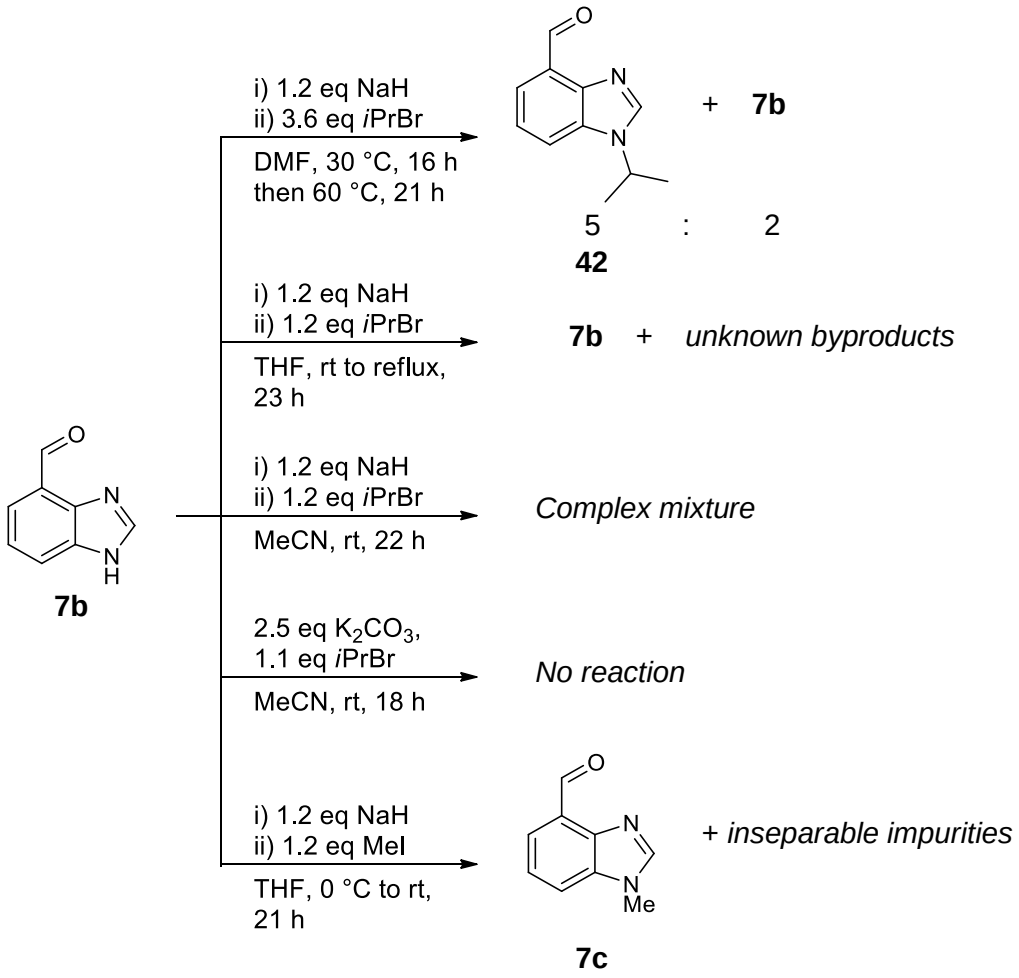

Scheme 2.23 *Various conditions employing different solvents, bases and electrophiles for the attempted N-alkylation of 4-formylbenzimidazole **7b**.*

Recalling the ease with which a Boc protecting group could be attached to **27**, it was wondered if the same could be done for **7b**. The *t*-butyl portion of the Boc group could facilitate purification by reducing the overall polarity of the molecule and improving its solubility in less polar solvents. Treatment of **7b** with Boc_2O and a catalytic amount of 4-DMAP in THF resulted in full conversion to the *N*-Boc aldehyde **7a**. Purified yields of **7a** ranged between 5 to 18 %, which may suggest some degree of decomposition of silica during flash chromatography. Nevertheless, the impurities associated with **7b** were much easier to separate from **7a**, and the quality of the product was most satisfactory. All existing

resonances in the ^{1}H NMR spectrum experienced a downfield shift following the introduction of the Boc group, most notably the singlet for the aldehyde proton, which now appeared at 10.83 ppm instead of 10.14 ppm. The new singlet at 1.72 ppm integrating for 9H betrayed the presence of the Boc *t*-butyl group. Two C=O stretching frequencies were seen in the IR spectrum at 1690 and 1748 cm^{-1}, corresponding to the aldehyde and carbamate functional groups respectively. Finally, the *m/z* = 269 peak in the ESI-MS spectrum was consistent with the sodium adduct of **7a**.

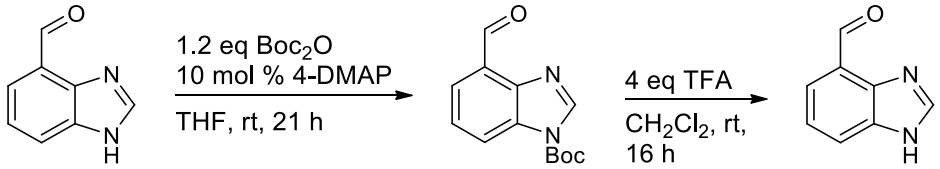

7b **7a**, 15 % **7b**, 65 %

Scheme 2.24 *Reversible Boc protection of 4-formylbenzimidazole* ***7b****.*

7a could be deprotected with excess trifluoroacetic acid (TFA) to regenerate **7b** in 65 % yield after a basic aqueous workup (Scheme 2.24). Samples of **7b** isolated via this protection/deprotection sequence are considerably cleaner than **7b** produced from the oxidation of **41**. Purer samples of **7b** could be efficiently methylated using the method described in Scheme 2.23, affording pure **7c** in 92 % yield without requiring any purification beyond an aqueous wash. It is important not to exceed the prescribed stoichiometry of NaH and methyl iodide, as **7c** will apparently undergo a second alkylation at the C2 position and simultaneous reduction of the aldehyde. The identity of this secondary reaction product was surmised from its ^{1}H NMR spectrum in which one of the aromatic proton signals are missing, but there are two new singlets at 3.51 and 3.86 ppm, each integrating for 3H. A logical assumption is that the two most acidic sites (N1 and C2) were deprotonated and then methylated. The conversion of the aldehyde group into the alcohol was deduced from the substitution of the downfield aldehyde peak with a singlet integrating for 2H at 4.98 ppm, which most likely represents the C*H*$_2$OH protons. Hydride reductions of carbonyl compounds[84] are very seldom accomplished using alkali metal hydrides such as NaH,[85] which is almost exclusively used as a strong Brønsted base for deprotonation. Recently, Chiba and coworkers made the astonishing discovery that NaH can act as a nucleophilic hydride transfer agent when used in conjunction with NaI.[86] It is believed that NaI activates the intrinsic hydride donor

capability of NaH by disrupting its ordered crystalline structure.[87] The NaH/NaI composite is particularly effective for reductive decyanations, but can also reduce polar π electrophiles such as amides, imines and aldehydes. Thus, it was reasoned that cooperative reactivity between excess NaH and NaI, a byproduct of methylation, may be responsible for the formation of the alcohol from **7c**.

The successful preparation of the various *N*-alkylated 4-formylbenzimidazoles **42**, **7a** and **7c** from **5** was a major coup which became the launch pad for the synthesis of the target diimine ligands. However, the low and erratic overall yields, subpar purity of the intermediates and tedious cycles of protection/deprotection meant that this route would be impractical in the long term, when scale-up becomes necessary. The eventual development of a more efficient route for the multigram synthesis of **7c** from the ester-substituted nitroaniline precursor **6** is discussed in the subsequent section.

2.2.3 Routes from methyl 2-amino-3-nitrobenzoate 6

The efficiency and reliability of the synthesis of **7c** from **6** offset the fact that **6** was more expensive than compound **5**. This is apparent from the very first step of the synthetic sequence. The iron-mediated reductive cyclisation of **6** enabled rapid access to **43** via a published one-pot procedure, which employed formic acid as the C2 carbon source and NH_4Cl as a reaction promoter (Scheme 2.25).[88] The NMR and MS spectra of the product are in excellent agreement with previously reported data.[83,88] Subsequent methylation of **43** with NaH and methyl iodide furnished **44** in quantitative yield. In place of the broad singlet at 12.56 ppm for the imidazole N*H*, there was a new singlet at 3.89 ppm which integrated for the three NCH_3 protons in the ^{1}H NMR spectrum of **44**. A mass increase consistent with one methyl group was also recorded by ESI-MS.

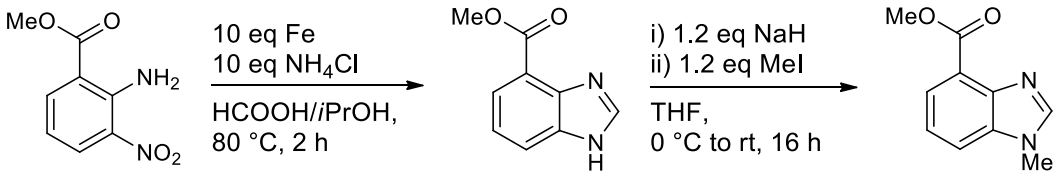

6 **43**, 94 % **44**, >99 %

Scheme 2.25 *Benzimidazole formation by reductive cyclisation of an ortho-nitroaniline and subsequent N-methylation.*

Next, the methyl ester was reduced into the alcohol using $LiAlH_4$ (Scheme 2.26). In accordance with expectations, the OCH_3 singlet is absent from the ^{1}H NMR

spectrum of **45**. The resonances for the CH_2 and O*H* protons are located at 4.92 and 5.13 ppm respectively. While **44** exhibits a strong IR absorption at 1710 cm^{-1} related to the ester carbonyl, **45** has instead a broad band at 3253 cm^{-1} signalling the presence of the hydroxyl group.

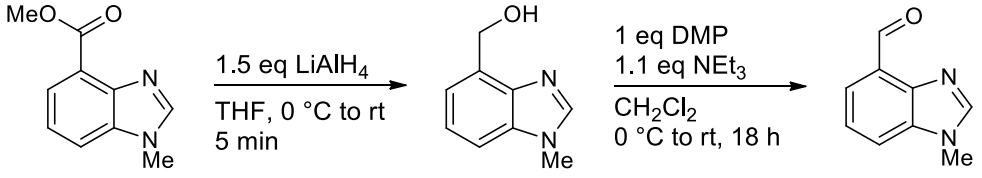

44 **45**, 90 % **7c**, 86 %

Scheme 2.26 *Hydride reduction of the methyl ester and oxidation of the resulting alcohol into an aldehyde.*

The DMP oxidation method used to prepare **7b** was just as effective for its *N*-methylated analogue, **7c**. Yields of **7c** consistently exceeded 80 %. Naturally, the ^{1}H NMR spectra of **7b** and **7c** are very similar, differing mainly by the additional singlet integrating for 3H at 3.97 ppm for the *N*-methyl protons. After an aqueous workup to remove the iodine-containing byproducts, **7c** was obtained as a solid which can vary in colour from orange to brown. The product usually appeared sufficiently pure by NMR spectroscopy, and was used directly for imine condensation without additional purification. **7c** can be recrystallised by slow evaporation from dichloromethane to give brown prisms suitable for X-ray diffraction. The molecular structure of **7c** is shown in Figure 2.3.

7c crystallises in the *C*2/*c* space group. One complete molecule of **7c** is the sole occupant of the asymmetric unit. Since all the atoms but C1 are sp^2 hybridised, the molecule is perfectly planar. Crystal packing does not seem to be influenced by significant π-stacking or hydrogen bonding interactions.

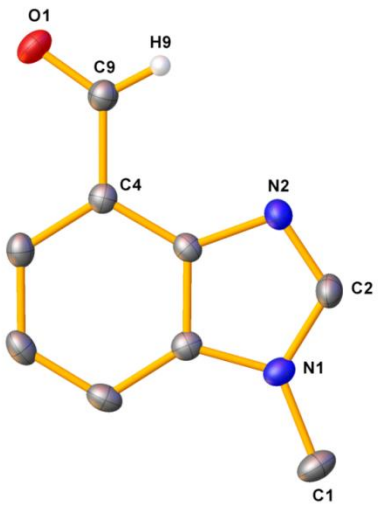

Figure 2.3 *Molecular structure of N-methyl-4-formylbenzimidazole,* ***7c****. Thermal ellipsoids are shown at the 50 % probability level. Aryl and methyl hydrogens are omitted for clarity. Selected bond lengths (Å) and angles (°): N1-C2 1.358(2), N2-C2 1.314(2), N1-C1 1.450(2), O1-C9 1.217(2), N1-C2-N2 114.40(14), O1-C9-H9 117.43(9).*

Previous experience with alkylating **7b** suggested that a methyl group would be the easiest to install. At this juncture, it would be premature to say whether the methyl substituent would be a boon or bane to the isolation of a free NM,NR NHC. Thus, there was not yet an overwhelming imperative to prepare analogues of **7** with bulkier *N*-substituents. Preliminary attempts to perform *N*-substitution with secondary or tertiary alkyl halides such as bromocyclohexane and 1-bromoadamantane were problematic, and seemed likely to require substantial optimisation to produce usable quantities of product. More promising results were obtained from transition metal-catalysed *N*-arylation. Buchwald and colleagues developed a method for the C–N coupling of 5-iodo-*m*-xylene and benzimidazole using a copper(I) catalyst that provided the arylated product in 91 % yield.[89] In this work, the same method was applied to **43**. After 23 hours, TLC analysis of the reaction mixture in 1:1 ethyl acetate/hexanes revealed the presence of two major species with R_f 0.1 and R_f 0.3 respectively (Scheme 2.27). These were separated by flash chromatography on silica gel. It should be noted that isolated yields were low (R_f 0.1 = 9 %; R_f 0.3 = 4 %), and the reaction was not optimised. Fortunately, there was sufficient product mass for NMR spectroscopy. The spectra of both fractions featured the same number and pattern of resonances, but could be distinguished based on subtle differences in the chemical shift. Two additional resonances between 7 – 7.2 ppm and one

more around 2.4 ppm consistent with a *m*-xylene substituent were found in each spectrum. This suggested that the *N*-arylation was not regioselective, and the two products were the N1- and N3-arylated species **46** and **47** respectively. It was not possible to identify which isomer was which based on NMR spectroscopy data alone, and single crystals of either isomer could not be obtained. It is curious that N3-arylation occurred despite the steric hindrance posed by the C4 methyl ester substituent, when the less bulky methyl or formyl substituents were sufficient to ensure exclusive N1 alkylation for **27** and **7b**. It is possible that one of the ester O atoms and the N3 atom form a favourable two-point interaction with the copper(I) centre that facilitates subsequent alkylation at N3 to give **47**.

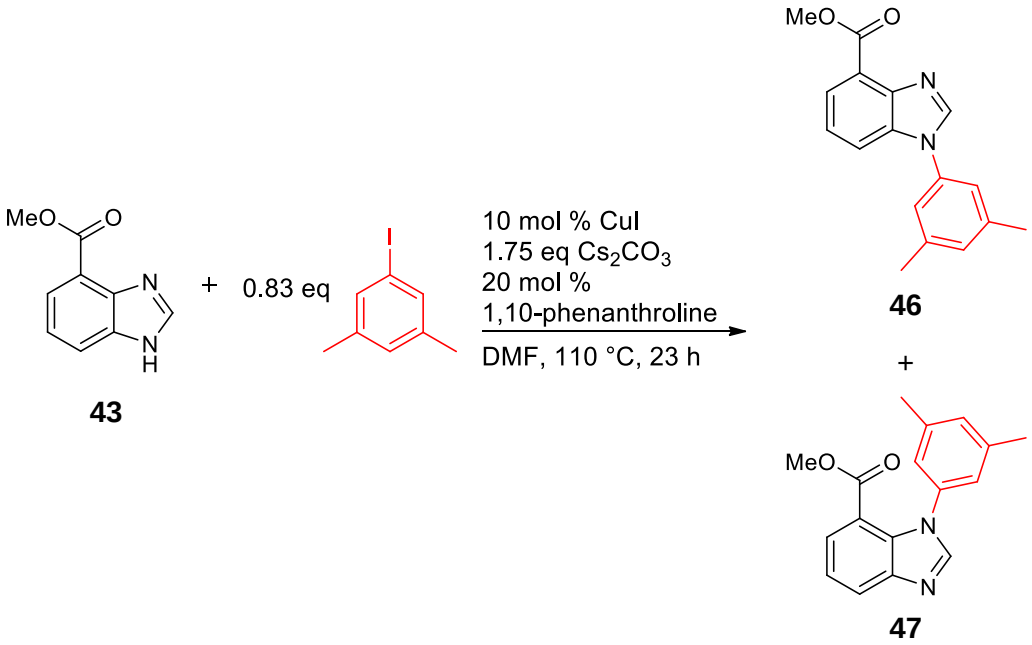

Scheme 2.27 *Non-regioselective copper(I)-catalysed N-xylenation of 4-methyl ester benzimidazole.*

2.2.4 Condensation reactions of 7 with *o*-phenylenediamine

Imine synthesis involving the condensation of an aldehyde to a primary amine is usually straightforward,[90] and it was anticipated that the general methods for preparing salophen ligands[91–95] would be applicable to the synthesis of MeRLH$_2$.

Surprisingly, the reaction mixtures from the condensation of *o*-phenylenediamine with **7a** in THF at reflux produced ^{1}H NMR spectra that were more complex than expected (Scheme 2.28). The desired C_2-symmetric diimine **48** should only have 8 unique resonances which integrate for a total of 14H, but the spectra obtained

featured many more. The tendency of the compounds to streak on TLC plates made it difficult to gauge how many species were present, and attempts to fractionate the mixture by flash chromatography were unsuccessful. Nonetheless, the NMR spectrum was not completely inscrutable. It was plain that both starting materials had been consumed in their entirety, for none of their signals remained. Aldimine protons typically give rise to distinctive singlets above 9 ppm in ^{1}H NMR spectroscopy, but no signals were observed past 8.6 ppm. This suggested that the product(s) did not possess aldimine functionalities. The reaction outcome was unaltered in ethanol, whether the reaction was conducted at room temperature, or at reflux with excess **7a** and piperidine as a co-solvent. The addition of molecular sieves and/or an acid catalyst such as *p*-toluenesulfonic acid still led to the same products.

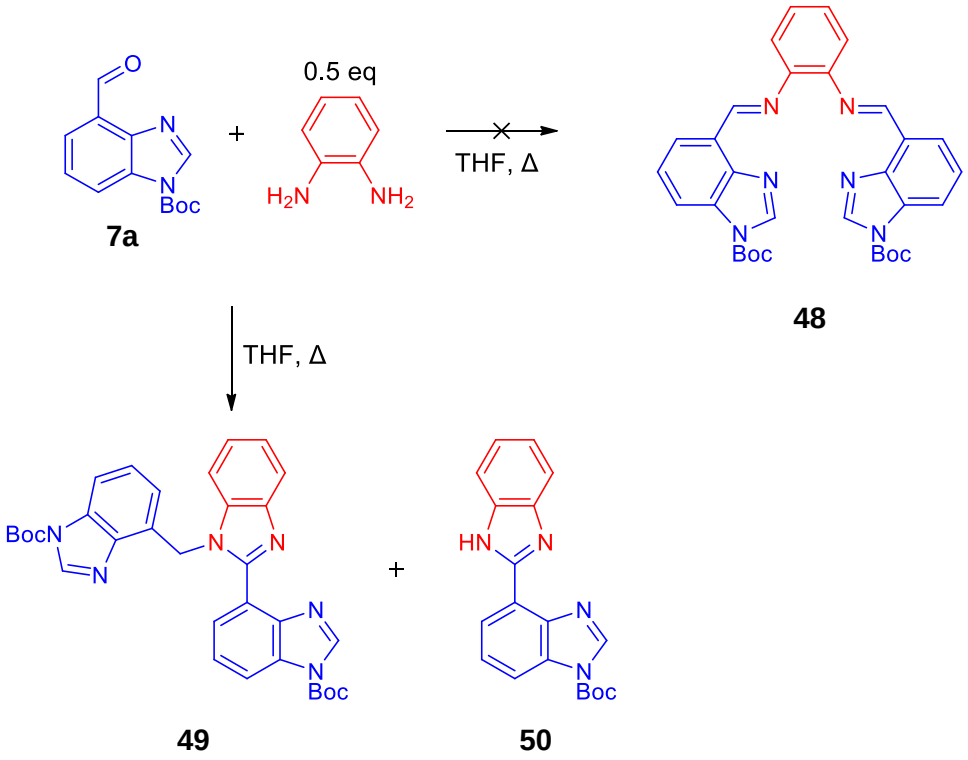

Scheme 2.28 *Cyclocondensation of aldehyde* ***7a*** *and o-phenylenediamine into 1,2-disubstituted and 2-substituted benzimidazoles*.

Fortunately, the minor product **50** would precipitate from the reaction mixture as an off-white solid that was pure by NMR spectroscopy. Its identification was instrumental in unravelling the chemistry at play. **50** exhibited one more resonance in the aromatic region of the ^{1}H NMR spectrum than would be expected for diimine **48**, which should only have seven. It was initially bewildering to learn that this product produced an ESI-MS peak at *m*/*z* = 335,

which would have been consistent with the [1:1 monoimine product + H]$^+$, yet the ^{1}H NMR spectrum did not exhibit any peaks that could be attributed to amino protons.

Single crystals of this product were grown by vapour diffusion of diethyl ether into a dichloromethane solution, enabling structural verification by SC-XRD. The data solved for the 2-substituted benzimidazolium salt **50**•HBr (Figure 2.4). Attempts to model the bromide ion as water, or chloride or iodide ions resulted in inflation of the R1 factor. The source of the bromide is unknown, and it is doubtful that any residual bromide from the NBS bromination would have been carried through so many synthetic steps. Nevertheless, it brought to attention the cyclisation reaction that was taking place, and provided guidance towards the conclusion that the other species present was the 1,2-substituted benzimidazole **49**.

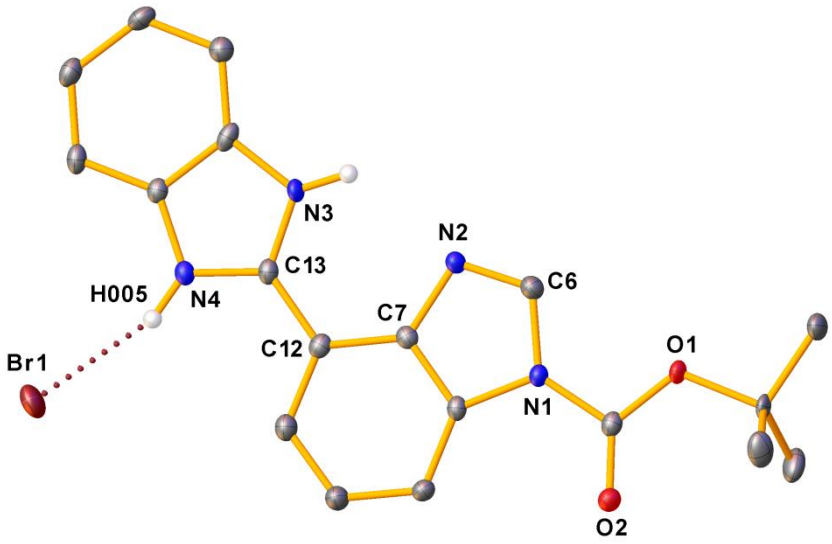

Figure 2.4 *Molecular structure of the 2-substituted benzimidazolium salt,* ***50****•HBr. Thermal ellipsoids are drawn at the 50 % probability level, and C-bound hydrogens are omitted for clarity. Selected bond distances (Å) and angles (°): N1–C6 1.393(3), N2–C6 1.296(3), N3–C13 1.344(3), N4–C13 1.341(3), C12–C13 1.451(3), Br1···H005 2.299(2), N3–C13–C12–C7 −0.5(3).*

The ^{1}H and ^{13}C NMR spectra for **50** wholly support the proposed structure. Notable features include the broad singlet at 14.07 ppm for the benzimidazole N*H*, and the relative integration of 8H:9H for the aromatic and *t*-butyl protons respectively. The most downfield peak in the ^{13}C NMR spectrum belongs to the

Boc carbonyl C and lies at 146.9 ppm, below the usual >160 ppm range for imine carbons. Isolated yields of **50** were low in the absence of any catalyst (3 – 17 %), but could be increased to 49 – 57 % when *p*-toluenesulfonic acid was added.

The tris(benzimidazole) **49** had no magnetic symmetry, and so exhibited 15 unique resonances in the ^{1}H NMR spectrum. Specific assignments for **49** were difficult to make because it defied isolation in its pure form; the chemical shifts of each resonance appeared to be sensitive to small changes in concentration or the presence of other species such as **50**, and tended to vary from sample to sample. Its most revealing spectral feature was the singlet around 6 ppm, which integrated for 2H and belonged to the NCH_2C protons. A correlation between this signal and a peak at 44 ppm in the ^{13}C NMR spectrum was detected using ^{1}H-^{13}C HSQC spectroscopy. Its molecular weight was verified by ESI-MS, in which the expected $[M+H]^+$ ion peak was found at *m/z* = 565.2.

Cyclisation is not an unusual result of condensations involving *o*-phenylenediamine. This tendency is often exploited in the construction of 1,2-disubstituted benzimidazoles,[96–98] and the competing mechanisms by which 1,2-disubstituted or 2-monosubstituted benzimidazoles are formed have been extensively probed.[97,99] The St. Clair Black group encountered the same setback while attempting to prepare an analogous diimine from 4,6-dimethoxy-7-formylindole and *o*-phenylenediamine, but could only obtain it as a metal complex through metal-templated condensation.[100] The higher degree of aromaticity in polybenzimidazoles **49** and **50** is probably a driving force for the cyclisation of *o*-phenylenediamine with aldehyde **7a** as the C2 carbon source. Curiously, benzimidazole formation is much less prevalent in the synthesis of salophen ligands, which have to be heated for cyclisation to occur.[101,102] As cyclisation appeared to be unavoidable with the present system, the phenylene-bridged ligand was never prepared in its free form. Instead, it was synthesised directly as its metal complex through metal-templated condensation. This will be discussed in greater detail in Chapter 3.

2.2.5 Condensation reactions of 7 with alkyldiamines

The formation of an aromatic benzimidazole ring is presumably the main thermodynamic incentive for cyclocondensation, aided by the restricted conformation of the phenylenediamine. It was reasoned that if this is not possible

and/or entropically unfavourable, for instance in the case of an aliphatic diamine, the desired diimine could be obtained instead. This prediction turned out to be correct, as the reactions of ethylenediamine with **7a** or **7c** in ethanol both yielded the respective diimines (Scheme 2.29).

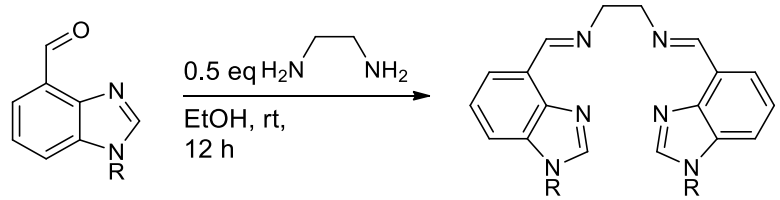

7a R = Boc
7c R = Me

51a R = Boc, 29 %
51b R = Me, 51 %

Scheme 2.29 *Synthesis of the ethylene-linked bis(benzimidazole) ligands.*

The NMR spectra of **51a**,**b** shared many similarities, and thus will be discussed jointly. Only 7 resonances were observed, confirming that the diimines have C_2 symmetry. The chemical shifts were unremarkable. The H_{imine} resonance was easily identified as the singlet residing farthest downfield, between 9.1 – 9.2 ppm. The peak at 158 ppm in the ^{13}C NMR spectrum was assigned to the imine carbon based on 2D NMR spectroscopy, as it demonstrated a multi-bond correlation to the ethylene CH_2 peak around 4 ppm. The relevant ion peaks at *m/z* = 517 $[M+H]^+$ and 344 $[M]^+$ were found in the mass spectrum of **51a** and **51b** respectively.

51b can be conveniently purified by recrystallisation from methanol/hexanes to give pale pink needles for which satisfactory elemental analysis was obtained. SC-XRD analysis of these needles validated the proposed structure (Figure 2.5). **51b** crystallised the $P4_2/n$ space group. The asymmetric unit consisted of one methanol solvent molecule and half the ligand, with the other half generated by symmetry. A hydrogen bonding interaction was detected between the hydroxyl group of the methanol and the unsubstituted benzimidazole nitrogen, with a contact distance of 1.84(2) Å. The flexibility of the ethylene bridge allowed the benzimidazole arms to be oriented facing away from each other. Due to the natural bend along the N3–C10–C10'–N3' bonds, the benzimidazoles were not coplanar with each other, but lay on parallel planes similar to a steps on a staircase. The shortest intermolecular centroid-to-centroid distances for the phenyl rings was 4.3630(9) Å, suggesting that π-stacking did not play a significant role in crystal packing.

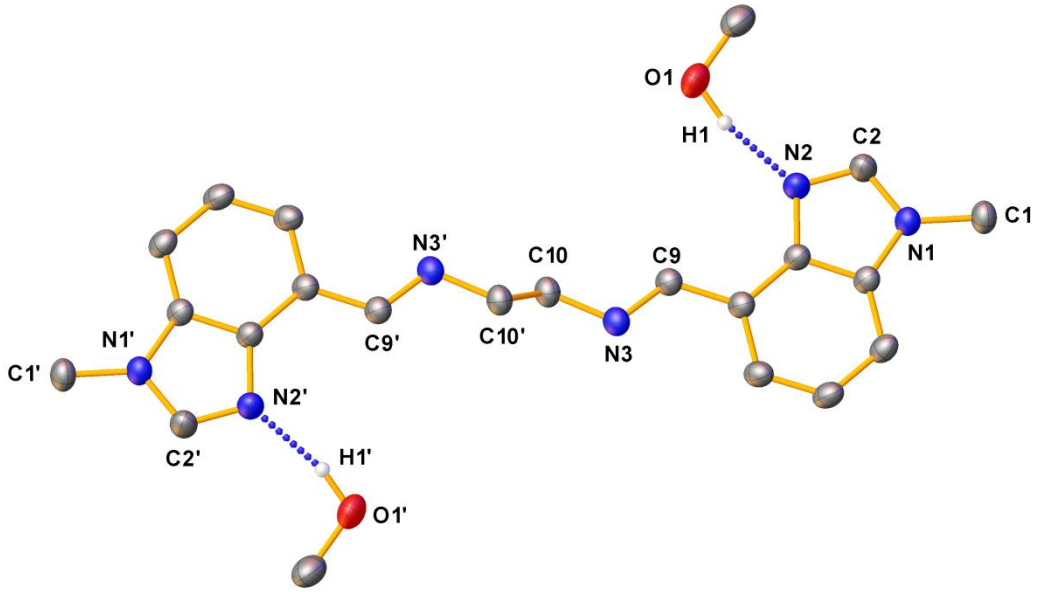

Figure 2.5 *Molecular structure of* ***51b****. Thermal ellipsoids are shown at the 50 % probability level. All C-bound hydrogens are omitted for clarity. Selected bond lengths (Å) and angles (°): N1-C2 1.3575(13), N2-C2 1.3228(14), N3-C9 1.2739(13), N3 C10 1.4620(13), C10-C10' 1.528(2), N2-H1 1.84(2), N2-C2-N1 113.92(9), C2-N2-C3 104.38(8), C2-N1-C4 106.58(8), C10-N3-C9 116.86(9).*

The ethylene bridge in **51a**,**b** should be capable of free rotation, as indicated by the equivalence of all the NCH_2 protons in the ^{1}H NMR spectrum. In contrast, a phenylene bridge should force the imine donors into fixed, relatively coplanar positions. The structure of the ligand could be fine-tuned by installing a cyclic aliphatic bridge such as a cyclohexyl group between the imines. This would endow the ligand with the rigidity of the phenylene linker, while retaining a slight backbone twist that is characteristic of the ethylene chain. The cyclohexyl group also adds a chiral element to the ligand, which is effectively the backbone-saturated analogue of **48**.

The condensation of **7c** and (1*R*,2*R*)-(−)-1,2-diaminocyclohexane was less straightforward, owing to challenges associated with purification. The reaction was performed under the same conditions used for **51a**,**b** (Scheme 2.30).

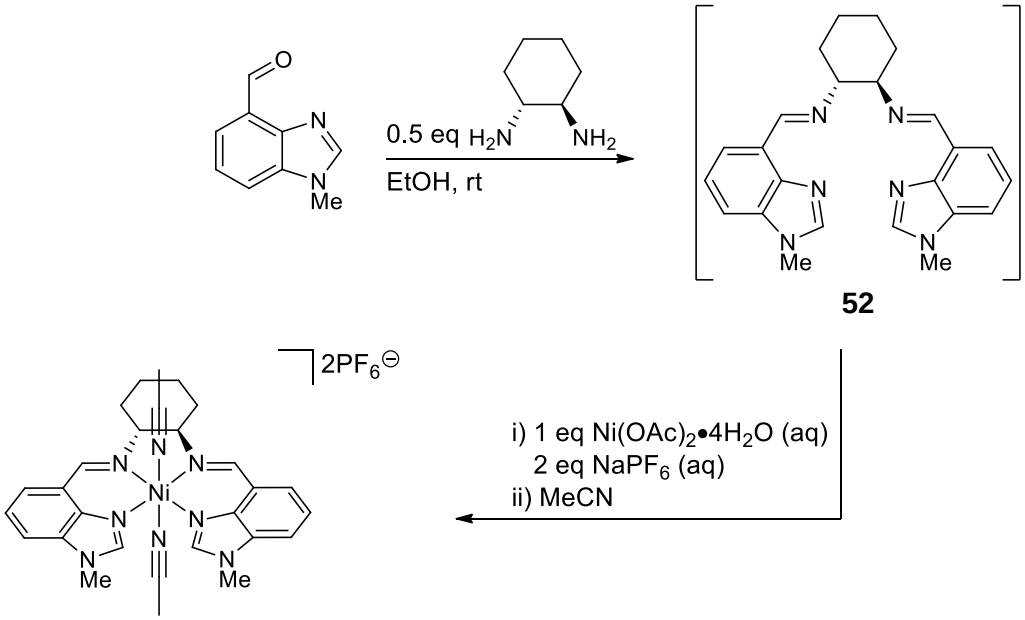

Scheme 2.30 *In situ generation of the cyclohexyl-bridged bis(benzimidazole) ligand* ***52*** *and isolation as a nickel(II) complex.*

After 40 minutes at room temperature, the ^{1}H NMR spectrum of the crude reaction mixture showed promising signs of the expected diimine **52** as the major product, with no trace of aldehyde remaining. Based on the number of resonances observed, the cyclic bridge did not desymmetrise the diimine. The presumed imine H resonance was a singlet at 8.96 ppm. A minor species suspected to be the 1:1 imine condensation is also present. Indeed, adding more **7c** to the NMR sample resulted in a decrease in the intensity of the presumed monoimine signals. EI-MS of the crude mixture failed to detect ion peaks for either the mono- or diimine products, possibly due to extensive fragmentation. However, **52** could be isolated as its nickel(II) complex by treatment with $Ni(OAc)_2•4H_2O$ and 2 equivalents of $NaPF_6$. The structure of the complex was verified by SC-XRD, providing indirect evidence for the successful formation of **52**. Since it was much easier to purify the complex than the free ligand, efforts to isolate the latter were discontinued in favour of a simultaneous condensation/complexation strategy, which will be elaborated upon in the subsequent chapter.

2.3 Conclusion

Based on a modular design concept, a diimine bis(benzimidazole) ligand was established as the synthetic target. The benzimidazole units constitute the carbene precursors, while the imine chelate donors and symmetric design are intended to prevent dimerisation of the carbenes by saturating the metal coordination sphere. Two scalable routes towards the key 1-methyl-4-formylbenzimidazole intermediate were developed from the commercially available substrates 2-amino-3-nitrotoluene and methyl 2-amino-3-nitrobenzoate. The latter route was found to be more efficient. Condensation of the aldehyde with *o*-phenylenediamine generally led to a 1,2-disubstituted benzimidazole with small amounts of a 2-monosubstituted benzimidazole. Cyclisation did not occur with aliphatic amines such as ethylenediamine and (1*R*,2*R*)-(−)-1,2-diaminocyclohexane, which reacted with the aldehyde to afford the desired diimine ligands. The following scheme illustrates the most efficient overall synthesis of the ethylene-linked *N*-methyl bis(benzimidazole) ligand.

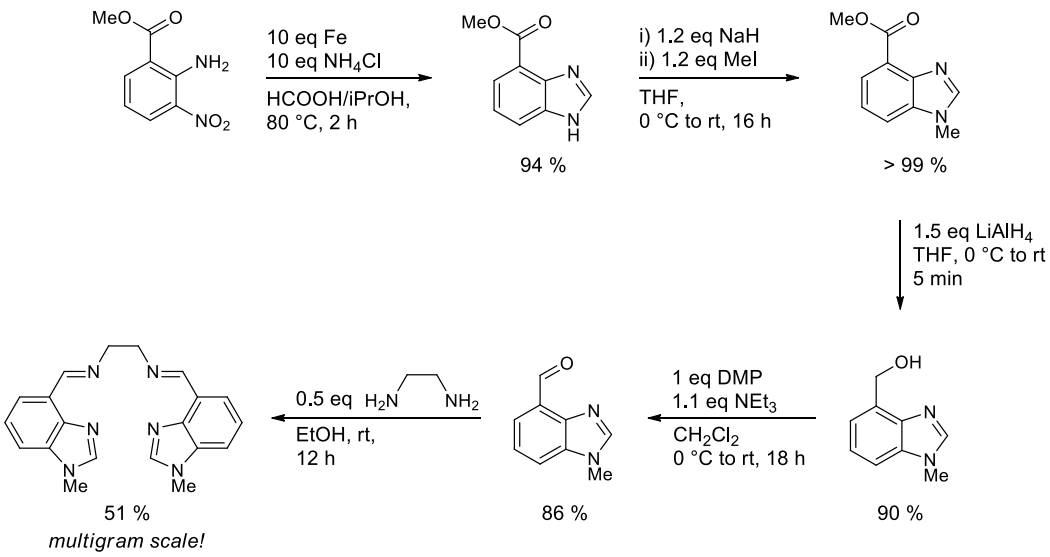

2.4 Experimental

2-Amino-3-nitrophenyl *tert*-butyl carbonate (10)

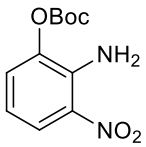

Boc anhydride (0.160 g, 0.733 mmol), 4-dimethylaminopyridine (0.003 g, 0.027 mmol) and 2-amino-3-nitrophenol (0.105 g, 0.680 mmol) were dissolved in THF (3 mL). After stirring at room temperature for 2 h, the solution was reduced to dryness to give a bright red oil. Purification by flash chromatography on silica gel eluting with 20 % ethyl acetate in hexanes afforded **10** as a yellow oil (0.140 g, 0.551 mmol, 81 % yield).

^{1}H NMR (400 MHz, $CDCl_3$): δ 8.02 (dd, *J* = 8.8, 1.2 Hz, 1H, CH_{Ar}), 7.37 (dd, *J* = 7.8, 1.1 Hz, 1H, CH_{Ar}), 6.69 (t, *J* = 8.3 Hz, 1H, CH_{Ar}), 6.20 (br s, 2H, NH_2), 1.57 (s, 9H, C(CH_3)$_3$).

^{13}C NMR (100 MHz, $CDCl_3$): δ 150.7 (*C*=O), 139.4 (C_{Ar}), 138.1 (C_{Ar}), 133.2 (C_{Ar}), 127.6 (CH_{Ar}), 123.3 (CH_{Ar}), 114.8 (CH_{Ar}), 85.0 ($C(CH_3)_3$), 27.6 ($C(CH_3)_3$).

IR (KBr, thin film) $\tilde{\nu}_{max}$ (cm^{-1}): 3502, 3388, 2981, 2358, 1765 (s), 1628 (s), 1580, 1528 (s), 1452, 1395, 1371, 1329, 1269, 1253, 1200, 1140 (s), 1047 (w), 904, 871, 845, 809, 799, 779, 737, 668.

HRMS–ESI (*m/z*): $[M + Na]^+$ calcd for $C_{11}H_{14}N_2O_5Na$, 277.0801; found, 277.0801.

2,3-Diaminophenol (20)

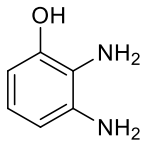

In a Schlenk flask, $Pd(dba)_2$ (0.022 g, 0.037 mmol) was suspended in a methanol (7 mL) solution of 2-amino-3-nitrophenol (0.102 g, 0.663 mmol). The flask was partially evacuated and backfilled with hydrogen gas. After stirring at room temperature for 16 hours, the red solution turned a clear, pale pinkish brown colour, which gradually turned dark brown upon exposure to air. The

reaction mixture was filtered through a Celite pad and reduced to dryness to give a dark grey-brown crystalline solid (0.087 g, >99 % yield), which was used in subsequent transformations without further purification. The spectral properties of **20** were in reasonable agreement with previously reported values.[30]

^{1}H NMR (400 MHz, $(CD_3)_2SO$): δ 8.71 (s, 1H), 6.25 (t, J = 7.93 Hz, 1H), 6.11 – 6.08 (m, 2H), 4.11 (br s, 4H).

***N*,*N*-Di-Boc-2-nitro-5-methylaniline (22)**

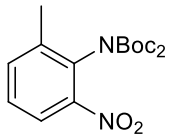

Compound **22** was prepared using a method previously described in the literature.[44] 2-amino-3-nitrotoluene (1.00 g, 6.57 mmol), 4-dimethylaminopyridine (0.0857 g, 0.701 mmol) and Boc anhydride (4.30 g, 19.7 mmol) were dissolved in THF (50 mL) in a pressure tube, The clear yellow solution was stirred magnetically at 70 °C for 21 h. The clear orange solution was reduced to dryness. The resulting orange oil was taken up in ethyl acetate (50 mL), and washed with 0.5 M HCl (50 mL). The aqueous layer was extracted once with ethyl acetate (25 mL). The combined organic fractions were washed with brine (50 mL), dried over sodium sulfate, filtered and concentrated to afford **22** as a yellow oil from which large colourless crystals would slowly form upon standing (2.66 g, >99 % yield).

^{1}H NMR (400 MHz, $CDCl_3$): δ 7.81 (d, *J* = 8.1 Hz, 1H, C*H*$_{Ar}$), 7.48 (d, *J* = 7.4 Hz, 1H, C*H*$_{Ar}$), 7.34 (t, *J* = 7.9 Hz, 1H, C*H*$_{Ar}$), 2.27 (s, 3H, C*H*$_3$), 1.34 (s, 9H, C(C*H*$_3$)$_3$).

^{13}C NMR (100 MHz, $CDCl_3$): δ 149.8 (N*C*=O), 146.4 (*C*$_{Ar}$), 138.9 (*C*$_{Ar}$), 135.1 (*C*H$_{Ar}$), 131.8 (*C*$_{Ar}$), 128.2 (*C*H$_{Ar}$), 122.6 (*C*H$_{Ar}$), 83.3 (*C*(CH$_3$)$_3$), 27.7 (C(*C*H$_3$)$_3$), 17.6 (Ar-*C*H$_3$).

IR (solid) $\tilde{\nu}_{max}$ (cm^{-1}): 2984 (w), 1790, 1751, 1723, 1528, 1458 (w), 1393 (w), 1370, 1355, 1319, 1278, 1252, 1244, 1153,1120 (s), 1093 (s), 1006, 875, 849, 812, 803, 778, 751, 668.

HRMS–ESI (*m/z*): $[M + Na]^+$ calcd for $C_{17}H_{24}N_2O_6Na$, 375.1532; found, 375.1520.

mp: 72 – 75 ˚C

Crystal data: $C_{17}H_{24}N_2O_6$, M = 352.39, monoclinic, a = 23.1677(5), b = 16.0033(4), c = 15.6451(4) Å, α = 90, β = 103.7190(10), γ = 90 °, U = 5635.1(2) Å^3, T = 135.15 K, space group $P2_1/c$ (no. 14), Z = 12, 103112 reflections measured, 11126 unique (R_{int} = 0.0305), 10331 > 4σ(F), R = 0.0364 (observed), R_w = 0.0950 (all data).

4-Methylbenzimidazole (27)

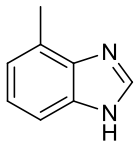

STEP 1 | **2,3-Diaminotoluene (26):** A Parr reactor vessel equipped with mechanical stirrer was charged with 2-amino-3-nitrotoluene (5.01 g, 32.9 mmol), $Pd(dba)_2$ (0.0916 g, 0.159 mmol) and methanol (75 mL). The vessel was pressurised with hydrogen gas (110 psi). After stirring at room temperature for 16 h, the brown solution was filtered through a Celite pad. The volatiles were removed under reduced pressure to give a dark brown solid. Yield = 4.16 g. This compound was used in the next step without further purification. The ^{1}H NMR spectrum of **26** was consistent with the published data.[103]

^{1}H NMR (400 MHz, $CDCl_3$): δ 6.66 – 6.62 (m, 3H, CH_{Ar}), 3.31 (br s, 4H, NH), 2.20 (s, 3H, CH_3).

STEP 2 | A solution of 2,3-diaminotoluene, **26** (2.57 g, 21.0 mmol) and *p*-toluenesulfonic acid monohydrate (0.40 g, 2.10 mmol) in triethyl orthoformate (11.5 mL, 69.1 mmol) was heated to reflux at 140 °C for 15 h. The dark brown solution was cooled to room temperature and volatiles were removed under reduced pressure. The resulting viscous, dark brown oil was filtered through a silica plug, eluting with 40:1 ethyl acetate/methanol. The clear orange solution was reduced to dryness to afford **27** as an orange-brown solid. Yield = 2.24 g (16.9 mmol, 81 % yield). The reported NMR and HRMS data are in good agreement with the literature values.[104]

^{1}H NMR (400 MHz, $CDCl_3$): δ 8.06 (s, 1H, NCHN), 7.48 (d, J = 8.0 Hz, 1H, CH_{Ar}), 7.21 (t, J = 8.0 Hz, 1H, CH_{Ar}), 7.10 (d, J = 8.0 Hz, 1H, CH_{Ar}), 2.63 (s, 3H, CH_3).

^{13}C NMR (100 MHz, $CDCl_3$): δ 140.2 (N*C*HN), 137.8, 136.9, 126.0, 123.3 (*C*H_{Ar}), 123.0 (*C*H_{Ar}), 112.6 (*C*H_{Ar}), 17.2 (*C*H_3).

IR (KBr, thin film) $\tilde{\nu}_{max}$ (cm^{-1}): 1614 (w), 1597 (w), 1485 (s), 1441 (s), 1360 (m), 1290, 1275, 1250, 1163 (w), 1074, 947, 786 (m), 748 (s), 635.

HRMS–ESI (*m/z*): $[M + H]^+$ calcd for $C_8H_9N_2$, 133.0760; found, 133.0754.

mp: 142 ˚C

***tert*-Butyl 4-methyl-1*H*-benzo[*d*]imidazole-1-carboxylate (39)**

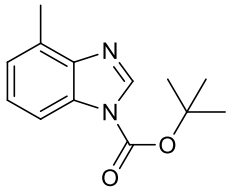

4-Methylbenzimidazole, **27** (1.89 g, 14.3 mmol) and 4-dimethylaminopyridine (0.177 g, 1.45 mmol) were dissolved in dry THF (47 mL) to give a clear orange solution. Boc anhydride (3.76 g, 17.2 mmol) was then added. The solution was stirred for 15 h at room temperature, and then evaporated to dryness. The resulting clear orange oil was taken up in ethyl acetate and washed with water (2 × 50 mL), followed by brine (50 mL). The organic layer was dried over sodium sulfate, filtered, and reduced to dryness to give a clear orange oil. Yield = 3.16 g (13.6 mmol, 95 %). The ^{1}H NMR spectral data are in excellent agreement with the literature.[105]

^{1}H NMR (400 MHz, $CDCl_3$): δ 8.43 (s, 1H, NC*H*N), 7.81 (d, *J* = 8.0 Hz, 1H, C*H*$_{Ar}$), 7.29 (t, *J* = 6.0 Hz, 1H, C*H*$_{Ar}$), 7.16 (d, *J* = 4.0 Hz, 1H, C*H*$_{Ar}$), 2.67 (s, 3H, Ar-C*H*$_3$), 1.70 (s, 9H, C(C*H*$_3$)$_3$).

^{13}C NMR (100 MHz, $CDCl_3$): δ 148.1 (N*C*=O), 142.8 (N*C*HN), 141.1, 131.0, 130.5, 125.2 (*C*H_{Ar}), 124.9 (*C*H_{Ar}), 111.9 (*C*H_{Ar}), 85.7 (*C*(CH_3)$_3$), 28.1 (C(*C*H_3)$_3$), 16.6 (Ar-*C*H_3).

IR (NaCl, thin film) $\tilde{\nu}_{max}$ (cm^{-1}): 2980, 1746 (s), 1606, 1510, 1495, 1418, 1367 (s), 1304, 1276 (s), 1258 (s), 1213, 1151 (s), 1128, 1115, 1064, 1002, 943, 847, 830, 781, 759, 686.

HRMS–ESI (*m/z*): $[M + H]^+$ calcd for $C_{13}H_{17}N_2O_2$, 233.1285; found, 233.1283.

***tert*-Butyl 4-(bromomethyl)-1*H*-benzo[*d*]imidazole-1-carboxylate (40)**

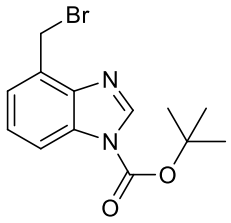

N-Bromosuccinimide (2.91 g, 16.4 mmol) and benzoyl peroxide (0.343 g, 1.42 mmol) were added to a stirring solution of benzimidazole **39** (3.44 g, 14.8 mmol) in carbon tetrachloride (73 mL). The orange reaction mixture was heated at 90 °C for 3 h. After cooling to room temperature, the mixture was washed with saturated sodium bicarbonate solution (30 mL), followed by water (30 mL), then brine (30 mL), and dried over sodium sulfate. The clear orange solution was reduced to dryness to give compound **40** as a clear, dark orange oil. Yield = 4.33 g (13.9 mmol, 94 %). The NMR spectroscopic data obtained match previously reported values.[105]

^{1}H NMR (400 MHz, $CDCl_3$): δ 8.48 (s, 1H, NC*H*N), 7.94 (d, *J* = 8.0 Hz, 1H, CH_{Ar}), 7.40 – 7.30 (m, 2H, CH_{Ar}), 4.94 (s, 2H, CH_2Br), 1.69 (s, 1H, C(CH_3)$_3$).

^{13}C NMR (100 MHz, $CDCl_3$): δ 147.9 (N*C*HN), 142.5, 142.3, 142.1, 129.8, 125.4, 125.0, 114.9 (*C*H_{Ar}), 85.9 (*C*(CH$_3$)$_3$), 28.1 (C(*C*H$_3$)$_3$), 28.0 (*C*H$_2$Br).

1*H*-Benzo[*d*]imidazole-4-carbaldehyde (7b)

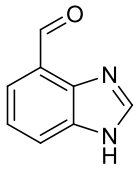

STEP 1 | **(1*H*-Benzo[*d*]imidazol-4-yl)methanol (41):** A yellow suspension of the benzyl bromide **40** (5.70 g, 18.3 mmol) and calcium carbonate (7.90 g, 79.0 mmol) in dioxane (35 mL) and deionised water (22 mL) was heated to 104 °C in an oil bath for 4 h. The mixture was filtered through a Celite pad, and a clear brown filtrate was obtained. The volatiles were removed under reduced pressure with heating to give **41** as a brown resin. This product was used in the next step without further purification. Yield = 3.93 g. The ^{1}H NMR spectroscopic and mass spectral data for **41** are consistent with the literature values.[106]

^{1}H NMR (400 MHz, $(CD_3)_2SO$): δ 12.45 (br s, 1H, N*H*), 8.18 (s, 1H, NC*H*N), 7.48 (d, *J* = 8.0 Hz, 1H, CH_{Ar}), 7.21 – 7.14 (m, 2H, CH_{Ar}), 5.23 (br s, 1H, O*H*), 4.86 (s, 2H, CH_2).

MS–EI (*m/z*): $[M]^+$ calcd for $C_8H_8N_2O$, 148; found, 148.

STEP 2 | A stirring brown suspension of the benzyl alcohol **41** (4.1608 g) and triethylamine (2.55 mL, 18.3 mmol) in dichloromethane (85 mL) was cooled in an ice bath. Dess–Martin periodinane (7.05 g, 16.6 mmol) was added to the reaction mixture, which was then allowed to gradually warm to room temperature and stirred for 12 h. A solution of sodium thiosulfate pentahydrate (5 g) in deionised water (75 mL) was added to the cloudy orange reaction mixture. After stirring for 1 hour, the mixture clarified. The reddish orange organic layer was separated, and washed with saturated sodium bicarbonate solution, followed by deionised water and brine. After drying over sodium sulfate, the organic layer was reduced to dryness to give **7b** as an orange solid. Yield = 1.39 g (9.48 mmol, 57 % over 4 steps). The NMR spectra are in reasonable agreement with previously reported values.[83]

^{1}H NMR (400 MHz, $CDCl_3$): δ 11.70 (br s, 1H, N*H*), 10.14 (s, 1H, C*H*O), 8.24 (s, 1H, NC*H*N), 8.12 (d, *J* = 8.0 Hz, 1H, CH_{Ar}), 7.77 (d, *J* = 8.0 Hz, 1H, CH_{Ar}), 7.45 (t, *J* = 8.0 Hz, 1H, CH_{Ar}).

^{13}C NMR (100 MHz, $CDCl_3$): δ 192.4 (*C*HO), 143.7 (NC_{Ar}), 142.3 (N*C*HN), 131.2 (*C*CHO), 129.1 (*C*H_{Ar}), 127.0 (*C*H_{Ar}), 122.3 (*C*H_{Ar}), 121.6 (NC_{Ar}).

IR (NaCl, thin film) $\tilde{\nu}_{max}$ (cm^{-1}): 1682 (s), 1613, 1597 (m), 1485 (m), 1385, 1362 (s), 1298 (w), 1263, 1231, 1217, 1165 (w), 1096, 1044 (w), 945 (w), 909 (w), 870 (w), 799 (m), 746 (m), 704 (m).

MS–EI (*m/z*): $[M]^+$ calcd for $C_8H_6N_2O$, 146; found, 146.

***tert*-Butyl 4-formyl-1*H*-benzo[*d*]imidazole-1-carboxylate (7a)**

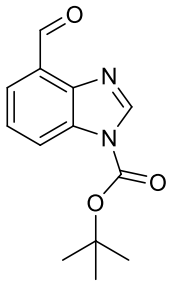

Boc anhydride (1.99 g, 9.12 mmol) and 4-dimethylaminopyridine (0.0958 g, 0.78 mmol) added to a solution of carbaldehyde **7b** (1.12 g, 7.66 mmol) in dry THF (28 mL). After stirring at room temperature for 21 hours, the reaction mixture was filtered through a Celite pad, and the filtrate was reduced to dryness. The resulting brown oil was taken up in ethyl acetate, and washed with deionised water (2 × 30 mL) and brine (30 mL). The organic layer was dried over sodium sulfate and the volatiles were removed *in vacuo* to give a dark brown oil (1.89 g). The crude product was purified by automated flash chromatography on silica gel (30% → 100% ethyl acetate in 40/60 petroleum spirits; R_f 0.3 in 30% ethyl acetate in 40/60 petroleum spirits). The pure product was obtained as a pale yellow solid. Yield = 0.29 g (1.17 mmol, 15 %).

^{1}H NMR (600 MHz, $CDCl_3$): δ 10.83 (s, 1H, C*H*O), 8.57 (s, 1H, NC*H*N), 8.28 (d, *J* = 8.2 Hz, 1H, CH_{Ar}), 7.92 (d, *J* = 7.7 Hz, 1H, CH_{Ar}), 7.52 (t, *J* = 7.9 Hz, 1H, CH_{Ar}), 1.72 (s, 9H, C(CH_3)$_3$).

^{13}C NMR (151 MHz, $CDCl_3$): δ 190.1 (*C*HO), 147.8 (N*C*=O), 144.9 (*C*$_{Ar}$NCH), 144.0 (N*C*HN), 132.6 (*C*$_{Ar}$NBoc), 127.2 (*C*$_{Ar}$CHO), 125.3 (*C*H$_{Ar}$), 124.0 (*C*H$_{Ar}$), 120.3 (*C*H$_{Ar}$), 86.7 (*C*(CH$_3$)$_3$), 28.2 (C(*C*H$_3$)$_3$).

IR (NaCl, thin flim) $\tilde{\nu}_{max}$ (cm^{-1}): 1748 (s), 1690 (s), 1605 (w), 1501, 1429 (m), 1370 (s), 1310, 1275, 1260, 1217 (w), 1152 (s), 1103, 843 (w), 781 (w), 760 (w).

HRMS–ESI (*m/z*): $[M + Na]^+$ calcd for $C_{13}H_{14}N_2O_3Na$, 269.0897; found, 269.0892.

Methyl 1*H*-benzo[*d*]imidazole-4-carboxylate (43)

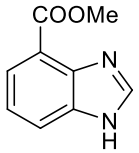

The title compound was prepared according to a published procedure.[88] Methyl 2-amino-3-nitrobenzoate (2.00 g, 10.2 mmol), iron powder (5.73 g, 103 mmol) and ammonium chloride (5.50 g, 103 mmol) were suspended in a mixture of 2-propanol (50 mL) and 85 % formic acid (51 mL). The slurry was heated in an 80 °C oil bath with stirring for 2 hours, and then filtered hot through a Celite pad. The clear dark brown filtrate was concentrated *in vacuo*, and redissolved in dichloromethane. The solution was washed with saturated sodium bicarbonate solution. The organic layer was separated, and the aqueous layer was extracted with dichloromethane (7 × 20 mL). The combined organic fractions were washed with brine, and dried over sodium sulfate. The solvent was evaporated under reduced pressure to afford **43** as a brown powder. Yield = 1.68 g (9.55 mmol, 94 %). The spectral data was consistent with reported values.[83]

^{1}H NMR (400 MHz, $(CD_3)_2SO$): δ 12.56 (br s, 1H, N*H*), 8.31 (s, 1H, NC*H*N), 7.97 (d, *J* = 8.0 Hz, 1H, CH_{Ar}), 7.85 (d, *J* = 8.0 Hz, 1H, CH_{Ar}), 7.32 (t, *J* = 8.0 Hz, 1H, CH_{Ar}), 3.95 (s, 3H, OCH_3).

^{13}C NMR (100 MHz, $(CD_3)_2SO$): δ 165.6 (*C*=O), 144.0, 143.8, 132.7, 124.5, 124.4, 121.1, 114.0, 52.0 (O*C*H_3).

IR (solid) $\tilde{\nu}_{max}$ (cm^{-1}): 1711, 1699 (s), 1597, 1498 (w), 1482, 1443 (m), 1408, 1358, 1305, 1272 (s), 1258 (s), 1223 (s), 1197, 1172, 1143, 1123, 1062 (w), 1025 (s), 945, 906, 815 (w), 753, 735, 635.

HRMS–ESI (*m/z*): $[M + H]^+$ calcd for $C_9H_9N_2O_2$, 177.0659; found, 177.0653.

Methyl 1-methyl-1H-benzo[d]imidazole-4-carboxylate (44)

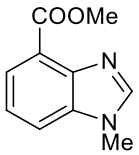

A solution of **43** (0.62 g, 3.52 mmol) in dry THF (15 mL) was added dropwise to a stirring suspension of sodium hydride (0.10 g, 4.28 mmol) in dry THF (25 mL)

at 0 °C under an argon atmosphere. After the evolution of hydrogen gas was complete, methyl iodide (265 µL, 4.26 mmol) was added dropwise to the cold solution. The dark brown reaction mixture was stirred for 16 hours at room temperature, and then reduced to dryness. The brown solid was redissolved in dichloromethane and washed with deionised water (5 mL). The organic layer was separated, and the aqueous layer was extracted with dichloromethane (3 × 3 mL). The combined organic fractions were washed with brine and dried over sodium sulfate. The volatiles were removed under reduced pressure, affording the title compound as a dark brown powder. Yield = 0.67 g (3.52 mmol, >99 %).

^{1}H NMR (600 MHz, $(CD_3)_2SO$): δ 8.31 (s, 1H, NC*H*N), 7.85 (d, *J* = 6.0 Hz, 1H, CH_{Ar}), 7.79 (d, *J* = 12.0 Hz, 1H, CH_{Ar}), 7.37 (t, *J* = 6.0 Hz, 1H, CH_{Ar}), 3.89 (s, 3H, NCH_3), 3.88 (s, 3H, OCH_3).

^{13}C NMR (100 MHz, $(CD_3)_2SO$): δ 166.4 (*C*=O), 146.1 (N*C*HN), 141.8 (C=NC_{Ar}), 135.7 (CH_3NC_{Ar}), 124.0 (CH_{Ar}), 121.6 (CH_{Ar}), 120.8 (O=CC_{Ar}), 115.1 (CH_{Ar}), 51.8 (NCH_3), 30.9 (OCH_3).

IR (NaCl, thin film) $\tilde{\nu}_{max}$ (cm^{-1}): 1710 (s), 1612, 1502 (m), 1437, 1420, 1352, 139, 1294, 1265 (s), 1226, 1220, 1194, 1127 (s), 1060, 1009, 992, 957, 781, 751 (s), 725, 626.

HRMS–ESI (*m/z*): $[M + H]^+$ calcd for $C_{10}H_{11}N_2O_2$, 191.0815; found, 191.0808.

(1-Methyl-1H-benzo[d]imidazol-4-yl)methanol (45)

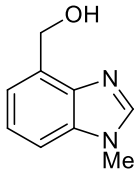

A solution of methyl ester **44** (0.53 g, 2.77 mmol) in dry THF (28 mL) was cooled in an ice bath. Freshly ground lithium aluminium hydride (0.16 g, 4.21 mmol) was added in small portions. The reaction mixture turned red. After stirring at 0 °C for 6 minutes, deionised water (160 µL) was added dropwise, followed by aqueous sodium hydroxide (160 µL), and deionised water (480 µL) once more. The reaction mixture was stirred at room temperature for 15 minutes. Sodium sulfate was added. The mixture was stirred for another 15 minutes before filtering

through Celite. The clear orange filtrate was reduced to dryness, furnishing **45** as an orange oil. Yield = 0.40 g (2.48 mmol, 90 %).

^{1}H NMR (400 MHz, $(CD_3)_2SO$): δ 8.13 (s, 1H, NC*H*N), 7.43 (dd, *J* = 7.0, 2.2 Hz, 1H, CH_{Ar}), 7.28 – 7.23 (m, 2H, CH_{Ar}), 5.13 (br s, 1H, O*H*), 4.92 (s, 2H, CH_2), 3.84 (s, 3H, NCH_3).

^{13}C NMR (100 MHz, $(CD_3)_2SO$): δ 144.3 (N*C*HN), 141.2 (C_{Ar}), 134.6 (C_{Ar}), 133.8 (*C*CH_2OH), 122.5 (*C*H_{Ar}), 119.1(*C*H_{Ar}), 108.8 (*C*H_{Ar}), 59.3 (*C*H_2), 31.2 (N*C*H_3).

IR (solid) $\tilde{\nu}_{max}$ (cm^{-1}): 3253 (br), 1502 (s), 1468, 1419, 1280, 1202, 1061, 1024 (s), 1005, 756 (s), 736 (s), 704, 668, 630.

HRMS–ESI (*m/z*): $[M + Na]^+$ calcd for $C_9H_{10}N_2ONa$, 185.0685; found, 185.0679.

1-Methyl-1H-benzo[d]imidazole-4-carbaldehyde (7c)

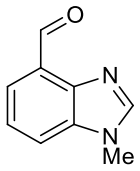

Triethylamine (0.31 mL, 2.22 mmol) and Dess–Martin periodinane (0.88 g, 2.07 mmol) were added to a stirring solution of **45** (0.33 g, 2.03 mmol) in dichloromethane (10 mL) at 0 °C. The orange-red suspension was allowed to warm to room temperature, and stirred for 18 hours. Ethyl acetate (10 mL), saturated sodium bicarbonate solution (10 mL) and sodium thiosulfate (1.36 g pentahydrate in 10 mL deionised water) were added to the reaction mixture, and stirred vigorously for 40 minutes. The organic layer was separated, and the aqueous layer was extracted with ethyl acetate (3 × 10 mL). The combined organic extracts were dried over sodium sulfate, and reduced to dryness to give orange needles. Yield = 0.28 g (1.76 mmol, 86 %). Crystals suitable for single crystal X-ray diffraction were grown by slow evaporation from dichloromethane.

H NMR (400 MHz, $CDCl_3$): δ 10.81 (s, 1H, C*H*O), 8.27 (s, 1H, NC*H*N), 7.90 (dd, *J* = 7.5, 1.0 Hz, 1H, CH_{Ar}), 7.70 (dd, *J* = 8.1, 1.0 Hz, 1H, CH_{Ar}), 7.48 (t, *J* = 7.8 Hz, 1H, CH_{Ar}), 3.97 (s, 3H, NCH_3).

^{13}C NMR (100 MHz, $CDCl_3$): δ 190.6 (*C*HO), 145.7 (NCHN), 144.0 (C_{Ar}N=CH), 135.8 ($C_{Ar}NCH_3$), 126.8 (*C*CHO), 122.9 (CH_{Ar}), 122.7 (CH_{Ar}), 115.5 (CH_{Ar}), 31.3 (NCH_3).

IR (solid) $\tilde{\nu}_{max}$ (cm^{-1}): 1680 (s), 1673 (s), 1606, 1496, 1489, 1436, 1417 (m), 1384 (m), 1333, 1257 (s), 1251 (s), 1061 (m), 972 (m), 890, 860 (s), 793, 777, 760, 642.

HRMS–ESI (*m/z*): $[M]^+$ calcd for $C_9H_9N_2O$, 161.0709; found, 161.0703.

Crystal data: $C_9H_8N_2O$, *M* = 160.18, monoclinic, *a* = 15.843(5), *b* = 7.3814(10), *c* = 14.175(3) Å, *α* = 90, *β* = 111.93(2), *γ* = 90 °, *U* = 1537.8(7) Å^3, *T* = 100 K, space group *C2/c* (no. 15), *Z* = 8, 9370 reflections measured, 1362 unique (R_{int} = 0.0410), 1248 > 4σ(*F*), *R* = 0.0418 (observed), R_w = 0.1105 (all data).

***tert*-Butyl 1*H*,1'*H*-[2,4'-bibenzo[*d*]imidazole]-1'-carboxylate (50)**

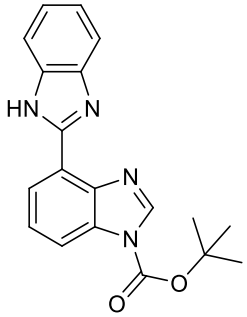

A clear dark orange solution of carbaldehyde **7a** (0.36 g, 1.46 mmol) and *o*-phenylenediamine (0.078 g, 0.72 mmol) in dry THF (5.4 mL) was heated to 70 °C in an oil bath. The reaction mixture turned clear brown after 15 minutes. After 4 hours, the reaction mixture was a red suspension, and the ^{1}H NMR spectrum of a crude aliquot at 4 hours revealed the complete disappearance of **7a**. The suspension was filtered, affording an off-white solid, which was rinsed with THF. Yield = 0.042 g (0.13 mmol, 17 %). Off-white needles suitable for SC-XRD could be crystallised by vapour diffusion of diethyl ether into a saturated dichloromethane solution.

^{1}H NMR (400 MHz, $CDCl_3$): δ 14.07 (br s, 1H, N*H*), 8.86 (d, *J* = 8.0 Hz, 1H, CH_{Ar}), 8.64 (s, 1H, NC*H*N), 8.05 (d, *J* = 12.0 Hz, 1H, CH_{Ar}), 7.91 – 7.88 (m, 2H, CH_{Ar}), 7.43 – 7.38 (m, 3H, CH_{Ar}), 1.73 (s, 9H, CH_3).

^{13}C NMR (100 MHz, $CDCl_3$): δ 146.9 (*C*=O), 146.0 (HN*C*N), 144.2 (N*C*HN), 140.9 (C_{Ar}), 131.6 (C_{Ar}), 130.4 (CH_{Ar}), 126.6 (CH_{Ar}), 126.3 (CH_{Ar}), 125.7 (CH_{Ar}), 120.0 (CH_{Ar}), 114.3 (CH_{Ar}), 111.5 (C_{Ar}), 87.7 (O*C*(CH_3)$_3$), 28.1 (C(*C*H$_3$)$_3$).

IR (NaCl, thin film) $\tilde{\nu}_{max}$ (cm^{-1}): 1755 (s), 1624 (m), 1607, 1568, 1559, 1504, 1468, 1408, 1397, 1368 (s), 1317 (s), 1281 (s), 1261, 1157, 1096, 1061 (w), 1009 (w), 991 (w), 920, 909, 843, 829, 800 (w), 787 (w), 746 (s), 731.

MS–ESI (*m/z*): $[M+H]^+$ calcd for $C_{19}H_{18}N_4O_2$, 335.2; found, 335.1.

Crystal data (HBr salt): $C_{38}H_{38}Br_2N_8O_4$, *M* = 830.58, monoclinic, *a* = 6.6413(2), *b* = 8.8151(2), *c* = 30.3052(7) Å, *α* = 90, *β* = 90, *γ* = 90 °, *U* = 1774.18(8) Å^3, *T* = 100 K, space group *P*2$_1$/*n* (no. 14), *Z* = 2, 12268 reflections measured, 3055 unique (R_{int} = 0.0299), 2736 > 4σ(*F*), *R* = 0.0338 (observed), R_w = 0.0725 (all data).

Di-*tert*-butyl-4,4'-((1*E*,1'*E*)-(ethane-1,2-diylbis(azanylylidene)) bis(methanylylidene))bis(1*H*-benzo[*d*]imidazole-1-carboxylate) (51a)

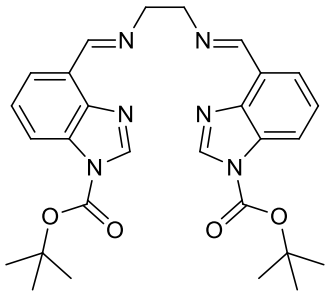

Ethylenediamine (14 µL, 0.21 mmol) was added in a single portion to a solution of carbaldehyde **7a** (0.10 g, 0.42 mmol) in absolute ethanol (0.80 mL). A white precipitate was formed. After stirring at room temperature for 15 hours, the reaction mixture was filtered to afford a white powder, which was rinsed with ethanol. Yield = 0.031 g (0.061 mmol, 29 %).

^{1}H NMR (400 MHz, $CDCl_3$): δ 9.18 (s, 1H, *H*C=N), 8.46 (s, 1H, NC*H*N), 8.03 – 7.98 (m, 2H, C*H*$_{Ar}$), 7.40 (t, *J* = 8.0 Hz, 1H, C*H*$_{Ar}$), 4.13 (s, 2H, C*H*$_2$), 1.70 (s, 9H, C(C*H*$_3$)$_3$).

^{13}C NMR (100 MHz, $CDCl_3$): δ 158.5 (*C*=N), 148.0 (*C*=O), 143.5 (C_{Ar}), 142.3 (N*C*HN), 131.7 (C_{Ar}), 127.6 (C_{Ar}), 125.3 (CH_{Ar}), 121.8 (CH_{Ar}), 116.2 (CH_{Ar}), 85.9 (O*C*(CH_3)$_3$), 62.3 (CH_2), 28.1 (C(*C*H$_3$)$_3$).

HRMS–ESI (*m/z*): $[M+H]^+$ calcd for $C_{28}H_{32}N_6O_4$, 517.2558; found, 517.2536.

(*N*^{1}*E*,*N*^{2}*E*)-*N*^{1},*N*^{2}-bis((1-Methyl-1*H*-benzo[*d*]imidazol-4-yl)methylene)ethane-1,2-diamine (51b)

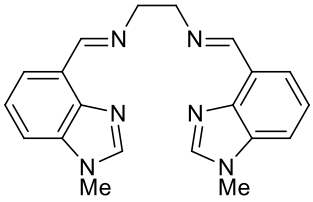

1-Methyl-4-formylbenzimidazole **7c** (2.69 g, 16.8 mmol) was dissolved in absolute ethanol (34 mL) at room temperature. Ethylenediamine (0.56 mL, 8.39 mmol) was added to the brown solution in two portions, allowing the reaction mixture to stir for 1 h between additions. The mixture was then stirred overnight at ambient temperature. Volatiles were removed under reduced pressure, and the resulting brown oil was taken up in methanol (30 mL), treated with petroleum spirits (5 mL), and cooled in a freezer. Fine, pale pink needles crystallised from the solution and were collected by vacuum filtration, rinsing with cold methanol. A second crop was obtained by reducing the filtrate to half its original volume, layering with petroleum spirits, and cooling the mixture overnight. Yield = 1.47 g (4.27 mmol, 51 %).

^{1}H NMR (600 MHz, $(CD_3)_2SO$): δ 9.14 (s, 1H, C*H*=N), 8.31 (s, 1H, NC*H*N), 7.80 (d, *J* = 7.4 Hz, 1H, CH_{Ar}), 7.68 (d, *J* = 7.6 Hz, 1H, CH_{Ar}), 7.34 (t, *J* = 7.7 Hz, 1H, CH_{Ar}), 4.06 (s, 2H, NCH_2), 3.90 (s, 3H, NCH_3).

^{13}C NMR (151 MHz, $(CD_3)_2SO$): δ 158.4 (*C*H=N), 145.8 (N*C*HN), 143.4, 135.6, 126.5, 122.6, 118.4, 112.7, 62.2 (N*C*H_2), 31.3 (N*C*H_3).

IR (solid) $\tilde{\nu}_{max}$ (cm^{-1}): 2876, 2844, 1641, 1608, 1494, 1435, 1412, 1261, 1253, 1030, 873, 795, 749.

HRMS–EI (*m/z*): $[M]^+$ calcd for $C_{20}H_{20}N_6$, 344.17494; found, 344.17364.

Anal. Calcd for $C_{20}H_{20}N_6$: C, 69.75; H, 5.85; N, 24.40. Found: C, 69.61; H, 6.01; N, 24.52.

mp: 206 ˚C (decomposition)

Crystal data: $C_{22}H_{28}N_6O_2$, M = 408.51, tetragonal, a = 22.124(3), b = 22.124(3), c = 4.3630(9) Å, α = 90, β = 90, γ = 90 °, U = 2135.6(6) Å^3, T = 100 K, space group $P4_2/n$ (no. 86), Z = 4, 35488 reflections measured, 3354 unique (R_{int} = 0.0477), 2931 > 4σ(F), R = 0.0506 (observed), R_w = 0.1547 (all data).

2.5 References

1 T. Kösterke, J. Kösters, E. U. Würthwein, C. Mück-Lichtenfeld, C. Schulte To Brinke, F. Lahoz and F. E. Hahn, *Chem. Eur. J.*, 2012, **18**, 14594–14598.

2 J. Ruiz and B. F. Perandones, *J. Am. Chem. Soc.*, 2007, **129**, 9298–9299.

3 J. Ruiz, Á. Berros, B. F. Perandones and M. Vivanco, *Dalton Trans.*, 2009, 6999.

4 G. Sini, O. Eisenstein and R. H. Crabtree, *Inorg. Chem.*, 2002, **41**, 602–604.

5 A. Ariafard, F. Zarkoob, H. Batebi, R. Stranger and B. F. Yates, *Organometallics*, 2011, **30**, 6218–6224.

6 D. R. Armstrong, W. Clegg, A. Hernán-Gómez, A. R. Kennedy, Z. Livingstone, S. D. Robertson, L. Russo and E. Hevia, *Dalton Trans.*, 2014, **43**, 4361–4369.

7 L. Xiang, J. Xiao and L. Deng, *Organometallics*, 2011, **30**, 2018–2025.

8 M. Y. Leow, *Synthesis and Characterisation of Novel Organometallic Carbene Complexes*, Honours thesis, University of Tasmania, Hobart, 2012.

9 R. W. Layer, *Chem. Rev.*, 1963, **63**, 489–510.

10 R. D. Patil and S. Adimurthy, *Asian J. Org. Chem.*, 2013, **2**, 726–744.

11 M. R. Grimmett, *Imidazole and Benzimidazole Synthesis*, Academic Press, 1st edn., 1997.

12 I. P. Beletskaya and A. V. Cheprakov, *Coord. Chem. Rev.*, 2004, **248**, 2337–2364.

13 F.-S. Han, *Chem. Soc. Rev.*, 2013, **42**, 5270.

14 A. H. Cherney, N. T. Kadunce and S. E. Reisman, *Chem. Rev.*, 2015, **115**, 9587–9652.

15 D. Ma and Q. Cai, *Acc. Chem. Res.*, 2008, **41**, 1450–1460.

16 A. Brennführer, H. Neumann, S. Klaus, T. Riermeier, J. Almena and M. Beller, *Tetrahedron*, 2007, **63**, 6252–6258.

17 S. Klaus, H. Neumann, A. Zapf, D. Strübing, S. Hübner, J. Almena, T. Riermeier, P. Groß, M. Sarich, W.-R. Krahnert, K. Rossen and M. Beller, *Angew. Chem. Int. Ed.*, 2006, **45**, 154–158.

18 A. Brennführer, H. Neumann and M. Beller, *Angew. Chem. Int. Ed.*, 2009, **48**, 4114–4133.

19 C. F. J. Barnard, *Organometallics*, 2008, **27**, 5402–5422.

20 K.-H. Pfoertner, K. Bernauer, F. Kaufmann and E. Lorch, *Helv. Chim. Acta*, 1985, **68**, 584–591.

21 X. Creary, M. E. Mehrsheikh-Mohammadi and S. McDonald, *J. Org. Chem.*, 1987, **52**, 3254–3263.

22 G. Voß and H. Gerlach, *Chem. Ber.*, 1989, **122**, 1199–1201.

23 S.-R. Li, C.-P. Lee, H.-T. Kuo, K.-C. Ho and S.-S. Sun, *Chem. Eur. J.*, 2012, **18**, 12085–12095.

24 M. Tobisu and N. Chatani, *Top. Curr. Chem.*, 2016, **374**, 41.

25 H. Zeng, Z. Qiu, A. Domínguez-Huerta, Z. Hearne, Z. Chen and C.-J. Li, *ACS Catal.*, 2017, **7**, 510–519.

26 A. R. Katritzky, B. Rachwal, S. Rachwal, P. J. Steel and K. A. Zaklika, *Heterocycles*, 1994, **38**, 2415–2422.

27 D. R. Buckle, K. A. Foster, J. F. Taylor, J. M. Tedder, V. E. Thody, R. A. B. Webster, J. Bermudez, R. E. Markwell and S. A. Smith, *J. Med. Chem.*, 1987, **30**, 2216–2221.

28 P. Boggu, E. Venkateswararao, M. Manickam, Y. Kim and S.-H. Jung, *Arch. Pharm. Res.*, 2017, **40**, 469–479.

29 M. C. Rezende, E. L. Dall'Oglio and C. Zucco, *Synth. Commun.*, 2001, **31**, 607–613.

30 R. J. Moreau, C. K. Skepper, B. A. Appleton, A. Blechschmidt, C. J. Balibar, B. M. Benton, D. I. Joseph E., B. Y. Feng, M. Geng, C. Li, M. K.

Lindvall, A. Lingel, Y. Lu, M. Mamo, W. Mergo, V. Polyakov, T. M. Smith, K. Takeoka, K. Uehara, L. Wang, J.-R. Wei, A. H. Weiss, L. Xie, W. Xu, Q. Zhang and J. de Vicente, *J. Med. Chem.*, 2018, **61**, 3309−3324.

31 J. Coates, *Encycl. Anal. Chem.*, 2006, 1–23.

32 Z. Cheraiet, S. Hessainia, S. Ouarna, M. Berredjem and N. E. Aouf, *Green Chem. Lett. Rev.*, 2013, **6**, 211–216.

33 H. K'tir, A. Amira, M. Berredjem and N.-E. Aouf, *Chem. Lett.*, 2014, **43**, 851–853.

34 S. V. Chankeshwara, R. Chebolu and A. K. Chakraborti, *J. Org. Chem.*, 2008, **73**, 8615–8618.

35 F. Houlihan, F. Bouchard, J. M. J. Fréchet and C. G. Willson, *Can. J. Chem.*, 1985, **63**, 153–162.

36 Y. Basel and A. Hassner, *J. Org. Chem.*, 2000, **65**, 6368–6380.

37 M. Frohn, V. Viswanadhan, A. J. Pickrell, J. E. Golden, K. M. Muller, R. W. Bürli, G. Biddlecome, S. C. Yoder, N. Rogers, J. H. Dao, R. Hungate and J. R. Allen, *Bioorg. Med. Chem. Lett.*, 2008, **18**, 5023–5026.

38 J. L. Rogers, L. Bayeh, T. H. Scheuermann, J. Longgood, J. Key, J. Naidoo, L. Melito, C. Shokri, D. E. Frantz, R. K. Bruick, K. H. Gardner, J. B. MacMillan and U. K. Tambar, *J. Med. Chem.*, 2013, **56**, 1739–1747.

39 T. De La Fuente, M. Martín-Fontecha, J. Sallander, B. Benhamú, M. Campillo, R. A. Medina, L. P. Pellissier, S. Claeysen, A. Dumuis, L. Pardo and M. L. López-Rodríguez, *J. Med. Chem.*, 2010, **53**, 1357–1369.

40 L. L. Xu, J. F. Zhu, X. L. Xu, J. Zhu, L. Li, M. Y. Xi, Z. Y. Jiang, M. Y. Zhang, F. Liu, M. C. Lu, Q. C. Bao, Q. Li, C. Zhang, J. L. Wei, X. J. Zhang, L. S. Zhang, Q. D. You and H. P. Sun, *J. Med. Chem.*, 2015, **58**, 5419–5436.

41 J. Shen, Z. Liu, H. Li and Q. Zhao, *Heterocycles*, 2008, **75**, 1907.

42 D. Ramsbeck, M. Buchholz, B. Koch, L. Böhme, T. Hoffmann, H. U. Demuth and U. Heiser, *J. Med. Chem.*, 2013, **56**, 6613–6625.

43 A. R. Katritzsky, R. P. Musgrave, B. Rachwal and C. Zaklika,

Heterocycles, 1995, **41**, 345–352.

44 S. Darnbrough, M. Mervic, S. M. Condon and C. J. Burns, *Synth. Commun.*, 2001, **31**, 3273–3280.

45 J. Howell and M. Rasmussen, *Aust. J. Chem.*, 1993, **46**, 1177.

46 G. A. Molander, *Chem. Rev.*, 1992, **92**, 29–68.

47 S. B. Laing and P. J. Sykes, *J. Chem. Soc. C*, 1968, 2915–2918.

48 S. Torii, H. Tanaka, T. Inokuchi, S. Nakane, M. Akada, N. Saito and T. Sirakawa, *J. Org. Chem.*, 1982, **47**, 1647–1652.

49 L. K. Sydnes, S. H. Hansen, I. C. Burkow and L. J. Saethre, *Tetrahedron*, 1985, **41**, 5205–5208.

50 B. Zhu, W. Zhang, R. Lee, Z. Han, W. Yang, D. Tan, K. W. Huang and Z. Jiang, *Angew. Chem. Int. Ed.*, 2013, **52**, 6666–6670.

51 L. Syper, *Tetrahedron Lett.*, 1966, **7**, 4493–4498.

52 D. J. Davies, M. Crowe, N. Lucas, J. Quinn, D. D. Miller, S. Pritchard, D. Grose, E. Bettini, N. Calcinaghi, C. Virginio, L. Abberley, P. Goldsmith, A. D. Michel, I. P. Chessell, J. N. C. Kew, N. D. Miller and M. J. Gunthorpe, *Bioorg. Med. Chem. Lett.*, 2012, **22**, 2620–2623.

53 A. Wohl and K. Jaschinowski, *Ber. Dtsch. Chem. Ges,* 1921, **54**, 476–484.

54 K. Ziegler, A. Späth, E. Schaaf, W. Schumann and E. Winkelmann, *Justus Liebigs Ann. Chem.*, 1942, **551**, 80–119.

55 C. Djerassi, *Chem. Rev.*, 1948, **43**, 271–317.

56 L. Horner and E. H. Winkelmann, *Angew. Chem.*, 1959, **71**, 349–365.

57 N. P. Buu-Hoi and J. Lecocq, *J. Chem. Soc.*, 1946, 830–832.

58 I. Kawasaki, N. Taguchi, Y. Yoneda, M. Yamashita and S. Ohta, *Heterocycles*, 1996, **43**, 1375–1379.

59 A. G. Mistry, K. Smith and M. R. Bye, *Tetrahedron Lett.*, 1986, **27**, 1051–1054.

60 A. D. Martin, A. R. Siamaki, K. Belecki and B. F. Gupton, *J. Org. Chem.*,

2015, **80**, 1915–1919.

61 B. D. Palmer, A. J. Kraker, B. G. Haitl, A. D. Panopoulos, R. L. Panek, B. L. Batley, G. H. Lu, S. Trumpp-Kallmeyer, H. D. H. Showalter and W. A. Denny, *J. Med. Chem.*, 1999, **42**, 2373–2382.

62 L. O'Donovan, M. P. Carty and F. Aldabbagh, *Chem. Commun.*, 2008, **1**, 5592.

63 B. Das, K. Venkateswarlu, M. Krishnaiah and H. Holla, *Tetrahedron Lett.*, 2006, **47**, 8693–8697.

64 H. Schmid and P. Karrer, *Helv. Chim. Acta*, 1946, **29**, 573–581.

65 P. Niño, M. Caba, N. Aguilar, E. Terricabras, F. Albericio and J. C. Fernàndez, *Indian J. Chem. B*, 2016, **55B**, 1117–1130.

66 S. Venkatraman, F. Velazquez, S. Gavalas, W. Wu, K. X. Chen, A. G. Nair, F. Bennett, Y. Huang, P. Pinto, Y. Jiang, O. Selyutin, B. Vibulbhan, Q. Zeng, C. Lesburg, J. Duca, L. Heimark, H. C. Huang, S. Agrawal, C. K. Jiang, E. Ferrari, C. Li, J. Kozlowski, S. Rosenblum, N. Y. Shih and F. George Njoroge, *Bioorg. Med. Chem.*, 2014, **22**, 447–458.

67 M. Movassaghi, O. K. Ahmad and S. P. Lathrop, *J. Am. Chem. Soc.*, 2011, **133**, 13002–13005.

68 M. Movassaghi and M. A. Schmidt, *Angew. Chem. Int. Ed.*, 2007, **46**, 3725–3728.

69 I. Villanueva-Margalef, D. E. Thurston and G. Zinzalla, *Org. Biomol. Chem.*, 2010, **8**, 5294–5303.

70 W.-H. Chiou, C.-L. Kao, J.-C. Tsai and Y.-M. Chang, *Chem. Commun.*, 2013, **49**, 8232--8234.

71 V. Sourdon, S. Mazoyer, V. Pique and J. P. Galy, *Molecules*, 2001, **6**, 673–682.

72 A. Podgoršek, S. Stavber, M. Zupan and J. Iskra, *Tetrahedron Lett.*, 2006, **47**, 1097–1099.

73 J. F. Honek, M. L. Mancini and B. Belleau, *Tetrahedron Lett.*, 1983, **24**, 257–260.

74 F. Mazzini, F. Galli and P. Salvadori, *Eur. J. Org. Chem.*, 2006, 5588–5593.

75 P. Zhang, R. Liu and J. M. Cook, *Tetrahedron Lett.*, 1995, **36**, 3103–3106.

76 T. Gan, R. Liu, P. Yu, S. Zhao and J. M. Cook, *J. Org. Chem.*, 1997, **62**, 9298–9304.

77 M. Al Hariri, O. Galley, F. Pautet and H. Fillion, *Eur. J. Org. Chem.*, 1998, 593–594.

78 C. H. M. Amijs, G. P. M. van Klink and G. van Koten, *Green Chem.*, 2003, **5**, 470.

79 D. Suarez, G. Laval, S.-M. Tu, D. Jiang, C. Robinson, R. Scott and B. Golding, *Synthesis*, 2009, 1807–1810.

80 N. Li, T. Yan, Z. Li, T. Thurn-Albrecht and W. H. Binder, *Energy Environ. Sci.*, 2012, **5**, 7888.

81 N. Kornblum, W. J. Jones and G. J. Anderson, *J. Am. Chem. Soc.*, 1959, **81**, 4113–4114.

82 Z. Li, J. Han, Y. Jiang, P. Browne, R. J. Knox and L. Hu, *Bioorg. Med. Chem.*, 2003, **11**, 4171–4178.

83 M. Hansen, S. E. Jacobsen, S. Plunkett, G. E. Liebscher, J. D. McCorvy, H. Bräuner-Osborne and J. L. Kristensen, *Bioorg. Med. Chem.*, 2015, **23**, 3933–3937.

84 H. C. Brown and S. Krishnamurthy, *Tetrahedron*, 1979, **35**, 567–607.

85 R. E. Gawley and D. D. Hennings, in *Encyclopedia of Reagents for Organic Synthesis*, John Wiley & Sons, Ltd, Chichester, UK, 2006.

86 P. C. Too, G. H. Chan, Y. L. Tnay, H. Hirao and S. Chiba, *Angew. Chem. Int. Ed.*, 2016, **55**, 3719–3723.

87 Z. Hong, D. Y. Ong, S. K. Muduli, P. C. Too, G. H. Chan, Y. L. Tnay, S. Chiba, Y. Nishiyama, H. Hirao and H. Sen Soo, *Chem. Eur. J.*, 2016, **22**, 7108–7114.

88 E. J. Hanan, B. K. Chan, A. A. Estrada, D. G. Shore and J. P. Lyssikatos,

Synlett, 2010, 2759–2764.

89 A. Klapars, J. C. Antilla, X. Huang and S. L. Buchwald, *J. Am. Chem. Soc.*, 2001, **123**, 7727–7729.

90 P. G. Cozzi, *Chem. Soc. Rev.*, 2004, **33**, 410–421.

91 S. I. Vagin, R. Reichardt, S. Klaus and B. Rieger, *J. Am. Chem. Soc.*, 2010, **132**, 14367–14369.

92 E. C. Escudero-Adán, J. Benet-Buchholz and A. W. Kleij, *Inorg. Chem.*, 2008, **47**, 4256–4263.

93 H. Chen, J. A. Cronin and R. D. Archer, *Inorg. Chem.*, 1995, **34**, 2306–2315.

94 S. Di Bella, I. Fragalà, I. Ledoux, M. A. Diaz-Garcia and T. J. Marks, *J. Am. Chem. Soc.*, 1997, **119**, 9550–9557.

95 R. D. Archer, H. Chen and L. C. Thompson, *Inorg. Chem.*, 1998, **37**, 2089–2095.

96 Y. S. Lee, Y. H. Cho, S. Lee, J. K. Bin, J. Yang, G. Chae and C. H. Cheon, *Tetrahedron*, 2015, **71**, 532–538.

97 L. Zhang, J. Xia, Y. Zhou, H. Wang and S. Wang, *Synth. Commun.*, 2012, **42**, 328–336.

98 N. Herrera Cano, J. G. Uranga, M. Nardi, A. Procopio, D. A. Wunderlin and A. N. Santiago, *Beilstein J. Org. Chem.*, 2016, **12**, 2410–2419.

99 R. Chebolu, D. N. Kommi, D. Kumar, N. Bollineni and A. K. Chakraborti, *J. Org. Chem.*, 2012, **77**, 10158–10167.

100 D. S. C. Black, D. C. Craig, N. Kumar and L. C. H. Wong, *J. Chem. Soc. Chem. Commun.*, 1985, 1172–1173.

101 X. Yang, R. A. Jones, R. J. Lai, A. Waheed, M. M. Oye and A. L. Holmes, *Polyhedron*, 2006, **25**, 881–887.

102 F. Z. Chiboub Fellah, J.-P. Costes, C. Duhayon, J.-C. Daran and J.-P. Tuchagues, *Polyhedron*, 2010, **29**, 2111–2119.

103 L. Wang, Z. Yang, M. Yang, R. Zhang, C. Kuai and X. Cui, *Org. Biomol.*

Chem., 2017, **15**, 8302–8307.

104 Z. Zhang, Q. Sun, C. Xia and W. Sun, *Org. Lett.*, 2016, **18**, 6316–6319.

105 G. Bridger, R. Skerlj, A. Haller, C. Harwig, D. Bogucki, T. R. Wilson, J. Crawford, E. J. McEachern, B. Atsma, S. Nan, Y. Zhou, D. Schols, C. D. Smith and R. M. Di Fluri, *Patent No. WO2002034745*, 2002.

106 F. Berst, P. Furet and A. Marzinzik, *Patent No. WO2011157787*, 2011.

3 Synthesis and structural studies of $MeRLH_2$ transition metal complexes

Although the $MeRLH_2$ (R = en, Ph, Cy) ligand set (Figure 3.1) was designed for a square planar metal centre, variations in bridge flexibility could allow some of them to accommodate other geometries. For example, $Me(en)LH_2$ enjoys free rotation about the ethylene bridge. The fact that these ligands contain four N donor atoms does not necessarily guarantee that they will coordinate exclusively in a tetradentate fashion as intended. Ligand candidates with more rigid backbones, namely $MePhLH_2$ and $MeCyLH_2$, were included to safeguard against the possibility of non-tetradentate coordination in the deprotonation precursor complex.

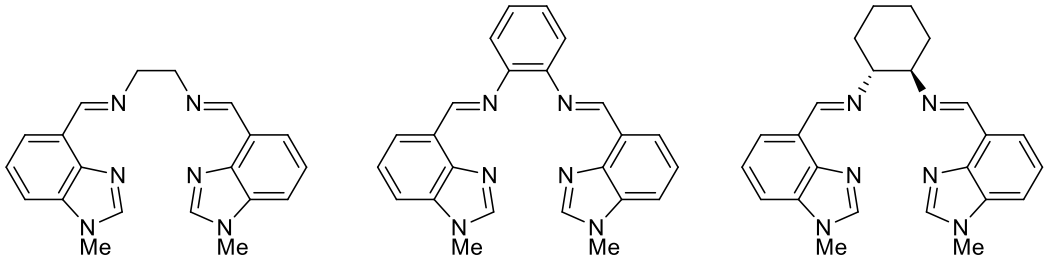

Figure 3.1 *The three key structures which make up the $MeRLH_2$ ligand set, featuring ethylene, 1,2-phenylene and (1R,2R)-(−)-1,2-cyclohexyl backbones.*

The range of flexibility within the $MeRLH_2$ ligand set presents an opportunity to investigate their compatibility with a series of transition metals. Thus, the search for the ideal deprotonation precursor was also an exploratory study to test the coordination capabilities of these ligands.

The base structure of $MeRLH_2$ is reminiscent of tetradentate Schiff base ligands, which also feature four coplanar coordination sites. They are predisposed towards the equatorial coordination of metals, leaving the axial sites available for interaction with potential substrates. As a testament to the enormous scope of transformations catalysed by salen or salophen complexes and their derivatives, numerous reviews have been dedicated to their powerful chemistry.[1–9] A notable member of the salen complex family is Jacobsen's catalyst, a manganese(III) species containing a chiral cyclohexyl diimine bridge (Figure 3.2). It is perhaps

best known for catalysing the enantioselective epoxidation of unfunctionalised olefins,[10] a transformation which helped forge a scalable pathway to an important side chain in the anti-tumour drug, taxol.[11] Its chromium(III) and cobalt(III) analogues were found to be effective catalysts in asymmetric epoxide ring-opening,[12] while its aluminium(III) congeners promoted the conjugate addition of azides to imides.[13]

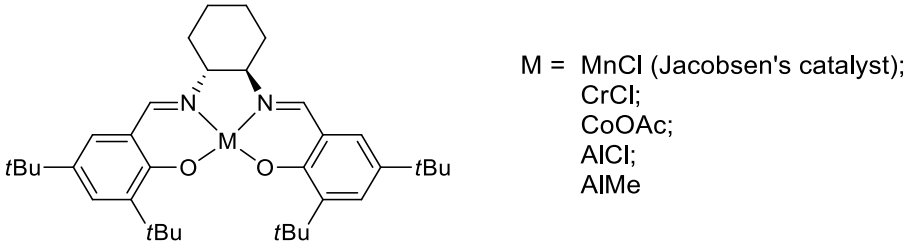

Figure 3.2 *Chiral salen catalysts for enantioselective transformations.*

Though they may appear quite similar at first glance, there is one important difference between $MeRLH_2$ and most salen-type ligands. The classic salen ligand binds to metals in a tetradentate fashion via two neutral imine N donor atoms and two negatively charged phenoxide O donor atoms. There are related *N*,*N'*,*N''*,*N'''* ligands where the phenoxide donors are replaced with amido nitrogen donors instead,[14–16] but the ligand is also dianionic in this case. In contrast, coordination complexes of $MeRLH_2$ would not feature any charge on the ligand.

The design of $MeRLH_2$ merges the linked bis(imine) motif from salen ligands with benzimidazoles, a prominent *N*-heterocycle with its own rich coordination chemistry. The incorporation of aromatic heterocycles such as benzimidazoles can boost the overall level of π-conjugation within a system. Thus, they are often used as building blocks to create extended π-systems with tunable photophysical properties. These systems are highly valued in the production of optical and electronic materials, where greater conjugation has been linked to better emissivity and conductivity.[17–20] Benzimidazoles and their complexes also make up a number of biologically active and sometimes pharmacologically relevant molecules.[21–28] It is plausible that $MeRLH_2$ complexes could find similar applications in catalysis, materials and medicinal chemistry as a consequence of these structural features. The insights gained from a thorough examination of their structural and spectroscopic properties may relay benefits to these fields.

Herein, the synthesis and characterisation of the nickel(II), copper(II), cobalt(II), zinc(II), silver(I) and palladium(II) complexes of $MeRLH_2$ are reported. The complexes will be evaluated based on their structural and spectroscopic properties, as well as practical aspects such as ease of synthesis and handling. Of particular importance is the distance between the two C2 carbon atoms where deprotonation would occur to form the free carbenes. If the carbene centres are situated closely to each other, the probability of entetraamine or macrocycle formation increases. Previous studies have shown that the presence of a bridge connecting two NHCs is conducive for dimerisation into the entetraamine, even when the *N*-substituents are very bulky.[29]

It was difficult to predict how the pre-carbene centres would interact with each other before the commencement of this investigation, as there were few reports of comparable tetradentate, non-macrocyclic complexes. One rare example is the bis(indolyl)nickel(II) complex **1**, which was prepared by the St. Clair Black research group and is depicted in Figure 3.3 below.[30]

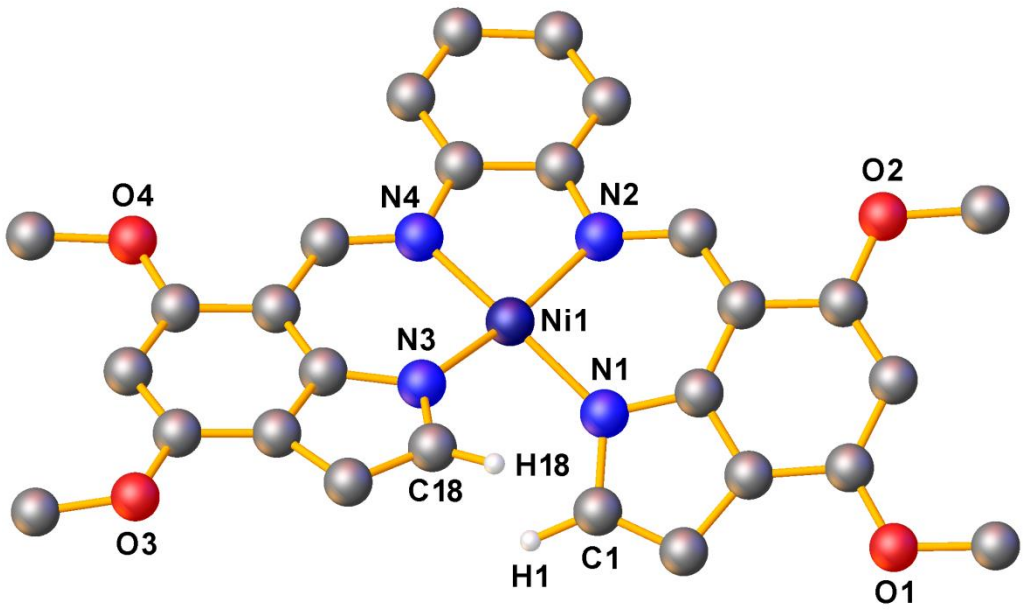

1

Figure 3.3 *Molecular structure of a tetradentate N,N',N'',N''' diimine bis(indolyl)nickel(II) complex*[30] ***1*** *adapted from the Cambridge Crystal Structure database*[31] *(database entry code: DAJLOP), showing the partial atom-numbering scheme. The lattice solvent molecule and all hydrogens apart from H1 and H18 have been omitted for clarity. All non-hydrogen atoms appear as arbitrarily sized radii.*

The ligand in **1** is an *N,N',N'',N'''* tetradentate Schiff base that has the same number of sp^2-hybridised spacers between each donor atom as $MePhLH_2$. The nickel(II) ion is situated within a distorted square planar coordination environment. This suggests that the coordination pocket in $MePhLH_2$ and its ethylene and cyclohexyl analogues could host a metal ion of similar size and geometry to nickel(II). Most of the geometric distortion visible in **1** was observed in the ligand itself. One indolyl unit is severely bent out of the plane on which the ligand backbone, the nickel(II) centre and the other indolyl unit lie. This presumably minimises the steric interactions between the H1 and H18 atoms. St. Clair Black and colleagues concluded that the large C1···C18 distance of 2.96 Å thwarted their best efforts to link the indole C1 and C18 atoms to form a macrocycle. They also noted that the ligand was not universally compatible with all transition metals. Presumably, this was a consequence of the strained, highly twisted indolyl ring. Alternative complexations were successful with cobalt(II) but not zinc(II) or copper(II).

This was encouraging in the context of the present endeavour, where a large distance between the C2 atoms is a desirable trait for the target complex. Given that the square planar nickel(II) ion was a reasonably good fit for the ligand in **1**, it was selected for initial screening with the $MeRLH_2$ ligands.

3.1 Nickel(II) complexes of $MeRLH_2$

3.1.1 Synthesis of nickel(II) complexes

A general method was developed for the preparation of transition metal complexes of $Me(en)LH_2$ (Scheme 3.1).

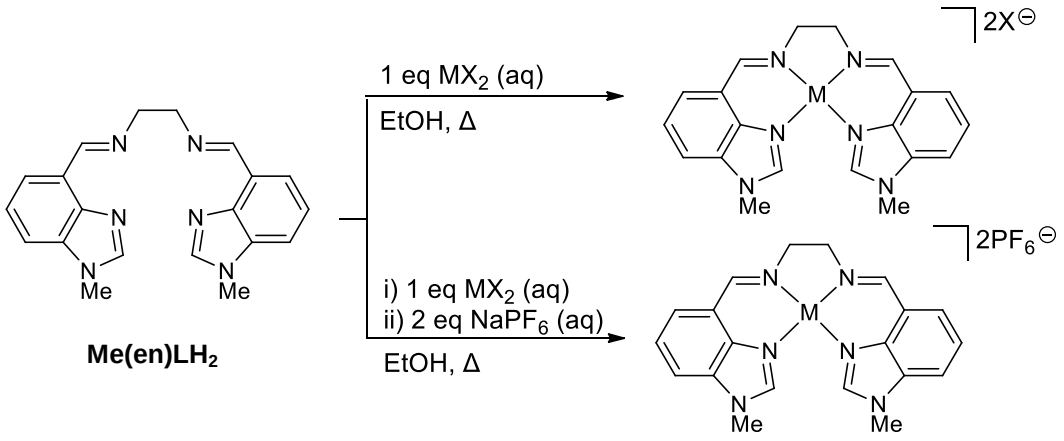

Scheme 3.1 *General syntheses of $Me(en)LH_2$ metal complexes.*

The nickel(II) complexes of Me(en)LH_2 were prepared according to the following one-pot procedure. First, the aqueous solution of a nickel(II) salt was added to a warm ethanolic solution of the ligand to produce a bis(aqua) adduct such as **2**[2BF_4] (Scheme 3.2). The counterions can be exchanged by adding $NaPF_6$ to produce a brown solid which readily precipitated from the reaction mixture. When $Ni(OAc)_2$•$4H_2O$ or $Ni(NO_3)_2$•$6H_2O$ were used as the nickel source, this brown solid was presumably the bis(aqua) complex [NiMe(en)$LH_2(H_2O)_2$]$(PF_6)_2$. This compound was not isolated, but used directly in the next step.

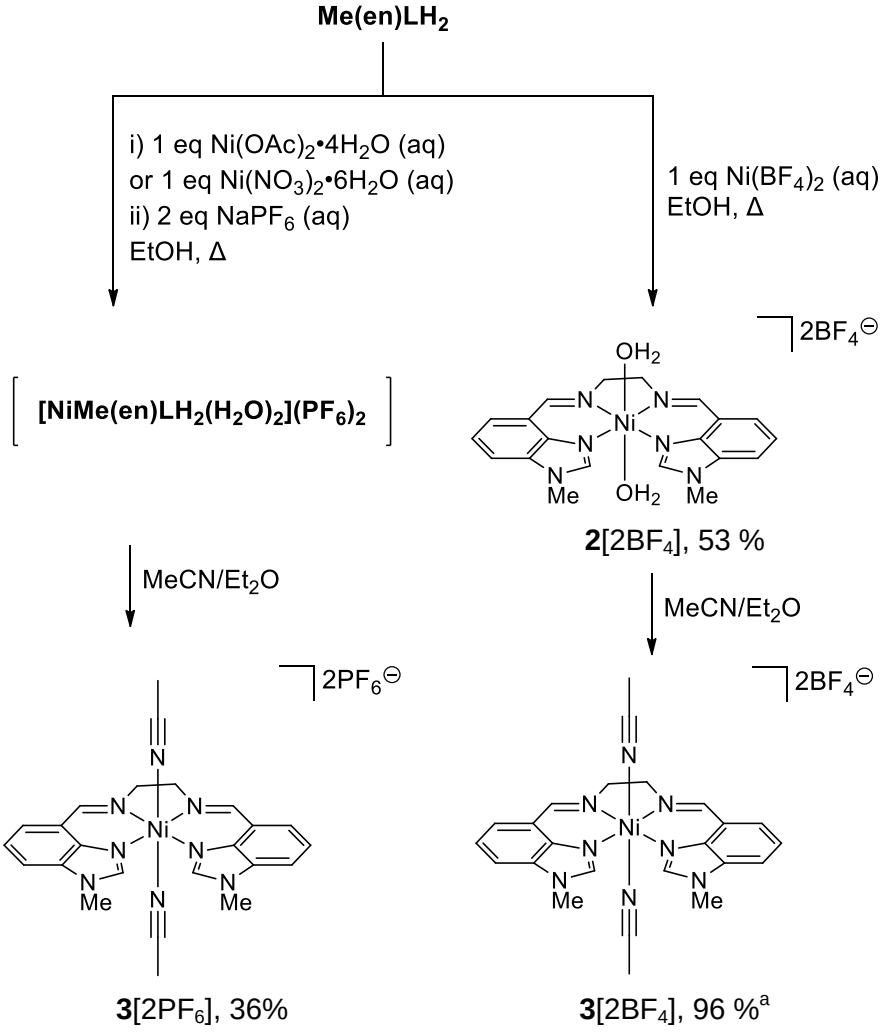

Scheme 3.2 *Synthesis of [NiMe(en)$LH_2(H_2O)_2$]$(BF_4)_2$* ***2****[2BF_4], [NiMe(en)$LH_2(MeCN)_2$]$(PF_6)_2$* ***3****[2PF_6], and [NiMe(en)$LH_2(MeCN)_2$]$(BF_4)_2$* ***3****[2BF_4]. [a]Isolated yield from one-step procedure described in Method A.*

Like most free carbenes, the target free NM,NR NHC is expected to be moisture-sensitive, as any trace of water may reprotonate the carbene. It is

therefore desirable to isolate a deprotonation precursor complex without any ligated or co-crystallised water molecules. The aqua ligands in **2**[2BF_4] and [NiMe(en)$LH_2(H_2O)_2$]$(PF_6)_2$ were readily displaced by acetonitrile upon dissolution, a process which was marked by an immediate colour change from pale brown to orange-brown or purple respectively. Vapour diffusion of diethyl ether into the acetonitrile solution produced single crystals of **3**[2PF_6] and **3**[2BF_4]. Alternatively, **3**[2BF_4] could be prepared more efficiently in a single step by reacting Me(en)LH_2 and $Ni(BF_4)_2$ in acetonitrile.

Since MePhLH_2 and MeCyLH_2 could not be obtained in their free forms, their complexes were prepared by metal-templated condensation (Scheme 3.3). The straightforward and convenient procedure effectively combines ligand formation and complexation into a single synthetic step. Similar one-pot procedures have been used to synthesise salen-type transition metal complexes with aliphatic[32,33] and aromatic[34] linkers between the N atoms, with yields comparable to those obtained through stepwise ligand formation and complexation.[33]

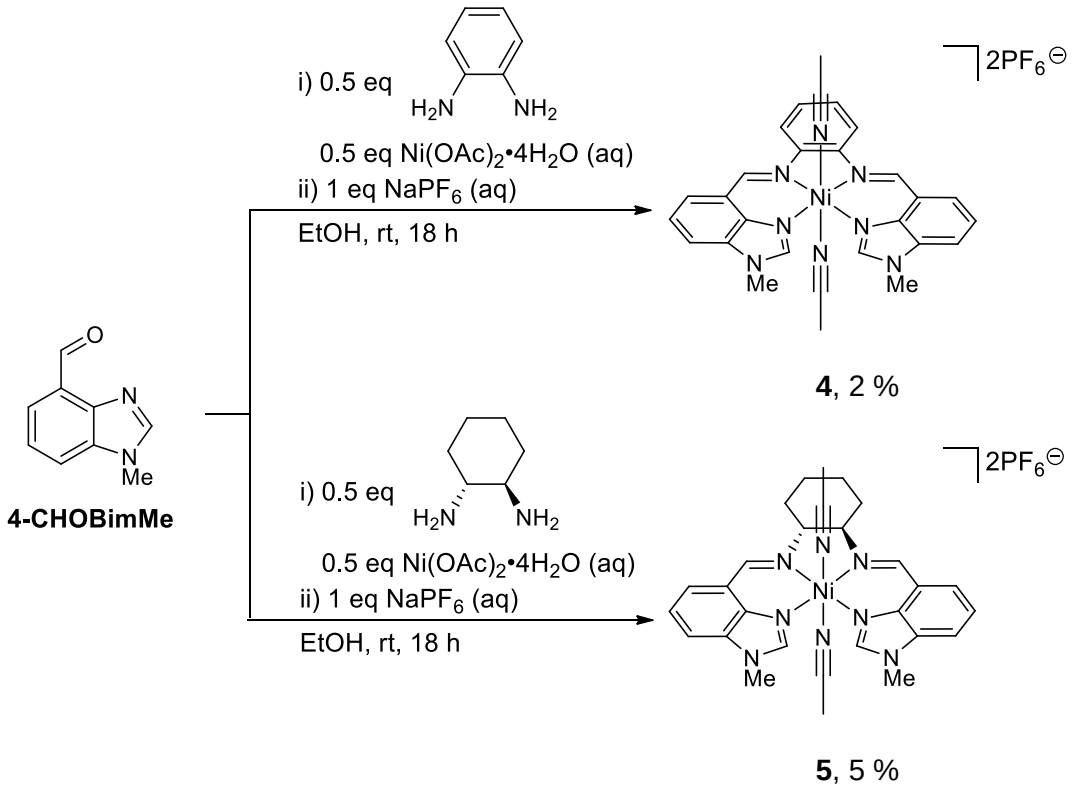

Scheme 3.3 *Metal-templated synthesis of $MeRLH_2$ complexes with cyclic backbones.*

A mixture of $Ni(OAc)_2$•$4H_2O$, the aldehyde 4-CHOBimMe and the cyclic diamine in a 1:2:1 molar ratio was dissolved in ethanol/water at room temperature.

The amine condensation partners for $MePhLH_2$ and $MeCyLH_2$ were *o*-phenylenediamine and (1*R*,2*R*)-(−)-1,2-diaminocyclohexane respectively. Two equivalents of $NaPF_6$ in water were added to this solution, inducing the precipitation of a brown solid. Treatment of this solid with acetonitrile/ether yielded the acetonitrile adducts $[NiMePhLH_2(MeCN)_2](PF_6)_2$, **4** and $[NiMeCyLH_2(MeCN)_2](PF_6)_2$, **5** as brown crystals in yields of 2 % and 5 % respectively.

A d^8 nickel(II) ion with a low spin electron configuration will adopt a square planar geometry. Consequently, square planar nickel(II) complexes are almost always diamagnetic, and exceptions to this rule are very rare.[35–37] It was therefore surprising to discover that the ^1H NMR spectra of all the nickel(II) complexes of $MeRLH_2$ displayed broad, contact-shifted resonances ranging from 0 – 110 ppm, consistent with the incorporation of a paramagnetic nickel(II) ion. Suspicions that octahedral complexes had formed were confirmed by X-ray diffraction of **2**[$2BF_4$], **3**[$2PF_6$], **3**[$2BF_4$], **4** and **5**. A detailed structural discussion is presented in Section 3.1.2. It has been observed that nickel(II) is inclined towards an octahedral geometry when coordinated to neutral imines and (benz)imidazoles,[38–40] which implies that benzimidazoles are weak field ligands. Nickel(II) complexes of (benz)imidazoles and other imine-like ligands such as azomethine[41] and aldoximate [42,43] are likewise six-coordinate. In a rather unusual case involving complex **6** which contains a ligand that structurally mimics $MeCyLH_2$, nickel(II) retains its square planar geometry despite exposure to a mixture of coordinating solvents, namely DMF and acetonitrile (Scheme 3.4).[44]

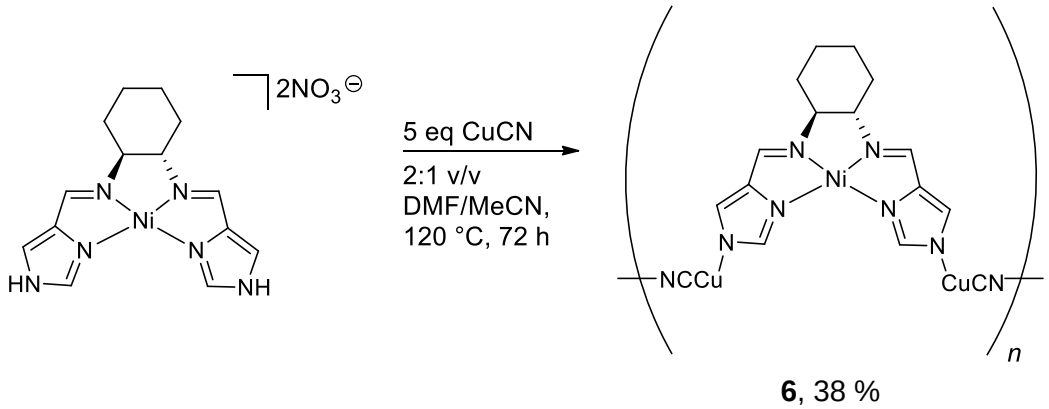

6, 38 %

Scheme 3.4 *N-metallation of a four-coordinate nickel(II) salen-type complex.*[44]

Presumably, nickel(II) binds preferentially to acetonitrile over water as the nitrile N is more electron rich than the O donor in water. The acceptance of more

electron rich donors could be an indication of insufficient electron donation from the $MeRLH_2$ ligand. The incorporation of more strongly electron-donating substituents on the ligand framework, or the replacement of the imines with more electron rich donors such as phosphines or NHCs may reduce the affinity of nickel(II) towards additional ligands. Possibly, further coordination at the axial positions could be hindered by installing very bulky substituents on the ethylene backbone of $Me(en)LH_2$. Alternatively, scorpionate pendant donors could be inserted into the ligand framework. Although this would not rectify the issue of octahedral complex formation, it could provide greater control over the occupants of the axial coordination sites. However, these non-trivial modifications were not attempted due to time constraints.

The identities of these complexes were supported by ESI-MS, revealing peaks at *m*/*z* = 201.05 {**2**[$2BF_4$], **3**[$2PF_6$], **3**[$2BF_4$]}, 225.06 (**4**), and 228.08 (**5**) that were consistent with the loss of the axial water or acetonitrile ligands from the complex cation. Dissociation of weakly coordinating “solvento" ligands from the parent ion is not unusual for octahedral complexes.[45–47] Complex **3**[$2PF_6$] underwent a colour change from purple to orange when the solid was heated to between 100 – 150 °C, which could be attributed to the thermally induced loss of MeCN. The dark brown colour of solid **4** lightened considerably at 280 °C, indicating a similar susceptibility to solvent loss. Yet, these complexes appeared to be stable to storage under vacuum at room temperature. Satisfactory elemental analyses for **4** and **5** showed that the crystal structures obtained were representative of the bulk composition. However, it should be noted that the lattice acetonitrile in **5** is removed upon drying the solid under vacuum, only to be replaced by water upon reintroducing the hygroscopic product to air.

In the interest of increasing solubility while minimising the probability of the metal centre preferentially coordinating to the counterion instead of a ligand donor site, the original acetate or nitrate counterions in the nickel salt precursor were exchanged for weakly coordinating PF_6 anions. On the surface, this appeared to be effective, as all the isolated complexes invariably showed the $MeRLH_2$ behaving as a tetradentate ligand. However, it was later discovered that the same result could be obtained when $Ni(OAc)_2{\bullet}4H_2O$ was used for the complexation without any subsequent counterion exchange. Perhaps this is a testament to the greater thermodynamic stability of the tetradentate $MeRLH_2$ complexes compared to the hypothetical mono-, di-, or tridentate derivatives, as predicted by the chelate effect. The $Ni(OAc)_2{\bullet}4H_2O$ complexation product was

crystallised as brown plates from ethanol/water. Its identity was established by SC-XRD as the hexacoordinate water-bound nickel(II) complex **2**[2OAc] with non-coordinating acetate ions (Scheme 3.6). Its molecular structure is illustrated in Figure 3.31 within the experimental section of this chapter. Even though the carboxylate O in the acetate ion is a potential donor, the nickel centre preferentially binds to water instead. The successful complexation of the nickel ion was also corroborated by ESI-MS with the detection of the desolvated cation peak at *m*/*z* = 201.05.

If water and acetonitrile were excluded from the complexation of Me(en)LH_2 with nickel(II) acetate, it is possible that the acetate ligands will then coordinate axially to the nickel(II) centre. Alternatively, the resulting complex may feature a four-coordinate metal centre with non-coordinating acetate ions. Regardless of the geometry at the nickel(II) centre, the predicted [NiMe(en)LH_2]$(OAc)_2$ complex could potentially undergo self-deprotonation to form [NiMe(en)L], as its coordination sphere would contain two equivalents of base in the form of the acetate ions (Scheme 3.5).

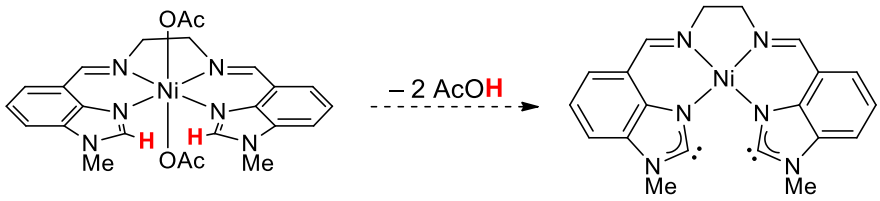

[NiMe(en)L$H_2$$(OAc)_2$] **[NiMe(en)L]**

Scheme 3.5 *Potential intramolecular deprotonation of the Ni$(OAc)_2$ complex to yield the target NM,NR NHC complex.*

NHC formation by "intramolecular" deprotonation with basic counterions such as acetates[48,49] and alkoxides[50] has been demonstrated in the literature, although the products are usually the NHC complexes and not the free carbene themselves. The synthesis of [NiMe(en)LH_2]$(OAc)_2$ was attempted by dissolving pre-dried Ni$(OAc)_2$ and Me(en)LH_2 in methanol under anhydrous, air-free conditions (Scheme 3.6). A small quantity of bright green needles were crystallised from the reaction mixture, and shown to be the tetranuclear nickel(II) aggregate **7** by X-ray diffraction. The vertices of the central cube-shaped cluster comprise four nickel(II) ions, which are bridged by the O atoms of four methoxide groups. One face of the cube is flanked by one Me(en)LH_2 unit, which is coordinated to two nickel ions in a bidentate fashion through one imine and one

benzimidazolyl N. This is the only instance of non-tetradentate coordination observed for the $MeRLH_2$ systems. The other two nickel centres are capped by chelating acetate groups. Bridging acetate ligands connect each of the N-bound nickel centres to the purely O-bound nickel centres. Although the tetramer was probably only a minor product, the ligand conformation in **7** showcases the highly flexible nature of the ethylene backbone.

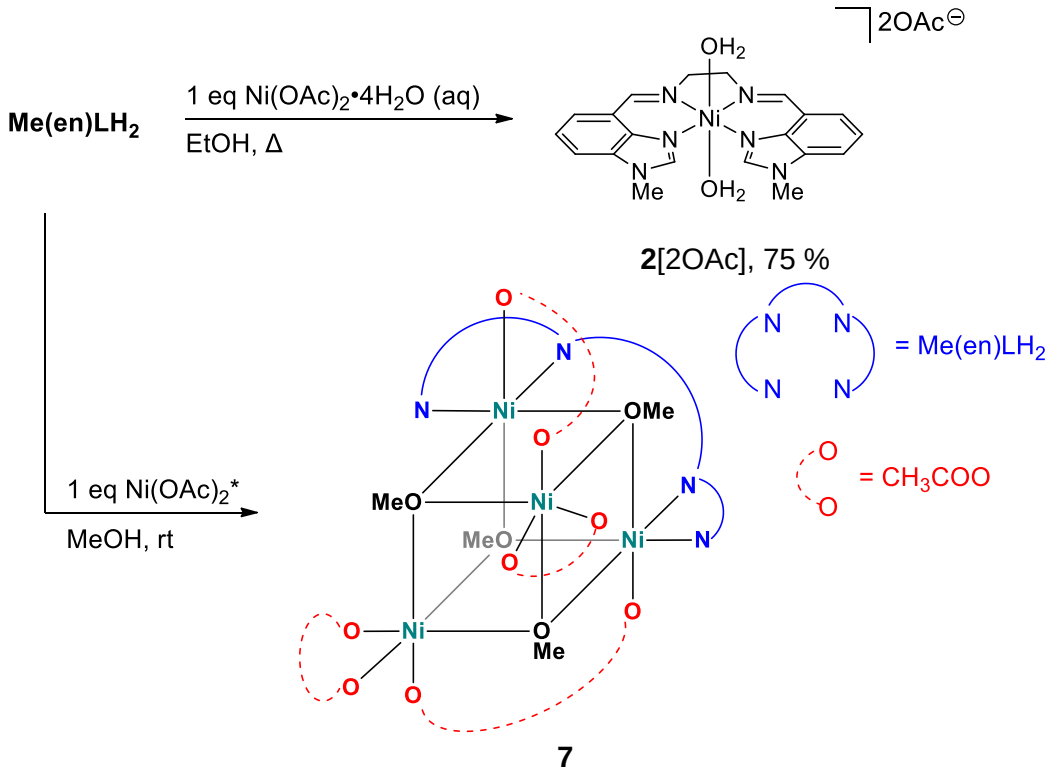

Scheme 3.6 *Reaction of $Me(en)LH_2$ with hydrated and heat-dried* nickel(II) acetate salts.*

It is believed that the formation of this unexpected byproduct was caused by thermal decomposition of nickel(II) acetate during the drying process. One study suggested that heating $Ni(OAc)_2•4H_2O$ at temperatures above 120 °C may lead to the formation of the basic nickel acetate species $0.86Ni(OAc)_2•0.14Ni(OH)_2$ after dehydration is achieved.[51] The capping methoxides in **7** could have arose from the deprotonation of methanol by this basic nickel acetate species.

3.1.2 Structural analysis of nickel(II) complexes of $MeRLH_2$

Single crystals of **2**[$2BF_4$] were obtained by slow evaporation from ethanol/water. This complex crystallised in the $P2_1/c$ space group, and the asymmetric unit comprised one $[NiMe(en)LH_2(H_2O)_2]^{2+}$ unit and two BF_4 anions (Figure 3.4 a).

(a)

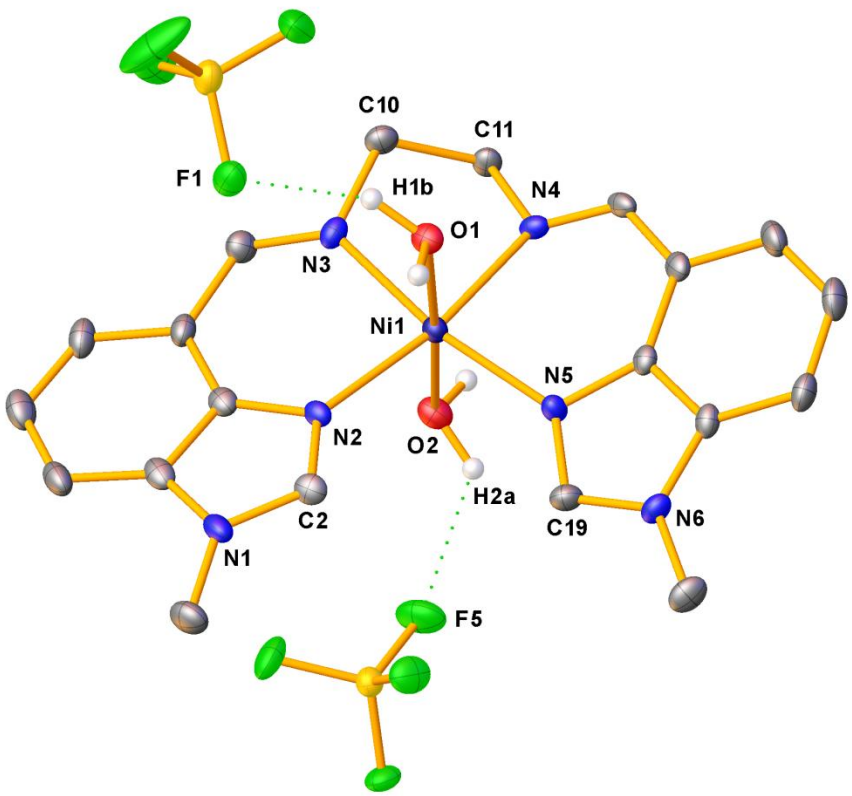

(b)

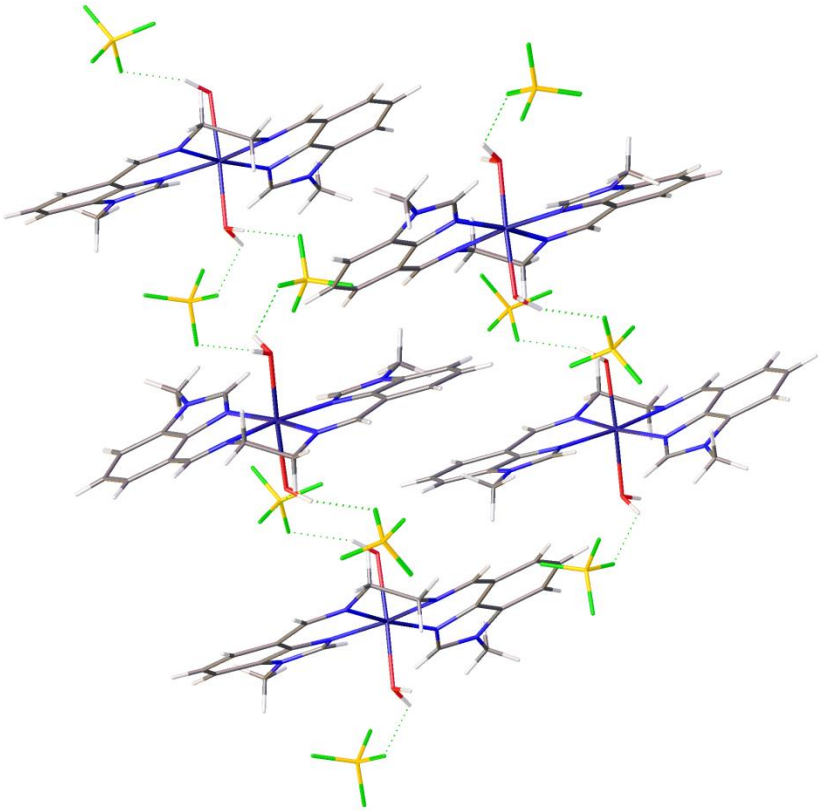

Figure 3.4 (a) *Structural representation of [NiMe(en)LH$_2$(H$_2$O)$_2$](BF$_4$)$_2$,* ***2****[2BF$_4$]. Thermal ellipsoids are drawn at the 50 % probability level. C-bound hydrogens are omitted for clarity.* ***(b)*** *Capped stick diagram showing hydrogen bonding networks within the crystal packing.*

Packing in the crystal was controlled by an extensive hydrogen bonding network built from the interaction between each proton on a water molecule and one F atom on a tetrafluoroborate anion [H1b···F1 *ca*. 1.942; H2a···F5 *ca*. 2.109 Å] (Figure 3.4 b).

The complex **3**[2BF_4] crystallised in the *C*2/*c* space group. The asymmetric unit contained one half of the C_2-symmetric cation, one lattice water molecule, and a disordered BF_4 anion that was modelled across two positions with refined occupancies of approximately 70:30 (Figure 3.5). The axial coordination of acetonitrile created solvent voids suitably sized for water in the lattice, and these water molecules interacted with the anions instead of the complex cation. Crystal packing was predominantly influenced by intermolecular face-to-face π-stacking of two benzimidazole phenyl rings with centroid separations of 3.5701(12) Å. The hydrogen bonding contacts H1a···F1 were measured at *ca*. 2.115 Å.

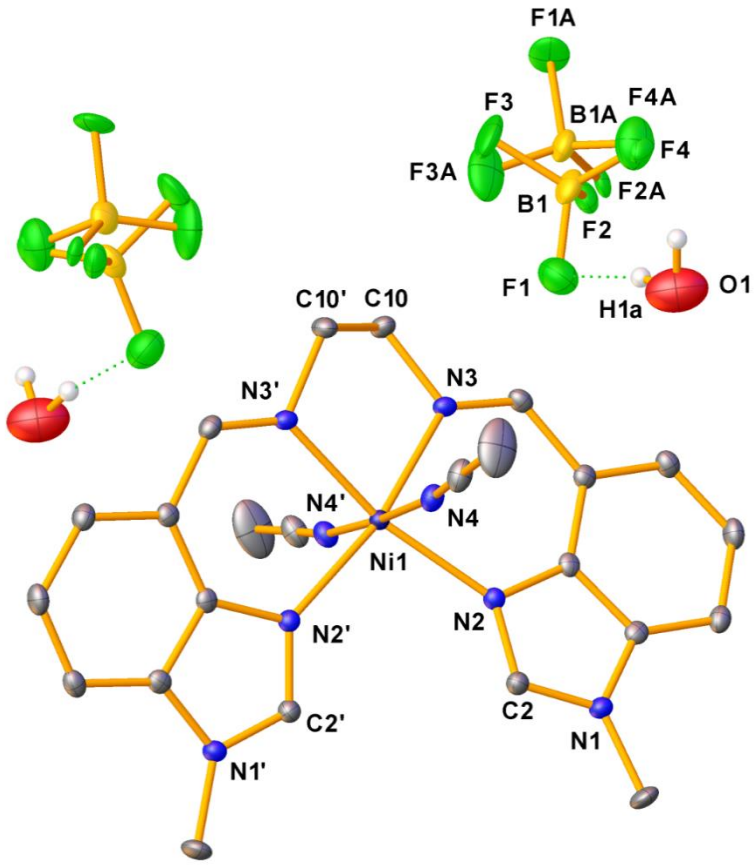

Figure 3.5 *Molecular structure of [NiMe(en)LH_2($MeCN)_2$]($BF_4)_2$,* ***3****[2BF_4] featuring disordered BF_4 anions with thermal ellipsoids at the 50 % probability level. C-bound hydrogen atoms are omitted for clarity.*

Significant bond lengths and angles for **2**[2BF_4] and **3**[2BF_4] are listed in Table 3.1. The equatorial Ni–N bond lengths fell within a similar narrow range {**2**[2BF_4] = 2.055(7)–2.084(7); **3**[2BF_4] 2.0611(12)–2.0788(12)} and were in good agreement with other octahedral nickel(II) complexes bearing N_4 ligands.[45] Minor deviations from the ideal octahedral geometry were evident from the equatorial *cis* N–Ni–N angles, which fall between 80–100 °. The sum of angles at the equatorial plane of the metal centre was *ca*. 360° for **2**[2BF_4], but slightly higher for **3**[2BF_4] (366 °). The axial Ni–O or Ni–N_{MeCN} bond distances were longer than the equatorial Ni–N bonds, which is typical of octahedral nickel(II) complexes.[52,53]

Table 3.1 *Summary of key bond lengths and angles for the [NiMe(en)$LH_2(Y)_2$]$(BF_4)_2$ (Y = H_2O, MeCN) complexes. Estimated standard deviations (ESDs) are given in parentheses.*

Bond lengths (Å) and angles (°)	[NiMe(en)$LH_2(H_2O)_2$]$(BF_4)_2$, **2**[2BF_4]	[NiMe(en)$LH_2(MeCN)_2$]$(BF_4)_2$, **3**[2BF_4]
Ni1–N2	2.055(7)	2.0611(12)
Ni1–N3	2.084(7)	2.0788(12)
Ni1–N4	2.069(7)	2.1107(13)
Ni1–N5	2.070(7)	–
Ni1–O1	2.121(6)	–
Ni1–O2	2.109(6)	–
N2–Ni1–N3	89.3(3)	89.90(5)
N2–Ni1–N5 N2–Ni1–N2’	100.7(3) –	99.97(7)
N3–Ni1–N3’	–	81.82(7)
N2–Ni1–N4	170.0(3)	87.47(5)
N3–Ni1–N4	80.9(3)	94.69(5)
N4–Ni1–N5	89.1(3)	–
C2···C19 C2···C2’	3.436(12) –	– 3.389(3)
N3–C10–C11–N4 N3’–C10’–C10–N3	−46.9(7) –	– −48.37(8)
Plane twist	0.8(3)	13.44(7)

The benzimidazole “arms” which wrap around the metal centre did not reside on the same plane as each other. One benzimidazole arm was twisted upwards of the metal coordination plane (defined by the four equatorial N donor atoms), while the other pointed downwards. The out-of-plane twisting of the benzimidazole arms increased the physical separation between their C2 atoms. The C2···C2’ (C2···C19 for **2**[2BF_4]) distance was slightly longer in **2**[2BF_4]. It was thought that the benzimidazole C2···C2’ distances could be related to other geometric parameters in the complex, which are illustrated in Figure 3.6: The bridge twist was measured as the torsion angle along the N–C–C–N bonds of the diimine linker. On the other hand, the plane twist was defined as the dihedral angle between two opposite N_{imine}–M–N_{Bim} (M = metal) least-squares calculated planes, and it approximates the distortion from planarity along the equatorial plane. The ideal plane twist should amount to 0 ° in an octahedral or square planar complex, and 90 ° for a tetrahedral complex.

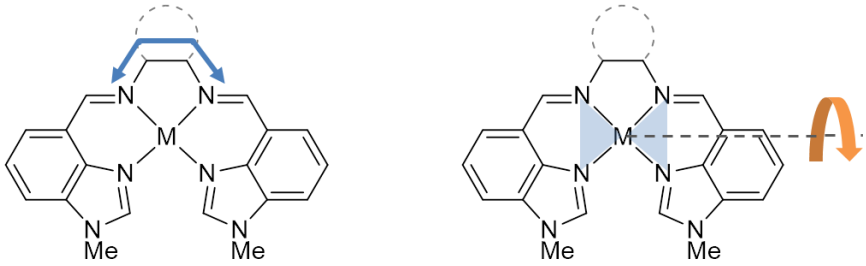

(a) Bridge twist (b) Plane twist

Figure 3.6 *Quantifying deviations from planarity using* ***(a)*** *the dihedral angle along the diimine bridge and* ***(b)*** *the angle between the two metal coordination planes, indicated in blue.*

As seen in **2**[2BF_4] and **3**[2BF_4], the MeRLH_2 ligand in **3**[2PF_6], **4** and **5** adopted a conformation that is reminiscent of organic helicene compounds[54] around the metal centre. Important bond lengths and angles for these three complexes are summarised in Table 3.2.

The asymmetric unit of **3**[2PF_6] contained one half of the complex cation, one PF_6 anion and one lattice-bound water molecule (Figure 3.7). The large H_{water}···F and O_{water}···H_{MeCN} distances of *ca*. 2.22 and 2.77 Å respectively suggest an absence of hydrogen bonding interactions between the water molecule and the complex or the PF_6 anions. Crystal packing was governed by intermolecular π-stacking between the benzimidazole phenyl rings, with centroid separations of

3.641(2) Å. The counteranion variation had little effect on the bond distances and packing arrangement for **3**[2PF_6] and **3**[2BF_4].

Table 3.2 *Summary of key bond lengths and angles for the [NiMeRLH_2(MeCN)$_2$](PF_6)$_2$ series of complexes. ESDs are given in parentheses.*

Bond lengths (Å) and angles (°)	[NiMe(en)LH_2 (MeCN)$_2$](PF_6)$_2$, **3**[2PF_6]	[NiMePhLH_2 (MeCN)$_2$](PF_6)$_2$, **4**	[NiMeCyLH_2 (MeCN)$_2$](PF_6)$_2$, **5**
Ni1–N2 Ni2–N7	2.083(2) –	2.0436(16) –	2.070(3) 2.052(3)
Ni1–N3 Ni2–N8	2.088(2) –	2.0813(16) –	2.074(3) 2.086(3)
Ni1–N4 Ni2–N9	2.102(2) –	2.1411(17) –	2.104(3) 2.118(3)
N2–Ni1–N3 N7–Ni2–N8	89.21(9) –	91.42(6) –	90.35(11) 91.60(11)
N2–Ni1–N2’ N7–Ni2–N7’	80.95(13) –	97.26(9) –	99.22(16) 97.86(16)
N3–Ni1–N3’ N8–Ni2–N8’	101.48(13) –	80.73(9) –	80.12(16) 81.09(16)
N2–Ni1–N4 N7–Ni2–N9	95.03(9) –	87.64(6) –	91.01(11) 88.52(11)
N3–Ni1–N4 N8–Ni2–N9	87.52(9) –	98.33(6) –	91.24(11) 98.98(11)
C2···C2’ C18···C18’	3.435(6) –	3.241(4) –	3.489(7) 3.362(7)
N3–C10–C10’–N3’ N8–C26–C26’–N8’	51.72(13) –	0.13(13) –	−49.87(13) −53.77(12)
Plane twist Ni1 Plane twist Ni2	9.93(12) –	9.54(7) –	2.12(15) 15.43(15)

(a)

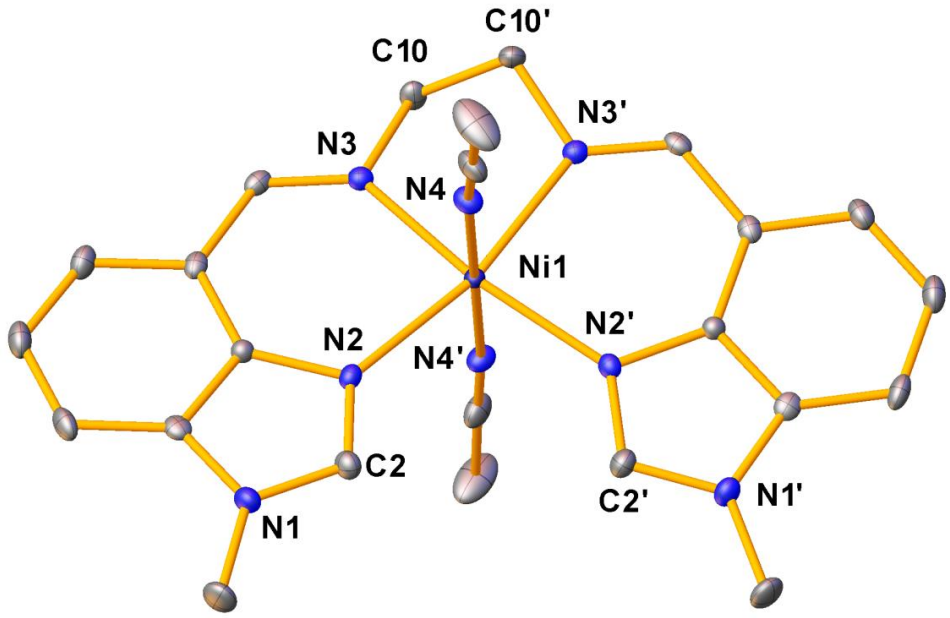
C10'
C10
N3'
N3
N4
Ni1
N2
N4'
N2'
C2
C2'
N1'
N1

(b)

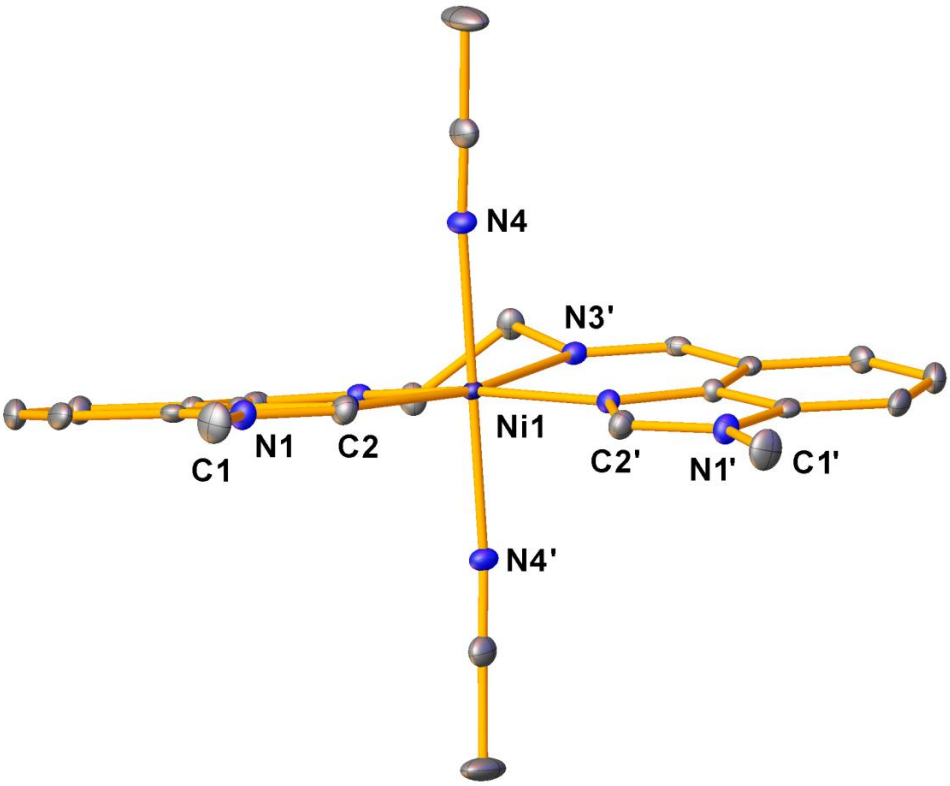
N4
N3'
Ni1
N1
C2
C2'
N1'
C1'
C1
N4'

(c)

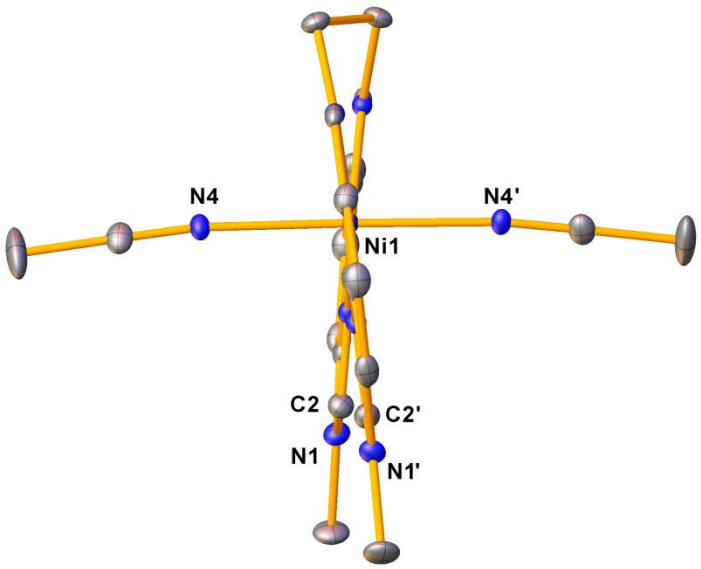

Figure 3.7 *Perspective views of the molecular structure of [NiMe(en)LH$_2$(MeCN)$_2$](PF$_6$)$_2$,* ***3****[2PF$_6$], showing* ***(a)*** *the equatorial coordination plane and* ***(b)*** *the subtle pseudo-helical conformation of the ligand, noting* ***(c)*** *the narrow spacing between the C2 and C2' atoms. Thermal ellipsoids are drawn at the 50 % probability level. All hydrogens, counteranions and lattice water molecules are omitted for clarity.*

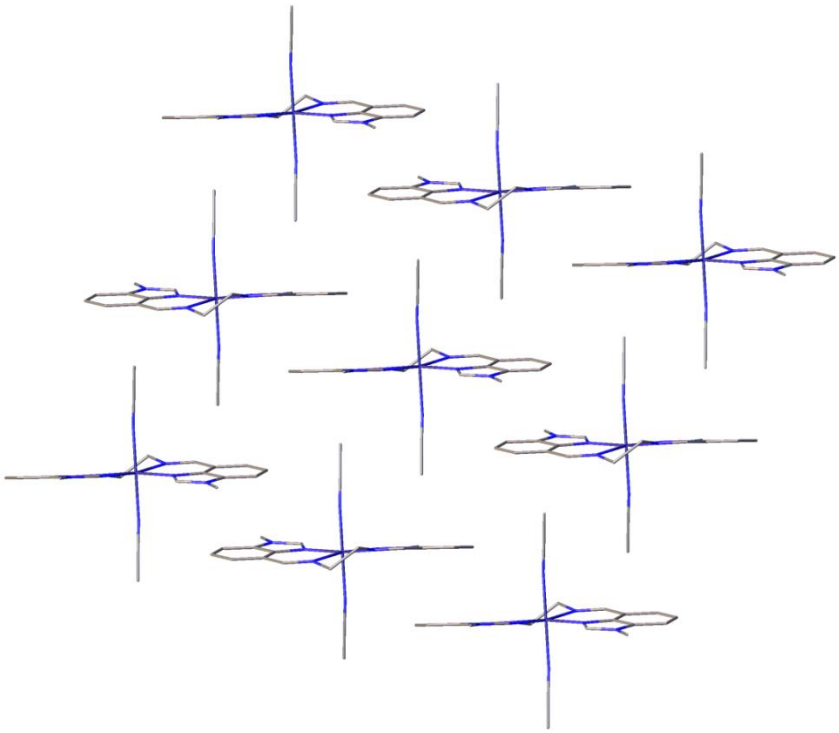

Figure 3.8 *Stick view of the crystal packing in* ***3****[2PF$_6$].*

Complex **4** crystallised in the monoclinic *C*2/*c* space group, and its asymmetric unit consisted of half the cationic complex and a hexafluorophosphate ion. The grown structure is depicted in Figure 3.9. The additional benzene ring in the linker unit may enhance the π-stacking ability of the complex cations. Each phenyl ring of a benzimidazole was overlaid by the phenylene linker of an adjacent cation, and vice versa in a stepped arrangement. The centroid-to-centroid distances were 3.6884(7) Å each.

(a)

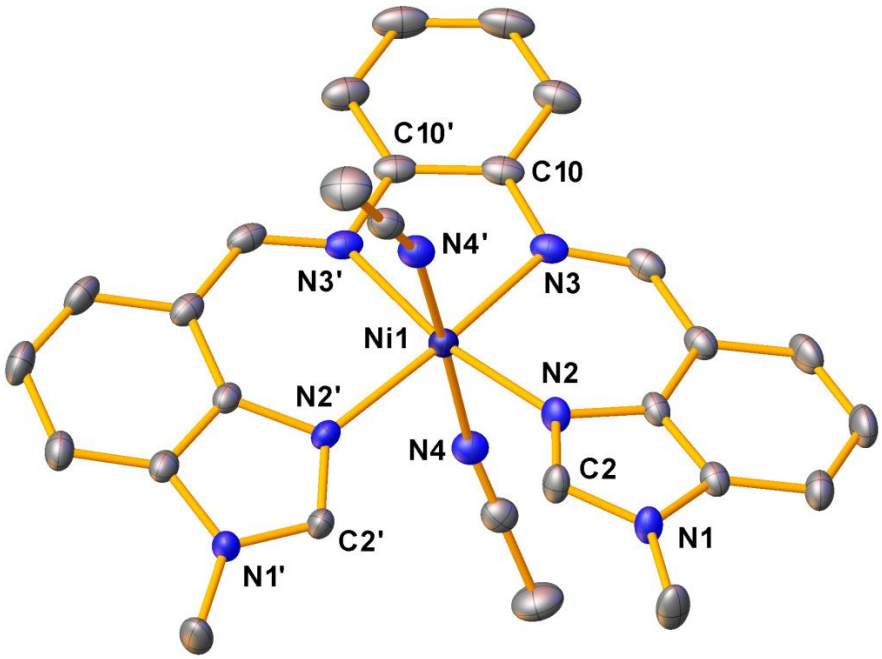

(b)

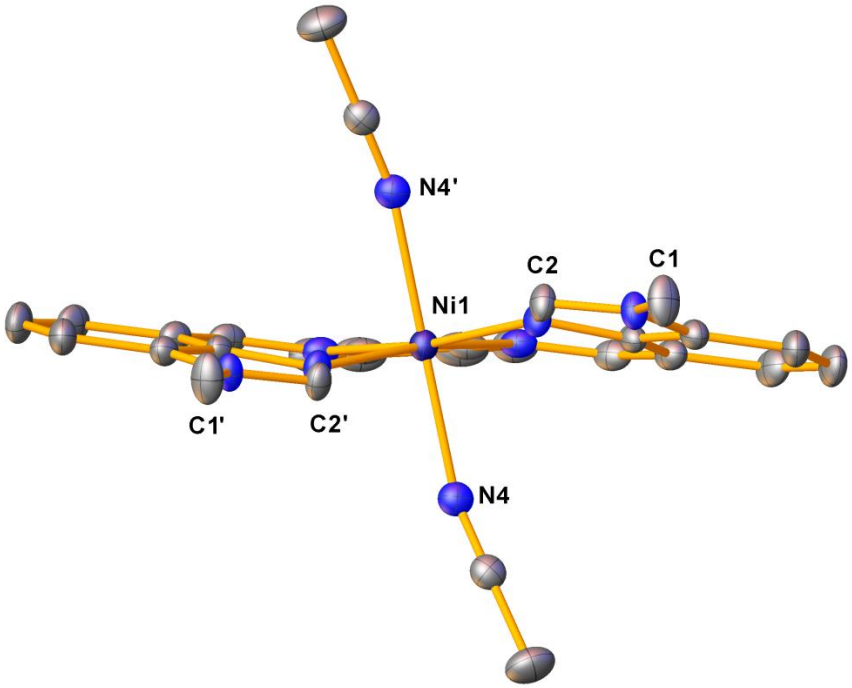

(c)

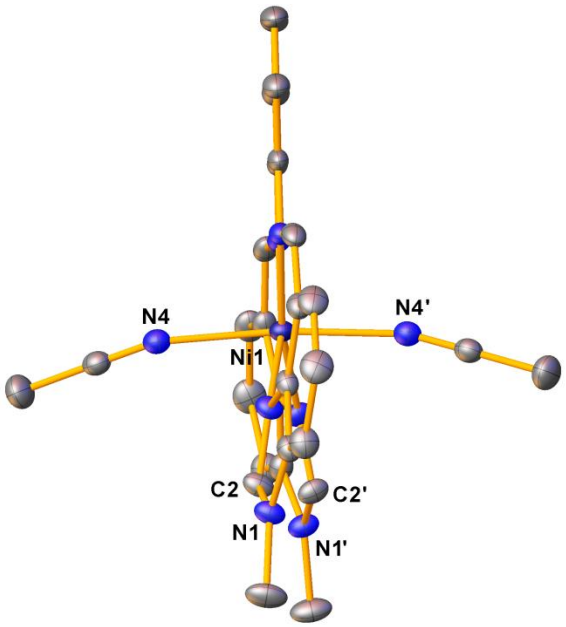

Figure 3.9 *Perspective views of the molecular structure of [NiMePhLH$_2$(MeCN)$_2$](PF$_6$)$_2$, **4**, highlighting **(a)** the equatorial coordination plane, **(b)** the slight helical twist of the ligand and **(c)** increased planarity along the bridge relative to **3**[2PF$_6$]. Thermal ellipsoids are shown at the 50 % probability level. All hydrogens and counteranions are omitted for clarity.*

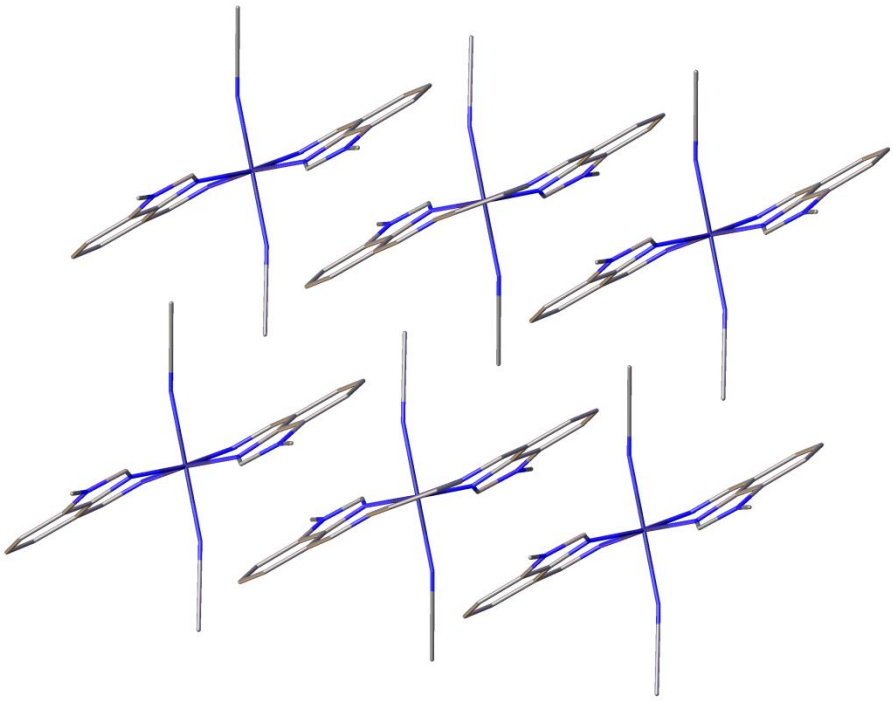

Figure 3.10 *Stick view of the crystal packing of the complex cations in **4**.*

(a)

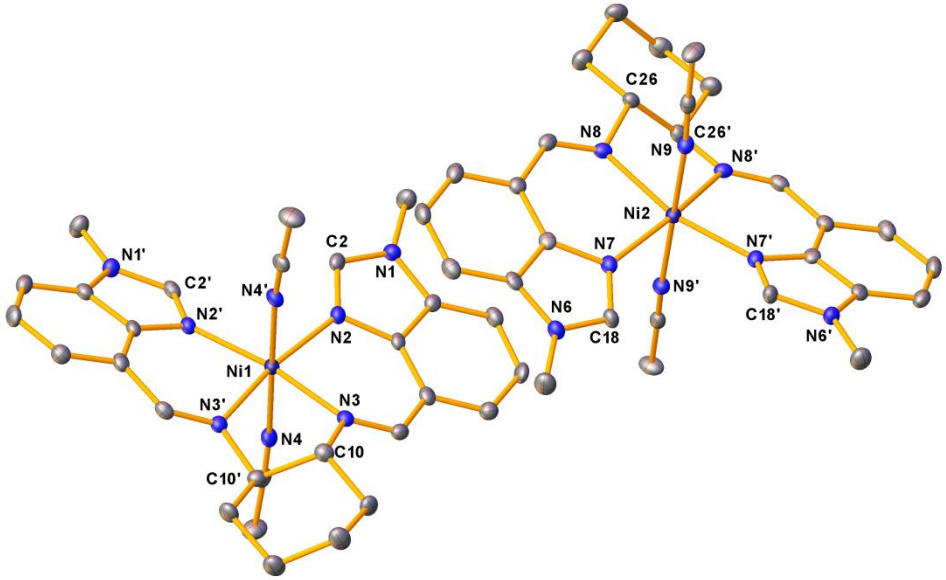
C26
N8
C26'
N9
N8'
Ni2
C2
N7
N7'
N1'
N1
N4'
N9'
C2'
N2'
N6
C18'
N2
C18
N6'
Ni1
N3'
N3
N4
C10
C10'

(b)

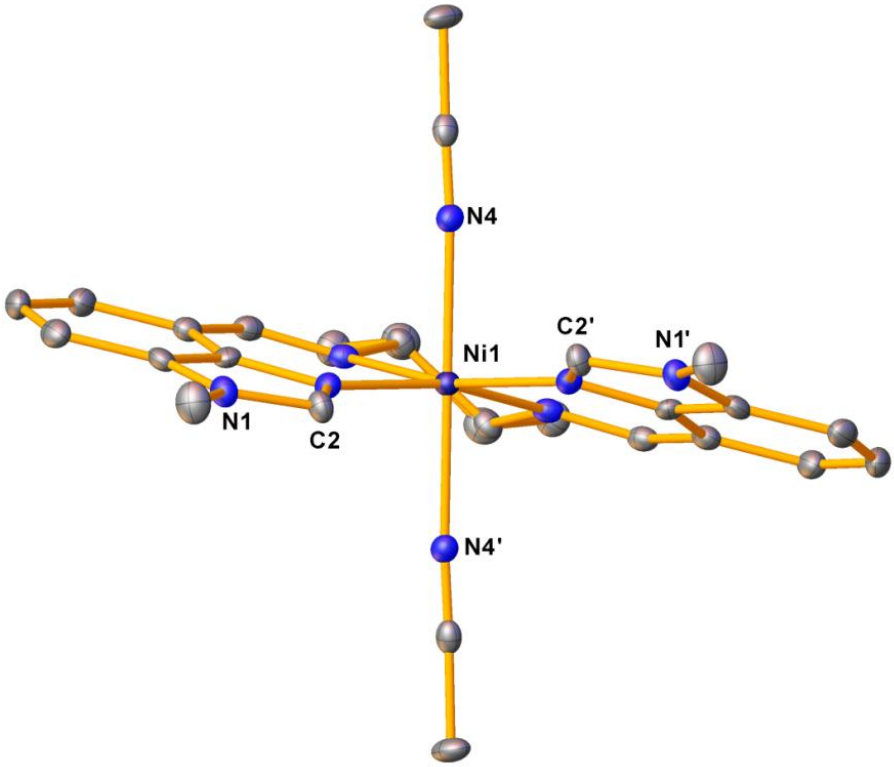
N4
C2'
N1'
Ni1
N1
C2
N4'

(c)

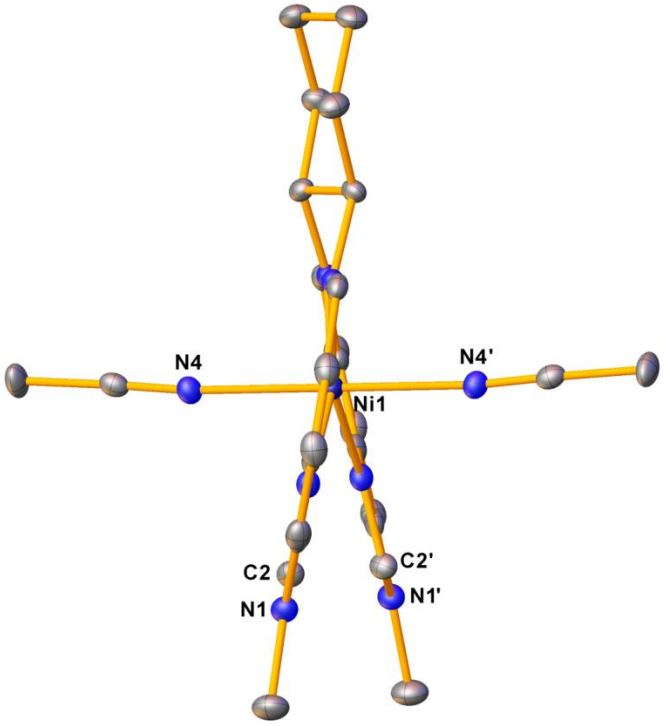

Figure 3.11 (a) *Two crystallographically distinct units of the complex cation in* $[NiMeCyLH_2(MeCN)_2](PF_6)_2$, ***5****. Alternative perspectives of the Ni1 cation reveal the* ***(b)*** *helicene-like coiling of the ligand around the metal centre and* ***(c)*** *widening of the spacing between the C2 and C2' atoms relative to* ***3****[2*PF_6*] and* ***4****. Thermal ellipsoids are shown at the 50 % probability level. All hydrogens, counteranions and lattice-bound acetonitrile molecules are omitted for clarity.*

The dark brown prisms of **5** crystallised in the non-centrosymmetric $P2_12_12$ space group. The asymmetric unit includes each half of two chemically equivalent but crystallographically distinct complex cations, two complete PF_6 ions and two co-crystallised acetonitrile molecules. Perspective views of the cationic complex are displayed in Figure 3.11. The bond lengths and angles of each complex unit were similar enough to each other that only the lengths and angles of one (labelled A) will be discussed. Here too, face-to-face π-stacking was seen between the arene portions of the benzimidazolyl rings in units A and B, with ring centroids spaced 3.6101(15) Å apart (Figure 3.12).

The bond lengths were generally very similar for **3**[2PF_6], **4** and **5**. Like **2**[2BF_4] and **3**[2BF_4], the axial Ni–N bonds were longer than the equatorial Ni–N bonds, as is characteristic for octahedral complexes.

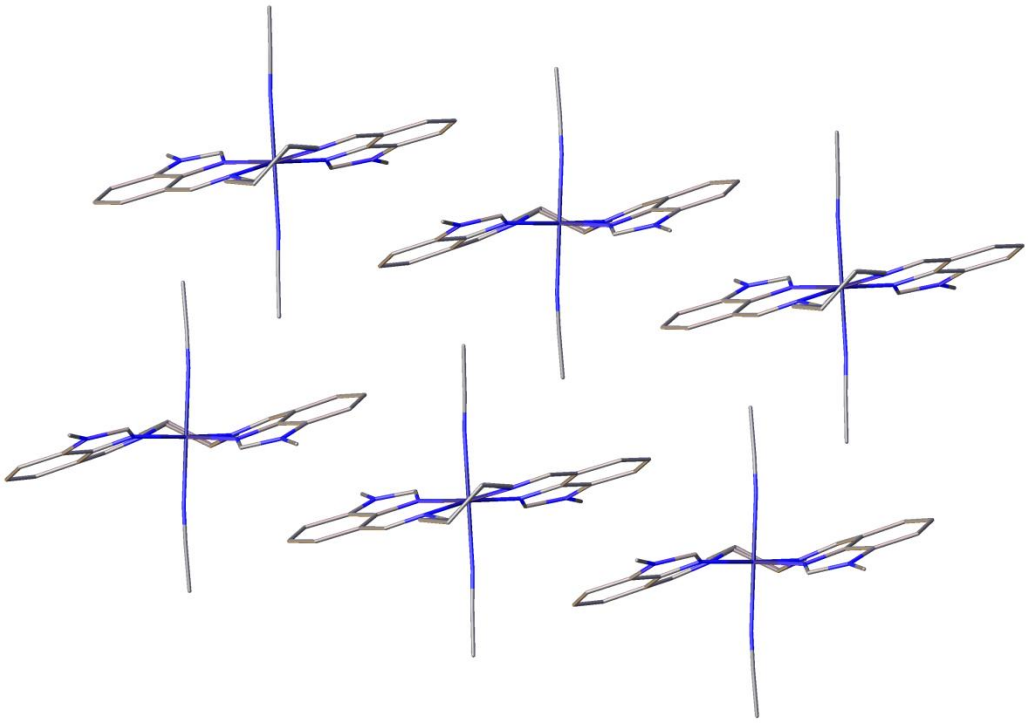

Figure 3.12 *Stick view showing intermolecular π-stacking between the complex cations of* ***5****.*

Complexes **4** and **5** featured comparable N2–Ni1–N2’ (and N7–Ni1–N7’) angles, whereas the corresponding angle for the ethylene analogue **3**[2PF_6] was *ca*. 20 ° narrower. This presumably originated from the limited ability of the cyclic backbones to bend out of plane, which is necessary to increase the vertical separation between the C2 atoms in **4** and **5**. Instead, the benzimidazoles were spread apart in the horizontal direction, and in this way, the steric repulsion between the C2-bound hydrogen atoms could be minimised. This was least effective in the highly rigid complex **4**, which had the shortest C2···C2’ distance, followed by $\mathbf{5}_B$ < **3**[2PF_6] < $\mathbf{5}_A$. Bridge twisting of similar magnitudes were observed in **3**[2PF_6] and **5**, but was virtually non-existent in the phenylene-linked **4**. To compensate, the ligand’s pseudo-helix angle was visibly larger in **4** than in **3**[2PF_6] and **5**, where distortions from the ideal octahedral geometry could be distributed across the ligand and not just the benzimidazole arms. Bond lengths and angles for the imidazolyl portion of the ligand were unremarkable and did not vary significantly within the series, showing no signs of the out-of-plane distortion observed in the indolyl complex **1**.

In an isolated incident, a small quantity of orange crystals of the four-coordinate [NiMe(en)LH_2](PF_6)$_2$ complex **8** was obtained when the presumed aqua adduct

was recrystallised from acetone/diethyl ether (Figure 3.13). The ^{1}H NMR spectrum of these crystals in d_6-acetone still bore paramagnetic resonances, but this could be due to coordination of trace water in the solvent to the nickel centres to regenerate the octahedral complex.

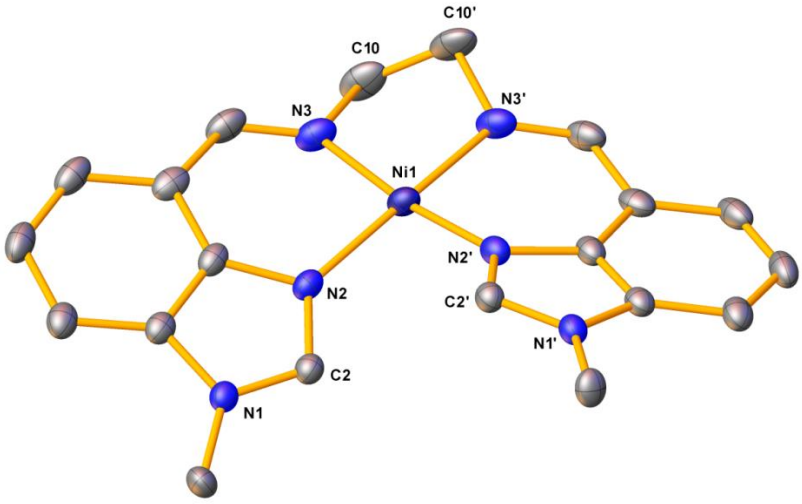

8

Figure 3.13 *Molecular structure of the four coordinate complex [NiMe(en)LH$_2$](PF$_6$)$_2$* ***8****. Hydrogen atoms and counterions are omitted for clarity. Thermal ellipsoids are shown at the 50 % probability level. Selected bond lengths or atom-to-atom distances (Å) and angles (°): Ni1–N2 1.893(2), Ni1–N3 1.913(2), N2–Ni1–N2' 93.58(13), N3–Ni1–N3' 84.38(15), N2–Ni1–N3 91.41(10), N3–C10–C10'–N3' 45.47(13), plane twist 9.33(13), C2···C2' 2.976(5).*

Like **3**[2BF$_4$], **3**[2PF$_6$] and **4**, crystals of **8** grew in the *C*2/*c* space group with an asymmetric unit that contained only half the complex cation and one PF$_6$ anion. As expected, the four-coordinate complex displayed a distorted square planar geometry. It should be emphasised that this outcome was difficult to reproduce, and so complex **8** could not be used as a deprotonation precursor despite possessing the desired geometry. Nevertheless, it was useful for comparing the structures of the four- and six-coordinate nickel(II) complexes of Me(en)LH$_2$.

The N–Ni–N angles were closer to 90° in **8** than in the octahedral **3**[2PF$_6$]. The Ni–N2(3) bond lengths {1.893(2)–1.913(2) Å} were roughly 0.2 Å shorter than in **3**[2PF$_6$], perhaps a reflection of the absence of additional electron donation from

the acetonitrile ligands. The Ni–N bond lengths in **1** compared well to **8**, falling between 1.876–1.906 Å.

Notably, every octahedral complex in the nickel(II) series featured a C2···C2' distance that exceeded that of **1** {2.96 Å} and **8** {2.976(5) Å}. The shorter Ni–N bonds in the two square planar complexes resulted in the *N*-heterocyclic arms being drawn inwards to the metal centre. Consequently, the benzimidazole arms in **8** were pushed further out of the nickel(II) coordination plane. The degree of skewing was aptly illustrated by the dihedral angle along C2–N2–Ni1–N2', which is greater in **8** {−23.15(19) °} than in **3**[2PF_6] {7.6(2) °}, **4** {−12.44(13) °} or **5** {15.3(3) °, −16.6(3) °}. The more exaggerated twisting in **8** results in less efficient π-stacking of the phenyl rings, as evidenced by the larger centroid-to-centroid distance of 3.730(2) Å (Figure 3.14).

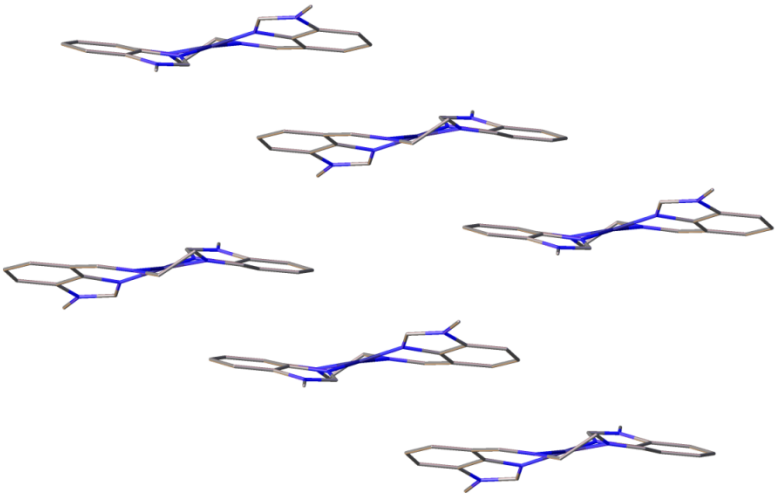

Figure 3.14 *Stick representation of crystal packing in* ***8****.*

In contrast to the phenylene-bridged complex **1**, both halves of the complex cation in **8** were geometrically equivalent. The more flexible chelate ring in the ethylene-bridged complex allowed for more variation in the positioning of the benzimidazoles. By comparison, the chelate ring created by the phenylene unit in **1** was highly planar. Accordingly, the skewing of the benzimidazole arms was most extreme in **1**, which featured a larger dihedral angle of 35.5 ° along C18–N3–Ni1–N1.[30]

Overall, the equatorial coordination planes in **3**[2BF_4], **3**[2PF_6], **4**, **5** and **8** exhibited minor deviations from planarity, with average plane twists of around 10 °. These deviations were much smaller in **2**[2BF_4], **2**[2OAc] and $\mathbf{5}_A$, where the plane twist was less than 3 °.

[NiMe(en)$LH_2(H_2O)_2$]$(OAc)_2$, **2**[2OAc], crystallised in the *C*2/*c* space group with an asymmetric unit comprising half the C_2-symmetric cation, an acetate ion and one co-crystallised methanol molecule. The acetate ion acted as a hydrogen bond acceptor for the Ni-bound water molecule, and the methanolic hydroxyl proton. Unlike complexes **2**[2BF_4] and **3**–**5**, the axial Ni–O bond {2.0798(12) Å} did not exhibit the characteristic lengthening relative to the equatorial Ni–N bonds {2.0620(15)–2.0935(15) Å}. In all other respects, the structure of **2**[2OAc] was very similar to **2**[2BF_4] and does not merit further discussion.

The $Ni^{II}_4(\mu_3\text{-OMe})_4$ core in **7** (Figure 3.15) is an interesting departure from the mononuclear complexes examined so far. Polynuclear metallic clusters such as Ni_4O_4 have unique magnetic characteristics that may be exploited in the assembly of new single molecule magnets for molecular electronics.[55–57] There are several recurring structural motifs in previously reported $Ni^{II}_4(\mu_3\text{-OMe})_4$ cubanes which partly resemble the features of **7**. For example, Ni(II) centres are often bridged by acetate[58–60] and sometimes pivalate[61,62] groups. The nickel(II) octahedral coordination sphere is frequently completed by bidentate *O*,*O*'-ligands derived from *o*-phenoxybenzaldehyde[63–66] or the ubiquitous acac[67–69] ligand. Bidentate *N*,*N*'-ligands are comparatively rare in Ni_4O_4 clusters, and tend to be simple amines such as 1,3,5-triaminocyclohexane[70] or *o*-phenylenediamine.[62] Complex **7** is the first example of benzimidazole coordination to a $Ni^{II}_4(\mu_3\text{-OMe})_4$ cubane. Me(en)LH_2 can be viewed as an unusual extended bridge between the two Ni atoms to which it was chelated.

Complex **7** crystallised in the monoclinic space group *C*2/*c*. The asymmetric unit contained half the cluster which resides on a crystallographic C_2 axis and several highly disordered methanol and water molecules in the lattice. Modelling of these co-crystallised molecules was unsuccessful, and their contribution was removed using a solvent mask procedure[71] implemented in OLEX2. Four solvent-accessible voids were identified, each with an estimated volume of 233.4 $Å^3$ and an electron count of 79. The R1 values before and after the application of the solvent mask were 15.45 % and 5.66 %, respectively.

(a)

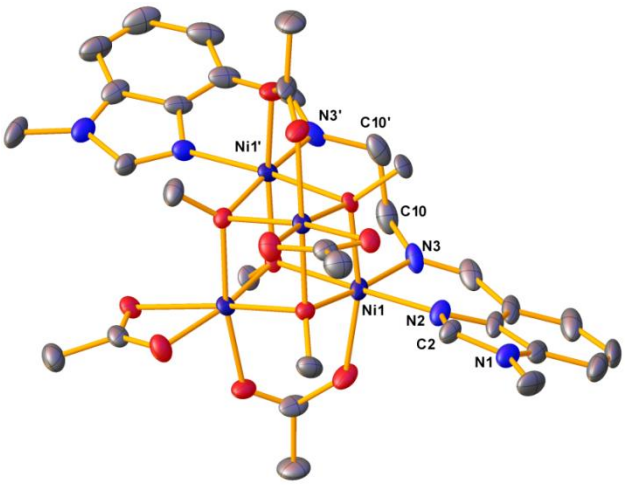

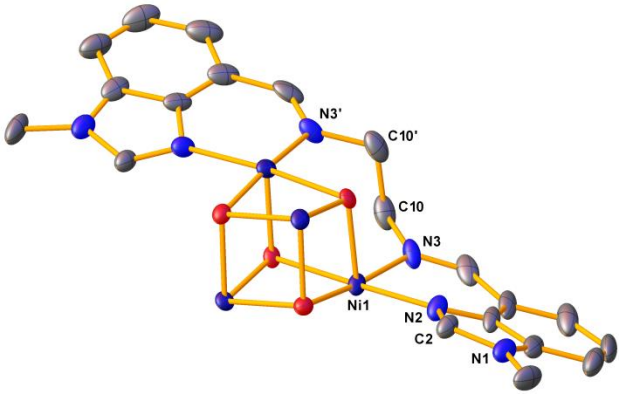

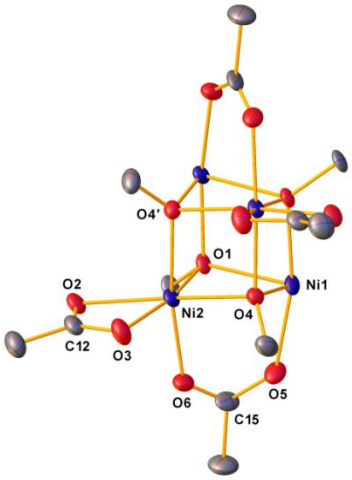

(b) (c)

Bond lengths (Å)		Bond angles (°)	
Ni1–N2	2.072(4)	N2–Ni1–N3	88.22(16)
Ni1–N3	2.131(4)	O4–Ni1–O1	84.35(11)
Ni1–O1	2.114(3)	O4–Ni1–O5	90.94(13)
Ni1–O1’	2.041(3)	O4–Ni1–O1’	80.62(11)
Ni1–O4	2.100(3)	Ni1–O1’–Ni1’	100.56(11)
Ni1–O5	2.061(3)	Ni1–O1’–Ni2’	99.83(12)
Ni2–O1	2.034(3)	O2–Ni2–O3	62.06(12)
Ni2–O2	2.114(3)	O4–Ni2–O1	88.71(12)
Ni2–O3	2.101(3)	O4–Ni2–O4’	82.86(11)
Ni2–O4	2.013(3)	O6–Ni2–O1	89.75(13)
Ni2–O4’	2.050(3)	Ni2–O4’–Ni2’	97.14(11)
Ni2–O6	2.047(3)	O2–Ni2–O4’	95.42(11)

Figure 3.15 *Molecular structure of complex **7** **(a)** in its entirety; **(b)** showing only the Ni_4O_4 core and $Me(en)LH_2$ ligand; **(c)** with $Me(en)LH_2$ hidden from view. Hydrogen atoms are omitted for clarity. Thermal ellipsoids are drawn at the 50 % probability level. Selected bonds and angles are shown in the table.*

The dihedral angle along the ethylene bridge was 107 °, approximately double the equivalent angle in **3**[2PF_6]. The C2 and C2' atoms were separated by a distance of 8.397(8) Å. These figures confirmed what was obvious upon visual inspection: The benzimidazole arms in Me(en)LH_2 were spread fan-like, far apart from each other. This should be impossible for the more conformationally rigid MePhLH_2 and MeCyLH_2. The benzimidazole arms were clearly not coplanar, as each half of the ligand was coordinated to a vertex that was diagonally opposite to the other.

The ligand environments of Ni1 and Ni2 were differentiated by the equatorial coordination plane, which was filled in two sites by Me(en)LH_2 or a chelating acetate group. Ni2 exhibits greater distortion from the ideal octahedral geometry as a consequence of the 4-membered acetate chelate ring, which resulted in a narrow bite angle of 59.94(12) °. In contrast, the N2–Ni1–N3 bite angle {88.22(16) °} was much closer to the ideal 90 ° for an octahedral complex. The range for all other O–Ni–O angles and Ni–O bond lengths were quite similar between the Ni1 {79.29(11)–94.54(15)°; 2.041(3)–2.131(4) Å} and Ni2 {82.01(12)–98.52(13)°; 2.013(3)–2.114(3) Å} centres.

Although the Ni_4O_4 core featured Ni–O bond lengths that were close to uniform {2.013(3)–2.114(3) Å}, the Ni–O–Ni and O–Ni–O angles of 91.03(11)–100.56(11) ° and 79.29(11)–88.71(12) ° were more variable. The long Ni···Ni distances {2.9596(10) – 3.1963(13) Å} were not suggestive of metal–metal bonding. Overall, the geometric parameters of **7** were in excellent agreement with the bond lengths and angles of a closely related $Ni^{II}_4(\mu_3\text{-OMe})_4$ containing 1,2-diamino-4,5-dimethylbenzene and pivalate ligands.

Given the difficulty of acquiring anhydrous nickel(II) acetate and assessing its purity, this was not pursued any further. There were also other reasons to seek better alternatives to nickel(II). For one, all these nickel complexes were paramagnetic, rendering real-time reaction monitoring by NMR spectroscopy more difficult to interpret. This left SC-XRD as the main method available for meaningful characterisation of the reaction products. The prospect of relying so heavily on the ability to obtain suitable crystals was less appealing, and alternative metals were assessed for the synthesis of deprotonation precursors.

3.2 Synthesis, structure and attempted oxidation of cobalt(II) complexes of Me(en)LH_2

St Clair Black and coworkers reported the preparation of cobalt(II) complexes featuring indolyl ligands which had coordination environments similar to $MeRLH_2$.[30,72] The solid state structures of these complexes could not be determined, but it was inferred from their FAB mass spectra and IR spectra that the cobalt(II) ion assumed a square planar geometry. Whether a four-coordinate cobalt(II) complex will adopt a tetrahedral or square planar geometry is largely dependent on the conformation of the ligand(s). Unlinked imidazole,[73–75] pyrazole[74] or diimine[76] ligands tend to produce tetrahedral complexes, whereas the more constrained porphyrin,[77] NacNac[78,79] or macrocyclic imine[80,81] ligands give rise to square planar complexes. The coordination geometry in $MeRLH_2$ may be simulated by ring-opened porphyrin complexes, in which the CoN_4 units were arranged in a distorted square planar[82] or tetrahedral[83] configuration. Based on those trends, it was anticipated that the four-coordinate complexes of Me(en)LH_2 could be obtained from cobalt(II).

The crude product from the reaction of $Co(OAc)_2{\bullet}4H_2O$ with Me(en)LH_2 and $NaPF_6$ was dissolved in acetonitrile, and recrystallised by vapour diffusion with diethyl ether to afford complex **9** as orange blocks (Scheme 3.7). Despite the good crystal quality, the crystallographic modelling for **9** was problematic and anisotropic refinement was not possible. As such, the SC-XRD data was only used to establish atom connectivity. The resulting octahedral cobalt(II) complex appeared to be isostructural to the nickel(II) complex **3**[$2PF_6$], with Me(en)LH_2 occupying the equatorial coordination plane, and acetonitrile ligands in the two apical positions. Six broadened resonances were observed over the range of 6 – 110 ppm in the ^{1}H NMR spectrum of the crystallised sample, confirming the paramagnetic nature of the cobalt(II) species. The major species detected in the ESI mass spectrum was the desolvated $[CoMe(en)LH_2]^{2+}$ ion, which was unsurprising given that similar desolvations were observed for other cobalt(II) acetonitrile complexes.[47,84] The imine C=N stretching frequency in the IR spectrum of **9** demonstrated an increase of 12 cm^{-1} relative to the free ligand.

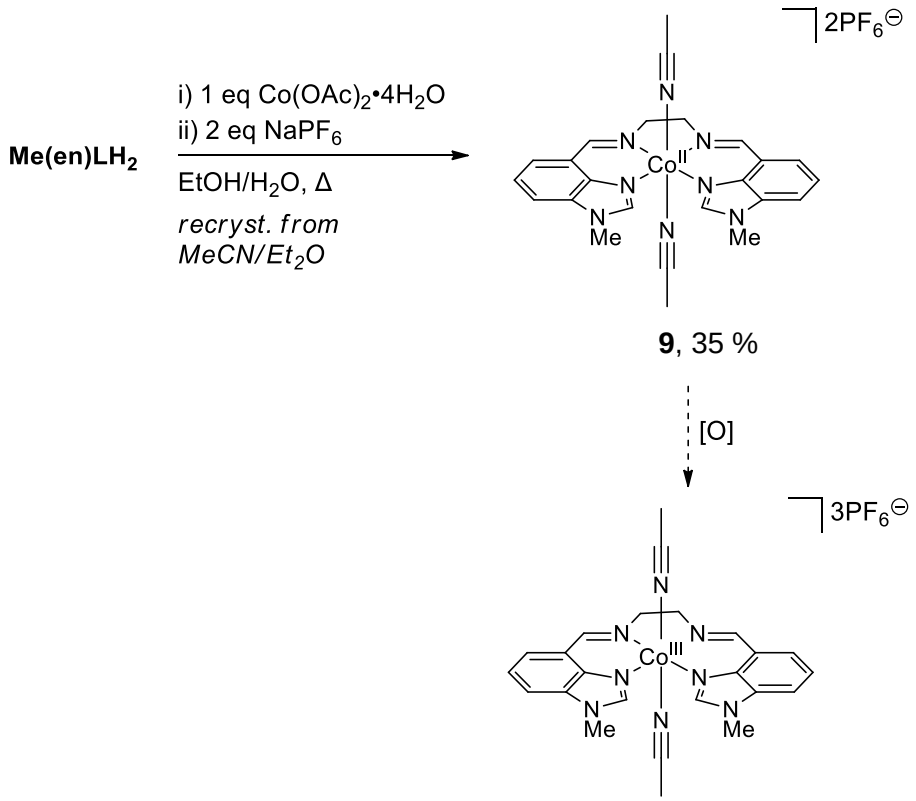

Scheme 3.7 *Synthesis of [CoMe(en)LH$_2$(MeCN)$_2$](PF$_6$)$_2$,* ***9*** *and proposed oxidation into the cobalt(III) complex.*

On one occasion, the recrystallisation of **9** was accompanied by a small amount of slightly darker orange crystals. SC-XRD analysis of these crystals revealed that they were [CoMe(en)LH$_2$(OAc)](PF$_6$) **10** (Figure 3.16). The formation of the cobalt(II) acetate product indicated incomplete anion exchange in that instance, and was attributed to a slight deficit of NaPF$_6$. In this severely distorted octahedral complex, the acetate ligand coordinated to the cobalt ion in a bidentate fashion. The cobalt(II) ion, N_{imine} and one of the N_{Bim} atoms of Me(en)LH$_2$ were approximately coplanar. One of the acetate O atoms resided in what may be considered the fourth equatorial coordination site, although it was offset from the aforementioned Co/N2/N3/N4 plane. One of the benzimidazole arms was bent downwards, and its coordinated N atom occupied the remaining pseudo-axial position. This resulted in a greater separation of the benzimidazole C2 atoms [C2···C19 3.616(3) Å], and a much larger plane twist [140.67(8)°] compared to the other mononuclear octahedral complexes of Me(en)LH$_2$ studied so far. The M–N bonds {2.0589(19)–2.1339(19) Å} were longer in **10** than in **3**[2PF$_6$] {2.083(2)–2.088(2) Å}. The Co–N bonds were shorter than the asymmetrical Co–O bonds [2.1463(17), 2.2791(17) Å]. Similar Co–N and Co–$O_{acetate}$ bond distances were reported for a $Co^{II}N_4$ quarterpyridine complex.[85]

The crystal lattice included a non-coordinating water molecule, which was involved in hydrogen bonding with a fluorine atom of an adjacent PF_6 anion, and one acetate O in the cationic complex.

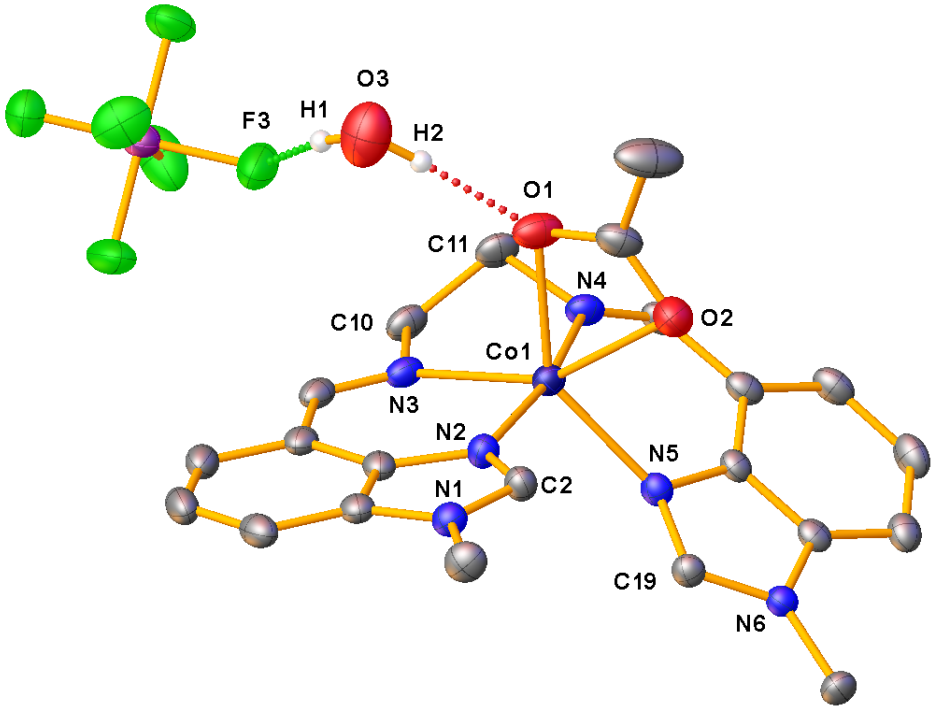

10

Bond lengths and distances (Å)		Bond angles (°)	
Co1–N2	2.0589(19)	N2–Co1–N3	89.99(7)
Co1–N3	2.1318(18)	N3–Co1–N4	77.71(7)
Co1–N4	2.1339(19)	N4–Co1–N5	86.12(7)
Co1–N5	2.0880(18)	N2–Co1–N5	99.55(7)
Co1–O1	2.1463(17)	O1–Co1–O2	58.86(6)
Co1–O2	2.2791(17)	N3–C10–C11–N4	51.06(19)
C2···C19	3.616(3)	Plane twist	140.67(8)

Figure 3.16 *Molecular structure of [CoMe(en)LH_2(OAc)](PF_6)* **10** *with selected bonds and angles. Thermal ellipsoids are drawn at the 50 % probability level. All C-bound hydrogens and lattice solvent are omitted for clarity.*

The formation of octahedral cobalt(II) complexes mirrored the results obtained with nickel(II), strengthening the notion than the imine-type nitrogens in $MeRLH_2$ are insufficiently strong donors to limit the coordination number to four. Drew and coworkers found that the metal centres in their macrocyclic tetraimino-dicobalt(II) complexes adopted tetrahedral geometries when the co-ligands were halides or

thiolate, but preferred trigonal bipyramidal geometries in the case of phenoxide or thiocyanate co-ligands.[86] These results were rationalised using Pauling's electroneutrality principle.[87] "Hard" or electronegative ligands such as phenoxide or thiocyanate were less effective at counteracting the positive charge on the metal centre, leading to an increase in coordination number to include additional ligands such as MeCN. As imino and benzimidazole nitrogens can also be classified as hard donors, this may explain the prevalence of higher coordination numbers in complexes of $MeRLH_2$.

Since complex **9** contained a d^7 metal ion, it presented the same spectroscopic challenges as its paramagnetic nickel(II) predecessors. Plans to circumvent this involved the conversion of the cobalt(II) ion into its diamagnetic cobalt(III) state. Complex **9** was stable when stored at bench conditions; that is, exposure to air alone did not trigger a change in oxidation state. $AgSbF_6$ has been used to generate a cobalt(III) species *in situ* from a cobalt(II) precursor.[88,89] In order to maintain consistency of the counterions, **9** was treated with 1 equivalent of $AgPF_6$ as the oxidant, stirring in MeCN at room temperature for 18 days. A fine grey deposit presumed to be elemental silver was removed by filtration, leaving an orange-brown residue that could not be redissolved in acetonitrile or methanol. Suspending the residue in CH_2Cl_2 also failed to solubilise it, but resulted in a colour change to a very dark green.

The ^1H NMR spectrum of this poorly soluble green solid contained only resonances in the diamagnetic range, and revealed the presence of several $Me(en)LH_2$-related species with one dominant component. These signals did not match those of the free ligand, suggesting that demetallation had not occurred. Transmetallation with Ag(I) also seemed unlikely, as the colour, solubility and spectroscopic characteristics of this complex did not resemble those of the silver(I) complexes which will be reported in a subsequent section. Presumably, the diamagnetic species are Co(III) complexes of $Me(en)LH_2$, although the role of dichloromethane in the reaction (if any) is unclear. The poor solubility of the oxidation products precluded further purification or characterisation.

The possibilities for accessing the cobalt(III) complex were far from exhausted. A number of alternative oxidation methods for cobalt(II) are known. Cerium(IV) salts[90] or *N*-bromohexamethyldisilazane[91] have been successfully used as oxidising agents for such a transformation. Bubbling oxygen gas through a solution of the cobalt(II) complex may also be effective, although the oxidation

process can be slow.[92] Alternatively, the diamagnetic complex could be prepared directly from the complexation of Me(en)LH_2 with a cobalt(III) source such as $Na_3[Co(CO_3)_3]$•$3H_2O$.[93] The studies by Drew and colleagues[86] suggest that Me(en)LH_2 alone may not stabilise a trivalent cobalt, and that the substitution of the weakly coordinating PF_6 anion with more polarisable counterions may be required. These strategies were ultimately left untested, as other metals being screened in parallel to the cobalt studies produced complexes which were more promising deprotonation precursors.

3.3 Copper(II) complexes of Me(en)LH_2

Being a d^9 ion, copper(II) must always be paramagnetic. It exhibits highly variable coordination geometries, which the enterprising chemist could view as an opportunity to visualise how Me(en)LH_2 might accommodate non-octahedral metal centres. These studies could help inform the long term goal of using MeRLH_2 complexes in catalysis, where there is no need to be limited by the requirement for diamagnetism. To this end, two copper(II) complexes were prepared: One from $Cu(NO_3)_2$•$2.5H_2O$, and one from $CuCl_2$ (Scheme 3.8).

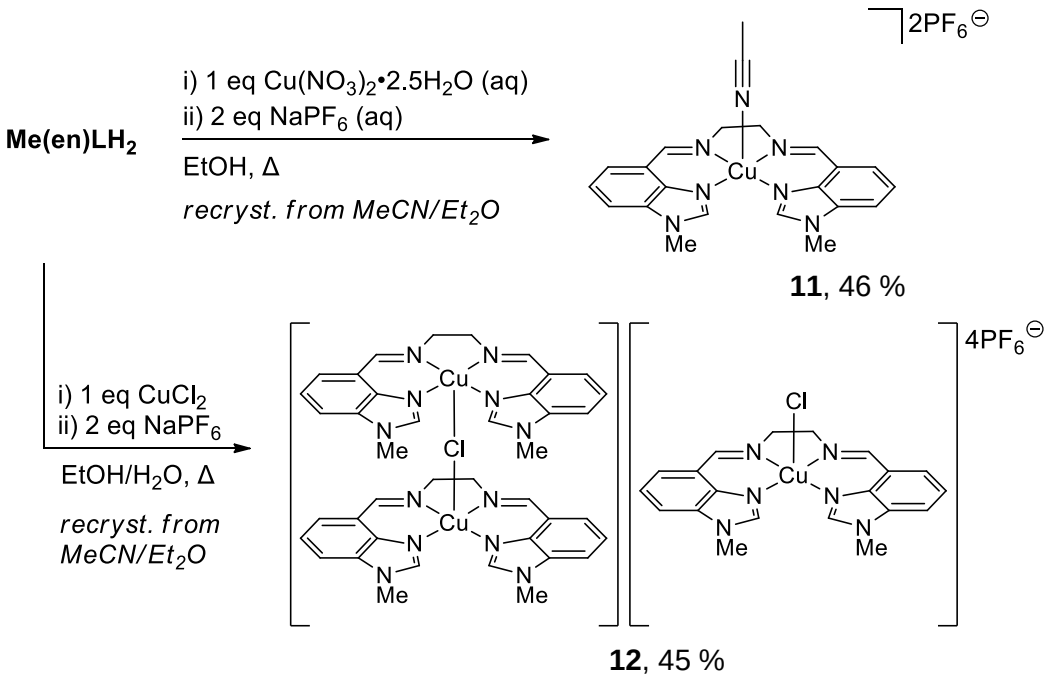

Scheme 3.8 *Counterion effects on the apical site occupant in square pyramidal copper(II) complexes of Me(en)LH_2.*

When $Cu(NO_3)_2$•$2.5H_2O$ was used as the starting material, [CuMe(en)LH_2(MeCN)]$(PF_6)_2$, **11** was obtained as deep blue blocks upon

crystallisation from acetonitrile/diethyl ether. Its molecular structure was analysed by SC-XRD as the pentacoordinate acetonitrile adduct (Figure 3.17). Consistent with this, the expected $[CuMe(en)LH_2]^{2+}$ cation at *m*/*z* = 204 was identified in the ESI mass spectrum, revealing a loss of the coordinated MeCN. A similar desolvation was observed for the acetonitrile adducts **3**[$2PF_6$], **3**[$2BF_4$] and **9**. Three contact-shifted resonances between 5 – 11 ppm could be discerned from the ^{1}H NMR spectrum of **11** recorded in CD_3CN over the −200 to 200 ppm range, corroborating the complexation of a paramagnetic copper(II) ion. The remaining shifts were possibly too broad to be identified. The elemental composition of **11** was in excellent agreement with the solid state structure.

Interestingly, the counteranion exchange with $NaPF_6$ was only partially effective when $CuCl_2$ was used as the copper source. Recrystallisation of the crude product from acetonitrile/diethyl ether furnished **12** as blue crystalline blocks which were identified by SC-XRD as a 1:1 mixture of two discrete complex cations: a chloride-bridged dimer $\{[CuMe(en)LH_2]_2Cl\}^{3+}$ and a mononuclear $[CuMe(en)LH_2Cl]^+$. Charge balance was maintained by four non-coordinating PF_6 anions, indicating that anion exchange was at least successful for the chlorides that were not involved in coordination.

Presently, it is uncertain whether the 1:1 mixture of monomeric and dimeric chloride-bridged copper(II) complexes was representative of the bulk product. The results from elemental analysis were more consistent with a formulation of $\{[CuMe(en)LH_2]_2Cl\}(PF_6)_3$. The ESI mass spectrum of **12** did not provide unequivocal evidence for the dinuclear cation. The expected peak at *m*/*z* = 283 for $\{[CuMe(en)LH_2]_2Cl\}^{3+}$ was not detected. Instead, two peaks were found at *m*/*z* = 204 and 442, matching the calculated values for a $[CuMe(en)LH_2]^{2+}$ fragment and $[CuMe(en)LH_2Cl]^+$ ion respectively. This may be indicative of dimer dissociation under ionisation conditions. The ^{1}H NMR spectrum in CD_3CN confirmed the paramagnetic nature of the complex. Four broad resonances appearing in the 5 – 30 ppm range could be assigned to **12**. The chemical shifts were similar to, yet distinct from those observed for **11**, showing that the copper(II) ions in both complexes retained their different ligand environments in the solution state. The retention of the chloride but not the nitrate was easily justified, since chloride is generally a stronger ligand than nitrate or acetonitrile. This shows that the choice of counterion in the metal precursor can affect the reaction outcome, even if anion exchange with $NaPF_6$ is performed.

The formation of the Cu2 dimer suggests that some of the chloride ligands in the presumed [CuMe(en)LH_2Cl]Cl intermediate were exchanged for PF_6 anions, along with the non-coordinating chloride ions. A greater excess of $NaPF_6$ may encourage more complete anion exchange, although a similar exchange between a $CuCl_2$ imidazole/imine complex with an excess 1 equivalent of NH_4NO_3 only succeeded in removing half the chloride ions (Scheme 3.9).[94] It is plausible that the Cu–Cl bond is simply more thermodynamically favourable for the product complex than a $Cu–O_{nitrate}$ or $Cu–N_{MeCN}$ bond.

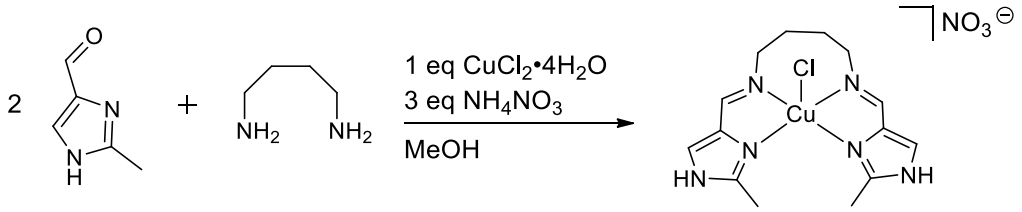

Scheme 3.9 *Formation of a mixed chloride/nitrate complex of copper(II) despite the presence of excess NH_4NO_3.*

3.3.1 Solid state structural studies of CuMe(en)LH_2 complexes

Complex **11** crystallised in the *P*2_1/*c* space group, and its asymmetric unit was made up of the complex cation and two PF_6 anions. The copper(II) atom adopted a square pyramidal geometry where the four N donors in Me(en)LH_2 filled the equatorial positions, while one MeCN occupied the apical site (Figure 3.17). The complex exhibited a slight tetrahedral distortion along the square base, with a plane twist (Figure 3.6 b) of 23.58(7) °, larger than those observed for the octahedral nickel(II) complexes. The $Cu–N_{MeCN}$ bond was nearly 0.4 Å longer than the other Cu–N bonds, and about 0.2 Å longer than the $Ni–N_{MeCN}$ bonds in the MeRLH_2 complexes. The bond lengths in **11** were very similar to those reported for another $Cu^{II}N_5$ square pyramidal complex bearing a tripodal bis(imidazole) ligand.[95] Like many other square pyramidal copper(II) complexes, the axial bond in **11** exhibited Jahn-Teller elongation relative to the basal bonds.[44,47,95–97] Additionally, it has been noted that other copper imine/imidazole complexes had $Cu–N_{imine}$ bonds that were longer than the $Cu–N_{imidazole}$ bonds, and this was also observed for **11**.[97]

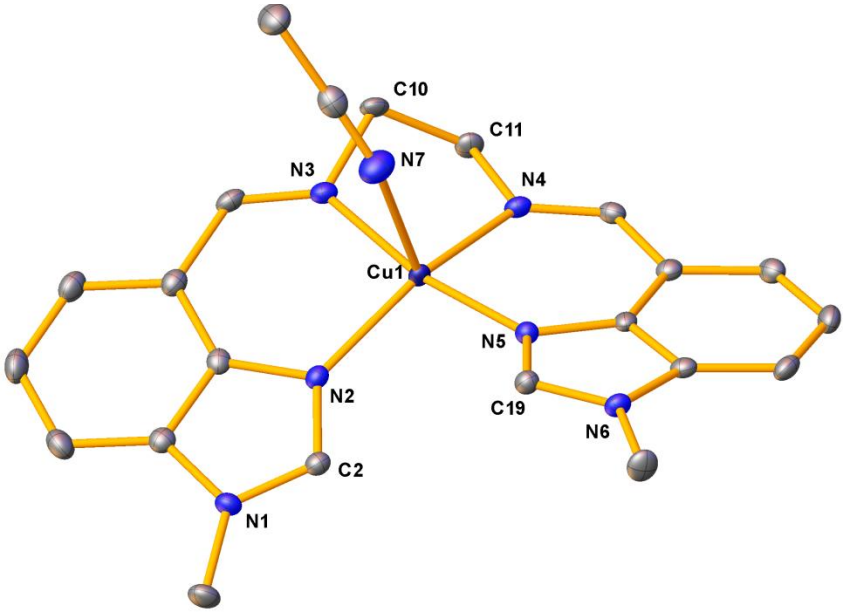

Bond lengths and distances (Å)		Bond angles (°)	
Cu–N2	1.9938(16)	N2–Cu–N3	91.62(6)
Cu–N3	2.0059(16)	N2–Cu–N5	98.04(6)
Cu–N4	2.0199(16)	N3–Cu–N4	82.84(6)
Cu–N5	1.9865(16)	N4–Cu–N5	91.25(7)
Cu–N7	2.3789(19)	N2–Cu–N7	97.30(7)
C2···C19	3.299(3)	N3–C10–C11–N4	−48.91(16)
		C2–N2–Cu1–N5	−7.2(2)

Figure 3.17 *Molecular structure and selected bonds and angles of [CuMe(en)LH$_2$(MeCN)](PF$_6$)$_2$,* ***11****. Hydrogen atoms and counterions are omitted for clarity. Thermal ellipsoids are shown at the 50 % probability level.*

Each cation in **11** was linked to two other cations in the crystal lattice by π-stacking of the arene rings, forming long strands which are arranged in rows on top of each other (Figure 3.18). The π-stacking distances [3.5582(17), 3.6215(16) Å] were comparable to those seen in the octahedral Ni(II) complexes, suggesting that the square pyramidal geometry did not result in improved packing efficiency.

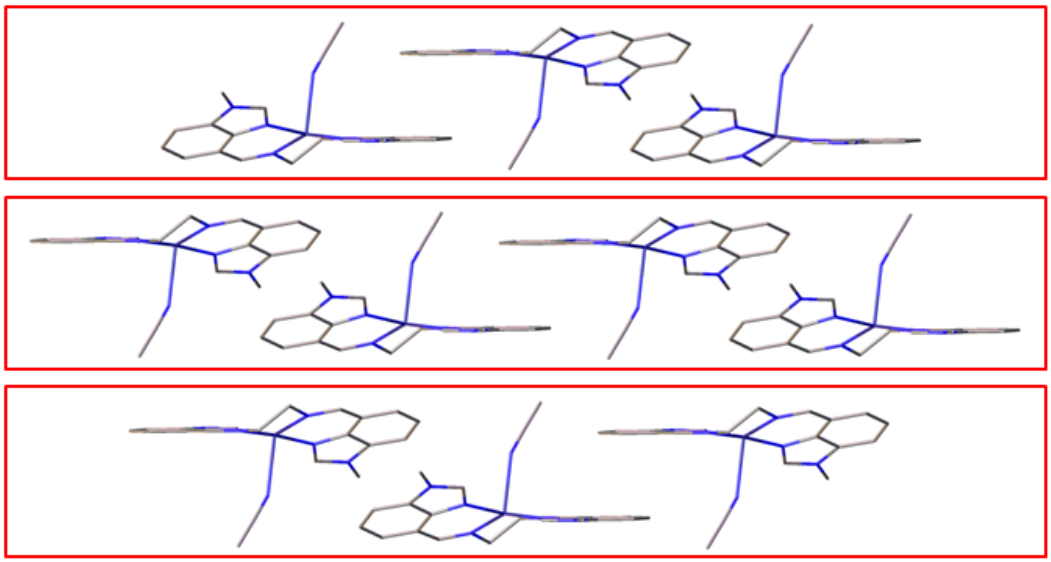

Figure 3.18 *Crystal packing in [CuMe(en)LH$_2$(MeCN)](PF$_6$)$_2$,* ***11****.*

The chloride complex **12** crystallised in the triclinic space group, *P*-1. Half the dimeric cation, one complete mononuclear cation, and two and a half PF_6 anions formed the asymmetric unit. The other half of the dimer was generated by symmetry through the crystallographic inversion centre at Cl2. The cationic structures are depicted in Figure 3.19.

The incomplete anion residue exhibited rotational disorder, which was modelled over two positions and refined to a 50:50 occupancy. No sensible refinement could be achieved for a disordered solvent molecule believed to be diethyl ether that was also present in the lattice. The total solvent-accessible volume was estimated to be 161.5 Å^3. The largest of the three voids had a calculated volume of 121.8 Å^3 and an electron count of 64, which could be in line with one diethyl ether molecule and two water molecules. This electron density was treated as a diffuse contribution to the overall scattering using the solvent mask procedure implemented in OLEX2, leading to a decrease in the converged R1 value from 7.90 % to 4.95 %.

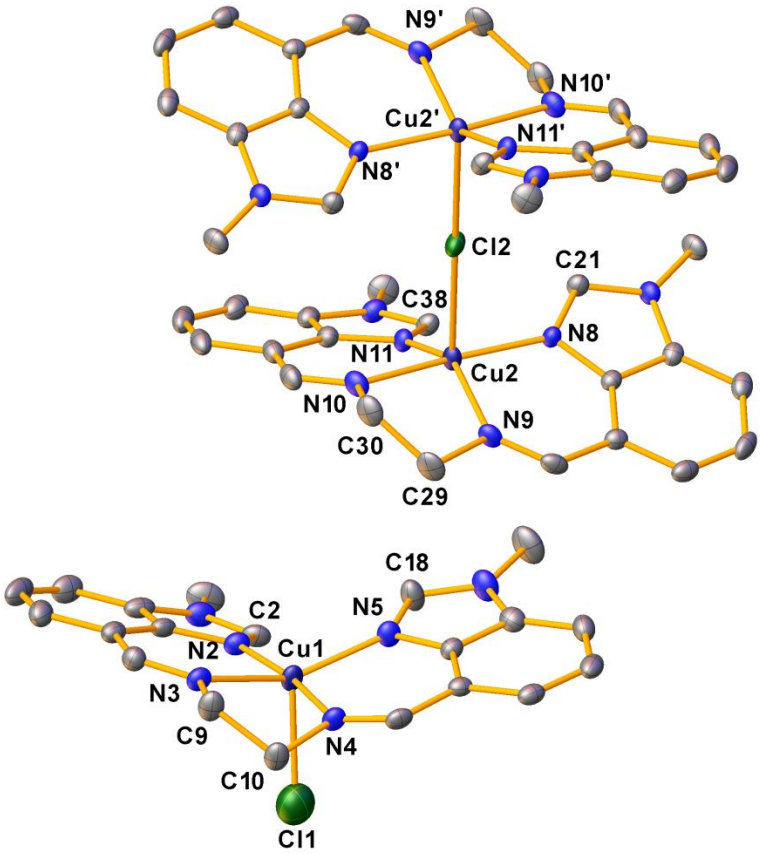

Bond lengths and distances (Å)		Bond angles (°)	
Cu1–N2	1.993(3)	N2–Cu1–N3	90.95(12)
Cu1–N3	2.031(3)	N2–Cu1–N5	97.19(12)
Cu1–N4	2.013(3)	N3–Cu1–N4	81.51(12)
Cu1–N5	2.007(3)	N3–C9–C10–N4	47.3(3)
Cu1–Cl1	2.4924(17)	Plane twist (Cu1)	20.94(12)
C2···C18	3.247(5)		
Cu2–N8	1.965(3)	N8–Cu2–N11	95.79(11)
Cu2–N9	2.039(3)	N8–Cu2–N9	91.19(12)
Cu2–N10	1.991(3)	N9–Cu2–N10	82.51(12)
Cu2–N11	2.007(3)	N9–C29–C30–N10	46.1(3)
Cu2–Cl2	2.6034(5)	Plane twist (Cu2)	25.11(12)
C21···C38	3.242(5)		

Figure 3.19 *Thermal ellipsoid representation of the mixed cation copper(II) complex* ***12*** *at the 50 % probability level with selected bond lengths and angles. All hydrogen atoms and non-coordinating counterions are omitted for clarity.*

There are numerous complexes bearing the square pyramidal $Cu^{II}N_4Cl$ binding motif where the axial chloride is non-bridging,[94,98,99] but fewer examples where the chloride forms a linear bridge to another copper atom. The Cu1 cation with the terminal chloride was crystallographically similar to **11**, albeit with a slightly longer axial bond. The Cu2–Cl2–Cu2' bridge in the dinuclear cation was linear based on crystallographic symmetry (angle of 180 °). The Cu2–Cl2 bond {2.6034(5) Å} was slightly longer than the Cu1–Cl1 bond {2.4924(17) Å}. In the only other example of a directly comparable pair of square pyramidal copper(II) complexes featuring terminal and bridging chlorides, the reverse situation was observed, where the Cu–(μ-Cl) bond was the shorter of the two by 0.04 Å.[100] Apart from this observation, the bond lengths and angles of **12** were in agreement with those of previously reported square pyramidal $Cu^{II}N_4Cl_{(terminal)}$[94,98,101] and $Cu^{II}N_4(\mu\text{-}Cl)$[102–104] complexes bearing *N*-heterocyclic ligands such as pyridine, imidazole or pyrazole. Both the Cu1 and Cu2 cations shared a characteristic that is common to most $Cu^{II}N_4Cl$ complexes: The Cu–Cl bond is much longer than the Cu–N bonds, including the $Cu–N_{MeCN}$ bond in **11**.

Copper in the +1 oxidation state is a diamagnetic d^{10} metal ion which usually forms trigonal planar or tetrahedral complexes. The reaction of $Me(en)LH_2$ with $[Cu(MeCN)_4](PF_6)$ or CuI gave rust-coloured powders that were highly insoluble in most organic solvents, thus discouraging further attempts to study their properties or application as deprotonation precursors.

3.4 Synthesis and structure of a zinc(II) complex of $Me(en)LH_2$

Following a string of attempts at complexation with transition metals which persistently yielded paramagnetic products, attention was turned to a metal ion whose d electrons can only have a total spin of 0. The two options that immediately come to mind are titanium(IV), whose d orbitals are vacant on account of its lack of d electrons, and zinc(II) which has 10 d electrons and therefore fully occupied d orbitals. In both situations, the possibility of there being unpaired electrons is eliminated. However, common titanium(IV) reagents such as $TiCl_4$ are rather reactive and require special handling. Furthermore, the hypothetical Ti(IV) complex would have a residual +2 charge upon deprotonation. For those reasons, zinc(II) emerged as the more attractive option, as its inorganic salts are more easily handled.

$Zn(NO_3)_2•6H_2O$ and $NaPF_6$ were added as aqueous solutions to a solution of $Me(en)LH_2$ in warm ethanol. The product precipitated as an off-white solid in

67 % yield, and could be recrystallised on a small scale by slow evaporation from ethanol/water to give pale pink needles. This product was crystallographically characterised as the aqua complex with the formula $[ZnMe(en)LH_2(H_2O)](PF_6)_2$, **13** (Figure 3.20). The peak at *m*/*z* = 204.05 detected in the ESI mass spectrum of the product was consistent with the desolvated $[ZnMe(en)LH_2]^{2+}$ cation.

As expected, the ^{1}H and ^{13}C NMR spectra for **13** in d_6-DMSO contained only well-defined resonances which were typical of a diamagnetic zinc(II) complex. Only seven signals were observed, indicating that a plane of symmetry bisects the ethylene bridge through the Zn–O bond, separating the magnetically equivalent halves of the molecule. If present, the resonance for the coordinated water in the ^{1}H NMR spectrum was indistinguishable from the residual water peak. It is conceivable that the aqua ligand was displaced by DMSO in solution, as $Zn^{ii}N_4$ complexes with O-bound DMSO ligands are known.[105,106] All but one signal displayed a downfield shift relative to the free ligand, which may suggest electron density donation from the ligand to the metal centre. The imine singlet experienced a minor upfield shift upon coordination.

Unfortunately, the sparing solubility of **13** in common organic solvents precluded it from use in deprotonation trials. Attempts to displace the coordinated water with acetonitrile to increase the solubility of the complex were unsuccessful.

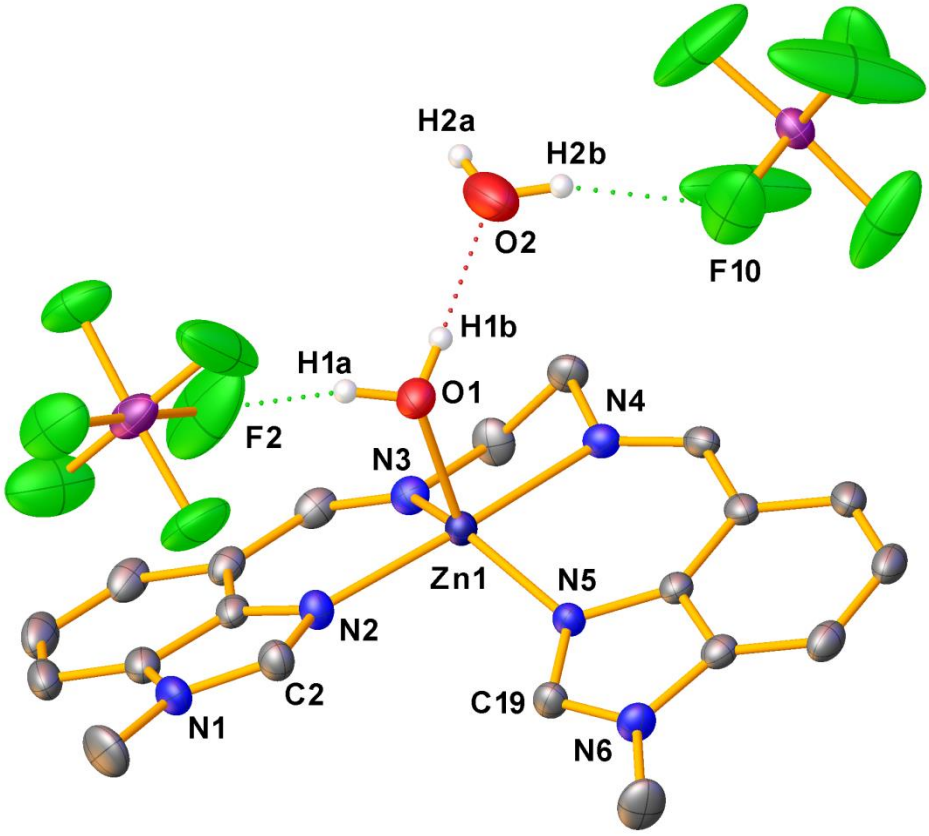

13

Figure 3.20 *Molecular structure of [ZnMe(en)LH$_2$(H$_2$O)](PF$_6$)$_2$,* ***13*** *showing 50 % probability ellipsoids. C-bound hydrogens are omitted for clarity. Selected bond lengths (Å) and angles (°): Zn1–O1 2.043(3), Zn1–N2 2.074(3), Zn1–N3 2.084(3), Zn1–N4 2.168(3), Zn1–N5 2.037(3), N2–Zn1–N5 100.93(13), N2–Zn1–N3 90.92(13), N3–Zn1–N4 79.16(13), N4–Zn1–N5 86.74(12), N2–Zn1–O1 92.02(12), N5–Zn1–O1 108.03(12), N2–Zn1–N4 170.05(13), N3–Zn1–N5 142.52(13), N3–C10–C11–N4 48.5(4), C2–N2–Zn1–N5 35.9(4), C2···C19 3.430(6), plane twist 23.73(13).*

As is common for zinc(II) complexes, the five-coordinate metal ion in **13** adopted a square pyramidal geometry. The central zinc atom was bound to four nitrogen atoms in Me(en)LH$_2$ in the equatorial plane, and the oxygen atom of one water molecule in the axial position. The Zn–N bond lengths and angles were unexceptional, and were similar to those in Chen and coworkers' zinc(II) complex **14** which bore a polydentate ligand with imidazole and imine donors (Figure 3.21).[39] The equatorial M–N bonds were shorter in **13** than in the

copper(II) complex **11**. These differences probably arose from Jahn-Teller distortions in the former.

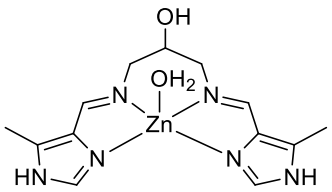

14

Figure 3.21 *A zinc(II) aqua complex of 1,3-bis[(4-methyl-5-imidazol-1-yl)ethylideneamino]propan-2-ol prepared by Chen and colleagues.*[39]

Both of the *trans* N–Zn–N angles in **14** were 155.81(12) °, positioning the zinc atom 0.413(2) Å above the N_4 plane and lending the complex a distorted square pyramidal shape. The stronger $Zn–O_{water}$ interaction manifested as a shorter bond length {2.028(4) Å}. By comparison, one of the *trans* N–Zn–N angles in **13** was close to linear while the other was smaller {170.05(13)° vs. 142.52(13)°}, indicating that N3 and N5 were situated further below the ideal square planar base of the coordination pyramid than N2 and N4. This asymmetrical distortion of the square base in **13** coincided with its larger $N_{imine}–Zn–N_{imidazole}$ chelate ring size, relative to **14**.

The coordinated water molecule participated in hydrogen bonding with the fluorine on one PF_6 anion, and the O atom of a lattice-bound water molecule. Consequently, vast continuous hydrogen bonding networks were formed within the crystal lattice. The extended two dimensional stacking of the cations could be likened to tiles on a V-shaped roof (Figure 3.22). The hydrogen bonding network runs through the inner channel of the roof structure, tilting one “tile” towards another to form the V arrangement.

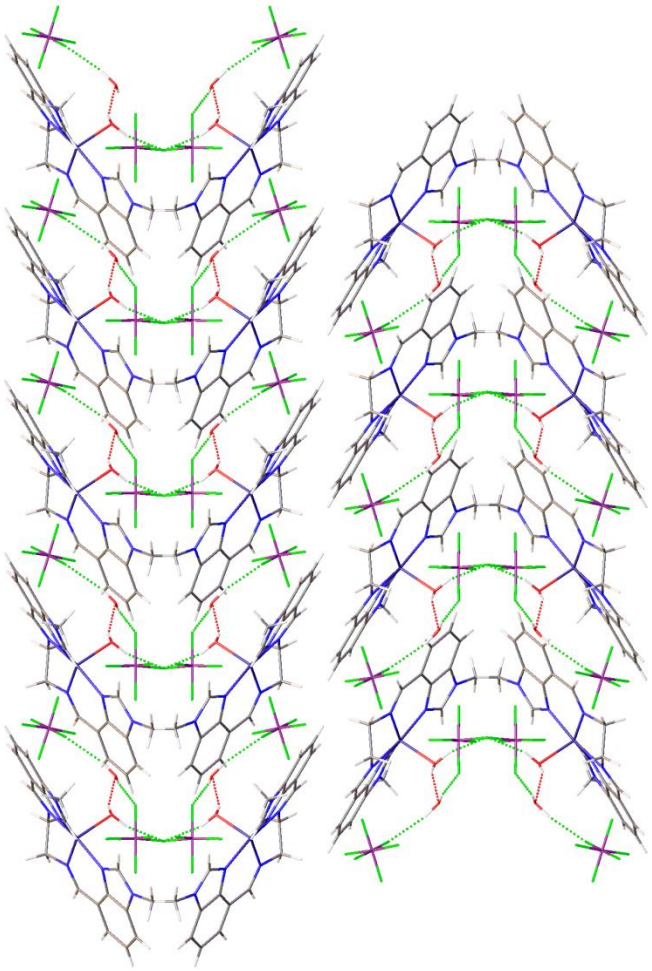

Figure 3.22 *Roof tile packing in* ***13****, which is controlled by hydrogen bonding networks formed between the water molecules and* PF_6 *anions.*

3.5 Silver(I) complexes of Me(en)LH_2

Silver(I) typically forms diamagnetic two-coordinate linear complexes. Four-coordinate silver(I) complexes are also frequently encountered and usually assume tetrahedral geometries, although square planar arrangements do occur.[107] So far, this investigation had not uncovered any tetrahedral complexes, so the question of how Me(en)LH_2 would arrange itself in this mode remained unanswered. Another factor motivating the search for silver(I) complexes is their history of being excellent transmetallation reagents, and thus may have potential as precursors to other Me(en)LH_2 complexes.

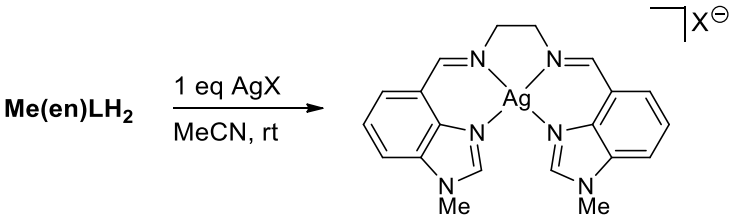

15[SbF_6] X = SbF_6, 89 %
15[OAc] X = OAc, 9 %

Scheme 3.10 *Synthesis of silver(I) complexes of Me(en)LH_2.*

[AgMe(en)LH_2](SbF_6) was prepared by combining $AgSbF_6$ directly with an equimolar amount of Me(en)LH_2 in acetonitrile at room temperature, which resulted in the immediate precipitation of **15**[SbF_6] as a pale yellow microcrystalline powder. The ^{1}H NMR spectrum in d_6-DMSO showed only one set of seven signals, an indication of C_2 symmetry in the sole species in solution. These resonances were spread over a smaller range (4.0 – 8.9 ppm) relative to the free ligand (3.8 – 9.1 ppm). Upon complexation, downfield shifts were observed for the resonances corresponding to the six phenyl and two C2 protons, the latter appearing as a broadened singlet. The H_{imine} singlet is moved slightly upfield. SC-XRD analysis confirmed the structures of **15**[SbF_6] as the four-coordinate complex, depicted in Figure 3.23.

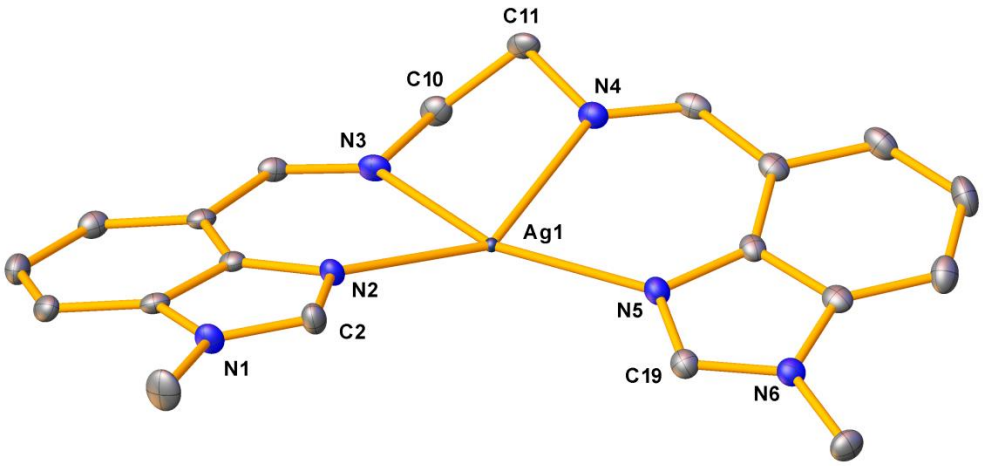

Bond lengths (Å)		Angles (°)	
Ag1–N2	2.229(2)	N2–Ag1–N3	80.23(8)
Ag1–N3	2.494(2)	N3–Ag1–N4	70.40(7)
Ag1–N4	2.460(2)	N4–Ag1–N5	80.82(8)
Ag1–N5	2.244(2)	N2–Ag1–N5	132.25(8)
C2···C19	4.716(4)	N3–C10–C11–N4	58.8(2)
		C2–N2–Ag1–N5	3.2(3)
		Plane twist	22.63(8)

Figure 3.23 *Molecular structure and selected bond lengths and angles for [AgMe(en)LH$_2$](SbF$_6$),* ***15****[SbF$_6$]. The counterion and all hydrogens are omitted for clarity. Thermal ellipsoids are shown at the 50 % probability level.*

Complex **15**[SbF$_6$] exhibited packing polymorphism. Recrystallisation from a saturated acetonitrile solution gave a mixture of prismatic (polymorph α) and fine, needle-shaped (polymorph β) yellow crystals. Both polymorphs of the complex crystallised in the *P*−1 space group. In polymorph α, the asymmetric unit was made up of the [AgMe(en)LH$_2$]$^+$ cation and one SbF$_6$ anion. The cations were arranged head-to-tail as extended overlapping chains (Figure 3.24).

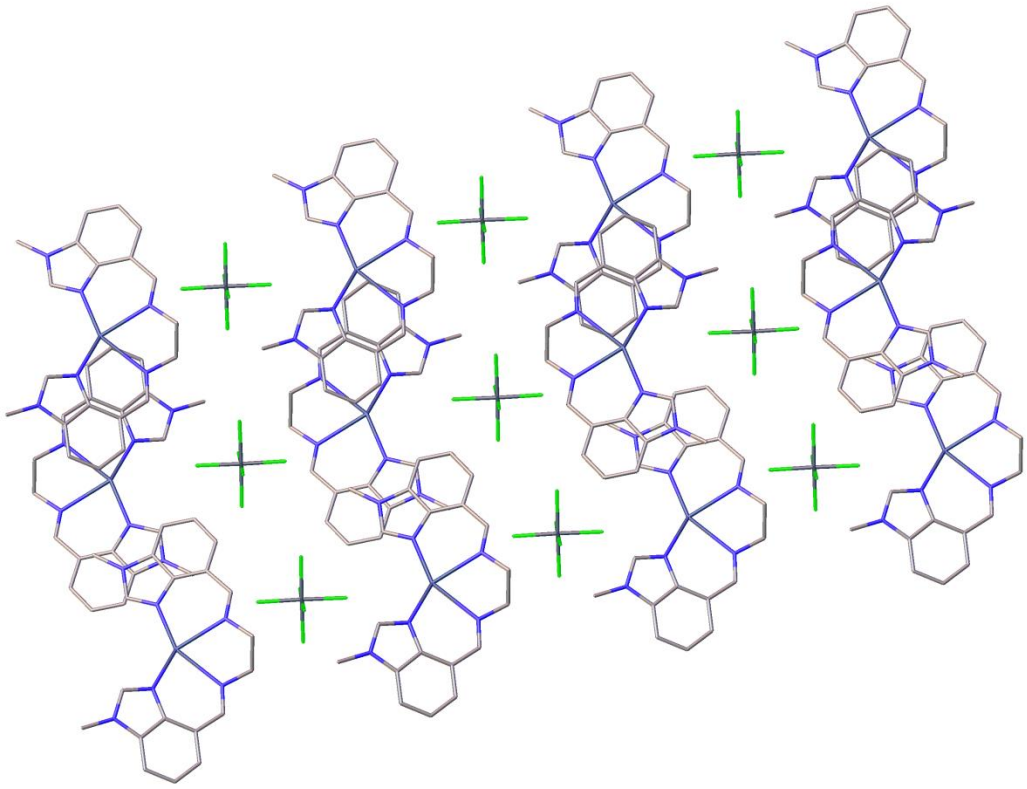

Figure 3.24 *Capped stick representation of the crystal packing in polymorph α of* ***15****[SbF_6]. Hydrogen atoms are omitted for clarity.*

The asymmetric unit in polymorph β consisted of two distinct columns, which each comprise 4 cations stacked on top of each other. The Ag···Ag distance between each layer in the stack ranged between 3.496–3.884 Å, which were larger than the sum of van der Waals radii of two Ag atoms (3.44 Å). Hence, the Ag atoms were too far apart to suggest the presence of any metal-metal interactions in the organisation of the layers. Crystal packing involved the stacking of the asymmetric units into infinite columns (Figure 3.25). The voids between the columns were occupied by the SbF_6 anions. Two of the SbF_6 anions exhibited rotational disorder; however, this was not modelled.

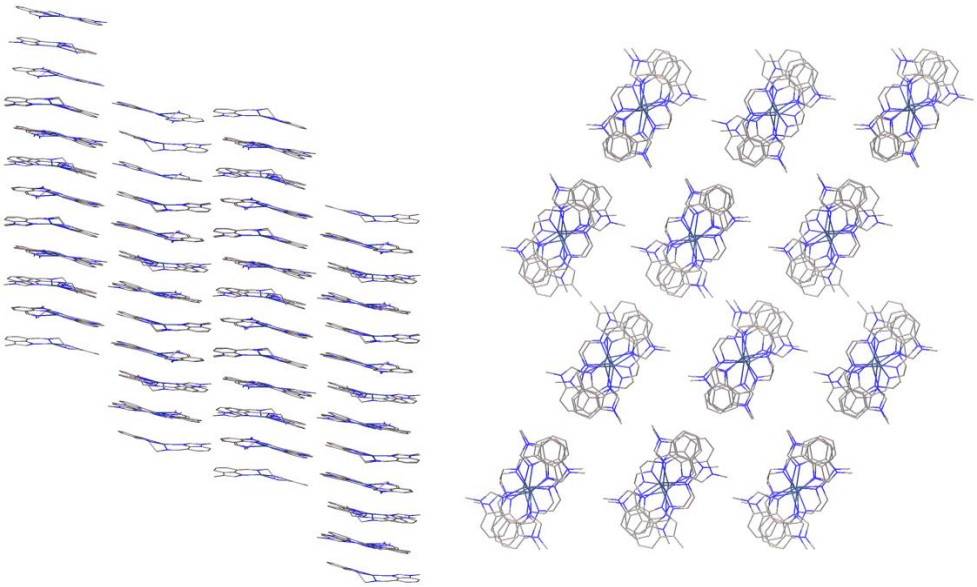

(a) (b)

Figure 3.25 *Capped stick illustrations of crystal packing in polymorph β of* ***15****[SbF_6]. The cationic units are arranged as infinite columnar stacks. Counterions and hydrogens are omitted for clarity.*

At a cursory glance, one might mistake the molecular structure of **15**[SbF_6] for the desired tetrahedral complex. Upon closer examination, some severe distortions become apparent. The *cis* N–Ag–N angles deviated greatly from the ideal 109.5 ° for a tetrahedral complex: Three of them ranged from 70.40(7)–80.82(8)°, while the N2–Ag1–N5 angle {132.25(8) °} in particular was much wider. The Ag–N2(5) bond distances {2.229(2), 2.244(2) Å} were similar to previously reported Ag–N_{Bim} bonds.[108] The Ag–N3(4) bond distances {2.494(2) and 2.460(2) Å} were significantly longer than the Ag–N2(5) or other Ag–N_{imine} bonds,[76] but were within range of Ag–$N_{pyrazole}$ bonds.[107] These suggest that the Ag–N3(4) interactions were weak, and perhaps forced out of proximity to the pseudo-linear coordination environment along N2–Ag–N5. In view of the acute plane twist of 22.63(8) °, the disparity between the Ag–N2(5) and Ag–N3(4) bond lengths, and the fact that most of the *cis* N–Ag–N angles were acute, **15**[SbF_6] is more aptly described as a distorted square planar[107] rather than a distorted tetrahedral complex. As a consequence of the wide N_{Bim}–Ag–N_{Bim} angle, the C2···C2 distances in the silver(I) complexes were the largest observed for all mononuclear Me(en)LH_2 complexes by a margin of at least 1 Å.

The Ag–N interactions were possibly fluxional in solution, which may account for the broadening of the H_{C2} resonance as the silver ion reversibly associated with

the imine N donors. This lessens the stabilising effect of the pendant donors, resulting in demetallation of **15**[SbF_6] upon exposure to base (Scheme 3.11). ^{1}H NMR spectroscopy monitoring of this reaction in d_6-DMSO showed shifts of the Me(en)LH_2 resonances that were consistent with the reformation of the free ligand, accompanied by the deposition of a fine grey solid believed to be metallic silver.

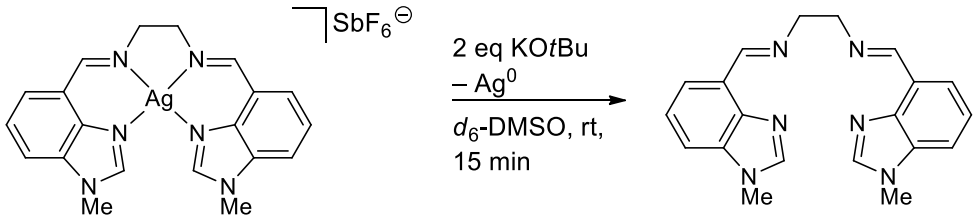

15[SbF_6]

Scheme 3.11 *Demetallation of **15**[SbF_6] under basic conditions.*

The demetallation of **15**[SbF_6] and weak Ag–N coordination could be linked to Me(en)LH_2 being ill-suited for tetrahedral coordination. The ligand would have to fold such that one benzimidazole/imine "arm" would be orthogonal to the other, but all complexes observed so far generally showed both halves of the ligand being approximately coplanar. It was considered that a slightly more coordinating counterion such as acetate could be used instead of hexafluoroantimonate to fill part of the Ag(I) tetrahedral coordination sphere, allowing the remainder to be completed by Me(en)LH_2 acting as a mono- or bidentate ligand. The analogous trifluoroacetate ion has been shown to form chelate or bridging complexes through the carboxylate unit.[108] Alternatively, methylene spacers could be added to the bridge or pendant arms for increased ligand flexibility.

15[OAc] was prepared from AgOAc via the same procedure used for **15**[SbF_6]. The ^{1}H and ^{13}C NMR spectra of **15**[OAc] were very similar to that of **15**[SbF_6], with the same broadened H_{C2} resonance observed, suggesting that changing the counterion had not affected the coordination mode. This was confirmed by SC-XRD, which once again showed the silver(I) ion in a pseudo-tetracoordinate environment. The acetate ions were non-coordinating and did not exhibit hydrogen bonding interactions. The elongated thermal ellipsoids for C10, C11, C30 and C31 were suggestive of disorder within the ethylene backbone. Although this was left unmodelled, the general structure of the complex was clear. Noteworthy differences between **15**[OAc] and its hexafluoroantimonate

counterpart were enlarged N_{imine}–Ag–N_{imine} bite angles and minimal plane twists (thus higher planarity of the Ag coordination environment), which led to considerably shorter distances between the benzimidazole C2 atoms.

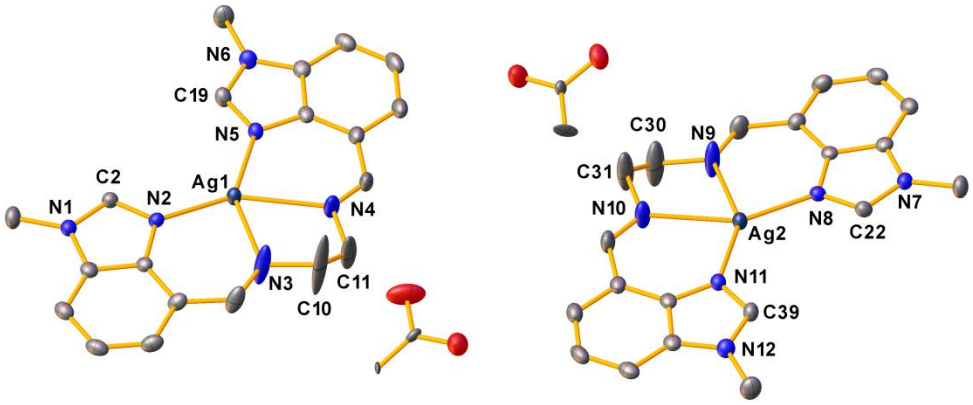

Figure 3.26 *Molecular structures of the asymmetric unit of [AgMe(en)LH_2](OAc),* ***15****[OAc]. All hydrogens are omitted for clarity. Thermal ellipsoids are shown at the 50 % probability level. Selected bond lengths (Å) and angles (°): Ag1–N2 [Ag2–N8] 2.216(3) [2.212(3)], Ag1–N3 [Ag2–N9] 2.485(4) [2.523(4)], N2–Ag1–N5 [N8–Ag2–N11] 131.00(11) [131.50(11), N3–Ag1–N4 [N8–Ag2–N11] 68.71(14) [68.83(13)], C2···C19 [C22··C39] 4.571(6) [4.578(6)], plane twist Ag1 [Ag2] 2.5(2) [4.3(2)].·*

15[OAc] is theoretically capable of self-deprotonation, and unlike the related nickel(II) complex **2**[2OAc], its structure was free from coordinated or lattice water molecules that may interfere with the deprotonation. Heating **15**[OAc] at 90 °C for 17 hours in anhydrous d_6-DMSO did not result in the disappearance of any resonances in the original spectrum or desymmetrisation of the complex, indicating that deprotonation did not occur and that the complex had good thermal stability. The silver(I) complexes showed no photosensitivity and were stable for months when stored in air.

3.6 Palladium(II) complexes of $MeRLH_2$

3.6.1 Synthesis and reactivity of palladium(II) complexes of $MeRLH_2$

Palladium(II) eventually became the prime candidate for complexation, after it was established that the Ni^{II}, Co^{II}, Zn^{II}, Cu^{II} and Ag^{I} complexes were unsatisfactory deprotonation precursors. Not only is palladium(II) reliably square

planar, it is also always diamagnetic, and the predictability of its coordination behaviour is worthy compensation for the higher cost of the precursor salts.

Initial attempts to prepare a $Pd^{II}Me(en)LH_2$ complex employed $Pd(OAc)_2$ as the metal source in hopes of obtaining a self-deprotonating complex. The addition of $Pd(OAc)_2$ to a solution of $Me(en)LH_2$ in d_6-DMSO produced a chalky purple precipitate. The heterogeneous mixture was heated at 50 °C to improve the resolution of its ^1H NMR spectrum by solubilising all the components. Unfortunately, the resulting clear dark purple solution possessed a complex ^1H NMR spectrum which could not be interpreted, although it was suggestive of decomposition.

$PdBr_2COD$ was then identified as a viable alternative palladium(II) source, as it was easy to prepare and had less reactive counteranions. The COD released during complexation could be conveniently evaporated from the mixture. This bright orange precursor typically undergoes striking colour changes upon complexation, providing a useful visual indicator of reaction progress. There were concerns that ligand denticity may fall below four if the bromides were to occupy part of the metal coordination sphere. One such possibility is illustrated in Scheme 3.12. Fortunately, the chelate effect stabilisation by $Me(en)LH_2$ was sufficient to ensure the sole formation of the desired tetradentate complex.

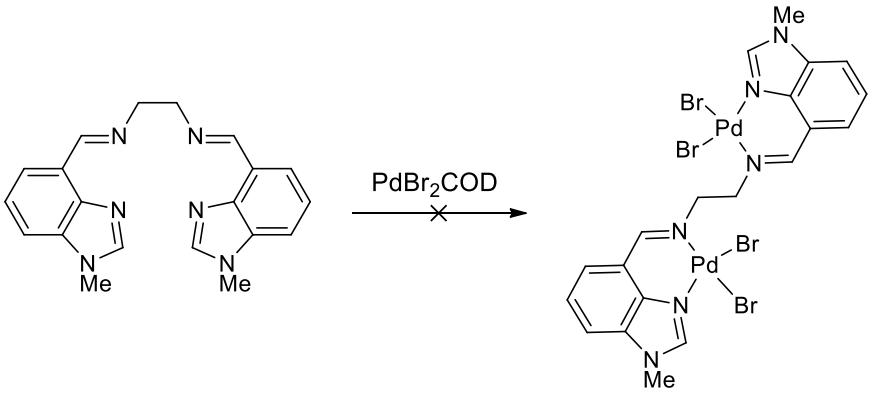

Scheme 3.12 *Possible but unobserved bidentate coordination of $Me(en)LH_2$ to palladium(II), leading to a bimetallic complex.*

Two ethylene-bridged ligands with different *N*-substituents, $Boc(en)LH_2$ and $Me(en)LH_2$ were tested for the complexation of $PdBr_2COD$ (Scheme 3.13). Both ligands gave the expected tetradentate complexes, coordinating only through the N donors.

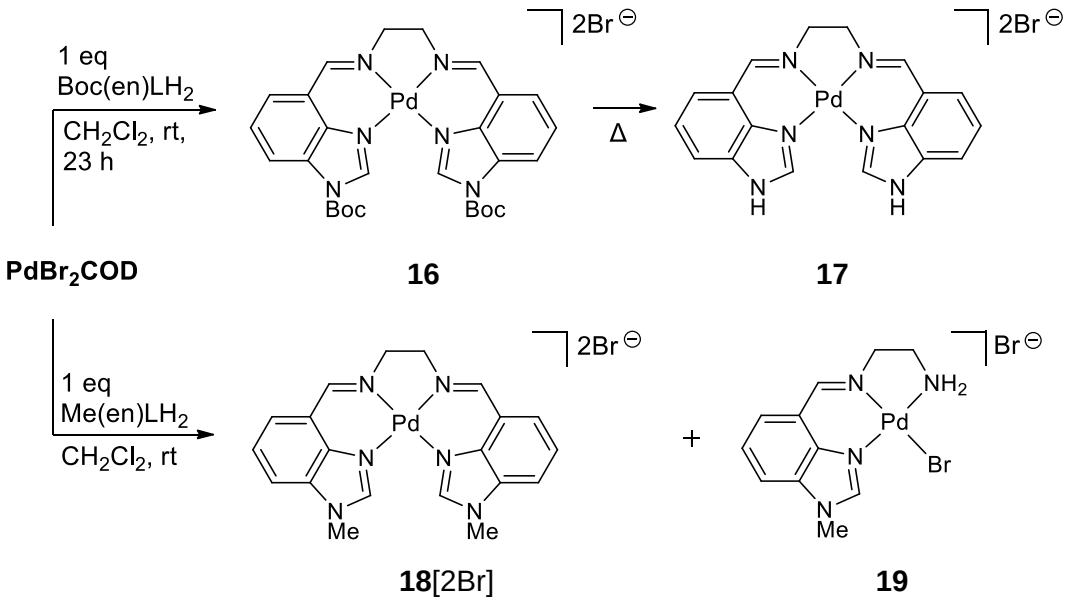

Scheme 3.13 *Preparation and degradation of palladium(II) bromide complexes of Boc(en)LH_2 and Me(en)LH_2.*

The structures of **17**, **18**[2Br] and **19** were elucidated by a combination of SC-XRD and NMR spectroscopy. The C_2 symmetry of **16** and **18**[2Br] was reflected in their ^{1}H NMR spectra, which contained only 7 signals. In contrast to the broadened H_{C2} peak in ^{1}H NMR spectra of the silver(I) complexes **15**[SbF_6] and **15**[OAc], the corresponding resonances for **17** and **18**[2Br] were sharp and well-defined, indicating that the Pd–N bonds were not fluxional in solution.

The *N*-Boc substituent in **16** was unstable and prone to cleavage upon heating or prolonged storage, giving [PdH(en)LH_2]Br_2, **17**. The upfield singlet for the *t*Bu group in the ^{1}H NMR spectrum was replaced by a downfield broad singlet integrating for 2H, consistent with the unprotected imidazole N*H*.

Unlike the relatively inert *N*-methyl group in Me(en)LH_2, the *N*-Boc group contains weakly Lewis basic carbonyl donors. X-ray quality crystals of **16** could not be obtained, thus it was not possible to ascertain whether the carbamate functionality had any interaction with the palladium centre. It was thought that the Boc group would confer greater solubility to the complex, but **16** and **17** had similarly poor solubilities in MeCN, MeOH, DCM and $CDCl_3$, and were only sparingly soluble in DMSO.

Anion exchange was initially deemed unnecessary for **18**[2Br] as the bromides were not coordinating to the palladium(II) centre. In fact, it was seen as a potential advantage because the precipitation of an insoluble bromide salt could

later be used as the driving force for deprotonation. Unfortunately, the synthesis of **18**[2Br] was plagued by the persistent formation of a side product, the tridentate *N*,*N'*,*N''*-monoimine complex **19** in variable amounts. The ^{1}H NMR spectrum contained signals for both complexes. Resonances for **19** were assigned based on 2D NMR spectroscopy and by subtracting the spectrum of a pure sample of **18**[2Br]. The ^{1}H and ^{13}C NMR chemical shifts of **19** were differentiated from those of **18**[2Br] primarily by the presence of two additional signals belonging to the CH_2 and NH_2 protons, integrating for 2H each. This was of course due to the desymmetrisation of the complex following the cleavage of one of the imine C=N bonds. In the ^{1}H NMR spectrum, the CH_2NH$_2$, CH_2CH=N and NH_2 protons appeared as multiplets around 2.7, 4.0 and 5.64 ppm respectively. ^{1}H COSY correlations were found between the CH_2NH$_2$ protons and the adjacent methylene and amino protons. The absence of any correlations to the multiplet at 5.64 ppm in the ^{1}H-^{13}C HSQC spectrum supported its assignment as the primary amine.

It was initially thought that the monoimine complex **19** was formed by hydrolysis of the ligand by the moisture in the reaction mixture. However, this was swiftly refuted as the formation of **19** still occurred despite conducting the reaction under anhydrous conditions. This decomposition pathway may be unique to palladium, as the monoimine products were not detected after complexation with other metals, although this may in part be due to the difficulty in studying the paramagnetic species by NMR spectroscopy. The formation of **19** was never accompanied by any amount of 4-CHOBimMe that was detectable in the ^{1}H NMR spectra, rendering inadequate the hypothesis that the imine was simply hydrolysed by adventitious water in the reaction.

Unfortunately, **18**[2Br] and the monoimine **19** could not be separated by chromatographic means or recrystallisation, owing to their similarly low solubilities even in highly polar solvents such as methanol and DMSO. [PdMe(en)LH$_2$]Br$_2$ **18**[2Br] could be selectively crystallised from the mixture by slow evaporation of DMSO over several weeks, but this was impractical to do on a preparative scale.

Sensing that the halide ions were responsible for the poor solubility of **18**[2Br], several anion exchange reactions with silver(I) salts were performed with limited success. The impure **18**[2Br] was stirred in methanol at room temperature with 2 equivalents of AgPF$_6$, AgSbF$_6$, AgOTf and AgOTs respectively. None of the

exchanges resulted in marked improvements in solubility, and most of the reaction mass remained as the solid.

The low yields and questionable reproducibility of the halide abstractions, coupled with the cost of upscaling the use of silver reagents, prompted a search for palladium(II) precursors with labile ligands and lipophilic, non-coordinating counteranions, such as $[Pd(MeCN)_4](BF_4)_2$.

The reaction of $[Pd(MeCN)_4](BF_4)_2$ and $Boc(en)LH_2$ in acetonitrile gave a poorly soluble precipitate that was believed to be $[PdH(en)LH_2](BF_4)_2$, based on ^1H and ^{13}C NMR spectroscopy and mass spectrometry. Although care was taken not to heat the mixture, the complex was clearly still sensitive to deprotection. The NH group could potentially undergo post-synthetic modification such as substitution with alkyl halides, but this was not attempted due to the low yields of the presumed $[PdH(en)LH_2](BF_4)_2$.

Fortunately, a similar and more conveniently prepared reagent $[Pd(MeCN)_4](OTf)_2$ gave the desired complexes **18**[2OTf], **20** and **21** cleanly in reasonable yields. Their syntheses are described in Scheme 3.14. Elemental analysis for all three complexes satisfied the $[PdMeRLH_2](OTf)_2$ formulation.

18[2OTf] was synthesised as a pale yellow solid by dissolving equimolar quantities of $[Pd(MeCN)_4](OTf)_2$ and $Me(en)LH_2$ in acetonitrile at ambient temperature. The ^1H and ^{13}C NMR peaks for C2-H shifted downfield upon coordination, which may signify loss of electron density from the imidazolyl moiety. The imine resonance also shifted downfield in the ^{13}C NMR spectrum, but exhibited a slight upfield shift in the ^1H NMR spectrum. The latter may be caused by the proximity of the shielding metal orbitals.

The phenylene-bridged analogue **20** was prepared by the palladium-templated condensation of 4-CHOBimMe and *o*-phenylenediamine. Complex **20** promptly precipitated from the reaction mixture as a chartreuse yellow powder. The formation of the ligand on the metal was confirmed by ^1H and ^{13}C NMR spectroscopy, where a new singlet at 9.81 ppm for the imine C*H* replaced the resonances belonging to the aldehyde and amino protons. A correlation between the imine proton and the bridge C–N was found in the ^1H-^{13}C HMBC spectrum, further supporting the presence of a newly created imine C=N bond. The most abundant peak in the ESI-MS spectrum was located at *m*/*z* = 249 with

characteristic palladium isotope satellites, consistent with the presence of the $[PdMePhLH_2]^{2+}$ cation.

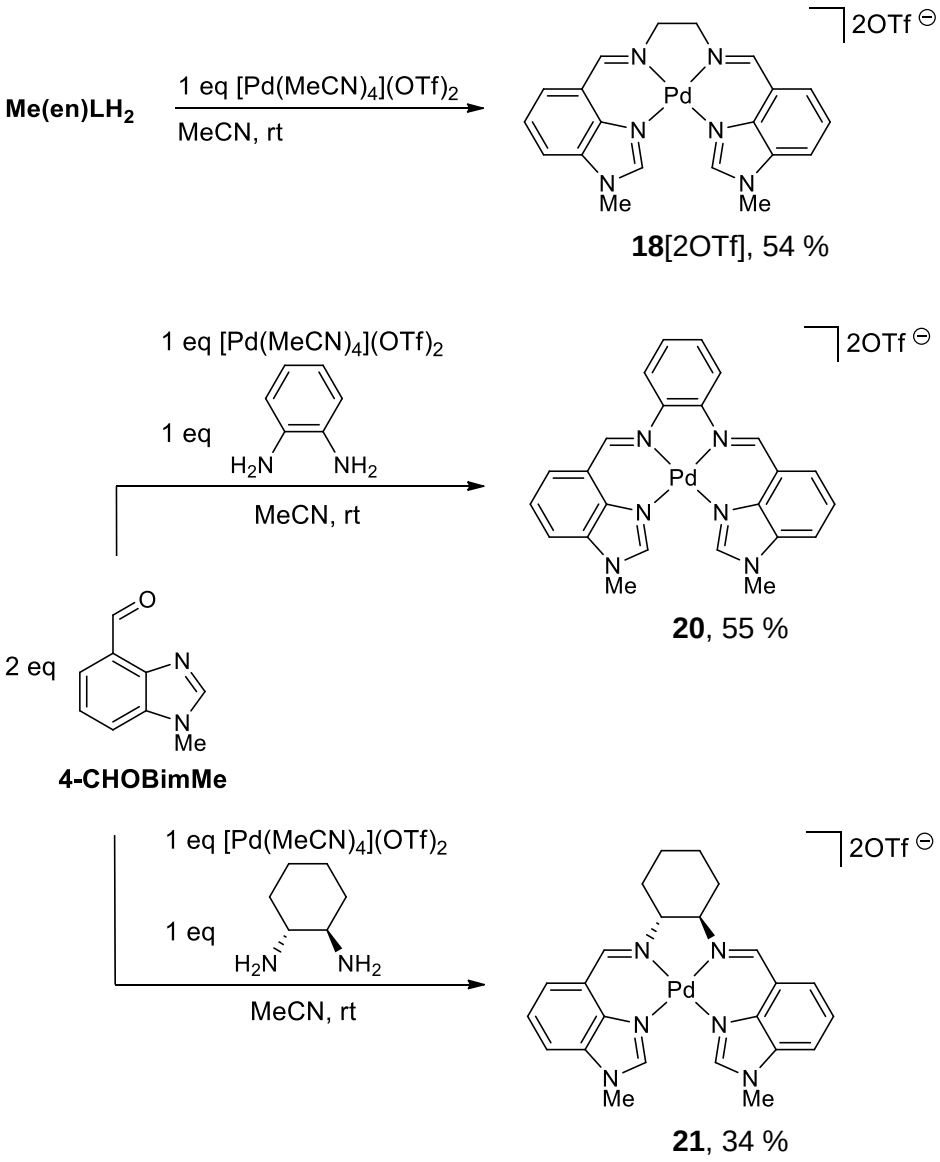

Scheme 3.14 *Synthesis of palladium(II) triflate complexes of* $MeRLH_2$.

Likewise, the reaction of $[Pd(MeCN)_4](OTf)_2$ with 1 equivalent of (1*R*,2*R*)-(−)-1,2-diaminocyclohexane and two equivalents of 4-CHOBimMe in acetonitrile cleanly afforded $[PdMeCyLH_2](OTf)_2$, **21**, as a yellow solid which could be purified by recrystallisation from acetonitrile. Unfortunately, the resulting needles were particularly prone to twinning and solvent loss, and suitable samples could not be grown for X-ray diffraction regardless of the crystallisation solvent. The success of the condensation reaction was evident from the ^{1}H NMR spectrum, which featured the trademark downfield singlet of the imine protons at 8.88 ppm, with no trace of aldehyde or amine singlets. Five distinct resonances were

observed between 1.4 – 3.9 ppm for each of the diastereotopic protons on the cyclohexyl ring. Additionally, a correlation between the imine carbon at 157.0 ppm and the vicinal cyclohexyl ring C*H* between 3.91 – 3.92 ppm was identified in the ^{1}H-^{13}C HMBC spectrum. Despite the incorporation of a chiral element, the $[PdMeCyLH_2]^{2+}$ cation still contained a C_2 axis of symmetry that bisects the cyclohexyl ring through the palladium centre. The presence of a coordinated palladium(II) ion was confirmed by an intense peak at *m*/*z* = 253 for $[PdMeCyLH_2]^{2+}$ in the ESI-MS spectrum.

It appears that the use of the triflate precursor is necessary for the template reactions to proceed smoothly. When $[Pd(MeCN)_2Br_2]$ or $[Pd(MeCN)_4]Br_2$ were subjected to template condensations with 4-CHOBimMe and *o*-phenylenediamine, the ^{1}H NMR spectra of the resulting mixtures were difficult to interpret and indicated the presence of multiple species. For the reaction with $[Pd(MeCN)_2Br_2]$, the crude mixture contained resonances consistent with $[PdMePhLH_2]^{2+}$ by ^{1}H NMR spectroscopy. However, the complex could not be separated from the other byproducts present. The inert halide ligands may have contributed to the poor performance of the palladium(II) bromide precursors, as they may be harder to displace without a pre-formed tetradentate ligand.

Although the solubility of the palladium(II) triflate complexes surpassed that of the bromide complex **18**[2Br], they were still limited to DMSO, acetonitrile and methanol. They were not soluble to any significant degree in boiling THF, toluene or hexanes, which are the preferred solvents for free carbene synthesis.

The crystal structures of $[NiMePhLH_2(MeCN)_2](PF_6)_2$ **4**, $[NiMeCyLH_2(MeCN)_2](PF_6)_2$ **5** and $[PdMePhLH_2](OTf)_2$ **20** all suggest that these cyclic-bridged ligands are unlikely to accommodate more than one metal centre, as that would require considerable distortion of the benzimidazolyl arms. However, the same could not be said for the ethylene analogues, which are capable of adopting a pseudo-*trans* configuration about the ethylene backbone or spreading out the benzimidazole arms in a fan-like fashion. If the complexation is conducted with excess palladium(II), perhaps the formation of bimetallic complexes could be possible (Scheme 3.15). The availability of a diamagnetic metallating agent enabled reaction monitoring by ^{1}H NMR spectroscopy, which was not previously feasible with the paramagnetic nickel(II) complex series.

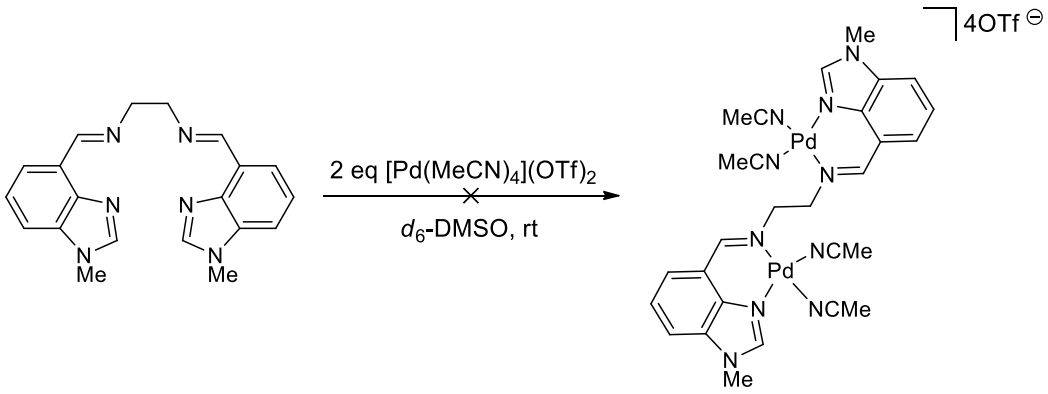

Scheme 3.15 *Formation of the dipalladium(II) Me(en)LH$_2$ complex does not occur even when excess palladium(II) is used.*

Two equivalents of [Pd(MeCN)$_4$](OTf)$_2$ were dissolved in d_6-DMSO to give an intensely orange solution, into which 1 equivalent of Me(en)LH$_2$ in d_6-DMSO was delivered dropwise over 20 seconds at room temperature. The ^{1}H NMR spectrum of the mixture was recorded after 10 minutes, and revealed only the 1:1 complex **18**[2OTf] and acetonitrile. Of course, [Pd(MeCN)$_4$](OTf)$_2$ is not easily distinguished from free acetonitrile by ^{1}H NMR spectroscopy, and it is possible that the bimetallic product depicted in Scheme 3.15 would share many spectral similarities with **18**[2OTf]. The addition of a second equivalent of Me(en)LH$_2$ merely increased the intensity of the signals believed to be those of **18**[2OTf], instead of adding a distinct set of resonances that might be expected if the bimetallic product was being converted into **18**[2OTf]. Visually, the reaction mixture became progressively less orange and more pale yellow in colour as more ligand was added, which would be consistent with the uptake of [Pd(MeCN)$_4$](OTf)$_2$ in the complexation reaction to form **18**[2OTf]. It was also telling that Me(en)LH$_2$ was not detected in the ^{1}H NMR spectra of the reaction mixture until a total of 3 equivalents of Me(en)LH$_2$ had been added. If the bimetallic product had formed and was slow to react with additional ligand, unreacted Me(en)LH$_2$ would have been observed after the second equivalent was added. Together, these observations indicated that the chelate effect is quite dominant and leads to the selective formation of the 1:1 product, regardless of the reaction stoichiometry. This stands in contrast to St. Clair Black's structurally analogous indolyl ligands, which formed homobimetallic complexes with 2.4 equivalents of iridium(I) or rhodium(I) (Scheme 3.16).[109]

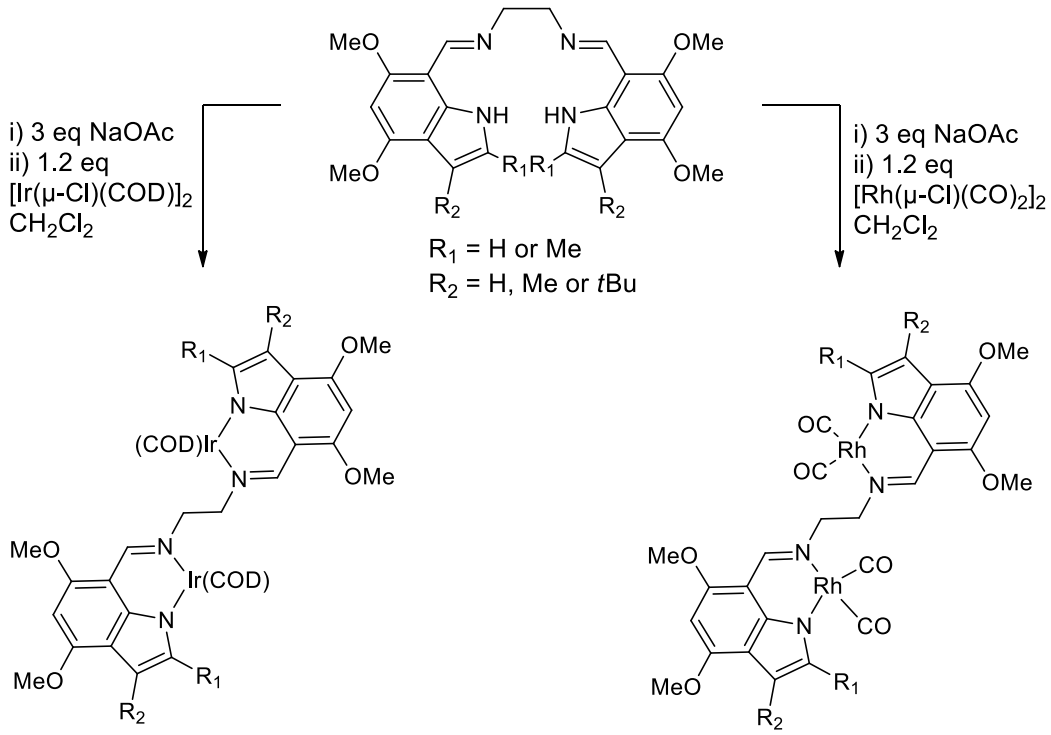

Scheme 3.16 *Preparation of binuclear iridium(I) and rhodium(I) complexes from ethylene-linked bis(indolyl) ligands.*[109]

3.6.2 Structural analysis of palladium(II) complexes of MeRLH$_2$

[PdH(en)LH$_2$]Br$_2$ **17** crystallised in the *Ac*2*m* space group. The asymmetric unit consists of two complete [PdH(en)LH$_2$]$^{2+}$ cations, as well as highly disordered bromide ions and lattice solvent molecules which were most likely water. As the disorder could not be modelled satisfactorily, the data only served to confirm the atom connectivity. The structure of the cationic unit in **17** was unexceptional. Hence, most of the structural discussion surrounding the ethylene-bridged palladium(II) complexes will be reserved for the *N*-methylated analogues **18**[2Br] and **18**[2OTf].

Complex **18**[2Br] crystallised in the *P*2$_1$/*c* space group. The asymmetric unit contains a complete cationic [PdMe(en)LH$_2$]$^{2+}$ residue, two bromide ions and one lattice water molecule (Figure 3.27). Each hydrogen atom on the water molecule participated in a short-range hydrogen interaction with a bromide ion.

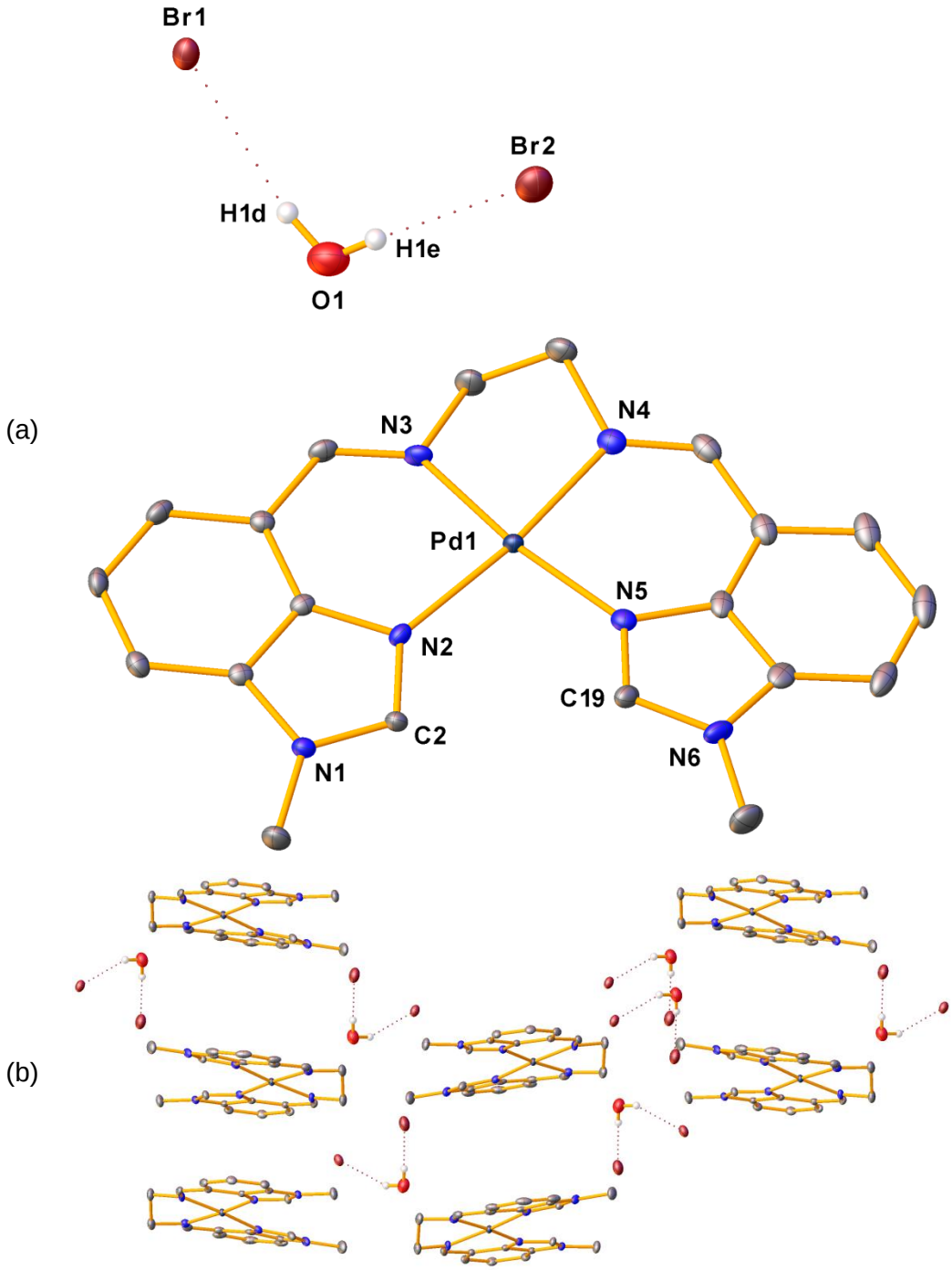

Figure 3.27 ***(a)*** *Molecular structure and* ***(b)*** *packing of* $[PdMe(en)LH_2]Br_2$, ***18****[2Br] showing 50 % probability ellipsoids and a partial atom-numbering scheme. All C-bound hydrogens are omitted for clarity. Selected bond lengths (Å) and angles (°): Pd1–N2 2.032(3), Pd1–N3 2.018(3), Pd1–N4 2.013(4), Pd1–N5 2.038(3), N2–Pd1–N3 90.35(13), N2–Pd1–N4 172.50(13), N2–Pd1–N5 97.16(14), N3–Pd1–N4 82.16(14), N4–Pd1–N5 90.33(14), C2···C19 3.186(6), plane twist 0.66(13).*

The tridentate monoimine complex **19** crystallised in the $P2_12_12_1$ space group, and featured an asymmetric unit comprising two chemically identical but crystallographically distinct cation units, two non-coordinating bromide ions, and one dichloromethane molecule in the lattice. Since the structural parameters of the two independent cation units were very similar, only one of them is shown in Figure 3.28. Each non-coordinating bromide ion acted as a hydrogen bond acceptor for one of the protons on the amine, whereas half the coordinated bromides displayed hydrogen bond interactions with methylene protons of the lattice CH_2Cl_2. The Pd–N bond lengths in **19** did not differ significantly from those in **18**[2Br], and both were within the expected range for Pd–$N_{(benz)imidazole}$[110,111] and Pd–N_{imine}[112,113] bonds. Although the plane twist was larger in **19** than **18**[2Br], the absolute difference was negligible.

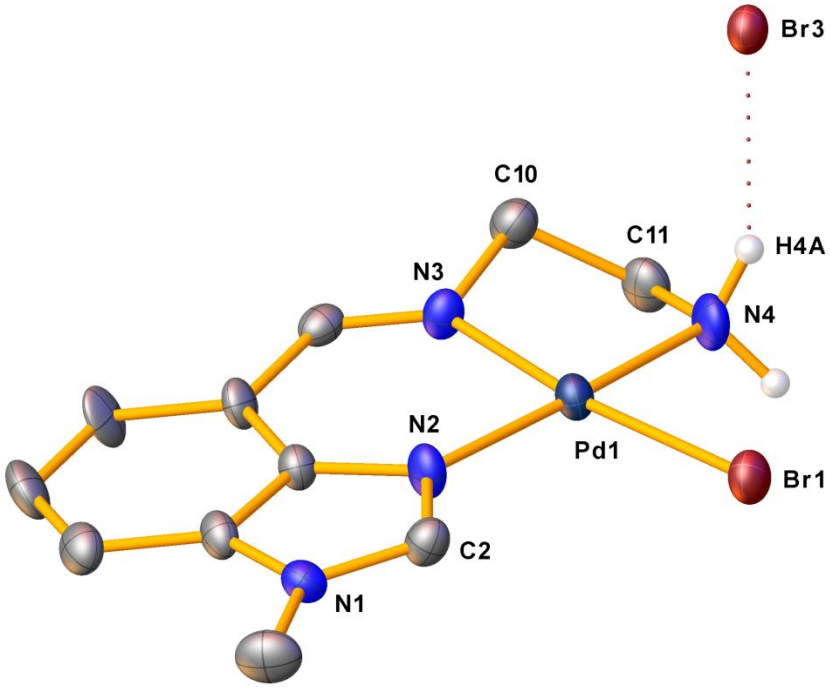

Figure 3.28 *Molecular structure of the monoimine palladium complex* ***19****. C-bound hydrogen atoms are omitted for clarity. Thermal ellipsoids are shown at the 50 % probability level. Selected bond lengths (Å) and angles (°): Pd1–N2 2.014(9), Pd1–N3 2.019(9), Pd1–N2 2.009(9), Pd1–Br1 2.4286(15), N2–Pd1–N3 91.2(4), N3–Pd1–N4 84.2(4), N4–Pd1–Br1 90.1(3), N3–Pd1–N4 94.5(3), plane twist 3.1(5).*

Important bond lengths and angles for **18**[2OTf] and **20** are summarised in Table 3.3. The minimal distortions in the metal coordination plane confirmed that the ligands fulfilled the design goal of complementing a square planar metal centre.

The tetradentate complex **18**[2OTf] crystallised from toluene in the $P2_1/c$ space group (Figure 3.29). The asymmetric unit comprised half the C_2-symmetric cation, one complete anion residue and half a toluene molecule. Each H_{C2} was a hydrogen bond donor to an O atom on a neighbouring triflate anion.

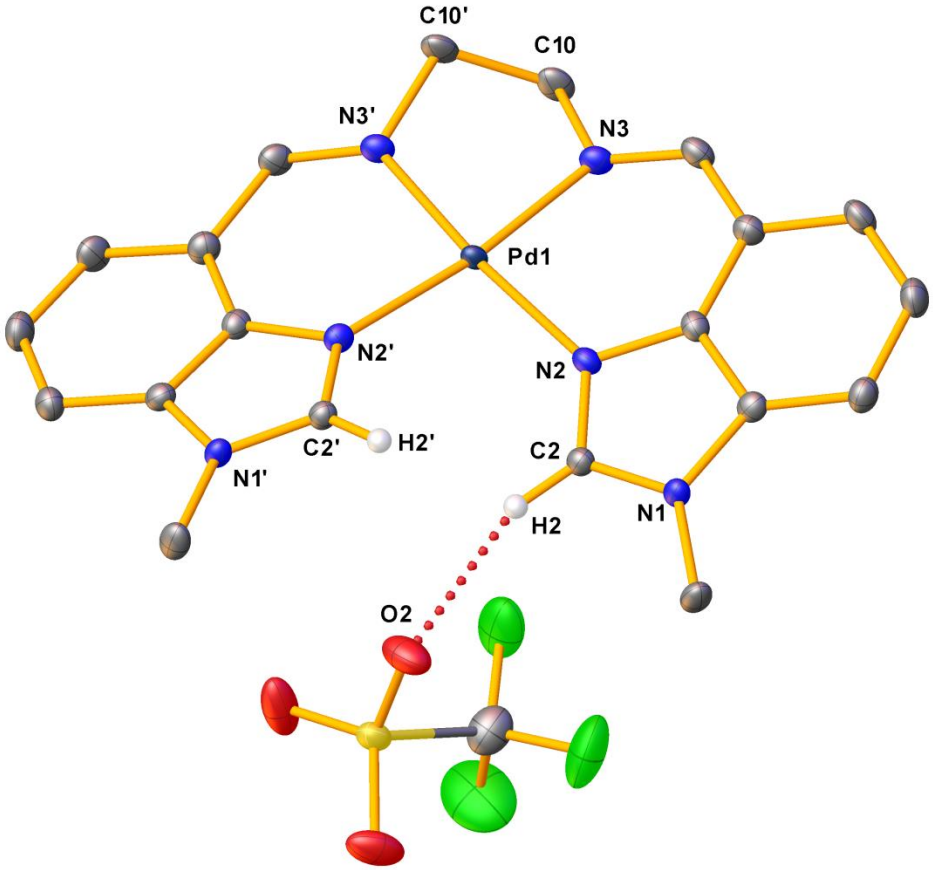

Figure 3.29 *Molecular structure of [PdMe(en)LH$_2$](OTf)$_2$,* ***18****[2OTf]. Non-hydrogen bonding protons and one lattice-bound toluene molecule are omitted for clarity. H2' interacts with the O atom on a symmetry-generated triflate ion which is not shown here. Thermal ellipsoids are shown at the 50 % probability level.*

(a)

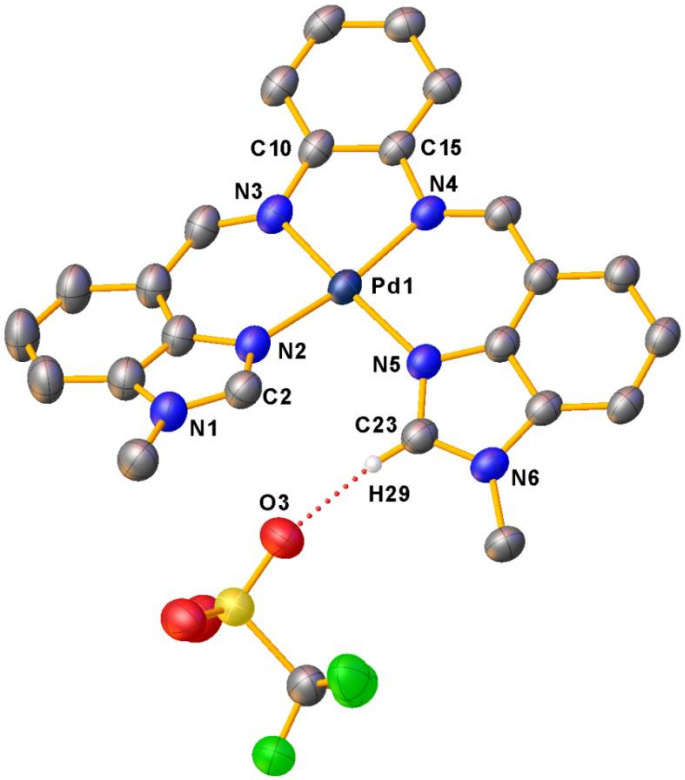

(b)

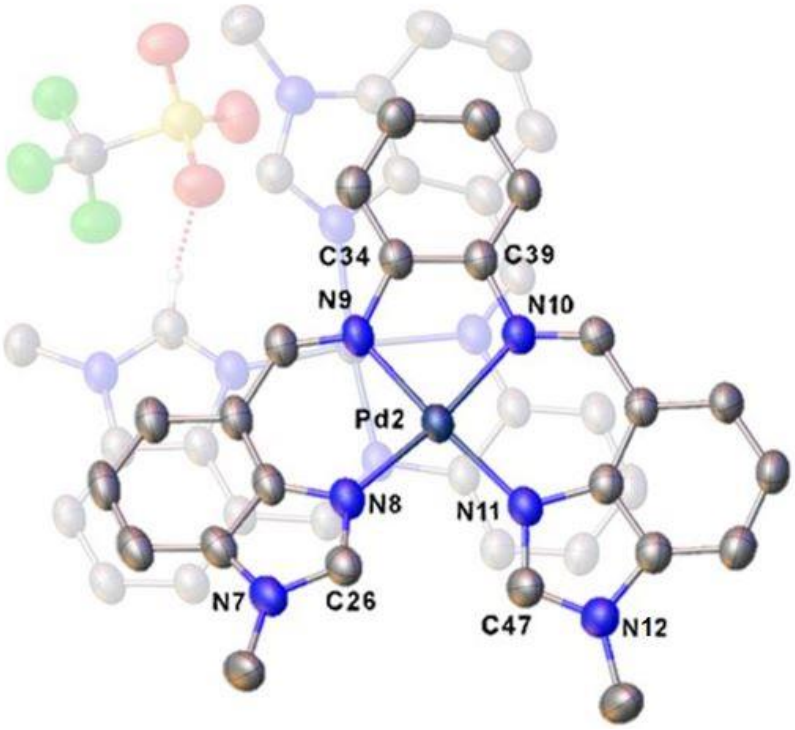

Figure 3.30 *Molecular structures of two crystallographically independent complex cations of [PdMePhLH$_2$](OTf)$_2$,* ***20****. Thermal ellipsoids are shown at the 50 % probability level. The H$_{C2}$···O hydrogen bond in part* ***(a)*** *is absent in part* ***(b)****.*

Table 3.3 *Selected bond lengths and angles for the [PdMeRLH$_2$](OTf)$_2$ complexes.*

Bond lengths (Å) and angles (°)	[PdMe(en)LH$_2$](OTf)$_2$, **18**[2OTf]	[PdMePhLH$_2$](OTf)$_2$, **20**
Pd1–N2 Pd2–N8	2.024(3) –	2.104(3) 2.014(3)
Pd1–N3 Pd2–N9	2.012(3) –	2.020(3) 2.019(3)
Pd1–N4 Pd2–N10	–	2.017(3) 2.019(3)
Pd1–N5 Pd2–N11	–	2.019(3) 2.011(3)
N2–Pd1–N2’ N2–Pd1–N5 N8–Pd2–N11	95.85(15) – –	– 94.15(11) 94.13(11)
N3–Pd1–N3’ N3–Pd1–N4 N9–Pd2–N10	82.51(15) – –	– 82.47(11) 82.31(10)
N2–Pd1–N3 N8–Pd2–N9	90.88(11) –	91.90(11) 91.57(11)
N4–Pd1–N5 N10–Pd2–N11	–	92.47(10) 92.58(11)
C2–N2–Pd1–N2’ C2–N2–Pd1–N5 C26–N8–Pd2–N11	14.6(4) – –	– 28.3(3) 23.2(3)
N3–C10–C10’–N3’ N3–C10–C15–N4 N9–C34–C39–N10	46.08(16) – –	– −1.3(3) −6.1(3)
C2···C2’ C2···C23 C26···C47	3.165(6) – –	– 3.196(5) 3.138(5)
Plane twist	3.70(15)	(a) 10.41(11) (b) 8.04(10)

Two chemically equivalent but crystallographically distinct molecules were found in the asymmetric unit of **20** (Figure 3.30). These two molecules had very similar structural parameters. The most significant difference between the two was the distances between the C2 atoms on the benzimidazoles. One of the benzimidazoles in Figure 3.30 (a) was twisted further out of the coordination

plane, creating a larger C2···C23 distance. The additional distortion was stabilised by a hydrogen bonding interaction between the C2 proton and the O atom on a triflate anion.

The C2···C2' distances were slightly shorter in **18**[2OTf] and **20** than their octahedral nickel(II) counterparts **3**[2PF_6] and **4**, but longer than the distance observed for the square planar nickel(II) complexes **1** and **8**. The C2···C2' distances correlated well with the Pd–N bond distances, which were intermediate to the Ni–N bond lengths in the octahedral and square planar nickel(II) complexes. A similar correlation could be seen with the C2–$N_{imidazole}$–M–$N_{imidazole}$ torsion angles, which was largest in **1**, followed by **20** and **8**, then **5** and **18**[2OTf]. These trends suggest that the complexes with a flexible bridge and longer M–N bond lengths will exhibit greater C2···C2' distances and less pronounced skewing of the benzimidazole arms.

3.7 Conclusion

In closing, the syntheses and characterisation of various transition metal complexes of Me(en)LH_2, MePhLH_2 and MeCyLH_2 were reported. Barring two exceptions, all the complexes obtained were mononuclear with one tetradentate MeRLH_2 ligand. As predicted, the solid state structures of the complexes showed that metals which were square planar or had an equivalent four-point plane exhibited good compatibility with the MeRLH_2 systems.

Nickel(II) typically formed octahedral complexes with the MeRLH_2 ligands, although one case of square planar coordination was reported. Cobalt(II) also assumed octahedral geometries when coordinated to Me(en)LH_2, whereas reactions with copper(II) and zinc(II) produced square pyramidal complexes. The coordination sphere was generally completed by coordinating solvents such as acetonitrile or water. The presence of these solvento ligands were less desirable in deprotonation precursors as the complexes could undergo desolvation, thus complicating any subsequent accurate determination of base stoichiometry. Furthermore, the aqua ligands may reprotonate the NM,NR NHC. Silver(I) complexes of Me(en)LH_2 were pseudo-tetracoordinate, with wide bite angles and long Ag–N bonds that were strongly suggestive of an underlying preference for linear binding modes. The $AgSbF_6$ complex underwent demetallation upon treatment with a strong base. Me(en)LH_2 and MePhLH_2 complexes of palladium(II) featured square planar geometries.

The reaction outcomes, specifically the success of anion exchange with $NaPF_6$, could be sensitive to the counterions in the precursor metal salt: Copper(II) nitrate afforded the monomeric acetonitrile complex, whereas copper(II) chloride produced chloride-bridged dimers. Nickel(II)- or palladium(II)-templated condensation cleanly afforded the respective $MeCyLH_2$ and $MePhLH_2$ complexes when the reaction mixture contained only weakly coordinating acetate, PF_6 or OTf anions. Similar condensations involving palladium(II) precursor salts containing bromide ions gave intractable mixtures. The adverse influence of bromide ions was also evident from the persistent formation of a *N*,*N'*,*N''*-tridentate palladium(II) complex byproduct when $PdBr_2COD$ was used as the metal source for complexation with $Me(en)LH_2$.

Nickel(II) complexes containing the more rigid cyclohexyl or phenylene bridge had a wider N_{Bim}–Ni–N_{Bim} angle and a shorter C2···C2 distance than their ethylene-bridged counterpart. In contrast, the bridge rigidity manifested in the phenylene-bridged palladium(II) complex as a larger plane twist.

Of all the complexes prepared, the palladium(II) triflate series were deemed the most suitable candidates to progress to deprotonation trials, as they fulfilled the following criteria:

a) Diamagnetic, facilitating reaction monitoring by NMR spectroscopy;
b) Reliable square planar coordination geometry;
c) Absence of moisture from coordination sphere and crystal lattice;
d) Oxidation state of +2 to balance the charge of the NM,NR NHCs;
e) Convenient to prepare and purify, even relative to their bromide analogues.

3.8 Experimental

[NiMe(en)LH$_2$(H$_2$O)$_2$](BF$_4$)$_2$ (2[2BF$_4$]**)**

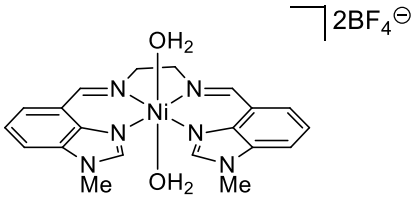

Me(en)LH$_2$ (0.200 g, 0.581 mmol) was dissolved in ethanol (10 mL) with warming. An aqueous solution of 50 % w/v nickel(II) tetrafluoroborate (190 µL, 0.581 mmol) was diluted with water (0.5 mL), and added dropwise to the ligand solution, which turned a slightly darker brown colour. The solution was cooled at 4 °C for 2 days. The reaction mixture was evaporated to dryness, and the resulting brown solid was washed with deionised water. Yield = 0.189 g (0.308 mmol, 53 %).

IR (solid) $\tilde{\nu}_{max}$ (cm^{-1}): 3533 (br m), 3481 (m), 1646 (s), 1520, 1447, 1368, 1339, 1288, 1222, 1049 (s), 1026 (br s), 1009, 903, 799, 760, 739, 723, 612.

HRMS–ESI (*m*/*z*): [M – 2H$_2$O – 2BF$_4$]$^{2+}$ calcd for C$_{20}$H$_{20}$N$_6$Ni, 201.0542; found, 201.0541.

mp: 324 – 326 °C (dec.)

Crystal data: C$_{20}$H$_{24}$N$_6$O$_2$B$_2$F$_8$Ni, M = 612.78, monoclinic, a = 14.5898(8), b = 10.3194(5), c = 17.8046(9) Å, α = 90, β = 110.037(2), γ = 90 °, U = 2518.4(2) Å^3, T = 100.08 K, space group $P2_1/c$ (no. 14), Z = 4, 42205 reflections measured, 4961 unique (R_{int} = 0.0460), 4738 > 4σ(F), R = 0.1043 (observed), R_w = 0.2941 (all data).

[NiMe(en)LH$_2$(H$_2$O)$_2$](OAc)$_2$ (2[2OAc]**)**

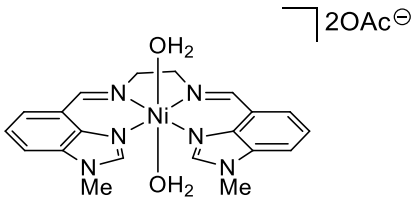

Nickel(II) acetate tetrahydrate (0.0515 g, 0.207 mmol in 3 mL ethanol) was added to a clear orange solution of Me(en)LH$_2$ (0.0726 g, 0.211 mmol) in warm

ethanol (3 mL) with swirling. The solution turned a clear brown colour. After standing at room temperature for 6 days, the reaction mixture was evaporated to dryness to afford a light brown solid. The solid was dissolved in methanol, and diethyl ether was added to crystallise the product as single brown prisms suitable for X-ray diffraction. Yield = 0.0877 g (0.157 mmol, 75 %).

IR (solid) $\tilde{\nu}_{max}$ (cm^{-1}): 3107 (br), 1644 (s), 1568 (s), 1516, 1425, 1390, 1364, 1338, 1284, 1219, 1096, 1037, 937, 804 (m), 763 (s), 739, 602.

HRMS–ESI (*m*/*z*): $[M - 2H_2O - 2CH_3COO]^{2+}$ calcd for $C_{20}H_{20}N_6Ni$, 201.0546; found, 201.0542.

mp: 242 ˚C (dec.)

Crystal data: $C_{26}H_{38}N_6O_8Ni$, *M* = 621.33, monoclinic, *a* = 14.6197(4), *b* = 13.6202(4), *c* = 16.2825(4) Å, *α* = 90, *β* = 114.2260(10), *γ* = 90 °, *U* = 2956.69(14) $Å^3$, *T* = 100.03 K, space group *C*2/*c* (no. 15), *Z* = 4, 24669 reflections measured, 2613 unique (R_{int} = 0.0306), 2488 > 4σ(*F*), *R* = 0.0346 (observed), R_w = 0.0932 (all data).

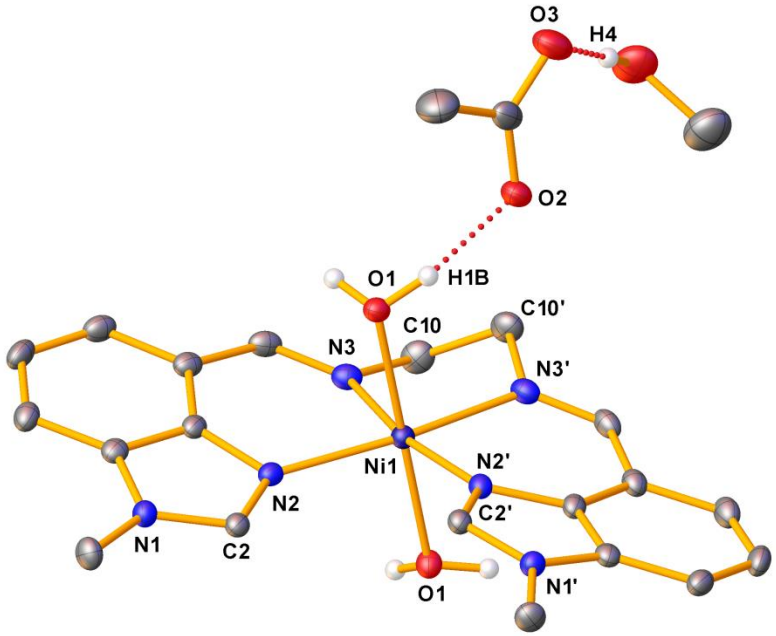

Figure 3.31 *Molecular structure of [NiMe(en)LH$_2$(H$_2$O)$_2$](OAc)$_2$,* ***2****[2OAc]. Thermal ellipsoids are drawn at the 50 % probability level. All C-bound hydrogen atoms are omitted for clarity.*

[NiMe(en)LH$_2$(MeCN)$_2$](PF$_6$)$_2$ (3[2PF$_6$]**)**

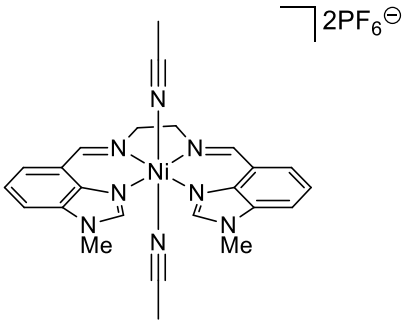

Me(en)LH$_2$ (0.0700 g, 0.203 mmol) was dissolved in ethanol (3 mL) with warming. Aqueous solutions of nickel(II) acetate tetrahydrate (0.0509 g, 0.205 mmol) and sodium hexafluorophosphate (0.0730 g, 0.435 mmol) were added, in that order, to the ligand solution with swirling. Water was added until a precipitate formed. The brown mixture was stirred for 1 h at room temperature. A light brown solid was collected by vacuum filtration, and a second crop of product was grown by slow evaporation of the filtrate. The combined crops were dissolved in acetonitrile to give a clear purple solution, from which a purple solid was crystallised by vapour diffusion of diethyl ether. Yield = 0.0555 g (0.0716 mmol, 36 %).

IR (solid) $\tilde{\nu}_{max}$ (cm^{-1}): 1700 (w), 1653 (m), 1633, 1603 (w), 1528 (m), 1446, 1426 (w), 1404, 1397, 1367, 1337, 1286, 1261, 1246, 1218, 1099, 1077, 1037, 948 (w), 901, 822 (br s), 795 (s), 754 (s), 735 (s), 722 (s), 627 (s).

HRMS–ESI (*m*/*z*): [M – 2CH$_3$CN – 2PF$_6$]$^{2+}$ calcd for C$_{20}$H$_{20}$N$_6$Ni, 201.0546; found, 201.0540.

Anal. Calcd for C$_{24}$H$_{26}$N$_8$P$_2$F$_{12}$Ni(OH$_2$)$_2$: C, 35.52; H, 3.73; N, 13.82. Found: C, 35.13; H, 3.58; N, 14.05.

mp: 340 ˚C (dec.)

Crystal data: C$_{24}$H$_{30}$N$_8$OF$_{12}$P$_2$Ni, *M* = 795.2, monoclinic, *a* = 12.3894(15), *b* = 19.330(2), *c* = 13.1965(16) Å, *α* = 90, *β* = 95.875(4), *γ* = 90 °, *U* = 3143.9(7) Å^3, *T* = 99.99 K, space group *C*2/*c* (no. 15), *Z* = 8, 21131 reflections measured, 2792 unique (R_{int} = 0.0439), 2748 > 4σ(*F*), *R* = 0.0532 (observed), R_w = 0.1369 (all data).

[NiMe(en)$LH_2$$(MeCN)_2$]$(BF_4)_2$ (3[2BF_4]**)**

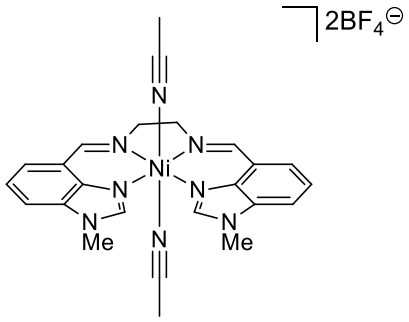

Method A: Me(en)LH_2 (0.0467 g, 0.136 mmol) was dissolved in acetonitrile (4 mL) with warming. An aqueous solution of 50 % w/v nickel(II) tetrafluoroborate (43 µL, 0.136 mmol) was added to the ligand solution, which turned a clear brown colour. The reaction mixture was reduced to dryness to give a pale pink crystalline solid. Yield = 0.0860 g (0.131 mmol, 96 %).

Method B: [NiMe(en)$LH_2$$(H_2O)_2$]$(BF_4)_2$, **2**[2$BF_4$] (0.0559 g, 0.0912 mmol) was dissolved in acetonitrile with warming, producing a clear orange-brown solution. Vapour diffusion of diethyl ether into this solution afforded **3**[2BF_4] as orange-brown prisms. Yield = 0.0527 g (0.0801 mmol, 88 %).

IR (solid) $\tilde{\nu}_{max}$ (cm^{-1}): 1647 (s), 1525 (s), 1447, 1424, 1368, 1338, 1285, 1245, 1221, 964, 796, 761, 754.

HRMS–ESI (*m*/*z*): $[M - 2CH_3CN - 2BF_4]^{2+}$ calcd for $C_{20}H_{20}N_6Ni$, 201.0542; found, 201.0546.

mp: 324 ˚C (dec.)

Crystal data: $C_{24}H_{28}N_8OB_2F_8Ni$, M = 677.96, monoclinic, a = 12.2889(3), b = 18.5661(4), c = 12.7150(3) Å, α = 90, β = 97.0545(9), γ = 90 °, U = 2879.05(12) $Å^3$, T = 100 K, space group $C2/c$ (no. 15), Z = 4, 19692 reflections measured, 2553 unique (R_{int} = 0.0357), 2304 > 4σ(F), R = 0.0261 (observed), R_w = 0.0624 (all data). Positional disorder in the BF_4 anions was modelled over two positions, with refined occupancies of 70:30.

[NiMePhLH$_2$(MeCN)$_2$](PF$_6$)$_2$ (4)

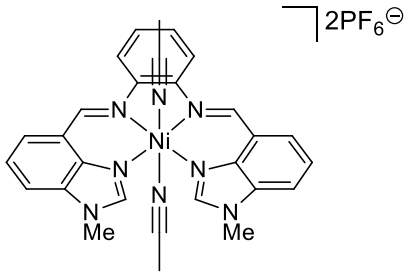

4-CHOBimMe (0.0915 g, 0.571 mmol), *o*-phenylenediamine (0.0339 g, 0.314 mmol) and nickel(II) acetate tetrahydrate (0.0739 g, 0.299 mmol) were dissolved in ethanol (4 mL) with warming to give a clear dark brown solution. Sodium hexafluorophosphate (0.106 g, 0.629 mmol in 6 mL water) was added, and a brown precipitate was produced. The brown solid was collected by vacuum filtration, washed with water and redissolved in warm acetonitrile (1 mL). Diethyl ether (4 mL) was added to precipitate **4** as a dark brown powder. Yield = 0.0074 g (0.00899 mmol, 2 %). The sample was recrystallised by vapour diffusion of diethyl ether into acetonitrile to give brown prisms suitable for X-ray diffraction.

IR (solid) $\tilde{\nu}_{max}$ (cm^{-1}): 1622, 1609, 1571 (s), 1525 (s), 1451, 1430, 1387, 1371, 1300, 1258,1228, 1193, 1087, 822 (s), 754 (s), 740 (s), 717.

HRMS–ESI (*m*/*z*): [M – 2PF$_6$ – 2CH$_3$CN]$^{2+}$ calcd for C$_{24}$H$_{20}$N$_6$Ni, 225.0551; found, 225.0559.

Anal. Calcd for C$_{28}$H$_{26}$N$_8$P$_2$F$_{12}$Ni: C, 40.85; H, 3.18; N, 13.61. Found: C, 40.71; H, 3.25; N, 13.43.

mp: 330 ˚C (dec.)

Crystal data: C$_{28}$H$_{26}$N$_8$P$_2$F$_{12}$Ni, *M* = 823.19, monoclinic, *a* = 16.7156(5), *b* = 15.1812(4), *c* = 12.9787(4) Å, *α* = 90, *β* = 93.6730(10), *γ* = 90 °, *U* = 3286.75(17) Å^3, *T* = 150 K, space group *C2/c* (no. 15), *Z* = 4, 17111 reflections measured, 2893 unique (R_{int} = 0.0371), 2751 > 4σ(*F*), *R* = 0.0405 (observed), R_w = 0.1091 (all data).

[NiMeCyLH$_2$(MeCN)$_2$](PF$_6$)$_2$ (5)

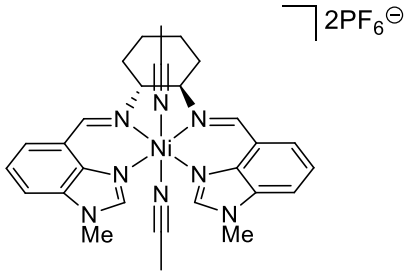

4-CHOBimMe (0.201 g, 1.25 mmol) and (1*R*,2*R*)-(−)-1,2-diaminocyclohexane (0.0718 g, 0.629 mmol) were dissolved in ethanol (3 mL) with warming to give a clear dark brown solution. Nickel(II) acetate tetrahydrate (0.155 g, 0.624 mmol in 2 mL water) and sodium hexafluorophosphate (0.220 g, 1.31 mmol in 2 mL water) were added successively with swirling. A brown precipitate formed, and the solid was collected by vacuum filtration and washed with water. The solid was dissolved in acetonitrile, and ether was added to crystallise the product as dark brown solid. The product was purified by two successive recrystallisations by vapour diffusion of diethyl ether into acetonitrile, which also afforded crystals suitable for X-ray diffraction. Yield = 0.0267 g (0.0322 mmol, 5 %).

IR (solid) $\tilde{\nu}_{max}$ (cm^{-1}): 2938 (w), 2869 (w), 1639, 1604, 1523 (m), 1451, 1423, 1368, 1286, 1250, 1217, 1078, 832 (s), 758 (s), 738 (s), 628.

HRMS–ESI (*m*/*z*): [M – 2PF$_6$ – 2CH$_3$CN]$^{2+}$ calcd for $C_{24}H_{26}N_6Ni$, 228.0786; found, 228.0793.

Anal. Calcd for $C_{28}H_{32}N_8P_2F_{12}Ni(H_2O)_2$: C, 38.85; H, 4.19; N, 12.95. Found: C, 39.05; H, 4.03; N, 12.91.

mp: 320 ˚C (dec.)

Crystal data: $C_{32}H_{28}N_{10}P_2F_{12}Ni$, M = 911.37, orthorhombic, a = 11.8495(3), b = 13.0514(3), c = 24.7222(5) Å, α = 90, β = 90, γ = 90 °, U = 3823.35(15) Å^3, T = 99.99 K, space group $P2_12_12$ (no. 18), Z = 4, 22454 reflections measured, 6724 unique (R_{int} = 0.0310), 6186 > 4σ(F), R = 0.0293 (observed), R_w = 0.0718 (all data).

{Ni_4(μ-OCH_3)$_4$[Me(en)LH_2]$(OAc)_2$} (7)

Nickel(II) acetate tetrahydrate placed under vacuum and heated to 100 °C for 5 h, after which the yellowish green powder ceased bumping. The resulting sample was presumed to be anhydrous nickel(II) acetate. In an inert atmosphere glovebox, nickel(II) acetate (0.0486 g, 0.275 mmol) and Me(en)LH_2 (0.0981 g, 0.285 mmol) were stirred in dry methanol (8 mL) for 3 days at ambient temperature. The clear pale brown solution was reduced to a third of its original volume *in vacuo* and left to stand. Small amounts of **7** crystallised from this solution as pale green needles.

Crystal data: $C_{32}H_{44}N_6O_{12}Ni_4$, M = 939.56, monoclinic, a = 19.4371(6), b = 13.4882(6), c = 16.7994(6) Å, α = 90, β = 94.331(2), γ = 90 °, U = 4391.7(3) Å^3, T = 100 K, space group $C2/c$ (no. 15), Z = 8, 65758 reflections measured, 3892 unique (R_{int} = 0.0719), 3603 > 4σ(F), R = 0.0566 (observed), R_w = 0.1262 (all data). Four voids with a total volume of 931.1 Å^3 containing disordered methanol and water molecules were found in the unit cell. A satisfactory model for the disorder could not be found. Hence, the OLEX2 solvent mask routine was applied to mask the disordered electron density.

[NiMe(en)LH_2]$(PF_6)_2$ (8)

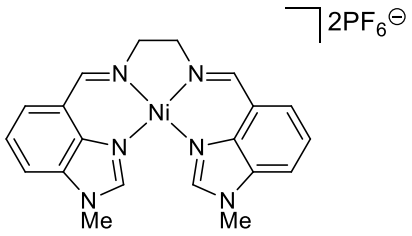

The initial light brown precipitate obtained from ethanol/water during the synthesis of [NiMe(en)LH_2(MeCN)$_2$]$(PF_6)_2$, **3**[2PF_6] was dissolved in acetone. Vapour diffusion of diethyl ether into this solution afforded dark orange blocks which were suitable for X-ray diffraction.

Crystal data: $C_{20}H_{20}N_6F_{12}P_2Ni$, M = 693.07, monoclinic, a = 18.128(5), b = 11.049(4), c = 14.949(5) Å, α = 90, β = 125.513(16), γ = 90 °, U = 2437.1(14) Å^3, T = 99.99 K, space group $C2/c$ (no. 15), Z = 4, 13684 reflections measured, 2152 unique (R_{int} = 0.0507), 1740 > 4σ(F), R = 0.0366 (observed), R_w = 0.0870 (all data).

[CoMe(en)LH$_2$(MeCN)$_2$](PF$_6$)$_2$ (9)

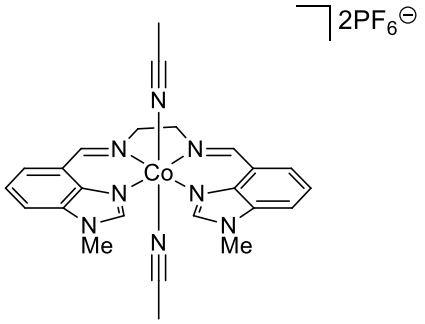

Cobalt(II) acetate tetrahydrate (0.0732 g, 0.294 mmol) and sodium hexafluorophosphate (0.0985 g, 0.586 mmol) were each dissolved in water (1 mL and 2 mL respectively). The cobalt solution was added to a solution of Me(en)LH$_2$ (0.102 g, 0.295 mmol) in warm ethanol (4 mL) with swirling. The solution turned brown immediately. The sodium hexafluorophosphate solution was then added, and a whitish precipitate formed. The solid was collected by vacuum filtration and dissolved in acetonitrile to give a clear orange solution. Vapour diffusion of diethyl ether into the solution gave orange-red blocks, which were collected by vacuum filtration and washed with 1:3 acetonitrile/diethyl ether. The mother liquor was concentrated and cooled to – 20 °C to afford a second crop of crystals. Yield = 0.0789 g (0.102 mmol, 35 %). During one recrystallisation attempt, a small number of darker orange prisms of the acetate complex were **10** formed in addition to **9**.

IR (solid) $\tilde{\nu}_{max}$ (cm^{-1}): 1700 (m), 1653 (m), 1646, 1636, 1602, 1560 (w), 1528 (m), 1507, 1445, 1423 (w), 1399, 1369, 1341, 1284, 1263, 1245, 1222, 1098, 1083, 1038, 902, 820 (br s), 799 (s), 757 (s), 738 (s), 722 (s), 626 (m).

HRMS–ESI (*m*/*z*): [M – 2CH$_3$CN – 2PF$_6$]$^{2+}$ calcd for C$_{20}$H$_{20}$N$_6$Co, 201.5541; found, 201.5535.

mp: 328 – 330 °C (dec.)

Crystal data for cobalt(II) acetate byproduct, 10: C$_{24}$H$_{28}$N$_7$O$_3$F$_6$PCo, M = 666.43, triclinic, a = 10.2676(4), b = 11.5136(5), c = 12.3200(5) Å, α = 84.629(2), β = 89.837(2), γ = 73.854(2) °, U = 1392.44(10) Å^3, T = 150 K, space group P–1 (no. 2), Z = 2, 46450 reflections measured, 4897 unique (R_{int} = 0.0479), 4417 > 4σ(F), R = 0.0344 (observed), R_w = 0.0783 (all data).

[CuMe(en)LH_2(MeCN)]$(PF_6)_2$ (11)

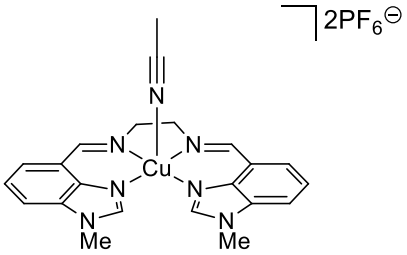

Copper(II) nitrate hemipentahydrate (0.105 g, 0.450 mmol in 2 mL water) and sodium hexafluorophosphate (0.155 g, 0.924 mmol in 2 mL water) were added to a solution of Me(en)LH_2 (0.160 g, 0.463 mmol) in ethanol (4 mL). After standing at room temperature overnight, a dark blue powder was collected by vacuum filtration. The powder was dissolved in warm acetonitrile. Vapour diffusion of diethyl ether into the solution gave dark blue crystalline blocks which were suitable for X-ray diffraction studies. Yield = 0.153 g (0.207 mmol, 46 %).

IR (solid) $\tilde{\nu}_{max}$ (cm^{-1}): 1639, 1604, 1527 (m), 1448, 1428 (w), 1400 (w), 1369, 1295, 1249, 1221, 1091, 1040, 989, 909, 823 (br s), 798 (s), 760, 755, 740, 722, 631, 624.

HRMS–ESI (*m*/*z*): $[M - CH_3CN - 2PF_6]^{2+}$ calcd for $C_{20}H_{20}N_6Cu$, 203.5517; found, 203.5512.

Anal. Calcd for $C_{22}H_{23}N_7P_2F_{12}Cu$: C, 35.76; H, 3.14; N, 13.27. Found: C, 35.91; H, 3.05; N, 13.31.

mp: 312 – 314 ˚C (dec.)

Crystal data: $C_{22}H_{23}N_7F_{12}P_2Cu$, M = 738.95, monoclinic, a = 16.0849(5), b = 8.2696(3), c = 20.6133(7) Å, α = 90, β = 92.361(2), γ = 90 °, U = 2739.56(16) $Å^3$, T = 100.01 K, space group $P2_1/c$ (no. 14), Z = 4, 28544 reflections measured, 4859 unique (R_{int} = 0.0301), 4451 > 4σ(F), R = 0.0286 (observed), R_w = 0.0736 (all data).

{[Me(en)LH$_2$]$_2$Cu}[CuClMe(en)LH$_2$](PF$_6$)$_3$ (12)

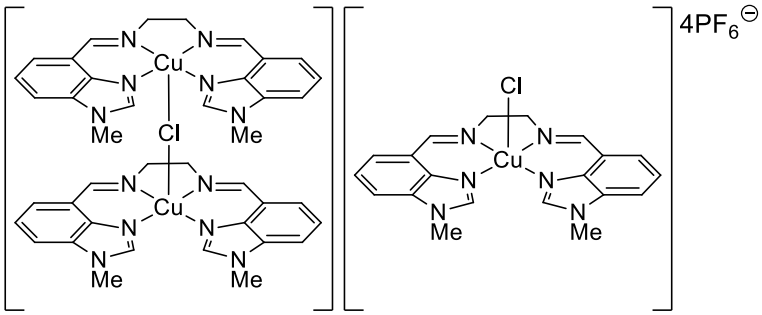

A solution of copper(II) chloride (0.0429 g, 0.319 mmol in 1 mL water) was added to a clear brown solution of Me(en)LH$_2$ (0.124 g, 0.360 mmol) in warm ethanol (3 mL). A dark blue solution formed instantly. Sodium hexafluorophosphate (0.122 g, 0.725 mmol in 1 mL water) was added to the blue solution with swirling, upon which an azure precipitate formed. The reaction mixture was left to stand overnight at room temperature. The azure powder was collected by vacuum filtration and redissolved in hot acetonitrile. Vapour diffusion of the resulting deep green solution afforded complex **12** as blue crystalline blocks. Yield = 0.0917 g (0.0713 mmol, 45 %).

IR (solid) $\tilde{\nu}_{max}$ (cm^{-1}): 1639, 1603, 1525 (m), 1447, 1398 (w), 1368, 1339, 1296, 1248, 1219 (m), 1090, 1038, 983, 906, 822 (br s), 755 (s), 738, 722, 623.

HRMS–ESI (*m*/*z*): [M – 4PF$_6$]$^{n+}$ calcd for [C$_{20}$H$_{20}$N$_6$ClCu]$^+$, 442.0729; found, 442.0711. Calcd for [C$_{20}$H$_{20}$N$_6$Cu]$^{2+}$, 203.5517; found, 203.5510.

Anal. Calcd for C$_{40}$H$_{40}$N$_{12}$P$_3$ClF$_{18}$Cu$_2$: C, 37.35; H, 3.13; N, 13.07. Found: C, 37.40; H, 2.99; N, 13.06.

mp: 280 ˚C (dec.)

Crystal data: C$_{80}$H$_{80}$N$_{24}$Cl$_3$P$_5$F$_{30}$Cu$_4$, *M* = 2463.04, triclinic, *a* = 11.1628(3), *b* = 11.5100(3), *c* = 19.3590(5) Å, *α* = 84.1730(10), *β* = 76.8630(10), *γ* = 81.1340(10) °, *U* = 2387.56(11) Å^3, *T* = 100 K, space group *P*–1 (no. 2), *Z* = 1, 76447 reflections measured, 8417 unique (R_{int} = 0.0396), 7552 > 4σ(*F*), *R* = 0.0495 (observed), R_w = 0.1233 (all data). The unit cell contained 3 solvent-accessible voids with a combined volume of 161.5 Å^3 and a total electron count of 67. No sensible model could be found for the

disordered solvent(s). Hence, the OLEX2 solvent mask routine was applied to mask the disordered electron density.

[ZnMe(en)LH_2(H_2O)](PF_6)$_2$ (13)

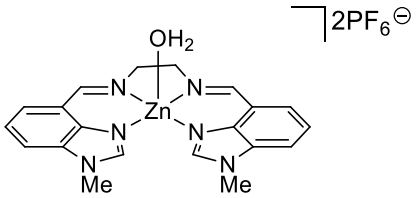

Zinc(II) nitrate hexahydrate (0.0630 g, 0.212 mmol in 1 mL water) was added to a solution of Me(en)LH_2 (0.0709 g, 0.206 mmol) in warm ethanol (4 mL) with swirling. Sodium hexafluorophosphate (0.0699 g, 0.416 mmol in 1 mL water) was then added to the clear peach solution, and a small quantity of fine white precipitate was formed. Slow evaporation of ethanol from the reaction mixture over 3 days yielded more fine white powder, mingled with peach crystalline rods which were of suitable quality for single crystal X-ray diffraction. The solid material was collected by vacuum filtration. Yield = 0.0993 g (1.38 mmol, 67 %).

^{1}H NMR (600 MHz, $(CD_3)_2SO$): δ 9.24 (br s, 1H, NC*H*N), 9.00 (s, 1H, C*H*=N), 8.14 (d, *J* = 8.3 Hz, 1H, CH_{Ar}), 7.88 (d, *J* = 7.2 Hz, 1H, CH_{Ar}), 7.70 (t, *J* = 7.8 Hz, 1H, CH_{Ar}), 4.15 (s, 3H, NCH_3), 4.08 (s, 2H, NCH_2).

^{13}C NMR (151 MHz, $(CD_3)_2SO$): δ 165.6 (*C*H=N), 146.7 (N*C*HN), 137.0 (C_{Ar}NMe), 134.0 (*C*H_{Ar}), 129.7 (C_{Ar}), 124.3 (*C*H_{Ar}), 121.9 (C_{Ar}), 116.6 (*C*H_{Ar}), 57.08 (N*C*H_2), 32.2 (N*C*H_3).

IR (solid) $\tilde{\nu}_{max}$ (cm^{-1}): 1659, 1643, 1522, 1446, 1407, 1369, 1288, 1246, 1226, 1220, 1153 (s), 1072, 1036, 988, 902, 830 (s), 799 (s), 795 (s), 762, 757 (s), 731, 721.

HRMS–ESI (*m*/*z*): [M – H_2O – 2PF_6]$^{2+}$ calcd for $C_{20}H_{20}N_6Zn$, 204.0520; found, 204.0515.

mp: 304 – 308 ˚C (dec.).

Crystal data: $C_{20}H_{24}N_6O_2P_2F_{12}Zn$, *M* = 735.78, monoclinic, *a* = 8.6119(2), *b* = 30.3008(8), *c* = 11.1542(3) Å, *α* = 90, *β* = 109.5790(10), *γ* = 90 °, *U* = 2742.37(12) Å^3, *T* = 150 K, space group $P2_1/c$ (no. 14), *Z* = 4, 44895 reflections measured, 4866 unique (R_{int} = 0.0279), 4791 > 4σ(*F*), *R* = 0.0615 (observed), R_w = 0.1467 (all data).

[AgMe(en)LH_2](SbF_6) (15[SbF_6])

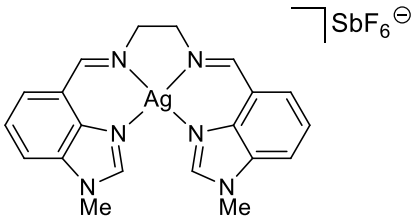

In a glovebox with a nitrogen atmosphere, Me(en)LH_2 (0.099 g, 2.86 mmol) was suspended in anhydrous acetonitrile (8 mL) at room temperature. Silver(I) hexafluoroantimonate (0.098 g, 2.84 mmol) was added to the stirring orange suspension, which turned slightly yellower. The reaction mixture was removed from the glovebox, and stirred at ambient conditions for 4 days. The mixture was reduced to dryness to give **15**[SbF_6] as a yellow solid. Yield = 0.174 g (2.53 mmol, 89 %). Crystals suitable for X-ray diffraction were grown from a saturated acetonitrile solution.

^{1}H NMR (400 MHz, $(CD_3)_2SO$): δ 8.84 (s, 1H, *CH*=N), 8.82 (br s, 1H, NC*H*N), 7.91 (d, *J* = 8.1 Hz, 1H, CH_{Ar}), 7.67 (d, *J* = 7.3 Hz, 1H, CH_{Ar}), 7.55 (t, *J* = 7.8 Hz, 1H, CH_{Ar}), 4.01 (br s, 2H, NCH_2), 4.00 (s, 3H, NCH_3).

^{13}C NMR (100 MHz, $(CD_3)_2SO$): δ 164.4 (*C*H=N), 147.7 (N*C*HN), 139.3 (C_{Ar}), 135.1 (C_{Ar}), 129.3 (*C*H_{Ar}), 124.7 (C_{Ar}), 123.8 (*C*H_{Ar}), 115.0 (*C*H_{Ar}), 62.7 (N*C*H_2), 32.0 (N*C*H_3).

IR (solid) $\tilde{\nu}_{max}$ (cm^{-1}): 2834 (w), 1641 (m), 1609, 1511 (m), 1425, 1386, 1360, 1340, 1282, 1261, 1224, 1155 (w), 1094, 1073, 1025, 975, 926, 896, 790 (m), 746 (s), 730, 718, 656 (s).

HRMS–ESI (*m*/*z*): [M – SbF_6]$^+$ calcd for $C_{20}H_{20}N_6Ag$, 451.0795; found, 451.0797.

Anal. Calcd for $C_{20}H_{20}N_6SbF_6Ag$: C, 34.91; H, 2.93; N, 12.21. Found: C, 34.91; H, 2.86; N, 12.15.

mp: 290 ˚C (dec.)

Crystal data for polymorph α, yellow prisms: $C_{20}H_{20}N_6F_6SbAg$, *M* = 688.04, triclinic, *a* = 7.3771(2), *b* = 11.4125(3), *c* = 13.6585(4) Å, *α* = 89.7130(10), *β* = 84.1590(10), *γ* = 77.9980(10) °, *U* = 1118.79(5) Å^3, *T* = 101.3 K, space group *P*-1 (no. 2), *Z* = 2, 29562 reflections measured,

3947 unique (R_{int} = 0.0370), 3655 > 4σ(F), R = 0.0208 (observed), R_w = 0.0457 (all data).

Crystal data for polymorph β, yellow needles: $C_{160}H_{160}N_{40}F_{48}Sb_8Ag_8$, M = 5504.31, triclinic, a = 14.207(3), b = 26.292(5), c = 26.683(5) Å, α = 111.91(3), β = 91.80(3), γ = 92.93(3) °, U = 9221(4) Å^3, T = 293 K, space group P-1 (no. 2), Z = 2, 164790 reflections measured, 52914 unique (R_{int} = 0.0264), 50204 > 4σ(F), R = 0.0406 (observed), R_w = 0.1099 (all data).

[AgMe(en)LH$_2$](OAc) (15[OAc]**)**

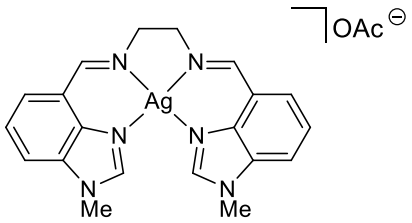

Silver(I) acetate (0.0469 g, 0.281 mmol) was added to a solution of Me(en)LH$_2$ (0.0985 g, 0.286 mmol) in acetonitrile (10 mL). A fine yellow precipitate was visible after 1 minute. The reaction mixture was allowed to continue stirring for 16 h at room temperature. The suspension was warmed to redissolve all components, filtered, and then vapour diffused with diethyl ether to produce golden prisms suitable for X-ray diffraction. Yield = 0.0136 g (0.0266 mmol, 9 %).

^{1}H NMR (400 MHz, $(CD_3)_2SO$): δ 8.88 (s, 1H, *CH*=N), 8.77 (br s, 1H, NC*H*N), 7.75 (d, J = 8.0 Hz, 1H, CH_{Ar}), 7.65 (d, J = 7.4 Hz, 1H, CH_{Ar}), 7.40 (t, J = 7.7 Hz, 1H, CH_{Ar}), 3.99 (br s, 2H, NCH_2), 3.92 (s, 3H, NCH_3).

^{13}C NMR (100 MHz, $(CD_3)_2SO$): δ 162.1 (*C*H=N), 147.2 (NCHN), 140.9 (C_{Ar}), 135.2 (C_{Ar}), 125.2 (C_{Ar}), 123.2 (*C*H$_{Ar}$), 123.2 (*C*H$_{Ar}$), 114.0 (*C*H$_{Ar}$), 62.6 (N*C*H$_2$), 31.6 (N*C*H$_3$).

IR (solid) $\tilde{\nu}_{max}$ (cm^{-1}): 1718, 1639 (s), 1558, 1437, 1394, 1358, 1340, 1283, 1261, 1226, 1093, 1022, 895, 792, 755, 746 (s).

HRMS–ESI (*m*/*z*): [M – CH_3COO]$^+$ calcd for $C_{20}H_{20}N_6Ag$, 451.0795; found, 451.0797.

Anal. Calcd for $C_{22}H_{23}N_6O_2Ag(OH_2)_2$: C, 48.27; H, 4.97; N, 15.25. Found: C, 48.19; H, 5.25; N, 15.36.

mp: 132 ˚C

Crystal data: $C_{22}H_{23}N_6O_2Ag$, M = 511.33, monoclinic, a = 45.2670(10), b = 7.6105(2), c = 24.2439(5) Å, α = 90, β = 108.0980(10), γ = 90 °, U = 7938.9(3) Å^3, T = 103.75 K, space group $C2/c$ (no. 15), Z = 16, 56124 reflections measured, 7015 unique (R_{int} = 0.0274), 6758 > 4σ(F), R = 0.0400 (observed), R_w = 0.0970 (all data).

[PdBoc(en)LH$_2$]Br$_2$ (16) and [PdH(en)LH$_2$]Br$_2$ (17)

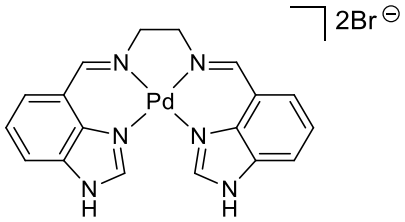

Dibromo(1,5-cyclooctadiene)palladium(II) (0.0102 g, 0.0272 mmol) and Boc(en)LH$_2$ (0.0149 g, 0.0288 mmol) were added to a flame-dried Schlenk tube under an argon atmosphere. Anhydrous dichloromethane (5 mL) was added, and the resulting pale yellow suspension was swirled vigorously while heat was applied until the reaction mixture began to boil. The reaction mixture was then stirred at room temperature for 23 h. Compound **16** was collected by filtration as a pale peach-coloured precipitate and identified by ^{1}H NMR spectroscopy. Upon storage at bench conditions for 2 months or after extended heating as a DMSO solution, the complex changes into a pale yellow colour. This new species was characterised as **17** by NMR spectroscopy and mass spectrometry. Single crystals of **17** were obtained from d_6-DMSO for X-ray diffraction studies. Regrettably, the yields were not recorded due to challenges imposed by the small reaction scale.

^{1}H NMR for **16** (400 MHz, $(CD_3)_2SO$): δ 9.76 (s, 1H), 9.16 (s, 1H), 8.52 (d, J = 8.2 Hz, 1H, CH_{Ar}), 8.26 (d, J = 7.4 Hz, 1H, CH_{Ar}), 7.98 (t, J = 8.0 Hz, 1H, CH_{Ar}), 4.28 (s, 2H, NCH_2), 1.74 (s, 9H, C(CH_3)$_3$).

^{1}H NMR for **17** (400 MHz, $(CD_3)_2SO$): δ 14.80 (br s, 1H, NH), 9.45 (s, 1H, NCHN), 9.07 (s, 1H, HC=N), 8.24 (d, J = 8.2 Hz, 1H, CH_{Ar}), 8.11 (d, J = 7.4 Hz, 1H, CH_{Ar}), 7.78 (t, J = 7.8 Hz, 1H, CH_{Ar}), 4.24 (s, 2H, NCH_2).

^{13}C NMR for **17** (100 MHz, $(CD_3)_2SO$): δ 162.9 (H*C*=N), 147.4 (N*C*HN), 132.0 (*C*H$_{Ar}$), 131.7 (*C*$_{Ar}$), 131.4 (*C*$_{Ar}$), 126.2 (*C*H$_{Ar}$), 122.0 (*C*$_{Ar}$), 121.2 (*C*H$_{Ar}$), 62.8 (N*C*H$_2$).

MS–ESI (*m*/*z*): $[M - 2Br]^{2+}$ calcd for $C_{18}H_{16}N_6Pd$, 211.0; found, 210.8.

Crystal data: $C_{40}H_{40}N_{12}Pd_2Br_4$, *M* = 1221.28, orthorhombic, *a* = 14.377(3), *b* = 13.629(3), *c* = 37.795(8) Å, *α* = 90, *β* = 90, *γ* = 90 °, *U* = 7406(3) Å^3, *T* = 173.15 K, space group *Ac*2*m* (no. 39), *Z* = 16, 43842 reflections measured, 12596 unique (R_{int} = 0.0799), 10790 > 4σ(*F*), *R* = 0.0638 (observed), R_w = 0.1727 (all data).

[PdMe(en)LH$_2$]Br$_2$ (18[2Br]**)**

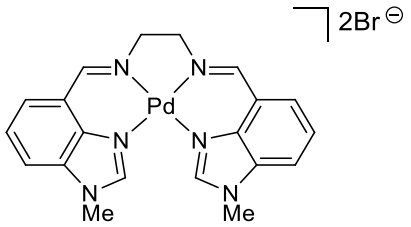

Dibromo(1,5-cyclooctadiene)palladium(II) (0.130 g, 0.350 mmol) was dissolved in dichloromethane (9 mL), and then added to a cold solution of Me(en)LH$_2$ (0.120 g, 0.349 mmol) in dichloromethane (4 mL). The reaction mixture became a thick pale brown suspension, which was stirred for 4 h at room temperature. A mixture of **18**[2Br] and **19** was obtained as a brown powder upon filtration. Yield = 0.176 g. **19** comprised approximately 45 % of the crude product, as estimated by ^{1}H NMR spectroscopy. Vapour diffusion of dichloromethane into a methanolic solution of **18**[2Br]/**19** afforded the former as yellow rods, suitable for X-ray diffraction. Alternatively, slow evaporation from a DMSO solution afforded very small quantities of **18**[2Br] as pale yellow rods that were pure by ^{1}H NMR spectroscopy.

^{1}H NMR (400 MHz, $(CD_3)_2SO$): δ 9.52 (s, 1H, NC*H*N), 9.05 (s, 1H, C*H*=N), 8.39 (d, *J* = 7.7 Hz, 1H, C*H*$_{Ar}$), 8.15 (d, *J* = 7.1 Hz, 1H, C*H*$_{Ar}$), 7.85 (dd, *J* = 7.9, 7.8 Hz, 1H, C*H*$_{Ar}$), 4.22 (br s, 5H, NC*H*$_2$ and NC*H*$_3$).

^{13}C NMR (100 MHz, $(CD_3)_2SO$): δ 162.6 (*C*H=N), 148.8 (N*C*HN), 133.2 (*C*$_{Ar}$), 131.8 (*C*$_{Ar}$), 131.7 (*C*H$_{Ar}$), 126.01 (*C*H$_{Ar}$), 122.1 (*C*$_{Ar}$), 120.1 (*C*H$_{Ar}$), 62.8 (N*C*H$_2$), 33.7 (N*C*H$_3$).

HRMS–ESI (*m*/*z*): [M – 2Br]$^{2+}$ calcd for $C_{20}H_{20}N_6Pd$, 225.0387; found, 225.0381.

mp: 315 ˚C (dec.)

Crystal data: $C_{20}H_{22}N_6Br_2PdO$, M = 628.66, monoclinic, a = 8.2049(5), b = 20.7704(14), c = 12.6967(10) Å, α = 90, β = 102.615(4), γ = 90 °, U = 2111.5(3) Å^3, T = 100.15 K, space group $P2_1/c$ (no. 14), Z = 4, 27139 reflections measured, 3740 unique (R_{int} = 0.0404), 3606 > 4σ(F), R = 0.0314 (observed), R_w = 0.0812 (all data).

[PdMe(en)LH$_2$](OTf)$_2$ (18[2OTf**])**

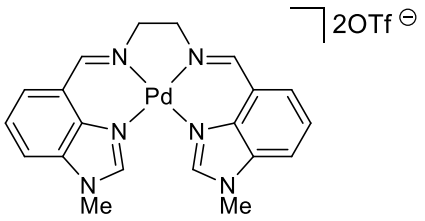

A solution of tetrakis(acetonitrile)palladium(II) bis(trifluoromethanesulfonate) (0.111 g, 0.322 mmol) in acetonitrile (2 mL) was added dropwise to a warm suspension of Me(en)LH$_2$ (0.183 g, 0.322 mmol) in acetonitrile (6 mL) in a glovebox. Within 1 minute, all the solids dissolved to give a clear golden solution. Shortly after, a fine pale yellow solid crystallised from the solution. The mixture was stirred for another 40 minutes at room temperature. The solid was collected by vacuum filtration and washed with 1:1 acetonitrile/diethyl ether. Yield = 0.131 g (0.174 mmol, 54 %). Crystals suitable for X-ray diffraction were grown from slow cooling of a warm acetonitrile/toluene solution.

^{1}H NMR (400 MHz, (CD$_3$)$_2$SO): δ 9.43 (s, 1H, NC*H*N), 9.03 (s, 1H, C*H*=N), 8.38 (d, J = 8.3 Hz, 1H, CH_{Ar}), 8.15 (d, J = 7.5 Hz, 1H, CH_{Ar}), 7.85 (t, J = 8.0 Hz, 1H, CH_{Ar}), 4.22 (br s, 2H, NCH_2), 4.21 (s, 3H, NCH_3).

^{13}C NMR (100 MHz, (CD$_3$)$_2$SO): δ 162.2 (*C*H=N), 148.3 (N*C*HN), 132.7 (C_{Ar}NMe), 131.3 (*C*H$_{Ar}$), 131.2 (C_{Ar}), 125.6 (*C*H$_{Ar}$), 121.6 (C_{Ar}), 119.6 (*C*H$_{Ar}$), 62.3 (N*C*H$_2$), 33.2 (N*C*H$_3$).

IR (solid) $\tilde{\nu}_{max}$ (cm^{-1}): 3117 (w), 1636, 1610, 1530 (m), 1450, 1369, 1249 (s), 1225 (s), 1149, 1091 (m), 1029 (s), 914, 800 (s), 756 (s), 746, 724 (w), 637, 620.

HRMS–ESI (*m*/*z*): $[M - 2CF_3SO_3]^{2+}$ calcd for $C_{20}H_{20}N_6Pd$, 225.0387; found, 225.0390.

Anal. Calcd for $C_{22}H_{20}N_6O_6S_2F_6Pd$: C, 35.28; H, 2.69; N, 11.22; S, 8.56. Found: C, 35.05; H, 2.53; N, 11.10; S, 8.29.

mp: 346 ˚C (dec.)

Crystal data: $C_{29}H_{28}F_6N_6O_6PdS_2$, M = 841.09, monoclinic, a = 9.5700(2), b = 10.7023(3), c = 16.3415(4) Å, α = 90, β = 102.7670(10), γ = 90 °, U = 1632.33(7) Å^3, T = 120 K, space group $P2/c$ (no. 13), Z = 2, 17809 reflections measured, 2884 unique (R_{int} = 0.0372), 2794 > 4σ(F), R = 0.0360 (observed), R_w = 0.0945 (all data).

(*E*)-*N*^{1}-((1-methyl-1*H*-benzo[*d*]imidazol-4-yl)methylene)ethane-1,2-diaminepalladium(II) bromide (19)

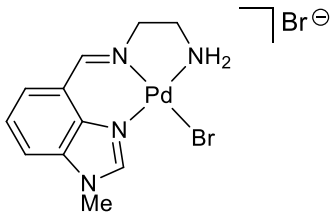

19 was obtained as a mixture with **18**[2Br] according to the preceding procedure. Recrystallisation of the **18**[2Br]/**19** mixture was accomplished by vapour diffusion of dichloromethane into a methanolic solution. This produced single crystals of both compounds which were suitable for X-ray diffraction.

^{1}H NMR (400 MHz, $(CD_3)_2SO$): δ 9.09 (s, 1H, NC*H*N), 8.80 (s, 1H, C*H*=N), 8.21 (d, J = 8.2 Hz, 1H, CH_{Ar}), 8.00 (d, J = 7.4 Hz, 1H, CH_{Ar}), 7.70 (t, J = 7.9 Hz, 1H, CH_{Ar}), 5.68 – 5.60 (m, 2H, NH_2), 4.09 (s, 3H, CH_3), 4.05 – 3.97 (m, 2H, CH_2), 2.74 – 2.65 (m, 2H, CH_2NH$_2$).

^{13}C NMR (100 MHz, $(CD_3)_2SO$): δ 160.4 (*C*H=N), 148.6 (N*C*HN), 133.4 (C_{Ar}), 131.0 (*C*H$_{Ar}$), 130.7 (C_{Ar}), 125.4 (*C*H$_{Ar}$), 122.4 (C_{Ar}), 119.5 (*C*H$_{Ar}$), 64.7 (N*C*H$_2$), 46.1 (*C*H$_2$NH$_2$), 33.7 (N*C*H$_3$).

Crystal data: $C_{23}H_{30}N_8Br_4Cl_2Pd_2$, M = 1021.85, orthorhombic, a = 6.7500(13), b = 21.662(4), c = 22.569(5) Å, α = 90, β = 90, γ = 90 °, U = 3300.0(11) Å^3, T = 173.15 K, space group $P2_12_12_1$ (no. 19), Z = 4,

40001 reflections measured, 10474 unique (R_{int} = 0.0634), 9888 > 4σ(F), R = 0.0717 (observed), R_w = 0.1958 (all data).

[PdMePhLH$_2$](OTf)$_2$ (20)

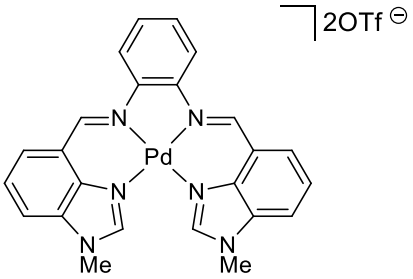

In a glovebox, dry acetonitrile (6 mL) was added to a vial containing 4-CHOBimMe (0.228 g, 1.42 mmol), *o*-phenylenediamine (0.075 g, 0.69 mmol), and tetrakis(acetonitrile)palladium(II) bis(trifluoromethanesulfonate) (0.40 g, 0.70 mmol). After stirring for 1 minute, the brown solution became a green slurry. The slurry was filtered to give **20** as a chartreuse yellow powder. The filtrate was concentrated and cooled to – 20 °C overnight to give a second crop, which was collected by vacuum filtration. Yield = 0.31 g (0.39 mmol, 55 %). Crystals suitable for X-ray diffraction were grown from a saturated acetonitrile solution.

^{1}H NMR (600 MHz, $(CD_3)_2SO$): δ 9.81 (s, 1H, C*H*=N), 9.55 (s, 1H, NC*H*N), 8.49 – 8.48 (m, 2H, CH_{Ar}), 8.39 (d, J = 7.5 Hz, 1H, CH_{Ar}), 7.94 (app. t, J = 7.8, 8.0 Hz, 1H, CH_{Ar}), 7.74 – 7.73 (m, 1H, CH_{Ar}) 4.23 (s, 3H, NCH_3).

^{13}C NMR (151 MHz, $(CD_3)_2SO$): δ 159.1 (*C*H=N), 148.8 (N*C*HN), 144.4 (C_{Ar}), 134.0 (*C*H$_{Ar}$), 133.1 (C_{Ar}), 131.8 (C_{Ar}), 131.6 (*C*H$_{Ar}$), 126.2 (*C*H$_{Ar}$), 122.4 (C_{Ar}), 121.6 (*C*H$_{Ar}$), 120.3 (*C*H$_{Ar}$), 33.9 (N*C*H$_3$).

IR (solid) $\tilde{\nu}_{max}$ (cm^{-1}): 3108 (w), 3044 (w), 1612, 1593, 1562 (s), 1531 (s), 1501, 1456, 1425, 1386, 1306, 1275 (s), 1256 (s), 1241 (s), 1222 (s), 1157, 1087, 1054, 1025, 979 (w), 961 (w), 932, 797, 773, 742 (s), 734 (s).

HRMS–ESI (*m*/*z*): [M – 2CF$_3$SO$_3$]$^{2+}$ calcd for $C_{24}H_{20}N_6Pd$, 249.0387; found, 249.0392.

Anal. Calcd for $C_{26}H_{20}N_6O_6S_2F_6Pd$: C, 39.18; H, 2.53; N, 10.54; S, 8.05. Found: C, 38.98; H, 2.31; N, 10.26; S, 7.75.

mp: 320 ˚C (decomposition)

Crystal data: $C_{52}H_{42}N_{12}F_{12}O_{13}S_4Pd_2$, M = 1612.01, monoclinic, a = 16.832(3), b = 26.357(5), c = 13.984(3) Å, α = 90, β = 104.99(3), γ = 90 °, U = 5993(2) Å^3, T = 293 K, space group $P2_1/c$ (no. 14), Z = 8, 100387 reflections measured, 16761 unique (R_{int} = 0.0333), 14647 > 4σ(F), R = 0.0595 (observed), R_w = 0.1739 (all data).

[PdMeCyLH$_2$](OTf)$_2$ (21)

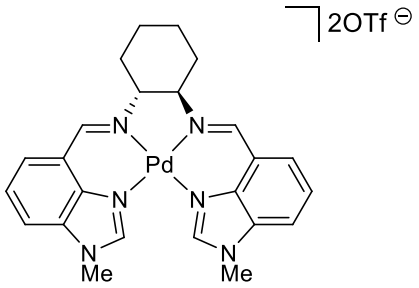

4-CHOBimMe (0.204 g, 1.27 mmol) was dissolved in warm dry acetonitrile (6 mL) in a glovebox. A solution of (1*R*,2*R*)-(−)-1,2-diaminocyclohexane (0.072 g, 0.64 mmol) in acetonitrile (2 mL) was added dropwise to the stirring aldehyde solution. The clear brown solution was stirred at room temperature for 10 minutes, and tetrakis(acetonitrile)palladium(II) bis(trifluoromethanesulfonate) (0.360 g, 0.63 mmol) was added in a single portion. A fine yellow solid precipitated instantly. After stirring for 20 minutes, the reaction mixture was filtered, and the collected solid was washed with 1:1 acetonitrile/diethyl ether (10 mL). Yield = 0.177 g (0.22 mmol, 34 %).

^{1}H NMR (600 MHz, $(CD_3)_2SO$): δ 9.41 (s, 1H, NC*H*N), 8.86 (s, 1H, C*H*=N), 8.38 (d, J = 8.2 Hz, 1H, CH_{Ar}), 8.31 (d, J = 7.5 Hz, 1H, CH_{Ar}), 7.86 (app. t, J = 8.1, 7.6 Hz, 1H, CH_{Ar}), 4.20 (s, 3H, NCH_3), 3.92 – 3.91 (m, 1H, CH_{Cy}N), 2.82 (d, J = 11.6 Hz, 1H, CH_{2a}), 1.98 (d, J = 8.6 Hz, 1H, CH_{2b}), 1.85 – 1.84 (m, 1H, CH_{2a}), 1.45 – 1.42 (m, 1H, CH_{2b}).

^{13}C NMR (151 MHz, $(CD_3)_2SO$): δ 157.0 (*C*H=N), 146.6 (N*C*HN), 131.0 (C_{Ar}), 130.3 (*C*H$_{Ar}$), 129.5 (C_{Ar}), 123.9 (*C*H$_{Ar}$), 120.3 (C_{Ar}), 117.9 (*C*H$_{Ar}$), 71.2 (*C*H$_{Cy}$), 31.7 (N*C*H$_3$), 28.2 (*C*H$_{2a}$), 22.3 (*C*H$_{2b}$).

IR (solid) $\tilde{\nu}_{max}$ (cm^{-1}): 3117 (w), 2982 (w), 1636, 1612, 1530, 1454, 1370, 1295, 1269 (s), 1249 (s), 1225 (s), 1164 (s), 1052 (w), 1031 (s), 1025 (s), 914 (w), 798 (s), 755 (s), 638 (s), 620.

HRMS–ESI (*m/z*): $[M - 2CF_3SO_3]^{2+}$ calcd for $C_{24}H_{24}N_6Pd$, 252.0621; found, 252.0619.

Anal. Calcd for $C_{26}H_{26}N_6O_6S_2F_6Pd$: C, 38.89; H, 3.26; N, 10.46; S, 7.99. Found: C, 38.93; H, 3.16; N, 10.34; S, 7.81.

mp: 350 – 352 ˚C (dec.)

3.9 References

1 D. A. Atwood and M. J. Harvey, *Chem. Rev.*, 2001, **101**, 37–52.

2 P. G. Cozzi, *Chem. Soc. Rev.*, 2004, **33**, 410–421.

3 C. J. Whiteoak, G. Salassa and A. W. Kleij, *Chem. Soc. Rev.*, 2012, **41**, 622–631.

4 K. C. Gupta and A. K. Sutar, *Coord. Chem. Rev.*, 2008, **252**, 1420–1450.

5 T. Katsuki, *Coord. Chem. Rev.*, 1995, **140**, 189–214.

6 L. Canali and D. C. Sherrington, *Chem. Soc. Rev.*, 1999, **28**, 85–93.

7 C. Baleizão and H. Garcia, *Chem. Rev.*, 2006, **106**, 3987–4043.

8 D. J. Darensbourg, *Chem. Rev.*, 2007, **107**, 2388–2410.

9 T. Katsuki, *Synlett*, 2003, **3**, 281–297.

10 E. N. Jacobsen, W. Zhang, A. R. Muci, J. R. Ecker and L. Deng, *J. Am. Chem. Soc.*, 1991, **113**, 7063–7064.

11 L. Deng and E. N. Jacobsen, *J. Org. Chem.*, 1992, **57**, 4320–4323.

12 E. N. Jacobsen, *Acc. Chem. Res.*, 2000, **33**, 421–431.

13 J. K. Myers and E. N. Jacobsen, *J. Am. Chem. Soc.*, 1999, **121**, 8959–8960.

14 A. Kochem, G. Gellon, N. Leconte, B. Baptiste, C. Philouze, O. Jarjayes, M. Orio and F. Thomas, *Chem. Eur. J.*, 2013, **19**, 16707–16721.

15 I. Karamé, M. L. Tommasino, R. Faure and M. Lemaire, *Eur. J. Org. Chem.*, 2003, 1271–1276.

16 M. Vázquez, M. R. Bermejo, J. Sanmartín, A. M. García-Deibe, C. Lodeiro and J. Mahía, *J. Chem. Soc. Dalton Trans.*, 2002, **38**, 870.

17 M. Zhao, M. Samoc, P. N. Prasad, B. A. Reinhardt, M. R. Unroe, M. Prazak, R. C. Evers, J. J. Kane, C. Jariwala and M. Sinsky, *Chem. Mater.*, 1990, **2**, 670–678.

18 B. Xiao, H. Han, X. Meng, Y. Song, Y. Fan, H. Hou and Y. Zhu, *Inorg.*

Chem. Commun., 2004, **7**, 378–381.

19 C. H. Chen, W. S. Huang, M. Y. Lai, W. C. Tsao, J. T. Lin, Y. H. Wu, T. H. Ke, L. Y. Chen and C. C. Wu, *Adv. Funct. Mater.*, 2009, **19**, 2661–2670.

20 J. Kulhánek and F. Bureš, *Beilstein J. Org. Chem.*, 2012, **8**, 25–49.

21 P. Forche Asobo, H. Wahe, J. T. Mbafor, A. E. Nkengfack, Z. T. Fomum, E. F. Sopbue and D. Döpp, *J. Chem. Soc. Perkin Trans. 1*, 2001, 457–461.

22 R. W. Bürli, D. McMinn, J. A. Kaizerman, W. Hu, Y. Ge, Q. Pack, V. Jiang, M. Gross, M. Garcia, R. Tanaka and H. E. Moser, *Bioorg. Med. Chem. Lett.*, 2004, **14**, 1253–1257.

23 H. Göker, S. Özden, S. Yıldız and D. W. Boykin, *Eur. J. Med. Chem.*, 2005, **40**, 1062–1069.

24 P. S. Charifson, A.-L. Grillot, T. H. Grossman, J. D. Parsons, M. Badia, S. Bellon, D. D. Deininger, J. E. Drumm, C. H. Gross, A. LeTiran, Y. Liao, N. Mani, D. P. Nicolau, E. Perola, S. Ronkin, D. Shannon, L. L. Swenson, Q. Tang, P. R. Tessier, S.-K. Tian, M. Trudeau, T. Wang, Y. Wei, H. Zhang and D. Stamos, *J. Med. Chem.*, 2008, **51**, 5243–5263.

25 D. J. Parks, W. H. Parsons, R. W. Colburn, S. K. Meegalla, S. K. Ballentine, C. R. Illig, N. Qin, Y. Liu, T. L. Hutchinson, M. Lou Lubin, D. J. Stone, J. F. Baker, C. R. Schneider, J. Ma, B. P. Damiano, C. M. Flores and M. R. Player, *J. Med. Chem.*, 2011, **54**, 233–247.

26 F. Arjmand, S. Parveen, M. Afzal and M. Shahid, *J. Photochem. Photobiol. B*, 2012, **114**, 15–26.

27 M. Tonelli, E. Gabriele, F. Piazza, N. Basilico, S. Parapini, B. Tasso, R. Loddo, F. Sparatore and A. Sparatore, *J. Enzyme Inhib. Med. Chem.*, 2018, **33**, 210–226.

28 L. Li, Y. S. Wong, T. Chen, C. Fan and W. Zheng, *Dalton Trans.*, 2012, **41**, 1138–1141.

29 F. E. Hahn, L. Wittenbecher, D. Le Van and R. Fröhlich, *Angew. Chem. Int. Ed.*, 2000, **39**, 541–544.

30 D. S. C. Black, D. C. Craig, N. Kumar and L. C. H. Wong, *J. Chem. Soc. Chem. Commun.*, 1985, 1172.

31 C. R. Groom, I. J. Bruno, M. P. Lightfoot and S. C. Ward, *Acta Crystallogr. B*, 2016, **72**, 171–179.

32 J. Gao, F. Ross Woolley and R. A. Zingaro, *Org. Biomol. Chem.*, 2005, **3**, 2126–2128.

33 J. F. Cívicos, J. S. M. Coimbra and P. R. R. Costa, *Synthesis*, 2017, **49**, 3998–4006.

34 F. Dumur, E. Contal, G. Wantz and D. Gigmes, *Eur. J. Inorg. Chem.*, 2014, **2014**, 4186–4198.

35 T. Frömmel, W. Peters, H. Wunderlich and W. Kuchen, *Angew. Chem. Int. Ed. Engl.*, 1992, **31**, 612–613.

36 T. Frömmel, W. Peters, H. Wunderlich and W. Kuchen, *Angew. Chem. Int. Ed. Engl.*, 1993, **32**, 907–909.

37 A. J. Bridgeman, *Dalton Trans.*, 2008, 1989–1992.

38 S. Demir, T. K. Yazıcılar and M. Taş, *Inorg. Chim. Acta*, 2014, **409**, 399–406.

39 L. Long, X. Chen, X. Yu, Z. Zhou and L. N. Ji, *Polyhedron*, 1999, **18**, 1927–1933.

40 S.-R. Zheng, M. Pan, K. Wu, L. Chen, J.-J. Jiang, D.-W. Wang, J.-Y. Shi and C.-Y. Su, *Cryst. Growth Des.*, 2015, **15**, 625–634.

41 V. Kamat, A. Kotian, A. Nevrekar, K. Naik, D. Kokare and V. K. Revankar, *Inorg. Chim. Acta*, 2017, **466**, 625–631.

42 H. Miyasaka, A. Saitoh, S. Yanagida, C. Kachi-Terajima, K. Sugiura and M. Yamashita, *Inorg. Chim. Acta*, 2005, **358**, 3525–3535.

43 A. Saitoh, H. Miyasaka, M. Yamashita and R. Clérac, *J. Mater. Chem.*, 2007, **17**, 2002–2012.

44 Y.-L. Hou, S.-X. Li, R. W.-Y. Sun, X.-Y. Liu, S. W. Ng and D. Li, *Dalton Trans.*, 2015, **44**, 17360–17365.

45 S. Tashiro, A. Minoda, M. Yamada and M. Shionoya, *Inorg. Chem.*, 2009, **48**, 10093–10101.

46 M. Balamurugan, R. Mayilmurugan, E. Suresh and M. Palaniandavar, *Dalton Trans.*, 2011, **40**, 9413–9424.

47 P. G. Plieger, A. J. Downard, B. Moubaraki, K. S. Murray and S. Brooker, *Dalton Trans.*, 2004, 2157–2165.

48 H. -W Wanzlick and H. -J Schönherr, *Angew. Chem. Int. Ed. Engl.*, 1968, **7**, 141–142.

49 J. Berding, M. Lutz, A. L. Spek and E. Bouwman, *Organometallics*, 2009, **28**, 1845–1854.

50 C. Köcher and W. A. Herrmann, *J. Organomet. Chem.*, 1997, **532**, 261–265.

51 J. C. De Jesus, I. González, A. Quevedo and T. Puerta, *J. Mol. Catal. A: Chem.*, 2005, **228**, 283–291.

52 S. Tashiro, A. Minoda, M. Yamada and M. Shionoya, *Inorg. Chem.*, 2009, **48**, 10093–10101.

53 A. J. Jircitano and K. B. Mertes, *Inorg. Chem.*, 1983, **22**, 1828–1831.

54 Y. Shen and C.-F. Chen, *Chem. Rev.*, 2012, **112**, 1463–1535.

55 H. Andres, R. Basler, A. J. Blake, C. Cadiou, G. Chaboussant, C. M. Grant, H. Güdel, M. Murrie, S. Parsons, C. Paulsen, F. Semadini, V. Villar, W. Wernsdorfer and R. E. P. Winpenny, *Chem. Eur. J.*, 2002, **8**, 4867–4876.

56 G. Christou, D. Gatteschi, D. N. Hendrickson and R. Sessoli, *MRS Bull.*, 2000, **25**, 66–71.

57 D. Ruiz-molina, G. Christou and D. N. Hendrickson, *Mol. Cryst. Liq. Cryst. Sci. Technol., Sect. A*, 2000, **343**, 17–27.

58 W. L. Gladfelter, M. W. Lynch, W. P. Schaefer, D. N. Hendrickson and H. B. Gray, *Inorg. Chem.*, 1981, **20**, 2390–2397.

59 A. Pons-Balagué, N. Ioanidis, W. Wernsdorfer, A. Yamaguchi and E. C.

Sañudo, *Dalton Trans.*, 2011, **40**, 11765–11769.

60 A. Massard, G. Rogez and P. Braunstein, *Dalton Trans.*, 2014, **43**, 42–46.

61 G. Chaboussant, H. Güdel, S. Ochsenbein, A. Parkin, S. Parsons, G. Rajaraman, A. Sieber, A. A. Smith, A. Timco and R. E. P. Winpenny, *Dalton Trans.*, 2004, **17**, 2758–2766.

62 I. G. Fomina, Z. V. Dobrokhotova, G. G. Aleksandrov, O. Y. Proshenkina, M. L. Kovba, A. S. Bogomyakov, V. N. Ikorskii, V. M. Novotortsev and I. L. Eremenko, *Russ. Chem. Bull.*, 2009, **58**, 11–20.

63 S. H. Zhang, N. Li, C. M. Ge, C. Feng and L. F. Ma, *Dalton Trans.*, 2011, **40**, 3000–3007.

64 S. Zhang, Y. D. Zhang, H. H. Zhou, J. J. Guo, H. P. Li, Y. Song and H. Liang, *Inorg. Chim. Acta*, 2013, **396**, 119–125.

65 F. Kobayashi, R. Ohtani, S. Teraoka, W. Kosaka, H. Miyasaka, Y. Zhang, L. F. Lindoy, S. Hayami and M. Nakamura, *Dalton Trans.*, 2017, **46**, 8555–8561.

66 A. Zianna, M. Ristović Šumar, A. Hatzidimitriou, C. D. Papadopoulos and M. Lalia-Kantouri, *J. Therm. Anal. Calorim.*, 2014, **118**, 1431–1440.

67 M. A. Halcrow, J. Sun, J. C. Huffman and G. Christou, *Inorg. Chem.*, 1995, **34**, 4167–77.

68 S. Petit, P. Neugebauer, G. Pilet, G. Chastanet, A. Barra, A. B. Antunes, W. Wernsdorfer and D. Luneau, *Inorg. Chem.*, 2012, **51**, 6645–6654.

69 M. Salah El Fallah, E. Rentschler, A. Caneschi and D. Gatteschi, *Inorg. Chim. Acta*, 1996, **247**, 231–235.

70 G. J. T. Cooper, G. N. Newton, P. Kögerler, D. L. Long, L. Engelhardt, M. Luban and L. Cronin, *Angew. Chem. Int. Ed.*, 2007, **46**, 1340–1344.

71 B. Rees, L. Jenner and M. Yusupov, *Acta Crystallogr. D*, 2005, **61**, 1299–1301.

72 P. K. Bowyer, D. S. Black, D. C. Craig, A. D. Rae and A. C. Willis, *J. Chem. Soc. Dalton Trans.*, 2001, 1948–1958.

73 E. Bernarducci, P. K. Bharadwaj, J. A. Potenza and H. J. Schugar, *Acta Crystallogr. C*, 1987, **43**, 1511–1514.

74 M. Hvastijová, R. Boča, J. Kohout, L. Jäger, I. Císařová and J. Kožíšek, *Inorg. Chim. Acta*, 2003, **343**, 217–223.

75 L. Liu, X. Zhang, H. Liu, X. Zhang, G. Sun and H. Zhang, *Inorg. Chim. Acta*, 2014, **414**, 8–14.

76 C. Trumm, S. Stang, B. Eberle, E. Kaifer, N. Wagner, J. Beck, T. Bredow, N. Meyerbröker, M. Zharnikov, O. Hübner and H. J. Himmel, *Eur. J. Inorg. Chem.*, 2012, 3156–3167.

77 M. M. Olmstead, D. A. Costa, K. Maitra, B. C. Noll, S. L. Phillips, P. M. Van Calcar and A. L. Balch, *J. Am. Chem. Soc.*, 1999, **121**, 7090–7097.

78 J. Magull and A. Simon, *Z. Anorg. Allg. Chem.*, 1992, **615**, 81–85.

79 J. Jubb, L. F. Larkworthy, D. C. Povey and G. W. Smith, *Polyhedron*, 1993, **12**, 1179–1185.

80 J. C. Stevens, P. J. Jackson, W. P. Schammel, G. G. Christoph and D. H. Busch, *J. Am. Chem. Soc.*, 1980, **102**, 3283–3285.

81 D. C. Lacy, C. C. L. McCrory and J. C. Peters, *Inorg. Chem.*, 2014, **53**, 4980–4988.

82 S. Attar, A. L. Balch, P. M. Van Calcar and K. Winkler, *J. Am. Chem. Soc.*, 1997, **119**, 3317–3323.

83 R. G. Khoury, M. O. Senge, J. E. Colchester and K. M. Smith, *J. Chem. Soc. Dalton Trans.*, 1996, 3937–3950.

84 Y. Lan, D. K. Kennepohl, B. Moubaraki, K. S. Murray, J. D. Cashion, G. B. Jameson and S. Brooker, *Chem. Eur. J.*, 2003, **9**, 3772–3784.

85 E. C. Constable, M. J. Hannon, P. Harverson, M. Neuburger, D. R. Smith, V. F. Wanner, L. A. Whall and M. Zehnder, *Polyhedron*, 2000, **19**, 23–34.

86 M. G. B. Drew, F. S. Esho, A. Lavery and S. M. Nelson, *J. Chem. Soc. Dalton Trans.*, 1984, 545–556.

87 L. Pauling, *J. Chem. Soc.*, 1948, 1461–1467.

88 D.-G. Yu, T. Gensch, F. de Azambuja, S. Vásquez-Céspedes and F. Glorius, *J. Am. Chem. Soc.*, 2014, **136**, 17722–17725.

89 D. Zhao, J. H. Kim, L. Stegemann, C. A. Strassert and F. Glorius, *Angew. Chem. Int. Ed.*, 2015, **54**, 4508–4511.

90 M. L. Caste, C. J. Cairns, J. Church, W. Lin, J. C. Gallucci and D. H. Busch, *Inorg. Chem.*, 1987, **26**, 78–83.

91 A. A. Danopoulos, J. A. Wright, W. B. Motherwell and S. Ellwood, *Organometallics*, 2004, **23**, 4807–4810.

92 S.-M. Peng and V. L. Goedken, *Inorg. Chem.*, 1978, **17**, 820–828.

93 H. F. Bauer and W. C. Drinkard, *J. Am. Chem. Soc.*, 1960, **82**, 5031–5032.

94 M. Mimura, T. Matsuo, T. Nakashima and N. Matsumoto, *Inorg. Chem.*, 1998, **37**, 3553–3560.

95 Y. F. Song, W. Chen, J. Chu, G. Su, I. Mutikainen, U. Turpeinen and J. Reedijk, *Inorg. Chem. Commun.*, 2010, **13**, 1538–1541.

96 C. Desmarets, C. Policar, L. M. Chamoreau and H. Amouri, *Eur. J. Inorg. Chem.*, 2009, **2**, 4396–4400.

97 M. M. Bishop, L. F. Lindoy, A. Parkin and P. Turner, *Dalton Trans.*, 2005, 2563–2571.

98 S. J. James, A. Perrin, C. D. Jones, D. S. Yufit and J. W. Steed, *Chem. Commun.*, 2014, **50**, 12851–12854.

99 T. Murata, Y. Yakiyama, K. Nakasuji and Y. Morita, *Cryst. Growth Des.*, 2010, **10**, 4898–4905.

100 G. A. Bowmaker, C. Di Nicola, C. Pettinari, B. W. Skelton, N. Somers and A. H. White, *Dalton Trans.*, 2011, **40**, 5102–5115.

101 S. Godlewska, J. Jezierska, K. Baranowska, E. Augustin and A. Dołęga, *Polyhedron*, 2013, **65**, 288–297.

102 H.-L. Zhu, L.-M. Zheng, D.-G. Fu, P. Huang, W.-M. Bu and W.-X. Tang, *Inorg. Chim. Acta*, 1999, **287**, 52–60.

103 N. Li, F. Jiang, L. Chen, X. Li, Q. Chen and M. Hong, *Chem. Commun.*, 2011, **47**, 2327–2329.

104 S. S. Feng, J. F. Zheng, L. P. Lu, H. G. Lu, Z. Q. Gao and Y. H. Dong, *CrystEngComm*, 2016, **18**, 9077–9084.

105 R.-S. Lin, M.-R. Li, Y.-H. Liu, S.-M. Peng and S.-T. Liu, *Inorg. Chim. Acta*, 2010, **363**, 3523–3529.

106 M. J. Gunter, T. P. Jeynes and P. Turner, *Eur. J. Org. Chem.*, 2004, **2004**, 193–208.

107 J. D. Crowley and P. H. Bandeen, *Dalton Trans.*, 2010, **39**, 612–623.

108 C. Su, B. Kang, C. Du, Q. Yang and T. C. W. Mak, *Inorg. Chem.*, 2000, **39**, 4843–4849.

109 J. H. H. Ho, D. S. C. Black, B. A. Messerle, J. K. Clegg and P. Turner, *Organometallics*, 2006, **25**, 5800–5810.

110 M. S. Szulmanowicz, W. Zawartka, A. Gniewek and A. M. Trzeciak, *Inorg. Chim. Acta*, 2010, **363**, 4346–4354.

111 G.-H. Ning, T.-Z. Xie, Y.-J. Pan, Y.-Z. Li and S.-Y. Yu, *Dalton Trans.*, 2010, **39**, 3203–3211.

112 P. J. Bailey, A. Collins, P. Haack, S. Parsons, M. Rahman, D. Smith and F. J. White, *Dalton Trans.*, 2010, **39**, 1591–1597.

113 A. J. Jircitano, M. C. Colton and K. B. Mertes, *Inorg. Chem.*, 1981, **20**, 890–896.

4 Synthetic strategies towards NM,NR NHCs

Of the various transition metal complexes described in Chapter 3, the palladium(II) triflate complexes $[PdMe(en)LH_2](OTf)_2$ **1**.H_2, $[PdMeCyLH_2](OTf)_2$ **2**.H_2 and $[PdMePhLH_2](OTf)_2$ **3**.H_2 were most qualified to be precursors to free NM,NR NHCs (Figure 4.1). This chapter reports the application of several well-established approaches towards free NHCs to **1**.H_2 – **3**.H_2, as well as attempts to obtain NHC derivatives from **1**.H_2 or its free ligand, $Me(en)LH_2$. The general strategies used here for carbene formation have already been described in Chapter 1.

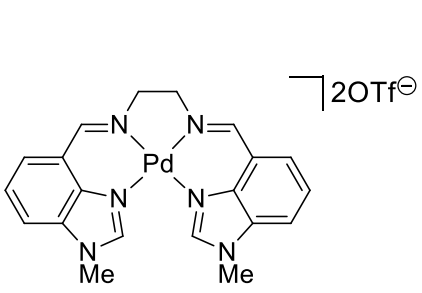

$[PdMe(en)LH_2](OTf)_2$,
1.H_2

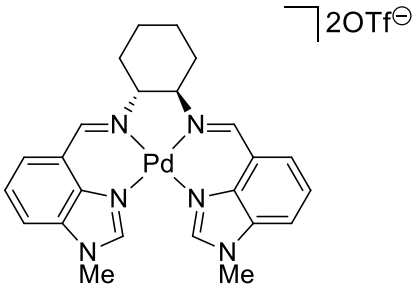

$[PdMeCyLH_2](OTf)_2$,
2.H_2

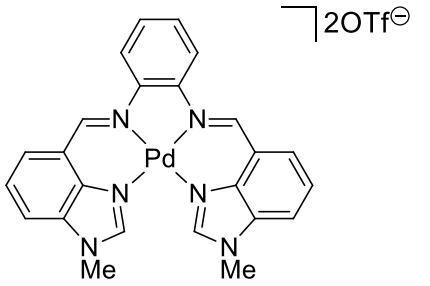

$[PdMePhLH_2](OTf)_2$,
3.H_2

Figure 4.1 *Three palladium(II) triflate complexes selected as precursors to free NM,NR NHCs.*

First, some general remarks should be made concerning the nature and intent of these studies. The objective was to screen reaction conditions that might be conducive to carbene formation from the precursor complexes or the ligand. The key variables are the base, the solvent and, where applicable, the second metal source. It is anticipated that the results would provide an indicator of the scope of bases and solvents that these precursors can tolerate, while offering insight

into their reactivity and the stability of the reaction products. Base selection cannot be determined solely on the basis of strength, as deprotonation outcomes can differ markedly while being specific to a base. For instance, deprotonation of IMes•HCl with an acetate or carbonate provides divergent reactivity to the mixed normal/abnormal and normal NHC complexes respectively (Scheme 4.1).[1]

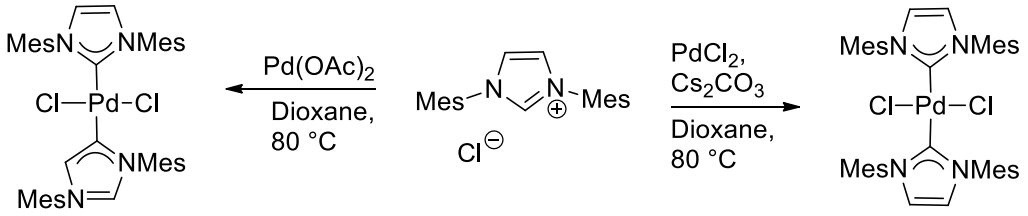

Scheme 4.1 *Base-dependent regioselective deprotonation of IMes•HCl produces palladium(II) complexes containing mixed normal/abnormal NHCs, or purely normal NHCs.*

Most of these screening studies were conducted as NMR scale reactions for practical reasons, such as the ability to monitor reactions in real time without expending large amounts of the precursors. The ideal outcome, of course, was the isolation of a free NM,NR NHC. Unfortunately, it was discovered that certain properties of these precursors necessitated slight deviations from what are considered to be the optimal conditions for carbene formation. Although this may have prevented the fulfilment of this goal, the findings from this study will be valuable for informing the design of future NM,NR NHC precursors.

One of the biggest limitations faced in these studies was the sparing solubilities of **1**.H_2 – **3**.H_2 and Me(en)LH_2 in common aprotic solvents such as THF, toluene and hexanes. These are the preferred solvents for carbene formation, as they are generally inert towards free NHCs. In order to achieve levels of solubility that were practical for analysis via NMR spectroscopy, it was best to dissolve compounds **1**.H_2 – **3**.H_2 and Me(en)LH_2 in DMSO, followed by acetonitrile or methanol. Methanol, being a protic solvent, was deemed unsuitable for carbene formation. The solubilities of **1**.H_2–**3**.H_2 were comparable despite their differences in steric bulk of the backbone unit. Hence, preliminary studies placed a heavier emphasis on **1**.H_2, as its ^{1}H NMR spectrum was the simplest of the three palladium(II) complexes.

(a) Direct deprotonation of a *N*-metallated precursor complex

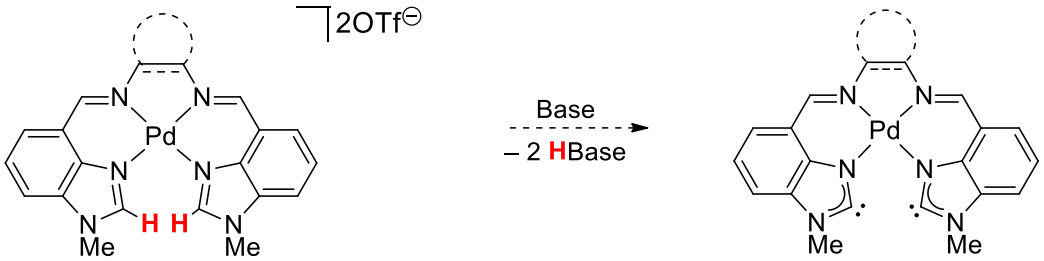

1.H_2 – **3**.H_2

(b) *In situ* generation and trapping of a NM,NR NHC from a *N*-metallated precursor complex using a secondary metal source or electrophile

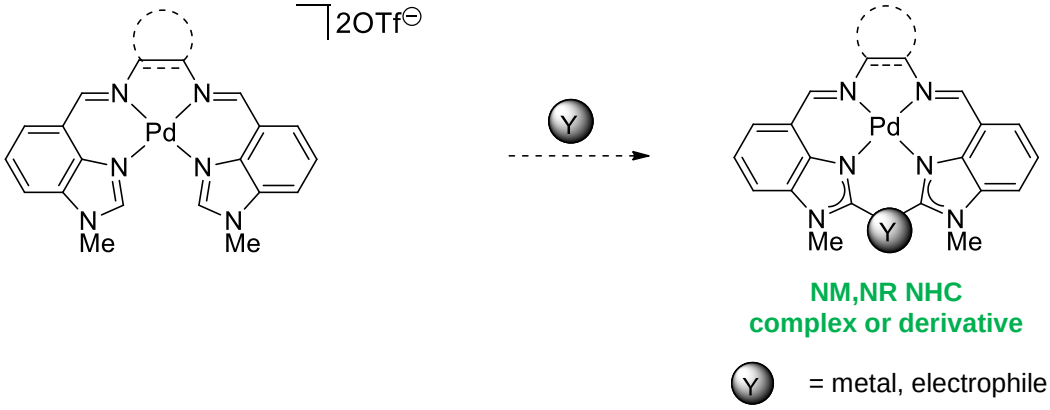

(c) Simultaneous or sequential deprotonation and *N*-metallation of a neutral azole ligand

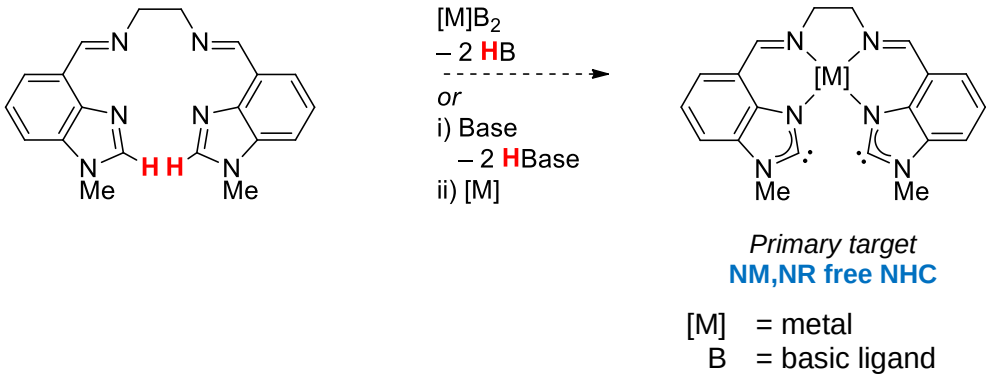

Figure 4.2 *General strategies for the synthesis of free NM,NR NHCs or their adducts.*

The strategies envisioned for carbene formation from the MeRLH$_2$ systems fall under three broad categories (Figure 4.2). The most direct method involves deprotonation of a [PdMeRLH$_2$](OTf)$_2$ complex at C2 with an appropriate base to

give the target free NM,NR NHC, PdMeRL **1**–**3** (Figure 4.2 a). The deprotonation of azolium salts is a tried and tested method for producing free carbenes, and it was hoped that the *N*-metallated benzimidazoles in $MeRLH_2$ complexes would behave in a similar manner to NR,NR azolium salts under these conditions. Carbene formation may also be observed indirectly by trapping the free NM,NR NHC with an electrophile, or as its metal complex using a secondary metal source (Figure 4.2 b). Although the latter results in a *N*,*C*-bimetallated complex instead of the target free carbene, it could be a useful fallback strategy in the event that the free carbene is too unstable for observation. Furthermore, the bimetallic complex would be an interesting study in its own right. For instance, more complex architectures could potentially be constructed from two different metals and the flexible $Me(en)LH_2$ ligand. Alternatively, complexation and deprotonation could be conducted simultaneously using a metal source with basic ligands (Figure 4.2 c). In principle, this method is attractive as it restricts the number of chemical species involved, which may reduce the likelihood of side reactions.

4.1 Attempted free carbene synthesis by direct deprotonation of $PdMeRLH_2$ complexes

Very strong bases such as NaH,[2,3] KO*t*Bu[2,4] and KHMDS[4,5] are usually required to deprotonate the C2 atom to produce a free carbene. Typically, deprotonation is performed in aprotic solvents such as hexane, toluene or THF, but owing to the poor solubility of the test compounds in these solvents and the desire to monitor these reactions by NMR spectroscopy, most of the reactions presented here were conducted in CD_3CN or d_6-DMSO. It should be acknowledged that some free NHCs may undergo C–H insertion reactions with acetonitrile or DMSO, although this is not always the case, particularly for unsaturated NR,NR NHCs.[6] For example, the carbene sites in I(*i*Pr),[7] IAd[8] and I*t*Bu[9] were reportedly stable in d_6-DMSO solutions at room temperature, although the latter two would undergo deuterium exchange at the C4 and C5 atoms on the backbone (Scheme 4.2). In fact, the free carbene in I*t*Bu did not attack DMSO even at temperatures as high as 145 °C.[9] Deuterium exchange along the backbone was also observed for IAd in CD_3CN, but the carbene remained unaltered.[8] It was only after prolonged heating that changes were seen in acetonitrile solutions of IAd, creating complex mixtures that presumably consisted of products from the base-catalysed self-condensation of acetonitrile.

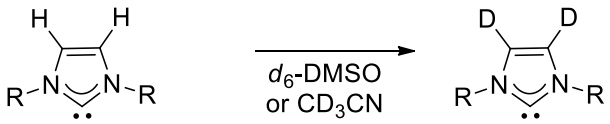

IAd R = 1-adamantyl
I*t*Bu R = *t*Bu

Scheme 4.2 *Deuterium exchange along the unsaturated backbone of some classical free carbenes.*

In contrast, the backbone-saturated SIMes readily inserted into acetonitrile at 23 °C to give a cyanomethylimidazoline in 70 % yield (Scheme 4.3 a). Similarly, deprotonation of the benzimidazolium salts **4a**-**c** with NaH in acetonitrile produced the insertion products **5a**-**c** (Scheme 4.3 b), and the analogous reaction occurred for the 1,3,4,5-tetramethylimidazolium salt.[10,11] Yet, this method was successful for the isolation of 1,2,4-triazol-5-ylidenes **8a**-**c** from their parent triazolium salts **7a**-**c** (Scheme 4.3 c).[12]

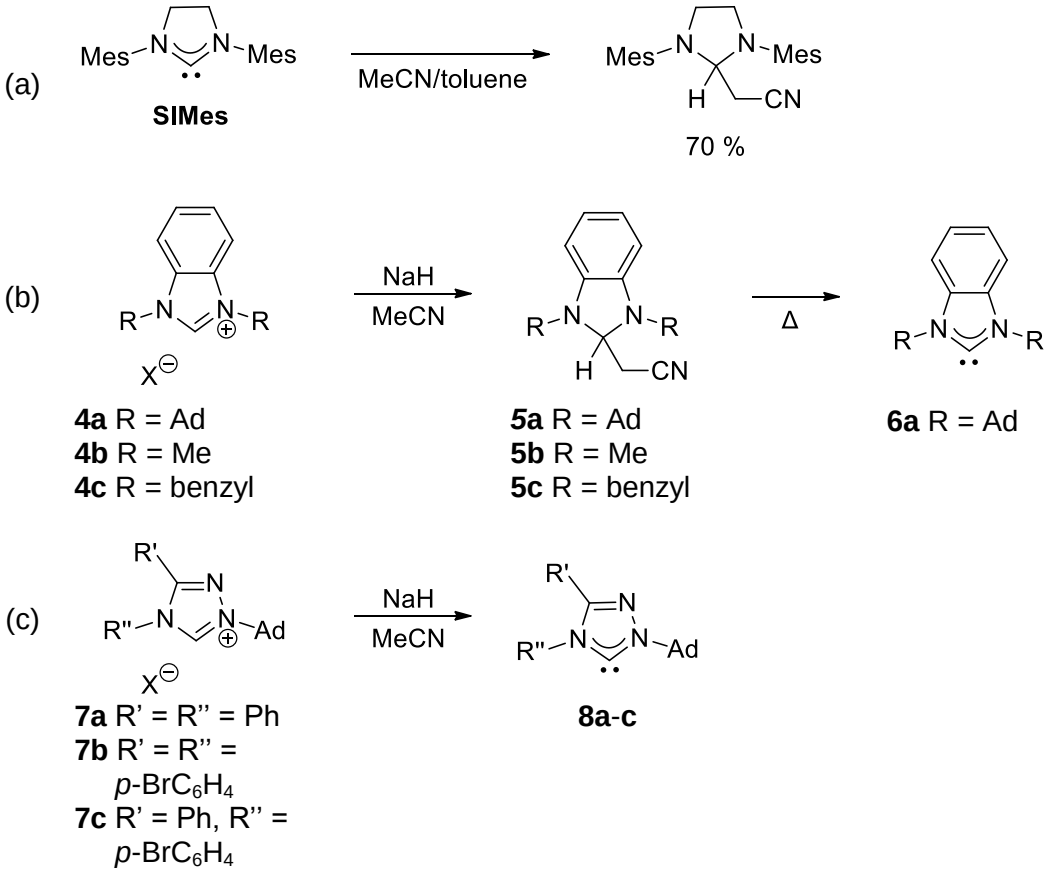

Scheme 4.3 *Insertion of acetonitrile into* ***(a)*** *1,3-dimesitylimidazolin-2-ylidene and* ***(b)*** *in situ generated benzimidazol-2-ylidenes.* ***(c)*** *Deprotonation of triazolium salts in acetonitrile to afford 1,2,4-triazol-5-ylidenes.*

The solid azoline **5a** could be heated at 180 °C to liberate acetonitrile, providing access to the corresponding free carbene.[10,11] However, heating the less sterically hindered azolines **5b**-**c** did not lead to the free carbenes. Presumably, the stronger C2–C bonds meant that other side reactions were favoured over α-elimination.

The propensity of a given NHC to insert into the acetonitrile C–H bond is likely linked to its nucleophilicity, which is in turn positively correlated with the pK_a of the parent azolium salt.[13,14] According to the empirical method developed by Mayr and coworkers,[15,16] the NHC types which were reactive towards acetonitrile (such as the imidazolin-2-ylidene, SIMes) were measurably more nucleophilic than the ones which were not (for example, the triazol-5-ylidenes).

These examples show that while MeCN and DMSO may not be ideal solvents for deprotonation, it is sometimes possible to isolate free carbenes from them. Any insertion products could potentially be used as precursors to a free carbene, or at least provide evidence for the intermediacy of one. The following experiments will use NMR spectroscopy to uncover any signs of the formation of free carbenes **1**–**3**, namely the disappearance of the H_{C2} singlet to indicate successful deprotonation. If the concentration of the sample permits study by ^{13}C NMR spectroscopy, the appearance of an extreme downfield peak in the ^{13}C NMR spectrum would be diagnostic of a new carbene atom. That said, the lack of a far downfield resonance does not necessarily prove the absence of a free carbene. As discussed in Chapter 1, anionic NHC carbene atoms often have chemical shifts that are closer to the aromatic range in ^{13}C NMR spectroscopy.

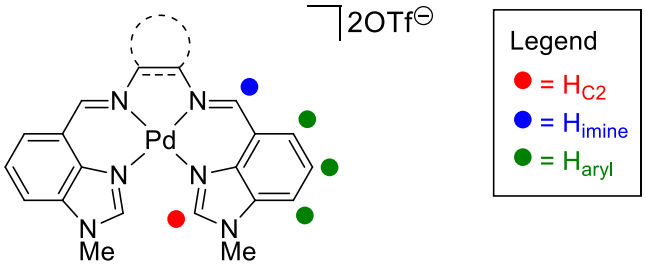

Figure 4.3 *Annotation of key protons in the [PdMeRLH$_2$](OTf)$_2$ complexes.*

All experiments were conducted using anhydrous reagents at room temperature unless otherwise specified. The reaction of **1**.H_2 with 2 equivalents of NaH in d_6-DMSO or CD_3CN resulted in decomposition after 5 minutes at room temperature. Conducting the reaction in THF at temperatures between −10 to

−84 °C failed to protect the free carbene product **1**, if it formed at all. Rather, the off-white solid that was filtered from the reaction fizzed vigorously when it was dissolved in d_6-DMSO for NMR spectroscopy, suggesting that the starting materials had not dissolved and therefore failed to react in cold THF. The ^{1}H NMR spectrum showed the same decomposition observed in the other instances where NaH was used.

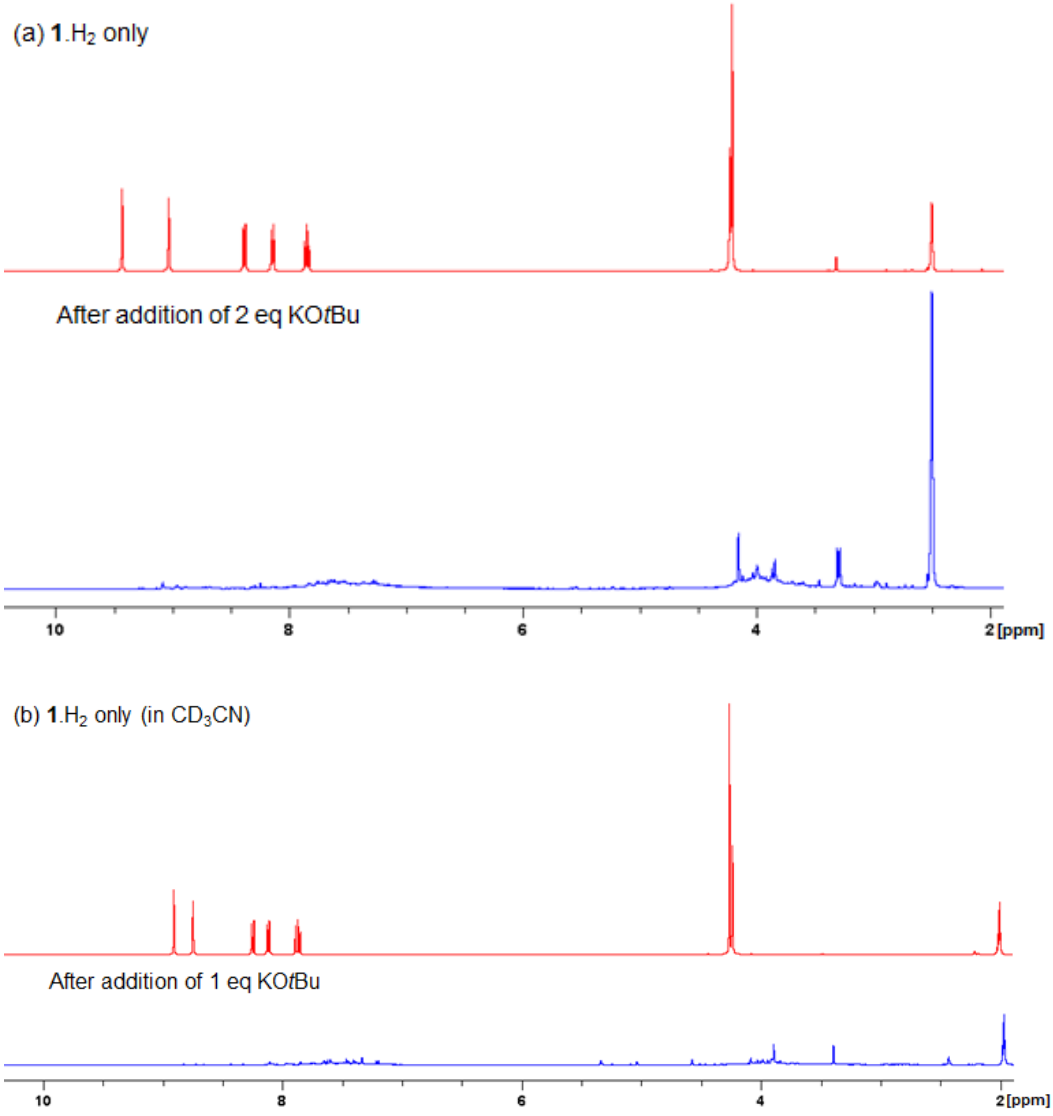

Figure 4.4 *^{1}H NMR spectra of **1**.H_2 before and after addition of **(a)** 2 equivalents of KOtBu in d_6-DMSO and **(b)** 1 equivalent of KOtBu in CD_3CN.*

Similar extents of decomposition were observed when 2 equivalents of KO*t*Bu, DBU or NaOMe were used as the base instead (Figure 4.4 a). The degree of degradation appeared to be proportional to the amount of base used, which indicates that base decomposition is not a catalytic process. For instance, when

only 0.6 equivalents of KO*t*Bu was added to **1**.H_2 in d_6-DMSO, **1**.H_2 was still the predominant species in solution, although a mixture of products was visible along the baseline of the ^{1}H NMR spectrum. The H_{imine} singlet had broadened considerably, but it is the H_{C2} resonance that was attenuated by the addition of D_2O, disappearing completely after 3 hours at room temperature.

Based on the results obtained with NaH, DBU and NaOMe, **1**.H_2 might be expected to decompose upon contact with another strong base, KHMDS. Contrary to expectations, this was not the case when 2 equivalents of KHMDS were added to a d_6-DMSO containing **1**.H_2. After 10 minutes, the ^{1}H NMR spectrum of the reaction mixture showed that all the resonances for **1**.H_2 had shifted on average 0.4 ppm upfield (Figure 4.5). There was also a substantial decrease in the intensity of the substrate signals, suggesting the precipitation of most of the reaction mass. A broad peak between 6.7 – 7.8 ppm obscured the base of the H_{aryl} signals. This spectral feature might hint at the aggregation of multiple species in solution.

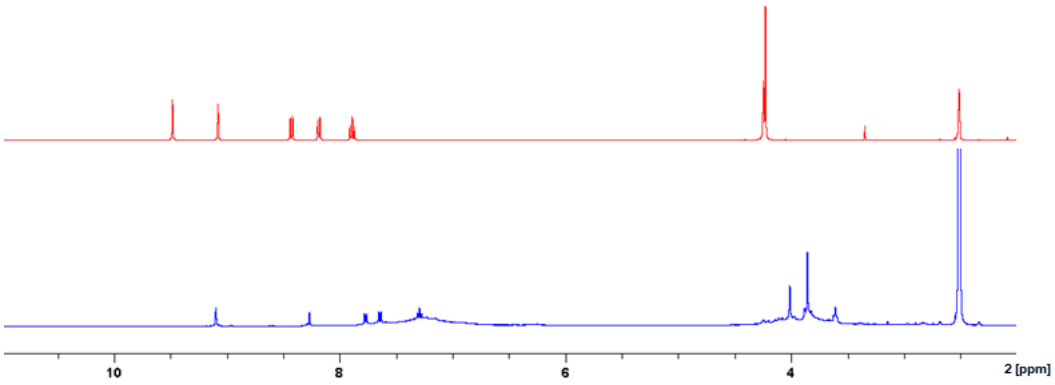

Figure 4.5 *^{1}H NMR spectra of **1**.H_2 before (top, red) and after treatment with 2 equivalents of KHMDS (bottom, blue) in d_6-DMSO. The vertical scale of the bottom spectrum relative to the top spectrum has been increased to ensure visibility of the resonances.*

Prompted by the broadening of the H_{C2} resonance when sub-stoichiometric amounts of KO*t*Bu were used, the investigation was expanded to include milder bases. Cs_2CO_3 was first chosen, as it is the most soluble of the carbonate bases. Even so, it was only partially dissolved in these small-scale reactions. When 2 equivalents of Cs_2CO_3 were added to a solution of **1**.H_2 in d_6-DMSO, the broadening of the H_{imine} peak was observed once more. An immediate reduction in the area of the H_{C2} peak occurred upon addition of excess D_2O. The intensity of the H_{imine} peak decreased by approximately 30 % after the mixture was left to

stand for 21 hours at room temperature, implying that deuterium exchange was taking place at both the imine and C2 (Figure 4.6).

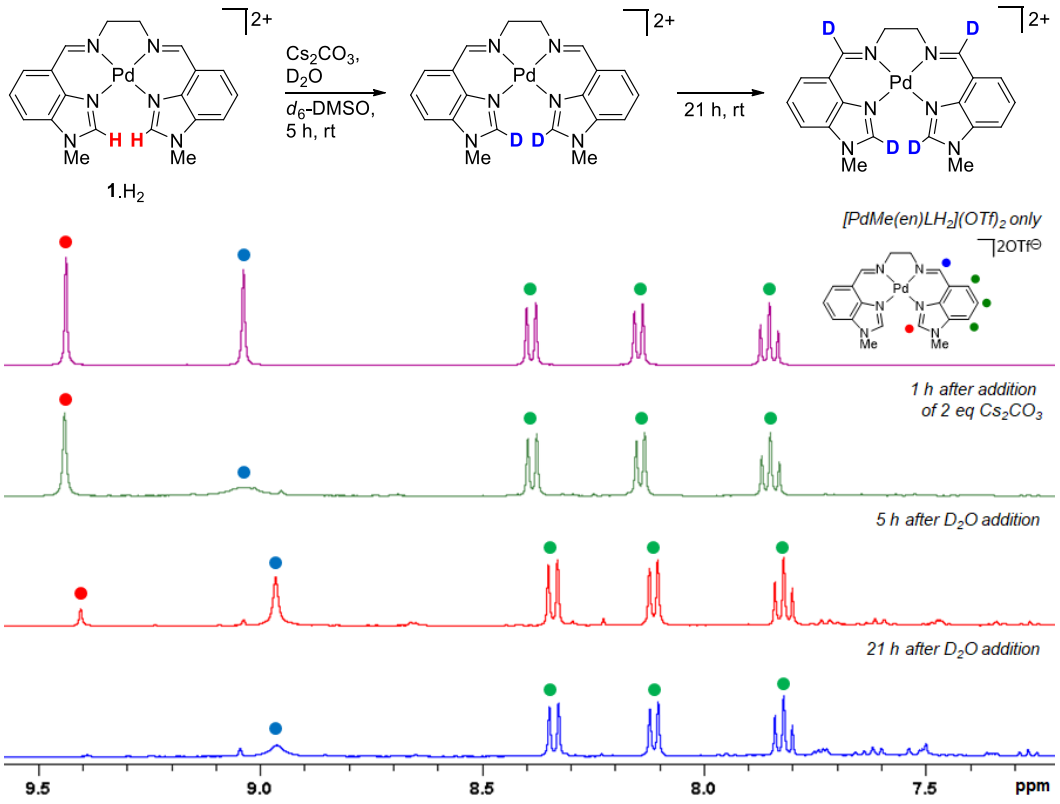

Figure 4.6 *^{1}H NMR spectra of **1**.H_2 in d_6-DMSO showing broadening of the H_{imine} singlet upon addition of base, and subsequent deuterium exchange of the imine and C2 protons with D_2O.*

After 6 days at room temperature, a small amount of 4-CHOBimMe appeared, indicating a very slow hydrolysis process. Small amounts of additional byproducts were also detected, but could not be identified. It is possible that some of the new minor peaks between 4.6 – 5.6 ppm belong to the *N*,*N'*,*N''*-monoimine palladium(II) complex. One could also consider the possibility that some of the aldehyde might react with **1** or another transient carbene species to form a species which resembles the Breslow intermediate. Imidazolium salts such as **9** are known to form adducts with benzaldehyde under mildly basic conditions (Scheme 4.4).[17] Even DABCO or 3-hydroxyquinuclidine which have pK_a values as low as 8 – 9 are sufficiently basic to generate the carbene, which then adds to the aldehyde to give adduct **10**.

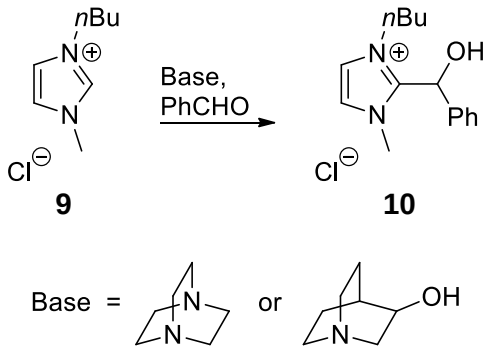

Scheme 4.4 *Reaction of an imidazolium-based ionic liquid with benzaldehyde.*

The formation of byproducts in this work appears to be a function of time and not the amount of Cs_2CO_3 employed. When the experiment was repeated with only 1 equivalent of Cs_2CO_3, the same amount of these byproducts was observed after a similar length of time. Complete disappearance of the H_{C2} singlet was seen 17 hours after D_2O was added to the reaction. H/D exchange of the imine proton was not observed in this case, possibly due to the shorter overall reaction time. Similar rates of deuterium exchange were achieved when Cs_2CO_3 was substituted with 2 equivalents of NaOAc. The rate of H/D exchange of H_{imine} can be significantly accelerated through the application of NaOH. With the stronger base, the size of the H_{imine} peak was halved within 15 minutes. For all bases except NaOH, the reaction mixture steadily turned into a dark purple colour after the base was added. Perhaps these reactions shared a common product that was highly coloured.

The results from the deuterium exchange studies offer some valuable insights. Firstly, deuterium exchange does not occur for **1**.H_2 at room temperature unless both base and D_2O are present. Complete exchange of H_{C2} can be achieved with less than 2 equivalents of base, suggesting that deuterium exchange can be a base-catalysed process.[18] In the absence of base, the d_6-DMSO solution of **1**.H_2 and D_2O must be heated at 160 °C for 3 days to attain significant degrees of H/D exchange at C2 and the imine. Secondly, H_{C2} is the most acidic proton in **1**.H_2. Hence, it is always completely exchanged before any other proton. The only other apparently exchangeable proton is H_{imine}, although its rate of exchange is slower. It is interesting to note that deuterium exchange on the backbone of IAd and I*t*Bu occurs without the need for an external base (Scheme 4.2), a reflection of the lower relative acidities of H_{C2} and H_{imine}.

It is well known that the C2 position in azolium salts is quite acidic due to the influence of the adjacent electronegative heteroatoms. Consequently, H/D exchange readily occurs at C2. An early example comes from a feasibility study of the deprotonation of a thiazolium cation, where the stability of the corresponding thiazol-2-ylidene was established by successful H/D exchange at C2.[19] Breslow found that the thiazolium salts **11a**-**b** would undergo rapid exchange at room temperature without the assistance of a basic catalyst (Scheme 4.5). The work of Bode and colleagues suggests that it is the weakly basic halide or acetate counterions in an azolium salt that help produce trace amounts of the corresponding NHC, which can then attack a suitable electrophile in a catalytic manner[20] or in Breslow's case, undergo deuteration.

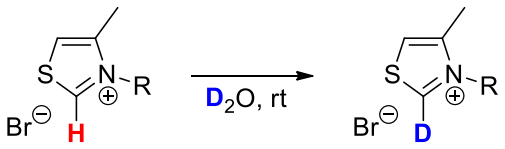

11a R = Me
11b R = Bn

Scheme 4.5 *Facile base-free deuterium exchange at the C2 position of thiazolium salts.*

Imidazolium cations exhibit a similar proclivity for isotopic H exchange, which is fastest at C2. H_{C2} acidity (and hence the rate of H/D exchange) is higher for imidazolium salts which are benzannulated[21,22] or contain strongly inductive *N*-aryl substituents instead of *N*-alkyl substituents.[23] By comparison, the C2 position is much less acidic in the neutral parent azoles, which leads one to expect the deprotonation of **1**.H_2 to be more challenging. N3-alkylation or protonation is essential for efficient isotopic H exchange, enhancing exchange rates by orders of magnitude.[24] Fortunately, N3-metallation also promotes the exchange, albeit to a lesser degree than alkylation or protonation.[25,26] The precise level of activation is dependent on the identity of the *N*-coordinated metal ion. All of this suggests that the C2 acidity in **1**.H_2 can be tuned by varying the *N*-substituents and metal ion. Perhaps by replacing the *N*-methyl group and palladium(II) with an electron-withdrawing aryl ring (such as 4-chlorophenyl) and a more activating metal ion respectively, H_{C2} can be removed under milder conditions.

Exchange can also occur at C4 and C5, although more forcing conditions are generally required.[27] Acyclic formamidine salts may also undergo H/D exchange

at C2, although in this case the process is much slower, to the point that it competes with imine hydrolysis.[23] This is in agreement with the slow deuterium exchange of H_{imine} in **1**.H_2 being accompanied by the appearance of 4-CHOBimMe.

It is proposed that in the presence of base but the absence of D_2O, the C2 and C_{imine} atoms are reversibly deprotonated. This process is too fast to be observed for C2 on the NMR time scale, but slow enough for C_{imine} that it results in broadening of the H_{imine} singlet. While this supports the belief that the free carbene can at least be formed transiently, the deprotonation of the imine might compete with C2 deprotonation if a base of sufficient strength is present in excess. This speculative imine deprotonation is somewhat reminiscent of iminium-derived carbenes: Bertrand and colleagues have shown that free aryl-[28] or alkylaminocarbenes[29] can be prepared by deprotonating the corresponding aldiminium salt. Later, Ellman and coworkers found that a similar carbene could be made by tautomerisation of the cyclic aldimine **12** into the protic NHC complex **13** in the presence of rhodium(I) (Scheme 4.6).[30]

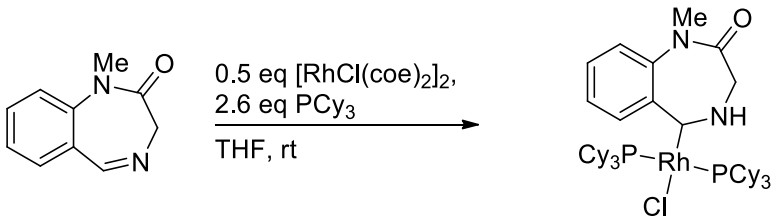

12 **13**, 35 – 50 % NMR yield

Scheme 4.6 *Metal-induced tautomerisation of an aldimine into a protic NHC.*

The carbenes reported by Bertrand and Ellman were neutral species, whereas the abstraction of H_{imine} from **1**.H_2 or **1** should result in gained anionic charge. This highly charged species is predicted to be more unstable than the neutral arylaminocarbenes, while sharing their potent nucleophilicity. It was noted earlier that **1**.H_2 did not tolerate strong bases well. The multitude of products formed under those circumstances may be explained as reactions of the imine-derived carbanion. More extensive screening might eventually reveal a base of just the right strength and specificity, such that C2 deprotonation occurs irreversibly without compromising the rest of the complex.

Another possibility is that the methylene unit adjacent to N_{imine} is deprotonated instead of C_{imine}, forming a 2-azaallyl anion (Figure 4.7). Such anions are highly

reactive nucleophiles, and their value in organic synthesis (particularly in cycloaddition reactions)[31,32] has been touted in a recent review.[33] They can be stabilised by the presence of aromatic or electron-withdrawing substituents on each end,[34–38] features which are mostly lacking in **1**.H_2. The intense colouration characteristic of 2-azaallyl anions may account for the deeply coloured reaction mixtures which pervade the deprotonation studies reported throughout this chapter.

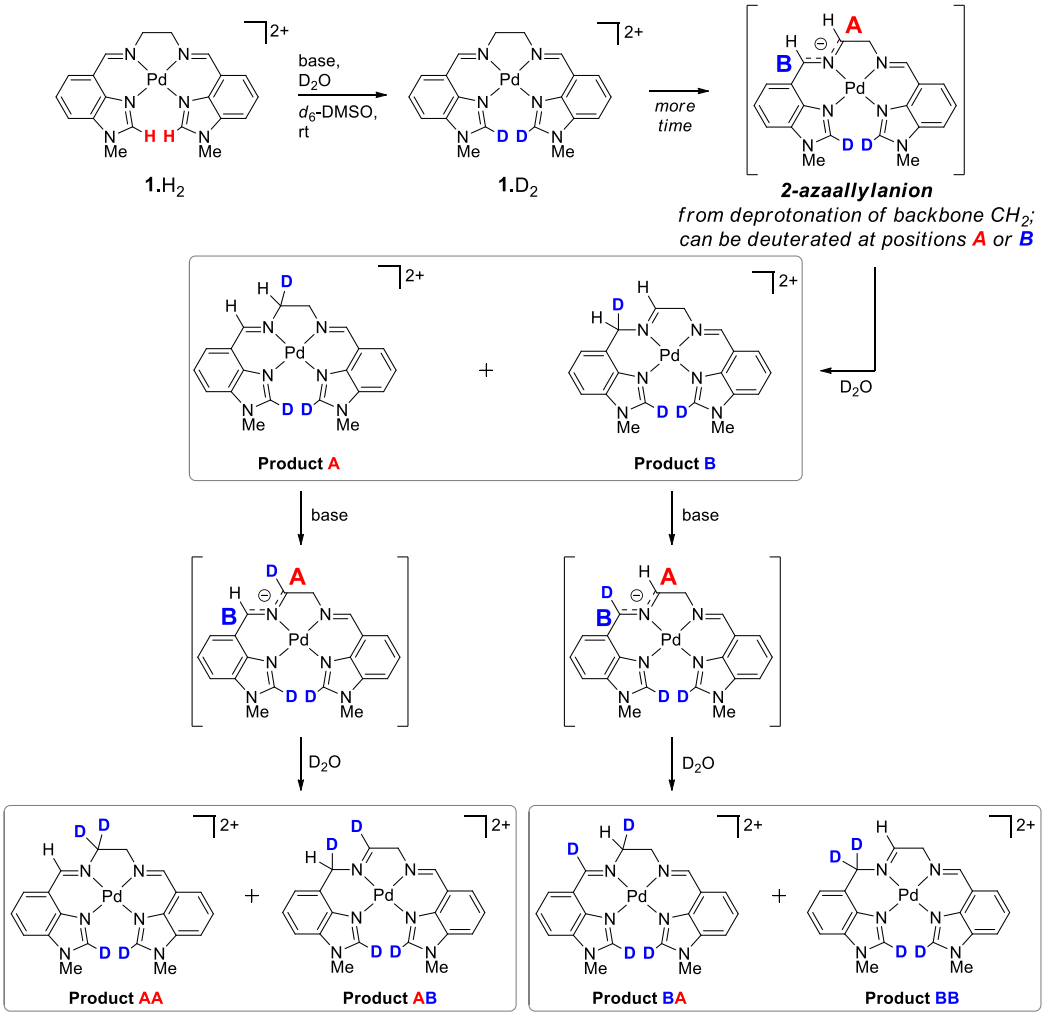

Figure 4.7 *Possible formation of a mixture of deuterated derivatives from* ***1***.H_2 *via a 2-azaallyl anion intermediate.*

In the presence of D_2O, the anion might be deuterated at either end to give products **A** or **B**, although the literature implies that deuteration at the less substituted carbon might be favoured.[37] Both species contain a H_{imine} and a CHD methylene group. Hence, the original H_{imine} resonance should be retained for **A**, and a new, similarly downfield H_{imine} singlet would appear for **B**. Suppose **A** and **B** undergo a second H/D exchange, leading to a mixture of four deuterated

species, two of which would be deuterated at C_{imine}. For every outcome, any attenuation of the original H_{imine} singlet should be accompanied by diminution of the CH_2 resonance as a consequence of deuteration. The ^{1}H NMR spectra do not unequivocally reflect this. A minor broadening of the CH_2 resonance was observed during H/D exchange. This resulted in partial overlap with the NCH_3 singlet and may have affected the accuracy of the integration of the CH_2 singlet, leading to values slightly below 2H (*ca.* 1.6H – 1.9H). If 2-azaallyl formation was occurring as illustrated in Figure 4.7, a more dramatic decrease in the size of the CH_2 singlet would be expected – at least 50 %. Furthermore, no new singlets consistent with H_{imine} in **B** or **BB** were observed. In light of the small number of experiments conducted here, it is acknowledged that further studies are required to fully evaluate the role (if any) that 2-azaallyl anions play in the deprotonation of **1**.H_2. Theoretically, **2**.H_2 is also capable of forming a 2-azaalyll anion, whereas such reactivity is not possible for **3**.H_2.

The complex product mixtures from the deprotonation of **1**.H_2 could also be the result of the transient carbene **1** participating in subsequent intra- or intermolecular reactions made possible by the flexible ethylene bridge. For example, imine-functionalised imidazolium salts such as **14a**-**b** are known to undergo intramolecular C–C bond formation in the presence of base.[39] It is believed that the formation of enamines **16a**-**b** proceeds via nucleophilic addition of the NHC intermediate **15a**-**b** to the imine (Scheme 4.7).

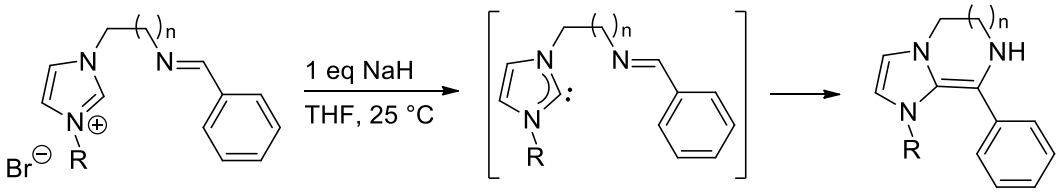

14a R = *i*Pr, n = 1 **15a-b** **16a-b**
14b R = *n*Pr, n = 2

Scheme 4.7 *Proposed mechanism for the formation of Breslow-type compounds by intramolecular addition of NHCs to imines.*[39]

Admittedly, such chemistry does not seem very feasible for **1**.H_2, given the steric congestion around C2 and significant ring strain that the products would experience. It may however be possible if partial ligand dissociation occurs. If similar transformations were occurring for **1**.H_2, the more rigid linkers in complexes **2**.H_2 and **3**.H_2 could protect the carbene by restricting substrate

access. While exposure of **1**.H_2 to less than 2 equivalents of KO*t*Bu resulted in broadening of the H_{imine} peak, the treatment of [PdMeCyLH_2](OTf)$_2$ **2**.H_2 with 1 equivalent of KO*t*Bu did not.

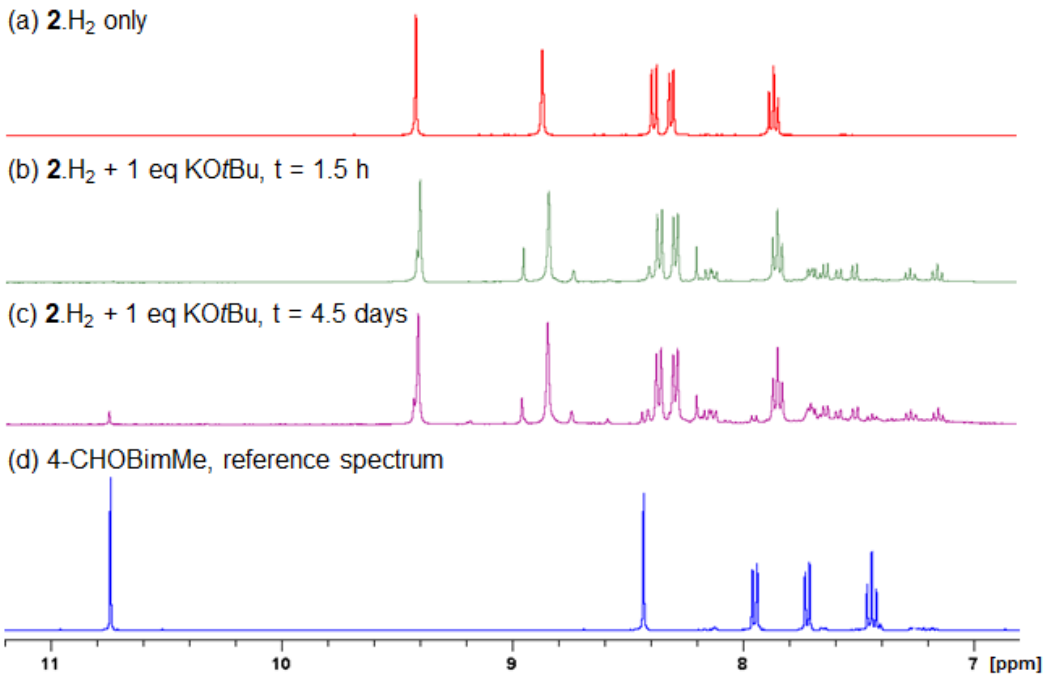

Figure 4.8 *^{1}H NMR spectra of **2**.H_2 **(a)** prior to base addition, **(b)** 1.5 hours and **(c)** 4.5 days after the addition of 1 equivalent of KOtBu, compared against **(d)** an authentic ^{1}H NMR spectrum of 4-CHOBimMe.*

The resulting ^{1}H NMR spectrum consisted of sharp peaks belonging to **2**.H_2, which was the major component in the mixture (Figure 4.8). Based on the number and pattern of the other H_{aryl} resonances, the minor component(s) might be a desymmetrised complex whose signals integrate for approximately 2:10 relative to **2**.H_2. After 1.5 hours at room temperature, the ratio of the new species to **2**.H_2 increased slightly to about 3:10, after which no further increase was seen. After 4.5 days, small traces of 4-CHOBimMe and minor overlapping species were visible in the spectrum, which was otherwise largely unchanged.

Next, the reaction of **2**.H_2 with a milder base was attempted. Treatment with 2 equivalents of Cs_2CO_3 in d_6-DMSO resulted in a ^{1}H NMR spectrum that consisted mostly of **2**.H_2 and traces of the desymmetrised species seen in the KO*t*Bu attempt (Figure 4.9).

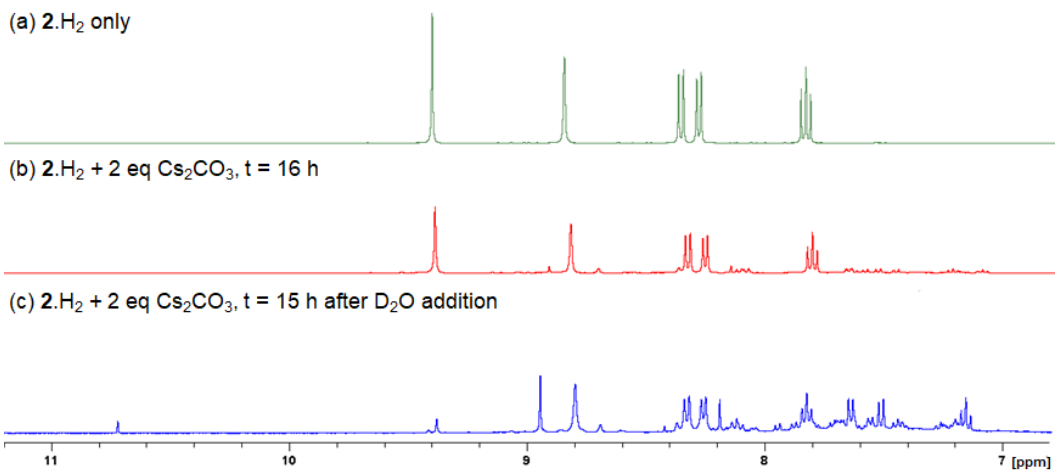

Figure 4.9 *^{1}H NMR spectra showing the formation of trace MeCyLH$_2$-derived species from **2**.H$_2$ after treatment with Cs$_2$CO$_3$, and subsequent degradation upon D$_2$O addition.*

The formation of the presumed desymmetrised species was slower with the carbonate base, even though the quantity of base was doubled. After 16 hours at room temperature, the degree of conversion was only half of what was achieved with KO*t*Bu in 1.5 hours. No aldehyde was observed at this point. Supposing that the new product(s) was **2**.H, **2** or a mixture thereof, adding D_2O should deuterate the carbenes and return the C_2 symmetry of the Pd(II) complex cation. D_2O addition did not result in the simplification of the ^{1}H NMR spectrum as hoped. Other peaks were still present, but greater overlaps in the resonances made it difficult to make definite assignments. There was a hint of another $MeCyLH_2$ derivative present, accompanied by a faint trace of 4-CHOBimMe, suggesting that the other component is a hydrolysis-related product. The area of the H_{C2} singlet of **2**.H_2 decreased noticeably after 15 hours. This indicates that **2**.H_2 will undergo exchange at C2 but does so more slowly than **1**.H_2, supporting the notion that more rigid linkers may retard reactions at C2. The "desymmetrised" species could also be formed in roughly the same amount by heating **2**.H_2 in d_6-DMSO at 40 °C with 2 equivalents of Hünig's base for 17 hours. No conversion occured at room temperature.

Since deuterium exchange at C2 occurs more slowly for **2**.H_2, perhaps the exchange was occurring at the more accessible imine site. The apparent asymmetry in the product(s) may arise not only from partial deprotonation, but also deprotonation at two different sites, for instance at one imine and one C2.

It seems that increasing the rigidity of the linkers makes the complexes more susceptible to imine hydrolysis, for $[PdMePhLH_2](OTf)_2$ **3**.H_2 was completely degraded by 2 equivalents of KO*t*Bu in d_6-DMSO after only 5 minutes. 4-CHOBimMe was the only identifiable species in the ^{1}H NMR spectrum. When the amount of KO*t*Bu was reduced to 1 equivalent, **3**.H_2 was still the major component by ^{1}H NMR spectroscopy after 4.5 days, though there was a gradual increase in the amount of 4-CHOBimMe.

3.H_2 is prone to imine hydrolysis even when a milder base such as Cs_2CO_3 was used, as evidenced by the persistent formation of small amounts of 4-CHOBimMe. The hydrolysis was not a rapid process under anhydrous conditions, as appreciable amounts of **3**.H_2 were still present after 2 days. As observed with **2**.H_2, the addition of 2 equivalents of Cs_2CO_3 did not result in the noticeable broadening of any of the ^{1}H NMR resonances for **3**.H_2. The addition of D_2O results in the complete decomposition of the complex within 5 minutes into a mixture of 4-CHOBimMe and other unidentified products. Possible decomposition pathways include the hydrolysis of **3**. Provided there is a suitably large excess of water, imidazol-2-ylidenes may undergo ring-opening hydrolysis instead of being protonated into the imidazolium cation.[40] Zuo and Braunstein found this to be the case for the iridium–NHC complex **17**, which hydrolysed under basic conditions to give **18** instead of the desired bis(carbene) chelate complex if the solvent was not rigorously dry (Scheme 4.8).[4]

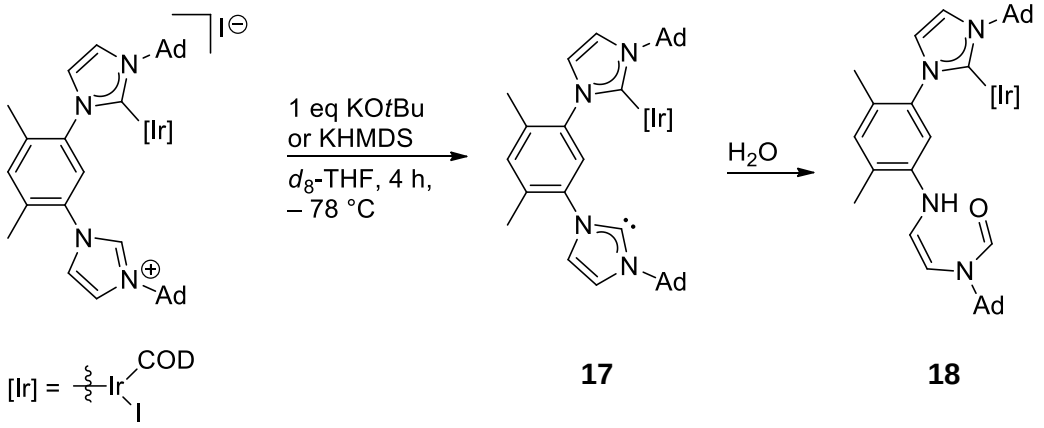

Scheme 4.8 *Ring-opening hydrolysis of a NHC fragment into an iminoformamide group.*

Subjecting **3**.H_2 to 2 equivalents of Hünig's base in d_6-DMSO produced a complex mixture after 24 hours. No starting material or significant amounts of 4-CHOBimMe were present. Given the frailty of **3**.H_2, it was not used in further

studies. Perhaps the greater steric strain imposed by the phenylene linker in **3**.H_2 increases its tendency to hydrolyse as a means of relieving this strain.

For ease of reference, the deprotonation conditions outlined in the preceding discussion are tabulated in Table 4.1.

Table 4.1 *Summary of base and solvent combinations tested for the synthesis of free NM,NR NHCs by direct deprotonation of precursor palladium(II) complexes.*

Precursor	Base	Solvent	Key outcomes
[PdMe(en)LH_2](OTf)$_2$, **1**.H_2	NaH, 2 eq	d_6-DMSO	Decomposition within 5 min
	NaH, 2 eq	CD_3CN	Decomposition within 5 min
	NaH, 2 eq	THF	−10 to −84 °C, decomp
	KO*t*Bu, 2 eq	d_6-DMSO	Decomposition
	KO*t*Bu, 1 eq	d_6-DMSO	Broadened H_{imine} resonance H/D exchange at C2 completed within 3 h at rt
	KO*t*Bu, 1 eq	CD_3CN	Messy after 30 min
	DBU, 2 eq	CD_3CN	Decomposition
	NaOMe, 2 eq	d_6-DMSO	Decomposition
	NaOMe, 1 eq	d_6-DMSO	Broadened H_{imine} resonance
	KHMDS, 2 eq	d_6-DMSO	Minor upfield shift of residual **1**.H_2 signals, appearance of broad hump around baseline
	Cs_2CO_3, 2 eq	d_6-DMSO	H/D exchange observed at C2, then imine
	Cs_2CO_3, 1 eq	d_6-DMSO	H/D exchange observed at C2
	NaOAc, 2 eq	d_6-DMSO	H/D exchange observed at C2
	NaOH	d_6-DMSO	H/D exchange observed at C2 then imine, at a higher rate than for Cs_2CO_3
[PdMeCyLH_2](OTf)$_2$, **2**.H_2	KO*t*Bu, 1 eq	d_6-DMSO	Mostly unreacted **2**.H_2 with appearance of a minor “desymmetrised” species, and eventually slow hydrolysis

	Cs_2CO_3, 2 eq	d_6-DMSO	Mostly unreacted **2**.H_2 with appearance of a minor "desymmetrised" species. D_2O addition results in slow H/D exchange at C2 and appearance of 4-CHOBimMe
	Hünig's base, 2 eq	d_6-DMSO	Minor conversion into "desymmetrised" species when heated to 40 °C.
[PdMePhLH_2](OTf)$_2$, **3**.H_2	KO*t*Bu, 2 eq	d_6-DMSO	Rapid decomposition
	KO*t*Bu, 1 eq	d_6-DMSO	Gradual hydrolysis
	Cs_2CO_3	d_6-DMSO	Slow hydrolytic decomposition, accelerated by addition of D_2O
	Hünig's base, 2 eq	d_6-DMSO	Complex mixture

4.2 Attempted indirect synthesis of the NM,NR NHC as its metal adduct

After multiple unsuccessful attempts at preparing the free carbene, there were growing concerns as to whether an inherent flaw existed in the ligand design. Any one or combination of features – the presence of an acidic H_{imine} or methylene, the flexibility of the ethylene linker, the small *N*-methyl substituent, or the benzimidazole scaffold – may limit the stability of the resulting free carbene to the extent that its isolation becomes inordinately difficult. A reasonable way to test this was to trap the carbene as its metal complex, and examine its structure for insight into the properties of the free carbene. Such a bimetallic complex could be interesting in its own right, as *C*,*N*-bimetallated NHCs are still relatively uncommon.

Although the bimetallic complex is expected to be more stable than the free carbene, the secondary complexation is not a trivial task. The selection of a metal for carbene coordination is subject to the same considerations that applied to the selection of the first metal. Preference should be given to a metal whose preferred geometry will allow it to occupy the coordination pocket between the two carbenes. Due to the proximity of the two carbenes, it was assumed that they will behave as a bidentate ligand. Once again, the second metallic fragment should ideally not disrupt the overall zero charge of the complex. In other words,

the charge of the secondary metal should be balanced by the appropriate number of coordinated counterions. This way, the complex unit remains neutral without the need for non-coordinating counterions.

The two potential carbene centres are better positioned for coordination to a tetrahedral or trigonal planar metal centre than a square planar or octahedral one (Figure 4.10). The ancillary ligands would then be less likely to crowd the *N*-methyl substituents of the carbenes.

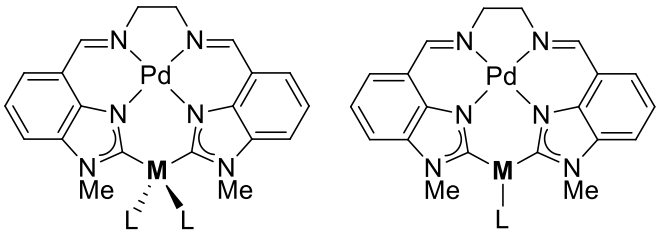

Figure 4.10 *Complexation of the NM,NR NHCs may be feasible with a secondary metal capable of adopting a* ***(a)*** *tetrahedral or* ***(b)*** *trigonal planar geometry.*

Attempts to prepare the bimetallic complex from $NiBr_2$ or $FeCl_2$ failed to produce any isolable species for crystallographic authentication. Most of the other commonly studied transition metals capable of tetrahedral geometries including cobalt(II) were discounted for being paramagnetic. This left silver(I), copper(I), and aluminium(III) as the main candidates.

The formation of the NHC complex is more thermodynamically favourable compared to free carbene formation from the imidazole. It should therefore be possible to accomplish using weaker carbonate, acetate or amine bases, which in turn could mitigate the number of side reactions on the ligand. Coordination to a metal stabilises NHCs, allowing for a wider range of solvents and conditions.

NHCs are also known to react with electrophiles such as sulfur, oxygen or CO_2 to form the corresponding thiourea, urea or ester. Accordingly, the successful isolation of these organic derivatives can be used as evidence for the presence of a carbene intermediate. However, this was not attempted due to time constraints.

4.2.1 Silver(I) as the secondary metal

As stated in Chapter 3, silver(I) is known to adopt a tetrahedral geometry in addition to the more commonly observed linear geometry. Initial attempts to prepare a tetrahedral silver(I) bisNHC complex of **1**.H_2 were adaptations of the silver oxide method pioneered by Lin and coworkers.[41] In theory, silver(I) oxide can deprotonate and metallate the C2 atoms on the benzimidazoles. The remainder of the coordination sphere can be completed by a coordinating solvent molecule such as MeCN. In CD_3CN, no reaction between **1**.H_2 and Ag_2O was visible by ^{1}H NMR spectroscopy, despite raising the temperature to 70 °C or adding a catalytic amount of KO*t*Bu (Figure 4.11 a). The addition of 2 equivalents of KO*t*Bu generated a mixture of species with overlapping resonances, but one particular set of signals was more prominent than the others (Figure 4.11 b). The doublets and triplet which typically correspond to the H_{aryl} resonances were visible. However, only one clearly identifiable singlet of comparable intensity was discerned at 8.8 ppm. This could be interpreted as the loss of H_{C2} and successful Ag complexation to form **1**[Ag]. This species could not be crystallised for SC-XRD.

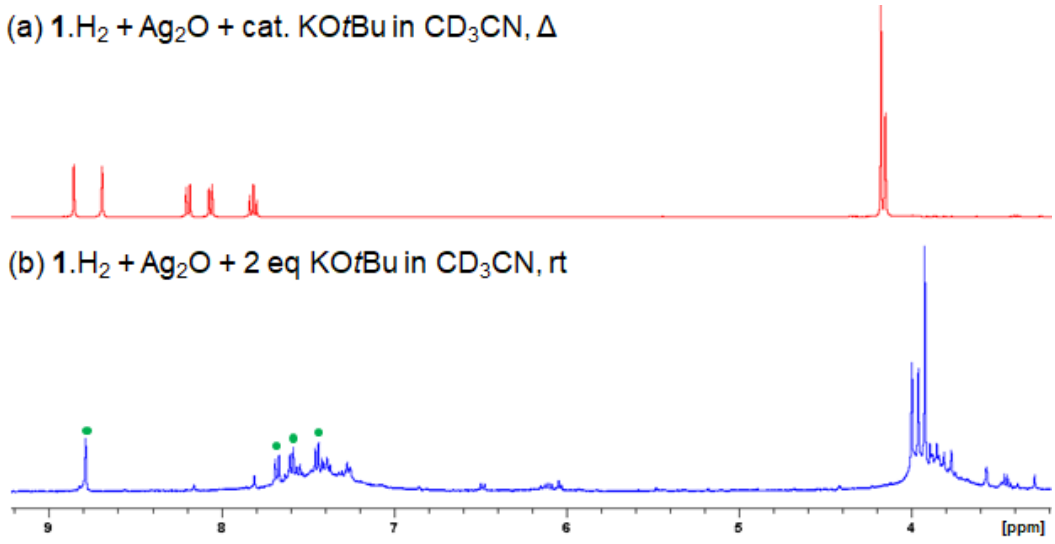

Figure 4.11 (a) *^{1}H NMR spectrum showing only unreacted **1**.H_2 in a mixture also containing Ag_2O and a catalytic amount of KOtBu.* ***(b)*** *Promising resonances suggestive of the NM,NR NHC complex **1**[Ag] (marked in green) are observed after adding a stoichiometric amount of KOtBu. Vertical scale in **(b)** has been enlarged relative to **(a)** to ensure readability despite low signal intensities.*

Interestingly, this product was not observed when the reaction was conducted in d_6-DMSO. A new broad peak between 6.5 – 7.9 ppm obscured the bases of the H_{aryl} resonances in the ^{1}H NMR spectrum, but otherwise the spectrum resembled starting material, albeit with a minor systematic upfield shift. Standing at room temperature for 1 day or heating to 80 °C did not result in the formation of new products. The absence of the presumed **1**[Ag] product in DMSO may stem from its inability to complete the Ag coordination sphere, due to its inferior ligand capability compared to MeCN.

Although silver(I) oxide is basic by nature, an external base was necessary to produce an observable change in the ^{1}H NMR spectrum. Similarly, silver(I) acetate alone did not appear to be sufficiently basic to deprotonate C2. To replicate the stoichiometry from the Ag_2O reactions, 2 equivalents each of AgOAc and acetonitrile (for completion of the Ag(I) tetrahedral coordination sphere) were heated at 60 °C with **1**.H_2 in d_6-DMSO. No differences in the composition of the mixture were revealed by ^{1}H NMR spectroscopy after 19 hours.

Since Ag_2O did not eliminate the need for an external base, a more soluble silver(I) salt was sought. Negligible conversion of **1**.H_2 occurred upon reaction with 2 equivalents of Cs_2CO_3, 2 equivalents of AgOTf and acetonitrile in d_6-DMSO, even after heating at 50 °C for 6 hours. This could be due to the depletion of available silver(I) as being sequestered as its carbonate salt, or it may highlight the need for extended reaction times or elevated temperatures when a base weaker than KO*t*Bu is used.

When NHC complexes of silver(I) are formed from azolium halide salts, the halides often coordinate to the silver atom. It is plausible that the secondary complexation could be more favourable if [PdMe(en)LH_2]Br_2 was used instead of **1**.H_2, given the stronger coordination ability of the bromide ions relative to MeCN.

4.2.2 Copper(I) as the secondary metal

Tetrahedral and trigonal planar geometries are fairly common amongst copper(I) complexes, and either geometry would be desirable for the secondary metal centre. It was hypothesised that the bimetallic product could be obtained by treatment of **1**.H_2 with KO*t*Bu in the presence of excess [$Cu(MeCN)_4$](PF_6), a convenient and soluble copper(I) source. The base was added in 1 equivalent

increments in an effort to minimise decomposition of the complex. Only trace products were detected in the ^{1}H NMR spectrum 30 hours after 2 equivalents of base were added. Adding yet another 2 equivalents of base led to total decomposition after only 5 minutes. Adding KO*t*Bu in smaller 0.5 equivalent increments reduced the extent of decomposition of **1**.H_2, but still produced complex mixtures of products that were difficult to interpret by ^{1}H NMR spectroscopy. This could mean that the reaction is incompatible with a strong base, despite the availability of a metal to trap the putative, highly sensitive NM,NR NHC. The mixture may also have been complicated by the presence of anion-scrambled products.

$Cu_2(OTf)_2$•benzene was then chosen as an alternative to $[Cu(MeCN)_4](PF_6)$, as it contained the same counterions as **1**.H_2. The copper(I) source and **1**.H_2 were dissolved in d_6-DMSO and treated with 2 equivalents of mild bases such as K_2CO_3 or NaOAc. With the former, only starting material was observed after heating at 50 °C for 20 hours, although a colour change from yellow to green was observed. It is possible that the copper(I) had been sequestered as the insoluble carbonate salt. On the other hand, treatment with NaOAc at 50 °C resulted in some conversion into promising products after 3 hours, although most of **1**.H_2 still remained. After 20 hours, traces of **1**.H_2 were detected by ^{1}H NMR spectroscopy, but most of the products had precipitated from solution.

At this point, it was questioned whether a copper(I) halide could be a better metal source than a copper(I) complex with labile and/or non-coordinating counterions. It seemed unlikely that the halide would cause scrambling with the weakly coordinating triflate ions from the parent complex, given the strength of the Cu–halogen bond. To explore this, two d_6-DMSO solutions of **1**.H_2 and CuCl were treated with 2 equivalents of NaOAc and Cs_2CO_3 respectively (Figure 4.12). In both cases, the ^{1}H NMR spectra revealed that concentrations of dissolved species dropped dramatically after 20 minutes, and only **1**.H_2 was observed in solution. Both mixtures were then heated at 40 °C for 5 hours in an attempt to encourage the dissolution of all components. After this period, the ^{1}H NMR spectra displayed a mixture of an estimated three species which seemingly contained Me(en)LH_2. In the case of NaOAc, the conversion was much lower and the spectrum was dominated by **1**.H_2. Halving the dosage of Cs_2CO_3 gave the same products in diminished yields.

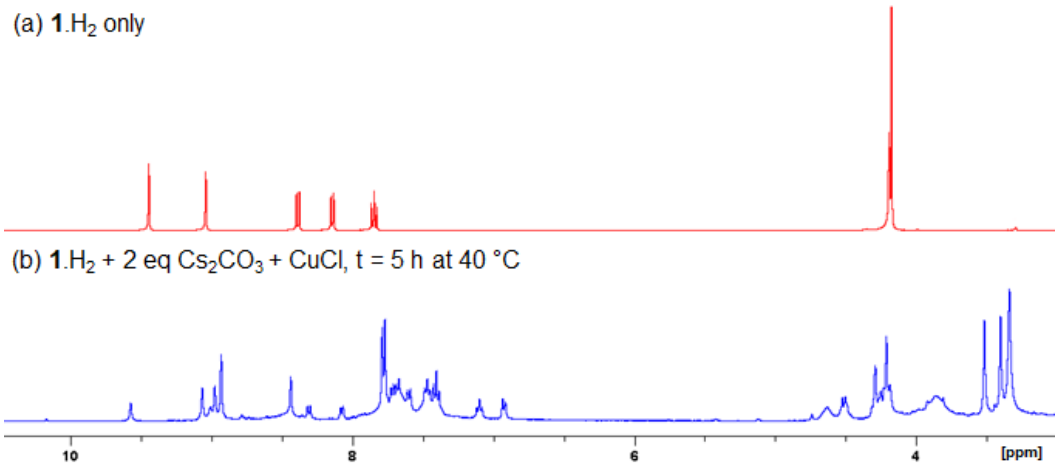

Figure 4.12 *Formation of multiple presumed Me(en)LH$_2$ derivatives from* ***(a) 1****.H$_2$ upon* ***(b)*** *treatment with a carbonate base and a copper(I) halide in an attempt to trap NM,NR NHC* ***1*** *as its copper(I) complex.*

To compare the effect of changing the halide in the Cs_2CO_3 reaction, CuI was used in place of CuCl, Once again, the ^{1}H NMR spectrum after 20 minutes merely exhibited signals consistent with **1**.H$_2$. After 19 hours, trace resonances that could be attributed to the desired Cu–NHC complex **1**[Cu] began to appear. Longer reaction times or heating the mixture resulted in an increase in other byproducts, although **1**.H$_2$ was not fully consumed. The concentration of the hopeful **1**[Cu] species did not increase significantly, nor could it be isolated. However, a weak correlation was detected between a carbon at 192 ppm and a ^{1}H resonance at 2.94 ppm in the ^{1}H-^{13}C HMBC spectrum. The correlation may have arisen from $^3J_{CH}$ coupling between a characteristically downfield carbenic carbon and the *N*-methyl protons. Unfortunately, further study and isolation of this species were impractical as it was only present in minute amounts.

The reaction was later conducted on a preparatory scale in hopes of crystallising some of the products for SC-XRD. **1**.H$_2$ and 2 equivalents of both KO*t*Bu and CuI were suspended in acetonitrile at 0 °C to see if the lower temperature promoted clean **1**[Cu] formation. Unfortunately, the ^{1}H NMR spectrum of the resulting dark red-brown solid was as messy as the other attempts, and no suitably crystalline products were obtained.

It did not escape notice that all the copper(I) halide reactions led to reddish-brown reaction mixtures with appreciable amounts of insoluble species. Previous attempts to make a CuI complex of Me(en)LH$_2$ led to a highly insoluble dark rust

coloured powder. It may be possible that the copper(I) displaced palladium(II) from Me(en)LH_2 and the resulting complex precipitated from solution.

Alkylamines have occasionally been used as bases in the preparation of transition metal NHC complexes.[1,42] Their excellent solubility in organic solvents and lower basicity compared to some inorganic bases could result in milder conditions for the complexation. When applied in 2 equivalents with CuI or $[Cu(MeCN)_4](PF_6)$, amine bases such as triethylamine, Hünig's base and morpholine generally resulted in little or no conversion of **1**.H_2, regardless of whether the mixture was heated or not. Broadening of the H_{C2} or H_{imine} resonances did not occur. Reactions involving NEt_3 or Hünig's base where CuI was the secondary metal source produced traces of the presumed **1**[Cu] species, as seen in the ^{1}H-^{13}C HMBC spectrum. Notably, an orange-yellow precipitate formed within 5 minutes of adding all reagents together in CD_3CN. Single needles of this solid were obtained by slow diffusion of separate acetonitrile solutions of CuI/Hünig's base and **1**.H_2. The structure of this product was authenticated by SC-XRD as $[PdMe(en)LH_2](CuI_3)$. Extended heating results in the deposition of a thin film of metallic copper, an expected byproduct of CuI_3^- formation. It is not particularly unusual for copper(I) halides to form Cu_nX_m type ions, but the copper:halide ratio can vary considerably according to the counterion and reaction solvent.[43] The formation of halocuprous ions sometimes accompanies successful complexation[44] and thus may not be of great detriment to the desired Cu–NHC formation, if it is compensated for by excess CuX.

Table 4.2 provides an overview of the conditions tested as part of this approach involving the *in situ* generation and trapping of NM,NR NHC as its complex.

Table 4.2 *Conditions used for the attempted synthesis of bimetallic NM,NR NHC complexes from the palladium(II) precursor complex* ***1****.*H_2*.*

Base	Solvent	Secondary metal (1 eq unless otherwise stated)	Key observations
KO*t*Bu, cat.	CD_3CN	Ag_2O	No reaction even at 70 °C
KO*t*Bu, 2 eq	CD_3CN	Ag_2O	Complex mixture with promising signs of **1**[Ag]
KO*t*Bu, 2 eq	d_6-DMSO	Ag_2O	Major identifiable spectral component is unreacted **1**.H_2

No external base	d_6-DMSO	AgOAc + 2 eq MeCN	No reaction at 60 °C
Cs_2CO_3	d_6-DMSO	AgOTf + 2 eq MeCN	No reaction at 50 °C
KO*t*Bu, 1 – 4 eq	d_6-DMSO	$[Cu(MeCN)_4](PF_6)$, 2 eq	Trace decomposition when ≤2 eq base used, further decomposition observed above 2 eq base
K_2CO_3, 2 eq	d_6-DMSO	$Cu_2(OTf)_2$•benzene	Only starting material observed at 50 °C
NaOAc, 2 eq	d_6-DMSO	$Cu_2(OTf)_2$•benzene	Gradual conversion at 50 °C, precipitation of unknown product(s), leaving trace **1**.H_2 in solution
NaOAc, 2 eq	d_6-DMSO	CuCl	Mixture of three apparent Me(en)LH_2 derivatives after heating at 40 °C
Cs_2CO_3, 2 eq	d_6-DMSO	CuCl	Mixture of three apparent Me(en)LH_2 derivatives after heating at 40 °C
Cs_2CO_3, 1 eq	d_6-DMSO	CuCl	Mixture of three apparent Me(en)LH_2 derivatives after heating at 40 °C, with more unreacted **1**.H_2 present compared to when 2 eq NaOAc or Cs_2CO_3 were used
Cs_2CO_3, 2 eq	d_6-DMSO	CuI	Trace conversion into possible **1**[Cu] complex
KO*t*Bu, 2 eq	MeCN	CuI, 2 eq	Reaction performed at 0 °C, complex ^{1}H NMR spectrum.
Hünig's base, 2 eq	CD_3CN	CuI	Trace conversion into potential **1**[Cu] complex, and formation of $[PdMe(en)LH_2](CuI_3)$ byproduct
NEt_3, 2 eq	CD_3CN	CuI	Trace conversion into potential **1**[Cu] complex, and formation of $[PdMe(en)LH_2](CuI_3)$ byproduct
Morpholine, 2 eq	CD_3CN	CuI	No conversion of **1**.H_2 at 60 °C
Hünig's base, 2 eq	CD_3CN	$[Cu(MeCN)_4](PF_6)$	No conversion of **1**.H_2 at 60 °C

4.3 Simultaneous complexation and deprotonation of Me(en)LH_2

The concept of achieving both complexation and free carbene formation in a single step was attractive for its elegance and simplicity. The strategy relies on the use of a metal source with basic ligands, and assumes that the metal will preferentially coordinate to the nitrogen atoms over the free carbenes. Considering the rapidity at which the complexes of Me(en)LH_2 form, it was expected that the rate of the initial complexation would exceed that of C2 deprotonation. It was hoped that Me(en)LH_2 would effectively sequester the metal ion, thus increasing the availability and basicity of the free anions in solution. Attempts to do so in a two-step process using $Pd(OAc)_2$ were described in Chapter 3. Here, alkylmetal compounds such as $AlEt_3$ and $ZnEt_2$ are considered as alternative reagents (Scheme 4.9). Their advantages are twofold: The alkyl anion has a higher pK_b than the acetate anion, and the sole byproduct of deprotonation, ethane is easily liberated from solution.

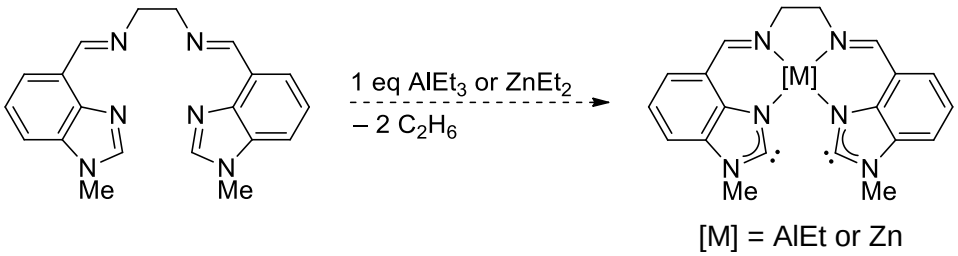

Scheme 4.9 *Proposed complexation and deprotonation of Me(en)LH_2 in a single step using triethylaluminium or diethylzinc.*

Reactions of $AlEt_3$ with similar tetradentate *N*,*N'*,*N''*,*N'''* ligands have led to pentacoordinate square pyramidal complexes with an ethyl group occupying the apical site.[45–47] The presence of the ethyl group may render the desired NM,NR NHC complex more soluble, facilitating its isolation. In the first attempt, $AlEt_3$ was added dropwise to a MeCN/toluene solution of Me(en)LH_2 at room temperature, and stirred for 45 minutes before being reduced to dryness. ^{1}H NMR spectroscopic analysis of the resulting solid revealed only unreacted ligand.

Deuterium exchange studies (discussed later) have suggested that H_{C2} is more acidic when the ligand is *N*-metallated. This might mean it could be easier to form the Al–NHC heterobimetallic complex from **1**.H_2 than it is to form the *N*-aluminated free carbene. Furthermore, aluminium(III) frequently adopts a tetrahedral coordination geometry which is compatible with **1**. With the goal of

obtaining this Pd/Al bimetallic complex, **1**.H_2 was treated with a stoichiometric equivalent of $AlEt_3$ in MeCN/toluene according to procedures adapted from the syntheses of Al(III) Schiff base complexes.[48,49] The reaction mixture was maintained at 80 °C to ensure a homogeneous solution. The initial yellow solution turned a pale pinkish red after 3.5 hours. After cooling to room temperature, a substantial amount of pale yellow crystals crystallised from the reaction mixture. These were identified by SC-XRD as **1**.H_2.

Finding no success with the aluminium reagent, attention was turned to the zinc alternative. $ZnEt_2$ was added to a THF solution of Me(en)LH_2 and stirred for 1 hour at room temperature. Unlike the reaction involving $AlEt_3$, a vivid colour change to bright red was observed. Attempts to obtain a crystalline product from this mixture were unsuccessful. The solution was reduced to dryness to give a bright fuchsia powder, which was identified as unreacted ligand using ^{1}H NMR spectroscopy. The stark colour change may simply be due to highly coloured trace products.

The alkylaluminium and alkylzinc reactions only resulted in the recovery of starting material. This is likely due to the high kinetic barrier for the activation of the M–R bond. In the context of NHC complex synthesis, these organometals are typically employed in adduct formation with pre-formed free NHCs.[50–52] In other words, $AlEt_3$ and $ZnEt_2$ are rarely used as bases for C–H deprotonation. The few examples of alkylmetals being used for direct NHC complex formation suggest that this route is deserving of further exploration. Direct zincation of 3-butyl-1-methylimidazolium bromide can be achieved with $ZnEt_2$ under solvent-free conditions.[53] Similarly, Tolman and colleagues prepared Zn-NHC complexes for lactide polymerisation by direct reaction of $ZnEt_2$ with IMes•HCl and IPr•HCl (Scheme 4.10 a).[54] Importantly, this method allowed access to complexes **20** and **21** featuring chelating pyridyl-NHCs that could not be prepared as the free carbenes, due to the presence of multiple acidic protons on the ligand (Scheme 4.10 b).

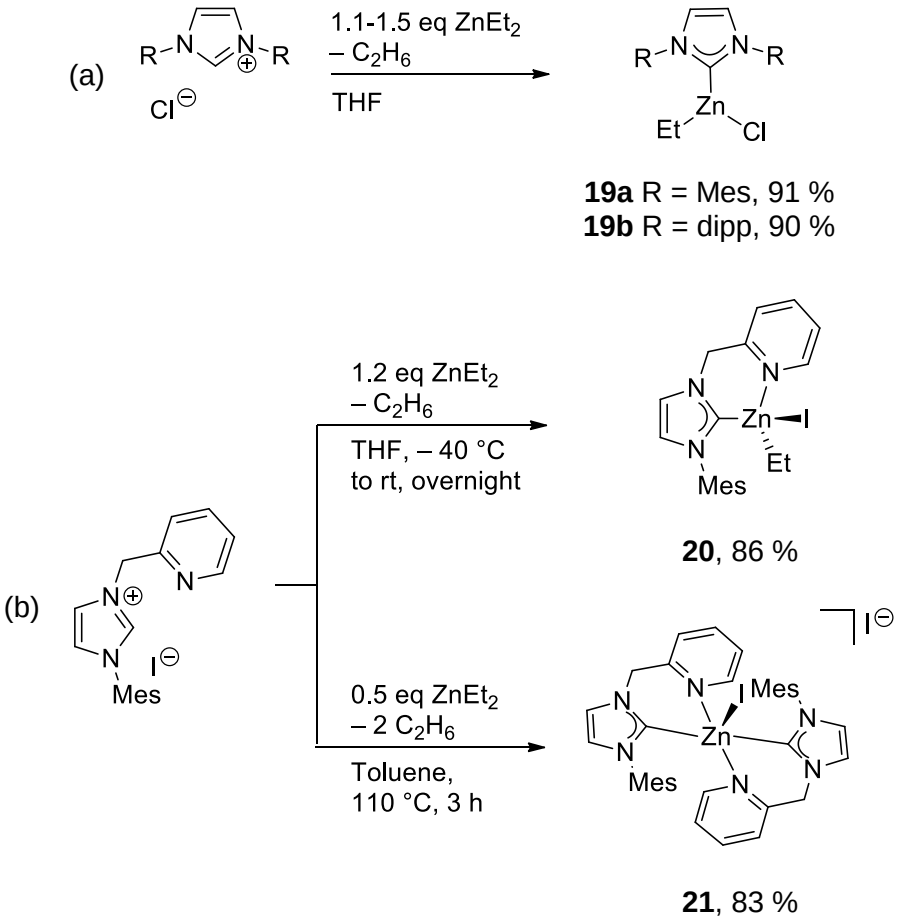

Scheme 4.10 *Direct synthesis of zinc(II) NHC complexes from imidazolium salts and diethylzinc.*[54]

Most of the reactions were performed at room temperature, and yields of the Zn–NHC complexes exceeded 80 %, showing that this strategy can be remarkably efficient. It was noted that **19a**-**b** were prone to NHC dissociation, a phenomenon sometimes associated with Zn–NHC complexes. The weaker affinity of Zn to NHCs could be advantageous for the present work as it might reduce the likelihood of Zn N,C-migration in the free NM,NR NHC.

Since the deprotonation of carbon acids by neutral organozinc reagents are notoriously sluggish, amidozinc bases have been suggested as promising alternatives. In particular, $Zn(TMP)_2$ is an effective base for the deprotonation of various functionalised substrates such as ketones, pyridines, sulfoxides and amides under mild conditions.[55] It also possesses good solubility in non-polar organic solvents, but its activity is not inhibited in polar or coordinating solvents such as CD_2Cl_2 or d_8-THF. $Zn(TMP)_2$ was thus prepared according to a published procedure[56] in order to examine its reactivity with $Me(en)LH_2$. Warm toluene solutions of $Me(en)LH_2$ and $Zn(TMP)_2$ were combined in one flask, giving

a cloudy orange-red solution which was stirred for 30 minutes at room temperature before being filtered and reduced *in vacuo*. However, colour appears to be a misleading indicator of reaction progress for the zinc(II) reactions. The ^{1}H NMR spectra of the solid and filtrate in C_6D_6 were consistent with unreacted Me(en)LH_2 and minor byproducts featuring the high-field resonances characteristic of the ethylzinc fragment. More forcing conditions or an additional donor ligand for Zn^{II} may be necessary to promote higher levels of conversion. It may also be worth exploring the use of mixed metal anionic zincate bases. The M[ZnR_2(TMP)] (M = Li, Na) class are renowned for their reactivity and chemoselectivity towards aromatic substrates, which generally surpass those of their monometallic parent components.[57,58]

4.4 Stepwise deprotonation and complexation of Me(en)LH_2

This route was first investigated as a control experiment to ascertain the involvement of the N-bound metal. It is unlikely that the free carbene can be prepared from the ligand prior to complexation, although this would be a remarkable achievement, as free anionic N,NR NHCs have not been reported. These studies may offer insight into the source of the persistent purple byproduct, which could be linked to a ligand-centred reaction, possibly involving C–C bond formation between the benzimidazole C2 atoms in Me(en)LH_2. The dimerisation of benzimidazol-2-ylidenes into entetraamines are well known,[59,60] and the dimers themselves are susceptible to spontaneous rearrangement, adding to the complexity of this reaction.[61] The formation of 2,2-bisbenzimidazoles from **1**.H_2 could also be occurring through a metal-mediated coupling process.[62–64]

When not bound to a metal, the ligand should be free to twist and rotate in solution. A carbene generated from the free ligand must surely be less shielded and thus more vulnerable to attack. Toluene was therefore selected as a more inert medium for deprotonation, even though Me(en)LH_2 was poorly soluble in it at room temperature. A pale peach suspension of Me(en)LH_2 and 2 equivalents of KO*t*Bu in d_8-toluene developed a familiar dark purple tinge after several hours at room temperature. Due to the low solubility of the species present, the ^{1}H NMR spectrum contained mostly residual solvent peaks. Other resonances appeared at 60 °C, but Me(en)LH_2 could not be identified in the spectrum. It is unknown whether these resonances were representative of the bulk reaction

mixture. Heating for 3 hours at 80 °C did not alter the ^{1}H NMR spectrum of the reaction mixture.

When D_2O was added, the reaction mixture instantly turned bright yellow. The ^{1}H NMR spectrum of the lemon yellow mixture resembled Me(en)LH_2, but with additional resonances. The yellow species might decompose over time, as more peaks appeared when the mixture was left to stand at room temperature for a few days. The reaction mixture was reduced to dryness, then fully dissolved in d_6-DMSO. The resulting ^{1}H NMR spectrum was cluttered, but still contained resonances for Me(en)LH_2, suggesting that not all of the ligand had reacted with the base, although this may have resulted from its sparing solubility in toluene. The presence of Me(en)LD_2 would have been good evidence for the formation of the free carbene Me(en)L, but it was at least clear that the latter was not a significant component of the spectrum. There is insufficient data to verify the identity of the other species or exclude the decomposition of Me(en)L. At this stage, the fate of the ligand in the presence of a strong base remains uncertain.

Dissatisfied by the inconclusive results, the focus was shifted from isolating the deprotonated ligand product(s) to using them for complexation. C2-Lithiated imidazoles have already been established as useful intermediates to carbene complexes,[65,66] in a similar fashion to using silver–NHC complexes as carbene transfer agents. This is usually driven by the precipitation of a lithium halide salt upon reaction of the lithiated azole with another metal halide salt (Scheme 4.11). Although reported examples usually culminate in metallation at C2 once the transition metal is introduced to the system, *N*,*N'*,*N''*,*N'''*-chelation may be favoured over the formation of a metal–NHC bond. If the latter product predominates, a second metal could still be inserted into the *N*,*N'*,*N''*,*N'''* coordination cavity to give the bimetallic complex. Thus, C2-lithiation of Me(en)LH_2 could be a pathway towards mono- or bimetallic complexes of Me(en)L.

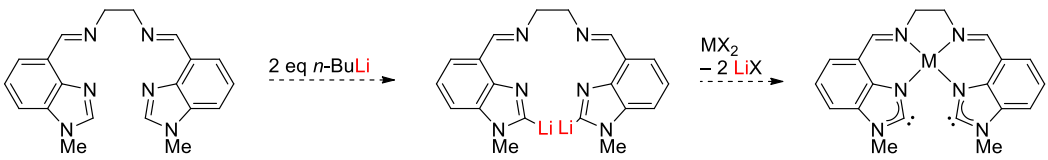

Scheme 4.11 *Proposed strategy towards NM,NR NHCs via C2-lithiation of Me(en)LH_2 followed by N-metallation and lithium salt elimination.*

With the aim of isolating the C2-lithiated Me(en)LH_2, 2 equivalents of *n*-BuLi were gradually added to a solution of the diimine in THF at room temperature. The resulting dark purple solution was stirred for another 40 minutes and its volume reduced before cooling to −20 °C. No products could be crystallised from the solution. The mixture was reduced to dryness, yielding a dark purple powder that was insoluble in C_6D_6. Its ^{1}H NMR spectra in both CD_3CN and d_6-DMSO were messy to the point of inscrutability. In order to determine whether the decomposition was caused by reaction with *n*-BuLi or the incompatibility of the product(s) with those solvents, the reaction was repeated without attempting to isolate the lithiated intermediate. Instead, 1 equivalent of $ZnCl_2$ was added as a diethyl ether solution. It was hoped that the zinc complex would be more stable or easier to crystallise. A slight cloudiness was observed, and the reaction mixture was left to stir overnight. Filtration of the reaction mixture afforded a purple solid. Subsequently, the volatiles from the filtrate were removed *in vacuo*, yielding a bright red powder. Both solids were poorly soluble in C_6D_6, and their ^{1}H NMR spectra in d_6-DMSO indicated the same extent of decomposition as before. Perhaps this decomposition could be curbed by performing the reaction at low temperatures and reducing the reaction times.

To examine the effect of *N*-metallation on the acidity of H_{C2}, 2 equivalents of Cs_2CO_3 were added to a solution of Me(en)LH_2 in d_6-DMSO. After 4 hours at room temperature, only clean Me(en)LH_2 could be seen in the ^{1}H NMR spectrum. D_2O was then added to the sample. No evidence of deuterium exchange was observed using ^{1}H NMR spectroscopy after 20 hours, but a small trace of 4-CHOBimMe appeared. The spectrum recorded after heating for 6 hours at 160 °C contained new Me(en)LH_2 derivatives. This shows that H_{C2} is less acidic in Me(en)LH_2 than its complexes, which can be rationalised as the metal centre drawing electron density away from the imidazole ring. In view of this, it is probably wiser to continue efforts to obtain the NHC from the complex instead of the free ligand, as the latter would require harsher conditions and risk more side reactions.

4.5 Conclusions and future outlooks

In summary, the $[PdMeRLH_2](OTf)_2$ (R = en, Cy, Ph) series of complexes were subjected to a variety of organic and inorganic bases in an effort to synthesise the free NM,NR NHC, PdMeRL. The complexes generally did not tolerate strong bases, while weak bases could only effect H/D exchange but not irreversibly deprotonate the C2 positions. Stronger bases can also induce H/D exchange at the imine. Attempts to trap PdMe(en)L as the heterobimetallic NM,CM complex with silver(I), copper(I) and aluminium(III) were unsuccessful. Alternative strategies involving the deprotonation of the $Me(en)LH_2$ ligand with $AlEt_3$ and $ZnEt_2$, or C2-lithiation followed by transmetallation with $ZnCl_2$ were discussed. The low kinetic basicity of the neutral organometal reagents failed to effect C2 deprotonation of $Me(en)LH_2$ or $[PdMe(en)LH_2](OTf)_2$, whereas C2-lithiation with an organolithium base resulted in decomposition. Overall, the results suggest that these conceived pathways to NM,NR NHC formation are often dominated by side reactions. It is proposed that these processes may involve the formation of a carbene at C2 and a carbanion at the imine, which then engage in intra- or intermolecular nucleophilic attack.

Clearly, one of the major setbacks experienced is the limited solubility of $Me(en)LH_2$ and the $MeRLH_2$ (R = en, Cy, Ph) complexes in common organic solvents. This restricted the range of practical reaction conditions, and prevented the use of lower temperatures or aprotic hydrocarbon solvents which are generally better suited to the synthesis of sensitive free carbene species. The incorporation of additional steric bulk around the bridge, benzimidazole phenyl ring or *N*-substituents could solve this issue, but fundamental design changes may be required to address the other problems that came to light. The observed H/D exchange at the imine highlighted the importance of not having multiple acidic protons in the carbene precursor. Future iterations of the precursor would benefit from the replacement of the aldimine with a secondary imine or an *N*-heterocyclic moiety such as pyridine.

The elusiveness of the free NM,NR NHC may be reflective of the fact that imidazol-2-ylidenes vastly outnumber their 4,5-benzannulated derivatives. This could be a sign that the enhanced stability of imidazol-2-ylidenes over their benzannulated analogues[67] may be essential for an isolable free NM,NR NHC. In the original design of the $MeRLH_2$ ligand system, the benzimidazole arene rings were intended to anchor the pendant imine donors, creating a planar

6-membered chelate ring. It is now clearer that having an *N*-heterocyclic structure from which stable carbenes can be more easily formed takes precedence over a fully sp^2 hybridised ligand to complement a square planar metal centre. It may be more synthetically challenging to fix an imine pendant donor onto an imidazole while maintaining the same highly planar coordination environment. Otherwise, it would result in either a less rigid sp^3 hybridised C–C arm (Figure 4.13 b) or a smaller 5-membered chelate ring (Figure 4.13 c). These modifications would have geometric as well as chemical consequences. An extended imine pendant with a flexible spacer would help adapt the ligand for coordination to a tetrahedral centre, as seen in a copper(I) imidazolyl complex prepared by Scheidt and colleagues.[68] The change to smaller chelate rings can increase the C2···C2 distances. Li and coworkers reported a cyclohexyl-bridged Schiff base nickel(II) complex that is a good model for the structure depicted in Figure 4.13 c (n = 5).[69] The C2···C2 distance is significantly longer (ca. 4.3 Å) in their complex, which may leave the carbene more exposed.

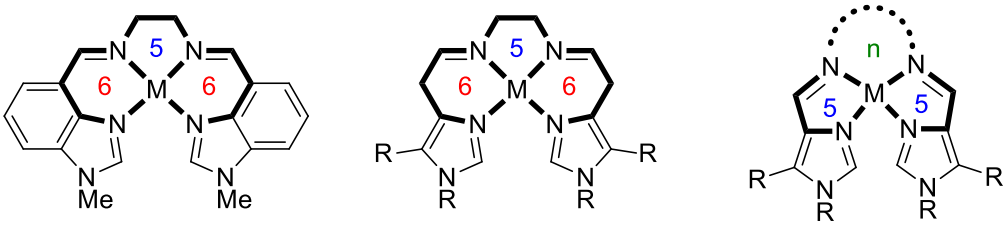

Figure 4.13 *Comparison of complexes containing* ***(a)*** *the original Me(en)LH*$_2$ *ligand and proposed imidazole-based analogues with* ***(b)*** *iminomethyl and* ***(c)*** *spacer-free imine linkers. Chelate rings are highlighted in bold.*

Although a small number of theoretical and experimental studies have shown that the electronic properties of imidazol-2-yl ligands warrant their description as anionic NHCs, virtually nothing is known about the nature of their free NM,NR NHC tautomers. During this investigation, a number of strategies to access these free NM,NR NHCs were explored. With further refinements of the complex design, the outlook is optimistic for the eventual isolation of a free NM,NR NHC. The spectroscopic and crystallographic data of this species, supported by theoretical modelling, will be necessary to shed light on whether the azolyl fragment will retain its NHC character when the carbenic atom is not part of a Lewis acid adduct.

The chief outcomes of this study as a whole are encapsulated in the following points:

a) A series of modular ligands dubbed "MeRLH_2" from which a free NM,NR NHC might be generated was rationally designed for proof-of-concept purposes;
b) A reliable and convenient multigram-scale synthesis for the ethylene-bridged diimine ligand Me(en)LH_2 and its key precursor aldehyde 4-CHOBimMe was developed;
c) An efficient metal-templated synthesis of the ligands MeCyLH_2 and MePhLH_2 from 4-CHOBimMe was identified;
d) MeRLH_2 complexes of transition metals such as nickel(II), copper(II), cobalt(II), silver(I), zinc(II) and palladium(II) were prepared and evaluated for their suitability for deprotonation trials, and the palladium(II) series of complexes were determined to be the most feasible precursors to NM,NR NHCs;
e) Deprotonation of the palladium(II) series of complexes and Me(en)LH_2 was attempted with a variety of inorganic and amine bases or alkylmetal reagents, but failed to deliver the desired free NM,NR NHCs, which also could not be trapped as their bimetallic NM,NR NHC complexes;
f) Improvements to ligand design that may be amenable to free NM,NR NHC synthesis were proposed based on the insight gained from the deprotonation and hydrogen/deuterium exchange studies of [PdMe(en)LH_2](OTf)$_2$.

4.6 Experimental

General method for NMR-scale deprotonation experiments:

In a glovebox with a dry nitrogen atmosphere, the precursor complex (such as **1**.H_2, **2**.H_2 or **3**.H_2) was dissolved in the appropriate deuterated solvent. The solution was transferred to an oven-dried Young's tube, which was then sealed. After an initial ^{1}H NMR spectrum was recorded, the solution was brought into the glovebox again, and the desired base and/or secondary metal source was added to the same tube. The reaction mixture was shaken vigorously to ensure thorough mixing of the reagents, and additional NMR spectra were recorded at suitable time intervals.

4.7 References

1 H. Lebel, M. K. Janes, A. B. Charette and S. P. Nolan, *J. Am. Chem. Soc.*, 2004, **126**, 5046–5047.

2 A. J. Arduengo, R. L. Harlow and M. Kline, *J. Am. Chem. Soc.*, 1991, **113**, 361–363.

3 X. Bantreil and S. P. Nolan, *Nat. Protoc.*, 2011, **6**, 69–77.

4 W. Zuo and P. Braunstein, *Dalton Trans.*, 2012, **41**, 636–643.

5 J. A. Wright, A. A. Danopoulos, W. B. Motherwell, R. J. Carroll and S. Ellwood, *J. Organomet. Chem.*, 2006, **691**, 5204–5210.

6 W. A. Herrmann and C. Köcher, *Angew. Chem. Int. Ed.*, 1997, **36**, 2162–2187.

7 R. W. Alder, P. R. Allen and S. J. Williams, *J. Chem. Soc. Chem. Commun.*, 1995, 1267–1268.

8 A. J. Arduengo, J. C. Calabrese, F. Davidson, H. V. Rasika Dias, J. R. Goerlich, R. Krafezyk, W. J. Marshall, M. Tamm and R. Schumtzler, *Helv. Chim. Acta*, 1999, **82**, 2348–2364.

9 M. K. Denk and J. M. Rodezno, *J. Organomet. Chem.*, 2000, **608**, 122–125.

10 N. I. Korotkikh, O. P. Shvaika, G. F. Rayenko, A. V. Kiselyov, A. V. Knishevitsky, A. H. Cowley, J. N. Jones and C. L. B. Macdonald, *Arkivoc*, 2005, **8**, 10–46.

11 N. I. Korotkikh, G. F. Rayenko and O. P. Shvaika, *Rep. Ukr. Acad. Sci.*, 2000, **2**, 135.

12 N. I. Korotkikh, G. F. Rayenko, O. P. Shvaika, T. M. Pekhtereva, A. H. Cowley, J. N. Jones and C. L. B. Macdonald, *J. Org. Chem.*, 2003, **68**, 5762–5765.

13 A. M. Magill, K. J. Cavell and B. F. Yates, *J. Am. Chem. Soc*, 2004, **126**, 8717–8724.

14 Z. Li, X. Li and J.-P. Cheng, *J. Org. Chem.*, 2017, **82**, 9675–9681.

15 B. Maji, M. Breugst and H. Mayr, *Angew. Chem. Int. Ed.*, 2011, **50**, 6915–6919.

16 A. Levens, F. An, M. Breugst, H. Mayr and D. W. Lupton, *Org. Lett.*, 2016,

18, 3566–3569.

17 V. K. Aggarwal, I. Emme and A. Mereu, *Chem. Commun.*, 2002, **2**, 1612–1613.

18 T. Junk and W. J. Catallo, *Chem. Soc. Rev.*, 1997, **26**, 401–406.

19 R. Breslow, *J. Am. Chem. Soc.*, 1957, **79**, 1762–1763.

20 J. Kaeobamrung, J. Mahatthananchai, P. Zheng and J. W. Bode, *J. Am. Chem. Soc.*, 2010, **132**, 8810–8812.

21 T. L. Amyes, S. T. Diver, J. P. Richard, F. M. Rivas and K. Toth, *J. Am. Chem. Soc.*, 2004, **126**, 4366–4374.

22 E. Buncel, H. A. Joly and J. R. Jones, *Can. J. Chem.*, 1986, **64**, 1240–1245.

23 E. M. Higgins, J. A. Sherwood, A. G. Lindsay, J. Armstrong, R. S. Massey, R. W. Alder and A. C. O'Donoghue, *Chem. Commun.*, 2011, **47**, 1559–1561.

24 E. Buncel and I. Onyido, *J. Label. Compd. Radiopharm.*, 2002, **45**, 291–306.

25 E. Buncel, O. Clement and C. Kl, *Acc. Chem. Res.*, 2000, **33**, 672–678.

26 C. R. Clark, A. G. Blackman and A. J. Clarkson, *J. Am. Chem. Soc.*, 2001, **123**, 8131–8132.

27 J. L. Wong and J. H. J. Keck, *J. Org. Chem.*, 1974, **39**, 2398–2403.

28 S. Solé, H. Gornitzka, W. W. Schoeller, D. Bourissou and G. Bertrand, *Science*, 2001, **292**, 1901–1903.

29 V. Lavallo, Y. Canac, C. Präsang, B. Donnadieu and G. Bertrand, *Angew. Chem. Int. Ed.*, 2005, **44**, 5705–5709.

30 M. W. Gribble, J. A. Ellman and R. G. Bergman, *Organometallics*, 2008, **27**, 2152–2155.

31 W. H. Pearson and P. Stoy, *Synlett*, 2003, 0903–0921.

32 W. H. Pearson, D. P. Szura and M. J. Postich, *J. Am. Chem. Soc.*, 1992, **114**, 1329–1345.

33 S. Tang, X. Zhang, J. Sun, D. Niu and J. J. Chruma, *Chem. Rev.*, 2018, **118**, 10393–10457.

34 T. Kauffmann, H. Berg and E. Köppelmann, *Angew. Chem. Int. Ed. Engl.*,

1970, **9**, 380–381.

35 T. Kauffmann, *Angew. Chem. Int. Ed. Engl.*, 1974, **13**, 627–639.

36 A. Dehnel and G. Lavielle, *Tetrahedron Lett.*, 1980, **21**, 1315–1318.

37 H. A. Houwing and A. M. Van Leusen, *J. Heterocycl. Chem.*, 1981, **18**, 1127–1132.

38 B. Fouchet, H. Joucla and J. Hamelin, *Tetrahedron Lett.*, 1981, **22**, 3397–3400.

39 S. Simonovic, J. C. Frison, H. Koyuncu, A. C. Whitwood and R. E. Douthwaite, *Org. Lett.*, 2009, **11**, 245–247.

40 O. Hollóczki, P. Terleczky, D. Szieberth, G. Mourgas, D. Gudat and L. Nyulászi, *J. Am. Chem. Soc.*, 2011, **133**, 780–789.

41 I. J. B. Lin and C. S. Vasam, *Comments Inorg. Chem.*, 2004, **25**, 75–129.

42 N. Coşkun and M. Çetin, *Tetrahedron*, 2010, **66**, 2053–2060.

43 G. A. Bowmaker, G. R. Clark, D. A. Rogers, A. Camus and N. Marsich, *J. Chem. Soc., Dalton Trans.*, 1984, 37–45.

44 C. Y. Su, Y. P. Cai, C. L. Chen, F. Lissner, B. S. Kang and W. Kaim, *Angew. Chem. Int. Ed.*, 2002, **41**, 3371–3375.

45 V. L. Goedken, H. Ito and T. Ito, *J. Chem. Soc., Chem. Commun.*, 1984, 1453–1454.

46 S. A. Ahmed, M. S. Hill, P. B. Hitchcock, S. M. Mansell and O. St John, *Organometallics*, 2007, **26**, 538–549.

47 H. F. S. Azpeitia, S. A. Cortes-Llamas, F. A. Vengoechea-Gómez, E. Rufino-Felipe, N. T. Crespo-Velasco and M.-Á. Muñoz-Hernández, *Main Group Chem.*, 2011, **10**, 127–140.

48 D. J. Darensbourg and D. B. Billodeaux, *Inorg. Chem.*, 2005, **44**, 1433–1442.

49 S. J. Dzugan and V. L. Goedken, *Inorg. Chem.*, 1986, **25**, 2858–2864.

50 W. Shih, C. Wang, Y. Chang, G. P. A. Yap and T. Ong, *Organometallics*, 2009, **28**, 1060–1067.

51 C. C. Tai, Y. T. Chang, J. H. Tsai, T. Jurca, G. P. A. Yap and T. G. Ong, *Organometallics*, 2012, **31**, 637–643.

52 H. Zhou, E. J. Campbell and S. T. Nguyen, *Org. Lett.*, 2001, **3**, 2229–

2231.

53 M. C. Law, K.-Y. Wong and T. H. Chan, *Green Chem.*, 2004, **6**, 241–244.

54 T. R. Jensen, C. P. Schaller, M. A. Hillmyer and W. B. Tolman, *J. Organomet. Chem.*, 2005, **690**, 5881–5891.

55 M. L. Hlavinka and J. R. Hagadorn, *Organometallics*, 2007, **26**, 4105–4108.

56 W. S. Rees, O. Just, H. Schumann and R. Weimann, *Polyhedron*, 1998, **17**, 1001–1004.

57 Y. Kondo, M. Shilai, M. Uchiyama and T. Sakamoto, *J. Am. Chem. Soc.*, 1999, **121**, 3539–3540.

58 M. Uchiyama, T. Miyoshi, Y. Kajihara, T. Sakamoto, Y. Otani, T. Ohwada and Y. Kondo, *J. Am. Chem. Soc.*, 2002, **124**, 8514–8515.

59 E. Çetinkaya, P. B. Hitchcock, H. Küçükbay, M. F. Lappert and S. Al-Juaid, *J. Organomet. Chem.*, 1994, **481**, 89–95.

60 J. W. Kamplain and C. W. Bielawski, *Chem. Commun.*, 2006, 1727–1729.

61 C. Holtgrewe, C. Diedrich, T. Pape, S. Grimme and F. E. Hahn, *Eur. J. Org. Chem.*, 2006, 3116–3124.

62 Q. Wang and S. L. Schreiber, *Org. Lett.*, 2009, **11**, 5178–5180.

63 T. Sekine, Y. Higuchi, T. Yamada and I. Murakoshi, *Chem. Pharm. Bull.*, 1989, **37**, 1987–1989.

64 S. Nishio, T. Somete, A. Sugie, T. Kobayashi, T. Yaita and A. Mori, *Org. Lett.*, 2012, **14**, 2476–2479.

65 F. Bonati, A. Burini, B. R. Pietroni and B. Bovio, *J. Organomet. Chem.*, 1989, **375**, 147–160.

66 H. G. Raubenheimer, L. Lindeque and S. Cronje, *J. Organomet. Chem.*, 1996, **511**, 177–184.

67 L. Pause, M. Robert, J. Heinicke and O. Kuhl, *J. Chem. Soc., Perkin Trans. 2*, 2001, 1383–1388.

68 J. A. Goodwin, G. A. Bodager, L. J. Wilson, D. M. Stanbury and W. R. Scheidt, *Inorg. Chem.*, 1989, **28**, 35–42.

69 Y.-L. Hou, S.-X. Li, R. W.-Y. Sun, X.-Y. Liu, S. W. Ng and D. Li, *Dalton Trans.*, 2015, **44**, 17360–17365.

Appendix

Substantial portions of sections 1.5.1 through 1.7 from Chapter 1 have been published as a review article, a copy of which is appended here.

catalysts

MDPI

Review

Non-Classical Anionic Naked *N*-Heterocyclic Carbenes: Fundamental Properties and Emerging Applications in Synthesis and Catalysis

Mei Yi Leow, Curtis C. Ho, Michael G. Gardiner and Alex C. Bissember *

School of Natural Sciences—Chemistry, University of Tasmania, Hobart, TAS 7001, Australia; mei.leow@utas.edu.au (M.Y.L.); curtis.ho@utas.edu.au (C.C.H.); michael.gardiner@utas.edu.au (M.G.G.)

* Correspondence: alex.bissember@utas.edu.au

Received: 1 November 2018; Accepted: 22 November 2018; Published: 4 December 2018

Abstract: Ongoing research exploring the chemistry of *N*-heterocyclic carbenes (NHCs) has led to the development and discovery of new NHC subclasses that deviate beyond Arduengo's prototypical *N*,*N*′-disubstituted imidazol-2-ylidene-based structures. These systems continue to enable and extend the fundamental role of NHC ligands in synthesis and catalysis. In this regard, the advent of protic NHCs has garnered particular interest. This derives in part from their applications to the selective preparation of unique molecular scaffolds and their unprecedented bifunctional reactivity, which can be exploited in transition metal-catalyzed processes. In comparison, the synthetic applications of closely related anionic naked NHCs remain rather underexplored. With this in mind, this review highlights the interesting fundamental properties of non-classical anionic naked NHCs, and focuses on their emerging applications in synthesis and catalysis.

Keywords: *N*-heterocyclic carbenes; non-classical NHCs; protic NHCs; naked NHCs; catalysis

1. Introduction

N-Heterocyclic carbenes (NHCs) have emerged as an integral component of contemporary coordination chemistry (Figure 1A). Since the isolation of the first stable free carbene species by Bertrand et al. in 1988 [1], and the first stable NHC by Arduengo et al. in 1991 [2], NHCs are now routinely utilized as versatile supporting ligands in metal complexes, and form the basis of many valuable catalyst systems that mediate an array of synthetic transformations [3–11]. The extent of research devoted to NHCs has led to the development and discovery of new NHC subclasses that have deviated from Arduengo's classical imidazol-2-ylidene based NHCs, thus expanding the structural and electronic diversity of this class of compounds and their associated applications. These modifications include forming carbenes on alternative carbon positions (i.e., abnormal or mesoionic carbenes) [12], featuring ring saturation [13], changing ring size [14–17], using fused ring systems [18–21], acyclic analogues [22], and even multidentate carbene ligands [23–30].

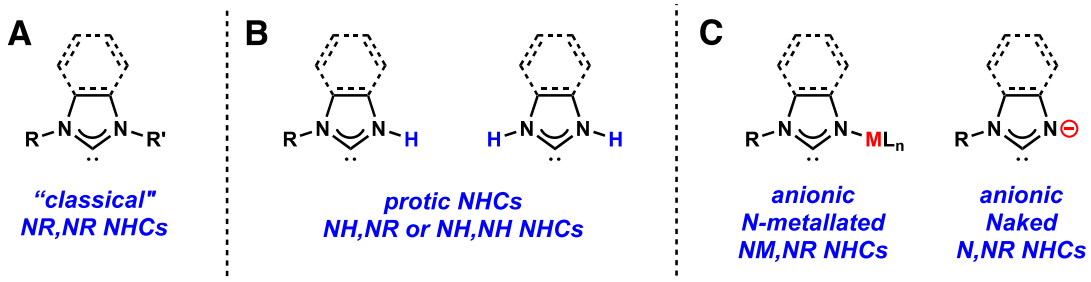

Figure 1. Substitution patterns of *N*-heterocyclic carbene (NHC) nitrogen atoms delineating: (**A**) "classical" NR,NR NHCs, (**B**) protic NH,NR or NH,NH NHCs, (**C**) and anionic NM,NR or naked N,NR NHCs.

A common feature of the aforementioned NHC subclasses is disubstitution of the NHC nitrogen atoms with alkyl or aryl substituents, which are collectively classified as "classical" NR,NR-NHC ligands (Figure 1A). Recent developments have led to the emergence of NHC ligands where one or both *N*-substituents are replaced with a hydrogen atom resulting in NH,NR or NH,NH-substitution patterns affording ligands known as protic NHCs (Figure 1B). These species have enjoyed significant interest owing to their unique ligand hydrogen bonding interactions and associated properties, which allow the corresponding NHC metal complexes to display valuable reactivity when applied in stereoselective macrocycle formation and catalytic processes, for example. Deprotonated NH,NR-NHCs represent another subclass of non-classical NHC ligands known as anionic naked N,NR NHCs, and are often isolated as their corresponding *N*-metalated complexes. These anionic NHCs differ from NHC ligands bearing anionic substituents and mixed abnormal/normal NHCs in that the unsubstituted nitrogen atom carries a formal negative charge (Figure 1C).

NHC chemistry has been the subject of many reviews highlighting their unique properties and applications in synthesis [3–11]. With this in mind, this review aims to provide an overview of recent advances in the preparation and synthetic applications of metal complexes bearing non-classical NHCs; in particular, anionic NM,NR-NHC and naked N,NR-NHC ligands. Progress in the preparation of the closely related protic NHCs and their applications in metal-mediated reactions will not be discussed in detail, as a recent review by Hahn and Kuwata covered this topic extensively [31]. To our knowledge, a review of anionic NM,NR-NHCs and naked N,NR-NHCs has not been published to date. Consequently, this review focuses on imidazole-based anionic NHCs with N,NR substitution patterns, thus excluding mixed normal/abnormal classical NR,NR NHCs which are anionic due to deprotonation of the azolium salt at two different sites (Figure 2) [32–36]. Specifically, the fundamental structural and electronic properties of these systems and their applications in synthesis are discussed. It should be noted that due to the emerging nature of this class of non-classical NHCs, only a handful of examples of the applications of these systems in catalysis have been reported to date. With this in mind, a primary aim of this review is to draw attention to the intrinsic and enabling fundamental properties of these anionic NM,NR-NHCs and naked N,NR-NHCs and highlight potential opportunities that may be explored to exploit the interesting and innate reactivity provided by this class of molecules in catalysis.

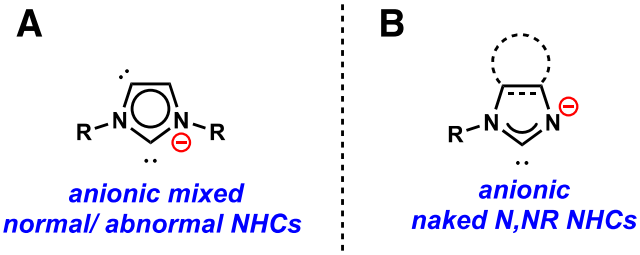

Figure 2. (**A**) Anionic Classical Mixed Normal/Abnormal *N*-Heterocyclic Carbenes (NHCs). (**B**) Anionic Naked N,NR NHCs.

2. Non-Classical NHCs and Their Metal Complexes

2.1. Protic NHC Metal Complexes

The most acidic proton in an NH,NR or NH,NH imidazolium salt is attached to the nitrogen atom, and not the C2 carbon. For this reason, the treatment of such a salt with base results in the regioselective deprotonation of the nitrogen atom and isomerization into the corresponding imidazole, rather than producing the free carbene. This has prevented the isolation of protic NHCs in their free form, and to date, these species have only been reported as their metal complexes. In principle, these protic NHC complexes could isomerize to the *N*-coordinated imidazole complex, but this is seldom observed in practice (Scheme 1) [37]. While imidazole is more thermodynamically stable than its protic free NHC tautomer, the high energy barrier that is calculated for the required 1,2-hydrogen shift suggests that the latter is kinetically favored [38,39]. Theoretical studies of the relative stabilities of the *C*-bound and *N*-bound tautomers suggest that strongly π-basic metal centers, hydrogen bonding at the N–H site(s), and the presence of ligands that cannot exert strong *trans* influences can stabilize the *C*-bound over the *N*-bound complex [40,41].

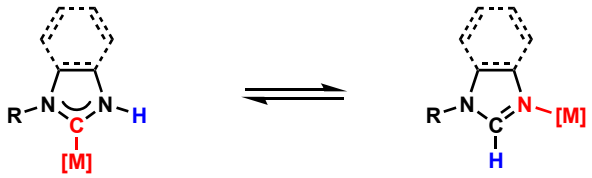

Scheme 1. Tautomeric forms of imidazole-based protic metal NHC complexes.

With the above-mentioned issues in mind, other strategies were developed to access protic NHC complexes, such as the metal-templated cyclisation of isocyanides and nitrogen-containing nucleophiles. Under basic conditions, a pre-coordinated metal isocyanide may be reacted with phenylisocyanate or phenylthioisocyanate to give protic NHC complexes bearing exocyclic oxy anions or thiolate functions, respectively (Scheme 2A) [42]. These versatile backbone substituents may undergo further alkylation or acylation, or act as monodentate donors. 2-bromoethylamine [43] and aziridine [44] may also be used as cyclization partners to form protic imidazolidin-2-ylidenes (Scheme 2B).

In cases where the isocyanide and nucleophile are contained within the same molecule, protic NHC complexes may be accessed via the intramolecular 1,2-addition across the C–N triple bond. This approach has been particularly successful in the preparation of backbone-saturated [45] and benzannulated protic NHCs (Scheme 2C) [46,47]. In a variation of this method, the isocyanide complex is generated in situ from an aminophosphinimine ligand [48]. Other methods involve the metalation of a preformed *N*-heterocycle bearing a labile *N*-protecting group that can later be cleaved to reveal the protic NHC complex (Scheme 2D) [49,50], C2 lithiation followed by transmetalation and *N*-protonation (Scheme 2E) [51–54], and finally the acid-induced or base-induced carbene/imidazole tautomerization from *N*-metalated imidazole metal complexes (Scheme 2F) [55,56].

In practice, the conversion of *N*-metalated imidazole complexes into their protic NHC tautomers is often the most convenient and versatile synthetic route, as post-metalation functionalization of the heterocycle can be difficult. The presence of chelating directors further encourages and stabilizes the resulting NHC metal complex, preventing tautomerization to the *N*-metalated form [57–65]. For example, Scheme 3A features an interesting transformation that converts osmium complex **1** to species **2,** and the transition metal center switches ligand donor atoms from nitrogen to the NHC carbon [58]. Presumably, the Lewis basicity of the chelating director influences *N*-metalation, as no *N*-metalated intermediate is observed in the presence of a pendant phosphine donor for the

transformation of complex **3** to species **4** (Scheme 3B) [57]. These types of transformations are thought to be operative in various proposed catalytic cycles involving protic NHC ligands displaying reversible deprotonation at the acidic N–H site.

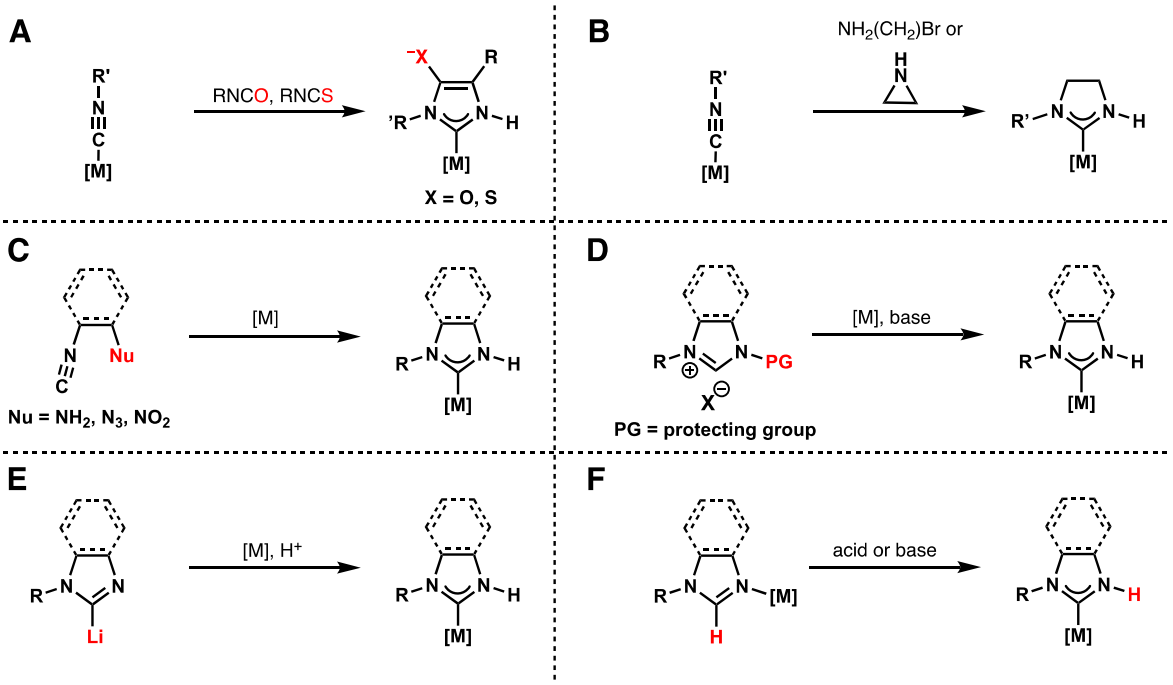

Scheme 2. Synthetic strategies for the preparation of protic NHC complexes: (**A**) metal-templated cyclization of isocyanides and nitrogen-containing nucleophiles; (**B**) metal-templated cyclisation of isocyanides with bromoethylamine or aziridine; (**C**) intramolecular metal isocyanide 1,2-addition; (**D**) metalation of pre-formed *N*-protected *N*-heterocycle followed by deprotection; (**E**) transmetalation of C2-lithiated *N*-heterocycle followed by *N*-protonation; (**F**) acid- or base-induced carbene/imidazole tautomerization from *N*-metalated imidazole metal complexes.

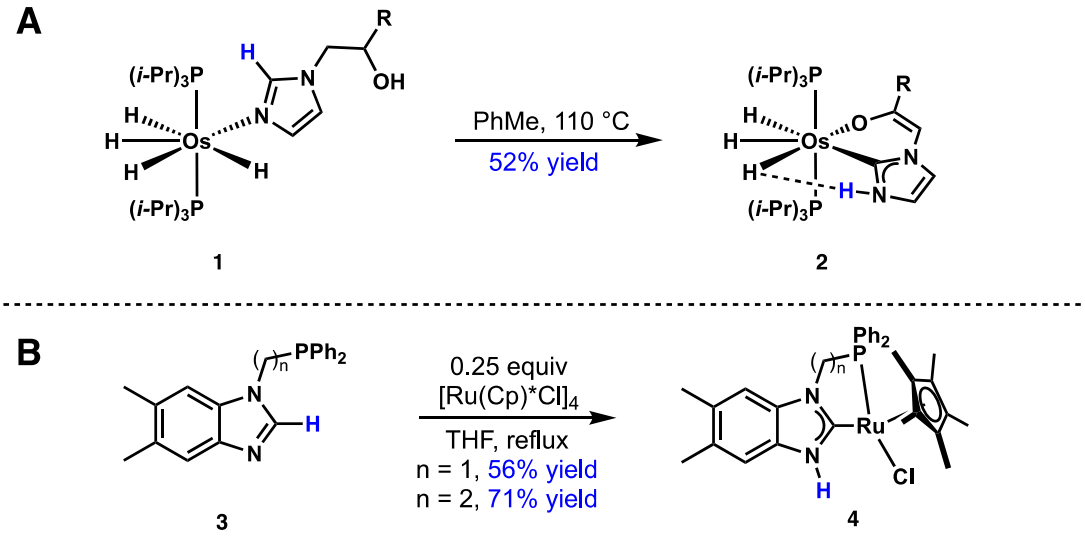

Scheme 3. Synthesis of a protic NHC complex by tautomerization of neutral imidazole-based ligands, facilitated by a pendant (**A**) oxygen donor [58] and (**B**) phosphine donor [57].

N-(2-Pyridyl)benzimidazole (**5**) can be allylated at the C2 position to give compound **6** in a Ru-catalyzed dehydrative C–C coupling reaction (Scheme 4) [59]. It is suggested that the process commences with the insertion of a ruthenium species into the C2–H bond of benzimidazole **5** to give

isolable intermediate **7**, which then coordinates to allyl alcohol. Next, the N–H proton and hydroxyl group in complex **8** are lost as water to give imidazol-2-yl allyl complex **9**. Facile elimination is expected due to the dual binding mode of the olefinic alcohol in species **8**. Reductive elimination of heterocycle **6** from intermediate **10** then occurs. Notably, compound **10** is also accessible via the stoichiometric reaction of species **7** and allyl alcohol. Similar processes are also proposed for the Rh-catalyzed intramolecular alkylation and the arylation of azoles, and analogous nitrogen/NHC carbon atom donor switching is invoked [59,66–68].

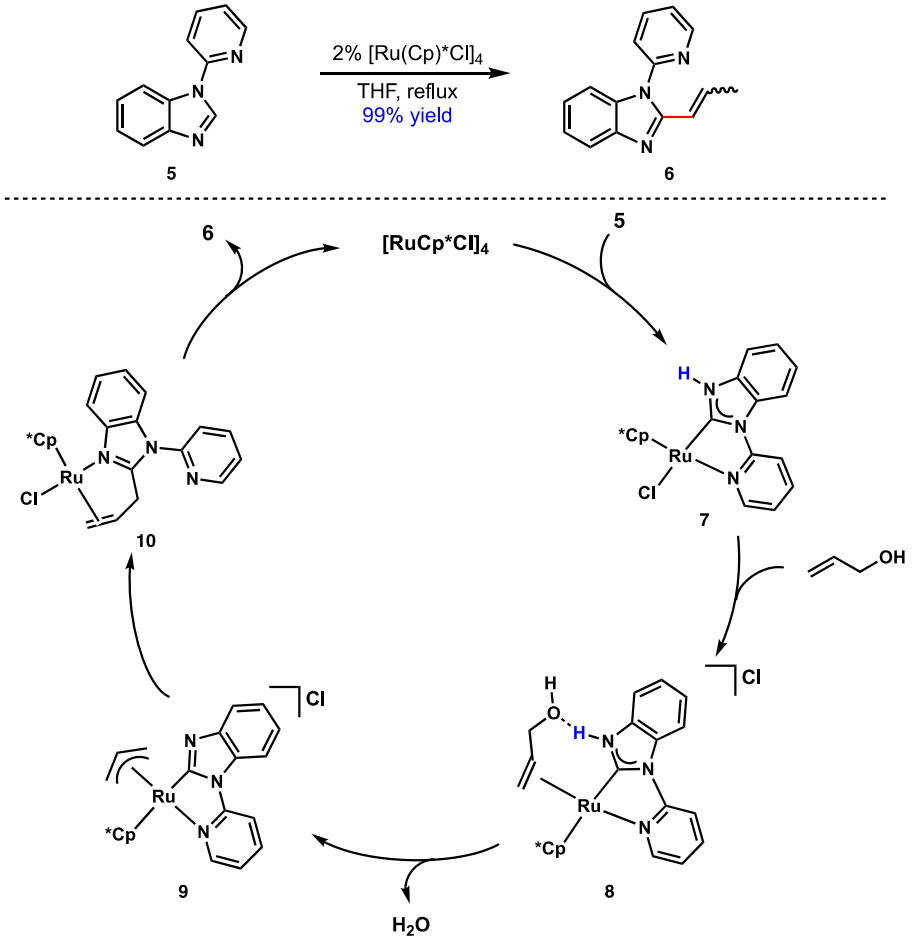

Scheme 4. Synthesis of a protic NHC complex by tautomerization of neutral imidazole ligands, facilitated by a pendant nitrogen donor: ruthenium-catalyzed dehydrative C–C coupling of a benzimidazole and allyl alcohol [59].

The above-mentioned examples reinforce suggestions that the deprotonation of the N–H site of a protic NHC generates an anionic nitrogen donor atom that may serve as a viable coordination site in the formation of naked N,NR NHC metal complexes, NM,NR-free NHC complexes, or even C/N bimetallic complexes. Indeed, deprotonation-induced reactions of protic NHC complexes have been developed to access a variety of transformations. This was first demonstrated by Angelici et al. in 1987 [69], in which the deprotonation of protic oxazolidin-2-ylidene iron complex **11** and the subsequent addition of electrophiles afforded a range of *N*-functionalized metal complexes **13** (Scheme 5). Hahn et al. have further exploited this reactivity for the template synthesis of organometallic macrocycles [70] and the stereoselective synthesis of facially coordinated tridentate mixed donor ligands [71–75]. Of particular interest is the intermediate **12**, which features a nitrogen atom bearing a formal negative charge, and its corresponding bimetallic complex **13c**. From the aforementioned examples, it is evident that studies involving protic NHCs have often uncovered interesting structures, which constitute so-called anionic NM,NR and naked N,NR NHCs (hereafter abbreviated collectively as N,NR NHCs).

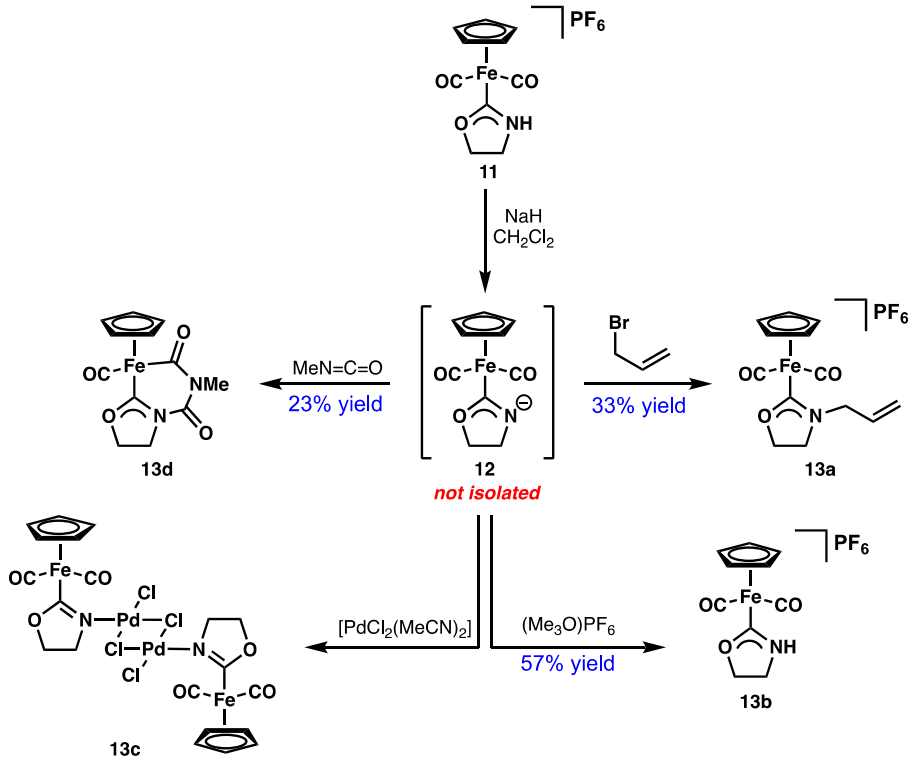

Scheme 5. Deprotonation-induced *N*-functionalization of an iron(II)-NHC complex.

2.2. Anionic NM,NR and Naked N,NR NHC Metal Complexes

N,NR NHCs were well-known before they became more widely recognized as anionic NHCs within the broader chemical community. In 1995, Boche et al. described a dimeric lithiated thiazol-2-yl compound **14** as a formyllithium equivalent (Figure 3) [76]. In contrast to common organolithium reagents such as methyllithium or butyllithium in which the alkyl component is typically regarded as a carbanion, these researchers argue that complex **14** exhibits a singlet carbene character in its crystal structure. A comparison with thiazole revealed that structure **14** experienced lengthening of the C2–N and C2–S bonds and shrinking of the N–C2–S angle from 115.1(8)° to 107.9(2)°, which mirrors the structural trends associated with moving from an imidazolium cation to an imidazol-2-ylidene. While the C2–N1 and C2–N3 bonds in imidazol-2-ylidenes are usually identical in length, a meaningful comparison cannot be made for species **14**, as the carbene carbon is flanked by two different heteroatoms.

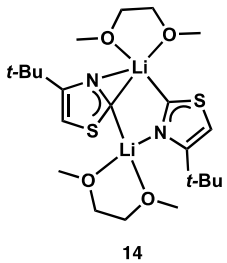

14

Figure 3. Lithiated 4-*tert*-butylthiazole **14** featuring C/N metalation.

Hahn et al. were the first to introduce the term "anionic NHC" when they reported complex **17**, which was one of the products isolated from the oxidative addition of zero-valent Group 10 metals to benzimidazole **15** (Scheme 6) [77]. These authors had previously alluded to the intermediacy of an anionic benzimidazole in the synthesis of protic NHC complexes via this oxidative addition route. It was determined that in the absence of a proton source, such as NH_4BF_4, an oxidative addition to

chloride **15** did not lead to protic NHC complexes **19** and **20**. Instead, N,NR complex **17** and its dimer **16** were obtained in a 4:1 ratio. The reaction of [$Pt(PPh_3)_4$] and 2-chloro-*N*-picolylbenzimidazole also afforded a similar dimeric product, suggesting that the formation of N(M),NR complexes under aprotic conditions may be generalized to other 2-halobenzimidazoles [77].

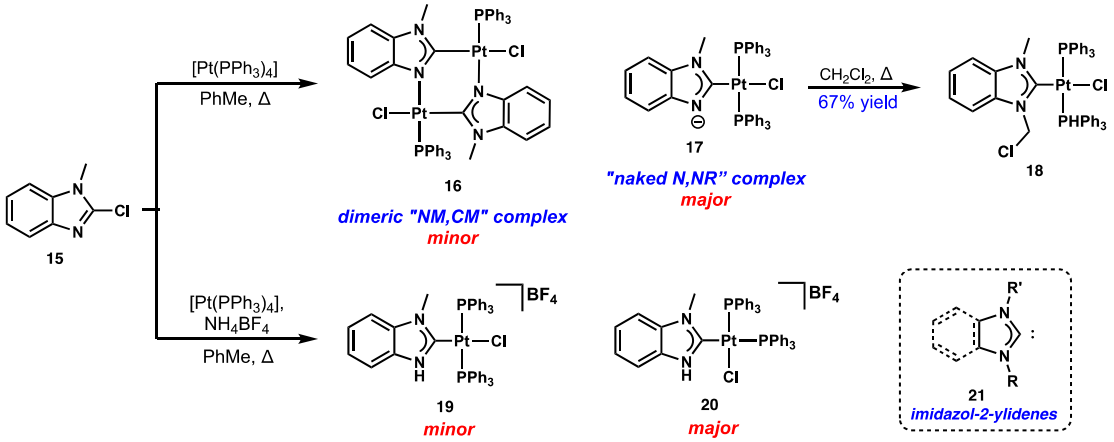

Scheme 6. Reaction products obtained from the oxidative addition of [$Pt(PPh_3)_4$] to 2-chloro-*N*-methylbenzimidazole (**15**) in the presence and absence of a proton source.

2.3. Carbene or Carbanion?

An important question that was posed when imidazol-2-ylidenes **21** were first discovered was whether deprotonation gives rise to a carbene or a carbanion. The Arduengo group endeavored to answer this question by using a combination of theoretical and experimental approaches. If the deprotonated azol-2-yl in question is indeed a carbanion, one should observe regions of high electron density or localized negative charge on a carbon atom that also participates in π-bonding interactions. However, Mulliken charge calculations for imidazol-2-ylidene estimate that most of the negative charge is borne by the nitrogen atoms, with only a small fraction residing on the carbene atom [78]. Electron density maps derived from the neutron diffraction data of 1,3,4,5-tetramethylimidazol-2-ylidene (IMe) showed that most of the electron density within the ring was localized on the nitrogen atoms. This is perhaps a predictable result in light of the higher electronegativity of nitrogen relative to carbon [78]. The π electron densities surrounding the C2–N and exocyclic C–N bonds are similarly low, indicating that bonds connected to C2 have a minimal double-bond character. A minima for π electron density was found on C2. In addition, deformation density maps reveal a concentrated region of electron density at C2 in the plane of the molecule, which evolved into a pronounced deficit above the plane. This is consistent with C2 having an in-plane lone pair and a vacant π-orbital. In contrast, other endocyclic atoms exhibit little distortion in their nuclear positions. The electron density maps generated by density functional theory (DFT) studies were in excellent agreement with the empirically derived maps, suggesting that accurate models of electron distribution in NHCs can be made this way. When taken together, these data strongly support the interpretation of IMe as a carbene rather than a carbanion.

It is instructive to employ the same structural and electronic reasoning developed by Boche and Arduengo to establish whether or not the N,NR complex **17** is a carbene. From a structural point of view, species **17** is perhaps best described as having partial azole and partial NHC character. *N*-methyladamantylbenzimidazole and benzimidazole will be used as references for the parent azole, as structural data for 2-chloro-*N*-methylbenzimidazole (**15**) is not available. The key bond lengths and angles are summarized in Table 1. Compared to the neutral azoles, the N1–C2–N3 angles in compounds **20** and **18** are smaller, which is a feature that is associated with NHC formation. The same decrease in the N1–C2–N3 angle is observed for complex **16**, albeit to a lesser extent. The C2–Pt bond lengths in complex **17**, its protonated form species **20**, and the chloromethylated form **18** are relatively

similar to one another, signifying that all three heterocycles possess similar donor/acceptor properties. This could mean that, similar to the other two complexes, structure **17** is also a carbene.

Table 1. Comparisons of fundamental structural and spectroscopic data for NH,NR (**20**), N,NR, (**17**), and NR,NR NHC (**18**) complexes relative to reference benzimidazoles.

Parameter	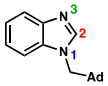		20; N3 = Protonated [77]	17; N3 = Naked	18; N3 = Alkylated
N1–C2–N3 (°)	114.83(11) [79]	114.41(17)	107.1(4)	111.37(17)	106.7(2)
C2–N1 (Å); "**A**"	1.3629(14) [79]	1.345(2)	1.350(6)	1.389(2)	1.351(3)
C2–N3 (Å); "**B**"	1.3096(14) [79]	1.312(2)	1.349(6)	1.319(3)	1.364(3)
ΔA–B (Å)	0.053	0.033	0.001	0.070	0.013
C2–Pt (Å)	-	-	1.972(4)	1.987(2)	1.973(2)
^{13}C NMR δC$_2$ (ppm)	144.3 ($CDCl_3$) [80]	141.9 (d_6-DMSO)	157.8 (CD_2Cl_2)	149.4 (CD_2Cl_2)	163.3 (CD_2Cl_2)

As noted earlier, another characteristic feature of NHC formation is the presence of C2–N1 and C2–N3 bonds of approximately equal lengths (but longer than the corresponding bonds in neutral azoles). This change is evident for the NHC complexes **20** and **18**, with a marked lengthening of the C2–N3 bond that ultimately results in a negligible difference between the C2–N1 and C2–N3 bond lengths. However, in species **17**, the C2–N1 bond becomes significantly longer than that in the neutral azoles and the NHC complexes, while the C2–N3 bond length is typical of neutral azoles. The disparity in C2–N1 and C2–N3 bond lengths for structure **17** exceeds the values observed for neutral azoles. This C2–N1 and C2–N3 bond length asymmetry appears to be characteristic of anionic azol-2-yl ligands in general [59,72].

Based largely on the stark difference in the C2–N1 and C2–N3 bond lengths, Hahn et al. initially assigned the structure-type **22b** to complex **17**, where the C2 atom and short C2–N1 bond are represented as an acyl-like anion and a double bond, respectively (Figure 4). However, this interpretation was contradicted by their natural bonding orbital (NBO) charge calculations for the N,NR ligand in species **17**. The calculated NBO charges suggest that the region with the highest electron density is found on N3 followed by N1, while C2 appears to be electron-deficient. DFT calculations support this, with these data indicating that the maximum negative electrostatic potential (of comparable value to Cl^-) is located close to N2. Overall, the NBO and DFT models of species **17** are more consistent with a carbene flanked by an anionic nitrogen, as depicted in structure **22a**.

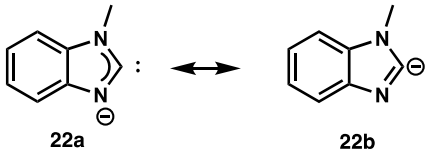

Figure 4. Possible carbenic (**22a**) and carbanionic (**22b**) resonance contributors for the N,NR ligand moiety in complex **17**.

Hahn et al. note that the C2 resonance appears further upfield in the ^{13}C NMR spectrum of complex **17** than for derivatives **19** and **18**. Although an extreme downfield shift is usually expected for a carbenic resonance, this may not necessarily suggest that the C2 within complex **17** is not a carbene. Rather, the upfield position of the resonance may be viewed as a consequence of the greater shielding experienced by C2, due to the higher electron density surrounding the adjacent anionic nitrogen. The upfield shift in the C2 resonance going from an NH/R,NR NHC complex to an N(M),NR NHC species has also been observed for other metals [65].

Finally, the reactivity of complex **17** further supports the assignment of the negative charge on N3 instead of C2. The dinuclear species **16** results from adduct formation between the Lewis basic unsubstituted nitrogen and the Lewis acidic metal center in a second molecule of species **17**.

The anionic nitrogen in complex **17** is strongly nucleophilic, and will attack electrophiles such as dichloromethane to produce the classical NHC complex **19**. On balance, the structural, electronic, and reactivity data provide sufficient justification that structure **17** can be considered an anionic NHC. However, the term has not been widely adopted, which is possibly due to the challenges involved in making the subtle distinction between a carbanion and an anionic carbene. Most of the N(M),NR compounds in the literature are still named azol-2-yls, which is perhaps for this reason.

2.4. Preparation of N(M),NR Complexes and Applications to Synthesis and Catalysis

N,NR complexes are probably most easily prepared by the deprotonation of an NH,NR complex with a suitable base [59,61,64]. Product **24** is generated from the treatment of the protic NHC complex **23** with NaOMe and NaH. Subsequent chloride abstraction results in the formation of derivative **25** featuring a vacant coordination site that can activate hydrogen and acetylene, affording products **26** and **27**, respectively (Scheme 7A). Similar to protic NHCs, species **24** can undergo *N*-methylation with methyl triflate to give a classical NR,NR NHC complex. The Ir–C2 bond length in complex **24** measures 2.059(3) Å, which is approximately 0.033 Å longer than the corresponding bond within structure **23**. This potentially suggests that in this example, the anionic NHC is a slightly weaker donor than its protic NHC congener. Related Ir(III) hydride complex **28** could be reduced to Ir(I) by hydride abstraction using *n*-butyllithium (Scheme 7B). Ensuing lithium adduct **29** is an NM,NR NHC complex, and its associated ^{13}C NMR spectrum features a signal that is consistent with a carbene resonance (δ 150 ppm). This is almost 20 ppm further downfield from the analogous ^{13}C NMR signal for complex **28**. Interestingly, the reaction of species **29** with methyl triflate or 1-iodobutane leads to alkylation at the metal instead of the nitrogen, and concomitant oxidation of the metal center to provide the corresponding Ir(III) compound **30**.

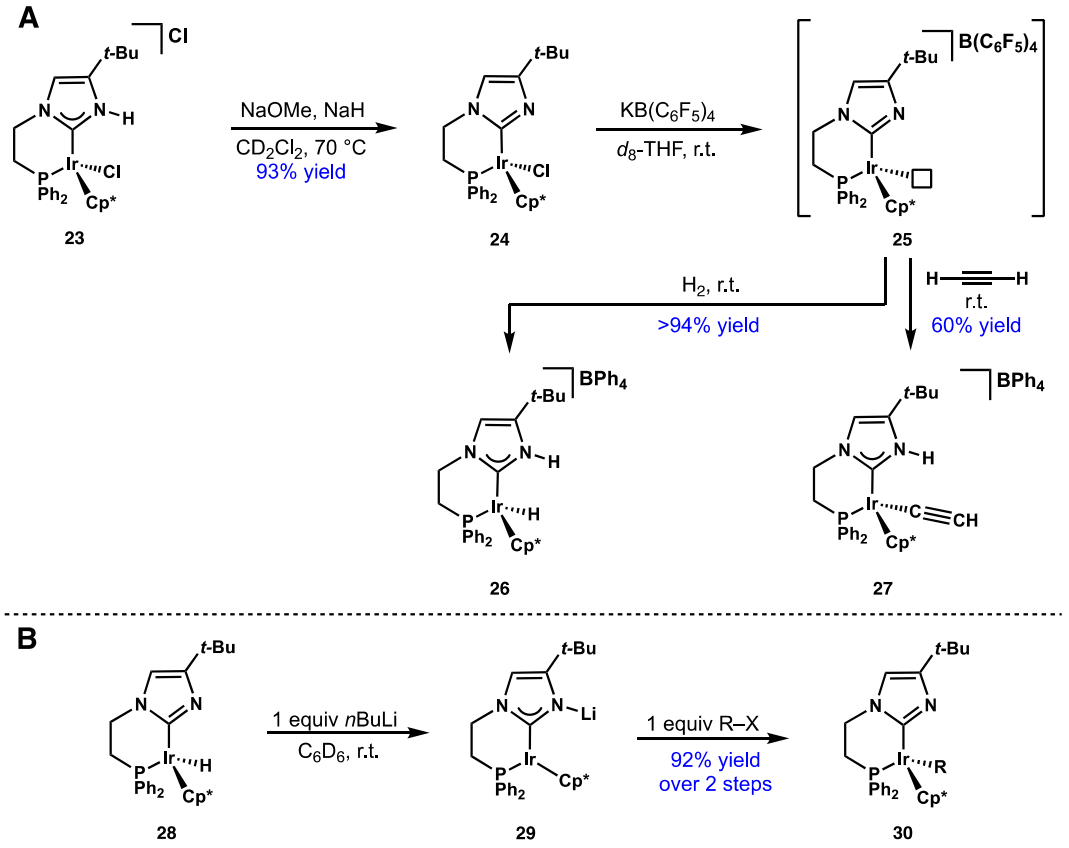

Scheme 7. (**A**) Anionic N,NR NHC complex formation from the deprotonation of a protic NHC complex. (**B**) Reduction of the iridium(III) center of a N,NR NHC complex to give a NM,NR complex, which can undergo alkylation on the metal.

The utility of heterobimetallic NM,NR complexes such as species **29** derives, in part, from their susceptibility to ligand exchange on the NHC-bound metal center, particularly when the exchange is driven by the precipitation of an insoluble lithium salt. Indeed, *N*-lithiated ruthenium complex **31** reacts with hydrogen, leading to the protic NHC/hydride complex **32**, and readily coordinates with ethylene to form **33** (Scheme 8) [61].

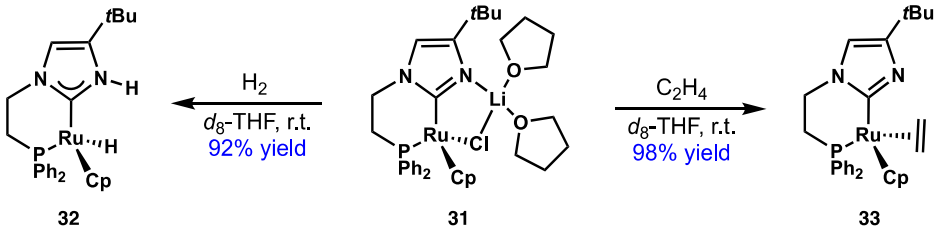

Scheme 8. Elimination of the *N*-coordinated metal in a heterobimetallic NM,NR NHC complex that facilitates ligand exchange at the metal center.

In some cases, metathesis occurs exclusively on N3, and the NHC-bound metal center is left unchanged when inorganic metal salts are used. Therefore, NM,NR NHC complexes may allow access to a variety of heterobimetallic complexes with bridging NHC ligands. For example, Cossairt and Flowers highlighted the potential of NM,NR NHC complexes as ligand transfer agents in their synthesis of a tridentate bis(carbene) complex **34** (Scheme 9) [63]. Lithiation affords heterobimetallic species **35**, and subsequent transmetalation provides access to new NM,NR NHC complexes, such as product **36**.

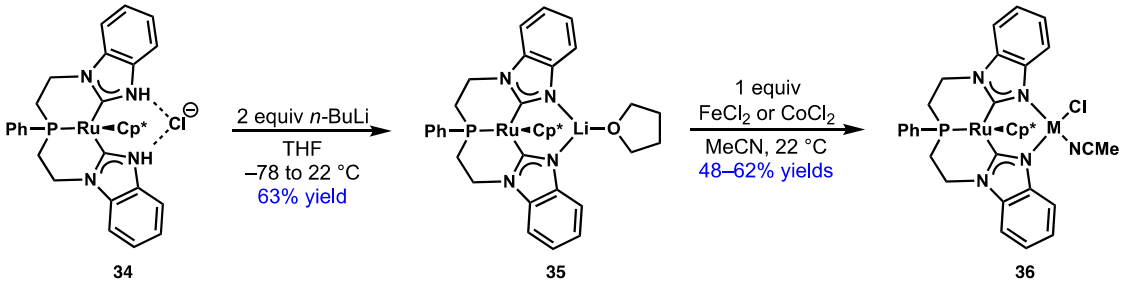

Scheme 9. Transmetalation at the anionic nitrogen site in NM,NR NHC complexes.

Anionic NHC complex **38** can be prepared from precursor **37** using the aforementioned base-assisted deprotonation method. However, the Brønsted acidity of the N–H moiety within a protic NHC complex can also be exploited under base-free conditions to deliver a N,NR NHC complex. For example, chloride abstraction from species **37** by $AgNO_2$ promotes an ensuing intramolecular proton migration. This generates a nitrosyl ligand from the nitrite ion via a dehydrative process, culminating in the formation of structure **38** after anion exchange with excess KOTf (Scheme 10) [59]. The authors also demonstrated that complexes **38** and **39** are interconvertible via acid/base-assisted protonation/deprotonation of the NHC nitrogen atom that enables switching between a protic and an anionic NHC motif. This property may find interesting applications in hydrogen transfer-type catalysis.

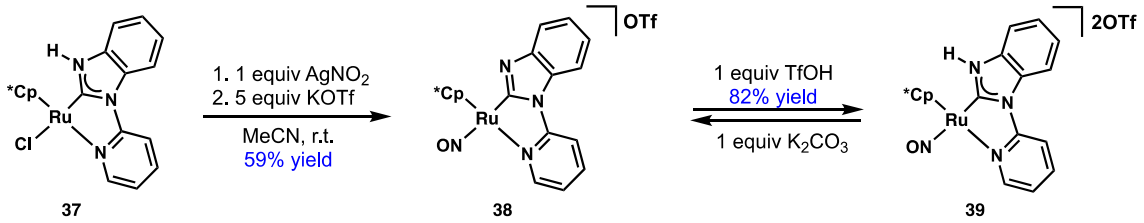

Scheme 10. Formation of a N,NR NHC complex **38** from protic NHC complexes **37** and **39** via the dehydrative conversion of a nitrite ion into a nitrosyl ligand under neutral conditions or base-assisted deprotonation.

Another method that has been used to access N,NR NHC complexes is the deprotonation and tautomerization of imidazole ligands. For example, the tris(*N*-methylimidazole)rhenium(I) complex **40a** can be deprotonated with KHMDS to give the N,NR NHC species **41**. Structure **41** was determined via NMR spectroscopy and single crystal X-ray diffraction (Scheme 11) [55]. A resonance at 182.4 ppm in the ^{13}C NMR spectrum was assigned to C2 within complex **41**. This represents the furthest downfield signal associated with all of the N,NR NHC complexes that have been specifically discussed in this review thus far. Furthermore, protonation with strong acids such as triflic or trifluoroacetic acid afforded the NH,NR NHC product **42**, which was consistent with the presence of the naked nitrogen moiety within intermediate **41**.

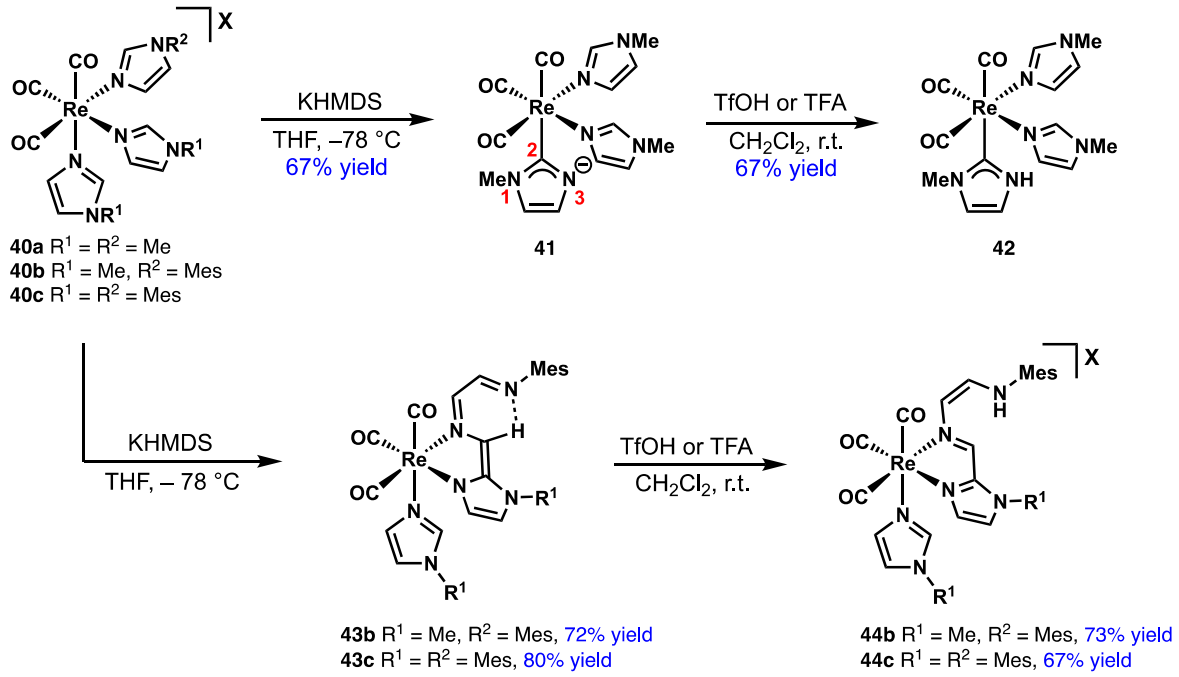

Scheme 11. Substituent-dependent formation of N(H),NR NHC complex **42** or ring-opening at *N*-alkylimidazole rhenium (I) complex **40**.

A topological analysis of the Laplacian of the electron density was performed for structures **41** and **42** using X-ray diffraction data. Complexes **41** and **42** both exhibited large non-bonded charge concentrations perpendicular to the plane at N3. Compound **41** also displayed an in-plane non-bonded charge concentration of similar magnitude at N3. However, the same was not true of product **42**, which instead showed a smaller bonded charge concentration. These observations are consistent with the presence of an in-plane lone pair on N3 for **41**, which is replaced by an N–H covalent interaction within structure **42**.

Interestingly, the *N*-substituents on the imidazole ligands have considerable bearing on the deprotonation outcome. If one or all of the methyl groups within complex **40a** are replaced with a

mesityl group, treatment with KHMDS results in the ring opening of an *N*-mesitylimidazole unit. It is thought that deprotonation takes place at the C2 position of one of the *N*-mesitylimidazole ligands, rapidly followed by the intramolecular attack of the NCHN moiety on an adjacent imidazole ligand by this nucleophilic C2 moiety. C–C coupling between the C2 atoms of two imidazole ligands and the ensuing ring-opening could furnish products **43b** and **43c**. DFT studies were employed to probe the reaction mechanism and suggest that the *N*-mesityl group enhances electron delocalization, and thus stabilizes, the transition state for the ring-opening step [81]. The amido-like nitrogen can be converted into the amine with the addition of acid to obtain species **44b** and **44c** in good yields. The N,NR NHC complex **41** can undergo a second metalation with $[AuCl(PPh_3)_2]$ to give the NM,NR NHC heterobimetallic complex **45** (Scheme 12) [81]. Notably, the imidazolyl fragment tautomerizes to the Re–N-bound form to accommodate the *C*-binding preference of the Au(I) center.

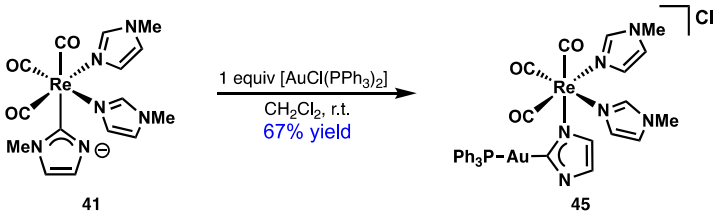

41 45

Scheme 12. Auration of N,NR rhenium(I) complex **41** involving tautomerization of the imidazolyl ligand.

A similar phenomenon has been observed in a manganese/gold system by Ruiz et al. (Scheme 13) [82]. In this case, manganese(I) imidazole complex **46** was transformed into the protic NHC complex **49**. The authors propose that the deprotonation of species **46** leads to an *N*-bound anionic species **47**, which isomerizes to *C*-bound analogue **48**. Although neither of these intermediates could be isolated, infrared spectroscopic analysis determined decreased ν(CO) frequencies (~10 cm^{-1} on average) that were consistent with NHC formation. This is a reflection of the stronger donor capability of NHCs compared to their corresponding imidazole counterparts. Metalation of the NHC complex **49** was accomplished under basic conditions. Presumably, the soft gold(I) center initially coordinates to the hard anionic nitrogen on the NHC ligand, and subsequently undergoes a 1,2-migration in order to bind with the softer carbene donor to afford heterobimetallic product **50**. The Mn–N bond within species **50** can be cleaved with perchloric acid to give the gold(I) protic NHC complex **51**. This demonstrates that NM,NR NHC complexes of manganese(I) may serve as NH,NR carbene transfer agents for gold(I) species, which represents a complementary approach to the Ag_2O transfer method. The latter strategy is limited to preparing NR,NR NHCs. The route depicted in Scheme 13 for the formation of manganese(I) protic NHC complexes can be extended to benzannulated heterocycles such as benzimidazole and benzoxazole. However, their use as carbene transfer agents is currently prevented by the instability of the corresponding manganese(I)/gold(I) heterobimetallic complexes [83].

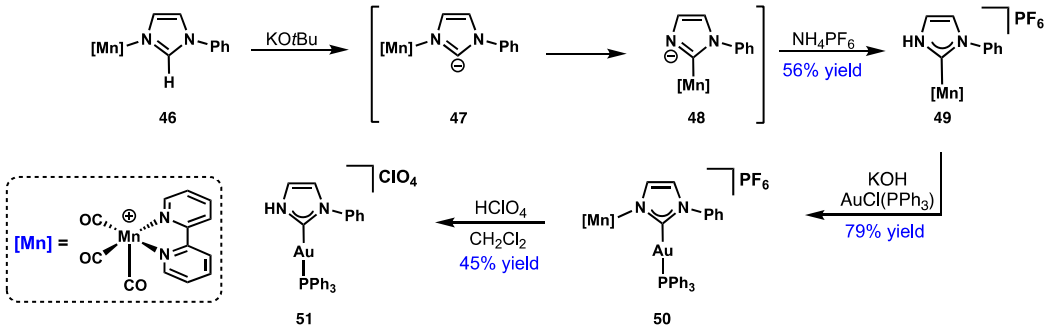

46 47 48 49 50 51

Scheme 13. Carbene transfer from a manganese(I) complex **49** to gold(I) complex **51** via heterobimetallic intermediate **50**.

Radius and Hering obtained N,NR platinum(II) complex **53** via the C–N bond cleavage of I(*i*Pr) (Scheme 14) [84]. When this reaction was conducted in nonpolar solvents, such as toluene or benzene, the reaction of [$Pt(PPh_3)_2(\eta^2$-$C_2H_4)$] (**52**) with excess I(*i*Pr) generated species **53** as the major product, which occurred presumably via homoleptic bis-NHC platinum(II) complex **54**. The evolution of propylene was detected during this transformation, which is consistent with the C–N bond cleavage of I(*i*Pr) that was observed. When the analogous reaction was performed in hexanes, complex **54** precipitated from solution, which prevented subsequent reactions with free I(*i*Pr). Indeed, the authors showed that reacting compound **54** with equimolar quantities of I(*i*Pr) also affords product **53**. Radius and Hering did not consider the imidazolyl fragment within complex **53** to display carbene character, which was in part because of the elongated Pt–$C_{imidazolyl}$ bond relative to the Pt–C_{NHC} bond. However, they acknowledged that this elongation may be due to the *trans* influence of the hydride ligand, and noted that a similar Pt–C_{NHC} bond length had been reported for an abnormal NHC complex [85].

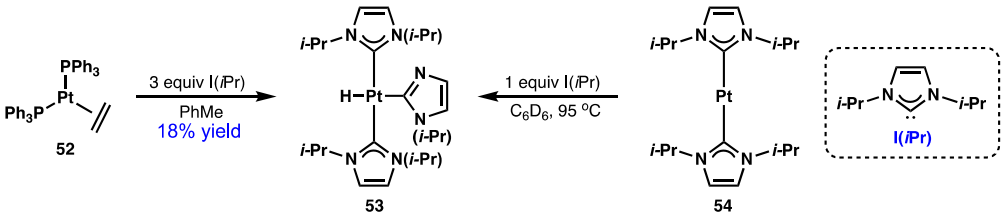

Scheme 14. Platinum-mediated C–N bond cleavage affording N,NR complex **53**.

Since the carbene and carbanion represent resonance forms of each other, it is possible that these assignments are strongly dependent on the identity of the coordinated metal, and as such, these designations must be made on a case-by-case basis. For example, the uranyl complex **55** exhibits exceptionally short U–C bonds and an extreme downfield ^{13}C NMR signal that is most consistent with a carbanionic imidazolyl ligand (Scheme 15) [86]. In contrast, the M–C bond lengths in the isomerized iron(II) and cobalt(II) derivatives **56a**,**b** fall within the normal range expected for their respective NHC complexes. The new U–N bond is slightly shorter than those previously observed for U–$N_{imidazole}$ complexes, which may be ascribed to the presence of a negative charge on the nitrogen atom. This suggests that the imidazolyl ligand may adopt the carbanionic resonance form when coordinated to the hard uranyl center, but undergoes electronic reconfiguration to become the carbene when bound to softer transition metal ions.

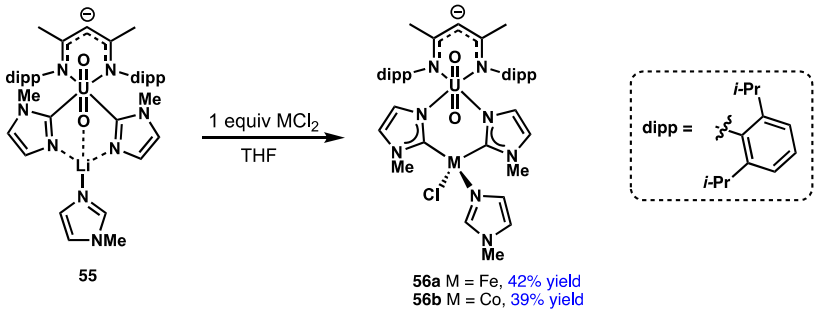

Scheme 15. Metalation and tautomerization of uranyl imidazolyl complex **55**.

Evidence consistent with the existence of NM,NR-free NHCs have also been reported. Indeed, Ruiz et al. speculated that one such species (**47**, Scheme 13) may be an intermediate formed during the deprotonation of compound **46**, prior to N–C migration of the manganese(I) ion [82]. Furthermore, it is conceivable that deprotonation and rhenium(I) migration onto the *C*-center from complex **40a** proceeds via an NM,NR-free NHC species (Scheme 11). However, the isolation of such NM,NR-free NHCs have not been disclosed. Theoretical studies have invoked the formation of NM,NR-free NHC complexes in intriguing metal-catalyzed transformations. For example, DFT studies undertaken by Ariafard

et al. exploring the mechanisms of two independent experimental reports of copper(I)-catalyzed carboxylation from the Hou and Nolan groups provide evidence implicating NM,NR-type free NHC complexes [87]. Hou et al. performed the direct insertion of CO_2 into the C2–H bond of various *N*-heterocycles under relatively mild conditions (Scheme 16) [88].

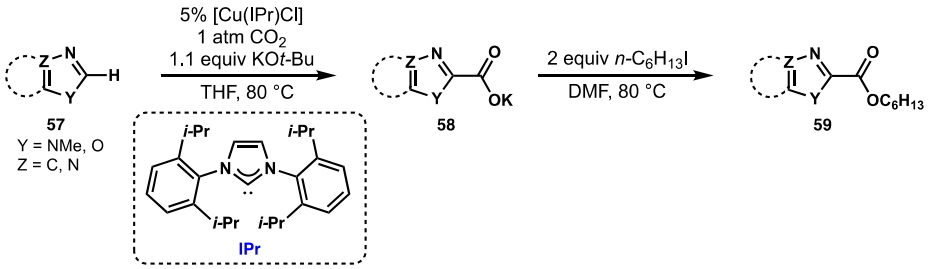

Scheme 16. Direct copper(I)-catalyzed carboxylation of aromatic C–H bonds within heterocycles **57**.

Nolan and Cazin employed the closely related [Cu(IPr)(OH)] catalyst to install ester functionalities onto heteroarenes and polyfluorinated benzenes. These authors also applied the same chemistry to carboxylate N–H bonds of imidazoles, pyrazoles, and even oxygen-containing heterocycles such as 2-oxazolidinone [89]. Hou et al. proposed the catalytic cycle shown in Scheme 17; this cycle featured copper(I) intermediates **60** and **61**, which were both isolated from the stoichiometric carboxylation of benzoxazole [88]. The mechanism that was put forward comprised three main steps: (i) first, the activation of the heterocyclic C–H bond by copper(I); (ii) CO_2 insertion into the Cu–C bond, (iii) and finally, salt metathesis with KO*t*-Bu to regenerate the active catalyst [Cu(IPr)(O*t*Bu)] and produce carboxylate salt **58**, which ultimately provides ester product **59**.

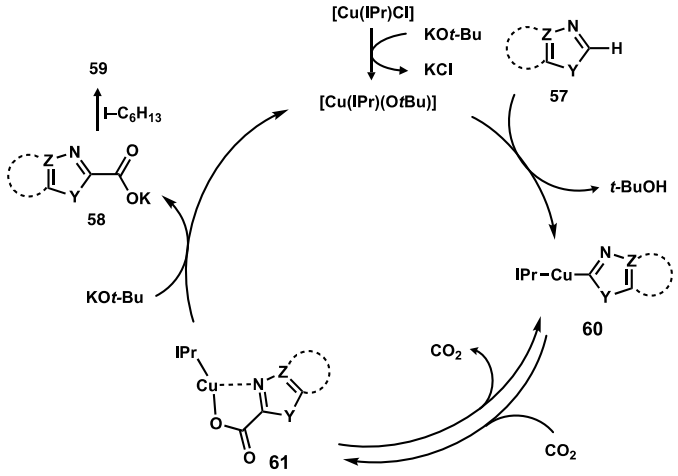

Scheme 17. Proposed mechanism for the copper(I)-catalyzed direct carboxylation of aromatic *N*-heterocycles **57**.

Although carbon dioxide is inexpensive, abundant, and low in toxicity, this species is a notoriously inert molecule due to its high thermodynamic stability. Thus, the independent reports disclosed by the Hou and Nolan groups represent significant advances in the development of efficient and alternative methods for harnessing carbon dioxide in synthesis, which may have important implications for future approaches for carbon capture, storage, and reuse. Furthermore, the relatively mild reaction conditions employed suggest the capacity for high functional group tolerance in these processes. In order to better understand the carboxylation process, Ariafard et al. conducted a detailed DFT investigation of the reaction mechanism proposed by Hou et al. [87].

Two possible pathways were identified for the first step of the catalytic cycle: namely, the protonolysis of [Cu(IPr)(OH)] by benzoxazole to form a copper(I) benzoxazole complex (Figure 5A).

Pathway I proceeds via a four-membered transition structure **TS-1a**, where proton transfer from benzoxazole to the OH ligand and benzoxazolyl migration to the copper species occur simultaneously. Alternatively, the reaction may occur via pathway II, which contains transition structure **TS-1b**, on which the copper complex interacts with the nitrogen instead of the carbon atom of benzoxazole during proton transfer to OH. The loss of water from **TS-1b** affords an NM,NR-free NHC, which then isomerizes into the *C*-metalated benzoxazolyl. Since **TS-1b** and **TS-1c** are lower in energy than **TS-1a**, the authors suggest that pathway II is more kinetically favorable than pathway I.

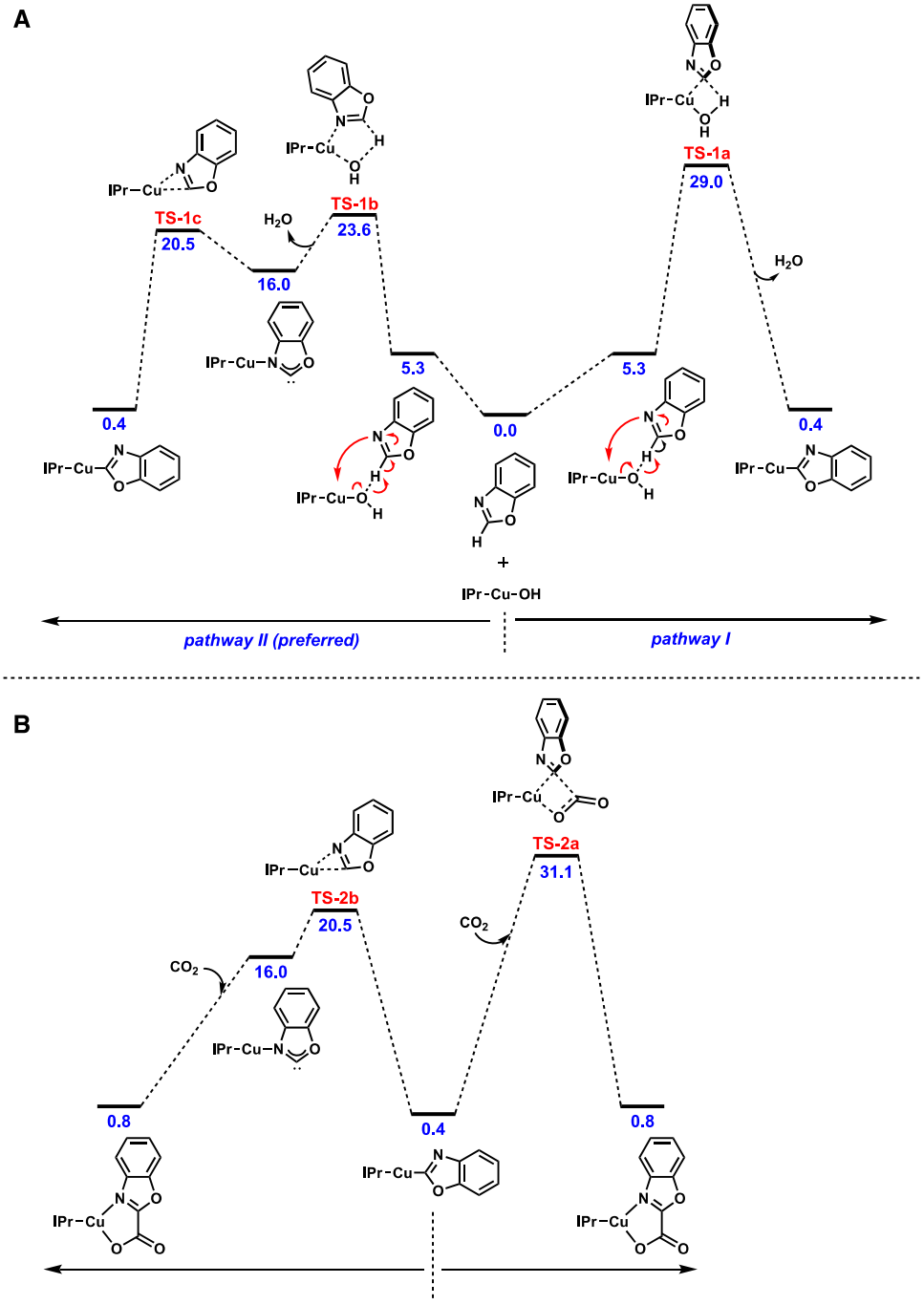

Figure 5. (**A**) Computed energy profiles for two possible pathways for the protonolysis of [Cu(IPr)(OH)] by benzoxazole determined via density functional theory (DFT). (**B**) Computed energy profiles for two possible CO_2 activation pathways from a copper benzoxazolyl complex determined via DFT. The relative free energies are given in kcal/mol.

The second step in the catalytic sequence concerns the insertion of carbon dioxide into the Cu–C bond of the copper(I) benzoxazolyl complex, resulting in a copper carboxylate complex (Figure 5B). The more conventional pathway III involves the nucleophilic attack of the Cu–C σ-bond on the electrophilic carbon atom within carbon dioxide, leading to four-membered transition structure **TS-2a**. The calculated energy barrier for this process is relatively high. However, Ariafard et al. were able to identify a second pathway with a lower energy barrier. This proposed mechanism, pathway IV, begins with the isomerization of the copper(I) benzoxazolyl complex into its *N*-metalated form. Remarkably, since the resulting NM,NR-free NHC is so much more nucleophilic than the Cu–C σ-bond, the functionalization of carbon dioxide is barrierless. The NM,NR-free NHC route also appeared to be the most energetically favorable for analogous CO_2 activation by a gold(I) species [90,91]. These findings highlight the dual functionality of NM,NR-free NHCs, which contain a Lewis acidic metal center and a Lewis basic free carbene, and suggest potential opportunities for these species to be exploited in cooperative catalysis.

Other instances of transformations that are cocatalyzed by an organometallic complex and a free NHC have been reported. For example, Yu and Zhang suggest that polyNHC dendrimer **62** can serve as both a ligand and a catalyst in the direct carboxylation into the C–H bond of terminal alkynes, enabling the synthesis of functionalized propiolic acids (Figure 6) [92]. These authors observed that the carboxylation of model substrate 4-nitro-1-ethynylbenzene proceeded most efficiently when only half a molar equivalent of CuCl (relative to the polyNHC) was employed. The yield of the propiolic acid product decreased markedly when a stoichiometric amount of CuCl was used, while no reaction occurred in the absence of CuCl. This prompted them to postulate that both the copper–NHC complex and the free NHC were required for optimal catalytic performance. Presumably, the [Cu(NHC)Cl] and free NHC fragments cooperatively activate both the terminal alkyne and carbon dioxide in the presence of a base. The NHC carboxylate coordinates to the proximal copper atom, facilitating the nucleophilic attack of the acetylide carbanion on the carboxylate carbon. This links the alkyne and carboxyl moieties within propiolic acid, which can be exchanged for another alkyne unit at the copper center.

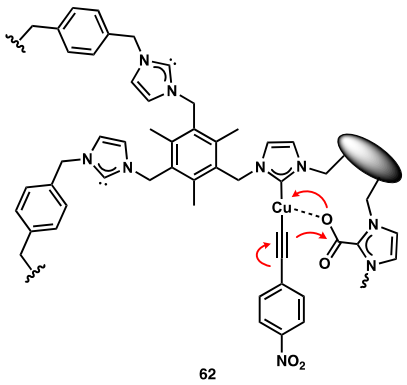

62

Figure 6. Cooperative CO_2 insertion into the C–H bond of terminal alkynes by copper(I) and a free carbene on a poly-NHC scaffold **62**.

In the dendrimer prepared by Yu and Zhang, the copper–NHC and free NHC are remote from each other. However, in Hou and Nolan's systems, the two functional sites in the putative NM,NR-free NHC intermediate are directly adjacent to each other. In fact, NM,NR-free NHCs could be viewed as the *N*-metalated tautomer **22a** (Figure 4). It has already been shown that complexes bearing structural motifs, such as **22a**, can activate hydrogen and acetylene gases, suggesting that it may be beneficial to ensure that the two complementary moieties are proximal. Given the general utility of the bifunctional ambident reactivity concept and encouraging evidence for the role of NM,NR-free NHCs in valuable carboxylation chemistry, further efforts directed toward the preparation and extensive study of these species is warranted. Certainly, this reactivity may extend beyond carbon dioxide to the activation of other inert small molecule feedstock chemicals.

To date, NM,NR-free NHCs have eluded isolation. Readers may have observed that there is little preventing the migration of the metal ion to the carbene, which forms the thermodynamically-favored complex in the preceding examples. DFT calculations estimate the energy separation between the copper–benzoxazolyl NM,NR-free NHC and its less energetic *C*-bound isomer at 15.4 kcal/mol (Figure 5). Perhaps with the appropriate structural modifications, this gap can be reduced to the point that the NM,NR-free NHC is stable enough to be isolated. Ideally, the barrier to tautomerization should be high so that the NM,NR-free NHC does not convert into the *C*-bound complex. The synthesis of protic NHC complexes encounter similar issues, so it is possible that strategies, such as using chelating pendant donors to direct the metal center onto a desired position, could be exploited in this domain.

3. Summary and Conclusions

Relative to the more established field of classical NHC chemistry, the fundamental understanding and applications of protic and naked NHCs is conspicuously lacking. The bonding nature of these non-classical carbenes remains a topic of debate and an area in which much remains to be discovered. As the knowledge and general understanding regarding the preparation and reactivity of protic and naked NHCs improves, their application in chemical synthesis will arguably become more widespread. It is possible that the synthetic applications of these systems may extend into chemical transformations that are traditionally performed by main group elements, such as a small molecule activation that is similar to the chemistry associated with frustrated Lewis pairs [93]. Furthermore, the aforementioned theoretical studies suggest the existence of *N*-metalated, NR-free NHC complexes in which the carbene moiety is available for cooperative reactivity [87].

Unlike classical NHCs, which tend to typically function solely as spectator ligands, the power of protic and naked NHC ligands relate to their non-innocent behavior, which is described by the bifunctional ambident reactivity concept. Their innate reactivity provides access to a rich variety of functionalized species, which lend themselves well to catalytic applications and processes that involve hydrogen bonding. The development of novel bifunctional catalysts may be enabled by utilizing this new subclass of NHCs. In addition, other applications may include exploiting these systems to facilitate the stereoselective synthesis of NHC-containing macrocycles and novel ligand scaffolds. Although protic and naked NHCs currently represent an emerging subclass of NHC molecules, their intrinsic properties and reactivity indicates that these systems have the capacity to contribute to broadening the power and scope of catalytic processes in the future.

Funding: This research received no external funding.

Acknowledgments: M.Y.L. thanks the University of Tasmania for a Tasmanian Graduate Research Scholarship.

Conflicts of Interest: The authors declare no conflict of interest.

References

1. Igau, A.; Grutzmacher, H.; Baceiredo, A.; Bertrand, G. Analogous α,α′-Bis-Carbenoid Triply Bonded Species: Synthesis of a Stable λ^3-Phosphinocarbene-λ^5-Phosphaacetylene. *J. Am. Chem. Soc.* **1988**, *110*, 6463–6466. [CrossRef]
2. Arduengo, A.J., III; Harlow, R.L.; Kline, M. A Stable Crystalline Carbene. *J. Am. Chem. Soc.* **1991**, *113*, 361–363. [CrossRef]
3. Herrmann, W.A.; Elison, M.; Fischer, J.; Kocher, C.; Artus, G.R.J. Metal Complexes of *N*-Heterocyclic Carbenes—A New Structural Principle for Catalysts in Homogeneous Catalysis. *Angew. Chem. Int. Ed.* **1995**, *34*, 2371–2374. [CrossRef]
4. Herrmann, W.A.; Kocher, C. *N*-Heterocyclic Carbenes. *Angew. Chem. Int. Ed.* **1997**, 2162–2187. [CrossRef]
5. Herrmann, W.A. *N*-Heterocyclic Carbenes: A New Concept in Organometallic Catalysis. *Angew. Chem. Int. Ed.* **2002**, *41*, 1290–1309. [CrossRef]
6. Crabtree, R.H. Carbenes in Synthesis and Homogeneous Catalysis. *Oil Gas Sci. Technol.* **2007**, *62*, 739–744. [CrossRef]

7. Hahn, F.E.; Jahnke, M.C. Heterocyclic Carbenes: Synthesis and Coordination Chemistry. *Angew. Chem. Int. Ed.* **2008**, *47*, 3122–3172. [CrossRef] [PubMed]
8. Öfele, K.; Tosh, E.; Taubmann, C.; Herrmann, W.A. Carbocyclic Carbene Metal Complexes. *Chem. Rev.* **2009**, *109*, 3408–3444. [CrossRef] [PubMed]
9. Díez-González, S.; Marion, N.; Nolan, S.P. *N*-Heterocyclic Carbenes in Late Transition Metal Catalysis. *Chem. Rev.* **2009**, *109*, 3612–3676. [CrossRef] [PubMed]
10. Bugaut, X.; Glorius, F. Organocatalytic umpolung: *N*-heterocyclic carbenes and beyond. *Chem. Soc. Rev.* **2012**, *41*, 3511–3522. [CrossRef]
11. Flanigan, D.M.; Romanov-Michailidis, F.; White, N.A.; Rovis, T. Organocatalytic Reactions Enabled by *N*-Heterocyclic Carbenes. *Chem. Rev.* **2015**, *115*, 9307–9387. [CrossRef] [PubMed]
12. Schuster, O.; Yang, L.; Raubenheimer, H.G.; Albrecht, M. Beyond Conventional *N*-Heterocyclic Carbenes: Abnormal, Remote, and Other Classes of NHC Ligands with Reduced Heteroatom Stabilization. *Chem. Rev.* **2009**, *109*, 3445–3478. [CrossRef] [PubMed]
13. Arduengo, A.J., III; Krafczyk, R.; Schmutzler, R.; Craig, H.A.; Goerlich, J.R.; Marshall, W.J.; Unverzagt, M. Imidazolylidenes, imidazolinylidenes and imidazolidines. *Tetrahedron* **1999**, *55*, 14523–14534. [CrossRef]
14. Davies, C.J.E.; Page, M.J.; Ellul, C.E.; Mahon, M.F.; Whittlesey, M.K. Ni(I) and Ni(II) ring-expanded *N*-heterocyclic carbene complexes: C–H activation, indole elimination and catalytic hydrodehalogenation. *Chem. Commun.* **2010**, *46*, 5151–5153. [CrossRef] [PubMed]
15. Hauwert, P.; Dunsford, J.J.; Tromp, D.S.; Weigand, J.J.; Lutz, M.; Cavell, K.J.; Elsevier, C.J. Zerovalent [Pd(NHC)(Alkene)$_{1,2}$] Complexes Bearing Expanded-Ring *N*-Heterocyclic Carbene Ligands in Transfer Hydrogenation of Alkynes. *Organometallics* **2013**, *32*, 131–140. [CrossRef]
16. Dunsford, J.J.; Cavell, K.J. Pd–PEPPSI-Type Expanded Ring *N*-Heterocyclic Carbene Complexes: Synthesis, Characterization, and Catalytic Activity in Suzuki–Miyaura Cross Coupling. *Organometallics* **2014**, *33*, 2902–2905. [CrossRef]
17. Türkmen, H.; Pape, T.; Hahn, F.E.; Çetinkaya, B. Annulated *N*-Heterocyclic Carbene Ligands Derived from 2-Methylaminopiperidine: Their Complexes and Catalytic Applications. *Organometallics* **2008**, *27*, 571–575. [CrossRef]
18. Martin, D.; Lassauque, N.; Donnadieu, B.; Bertrand, G. A Cyclic Diaminocarbene with Pyramidalized Nitrogen Atom: A Stable *N*-Heterocyclic Carbene with Enhanced Nucleophilicity. *Angew. Chem. Int. Ed.* **2012**, *51*, 6172–6175. [CrossRef] [PubMed]
19. Yang, B.-M.; Xiang, K.; Tu, Y.-Q.; Zhang, S.-H.; Yang, D.-T.; Wang, S.-H.; Zhang, F.-M. Spiro-fused six-membered *N*-heterocyclic carbene: A new scaffold toward unique properties and activities. *Chem. Commun.* **2014**, *50*, 7163–7165. [CrossRef] [PubMed]
20. Rao, B.; Tang, H.; Zeng, X.; Liu, L.; Melaimi, M.; Bertrand, G. Cyclic (Amino)(aryl)carbenes (CAArCs) as Strong σ-Donating and π-Accepting Ligands for Transition Metals. *Angew. Chem. Int. Ed.* **2015**, *54*, 14915–14919. [CrossRef] [PubMed]
21. Peris, E.; Crabtree, R.H. Recent homogeneous catalytic applications of chelate and pincer *N*-heterocyclic carbenes. *Coord. Chem. Rev.* **2004**, *248*, 2239–2246. [CrossRef]
22. Vignolle, J.; Cattoën, X.; Bourissou, D. Stable Noncyclic Singlet Carbenes. *Chem. Rev.* **2009**, *109*, 3333–3384. [CrossRef] [PubMed]
23. Mata, J.A.; Poyatos, M.; Peris, E. Structural and catalytic properties of chelating bis- and tris-*N*-heterocyclic carbenes. *Coord. Chem. Rev.* **2007**, *251*, 841–859. [CrossRef]
24. Pugh, D.; Danopoulos, A.A. Metal complexes with 'pincer'-type ligands incorporating *N*-heterocyclic carbene functionalities. *Coord. Chem. Rev.* **2007**, *251*, 610–641. [CrossRef]
25. Poyatos, M.; Mata, J.A.; Peris, E. Complexes with Poly(*N*-heterocyclic carbene) Ligands: Structural Features and Catalytic Applications. *Chem. Rev.* **2009**, *109*, 3677–3707. [CrossRef] [PubMed]
26. Hopkinson, M.N.; Ritcher, C.; Schedler, M.; Glorius, F. An overview of *N*-heterocylic carbenes. *Nature* **2014**, *510*, 485–496. [CrossRef] [PubMed]
27. Zhang, D.; Zi, G. *N*-heterocyclic carbene (NHC) complexes of group 4 transition metals. *Chem. Soc. Rev.* **2015**, *44*, 1898–1921. [CrossRef]
28. Peris, E. Smart *N*-Heterocyclic Carbene Ligands in Catalysis. *Chem. Rev.* **2018**, *118*, 9988–10031. [CrossRef]
29. Charra, V.; de Fremont, P.; Braunstein, P. Multidentate *N*-heterocyclic carbene complexes of the 3d metals: Synthesis, structure, reactivity and catalysis. *Coord. Chem. Rev.* **2017**, *341*, 53–176. [CrossRef]

30. Gardiner, M.G.; Ho, C.C. Recent advances in bidentate bis(*N*-heterocyclic carbene) transition metal complexes and their applications in metal-mediated reactions. *Coord. Chem. Rev.* **2018**, *375*, 373–388. [CrossRef]
31. Kuwata, S.; Hahn, F.E. Complexes Bearing Protic *N*-Heterocyclic Carbene Ligands. *Chem. Rev.* **2018**, *118*, 9642–9677. [CrossRef]
32. Liu, M.; Namyslo, J.C.; Nieger, M.; Polamo, M.; Schmidt, A. From betaines to anionic *N*-heterocyclic carbenes. Borane, gold, rhodium, and nickel complexes starting from an imidazoliumphenolate and its carbene tautomer. *Beilstein J. Org. Chem.* **2016**, *12*, 2673–2681. [CrossRef] [PubMed]
33. César, V.; Lugan, N.; Lavigne, G. A Stable Anionic *N*-Heterocyclic Carbene and Its Zwitterionic Complexes. *J. Am. Chem. Soc.* **2008**, *130*, 11286–11287. [CrossRef] [PubMed]
34. Danopoulos, A.A.; Monakhov, K.Y.; Braunstein, P. Anionic *N*-Heterocyclic Carbene Ligands from Mesoionic Imidazolium Precursors: Remote Backbone Arylimino Substitution Directs Carbene Coordination. *Chem. Eur. J.* **2013**, *19*, 450–455. [CrossRef] [PubMed]
35. Liddle, S.T.; Edworthy, I.S.; Arnold, P.L. Anionic tethered *N*-heterocyclic carbene chemistry. *Chem. Soc. Rev.* **2007**, *36*, 1732–1744. [CrossRef] [PubMed]
36. Benhamou, L.; César, V.; Gornitzka, H.; Lugan, N.; Lavigne, G. Imidazol-2-ylidene-4-olate: An anionic *N*-heterocyclic carbene pre-programmed for further derivatization. *Chem. Commun.* **2009**, 4720–4722. [CrossRef] [PubMed]
37. Wang, X.; Chen, H.; Li, X. Ir(III)-induced C-bound to *N*-bound tautomerization of a *N*-heterocyclic carbene. *Organometallics* **2007**, *26*, 4684–4687. [CrossRef]
38. Heinemann, C.; Thiel, W. Ab initio study on the stability of diaminocarbenes. *Chem. Phys. Lett.* **1994**, *217*, 11–16. [CrossRef]
39. McGibbon, G.A.; Heinemann, C.; Lavorato, D.J.; Schwarz, H. Imidazol-2-ylidene: Generation of a Missing Carbene and Its Dication by Neutralization- Reionization and Charge-Stripping Mass Spectrometry. *Angew. Chem. Int. Ed.* **1997**, *36*, 1478–1481. [CrossRef]
40. Häller, L.J.L.; Macgregor, S.A. Computational Study of the *C*- and *N*-Bound Tautomers of [Ru(Cl)(H)(CO)-(PPh_3)$_2$ (I*i*PrMe$_2$)] (I*i*PrMe$_2$ = 3-Isopropyl-4,5-dimethylimidazol-2-ylidene). *Eur. J. Inorg. Chem.* **2009**, *2009*, 2000–2006. [CrossRef]
41. Sini, G.; Eisenstein, O.; Crabtree, R.H. Preferential C-binding versus *N*-binding in imidazole depends on the metal fragment involved. *Inorg. Chem.* **2002**, *41*, 602–604. [CrossRef] [PubMed]
42. Fehlhammer, W.P.; Völkl, A.; Plaia, U.; Beck, G. Metallkomplexe funktioneller Isocyanide, XVI1) 1,3-Dipolare Cycloadditionen von Heteroallenen an die metallorganischen Nitrilylide [$(OC)_5$M–C≡N–CHR]$^-$ (M = Cr, W; R = CO_2Et). *Chem. Ber.* **1987**, *120*, 2031–2040. [CrossRef]
43. Michelin, R.A.; Zanotto, L.; Braga, D.; Sabatino, P.; Angelici, R.J. Transition-Metal-Promoted Cyclization Reactions of Isocyanide Ligands. Synthesis of Cyclic Diaminocarbenes from Isocyanide Complexes of Palladium(II) and Platinum(II) and X-ray Structure of *cis*-Br_2Pt[CN(C_6H_4-*p*-Me)CH_2CH_2N(H)](PPh_3). *Inorg. Chem.* **1988**, *27*, 93–99. [CrossRef]
44. Michelin, R.A.; Mozzon, M.; Zecca, M.; Corain, B.; Piazzi, O.; Zanotti, G. Palladium(II) cyclic carbene complexes from 3-isocyanopropylacrylate. X-ray structure of cis-{$PdCl_2$(PPh_3)[C–N(H)–$(CH_2)_3$–O–C(O)–CH–CH_2]}. *Inorg. Chim. Acta* **1990**, *174*, 3–7. [CrossRef]
45. Hahn, F.E.; Langenhahn, V.; Pape, T. Template synthesis of tungsten complexes with saturated *N*-heterocyclic carbene ligands. *Chem. Commun.* **2005**, *5*, 5390–5392. [CrossRef] [PubMed]
46. Kaufhold, O.; Flores-Figueroa, A.; Pape, T.; Hahn, F.E. Template Synthesis of Ruthenium Complexes with Saturated and Benzannulated NH,NH-Stabilized *N*-Heterocyclic Carbene Ligands. *Organometallics* **2009**, *28*, 896–901. [CrossRef]
47. Hahn, F.E.; Langenhahn, V.; Meier, N.; Lügger, T.; Fehlhammer, W.P. Template synthesis of benzannulated *N*-heterocyclic carbene ligands. *Chem. Eur. J.* **2003**, *9*, 704–712. [CrossRef]
48. Liu, C.Y.; Chen, D.Y.; Lee, G.H.; Peng, S.M.; Liu, S.T. Synthesis of cyclic diamino-substituted metal carbene complexes. *Organometallics* **1996**, *15*, 1055–1061. [CrossRef]
49. Brendler, E.; Hill, A.F.; Wagler, J. A donor-stabilized silanethione or a Si-substituted *N*-heterocyclic platinum carbene? *Chem. A Eur. J.* **2008**, *14*, 11300–11304. [CrossRef]
50. Dobereiner, G.E.; Chamberlin, C.A.; Schley, N.D.; Crabtree, R.H. Acyl protection strategy for synthesis of a protic NHC complex via *N*-acyl methanolysis. *Organometallics* **2010**, *29*, 5728–5731. [CrossRef]

51. Fehlhammer, W.P.; Bliß, T.; Fuchs, J.; Holzmann, G. Tetrakis (*N*-alkylimidazolin-2-yliden) palladium and -platin. *Zeitschrift für Naturforsch. B* **1992**, *59*, 79–89. [CrossRef]
52. Meier, N.; Hahn, F.E.; Pape, T.; Siering, C.; Waldvogel, S.R. Molecular recognition utilizing complexes with NH,NR-stabilized carbene ligands. *Eur. J. Inorg. Chem.* **2007**, 1210–1214. [CrossRef]
53. Bonati, F.; Burini, A.; Pietroni, B.R.; Bovio, B. Reactions of C-imidazolyllithium derivatives with Group Ib compounds: Tris[μ-(1-alkylimidazolato-N3,C2)]tri-gold(I) and -silver(I). Crystal structure of bis(1-benzylimidazolin-2-yliden)gold(I) chloride. *J. Organomet. Chem.* **1989**, *375*, 147–160. [CrossRef]
54. Raubenheimer, H.G.; Lindeque, L.; Cronje, S. Synthesis and characterization of neutral and cationic diamino carbene complexes of gold(I). *J. Organomet. Chem.* **1996**, *511*, 177–184. [CrossRef]
55. Huertos, M.A.; Pérez, J.; Riera, L.; Menéndez-Velázquez, A. From *N*-alkylimidazole ligands at a rhenium center: Ring opening or formation of NHC complexes. *J. Am. Chem. Soc.* **2008**, *130*, 13530–13531. [CrossRef] [PubMed]
56. Sundberg, R.J.; Bryan, R.F.; Taylor, I.F.; Taube, H. Nitrogen-Bound and Carbon-Bound Imidazole Complexes of Ruthenium Ammines. *J. Am. Chem. Soc.* **1974**, *96*, 381–392. [CrossRef]
57. Hahn, F.E.; Naziruddin, A.R.; Hepp, A.; Pape, T. Synthesis, characterization, and H-bonding abilities of ruthenium(II) complexes bearing bidentate NR,NH-carbene/phosphine ligands. *Organometallics* **2010**, *29*, 5283–5288. [CrossRef]
58. Eguillor, B.; Esteruelas, M.A.; García-Raboso, J.; Oliván, M.; Oñate, E.; Pastor, I.M.; Peñafiel, I.; Yus, M. Osmium NHC complexes from alcohol-functionalized imidazoles and imidazolium salts. *Organometallics* **2011**, *30*, 1658–1667. [CrossRef]
59. Araki, K.; Kuwata, S.; Ikariya, T. Isolation and interconversion of protic *N*-heterocyclic carbene and imidazolyl complexes: Application to catalytic dehydrative condensation of *N*-(2-Pyridyl)benzimidazole and allyl alcohol. *Organometallics* **2008**, *27*, 2176–2178. [CrossRef]
60. Miranda-Soto, V.; Grotjahn, D.B.; Cooksy, A.L.; Golen, J.A.; Moore, C.E.; Rheingold, A.L. A Labile and Catalytically Active Imidazol-2-yl Fragment System. *Angew. Chem. Int. Ed.* **2011**, *50*, 631–635. [CrossRef]
61. Miranda-Soto, V.; Grotjahn, D.B.; DiPasquale, A.G.; Rheingold, A.L. Imidazol-2-yl Complexes of Cp*Ir as Bifunctional Ambident Reactants. *J. Am. Chem. Soc.* **2008**, *130*, 13200–13201. [CrossRef] [PubMed]
62. Naziruddin, A.R.; Hepp, A.; Pape, T.; Hahn, F.E. Synthesis of Rhodium(I) Complexes Bearing Bidentate NH,NR-NHC/Phosphine Ligands. *Organometallics* **2011**, *30*, 5859–5866. [CrossRef]
63. Flowers, S.E.; Cossairt, B.M. Mono- and Dimetalation of a Tridentate Bisimidazole-Phosphine Ligand. *Organometallics* **2014**, *33*, 4341–4344. [CrossRef]
64. He, F.; Braunstein, P.; Wesolek, M.; Danopoulos, A.A. Imine-functionalised protic NHC complexes of Ir: Direct formation by C–H activation. *Chem. Commun.* **2015**, *51*, 2814–2817. [CrossRef] [PubMed]
65. Cepa, S.; Schulte To Brinke, C.; Roelfes, F.; Hahn, F.E. Hydrogen Activation by an Iridium(III) Complex Bearing a Bidentate Protic NH,NR-NHCˆPhosphine Ligand. *Organometallics* **2015**, *34*, 5454–5460. [CrossRef]
66. Wiedemann, S.H.; Lewis, J.C.; Ellman, J.A.; Bergman, R.G. Experimental and Computational Studies on the Mechanism of *N*-Heterocycle C−H Activation by Rh(I). *J. Am. Chem. Soc.* **2006**, *128*, 2452–2462. [CrossRef]
67. Hawkes, K.J.; Cavell, K.J.; Yates, B.F. Rhodium-Catalyzed C−C Coupling Reactions: Mechanistic Considerations. *Organometallics* **2008**, *27*, 4758–4771. [CrossRef]
68. Lewis, J.C.; Wu, J.Y.; Bergman, R.G.; Ellman, J.A. Microwave-Promoted Rhodium-Catalyzed Arylation of Heterocycles through C−H Bond Activation. *Angew. Chem. Int. Ed.* **2006**, *45*, 1589–1591. [CrossRef]
69. Johnson, L.K.; Angelici, R.J. Synthesis of Aminooxycarbene Complexes of Iron with *N*-Alkyl, -Allyl, and -Carbamoyl Groups. *Inorg. Chem.* **1987**, *26*, 973–976. [CrossRef]
70. Hahn, F.E.; Langenhahn, V.; Lügger, T.; Pape, T.; Le Van, D. Template Synthesis of a Coordinated Tetracarbene Ligand with Crown Ether Topology. *Angew. Chem. Int. Ed.* **2005**, *44*, 3759–3763. [CrossRef]
71. Kaufhold, O.; Stasch, A.; Edwards, P.G.; Hahn, F.E. Template Controlled Synthesis of a Coordinated [11]ane-P_2C^{NHC} Macrocycle. *Chem. Commun* **2007**, 1822–1824. [CrossRef] [PubMed]
72. Kaufhold, O.; Stasch, A.; Pape, T.; Hepp, A.; Edwards, P.G.; Newman, P.D.; Hahn, F.E. Metal Template Controlled Formation of [11]ane- P_2C^{NHC} Macrocycles. *J. Am. Chem. Soc.* **2009**, *131*, 306–317. [CrossRef]
73. Blase, V.; Pape, T.; Hahn, F.E. Template Synthesis of a Macrocycle with a Mixed NHC/phosphine Donor Set. *J. Organomet. Chem.* **2011**, *696*, 3337–3342. [CrossRef]

74. Flores-Figueroa, A.; Kaufhold, O.; Hepp, A.; Fröhlich, R.; Hahn, F.E. Synthesis of a Ruthenium(II) Complex Containing an [11]ane-P_2C^{NHC} (NHC = Imidazolidin-2-ylidene) Macrocycle. *Organometallics* **2009**, *28*, 6362–6369. [CrossRef]
75. Flores-Figueroa, A.; Pape, T.; Weigand, J.J.; Hahn, F.E. Template-Controlled Formation of an [11]ane- P2CNH^{C} Macrocyclic Ligand at an Iron(II) Template. *Eur. J. Inorg. Chem.* **2010**, 2907–2910. [CrossRef]
76. Boche, G.; Hilf, C.; Harms, K.; Marsch, M.; Lohrenz, J.C.W. Crystal Structure of the Dimeric(4-tert-Butylthiazolato)(glyme)lithium: Carbene Character of a Formyl Anion Equivalent. *Angew. Chem. Int. Ed.* **1995**, *34*, 487–489. [CrossRef]
77. Kösterke, T.; Kösters, J.; Würthwein, E.U.; Mück-Lichtenfeld, C.; Schulte To Brinke, C.; Lahoz, F.; Hahn, F.E. Synthesis of complexes containing an anionic NHC ligand with an unsubstituted ring-nitrogen atom. *Chem. Eur. J.* **2012**, *18*, 14594–14598. [CrossRef]
78. Arduengo, A.J.; Dixon, D.A.; Harlow, R.L.; Dias, H.V.R.; Booster, W.T.; Koetzle, T.F. Electron Distribution in a Stable Carbene. *J. Am. Chem. Soc.* **1994**, *116*, 6812–6822. [CrossRef]
79. Cernochvá, J.; Necas, M.; Kuritka, I.; Vicha, R. 1-(1-Adamantylmethyl)-1*H*-benzimidazole. *Acta Crystallogr. Sect. E* **2011**, *E67*, 2906. [CrossRef] [PubMed]
80. Hille, U.E.; Zimmer, C.; Vock, C.A.; Hartmann, R.W. First Selective CPB11B1 Inhibitors for the Treatment of Cortisol-Dependent Diseases. *ACS Med. Chem. Lett.* **2011**, *2*, 2–6. [CrossRef]
81. Huertos, M.A.; Pérez, J.; Riera, L.; Díaz, J.; López, R. Effect of the nature of the substituent in *N*-alkylimidazole ligands on the outcome of deprotonation: Ring opening versus the formation of *N*-heterocyclic carbene complexes. *Chem. Eur. J.* **2010**, *16*, 8495–8507. [CrossRef] [PubMed]
82. Ruiz, J.; Perandones, B.F. Base-Promoted Tautomerization of Imidazole Ligand to NHC & Subsequent Transmetalation Reaction. *J. Am. Chem. Soc.* **2007**, *129*, 9298–9299. [CrossRef] [PubMed]
83. Ruiz, J.; Berros, Á.; Perandones, B.F.; Vivanco, M. NHC–manganese(I) complexes as carbene transfer agents. *Dalton Trans.* **2009**, 6999. [CrossRef] [PubMed]
84. Hering, F.; Radius, U. From NHC to Imidazolyl Ligand: Synthesis of Platinum and Palladium Complexes d^{10}-[$M(NHC)_2$] (M = Pd, Pt) of the NHC 1,3-Diisopropylimidazolin-2-ylidene. *Organometallics* **2015**, *34*, 3236–3245. [CrossRef]
85. Fortman, G.C.; Scott, N.M.; Linden, A.; Stevens, E.D.; Dorta, R.; Nolan, S.P. Unusual reactivities of *N*-heterocyclic carbenes upon coordination to the platinum(II)–dimethyl moiety. *Chem. Commun.* **2010**, *46*, 1050–1052. [CrossRef]
86. Schettini, M.F.; Wu, G.; Hayton, T.W. Synthesis and reactivity of a uranyl-imidazolyl complex. *Chem. Commun.* **2012**, *48*, 1484–1486. [CrossRef]
87. Ariafard, A.; Zarkoob, F.; Batebi, H.; Stranger, R.; Yates, B.F. DFT studies on the carboxylation of the C-H bond of heteroarenes by copper(I) complexes. *Organometallics* **2011**, *30*, 6218–6224. [CrossRef]
88. Zhang, L.; Cheng, J.; Ohishi, T.; Hou, Z. Copper-catalyzed direct carboxylation of C-H bonds with carbon dioxide. *Angew. Chem. Int. Ed.* **2010**, *49*, 8670–8673. [CrossRef]
89. Boogaerts, I.I.F.; Fortman, G.C.; Furst, M.R.L.; Cazin, C.S.J.; Nolan, S.P. Carboxylation of N–H/C–H bonds using *N*-heterocyclic carbene copper(I) complexes. *Angew. Chem. Int. Ed.* **2010**, *49*, 8674–8677. [CrossRef]
90. Boogaerts, I.I.F.; Nolan, S.P. Carboxylation of C–H bonds using *N*-heterocyclic carbene gold(I) complexes. *J. Am. Chem. Soc.* **2010**, *132*, 8858–8859. [CrossRef]
91. Zhang, X.; Geng, Z.; Wang, Y.; Hou, X.; Wang, D. Theoretical studies on the mechanism of oxazole with CO2 catalyzed by gold(I) complexes. *J. Mol. Catal. A Chem.* **2012**, *363–364*, 31–40. [CrossRef]
92. Yu, D.; Zhang, Y. Copper- and copper–*N*-heterocyclic carbene-catalyzed C–H activating carboxylation of terminal alkynes with CO_2 at ambient conditions. *Proc. Natl. Acad. Sci. USA* **2010**, *107*, 20184–20189. [CrossRef] [PubMed]
93. Stephan, D.W.; Erker, G. Frustrated Lewis Pair Chemistry: Development and Perspectives. *Angew. Chem. Int. Ed.* **2015**, *54*, 6400–6441. [CrossRef] [PubMed]